

**Spatial and temporal relationship between
large-scale mass-failure events and turbidity currents:
a subsurface and outcrop investigation
of facies architecture evolution in deep-water
mass-transport deposit - influenced settings**

Riccardo Teloni

Submitted in accordance with the requirements for the degree of
Doctor of Philosophy

The University of Leeds
School of Earth and Environment

May 2017

The candidate confirms that the work submitted is his own and that appropriate credit has been given where reference has been made to the work of others.

This copy has been supplied on the understanding that it is copyright material and that no quotation from the thesis may be published without proper acknowledgement

© 2017 The University of Leeds and Riccardo Teloni

The right of Riccardo Teloni to be identified as Author of this work has been asserted by him in accordance with the Copyright, Designs and Patents Act 1988.

Acknowledgements

I have probably thought a thousand times how it would feel to lay down on this page all my feelings and the turbulent rollercoaster ride that accompanied my PhD, especially in the latter part of this, when *“the earth, considered from our earliest childhood as the type of solidity, has oscillated like a thin crust beneath our feet; and in seeing the laboured works of man in a moment overthrown, we feel the insignificance of his boasted power”* - Charles Darwin. And if I am now writing this page it is because of the wonderful people I have met during this long trip that showed me the pathway when I could only see mounded topography in front of me (maybe effects of the thesis?).

Impossible not to start with my fab-five Bill McCaffrey, Marco Patacci, Peter Haughton, Joris Eggenhuisen and Rob Butler that gave me the chance to work on a project that has evolved somewhat since initial conception and have provided me with all of the opportunities that it has entailed. Each of you has contributed greatly to this achievement. Among these, a special thanks is to be given to Bill and Marco. I want to thank you for the large portion of time and effort you invested in me. You motivated me to pursue my thoughts throughout the project and besides your scientific and technical support kept a sense of humour when I had lost mine.

I owe thanks to the Turbidites Research Group and to all the sponsor companies that through their involvement made this work possible. I also acknowledge Britannia Operator Limited and especially Peter Ablard, Rachel Preece, Steven Johansen and Adrian Machell, for providing advice and exchanging information on the Britannia Field during our annual meetings in Aberdeen.

Mason Dykstra and Fabiano Gamberi are thanked for having introduced me to the Casaglia MTD outcrop, as well as for their valuable advice in the numerous meetings held at conferences around the world.

A special thanks is also given to all the people of the Staff Building - post-docs and PhD students of the Geology Department, which contributed to make the office a great place to exchange ideas and knowledge (i.e., Jose's stock exchange lessons on the very early Monday mornings).

To all my friends and the fellowships which they belong: the “Latin lunch” led by our own Giacomino; the “night-out people” led by Aurelia with whom I spent many crazy moments with; the “WhatsApp Italian friends” helping me not to feel too far from them; the “footy-club” for the many matches and finally to all my ex-flatmates with whom I survived many “fiery” episodes, I thank you all.

Last, but not least, I wish to thank my special Lodi for showing me the ropes during the end, and to my wonderful-crazy family, as I like to call it, which has always provided me with un-ending support and the freedom to fly far from home. Maybe it is now time to be back... ..maybe only for a while, before the next adventure.

Abstract

Submarine landslides have been documented in many deep-water systems. Mass wasting processes and related emplacement of mass-transport deposits (MTDs) may reset the bathymetry of the seafloor through creation of erosional and depositional relief. MTD-related seafloor bathymetry may influence the dispersal patterns of subsequent sediment gravity flows, through reflection, deflecting, or ponding over a relatively small length scales (<1 km), and may thus exert major control on the architecture and internal heterogeneity of associated turbidites. The principal aim of this thesis is to better constrain the links between MTD-related seafloor bathymetry and facies variability in subsequent deposits.

Two case studies of MTD-influenced deep-water systems are presented: the subsurface Britannia Sandstone Fm. (Lower Cretaceous, UK North Sea) and the outcropping Marnoso-arenacea Fm. (Miocene, Central Italy). These studies document i) the different scales of seafloor rugosity created by the emplacement of MTDs and ii) the predictability of the effects of such bathymetry upon sandstone facies distribution and termination geometries. An original structural restoration exercise in the Britannia Sandstone Formation enabled construction of maps of the palaeobathymetry developed after each of four major mass transport events. Morphological features such as deep troughs provide pathways for the emplacement of relatively sandy, high net-to-gross deposits, whereas subtle rugosity produced hybrid event bed-prone deposits with marginal clay-rich banded facies adjacent to confining slopes. Field data from the Casaglia MTD enable the recognition of three different scales of rugosity on the upper MTD surface, the smallest of which effectively represents inter-well scale in the subsurface. Overlying sandstone deposits show evidence of flow deflection, confinement and ponding, with the latter resulting in thick mud caps and a taken net-to-gross.

The study emphasises that reservoir heterogeneity in sandstone deposits overlying MTDs is controlled by the shape, depth and size of the morphological features associated with the MTD, together with their elevation above the seafloor bathymetry in relationship to the thickness and direction of the depositing flows.

List of Contents

Acknowledgements	iii
Abstract	iv
List of Contents	v
List of Figures	xii
List of Tables	xx
Abbreviations	xxi
1 Introduction	1
1.1 Nature of the problem	1
1.2 Aims and objectives	2
1.3 Thesis structure	3
2 Deep-water sediment gravity flows: an overview of flow processes and associated deposits with focus on mass-transport deposit - turbidite association	6
2.1 Overview of sediment gravity flows and associated deposits	6
2.1.1 Slides, slumps and debris flows	10
2.1.2 Turbidity currents	11
2.1.3 Hybrid flows	18
2.2 Mass-failures and related deposits	22
2.2.1 Slope deformational processes and MTD triggering	23
2.2.2 Flow transformation.....	25
2.2.3 Classification schemes of mass-transport deposits	28
2.2.4 Mass transport deposits structural and geomorphological domains	30
2.2.5 Applications of MTDs studies	33
2.2.6 Identification of MTDs in the subsurface: a problem of scale	35
2.3 Interaction between MTD-related bathymetry and turbidity currents.....	38
2.4 Open research questions	47

3	Geology of the Lower Cretaceous in the Central North Sea and of the Britannia Field (UK sector)	49
3.1	Introduction	49
3.2	The regional tectonic setting of the Central North Sea	50
3.2.1	Pre-rifting phase (Palaeozoic).....	54
3.2.2	Syn-rifting phase (Triassic).....	54
3.2.3	Post-rifting phase (Cretaceous)	55
3.3	Britannia Sandstone Formation.....	58
3.3.1	Key stratigraphic intervals.....	62
3.3.2	Sediment source and fairways.....	64
3.3.3	Inherited facies scheme.....	67
3.3.4	Platform Area correlations	77
4	A revised facies scheme and correlation framework of the Britannia Sandstone Formation in the Platform Area	81
4.1	Introduction	81
4.2	Data and methods.....	82
4.3	Revised facies scheme	93
4.4	Revised correlation framework	104
4.4.1	Lower Reservoir	104
4.4.2	Middle Reservoir.....	104
5	Architecture of the MTD-dominated BSF in the Platform Area	115
5.1	Introduction	115
5.2	Geometry of the BSF in the Platform Area	117
5.3	Investigation of the origin of the wedge geometry.....	119
5.3.1	Assumptions and boundary conditions for palaeobathymetric modelling	121
5.3.2	Decompaction of the BSF to investigate differential compaction within the Lower-Middle Reservoir Section (Z10A-B58) in the PA	122
5.3.2.1	Decompaction equation (STEP 1).....	122
5.3.2.2	Selection of the values for initial porosity (ϕ) and compaction factor (c) for sand and mud (STEP 2).....	124

5.3.2.3	Calculation of the reservoir interval thicknesses (STEP 3).....	125
5.3.2.4	Calculation of the net/gross for the reservoir intervals (STEP 4) 126	
5.3.2.5	Decompaction of the reservoir intervals for the average middle point of the total thickness of Britannia reservoir calculated for all wells of the Platform Area (STEP 5).....	127
5.3.3	Decompaction of Valhall Shales below BSF in the PA	128
5.3.4	Causes of the creation of the wedge geometry of the Lower and Middle Reservoir in the PA.....	131
5.3.4.1	Early Cretaceous Valhall Shales - Under Britannia (Fig. 5.11-A) 135	
5.3.4.2	Lower-Middle Britannia (Fig. 5.11-B)	137
5.3.4.3	Upper Britannia (Fig. 5.11-C).....	138
5.3.4.4	Late Cretaceous-Cenozoic interval above Britannia (Fig. 5.11-D) 139	
5.4	Reconstruction of post-MTD palaeobathymetric surfaces	143
5.4.1	Methodology of the restoration	144
5.4.1.1	Identification of the continuity and discontinuity surfaces (STEP 1) 145	
5.4.1.2	Building the geometrical model to calculate the creation of accommodation space (STEP 2).....	145
5.4.1.3	Calculation of the coefficients of aggradation of sediments and differential creation of accommodation space to restore palaeobathymetry (STEP 3) 151	
5.4.2	Choice of parameters, issues and associated uncertainties which arose when applying the methodology to the dataset.....	153
5.4.2.1	Restoration of the palaeobathymetry at MTD-1 time	159
5.4.2.2	Restoration of the palaeobathymetry at MTD-2 time	162
5.4.2.3	Restoration of the palaeobathymetry at MTD-3 time	164
5.4.2.4	Restoration palaeobathymetry at MTD-3 time.....	166
5.5	MTD-related palaeobathymetries.....	168
5.5.1	MTDs of the Lower-Middle reservoir in the Platform Area	168

5.5.2	MTD character at different scales of observation	170
5.5.3	MTD-1	176
5.5.4	MTD-2	181
5.5.5	MTD-3	193
5.5.6	MTD-4	197
5.5.7	Creation of accommodation space associated with MTD emplacement.....	201
5.6	Discussion.....	204
5.6.1	Discussion on the workflow to build palaeobathymetries	204
5.6.2	Deformation during the Lower-Middle reservoir time and its relationship with the MTDs	209
5.6.2.1	Palaeo-slope modelling in the Platform Area.....	213
5.6.3	Clastic rate input associated with MTD emplacement.....	214
5.6.4	Implications outside the Platform Area.....	216
5.7	Conclusion	218
6	Sandstone deposition associated with MTDs-related topography: vertical and lateral sandstone lithofacies distribution influenced by pronounced vs subtle seafloor morphology shaped by large landslides in the Britannia Field 222	
	Abstract	222
6.1	Introduction	223
6.2	Dataset	227
6.3	Core facies.....	231
6.3.1	Lithology.....	231
6.3.2	Facies descriptions and interpretations.....	232
6.3.3	Bed/Zone thickness and internal organisation	233
6.3.4	Complicating factors	238
6.3.5	Grain size distribution and palaeoflow	238
6.4	Sandstone deposition in the Lower and Middle Reservoir	245
6.4.1	Zone 10A.....	249
6.4.2	Zone 10B (above MTD-1).....	255

6.4.3	Zone 40A (above MTD-2).....	263
6.4.4	Zone 40B (above MTD-3).....	269
6.4.5	Zone 40C (above MTD-4)	275
6.5	Effects of MTD deposition upon subsequent sandstone emplacement .	283
6.5.1	Lower and Middle Britannia Sandstone architecture.....	283
6.5.2	Interpretation of flow character based on vertical facies evolution within beds.....	289
6.5.3	Interpretation of lateral facies variations	292
6.6	Conclusions	297
7	Turbidite emplacement upon the irregular topography left by a large-scale MTD: the Casaglia MTD, Middle-Miocene Marnoso-arenacea, Central Italy .	299
	Abstract.....	299
7.1	Introduction.....	300
7.2	The Marnoso-arenacea Formation.....	301
7.2.1	Geological setting and stratigraphic setting	303
7.2.2	Fiorenzuola System	306
7.3	The Casaglia MTD.....	308
7.4	Dataset.....	310
7.4.1	Methodology	310
7.4.2	Location of the sedimentary logs.....	311
7.4.3	Lithology and lithofacies	313
7.4.4	Sandstones overlying the Casaglia MTD.....	313
7.4.5	Palaeocurrent data.....	320
7.5	MTD character	321
7.5.1	Casaglia sector (Sector A)	321
7.5.2	Bibbiana sector (Sector B)	321
7.5.3	Sambuca sector (Sector C).....	322
7.6	Reconstruction of the topography left by the Casaglia MTD.....	328
7.6.1	Log correlation panel.....	329
7.6.2	Scales of topographic rugosity left by MTDs.....	333

7.7	Turbidite character above the different scales of MTD-related topography	334
7.7.1	100s metres scale rugosity and sandstone infill (large-scale topography).....	334
7.7.2	Sandstone geometries related to 10s metres scale rugosity (local topography).....	339
7.7.2.1	Example I: Bibbiana outcrop	339
7.7.2.2	Example II: Sambuca outcrop	340
7.7.2.3	Example III: Campanara outcrop.....	340
7.7.3	Very small scale of rugosity (<1 m).....	344
7.7.4	Loading	344
7.7.5	Growth strata.....	345
7.8	Controls on turbidite character above MTD topography.....	348
7.9	Conclusions	353
8	Integration of subsurface and outcrop studies to investigate the influence of MTDs on subsequent turbidite deposition at different scales.....	356
8.1	The role of MTDs in shaping seafloor bathymetry	356
8.1.1	MTD-related topography from subsurface and outcrop datasets: size, geometry and wavelength of the rugosity over the upper surface of an MTD	357
8.1.2	Investigation of the small-scale MTD top rugosity of the Casaglia MTD to reduce inter-well uncertainty in the Britannia Field	359
8.2	Emplacement of turbidites above MTD-related bathymetry, with consideration of how turbidity currents adjust to different scales of rugosity.....	361
8.2.1	Nature of the substrate on subsequent flow transformation	361
8.2.2	Character of MTD rugosity on facies patterns	362
8.3	MTDs in deep-water settings: an important aspect for hydrocarbon exploration and reservoir characterisation	367
9	Conclusions and future work.....	370
9.1	Results from subsurface and outcrop datasets.....	370
9.2	Main outcomes.....	373
9.3	Recommendations for further work	376

Reference list	379
Appendix A – Britannia Platform Area well-dataset	421
Appendix B – Britannia Sandstone Fm. graphic logs	422
Appendix C – Britannia Sandstone Fm. decompaction	545
C.1 Choice of the porosity (ϕ) and compaction factor (c).....	545
C.2 Calculation of sand/mud decompaction coefficients for a chosen decompaction interval.....	548
C.3 Sand/mud decompaction coefficients sensitivities.....	551
C.4 Reservoir intervals thicknesses.....	553
C.5 Calculation of the net/gross through core inspection (a) and related sensitivities	553
C.6 Errors associated with the simplified decompaction workflow	556
Appendix D – Correlation panel of the Casaglia MTD	559

List of Figures

Fig. 2.1 – Schematic cartoon that shows the distribution of sedimentary environments in the shelf-slope-basin setting.	7
Fig. 2.2 – Block model illustrating the range of transport and deposition of sediments in deep water settings.	7
Fig. 2.3 – Nemeč's (1990) classification of slope deformational processes based on deposits and rheology.	9
Fig. 2.4 – Examples of the spectrum of sedimentary gravity flow behaviour and products determined by their sediment composition, concentration and dominant grain-support mechanism.	10
Fig. 2.5 – Schematic continuity of sediment deposition from a high-density flow, a low-density flow and fallout/hemipelagic deposition.	12
Fig. 2.6 – Generalised diagrams showing downslope changes in deep-water deposit organisation for coarse-grain supply and fine-grain supply.	15
Fig. 2.7 – Schematic diagrams showing respectively the temporal variation in flow at a fixed point in space and the spatial variation in flow velocity at a fixed time. .	18
Fig. 2.8 – Schematic flow transformation trends during run-out downstream.	20
Fig. 2.9 – Idealised hybrid event bed composed of typical five divisions with related descriptions and interpretations.	21
Fig. 2.10 – Dynamic classification and evolutionary scheme of MTDs which take into account genetic and evolutionary relationships between generating processes. ..	26
Fig. 2.11 – Cartoon representing an attempt to define evolutionary stages of matrix development through progressive stratal disruption of a thin-layered sequence. ...	27
Fig. 2.12 – 3D high resolution swath bathymetry showing an MTC in the offshore Gioia Basin, NE Sicily.	30
Fig. 2.13 – Geomorphologic elements of a mass-transport deposit and the likely occurrence of kinematic indicators relative to its various domains and schematic plan-view of the structural deformation in a mass-transport deposit, showing the variety of structures, and common locations where they may occur.	32
Fig. 2.14 – Seismic profiles across two portions of a prominent mass-transport deposit in Brunei deep-water margin showing typical features associated to MTDs.	34
Fig. 2.15 – Log-plot showing the relative scales of observation and resolution of different data sets used in studying deep-water settings.	35
Fig. 2.16 – Seismic and rock facies of various types and portions of MTDs showing the level of complexity that may be present in large-scale examples.	37

Fig. 2.17 – Schematic uniform and non-uniform flow change in relationship to topographic features at the basinal, flow and sub-flow scale.....	39
Fig. 2.18 – Schematic block model illustrating the influence of seafloor topography upon shelf, slope and basin floor depositional systems.	40
Fig. 2.19 – Examples of turbidite sandstone bodies above topography created by mass-transport deposits.	42
Fig. 2.20 – A series of RMS amplitude variance extractions on the MTC top surface from the Magdalena Fan in the Caribbean Sea.	43
Fig. 2.21 – Seismic section showing the generation of short and long wavelength topographic relief by the formation of imbricate stacks within a mass-transport deposit and cartoons showing the effects of underfilled versus overfilled accommodation on reservoir.	45
Fig. 2.22 – Illustration of the effect of flow size relative to topographic relief.....	46
Fig. 3.1 – Map showing the tectonic framework to NW Europe.....	51
Fig. 3.2 – Summary and reconstruction of the structural state of the Central North Sea during the Lower Jurassic.	52
Fig. 3.3 – Summary stratigraphic column for the Central North Sea area.	53
Fig. 3.4 – Regional palaeo-geography of the Aptian, Lower Cretaceous with sand fairway stretching from the Inner Moray Firth to the Outer Moray Firth, Central North Sea Triple Junction.....	55
Fig. 3.5 – Stratigraphic summary chart of the UK Central North Sea in the Outer Moray Firth, Viking Graben and Central Graben.....	57
Fig. 3.6 – Principal structural features around the Britannia Field.	59
Fig. 3.7 – Series of maps and cross-section of the Britannia Field.....	61
Fig. 3.8 – On the right the Britannia informal stratigraphic nomenclature and zonal calibration based on well 16/26-21.	62
Fig. 3.9 – Provenance and direction of turbidity currents and debris flows.....	66
Fig. 3.10 – Correlations of the Upper and Lower-to-Middle Britannia Sandstone Formation in the Platform Area.....	80
Fig. 4.1 – Platform Area of the Britannia Field.....	85
Fig. 4.2 – Dataset exported from ODM software. ODM allows to visualise all available data (wireline, core, etc.) in the same environment, helping interpretation of the depths of base and top of each interval for cored and uncored wells.	87
Fig. 4.3 – Facies core photograph of sandstones for sandy reservoir zones.....	99
Fig. 4.4 – Facies core photograph for debritic deposits and mudstones identified within the sandstone reservoir zones.	102

Fig. 4.5 – Core photographs of dewatering fabric recognised on sandstone facies.	103
Fig. 4.6 – Stratigraphic chart summarising the revised Britannia Field zonation in the Platform Area.	106
Fig. 4.7 – Correlations of the Lower and Middle Reservoir Section..	111
Fig. 4.8 – Comparison between earlier well correlation of the Lower-Middle Reservoir Section and new correlation along an east-to-west transect.	112
Fig. 4.9 - Fence diagram for the Lower and Middle Reservoir Section in the Platform Area.	113
Fig. 5.1 – NW-SE – oriented cross section through the BSF in the Platform Area, showing the development of a wedge geometry that thins towards the north-west of the deposits of the Lower and Middle Reservoir Section.	118
Fig. 5.2 – Seismic profile of the northern portion of the Witch Ground Graben across the Platform Area of the Britannia Field.	120
Fig. 5.3 – North-south seismic line across the flank of the Fladen Ground Spur under the Platform Area.	120
Fig. 5.4 – Concept of the successive stages in a decompaction exercise.	123
Fig. 5.5 – Seismic profile across the Platform Area calibrated with wells towards a north-to-south line.	128
Fig. 5.6 – Sketch of the methodology used to decompact the Valhall Shales interval.	129
Fig. 5.7 – Models that show the partial re-compaction of Valhall Shales at the base of BSF.	131
Fig. 5.8 – Comparison between fully decompacted deposits of the BSF and the Valhall Shales, and the partial compaction of sediments of the BSF and Valhall Shales at the top of the BSF.	132
Fig. 5.9 – Schematic model showing the creation of accommodation space within the Lower and Middle Reservoir Section and the analysis undertaken to identify possible differential compaction effects.	133
Fig. 5.10 – Isopach map showing the main structural features around the Platform Area.	135
Fig. 5.11 – Isopach maps showing the Lower Cretaceous-Quaternary stratigraphic intervals identified in Chapter 4.	141
Fig. 5.12 – Hypothesised geological evolution of the stratigraphic interval Bed58-Z10A of the Britannia deposits, showing the emplacement of the different reservoir intervals and their interplay with the MTDs.	146

Fig. 5.13 – Simplified plot showing differential creation of accommodation space within the Platform Area, as evidenced by the stratigraphic interval thickness Bed58-Z10A.....	148
Fig. 5.14 – Map showing the sectors identified by the clustering character of wells based on the accommodation space created within the Z10A-BED58 interval...	149
Fig. 5.15 – Scheme that shows how uniform/differential creation of accommodation was applied to wells.....	150
Fig. 5.16 – Model of the deformation applied to the well-dataset of the Platform Area in order to restore the palaeobathymetric surfaces of interest.	151
Fig. 5.17 – Model of the deformation applied to the well-dataset of the Platform Area in which the surfaces of interest are identified.	152
Fig. 5.18 – The Britannia Field (Platform Area) dataset in which wells are sorted on the depths of Z10A measured from the top of Bed 58.	155
Fig. 5.19 – Palaeo-datum restoration through time. The diagram shows the full reversed creation of accommodation history of the Lower and Middle Britannia deposits (Z10A-Bed 58 stratigraphic interval) in the Platform Area and the step-wise restoration of the Z10A palaeo-datum at each depositional event..	157
Fig. 5.20 – Restoration of the palaeobathymetry surface at the time of the MTD-1 (dashed line). Blue line represents the reconstructed palaeo-slope using the preserved tops of the Zone 10B.	161
Fig. 5.21 - Restoration of the palaeobathymetry surface at the time of the MTD-2	163
Fig. 5.22 – Restoration of the palaeobathymetric surface based on the reconstructed palaeo-horizontal at the time of the MTD-3.....	165
Fig. 5.23 – Restoration through time of the palaeo-horizontal datums (dashed lines) associated with the MTDs occurring within the Z10A-Bed 58 interval.	167
Fig. 5.24 – The three main sectors identified in the Platform Area based on different amounts of removal of the Britannia Sandstone stratigraphy.	169
Fig. 5.25 – WE-SE section integrating cored and uncored wells.	170
Fig. 5.26 – Representative core photos of the debrite facies groups recognised in this work.	172
Fig. 5.27 – Representative core log (well: 16/26-24) showing a range of sand and mud clasts surrounded by the muddy matrix within the MTD-3 interval.	173
Fig. 5.28 – Palaeobathymetric maps of the basal-upper topography associated with MTD-1, for reconstructed MTD1-time.	179
Fig. 5.29 – Palaeobathymetric maps of the basal-upper topography associated to MTD-2, for reconstructed MTD-2-time.	185

Fig. 5.30 – Relationship between the Z10B thickness in wells with preserved tops and reconstructed palaeobathymetric surface associated with MTD-1 in order to recognise remobilised stratigraphic intervals.	188
Fig. 5.31 – Palaeobathymetric maps of the basal topography associated to MTD-2, for reconstructed MTD-2-time.	191
Fig. 5.32 – Palaeobathymetric maps of the basal-upper topography associated with MTD-3, for reconstructed MTD-3-time.	195
Fig. 5.33 – Palaeobathymetric maps of the basal-upper topography associated to MTD-4, for reconstructed MTD-4-time.	199
Fig. 5.34 – Schematic NW-SE section to show the accommodation space at the sub-regional scale Platform Area.	201
Fig. 5.35 – Graph showing the topographic features associated with the large mass-transport and related deposits in terms of max evacuation, max MTD thickness and max positive topography on the reconstructed palaeo-slope.	202
Fig. 5.36 – Map showing the three main sectors identified in the Platform Area based on remobilisation area map.	203
Fig. 5.37 – Present day bathymetry of the MTD-2 top surface.	206
Fig. 5.38 – Bathymetry of the Upper surface of MTD-2 after decompaction of the BSF deposits.	207
Fig. 5.39 – Palaeobathymetry of the upper surface of the MTD-2 after decompaction of the BSF deposits and restoration at MTD-2 time, so after the emplacement of the hemipelagic Reddish Mudstones.	208
Fig. 5.40 – Deformation sequence between Z10A and Bed 58.	211
Fig. 5.41 – Relationship between bathymetry created by MTDs and differential creation of accommodation space recorded by the stratigraphic event.	212
Fig. 5.42 – Clastic input measured on wells per each zone of the Britannia stratigraphy grouped per reservoir section (Lower, Middle and Upper).	215
Fig. 5.43 – Reconstruction of the palaeobathymetric evolution of the Platform Area after the emplacement of MTD-1, 2, 3, 4.	221
Fig. 6.1 – Schematic illustration showing the effects of different degrees of confinement.	226
Fig. 6.2 - Platform Area of the Britannia Field.	229
Fig. 6.3 – Correlation of the Lower and Middle Britannia Sandstone Member. ...	231
Fig. 6.4 – Example logs of typical beds encountered in the Middle Britannia Formation.	236

Fig. 6.5 – Graphic sedimentary logs (wells B01, B07, 16/26-24 and B17) summarising typical zone/bed organisation and internal character of different reservoir units.....	237
Fig. 6.6 – Contour maps showing average and max grain size for four reservoir intervals and two event beds across the Platform Area.....	243
Fig. 6.7 – Well correlation panels of cored and uncored wells of the Lower and Middle Reservoir Section across the Platform Area.....	247
Fig. 6.8 – Palaeobathymetric map of the BSF in the Platform Area representing the basal surface of Zone 10A.....	251
Fig. 6.9 – Graphic sedimentary logs summarising facies and bed organisation of Zone 10A.....	253
Fig. 6.10 – Palaeobathymetric map of the upper topography associated with MTD-1 with pie charts showing proportion of lithofacies identified within Zone 10B in cored wells.....	259
Fig. 6.11 – Graphic sedimentary logs summarising facies and bed organisation present within Zone 10B.....	261
Fig. 6.12 – Palaeobathymetric map of the upper topography associated to MTD-2 with pie charts showing proportion of lithofacies identified within Zone 40A in cored wells.....	265
Fig. 6.13 – Graphic sedimentary logs summarising facies and bed organisation of Zone 40A.....	267
Fig. 6.14 – Palaeobathymetric map of the upper topography associated to MTD-3 with pie charts showing proportion of lithofacies identified within Zone 40B in cored wells.....	271
Fig. 6.15 – Graphic sedimentary logs summarising facies and bed organisation of Zone 40B.....	273
Fig. 6.16 – Palaeobathymetric map of the upper topography associated to MTD-4 with pie charts showing proportion of lithofacies identified within Zone 40C in cored wells (red dots).....	277
Fig. 6.17 – Graphic sedimentary logs of cored wells summarising facies and bed organisation of Zone 40C.....	279
Fig. 6.18 – Contour map showing the MTD-4-related topography and fence diagram of Zone 40C with related sandstone lithofacies distribution.....	281
Fig. 6.19 – Reconstruction of the depositional history of the Lower and Middle Britannia Reservoir in the Platform Area.....	287
Fig. 6.20 – Core examples of sand-rich HDT and mud-rich HEB recognised in the Lower and Middle BSF in the PA.....	291

Fig. 6.21 – Diagram showing the spatial relationship between the distributions of clean massive sands.....	293
Fig. 6.22 – Two conceptual sketches illustrating flow-topography interactions in the Lower and Middle Britannia within the Platform Area.....	295
Fig. 6.23 – Vertical profile sections of gravity flow portioning axially and orthogonal to flow direction.....	296
Fig. 7.1 – Simplified palaeogeographic reconstruction of the areal distribution of the main Tertiary basins developed within the Alps-Apennine orogenic system.	302
Fig. 7.2 – MAF crops out in the northern Apennines.....	305
Fig. 7.3 – Schematic stratigraphic log of the MAF deposits.	307
Fig. 7.4 – Geologic map of the field area, showing the outcropping portion of the Casaglia MTD, main stratigraphic and structural elements, and investigated sector of study (Casaglia, Bibbiana, Sambuca and Campanara).....	309
Fig. 7.5 – Satellite view of the study area.	312
Fig. 7.6 – Example of lithofacies defined in Table 7.2.....	319
Fig. 7.7 – Idealised cross-section of the Casaglia MTD, parallel to the SE-NW direction of the mass-failure movement, showing the external geometry and internal distribution of structures based on Lucente and Pini (2003) and adapted to the field observations in the investigated sectors.	323
Fig. 7.8 – Photomosaic of the Casaglia MTD near the Casaglia village, characterised by the presence of the olistostrome..	324
Fig. 7.9 – Overview of the outcrops in the Bibbiana sector, showing some of the major elements.	325
Fig. 7.10 – Photomosaic of the top and base of the Casaglia MTD in the Sambuca sector.....	326
Fig. 7.11 – Photomosaic of the Campanara outcrops.....	327
Fig. 7.12 – Stratigraphic correlation panels of sedimentary logs of the sandstones overlying the Casaglia MTD showing the spatial and vertical distribution of sandstone character.	331
Fig. 7.13 – Sedimentary logs illustrating variability of the character of the deposits overlying the Casaglia MTD in different locations.	338
Fig. 7.14 – Photomosaic showing sandstone bed onlap against the irregular top of the Casaglia MTD in the Bibbiana sector.....	342
Fig. 7.15 – Small scale rugosity developed on the upper surface of the Casaglia MTD in the Campanara sector and location of measured sections.	343
Fig. 7.16 – Outcrops of the MTD top in the Campanara sector.....	346

Fig. 7.17 – Top of the Casaglia MTD in the Campanara sector, characterised by metre-scale topography and by the presence of loading structures of the first sandstone bed above the MTD.....	347
Fig. 7.18 – Interpretative palinspastic block diagram of the Casaglia MTD emplacement and subsequent turbidite sandstone emplacement.	351
Fig. 7.19 – Sketch at a basinal scale illustrating how MTD-related topography can force the progressive down-current detachment of the upper turbulent flow from the lower axial dense part of a turbidity current.	352
Fig. 8.1 – Block diagrams showing the interaction between MTDs (pink) and sandstone deposits.....	366
Fig. 9.1 – Schematic representation of the MTD-related controls on turbidite deposition.	375
Fig. C-1 – Plots of log porosity versus depth for shales and sandstones	546
Fig. C-2 – Reconstructed porosity-depth curves for sands initial porosity taken by Bear and Weyl's (1973) table and reservoir porosities, compared against the Sclater and Christie curve.....	548
Fig. C-3 – Decompaction interval within the Britannia Field deposits. The sketch shows the decompaction intervals chosen for mud and sand, respectively placed at the base and middle average point of the reservoir.	550
Fig. C-4 – Graph showing the relationship between net/gross and gamma ray value for sand intervals on cored wells (reservoir interval Z10A-Bed 58).....	554
Fig. C-5 – Graph showing net/gross vs. gamma ray values for debritic intervals corresponding to MTDs on cored wells (reservoir interval Z10A-B58). Boxes show the concentration of sand clasts in MTDs: green = high; red = low.....	555

List of Tables

Table 3.1 – Summary of the revised Britannia reservoir zonation.....	64
Table 3.2 – Table showing a summary of the facies schemes proposed by different authors for the BSF.....	69
Table 4.1 – Dataset summary table for the Middle Reservoir Zone.....	84
Table 4.2 – Revised facies scheme used in this study for the cored wells of the Platform Area.....	97
Table 4.3 – Table showing the reservoir intervals recognised in this work and those revised from previous PhD works.....	107
Table 5.1 – Initial porosities and compaction factors used for various modelled lithologies in the North Sea basin, from Sclater and Chistie (1980).....	124
Table 5.2 – Porosity (%) of artificially mixed wet-packed sand (after Bear and Weyl, 1973).....	125
Table 5.3 – Sand proportion assigned to the lithologies in the Britannia Field reservoir.....	126
Table 5.4 – Facies table for the MTDs from core logs.....	175
Table 5.5 – Summary of the uniform and differential deformation rate assigned to each stratigraphic time event represented by hemipelagic markers and MTDs identified in the Z10A-Bed 58 interval (see section 5.4.1).....	210
Table 5.6 – Slope gradients measured between wells across the Platform Area and representing different times associated with the emplacement of the MTDs during the Lower and Middle Britannia Members.....	213
Table 6.1 – Dataset summary table.....	228
Table 6.2 – List of the core facies identified in the BSF in the PA.....	232
Table 6.3 – Mud content within facies division.....	289
Table 7.1 – Summary of the sedimentary logs of the sandstone interval overlying the Casaglia MTD.....	311
Table 7.2 – Facies scheme used in the study of the succession above the Casaglia MTD.....	315
Table C-1 – Summary of porosity values/facies in the Britannia Sandstone Fm. and reconstructed porosity near the surface calculated with the Table. 3.2 proposed by Bear and Weyl (1973).....	547
Table C-2 – Summary of the measured and reconstructed porosity at reservoir depth (3700-3800 m).....	548
Table C-3 – Britannia Field depth of intervals in the Platform Area.....	550

Table C-4 – Summary of the calculated decompaction coefficients for sand for different intervals and mud in function of interval and depth.	552
Table C-5 - Calculated decompaction coefficients for sand and mud in function of different 'model' interval thicknesses.	552
Table C-6 – Summary of the calculated min and max thickness value of the Britannia Field reservoir intervals.	553
Table C-7 – Tab shows the net/gross for selected reservoir intervals of well B01.	556
Table C-8 – Full decompaction step by step of the reservoir intervals (Z10A-MTD-6) in well B04 with comparison between the decompaction adopted for this work and the decompaction provided of sediment loading correction..	558

Abbreviations

SGF - Sediment gravity flow
MTD - Mass-transport deposit
LSMF - Large-scale mass-failure
HEB - Hybrid event bed
BSF - Britannia Sandstone Formation
FGS - Fladen Ground Spur
PA - Platform Area
MF - Moray Firth
LBR - Lower Britannia Reservoir (of the Britannia Field)
MBR - Middle Britannia Reservoir (of the Britannia Field)
UBR - Upper Britannia Reservoir (of the Britannia Field)
MAF - Marnoso-arenacea Formation

1 Introduction

1.1 Nature of the problem

Many deep marine clastic accumulations are built by gravity-driven events of various rheology, including: 1) non-cohesive, fluidal and relatively dilute (Newtonian) flows such as turbidity currents, in which particles are largely supported by fluid turbulence, 2) cohesive, laminar, relatively concentrated flows (non-Newtonian), such as slides, slumps, debris flows or in general large-scale mass-failures, and 3) rheologically heterogeneous hybrid flows (Talling et al., 2012 and references therein).

These different flow types leave deposits with differing characteristic morphologies – turbidity currents commonly deposit flat-topped or gently tapering deposits (or may leave channels of erosional, aggradational or mixed character), mass-failure flows typically are associated with mounded deposits with rugose tops and relatively abrupt margins, and hybrid flows can develop deposits of a mixed and heterogeneous internal character; their external geometry is similar to that of turbidites.

Different flow types therefore (1) variably influence the substrate encountered by subsequent flows, and (2) respond to bed topography in different ways; in particular sandy gravity flows are commonly strongly influenced by the change of bathymetric seafloor gradient, which affects the ability of gravity flows to erode, transport, and deposit sediments, as observed on modern sedimentary systems (e.g., Ercilla et al., 2002; Wynn et al., 2002a) and investigated in the laboratory (e.g., Garcia and Parker, 1989; Mulder and Alexander, 2001). Seafloor topography can be modified by a number of agents, such as a) tectonic controls (e.g., faults, subsidence, substrate mobility, etc.) or b) due to erosion by gravity flows such as turbidity currents and large mass-failure processes. The latter can reshape the seafloor through erosion, remobilisation and accumulation of large volumes of remobilised deposits associated with large-scale mass-failures (Norem et al., 1990; Masson et al., 1998; Gee et al., 1999, 2001, 2006; Frey Martinez et al., 2005; Moscardelli et al., 2006). Numerous studies have demonstrated that seafloor topography can be a significant control on deposition from sediment gravity flows (Pickering et al., 1989; Fisher, 1990; Thornburg et al., 1990; Cronin et al., 1998; Prather et al., 1998; Pickering and Corregidor, 2005). However, only a few studies have focused specifically on the interaction between sandy gravity flows and topographic features developed after the emplacement of mass-failure – related deposits (Weimer and Slatt, 2008; Kneller et al., 2016) either at outcrop (Armitage et al., 2009) or in the subsurface (Ortiz-Karpp et al., 2015). As a result, despite the remarkable progresses in the understanding of

deep-water depositional systems in the last few decades, this area of deep-water process sedimentology remains relatively poorly understood.

As well as being an important research area for academic sedimentology, the interaction between sandy gravity flows and mass-transport – related topographic features is also important for hydrocarbon exploration and production in deep-water settings, as sands deposited in association with mass transport deposits can host hydrocarbon reservoirs.

1.2 Aims and objectives

The overall aim of the research reported in this thesis is to contribute to an ongoing effort to better understand the role of mass-transport deposits (MTDs) in influencing the evolution of stratigraphic architecture in deep-water settings. Immediate aims are to investigate the spatio-temporal evolution of deep-water systems dominated by the interplay of large-scale mass-failures and sandy gravity flows, investigating the processes controlling the distribution and internal character of resultant sandy deposits in order to investigate the relationships between MTDs and turbidites. Thus the chapters of this thesis have the following objectives:

- To undertake a comprehensive up-to-date review of sedimentary gravity flows in deep water, in order to better describe and interpret different deposit characteristics from subsurface, core and outcrop datasets. A standardised terminology will be also adopted to attempt to avoid ambiguity that usually affects deposits and process description.
- To reconstruct the bathymetry of the seafloor subsequent to large-scale mass-failure events in ancient deep-water settings from both subsurface and outcrop datasets. This study aims to show how the emplacement of MTDs may reconfigure the topography of the seafloor.
- To investigate the deposition of classic turbidite facies and “slurried sandstone facies” (*sensu* Lowe and Guy, 2000) using subsurface data from the Lower Cretaceous Britannia Sandstone Formation, UK North Sea. This work also aims to study the controls on sandstone deposition due to MTD-related topography, proposing a novel depositional model to explain the development of the characteristic Britannia Sandstone facies linked to the rugose seafloor on top of the MTDs.
- To map the geometry of the upper surface of an MTD in outcrop; namely the Casaglia MTD in the Miocene Marnoso-arenacea Fm., Central Italy, where the MTD-related topography can be reconstructed at large (100s of metres) and in

some cases at small (10s of metres) scales. Above the MTD, sandstone event beds can be traced for 10s of kilometres, allowing observations of the contact character (e.g., onlap, pinch-out terminations) with the underlying Casaglia MTD to be made.

By combining the analysis from both subsurface and outcrop datasets, it is hoped that uncertainties in interpretation from individual datasets can be minimised, for instance those related to inter-well prediction in subsurface studies (for instance using wireline logs), or to the establishment of correlations at outcrop.

A final aim of the study is to allow better characterisation of the impact of geological reservoir heterogeneity on fluid flow prediction in production scenarios through development of a better understanding of the stratigraphic controls on reservoir compartmentalisation. It is hoped that new insight in this regard may have practical implications for the prediction, characterisation and development of hydrocarbon reservoirs in deep-water settings influenced by the presence of MTDs.

1.3 Thesis structure

The thesis comprises new findings from subsurface and outcrop case studies related to the interaction of deep-water sediment gravity flows with MTD's related topography, including well dataset, core logs and structural restoration workflows from the Britannia Field case study and sedimentary logs and correlational panel from the Casaglia field case study.

The principal results of this thesis (chapters 5, 6 and 7) have been written in manuscript form to facilitate submission for publication. The data presented consider a variety of scales from that of the larger depositional system to that of the individual bed. The results from the two case studies presented are discussed in terms of the generic insight they offer into MTDs, sandstones and hybrid deposits and the process that emplaced them.

The main case study is focused upon the subsurface Britannia Sandstone Formation, UK North Sea, and builds upon and extends the work of three earlier PhD projects (Barker, 2005; del Pino Sanchez, 2006; Eggenhuisen, 2009). This work is integrated with a complimentary outcrop study from the Casaglia MTD, Marnoso-arenacea Fm. (Central Italy).

In detail:

Chapter 2 provides the background to the study by summarising pertinent literature regarding gravity flow dynamics and deposits, including flow classification, evolution and interaction with topographic features on the seafloor with particular focus on the influence of large-scale mass-failures on sandstone deposition.

Chapter 3 provides a detailed review of the geology of the Lower Cretaceous in the Central North Sea with particular focus on the configuration and sedimentation of the Moray Firth. The Britannia Field (UK sector) Britannia Sandstone Formation are described at both large scale (Britannia Field) and small scale (the study area of the “Platform Area”, hereafter “PA”), framed within the geological history of the Northern North Sea.

Chapter 4 provides a revised facies scheme and correlation framework for the Britannia Sandstone Formation. The re-interpreted stratigraphic well correlations and the detailed reservoir characterisation of the Britannia Field in the study area are shown through wireline and core log description forming the basis for the investigation of the relationship between MTDs and sandstones.

Chapter 5 presents the reconstruction of the spatial and temporal evolution of large-scale mass-failures and associated MTDs in the Lower and Middle Reservoir Section of the Platform Area of the Britannia field through a detailed decompaction and structural restoration analysis of these deposits. This analysis is designed to allow instantaneous “post MTC” bathymetries of the PA to be reconstructed, placing a new constraint on evaluation of the geometry and origin of the BSF; different hypothesis that could have led the creation of accommodation space in the PA can be investigated. The advantages of the adopted decompaction and structural restoration workflow are discussed. In addition, detailed facies descriptions of the MTDs recognised in core are also presented to help interpreting their emplacement processes.

Chapter 6 expands upon the case study presented in Chapter 5 by documenting the sandstones character from core facies, including their spatial distribution and stratigraphic variations within the Platform Area in relation to the evolving palaeobathymetry.

Chapter 7 provides an outcrop case study from the Casaglia MTD, in the Marnoso-arenacea (Central Italy). Sedimentary logs of the sandstones immediately overlying the MTD allow both the reconstruction of the rugosity of the MTD upper surface and the recognition of the associated sandstone character.

Chapter 8 integrates the results of the subsurface and outcrop case studies to better understand the relationships between MTDs and turbidites. In particular this chapter synthesises early results to show i) the different scales of rugosity associated with MTDs on the basin floor, ii) the emplacement of turbidites over MTD-related bathymetry, and iii) the applied significance of the findings for hydrocarbon exploration and reservoir characterisation in MTD-prone systems.

Chapter 9 summaries the thesis findings and provides a list of future research pathways that could be developed building upon the insights from the thesis.

2 Deep-water sediment gravity flows: an overview of flow processes and associated deposits with focus on mass-transport deposit - turbidite association

The aim of this chapter is to provide a general process review and the concepts for a fundamental evaluation of the development of MTD-related bathymetry and related deposits in order to identify understudied aspects associated with MTDs.

2.1 Overview of sediment gravity flows and associated deposits

Deep-water sediments cover two-thirds of the Earth and these are conventionally termed “deep” when deposited beneath storm wave base (Hüeneke and Mulder, 2011), in order to exclude continental, deltaic, shallow marine and continental shelf deposits (Fig. 2.1 - Pyles and Slatt, 2000); the term “deep” is also conventionally used in hydrocarbon industry for depths greater than about 500 metres, somewhere in the shelf to upper continental slope region.

Deep-water deposits have received particular attention by the sedimentology community in the last 50 years, driven in part by the recognition that these deposits could represent important elements for the development of hydrocarbon reservoirs (see a recent review by Weimer and Slatt, 2008). However, the most rapid development of deep-water sedimentology has occurred relatively recently, mainly due to the depth and the inaccessible nature of this depositional environment. The first attempt at describing deep-water sediment processes was made by Migliorini (1943) who defined these flows as “*sediment-laden flows that move downslope because of their excess density*”; this was followed by the first definition of “*turbidite*” as the deposit of “*turbidity current*” and related to graded bed sequences by Kuenen and Migliorini, (1950).

Since then, substantial progress in the study of sedimentary gravity flows and their controlling factors has been made, thanks to a wealth of data from outcrop, experimental and modelling studies together with data from subsurface, helped by advances in technology (i.e., 3D seismic reflection data, cores and borehole image logs, conventional wireline logs, 3D geologic models and reservoir simulation). These advances have highlighted how sediments are transported down to deep-water environments by subaqueous sediment gravity flows (Fig. 2.2), which represent some of the largest events of sediment movement on Earth (Middleton and Hampton,

1976; Elmore et al., 1979; Masson et al., 1993; Normark et al., 1993; Piper et al., 1999).

Distribution of sediment environments in the shelf-slope-basin

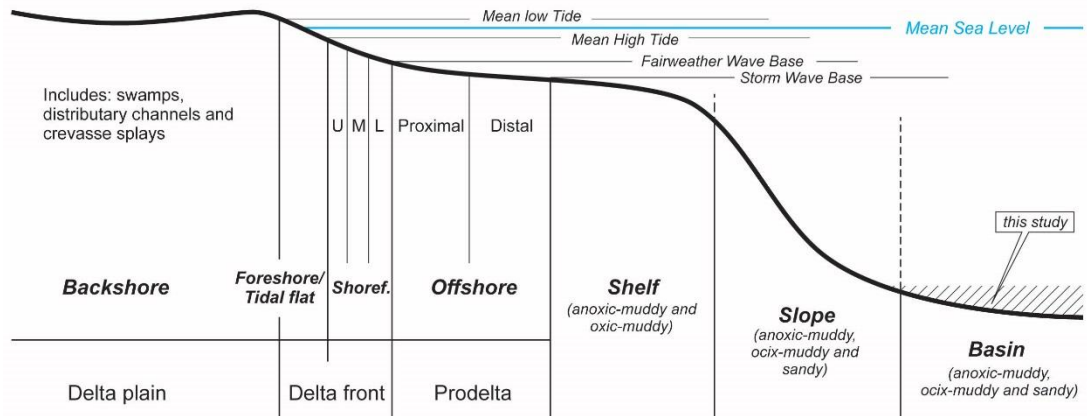


Fig. 2.1 – Schematic cartoon (vertical scale is exaggerated) that shows the distribution of sedimentary environments in the shelf-slope-basin setting (modified after Pyles and Slatt, 2000).

Deep-water sedimentation processes

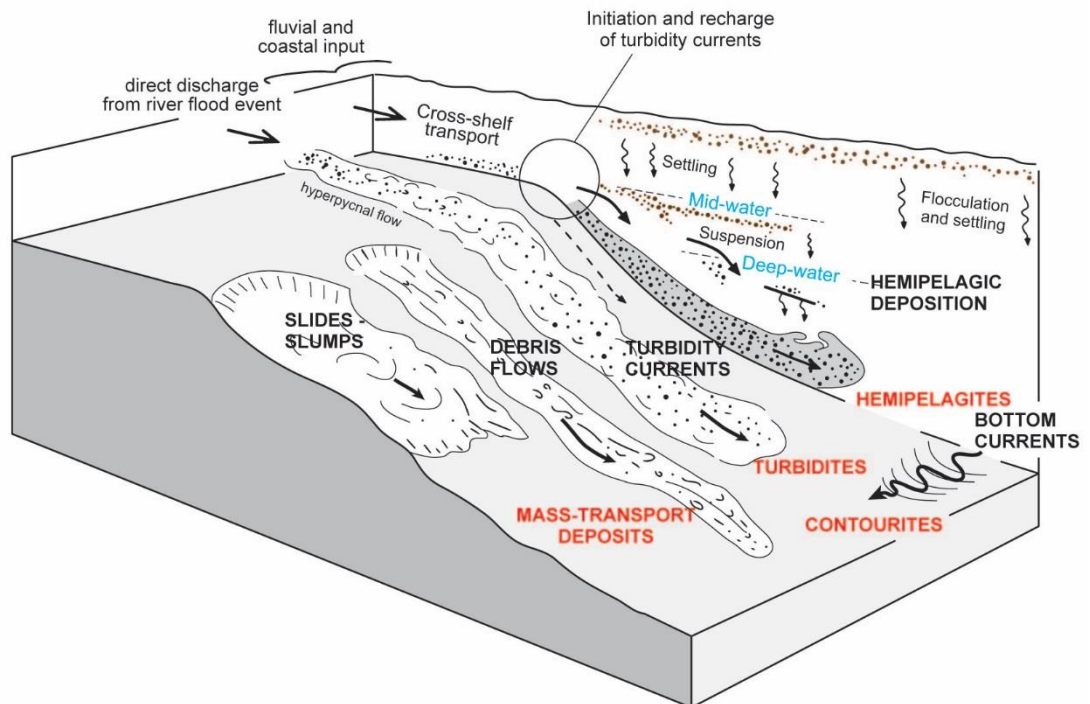


Fig. 2.2 – Block model illustrating the range of transport and deposition of sediments in deep water settings (modified after Stow and Mayall, 2000).

The wide range of sedimentary deposits documented in deep-water deposits have invoked a spectrum of gravity flow models for sediment transport (Fig. 2.3), characterised by different sediment grain size and concentration and by the different combinations of grain-support mechanisms (Bouma, 1962; Middleton and Hampton, 1976; Lowe, 1982, 1988).

Submarine gravity flows have been classified according to: 1) the mechanical behaviour (rheology) of the process (Dott, 1963; Mulder and Cochonat, 1996); 2) the particle-support mechanism (Middleton and Hampton, 1976; Nardin et al., 1979; Lowe, 1979, 1982; Stow et al., 1996); 3) the flow concentration observed in flow deposits (Mulder and Alexander, 2001); 4) the longitudinal change in their deposits (Mutti and Ricci Lucchi, 1975).

Process and products are described and classified upon different schemes. Matrix strength, grain-to-grain interactions, fluid support and turbulence are the four principal types of particle-support mechanism used to classify sedimentary gravity flows, and also represent the most commonly used classifications in the literature for present-day deep-sea environments (Smith, 1955; Sinclair, 1962; Kuenen and Menard, 1952; Middleton and Southard, 1984; Allen, 1991; Garcia, 1994; Mulder et al., 1997; Postma et al., 1988; Kneller and Buckee, 2000; McCaffrey et al., 2003). Classifications based on the recognition of the sedimentary facies and their evolution along the pathway of the flow are instead extensively used in descriptions of deposits, at outcrop and in the subsurface. By combining the above approaches, sedimentary gravity flows and their related deposits are traditionally ascribed to either: (A) slumps and/or slides, involving passive translation of intact or coherently deforming stratigraphy on a discrete basal detachment surface; (B) debris flows, involving en-masse deposition from laminar or slowly churning flows with or without cohesion, and (C) various types of turbidity currents that deposit grain-by-grain or layer-by-layer with significant sediment support by turbulence, although this may be suppressed near bed by high sediment concentrations. These submarine gravity flow types may evolve from one to another; as relatively concentrated slides become progressively more dilute as they mix with ambient water and lose sediment due to selective deposition. This results in a change from up-dip slides, slumps and debris flows to down-slope turbidity currents with the latter showing evidence for a later passage from high density to low-density flows towards the distal edge of the system. More recently (D) hybrid flow (slurry flow, *sensu* Lowe and Guy, 2000) has been recognised (Houghton et al., 2003, 2009; Talling et al., 2004, Talling, 2013), and is described below in more detail.

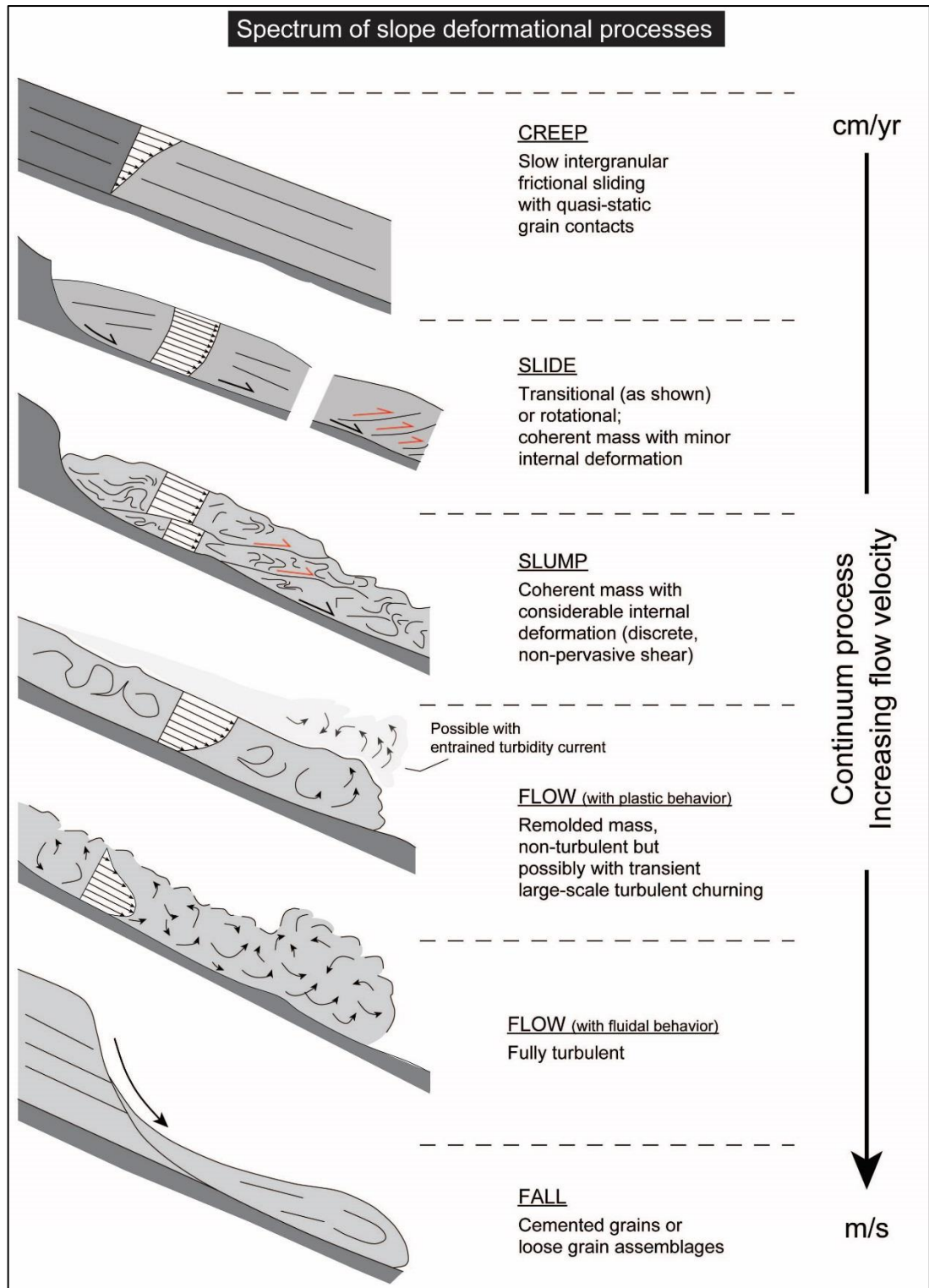


Fig. 2.3 – Nemeč's (1990) classification of slope deformational processes based on deposits and rheology. Slumps, slides and debris flow processes produce mass-transport deposits. The classification considers the rheology of the material being transported during mass-wasting (modified after Shipp et al., 2011, from Nemeč, 1990).

Sedimentary gravity flows and products

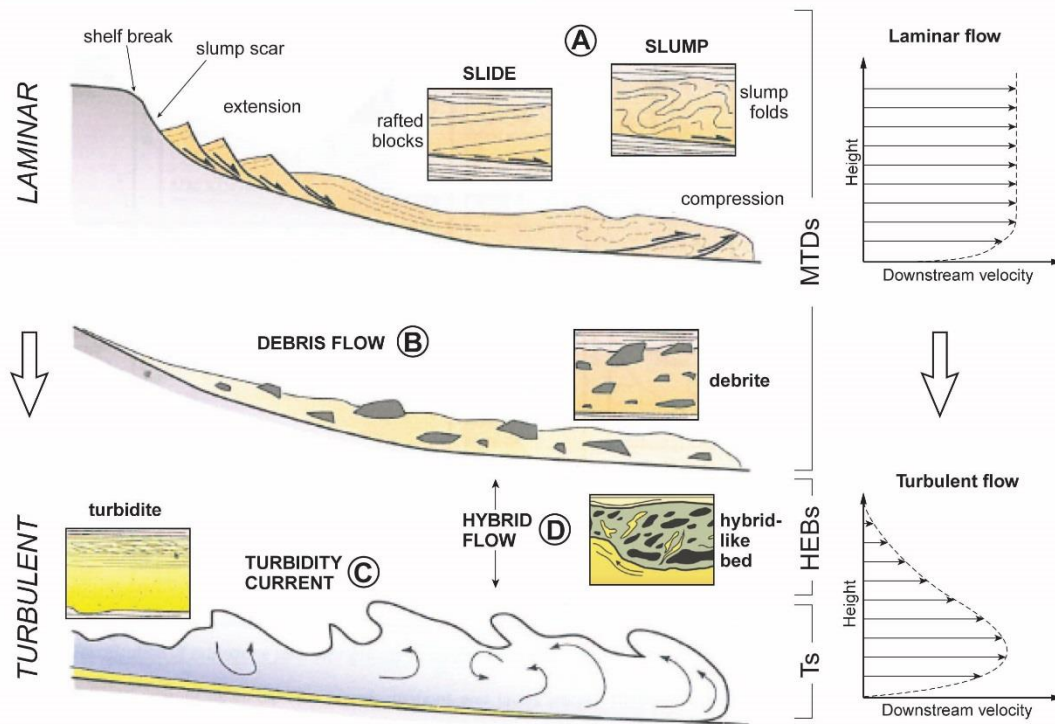


Fig. 2.4 – Examples of the spectrum of sedimentary gravity flow behaviour and products determined by their sediment composition, concentration and dominant grain-support mechanism. Sediment gravity flows may exhibit spatial and temporal variation in flow behaviour during a single event characterised by the interplay of multiple grain-support mechanisms.

In this work slides/slumps (A) and debris flows (B) are grouped together as mass-wasting processes given their cohesive behaviour and the chaotic and disorganised character of their products (mass-transport deposits) (Posamentier and Martinsen, 2011).

2.1.1 Slides, slumps and debris flows

Slides, slumps and debris flows represent sediment failures (mass-wasting processes) and correspond to the motion of large volumes of sediment or rock along a failure surface (Fig. 2.3), usually following the evolution of creeping (Nardin et al., 1979). These are usually not isolated structures and they may form complex structures with multiple phases of failure. Shanmugam et al., (1994) termed a slide as a block of sediment that has moved downslope with no internal deformation; a slump as a block that moves downslope on a glide plane or shear surface and undergoes rotational movements causing internal deformation; and a debris flow as resulting from an increase in mass disaggregation and mixing to the point where the sediment is an incoherent body that may contain folded, rotated blocks.

Mass-failures are commonly characterised by a cohesive character. They are usually characterised by a significant matrix strength that results from a high proportion of cohesive particles such as clay (>40% - clay-rich mudflows) and as fine silt (<25% - silty mudflows) that are capable of suppress turbulence and preventing differential grain settling (Hampton, 1975; Middleton and Hampton, 1976; Marr et al., 2001; Mulder and Alexander, 2001). They may move in part due to a water layer that is trapped under the head and part of the body of the flow, reducing the flow resistance at the flow/seafloor interface, and hence its erosional power (hydroplaning, Mohrig et al., 1996). The flows can maintain a laminar behaviour (Middleton and Hampton, 1973; Carter, 1975; Hampton, 1975; Marr et al., 2001) thanks to low permeability of the matrix that reduces the rate at which they mix with ambient water, keeping the density high (Stow et al., 1996). As soon as the yield-strength decreases and the shear stress increase, debris flows decelerate abruptly, depositing the transported material via en-masse freezing (Carter, 1975). The deposits are poorly sorted matrix clay-rich and clast-rich deposits, generally lacking internal stratification (Embley, 1976; Middleton and Hampton, 1976; Naylor, 1980; Mohrig et al., 1996). An irregular topography on their upper boundaries results in the associated seafloor being typically hummocky (Pickering et al., 1989). This is mainly due to the presence of abundant clasts of varying size, from m to 100s of m scale (boulder-size clasts of soft sediment or very large rafts or olistoliths) (Moscardelli et al., 2006, 2013; Moscardelli and Wood, 2008, 2016; Armitage et al., 2009; Masson et al., 2010; Jackson, 2011) that floated close to the upper surface of the flows (Johnson, 1970, 1984; Rodine and Johnson, 1976; Leigh and Hartley, 1992). Hampton (1972) and Marr et al. (2001) later demonstrated in the laboratory that the size of the carried blocks was inversely related to the density of the matrix of the flow, however, care is needed in scaling up such observations.

2.1.2 Turbidity currents

Non-cohesive gravity sediment flows have generally been further distinguished into 1) granular flows, where particle support is due to dispersive pressures resulting from grain-to-grain interactions, 2) water-dominated flows, where particles are supported by the upward force of the interstitial fluid (hindered settling), 3) and turbulent flows, where the sediment is supported mainly by the upward component of fluid turbulence (Mulder and Cochonat, 1996; Kneller and Buckee, 2000). However, inferring the grain-support mechanism of the flows from their deposits is often problematic, mainly due to the difficulties associated with their high spatial and temporal variability within the flow related to variations in velocity and sediment concentration; further these

mechanisms are recognised not to be mutually exclusive (Smith, 1955; Sinclair, 1962; Kuenen and Menard, 1952; Middleton and Southard, 1984; Allen, 1991; Garcia, 1994; Mulder et al., 1997; Postma et al., 1988; Kneller and Buckee, 2000; McCaffrey et al., 2003).

Turbidity currents are herein considered “suspension currents” (*sensu* Kneller and Buckee, 2000) where sediment and water are mixed and suspended as a “fluidal mixture” with fluid turbulence as the principal grain-support mechanisms. However, Bouma (1962) and Lowe (1982) showed that turbidity currents may exhibit turbulent or laminar-like (but non-cohesive) behaviour depending on local sediment concentration and associated dominant grain-support mechanism and expressed in their resulting deposits forming high-density (Lowe, 1982) and low-density (Bouma, 1962) turbidites (Fig. 2.5). In this regard, Bagnold (1962) suggested a limit of 9% sediment concentration by volume for full turbulent support of sediment, a value used as the threshold value to define turbidity currents *sensu stricto* (Hüeneke and Mulder, 2011).

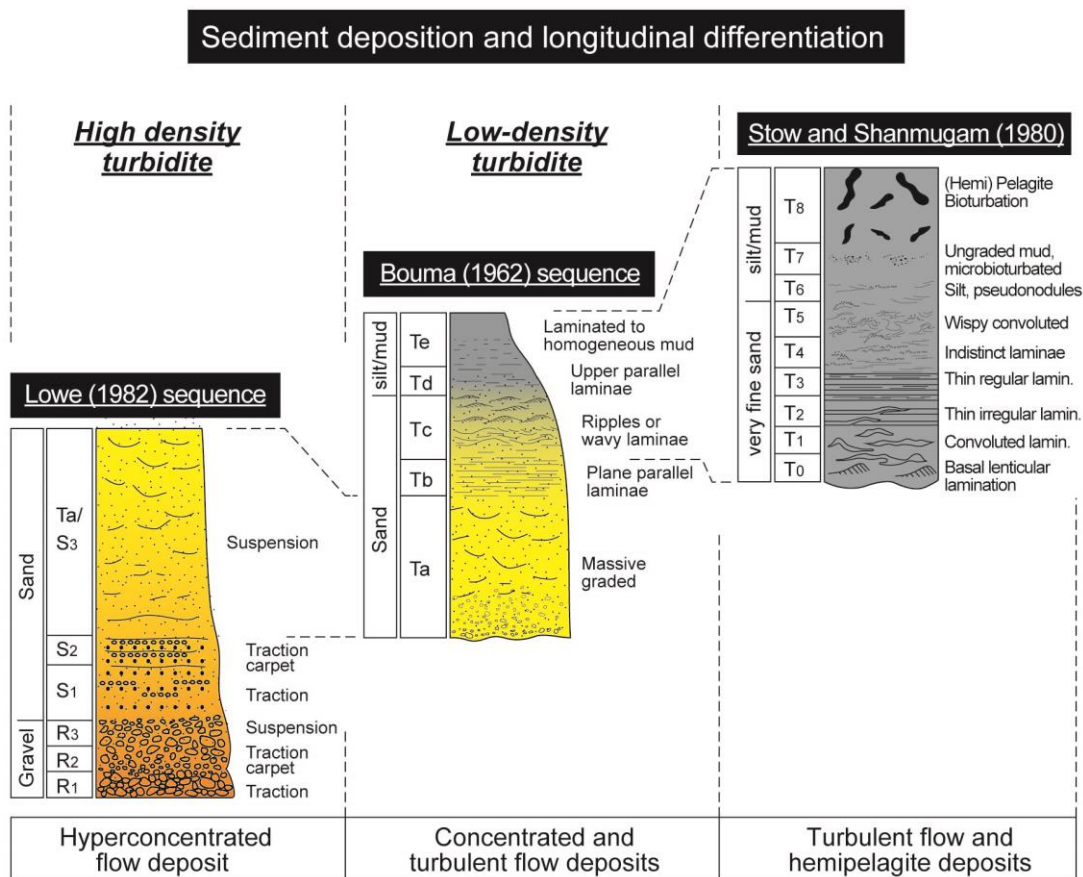


Fig. 2.5 – Schematic continuity of sediment deposition from a high-density flow (Lowe sequence: Lowe, 1982), a low-density flow (Bouma sequence: Bouma, 1962) and fallout/hemipelagic deposition (Stow and Shanmugam sequence: Stow and Shanmugam, 1980) (redrawn after Shanmugam, 2000).

The deposits of turbidity currents, turbidites, are often normally graded, representing the fallout of particles from a suspension. This mechanism is the origin of most of the vertical normal grading, typical of a single, waning, dilute surge-like turbidity currents (*sensu* Bouma, 1962, which represented the first model of gravity-flow deposition based on traction/suspension fallout process).

When present, scours and flute casts in some turbidite deposits represent the erosional surface at the base of the sequence caused by the passage of the energetic head of the current (Mulder et al., 2001). Groove, brush marks and casts, prod and bounce marks and casts are also typical at the base of turbidite deposits, generally produced by the drag or the impact or rolling of a clast along the basin floor, transported by the current (Lanteaume et al., 1967). Bouma (1962) distinguished five divisions (Ta-Te), from the lower to the upper part of a turbidite event bed (Fig. 2.5). The lower weakly graded Ta interval of a Bouma sequence arises due to the high concentration of sediment in the depositing flow, which prevents significant differential sedimentation of grains by size. The upper intervals of the Bouma sequence suggest the passage of the flow body with a turbulent regime and a progressively decreasing energy, depositing firstly an interval of planar lamination (Tb interval), ascribed to deposition under upper-flow-regime plane-bed conditions, and then a cross-laminated interval (Tc interval), representing the further decrease in energy in the middle part of the body. Planar laminations (Td) are ascribed to deposition under lower-flow-regime plane-bed conditions which represent the low energy distal part of the body current. Silty laminations (Te) are instead interpreted as the tail of the flow, dominated by passive particle fallout. Stow and Shanmugam (1980) described in detail the suspension fallout-dominated fine-grained parts of the turbidite sequence (Td-Te = T1-T8), characterised by intensification of bioturbation towards the top and interpreted as resulting from the interaction between hemipelagic sedimentation and the fine particles from the turbulent cloud (Fig. 2.5).

Additional divisions were proposed for different sedimentary structures recognised in coarser grained deposits by Lowe (1982) (Fig. 2.5). These deposits were interpreted as the product of bipartite currents, where the basal part is a hyper concentrated flow, with a laminar regime, and the upper part is a more dilute flow, in which turbulence progressively develops into the Bouma sequence. Coarse material, pebbles or gravels are reworked along the seafloor by the flow forming gravel waves of oriented clasts (unit R1). The competence of the flow increases upwards as the velocity of the flow increases progressively due to the less interaction and friction of the flow with the seafloor, forming an inverse grading within the moving basal flow. This interval is preserved when the basal flow increases its concentration and the flow freezes

(traction carpet of unit R2 in Fig. 2.5). When the grains at the top of the basal flow settle by suspension fallout, an R3 unit is formed, exhibiting normal grading. As coarse particles quickly become less abundant in the flow R1 and R2 only form lenses rather than massive beds. This sequence of processes is repeated during deposition of finer grain sizes, resulting in S1-S3 (S3 = Ta in Fig. 2.5).

The deposit sequences described above can be represented in a diagram that shows a schematic distribution of the particles along the run out of the flow as the result of the flow evolution along its pathway (Fig. 2.6). The Lowe sequence is usually associated with sand-rich source environments, where hyper-concentrated flows result in the deposition of structureless and coarse-grained beds (controlled by grain-to-grain interaction) and followed in a continuum by the Bouma sequence with normally graded deposits as the dilution of the flow increases with distance (Fig. 2.6-a).

In mud-dominated environments, debrites usually represent the result of the transformation of mass-failures, which capture any coarse fraction (pebbles to sand); any elutriation within the flow may facilitate the rapid formation of dilute clay- and silt-rich turbidity currents. Consequently, the Lowe sequence and the base of the Bouma sequence can be lacking and may be replaced by a zone of bypass or erosion. The upper intervals of the Bouma sequence are instead well developed (Hüeneke and Mulder, 2011; Fig. 2.6-b).

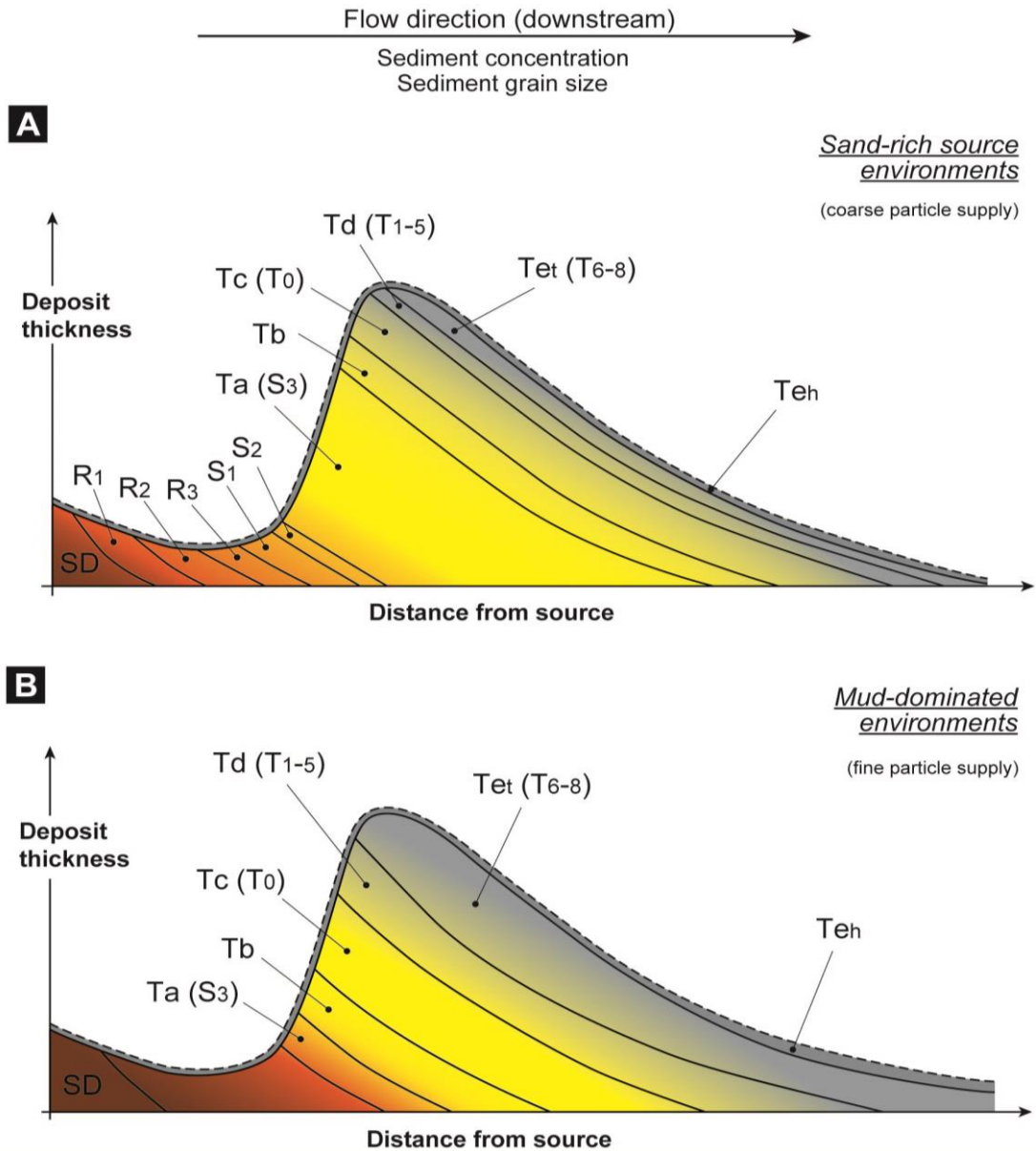


Fig. 2.6 – Generalised diagrams showing downslope changes in deep-water deposit organisation for (A) coarse-grain supply and (B) fine-grain supply. The horizontal line represents the base of the deposit whereas the vertical line drawn at each point along the run out of the flow shows schematic thickness and organisation of high- and low- density divisions deposited by sedimentary gravity flows after slump deposits (SD). Facies R (1-2-3), S (1-2-3), T (a-b-c-d-e) and T (0-1-2-3-4-5-6-7-8) are explained in Fig. 2.5. Tet and Teh indicates respectively turbiditic and hemipelagic mud (redrawn after Hüeneke and Mulder, 2011; from Lowe, 1982).

Experimental and theoretical work has shown how turbidity currents can develop spatially-variable structure in terms of velocity, turbulence, sediment concentration and grain size, and associated flow rheology (Kuenen and Menard, 1952; Middleton and Southard, 1984; Allen, 1991; Middleton, 1993; Garcia, 1994; Altinakar et al., 1996; Hand, 1997; Kneller et al., 1997; Parsons and García, 1998; Kneller and McCaffrey, 1999; Kneller and Buckee, 2000; Peakall et al., 2000; Choux and Druitt,

2002; McCaffrey et al., 2003; Choux et al., 2004; Baas et al., 2005). For example, particles with relatively higher settling velocities (e.g., larger or denser grains) tend to concentrate closer to the bottom, whereas particles with relatively lower settling velocities tend to be more evenly distributed through the flow height, resulting in vertical flow stratification in terms of sediment concentration (density stratification), grain size, composition and rheology (Rouse, 1939; Middleton and Southard, 1984; Stacey and Bowen, 1988; Zeng et al., 1991; Garcia, 1994; Kneller and McCaffrey, 1995, 1996; Kneller and Buckee, 2000; Buckee et al., 2001). The action of vertical gradients in horizontal velocity upon such density and grain size stratification can result in lower-settling velocity particles (e.g., larger, denser or more elongate particles) being hydraulic segregated and redistributed longitudinally towards the rear of the flow (Stacey and Bowen, 1988; Garcia and Parker, 1993; Garcia, 1994; Altinakar et al., 1996; Kneller and Buckee, 2000). Flows may further self-organise as faster travelling regions as the flow advance headwards until they reach equilibrium with the surrounding flow, thus flow structure undergoes a spatio-temporal transformation in terms of velocity, turbulence and sediment concentration, size and composition (McCaffrey et al., 2003). The term flow transformation refers to such temporal variation in flow characteristics (i.e., grain size, concentration, velocity, turbulence and rheology) and the instantaneous flow structure during downstream run-out. Study of sub-aerial pyroclastic flows and flume tank experiments with particulate gravity flows have provided insight into the range of flow transformations affecting sandy gravity flows (Kuenen and Menard, 1952; Middleton, 1967, 1970; Hampton, 1972; Middleton and Hampton, 1973; Fisher, 1983; Marr et al., 2001; Branney and Kokelaar, 2002; Mohrig and Marr, 2003; Baas et al., 2009, 2011; Sumner et al., 2009). Models attempting to predict the depositional record of sandy gravity flows evolution during downstream run-out, termed facies tracts, have traditionally been dominated by a downstream trend of increasing flow dilution, driven by mixing with the ambient fluid and sediment deposition, accompanied with an increase in turbulence intensity and downstream reduction in sediment concentration and grain size (Bouma, 1962; Walker, 1967, 1978; Hampton, 1972; Piper et al., 1985; Lowe, 1988, 1982; Allen, 1991; Stow et al., 1996; Mutti, 1992).

The deposit sequences introduced by Bouma (1962) and Lowe (1982) shown above are based on a single waning, surge-type turbidity current. However, this assumption does not account for the un-steadiness and non-uniformity of the flow related to spatial and temporal accelerations and decelerations (Kneller, 1995; Kneller and Branney, 1995).

Flows are unsteady if their mean velocity shows temporal variation when observed at an instant in time (Kneller, 1995; Kneller and Branney, 1995). When velocity increases with time a flow is waxing, whereas a flow is waning when its velocity decreases with time. The flow is instead considered steady when its velocity is constant in time (Fig. 2.7a).

Flows are considered uniform when their velocity is constant with distance, whereas they are considered non-uniform if they exhibit spatial velocity variation along the flow pathway. The flow is accumulative when its velocity increases with distance whereas it is depletive if its velocity decreases with distance (Fig. 2.7b).

The evolution of non-cohesive flows is also influenced by intrinsic properties, such as a) the *competence*, b) the *capacity* and c) the *efficiency* of the flow. These are interpreted as being responsible for the facies evolution as the consequence of the main hydrodynamic transformation occurring in a gravity flow along transport.

The flow competence is a measure of the maximum particle size that a non-cohesive flow can carry, which, in turn, depends on the slope gradient and on the particle-support mechanisms (Kneller and McCaffrey, 2003). The total amount of sediment that a non-cohesive flow can carry represents instead the *capacity* of a flow, related to fluid discharge and turbulence intensity (Kneller and McCaffrey, 2003; Dorrell et al., 2013).

The ability of a flow to carry sediment according to its clay content determines the efficiency of a non-cohesive flow (Mutti, 1979; Al Ja'Aidi et al., 2004). High efficiency flows can transport sediment over long distances and form well sorted deposits as elutriation acts during transport, whereas low-efficiency flows transport particles over short distance and generate poorly sorted deposits (Hüeneke and Mulder, 2011).

Flow steadiness and flow uniformity - velocity vs time - distance

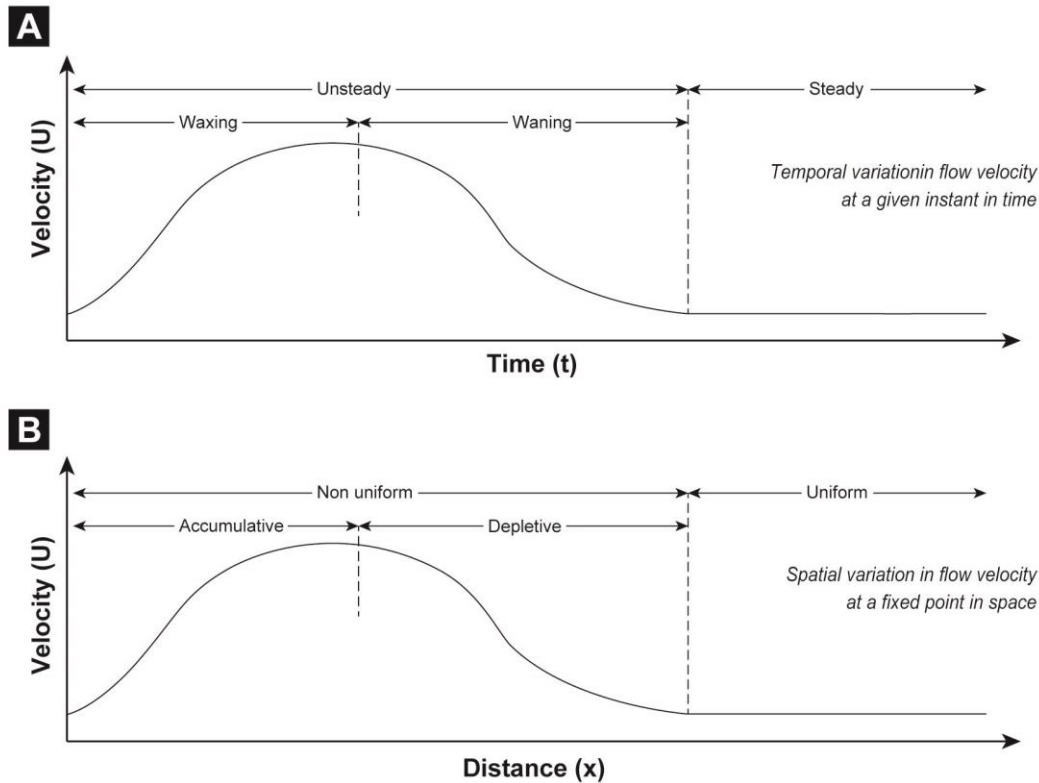


Fig. 2.7 – Schematic diagrams showing respectively (A) the temporal variation in flow at a fixed point in space and (B) the spatial variation in flow velocity at a fixed time (redrawn from Kneller, 1995; Kneller and Branney, 1995).

2.1.3 Hybrid flows

More recently, a range of mechanisms has been proposed resulting in a downstream transformation (partial or full) from relatively non-cohesive turbulent flow into more cohesive and higher density, laminar-like, turbulence suppressed flow (Wood and Smith, 1958a; Haughton et al., 2003, 2009; Talling et al., 2004, 2007b; Amy and Talling, 2006; Barker et al., 2008; Baas et al., 2009, 2011; Sumner et al., 2009; Kane & Pontén, 2012; Talling, 2013). Deposits containing co-genetic matrix-poor and matrix-rich sandstone facies, indicative of deposition beneath non-cohesive and relatively more cohesive flow states (Fig. 2.8), have been documented in a suite of deep-water depositional systems (Wood & Smith 1958; McCave and Jones, 1988; Van Vliet, 1978; Ricci Lucchi & Valmori, 1980; Lowe & Guy, 2000; McCaffrey & Kneller, 2001; Haughton et al., 2003, 2009; Talling et al., 2004; Sylvester and Lowe, 2004; Puigdefàbregas et al., 2004; Amy & Talling, 2006; Barker et al., 2008; Davis et al., 2009; Hodgson, 2009; Kane & Pontén, 2012; Lee et al., 2013; Talling, 2013; Patacci et al., 2014; Terlaky and Arnott, 2014; Fonesu et al., 2015).

These deposits (called hybrid event beds or HEBs by Haughton et al., 2009) are thought to record the downstream transformation of flows which became increasingly more cohesive (clay-rich) and turbulence-suppressed due to clay enrichment following the entrainment of muddy substrate and / or flow deceleration and reduction of flow shear stresses (Wood & Smith 1958; McCave and Jones, 1988; Haughton et al., 2003, 2009; Talling et al., 2004; Barker et al., 2008; Baas et al., 2009, 2011; Hodgson, 2009; Sumner et al., 2009; Kane & Pontén, 2012; Talling, 2013; Terlaky & Arnott, 2014). Using examples from ancient deep-water systems in the North Sea, Haughton et al. (2003, 2009) demonstrated the co-genetic relationship of matrix-poor and matrix-rich sandstone HEBs and proposed an “idealised” HEB divisions (Fig. 2.9). The authors interpreted the flows to become increasingly cohesive and turbulence-suppressed downstream (hybrid flow *sensu lato*, herein). However, particular emphasis was placed on the development of rheological heterogeneity along the length of near-bed flow with a forerunning non-cohesive (clay-poor) flow passing rearwards into a region of increasingly cohesive, turbulence suppressed flow (hybrid flow *sensu stricto*, herein). Flow transformation, and the emplacement of HEBs, has also been suggested to result from the vertical redistribution of non-cohesive material within the flow and development of vertical rheological stratification within the flow (e.g., Talling et al., 2007b, Kane and Pontén, 2012) without significant longitudinal heterogeneity in near-bed flow structure. These conceptual models are supported by, or were based upon, observations from experimental, variably clay-rich, turbulence-suppressed “transitional” flow types (Marr et al., 2001; Mohrig and Marr, 2003; Baas et al., 2009, 2011; Sumner et al., 2009). Experimental studies have demonstrated how co-genetic matrix-poor and matrix-rich sandstone can be deposited in the absence of a region of sandy non-cohesive flow (Sumner et al., 2009; Baas et al., 2011). Experimental studies of clay-rich flows have been valuable in demonstrating the influence of cohesive clay upon flow rheology style and vertical structure, as well as subsequent depositional character (Marr et al., 2001; Mohrig & Marr, 2003; Baas and Best, 2002; Baas et al., 2009, 2011; Sumner et al., 2009). However, the relatively short tanks or recirculating flume tanks used in these experiments are limited in their ability to effectively simulate the longitudinal structure, and its behaviour, within clay-rich flows (Kuenen & Menard, 1952; Middleton & Southard, 1984; McCaffrey et al., 2003; Choux et al., 2004; Baas et al., 2005). Thus it is unclear how observations from these experiments relate to conceptual models concerning the longitudinal structure of clay-rich flow types (i.e., hybrid flows *sensu stricto*, Haughton et al., 2003, 2009).

In summary, HEBs record the association of fluidal, non-cohesive flow, through various styles of transitional flow, to cohesive, turbulence-suppressed flow during a single sandy gravity flow event which may be expressed; 1) spatially across the flow (i.e., an instantaneous flow structure, Haughton et al., 2003, 2009); 2) temporally during larger-scale bulk transformation of the flow (Wood & Smith, 1958, McCave & Jones, 1988); or 3) both due to changing proportions of cohesive clay within the flow. The term hybrid event bed is used *sensu lato* herein as it makes no specific reference to a given flow rheology or flow structure and encompasses a wide range of potential flow character (i.e., cohesive or non-cohesive, turbulent or laminar).

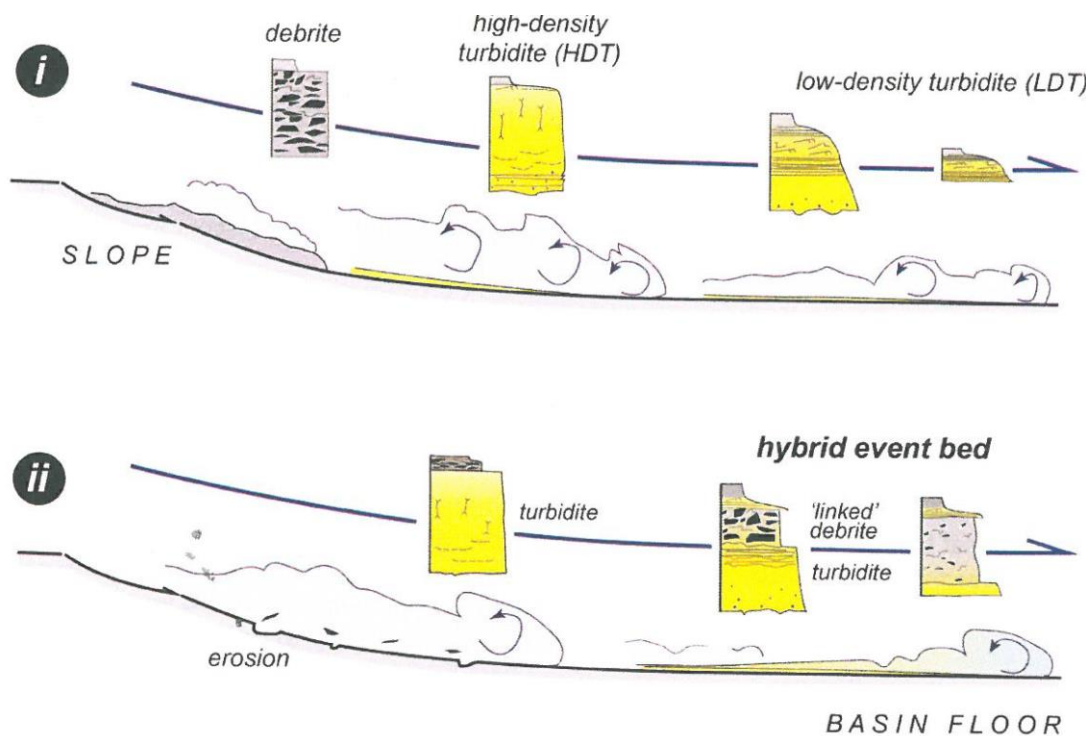


Fig. 2.8 – Schematic flow transformation trends during run-out downstream. 1) Traditional facies tract where the cohesive flow segregates sediment populations, increases dilution and, in turn, develops a turbulent behaviour. 2) 'Hybrid flow' model where the flow initially turbulent becomes cohesive distally (from Haughton et al., 2009).

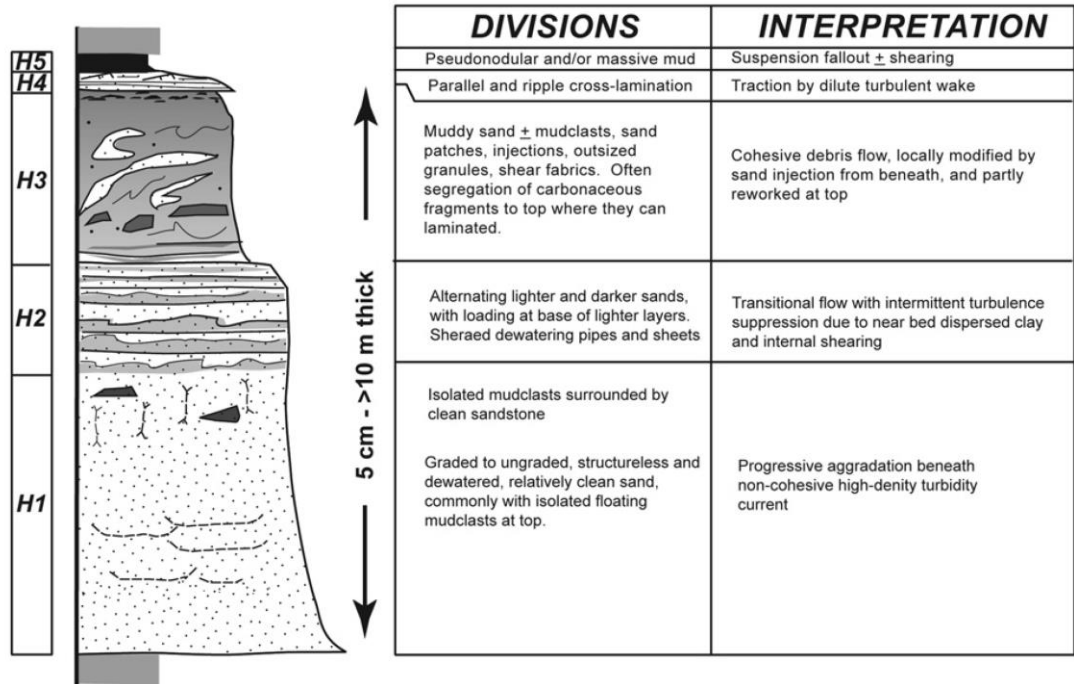


Fig. 2.9 – Idealised hybrid event bed composed of typical five divisions (H1–H5) with related descriptions and interpretations (from Haughton et al., 2009).

2.2 Mass-failures and related deposits

Submarine mass-transport deposits (MTDs) comprise marine sediments that have been remobilised, transported downslope, and redeposited by submarine landslides and comprise sediment packages emplaced during a single event of slope failure. The abundant presence of MTDs on submarine slopes and basin floors, in all geological settings, including rift, transform, convergent and passive continental margins, emerged with the improvement of side-scan sonar (Prior and Bornhold, 1985; Lipman et al., 1988; Moore et al., 1989, 1994; Watts and Masson, 1995, 2001; Labazuy, 1996; Masson, 1996; Roberts and Cramp, 1996; Masson et al., 1997, 1998, 2002; Urgeles et al., 1997; Urgeles et al., 1999; Gardner et al., 1999; Goldfinger et al., 2000; McAdoo et al., 2000; Krastel et al., 2001; Hafliðason et al., 2002; Laberg et al., 2002; Locat and Lee, 2002; Canals et al., 2004; Parsons et al., 2004), and high-resolution seismic data (Damuth, 1978; Savoye et al., 1990; Duperret et al., 1995; Evans et al., 1996; Mulder et al., 1997; Piper et al., 1997; Gardner et al., 1999; Bouriak et al., 2000; Bøe et al., 2000; Locat, 2001; Laberg et al., 2002; Lykousis et al., 2002; Nygard et al., 2002; Urgeles et al., 2002; Posamentier and Kolla, 2003; Hjelstuen et al., 2004; Homza, 2004; Lee et al., 2004; McGilvery and Cook, 2004; Gee et al., 2005; Posamentier, 2005; Schnellmann et al., 2005). The high spatial resolution provided by 3D seismic data allows detailed seafloor analysis, interpretation of the geomorphology and calculation of parameters such as seafloor slope angles at which failure may occur.

MTDs have also been described extensively from core (e.g., Tripsanas et al., 2008; Eggenhuisen et al., 2010) and outcrop studies (e.g., Kleverlaan, 1987; Macdonald, 1993; Shultz et al., 2005; Frey-Martínez et al., 2006; Moscardelli et al., 2006; Armitage et al., 2009; Bull et al., 2009; van der Merwe et al., 2009; Dykstra et al., 2011; Alves and Lourenço, 2010; Alves, 2015; Sobiesiak et al., 2016, 2017).

MTDs occur at all water depths. Large MTDs usually have dimensions of tens to hundreds of kilometres longitudinally, they are usually formed by shelf break or mid-slope failure, in contrast to smaller scale MTDs formed by collapse of canyon walls or failure on areas of elevated gradient on the flanks of salt diapirs or other areas of tectonically controlled fault steepening (Hampton et al., 1996; Masson et al., 2006; Posamentier and Walker, 2006). In some settings, up to 70% of the entire slope and deep-water stratigraphic column is composed of MTDs (Maslin et al., 2004). A variety of slope failures have been documented in numerous offshore oil provinces such as Israel (e.g., Frey Martinez et al., 2005), Norway (e.g., Bryn et al., 2005), and

the Niger Delta (e.g., Heiniö and Davies, 2006), and the Gulf of Mexico (e.g., Sawyer et al., 2007).

2.2.1 Slope deformational processes and MTD triggering

Submarine mass-failures generally involve un-lithified sediments from the upper part of the sedimentary column, but can also include partially compacted and marine-cemented sediments, or older, lithified materials (Maltman, 1994; Martinsen, 1994; Hafliðason et al., 2004). The character of the deposit prone to collapse partly determines the type of mass-failure that occurs. A failure of lithified deposit will usually result in a rock-fall or a granular debris flow, whereas an un-lithified source may move as one or a combination of turbidity current, grain-flow, debris flow, slump, slide and creeping slope (Brunden and Prior, 1984; Stow, 1986; Martinsen, 1994; Hampton et al., 1996; McAdoo et al., 2000).

Several classification schemes of submarine sediment mass-movements have been introduced through the years, and primarily used to classify sediment gravity flows (Mutti and Ricci Lucchi, 1978; Pickering et al., 1986; Ghibaudo, 1992) and to characterise the type of deposits (Kruit et al., 1976 and modified by Varnes, 1978; Nardin et al., 1979; Rupke, 1978; Stow et al., 1985; Stow, 1986; Stow et al., 1996; Nemeč, 1990), and may be based on rheology, product, climate, type of material moved, local geology, and triggering mechanisms (e.g., Dott, 1963; Ladd, 1935; Middleton and Hampton, 1976; Nardin et al., 1979; Ward, 1945; Hansen et al., 1984; Pierson and Costa, 1987; Martinsen, 1994; Mulder and Cochonat, 1996).

The majority of published classification schemes are scale-dependent or only applicable to limited case studies. Posamentier and Martinsen (2011) say that *“classification schemes should be simple, concentrate on descriptive and morphological factors, and direct the user towards genesis of a particular unit observed”*.

This section appraises published classification schemes for sediment gravity flows in order to find a common scheme that is able to summarise rheology, deposits and morphology of mass-failure events, primarily focusing on slides, slumps, and flows with plastic behaviour, all of which are mass flows in which the sediment is supported primarily by cohesion (i.e., the matrix has a finite yield strength) and/or by skeleton stresses (i.e., contacts between grains) (Hampton et al., 1996; Iverson, 1997, Posamentier and Martinsen, 2011). Nemeč (1990) developed a classification schemes based on previous classifications by Kruit et al. (1976), Rupke (1978), and

Stow (1986), where process and product are considered in a simplified way. The scheme is based on characterisation of mass-movement rheology which groups the processes into six categories (Fig. 2.3).

This classification shows a range from slow movement of coherent masses (creep), with little or no relative movement of individual grains (“quasi-static” grain contacts), to rapid mass movement of grains, which move almost entirely independently of other grains (falls of debris). This scheme also shows that the processes are a part of a process continuum. One process may evolve into another with time, or depositional effects of one process type may trigger other processes. This scheme is applicable both at outcrop and at seismic scale, and its use allows easier comparison between various settings (Posamentier and Martinsen, 2011).

The initiation of mass-movements is controlled by a number of factors that can be divided into those that affect the slope long-term stability and those that affect its short-term stability. When slope failures are more frequent and larger (e.g., volume, surface area, duration) during sea-level fall than during sea-level rise (Rouillard, 2010), a combination of processes including oversteepening, overloading (intensified by high sedimentation and progradation rates) and earthquakes are inferred to represent the principal trigger (Piper et al., 1997; Lamarche et al., 2008; Shanmugam, 2008; Tappin, 2010; Masson et al., 2011; Basilone et al., 2016).

Based on this consideration, several dominant controls on slope stability have been summarised by Lee (2009) as: (i) sediment delivery to the continental margins; its rate, volume and type, (ii) sediment thickness, (iii) changes in seafloor conditions, which can influence hydrate stability and the possible generation of free gas (Sharp and Samuel, 2004), (iv) variations in seismicity and, (v) changes in groundwater flow (Tappin, 2010; Mason Dykstra, 2005)

2.2.2 Flow transformation

MTDs, as described above, are the product of remobilisation of previously deposited sediments which during their movement downslope are subject to a progressive disruption and disaggregation through several interacting or overlapping mechanisms. The processes related to mass transport are mechanisms of stratal disruption, both inside the flow (e.g., partial disaggregation of still stratified blocks) and also outside the slide body (e.g., within the uppermost portion of the overriding substrate), and commonly involving non- to poorly lithified material (Fig. 2.10 - Lucente and Pini, 2003; Mutti et al., 2009b; Odonne et al., 2011; Ogata et al., 2010; Strachan, 2008; Talling et al., 2007c). In this scheme a broad spectrum of sedimentary products identified by Mutti et al. (2006) ranges from almost undeformed lithologies (e.g., slide blocks facies), passing through folded and boudinaged successions (e.g., slump facies), to block-in-matrix bodies (e.g., debris-flow facies), characterized by the occurrence of a strongly mixed, liquidized matrix (Fig. 2.10 - Mutti et al., 2006; Ogata et al., 2010).

Recognition of a “mixed” matrix, as described above reflects generation and maintenance of over-pressured conditions during mass transport triggering, translation and emplacement phases (Ogata et al., 2011). Ogata et al. (2011) observed that the matrix abundance may be used in discriminating low-mobility processes (i.e., syn-sedimentary shallow-level tectonic, slumps, gravitational spreading and creeping) from high-mobility ones (i.e., avalanches, block slides, debris- and blocky-flows). It is also possibly useful to conceptually separate slides with coherent behaviour from those with flow-like characteristics (Fig. 2.11).

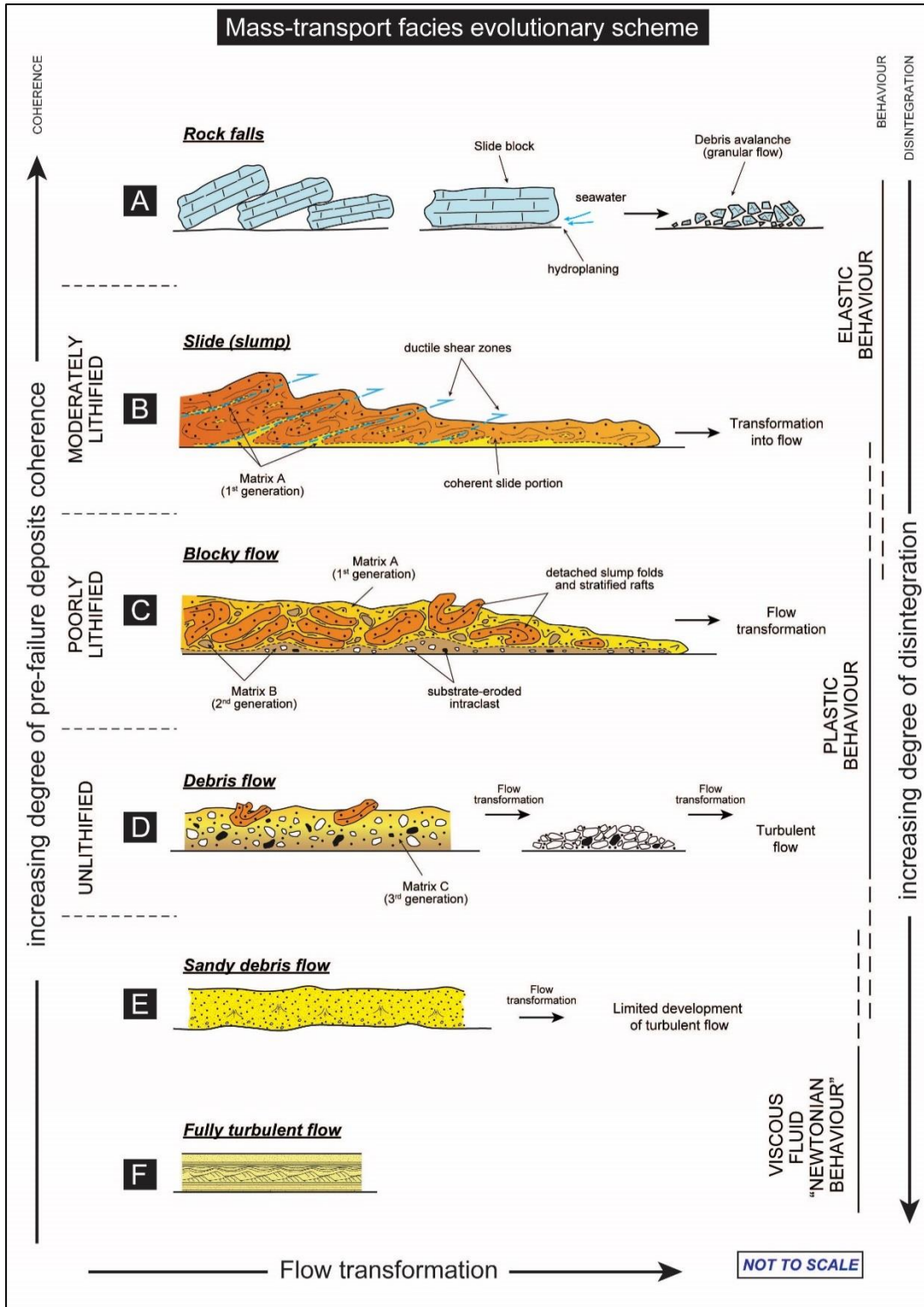


Fig. 2.10 – Dynamic classification and evolutionary scheme of MTDs which take into account genetic and evolutionary relationships between generating processes. This shows the possible relationships between slide, slump, blocky flow and debris flow deposits (left) and related structures, rheological behaviour and disruption degree (right). The possible linkage between the deposits and the lithification degree of the original (pre-failure) stratigraphic succession is shown on the right side. Block falls and turbidity currents are intended to represent the end-members of such broad spectrum of processes (modified after Ogata et al., 2012b; from Mutti et al., 2006).

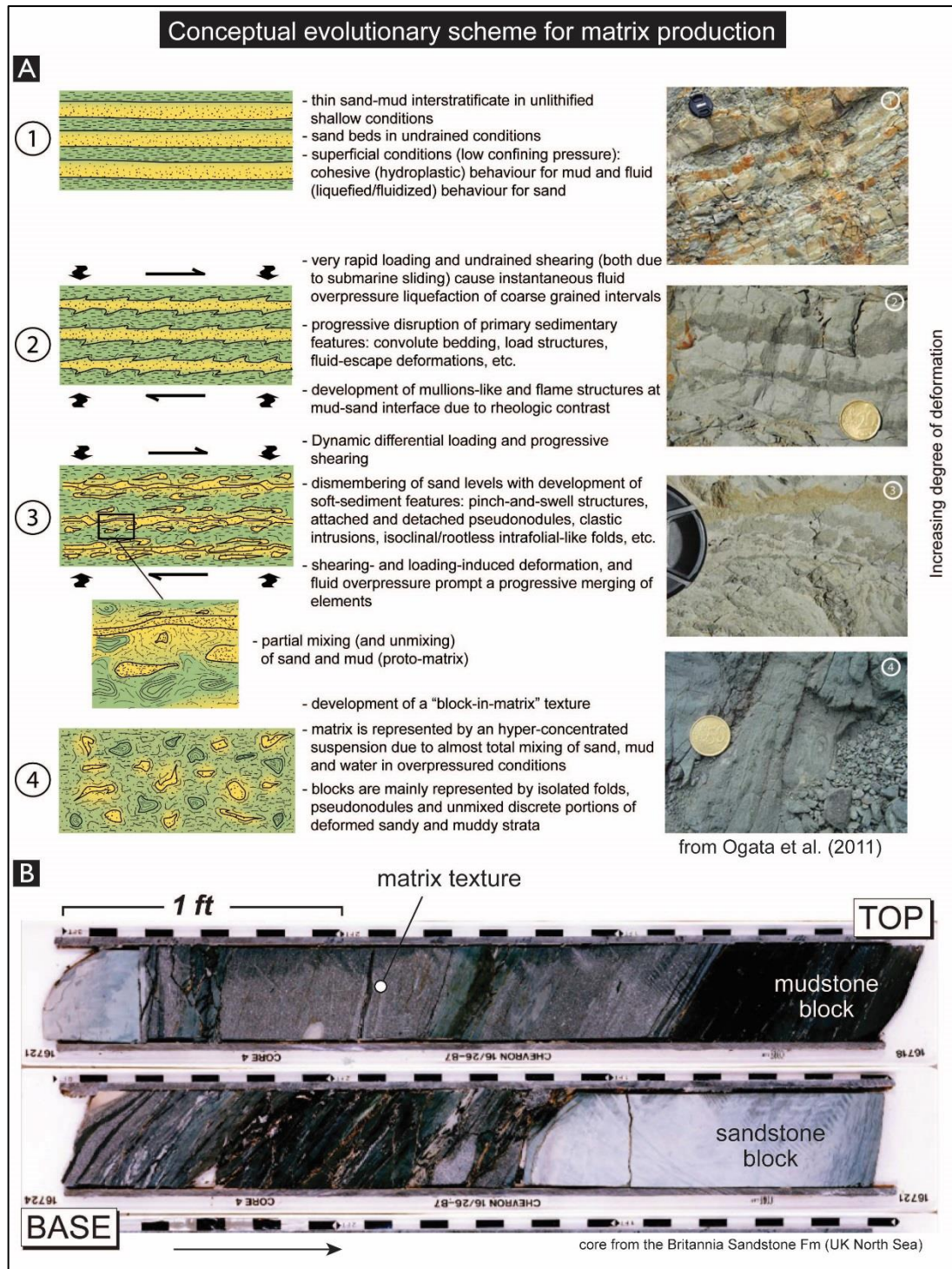


Fig. 2.11 – A) Cartoon representing an attempt to define evolutionary stages of matrix development through progressive stratal disruption of a thin-layered sequence (from Ogata et al., 2012a). B) Core example of debrite deposits from the Britannia Sandstone Fm., UK North Sea. The debrite shows a chaotic internal fabric with sand injections, mudclasts and floating quartz grains which give the characteristic “starry night” appearance (*sensu* Lowe and Guy, 2000).

2.2.3 Classification schemes of mass-transport deposits

Despite the great advances made in facies analysis, sequence stratigraphic studies, seismic acquisition and imaging techniques of deep-water deposits, Moscardelli and Wood (2008) show that in the 'modern' literature, the terminology used in MTD studies remains a confusing mix of terms compiled by scientists working in a variety of geological environments (Nardin et al., 1979; Shanmugam, 2002, 2000). Furthermore, Moscardelli and Wood (2008) also notice that in the literature submarine mass movements are broadly defined as "*movement of sediment driven by gravity (gravity-induced deposits)*" and, therefore, a huge spectrum of deposits can fall into the category, including slides, slumps, debris flows and turbidites".

Nardin et al. (1979) and later Nemec (1990) proposed a comprehensive classification system for submarine mass movement processes based on the interpretation of mode of transport and mechanical behaviour which can be inferred from the characteristics of the sedimentary deposits. However, this approach does not address the issues of grain-size distribution, sedimentation rate or slope gradient, which ultimately will influence boundary conditions for mechanical behaviour (Moscardelli and Wood, 2008), and could be used to address broader issues of causal mechanisms and pre-failure conditions of large-scale mass-failures.

The term mass-transport deposit (MTD) is commonly used synonymously in the literature with "mass transport complex", "mass-movement complex", "mass-gravity deposit"; it was first introduced by Peterson (1965) to describe a "generic" debris-flow deposit when understanding of mass-movement mechanics was still relatively poor and the use of a general term was justified (Posamentier and Martinsen, 2011).

Weimer (1989) introduced the term mass-transport complexes (MTCs) to define those features that occur at the base of depositional sequences and are overlain and/or overlapped by channel and levee sediments. Thus, in its original usage, the term MTC had a clear sequence stratigraphic connotation that was used to distinguish it from the generic term "slide" and as primarily a seismic facies description (Weimer, 1989). In their work Moscardelli and Wood (2008) use the term "mass-transport complex" (MTC) to group together slide, slump and debris flow products that can occur in the same event or depositional unit (Dott, 1963) as "gravity induced deposits" but the same authors (Moscardelli and Wood, 2016) refer to mass-transport deposits (MTDs) when they describe both deposits and processes of mass-failures. Mutti et al., 2006 differentiate MTDs and MTCs as two end-members, respectively: (a) a single-event unit developed at a scale below the seismic/cartographic scale (i.e., up to 10-20 m-thick), and as (b) an association of

two or more one-event units developed at the seismic/cartographic scale (10s to 100s of m-thick). Hence, the term MTC is used where multiple slope failures have coalesced into a larger unit or package (Gamberi et al., 2011; Hampton et al., 1996; Masson et al., 2006; Mulder and Cochonat, 1996; Posamentier and Walker, 2006; Varnes, 1978).

Sometimes these terms are misused, or just overused, to refer indiscriminately to both processes and products of large-scale mass failures. In order to better study and understand deposits from submarine mass-failures, an unambiguous terminology is required. For purposes of this work, slides, slumps and debrites will be considered constituents of MTDs when they are interpreted to co-occur in the same event or depositional unit (Dott, 1963), whereas MTCs will be mainly referred to the products of sliding movement, slumping and debris flow whose single or compound origin is difficult to determine.

Submarine landslides, slumps and debris flow can co-occur during the same slope instability event and result in the development of characteristic seafloor morphologies (Fig. 2.12). The geometry and internal deformation of MTDs is a consequence of the mechanisms of failure and the morphology of the slope over which translation occurs (Strachan, 2002; Lucente and Pini, 2003). Thus, the morphological characteristics of MTDs are commonly expressed by different geological structures or features that record information related to the type and direction of transport at the time of emplacement. These features are generally referred to as kinematic indicators (Fig. 2.13); they are geological structures that can unravel the history of mass-wasting from initiation, to its dynamic evolution and to the cessation of activity (Bull et al., 2009).

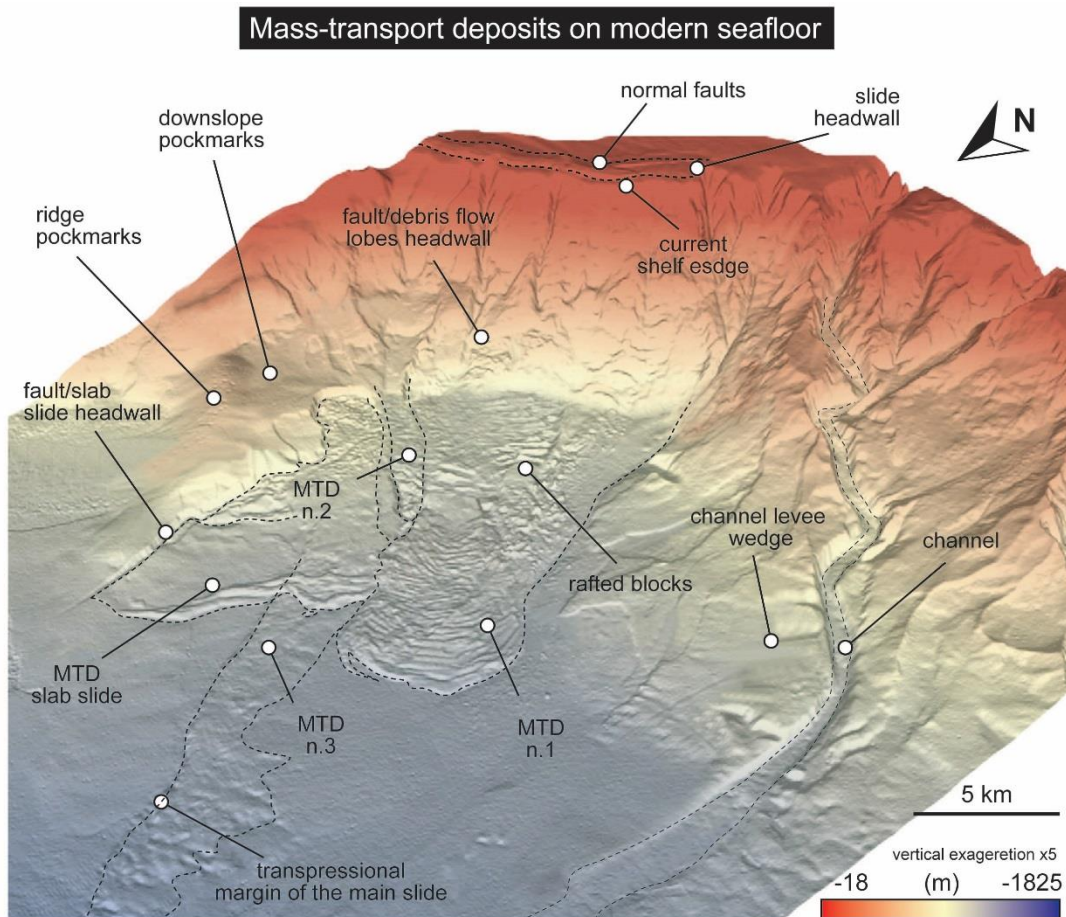


Fig. 2.12 – 3D high resolution swath bathymetry showing an MTC in the offshore Gioia Basin, NE Sicily. The MTC is the result of the stacking of different MTDs due to repeated failures of the shelf edge and upper slope area and of the nearby Villafranca slope. Vertical exaggeration of 5 (modified from Gamberi, 2010, Gamberi et al., 2011, and Rovere et al., 2013).

2.2.4 Mass transport deposits structural and geomorphological domains

MTDs can be organized into structural domains reflecting characteristic kinematics and strain (Lewis, 1971; Bull et al., 2009). These structural domains include (1) an ‘extensional domain’ located at the head of the failure containing predominantly extensional strain and a volume reduction relative to the stable slope, (2) a ‘translational domain’ in the mid-slope containing relatively undeformed strata, and (3) a ‘compressive domain’ at the toe of the failure reflecting contractional strain and a height increase with respect to the stable slope (Fig. 2.13). However, this classification comprises an oversimplification of the structural division of MTDs that are often observed in nature. In larger complexes of coalesced deposits, the tripartite scheme can be broken down into multiple sub-domains (Martinsen, 1994; Gardner et al., 1999).

The “headwall domain” is where sediment excavation/evacuation initiates, and in plan-view it usually appears as a composite arcuate feature (Fig. 2.13). On seismic

cross-sections, it is recognised as an excisional feature, where there is an abrupt reduction of stratigraphic section in a downslope direction. Immediately downslope, there is a region of marked extensional thinning, where the MTD is frequently cut by minor listric faults. Upslope of the headscarp, there is generally a region affected by smaller-scale faults and fractures (i.e., crown-cracks). Crown-cracks normally form in the undisplaced material adjacent to the headscarp because of extensional stresses developed by undermining during sediment removal. Crown-cracks represent the upslope propagation of slope instability during retrogressive failure and their identification is critical to highlight potential areas for future events of mass-wasting (review from Alves and Lourenço, 2010; Frey-Martinez, 2010; Alves, 2015).

The “translation domain” is the middle portion of the run-out of mass-failures characterised by the presence of translated blocks from the headwall area (Fig. 2.13). In this area it is usually possible to recognise ramp-flat-ramp structures. A ramp is defined as comprising a segment of the basal shear surface that cuts discordantly across bedding, whereas the ‘flat’ sections are bedding-parallel segments of the basal shear surface. The ramps, therefore, connect ‘flat’ segments of the basal shear surface at different stratigraphic levels (Trincardi and Argnani, 1990). Lucente and Pini (2003) suggested the ramp and flat geometry to be similar to shallow level deformation in accretionary wedges, and Gupta et al. (1999) assigned the terms “contractional” if the basal shear surface cuts up section and ‘extensional’ if it cuts down (Fig. 2.13). Gawthorpe and Clemmey (1985) and Trincardi and Argnani (1990) reported that most ramps trend perpendicular to the main flow or movement direction; rarer “slots” are ramps striking (sub-) parallel to the mass flow transport direction (O’Learly, 1986; Bull et al., 2009) (review from Omosanya, 2014).

The “toe domain” is the downslope limit of an MTD and it corresponds to the furthest extent of the area where sediment accumulates (Fig. 2.13). On seismic profiles, it is usually recognised as a zone of significant thickening of stratigraphic section. In shallow subsurface MTDs, where seismic resolution is the greatest, toe regions appear on dip-maps as areas of intense rugosity (Prior et al., 1984; Frey Martinez et al., 2005) with ridge-like features that are approximately arcuate, and convex downslope (Fig. 2.13). Frey-Martínez et al. (2006) subdivided the toe domain into those which are ‘frontally confined’, in which the translated mass is buttressed downslope against undisturbed strata; and ‘frontally emergent’ occurring when the translated mass has ramped up the basal shear surface and moved freely across the seafloor (review from Strachan, 2002; Omosanya, 2014).

Geomorphological division of a mass-transport deposit

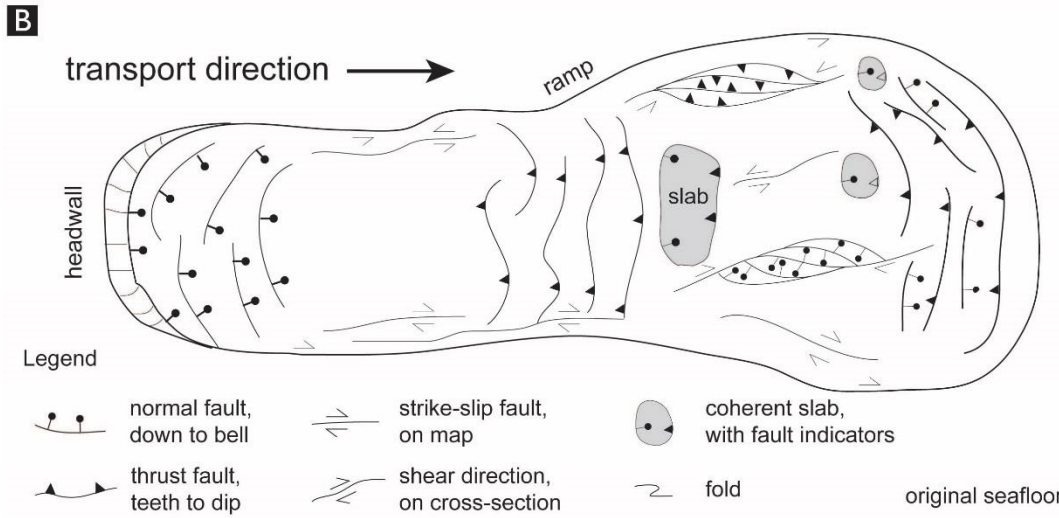
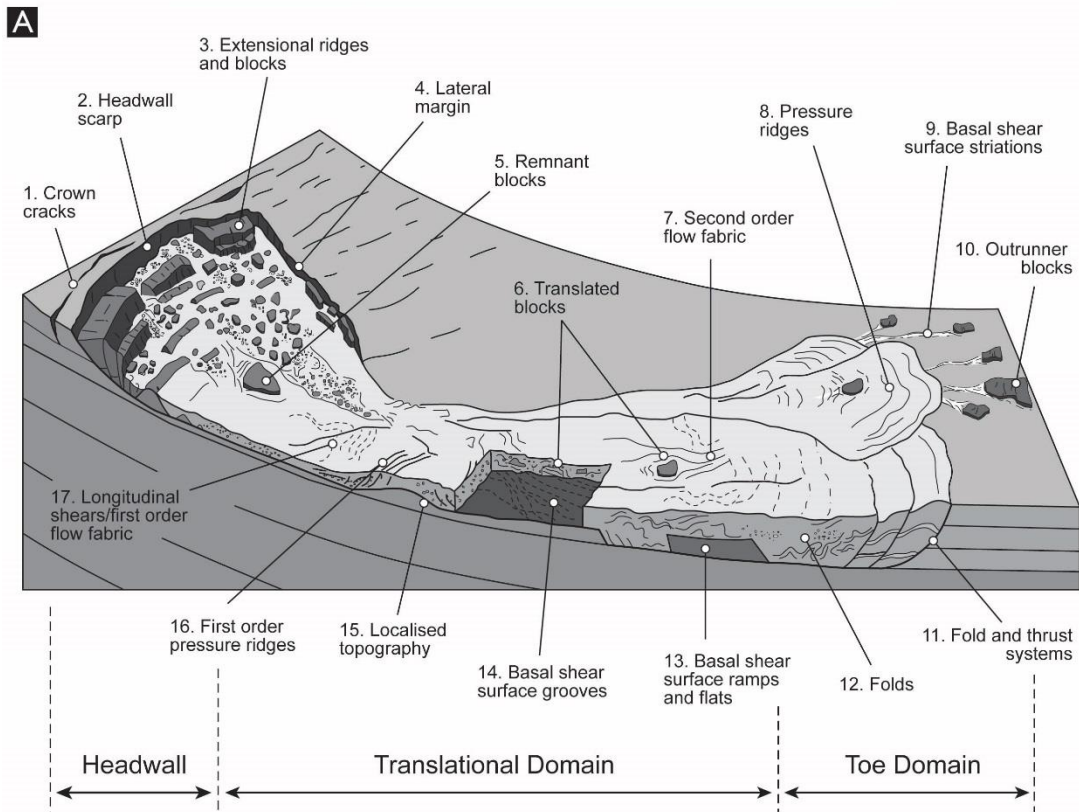


Fig. 2.13 – A) Geomorphologic elements of a mass-transport deposit and the likely occurrence of kinematic indicators relative to its various domains (redrawn after Prior et al., 1984). B) Schematic plan-view of the structural deformation in a mass-transport deposit, showing the variety of structures, and common locations where they may occur. Scale variable, from a few metres to hundreds of km (redrawn after M. Dykstra, 2005).

2.2.5 Applications of MTDs studies

During the last few decades MTDs have arguably been principally investigated by the academic world, whilst receiving less attention from geoscientists in the energy industry (Posamentier and Martinsen, 2011). The recent petroleum exploration of deeper water deposits has, however, led to the realisation that many aspects of these deposits are still poorly understood (Shipp et al., 2011), whilst recognising that better understanding of the mechanisms and consequences of mass-failure events can significantly influence offshore exploration and development (e.g., Piper and Normark, 1982; Piper et al., 1988; Loseth et al., 2003; Weimer and Shipp, 2004).

Although studies confirm that MTDs can act as reservoirs in oil and gas fields (Meckel, 2011), MTDs are rarely primary reservoirs and are certainly not primary exploration targets in siliciclastic settings (Weimer and Slatt, 2007). However, large slope failures and associated deposits have the potential to alter the original properties and architecture of reservoir intervals and to affect later sedimentation, prompting their academic study. In fact, mass-failures can modify the original stratification of the failed material, remixing the lithological compositions and altering the primary volumes of sediments (Beaubouef and Abreu, 2010). Such modifications are usually associated with a decrease in the net to gross, porosity and permeability of the reservoir deposits, the resulting complex lithologies may act as widespread seals, may influence migration pathways or play a role in trap generation (Shipp et al., 2004; Meckel, 2011). In this regard, MTDs represent important stratigraphic elements in many deep-water basins, traditionally identified as possible updip and lateral seals (Alves et al., 2014), due to the shear deformation and remolding associated with the movement downslope, that can enhance clay alignment and destroy large pore-throats. This is the case of the Jubilee gas field - Gulf of Mexico (Cardona et al., 2016) where remolded clayish deposits represented potential seal quality facies.

However, large-scale failures are also commonly erosive and they may result in deep and widely dispersed truncation and removal of underlying primary reservoir target, or may trigger seal failure with consequent vertical migration of hydrocarbons (Fig. 2.14 - Hafliadason et al., 2002, 2004; McGilvery and Cook, 2003).

MTD-related topography is another important feature to consider in hydrocarbon exploration because the rugose upper surface of these deposits may influence the distribution of subsequent sands, or at least compartmentalise the basal parts of overlying sandstone units (Shor and Piper, 1989; Cronin et al., 1998; Shultz et al., 2005; Armitage et al., 2009; Amerman et al., 2010). During late-stage transport,

MTDs may also experience deformation associated with the emplacement of turbidites above, which may contribute to an increase in upper MTD rugosity and subsequent creation of accommodation for sediments (Butler and McCaffrey, 2010; Kneller et al., 2016).

In addition, MTD presence in the shallow subsurface is an important factor that should be identified in any assessment of drilling hazards and in geotechnical studies for exploration and development planning (Molyneux et al., 2001; Lu and Shipp, 2011), because of their complex internal structure and inherent potential to contain local gas pockets and because the triggering of small- and large-scale slope-instabilities has the potential to put at risk installations and other anthropogenic structures on the seafloor (Barley, 1999; Weimer and Shipp, 2004; Butler and Turner, 2010; Mosher et al., 2010).

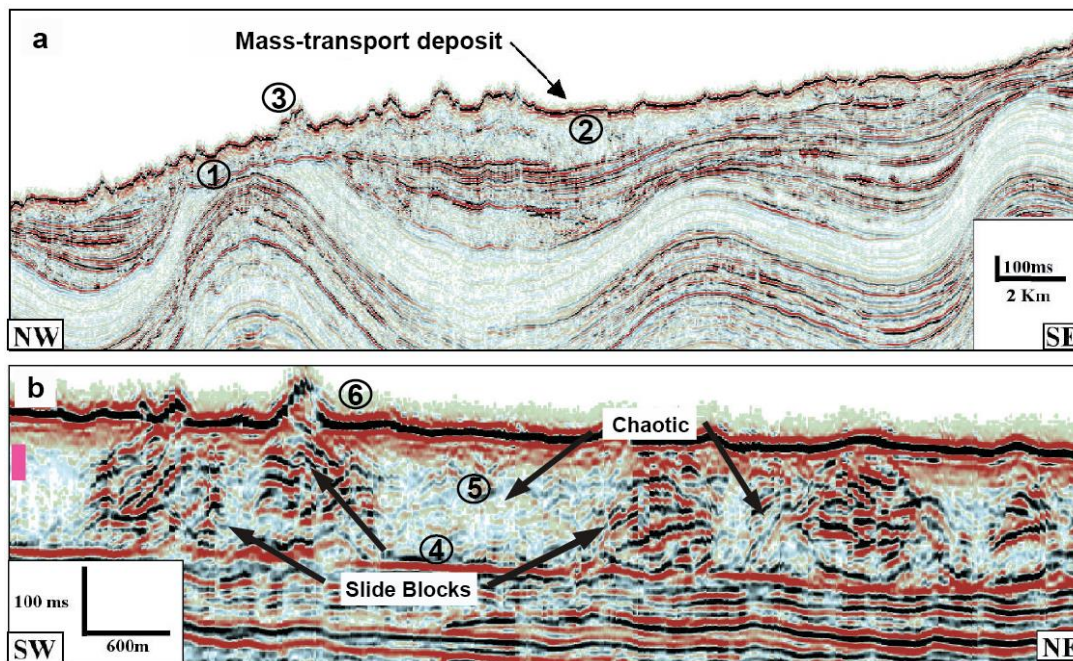


Fig. 2.14 – Seismic profiles across two portions of a prominent mass-transport deposit in Brunei deep-water margin showing typical features associated to MTDs. A) Seismic profile from up-dip area shows: (1) high-amplitude, basal reflection of the MTD that extends across the truncated fold; (2) chaotic reflections internal to the MTD; (3) irregular bathymetry developed on the upper surface of the MTD. B) Seismic profile down-dip of (A), highlighting: (4) the dipping basal surface of detachment; (5) the alternating facies from high-amplitude, irregularly bedded reflections (slide blocks) and low-amplitude chaotic reflections; (6) the irregular bathymetry caused by pelagic drape over the slide blocks (modified from McGilvery and Cook, 2003).

Processes of large en-masse movement of sediments also have the potential to generate tsunamis, posing a significant hazard to near-shore navigation and coastal

communities. Finally, a further consequence of large-scale failure events could be their triggering of episodic releases of methane into the atmosphere with possible consequences for global warming (Haq, 1995, 2009; Kvenvolden, 1993; Maslin et al., 1998, 2004, 2005).

2.2.6 Identification of MTDs in the subsurface: a problem of scale

The identification of MTDs in the subsurface is not always straightforward; different tools and techniques allow the observation of reservoir heterogeneities at different scales (Fig. 2.15), for instance microscopic (pore and grain scale), mesoscopic (vertical sequence in core or outcrop), macroscopic (inter-well) and megascopic (field-wide) scales (Krause et al., 1987).

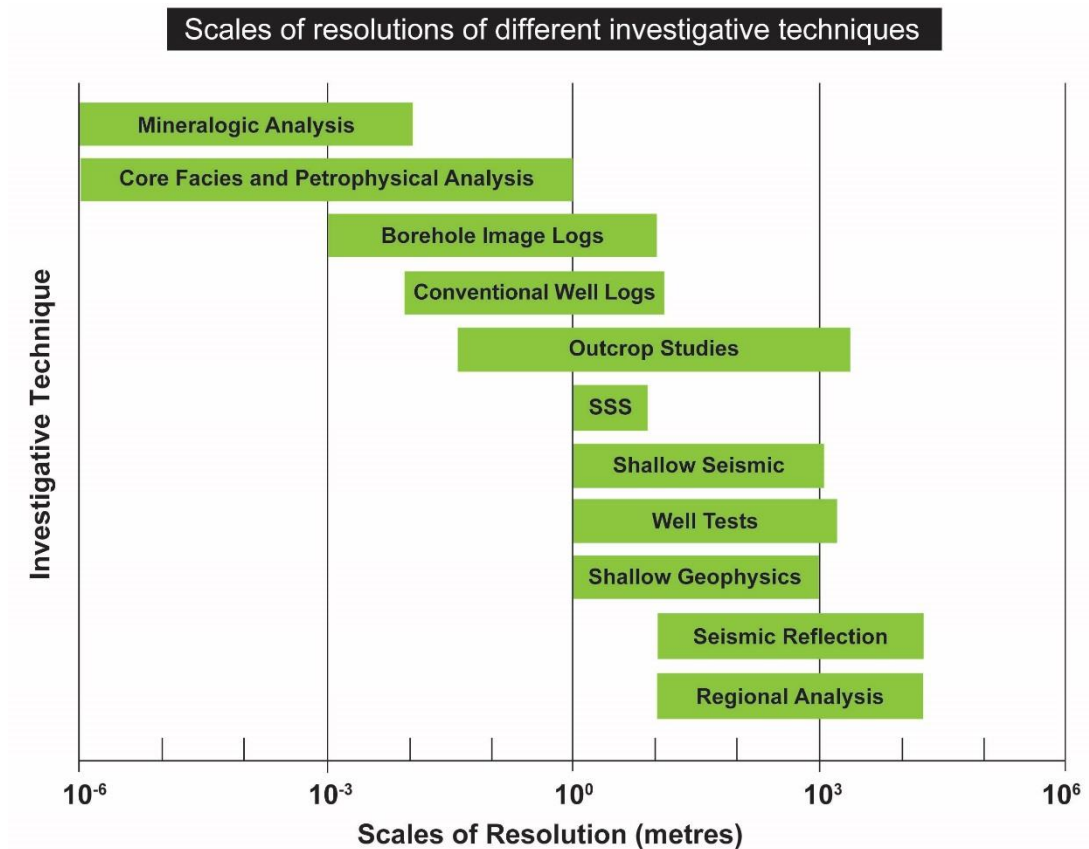


Fig. 2.15 – Log-plot showing the relative scales of observation and resolution of different data sets used in studying deep-water settings. SSS=side scan sonar (from Weimer and Slatt, 2007).

When imaged in seismic-reflection data (Fig. 2.16), MTDs commonly are inherently chaotic with transparent character (Fig. 2.14) though the relief of their rugose top surfaces is rarely imaged in typical petroleum industry seismic-reflection data due to resolution limitations (Posamentier and Kolla, 2003). In fact, the seismic expression of MTDs is strongly dictated by their lack of stratification and highly variable heterogeneous lithological character. High-resolution three-dimensional seismic-reflection data is often used to delineate some of the complicated characteristics and geometries associated with MTDs (e.g., Moscardelli and Wood, 2008; Bull et al., 2009), but is not always available.

Typical features associated with MTDs, such as the rugose surface topography and the disorganised reflections in profiles, prevent clear imaging in seismic-reflection data, especially for those sandstone deposits that overlie or underlie MTDs, causing misleading interpretations of the reservoir properties, as related to deposit geometries and lithofacies distributions (Armitage and Stright, 2010).

Outcrop analogues are commonly used to constrain physical geological properties of the MTDs, such as their internal heterogeneity and surface continuity, and of the overlying sandstones, such as bed thickness variations and lithofacies distribution, in order to reduce subsurface uncertainty and aid reservoir performance prediction (e.g., Slatt, 2000; Sullivan et al., 2000).

Outcrop and seismic character of mass-transport deposits

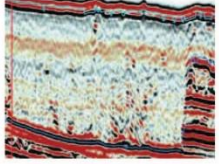
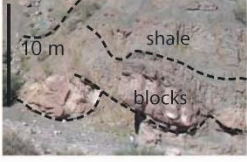
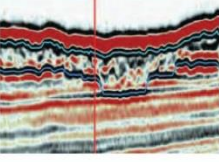
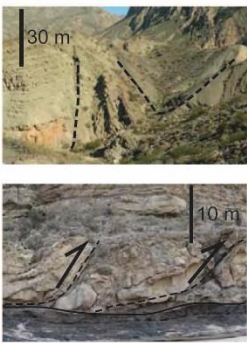
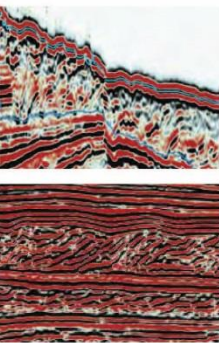
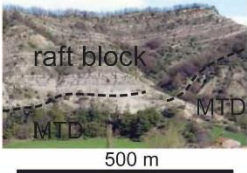
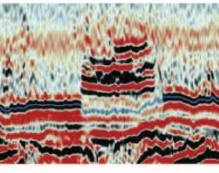
Outcrop Facies	Interpretation	Seismic Facies
	<p>Very chaotic deposits, highly deformed, often representing debrite deposits.</p>	
	<p>Small scale (10^1 to 10^2 m) blocks, internally deformed, which have probably been plucked up from the underlying strata.</p>	
	<p>Imbricated structures with a variable degree of deformation internal to the stratigraphy. Individual fault blocks can be internally coherent or deformed, and may form due to extension (C1) or compression (C2) (i.e. normal or reverse sense). Such through-going structures may form major fluid conduits.</p>	
	<p>Large scale (10^2 to 10^3 m) blocks representing big packages of stratigraphy that have been detached from the adjacent sea floor. These packages occasionally show a high degree of deformation along their margins.</p>	

Fig. 2.16 – Seismic and rock facies of various types and portions of MTDs showing the level of complexity that may be present in large-scale examples, but is beyond the resolution limitations of modern geophysical data. This figures also shows how the application of field-scale observations can help to restore sub-resolution information leading to an improved understanding of the depositional units resulting from mass-wasting events (modified from Kneller et al., 2016).

2.3 Interaction between MTD-related bathymetry and turbidity currents

2.3.1 Turbidity currents and topography

Sediment gravity flows may run out for long distances where the seafloor topography is relatively simple or where they are confined by channel morphology (10s – 100s km, Wynn et al., 2002b). Where sandy gravity flows occur in more topographically complex settings, their potential run-out distance can be reduced, or increased, and their character, including that of the depositional system they emplace, can be modified by interaction with seafloor topography (Miller et al., 1977; Fisher, 1990; Smith and Joseph, 2004 and references therein); these are non-uniformity effects. Systems affected by such processes can contain commercial hydrocarbon reserves (e.g., Gulf of Mexico, Kendrick, 2000; West Africa, Gee and Gawthorpe, 2007; North Sea, Barker et al., 2008, Davis et al., 2009) as seafloor topography can focus sand distribution and provide suitable traps through structural and or stratigraphic trapping (McCaffrey and Kneller, 2001; Prather, 2003). Seafloor topography can take a variety of forms (e.g., salt or mud diapirs, Beaubouef and Friedmann, 2000; fault-generated topography, Clark and Cartwright, 2009) and its expression on the seafloor may be static or dynamic depending upon sedimentation rates versus that of the processes generating topography (Fig. 2.17 - Prather et al., 1998; Grando and McClay, 2004; Mayall et al., 2010). Interaction with seafloor topography can modify sedimentary gravity flows in terms of their transport direction, velocity, turbulence and sediment concentration, suspension fall-out rate and rheology (Long, 1955; Pickering & Hiscott, 1985; Kneller et al., 1991; Edwards et al., 1994; Haughton, 1994; Kneller & McCaffrey, 1999; Lamb et al., 2004; Barker et al., 2008; Davis et al., 2009; Patacci et al., 2014). The nature of the modification depends upon a number of factors such as flow velocity, density, height, and degree of flow stratification, as well the height of the topographic obstacle (Fig. 2.17 - Kneller and Buckee, 2000; Kneller and McCaffrey, 1999). Such topographically-driven modification of the sedimentary gravity flows is referred to herein as flow confinement or confined flow, and may occur following flow interaction with a range of topographic features on the seafloor. Confined flows may also be contained (flow containment) where the height (Kneller and McCaffrey, 1999) and geometry of the topography is such that the majority of the flow is restricted within a depositional container; provided the flow is of sufficient magnitude such that it reaches the limits, and feel the effects of this containment (Kneller and Buckee, 2000; Al Ja'Aidi et al., 2004). Such confined and contained flow may occur in salt withdrawal mini-basins (Prather et al., 1998) and in small intra-continental rift or fore-arc basins (Pickering and Corregidor, 2000). Thus sedimentary gravity flows, and the depositional systems that they emplace, can be classified

depending upon whether they were: 1) unconfined, 2) confined but uncontained, or 3) contained. The effects of flow confinement can be manifested in the rock record (Fig. 2.18). Specifically, confinement may be indicated by the following observations: 1) disparate palaeoflow directions (e.g., sole structures versus tractional sedimentary structures higher within the bed (Pickering and Hiscott, 1985; Kneller et al., 1991; Haughton, 1994; Kneller, 1995; Kneller and McCaffrey, 1999; McCaffrey and Kneller, 2001; Felletti, 2002); 2) complex grain-size grading and arrangements of sedimentary structures (e.g., Pickering and Hiscott, 1985; Haughton, 1994); 3) distinct “combined” sedimentary structures considered to record oscillatory “seiches” or multidirectional flow (Marjanac, 1990; Tinterri, 2011). Additionally, where confined flows also experience containment, their deposits are typically characterised by greater thicknesses of both sandstone and overlying mud-caps compared to unconfined systems (e.g., ponded mud-caps Ricci Lucchi and Valmori, 1980; Pickering and Hiscott, 1985; Haughton, 1994).

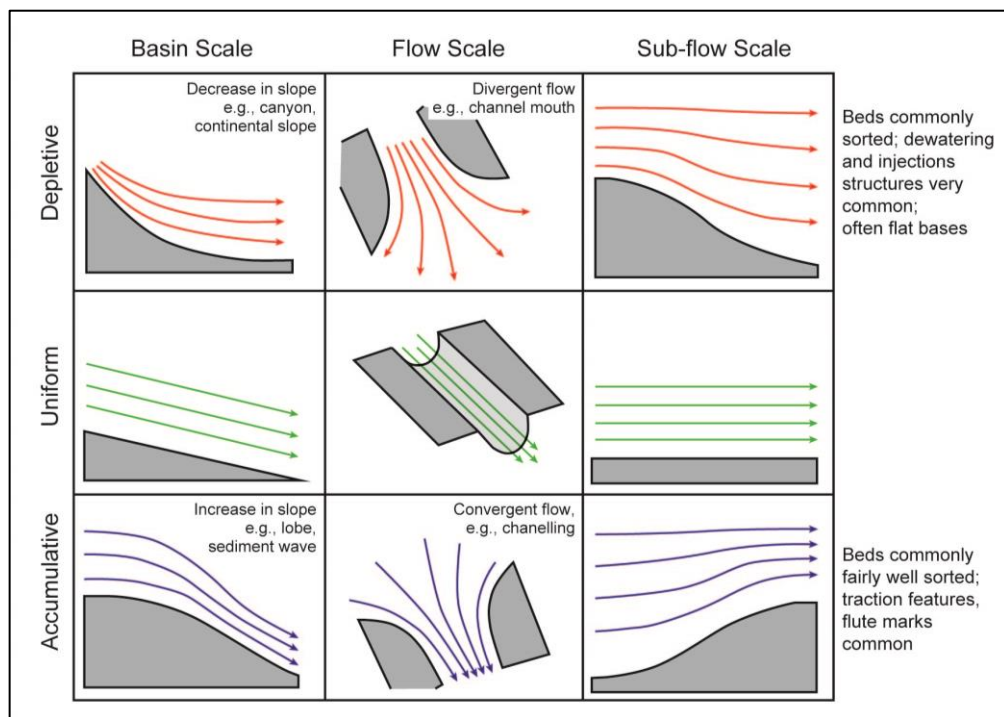


Fig. 2.17 – Schematic uniform and non-uniform flow change in relationship to topographic features at the basinal, flow and sub-flow scale. The flow is depletive when its velocity decreases with distance for example, when the flow spreads or when it moves on concave-up foot of slopes (basinal scale), where flow expands laterally beyond canyon- and channel-mouths (flow scale), or where flows expand vertically over downstream increases in gradient, associated, for example, with erosional topography (sub-flow scale). The flow is accumulative when its velocity increases with distance, for example, at increases in slope (basinal scale) where flow is confined or channelized (flow scale) or at decreases in convex-up slope (sub-flow scale). The flow is instead uniform when its velocity is constant with distance, for example along zones of constant gradient (basinal scale), where the degree of flow constriction is invariant (flow scale) or where the immediate gradient is the same as the mean local

gradient (sub-flow scale). Note: diagrams are not to scale (modified after McCaffrey and Kneller, 2004, from Kneller, 1995)

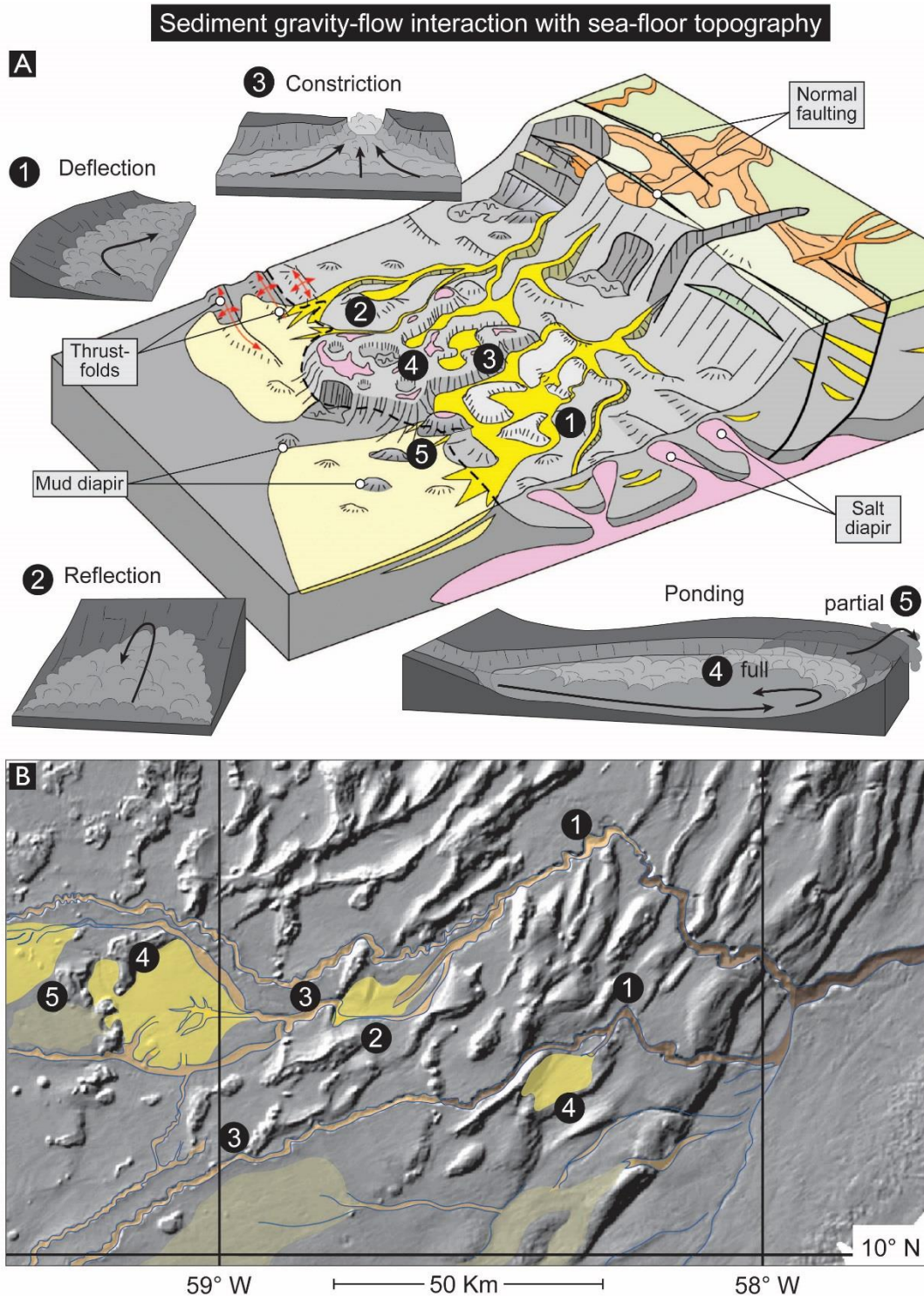


Fig. 2.18 – (A) Schematic block model illustrating the influence of seafloor topography upon shelf, slope and basin floor depositional systems (modified after Mayall et al., 2010, from Huyghe et al., 2004). Roman numbers highlight the topographic effects on gravity flows, as 1) deflection, 2) reflection, 3) constriction and 4) full and 5) partial ponding (after Patacci et al., 2015). (B) At the bottom, seafloor bathymetry of the southern Barbados accretionary prism where effect of topographic features on deep-water channel-lobe systems are highlighted. Flow from right to left (modified after Mayall et al., 2010, from Huyghe et al., 2004).

2.3.2 MTD-related bathymetry and turbidity currents

Large-scale failure events play an important role in shaping the seafloor (Posamentier and Martinsen, 2011) by a) removing large volumes of material which may leave behind submarine scars that can reach 1000s of km² on the seafloor, creating morphological relief up to 100s of metres high in the proximal area in relation to the mass-failure run out (Bugge et al., 1987; M. Dykstra, 2005; Gee et al., 2007; Omeru and Cartwright, 2015), and by b) depositing the remobilised material which usually form deposits of 10s of metres and locally even 100s of metres in thickness (see Fig. 2.19; Armitage et al., 2009; Jackson and Johnson, 2009; Dykstra et al., 2011).

The resultant MTD-related topography may affect sediment pathways (see Fig. 2.20; Brami et al., 2000; Ortiz-Karpf et al., 2015, 2017) and influence the behaviour of turbidity currents and thus their deposits (see Fig. 2.21; Armitage et al., 2009; Bernhardt et al., 2012; Kneller et al., 2016).

Kneller et al. (2016a) provided a detailed review of different styles of accommodation space associated with the emplacement of MTDs on the seafloor and the creation of relative bathymetric lows that may trap sediment or redirect sedimentary gravity flows, due to the influence of 1) the evacuated scar left by submarine failures in the up dip zone, 2) ponding against the mounded topography due to the en-masse deposition of the bulk of remobilised material, and 3) upper surface ponding linked to the relief developed on MTD upper surfaces along the translation and toe domains. The first two topographic features are commonly located on the upper slope, representing good sediment traps for sedimentary gravity flows moving downslope, which can be captured, contained or redirected before reaching the basin floor on an otherwise bypass-dominated slope (Armitage and Jackson, 2010; Olafiranye et al., 2013). Large-scale up dip ponding has been identified in outcrop (Lucente and Pini, 2003; M. Dykstra, 2005; Walker, 2008) and in seismic data from the Gulf of Mexico (Greene et al., 2006). In the third case, the surface ponding associated with topographic lows developed on the upper surface of MTDs has generally been related to the internal character of the MTD. This character may arise due to the presence of material incorporated within the bulk of the MTD (e.g., transported blocks; McGilvery and Cook, 2003; Alves and Cartwright, 2010; Alves and Lourenço, 2010; Alves, 2015; Moscardelli, 2014; Moscardelli and Wood, 2016; Sobiesiak et al., 2016, 2017), which can cause differential compaction effects (Alves, 2010). Another feature linked to the creation of accommodation space on top of MTDs is the

development of transverse troughs separated by ridges, whose size is generally proportional to the size and thickness of the MTD (Lee et al., 2004). These are usually associated with 1) the development of extensional faults within the proximal area of MTDs, creating topographic lows immediately overlying the subsided hanging wall block (Martinsen et al., 2000), and 2) thrust faults, which can generate negative and positive relief, tens of metres high and kilometres wide, commonly oriented orthogonal to the transport direction (Frey-Martínez et al., 2006; Dykstra et al., 2011).

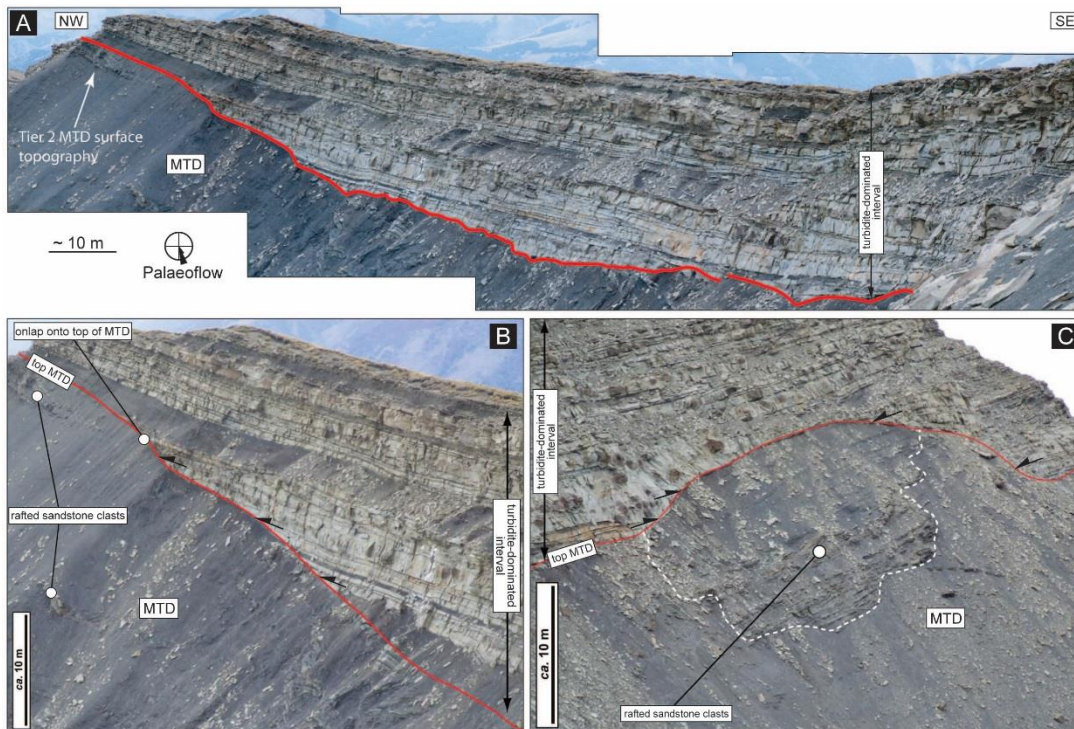


Fig. 2.19 – Examples of turbidite sandstone bodies above topography created by mass-transport deposits. A) Photomosaic of imbricated rafted blocks observed at the top of Unit 3 from the Upper Cretaceous Tres Pasos Formation, exposed on the Sierra Contreras, southern Chile. B-C) The MTDs are composed of sandstone clasts several 10s of meters in diameter buried within poorly-sorted and contorted silty shale beds upon which turbidite deposits onlap and pond (from Armitage et al., 2009).

Influence of MTDs on sandstone distribution

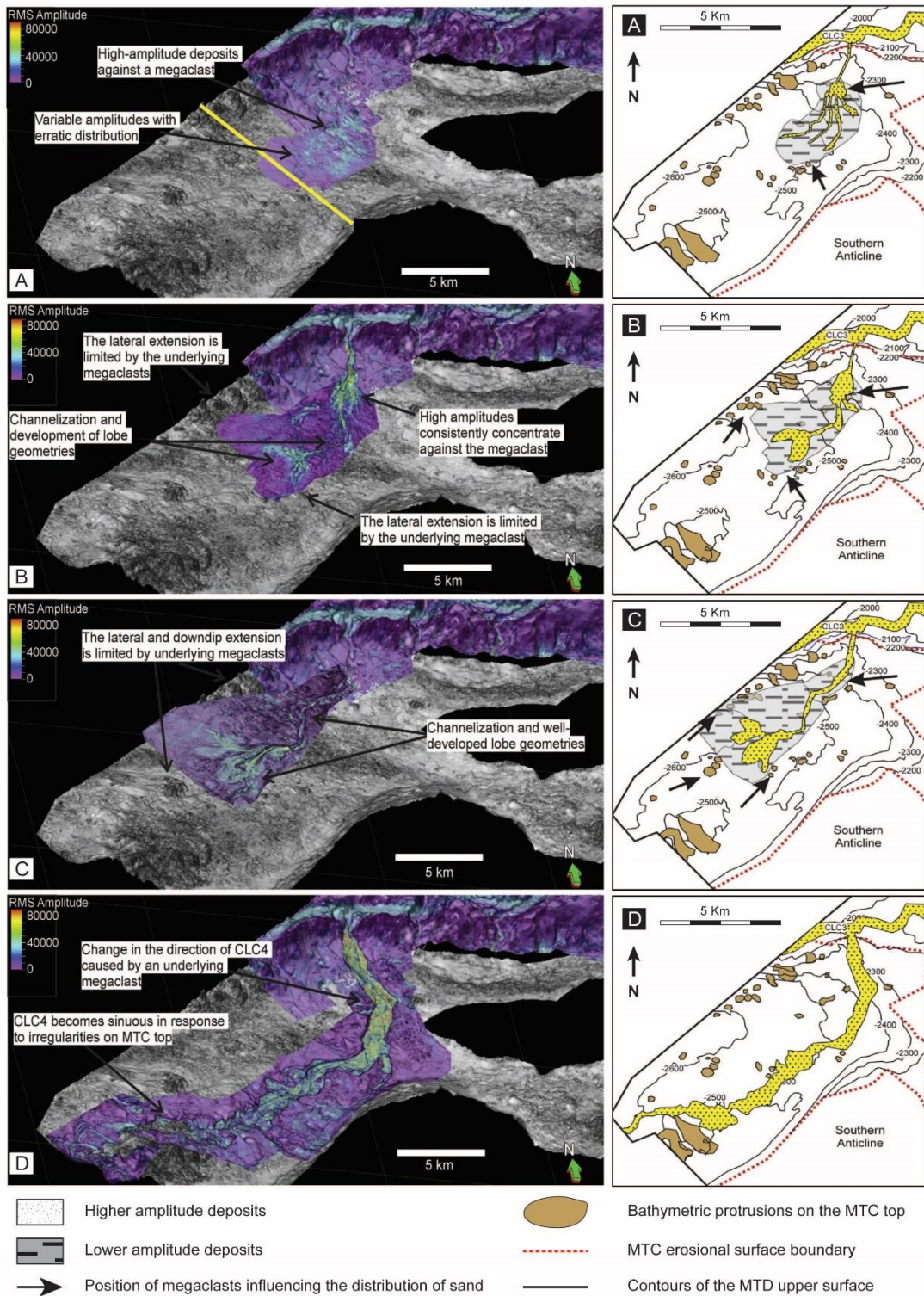


Fig. 2.20 – A series (A-D) of RMS amplitude variance extractions on the MTC top surface from the Magdalena Fan in the Caribbean Sea, off the northern coast of Colombia, showing the influence of MTD-related topography upon channel avulsion and the subsequent sediment dispersal patterns. On the right side the related schematic cartoons with contours constituting a proxy to the bathymetry underlying the lobes which highlight the interaction between the avulsion lobe deposits and the underlying bathymetric anomalies (from Ortiz-Karpf et al., 2015).

Kneller et al. (2016b) show that the nature of the sandstone reservoirs formed by turbidity currents ponding on top of MTDs is largely controlled by the scale and geometry of the topography. This can have different wavelengths, usually in the range of a few 100s of metres (Fairweather, 2014; Garyfalou, 2014), as described above; see also (Fig. 2.21-A). The scale of the topography plays an important role determining the spacing and the maximum thickness of isolated ponded sandstones (underfilled case), or shaping the form of the base of the reservoir (overfilled case), controlling the position of fluid contact/depth variation (Fig. 2.21-B-C; Kneller et al., 2016).

The internal character of ponded reservoirs is controlled by the style of progressive infill, which in turn depends on the nature of the sedimentary gravity flows in terms of size, thickness, efficiency and density (Kneller and McCaffrey, 1999; Kneller and Buckee, 2000; Meiburg and Kneller, 2010). Kneller et al. (2016b) show that when the thickness of the flows is equivalent to the high of the topographic relief, overspill may occur and deposition will result in a fill-and-spill style of sedimentation (Fig. 2.22-A; Prather et al., 1998; Sinclair and Tomasso, 2002; Brunt et al., 2004). The resulting ponded reservoirs may be coeval, although the deposits may not be connected (Fig. 2.22). Flows will mainly overrun topographic relief when they are thicker than the associated rugose topography (Fig. 2.22-A). In this latter case, despite the bypassing character of the flows, sand deposition is likely to be restricted into topographic lows, mainly due the sensitivity of turbidity currents to gradient changes associated with the topography (Kneller and McCaffrey, 1999), which facilitates amalgamation and the development of potential high net-to-gross. However, large flow size may also favour erosion of MTD-associated relief (typically comprising muddy material) producing layers of shale clasts within the ponded fill (Kneller et al., 2016).

Mass-transport deposits and reservoir properties

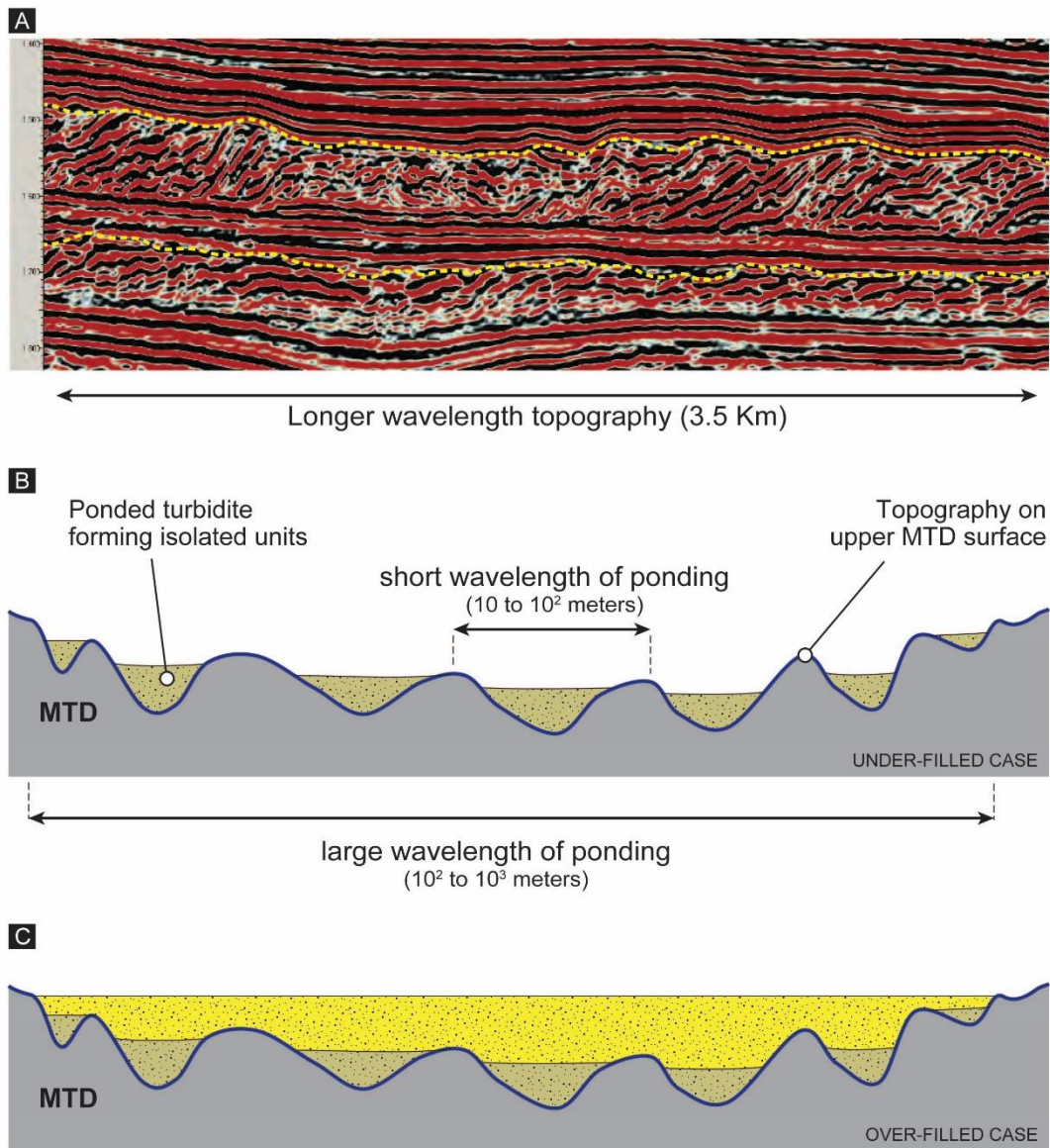
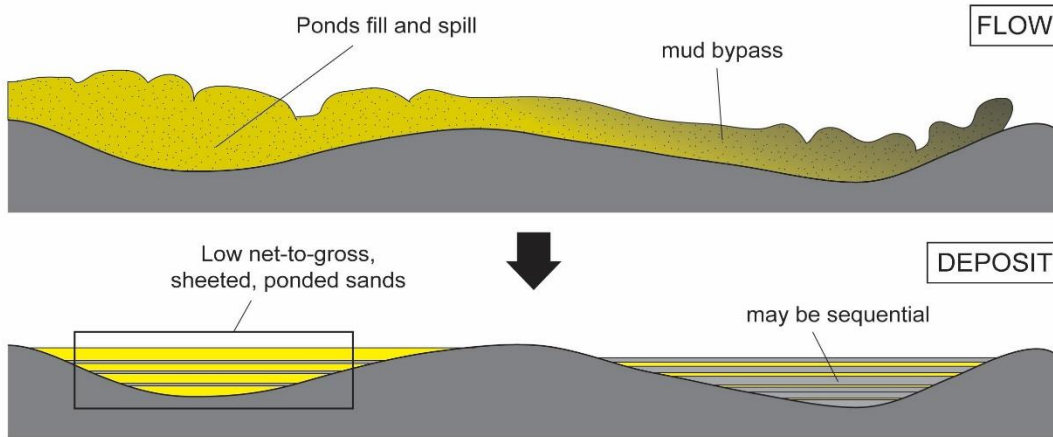


Fig. 2.21 – (A) Seismic section showing the generation of short and long wavelength topographic relief by the formation of imbricate stacks within a mass-transport deposit (seismic section from Kneller et al., 2016). Below, cartoons showing the effects of underfilled versus overfilled accommodation on reservoir. (B) Underfilling of topography by sandy turbidites producing isolated sand bodies. (C) Overfilling of topography producing continuous sand bodies with irregular bases (modified from Kneller et al., 2016).

MTD-related topographic reliefs and flow size

A FLOW PARTIALLY/WHOLLY CONFINED BY TOPOGRAPHY



B FLOW OUTSIZE WITH RESPECT TO TOPOGRAPHY

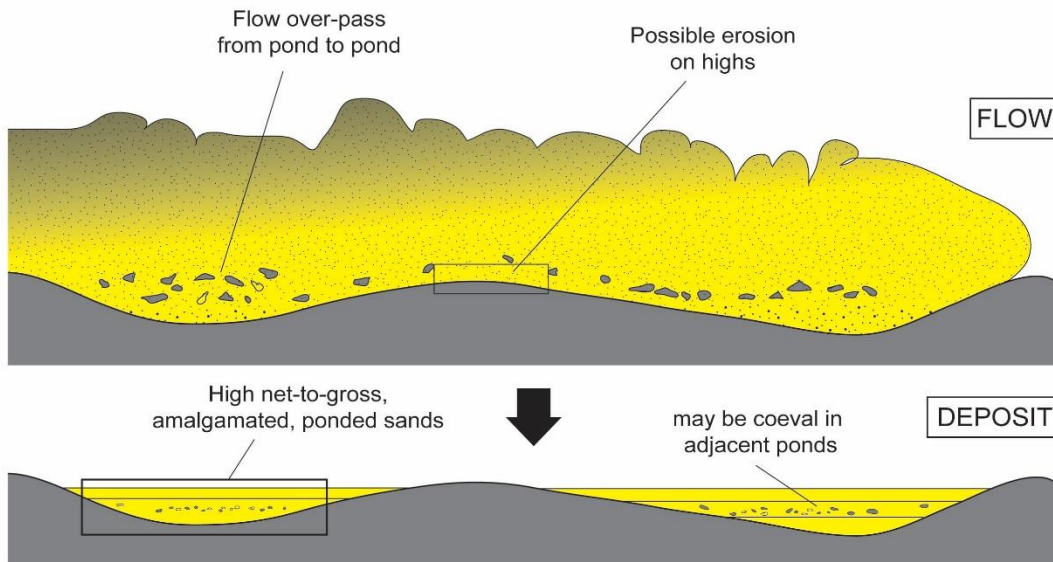


Fig. 2.22 – Illustration of the effect of flow size relative to topographic relief. (A) Where flows are ponded by the topography, updip ponds fill first, with progressive overspill of increasingly coarse sediment to downdip ponds, generating fills that coarsen and increase in net-to-gross upward. (B) Where flows are only partly ponded (flows larger than topography or interacting with positive three-dimensional topography-bumps with continuous valleys), fills of adjacent ponds will be coeval, possibly with bypass of mud to generate high net-to-gross ponded sands (modified from Kneller et al., 2016).

In conclusion, Kneller et al. (2016b) suggest that the topographic effects on the sandstone deposition will depend largely on 1) the relationship between the scale of the turbidity currents (thickness, stratification and grain size distribution) and the scale of rugosity developed on the upper topography of MTDs; 2) the orientation of the MTD development over the seafloor and the sedimentary gravity flow direction; 3) the pathway taken by the turbidity currents over the surface of the MTD; and 4) the ratio between areas with potential accommodation space and those without.

2.4 Open research questions

Substantial progress in the study of sedimentary gravity flows and their controlling factors, aided by advances in technology (i.e., 3D seismic reflection data, cores and borehole image logs, conventional wireline logs, 3D geologic models and reservoir simulation), has shown the commonplace occurrence of MTDs on continental slopes and basin plains.

Although MTDs have been studied since the early 1920s, much of the research has been conducted on features partially preserved at outcrop, which can afford both snapshots and views through the evolution of systems with extensive MTDs (e.g., Martinsen et al., 2000; Lucente and Pini, 2003). However, the incompleteness of outcrop examples has been a persistent obstacle to a more comprehensive, process based analysis of MTD triggers, emplacement mechanisms and deposits.

The study of MTDs is fundamental for better understanding the role of mass-wasting processes in shaping the fill of sedimentary basins (Norem et al., 1990; Masson et al., 1998; Gee et al., 1999, 2006; Frey Martinez et al., 2005; Richardson et al., 2011). In fact, they are responsible of the transport of significant amount of sediment to offshore areas, commonly comprising c. 10% to 30% of continental slope strata (Hjelstuen et al., 2007; Talling et al., 2007c; Hühnerbach and Masson, 2004; Mienert and Weaver, 2012). As a result, in hydrocarbon exploration and development, understanding the distribution of these transported masses is crucial to improving prediction of the presence and character of any reservoir sands deposited around them and to assess their seal potential.

The overall aim of the research reported in this thesis is to contribute to an ongoing effort to better understand the role of MTDs in influencing the evolution of stratigraphic architecture in deep-water settings. In this regard, the principal open research questions that arise following literature review on sediment gravity flows and especially on MTDs are:

- What is the size, geometry and wavelength of the rugosity over the upper surface of an MTD? – Scales of rugosity associated with MTDs on the basin floor will be described as relationship of length scale and morphology, using outcrop characterisation as a tool for reducing inter-well uncertainty in the subsurface.
- What is the role of MTDs in the alteration of accommodation space on the seafloor? – The reconstruction of palaeobathymetry of the seafloor will show some example of the size of accommodation space created/destroyed by the emplacement of MTDs.
- What is the effect of the presence of MTDs on turbidite systems and what is the relationship between MTD-related topography and turbidites distribution? – The emplacement of turbidites over MTD-related bathymetry will be shown from both subsurface and outcrop study in order to show how turbidity currents adjust to different scales of rugosity, how the nature of the substrate may influence subsequent flow transformation, and the impact of the character of rugosity on facies patterns.
- What role do MTDs play in applied contexts? - The presence of MTDs in deep-water settings is an important factor in hydrocarbon exploration and reservoir characterisation. The work detailed in this thesis may have applications in subsurface settings where reservoir characterisation of deep-water deposits influenced by the presence of MTDs is challenging, as is commonly the case where morphological features associated with MTDs are under the scale of seismic resolution.

This thesis aims to address these research questions through a subsurface case study (Britannia Field) and an outcrop case study (Casaglia MTD): both settings are characterised by the presence of MTDs.

3 Geology of the Lower Cretaceous in the Central North Sea and of the Britannia Field (UK sector)

3.1 Introduction

The Lower Cretaceous of the Central North Sea became the object of increasing interest after a number of significant oil and gas discoveries during the 70s which made it a focus for hydrocarbon exploration (Coperstake et al., 2003). In general, this interval is characterised by difficulties in seeing or interpreting sand and/or hydrocarbon presence using seismic data alone; such data are adversely affected by the presence of a thick chalk overburden (Chalk Group, <2000 feet) that attenuates the high frequency element to approximately 30 Hz and reduces vertical resolution to approximately 80 feet (Hill and Palfrey, 2003). Therefore, evaluating potential sweet spots within wide fairway tracts (e.g., Britannia Field) results in a very high dependence on well data and geological modelling (Sumner et al., 2005).

This chapter aims to introduce the geology of the Central North Sea together with a review of stratigraphy and the tectonic features developed during the pre-, syn-rift and post-rift development of the North Sea Basin in order to better understand the depositional environment of the Britannia Sandstone Formation (BSF) during the lower Cretaceous.

Thus, in summary, the Chapter objectives are:

- To briefly review the tectonic setting of the Central North Sea together with a brief general description of the pre-, syn- and post-rifting history of the North Sea;
- To review the stratigraphy of the Lower Cretaceous BSF;
- To review the inherited geological knowledge of the BSF as derived by previous workers on the Britannia Field;

3.2 The regional tectonic setting of the Central North Sea

The Central North Sea has been subject of intense study due to the significant exploration activity that occurred in this area in the last 40 years. Seismic data and extensive well databases increased understanding of the evolution of the North Sea Rift making this area one of the best studied rift systems in the world (Erratt et al., 1999; Millennium Atlas, 2003). Multiple compressional and extensional phases are recorded across the North Sea area, with major tectonic episodes represented by a) the Caledonian orogeny, b) the Variscan orogeny and c) the Triassic rifting (Ziegler, 1975) (Fig. 3.1).

The Caledonian orogenic belt extended from northern Norway and Greenland to the southern Appalachians and was formed by the early Palaeozoic accretion of magmatic arcs and continental fragments on to the North American continental craton, involving both dip-slip and strike-slip displacements; Jones et al. (1999) emphasise the importance of strike-slip movements relative to dip-slip displacements (Fig. 3.2) The history of the Caledonian orogeny (500-400 Ma) is well preserved on the SE of the Great Glen Fault and involved: a) development of a rift basin associated with a passive oceanic margin during the late Precambrian to Cambrian which, b) collapsed during the early stages of reversal in plate motion, before c) the development of a magmatic arc together with a fore-arc basin and its associated accretionary wedge. The Caledonian orogeny resulted in the fusion of the North America-Greenland and the North-West European continental masses (Wilson, 1966) with the Caledonian belt crossing the northern North Sea (Ziegler, 1975).

The Variscan orogeny (400-300 Ma) was another episode of progressive NW-directed accretion of magmatic arcs and older continental fragments onto the North American Craton (Coward, 1990). Thrust systems of the Variscan orogenic belt were activated during the main period of compression. At the same time southern Britain was influenced by spasmodic crustal extension. The extension direction is reconstructed to be NE-SW, likely associated with a pull-apart basin in a major strike slip shear (Ziegler, 1975). Rift basins in the northern Britain were produced by widespread extension of the early Carboniferous across NW Europe. Marine incursions from the "Variscan geosyncline" reached as far as the central North Sea (Coward, 1990).

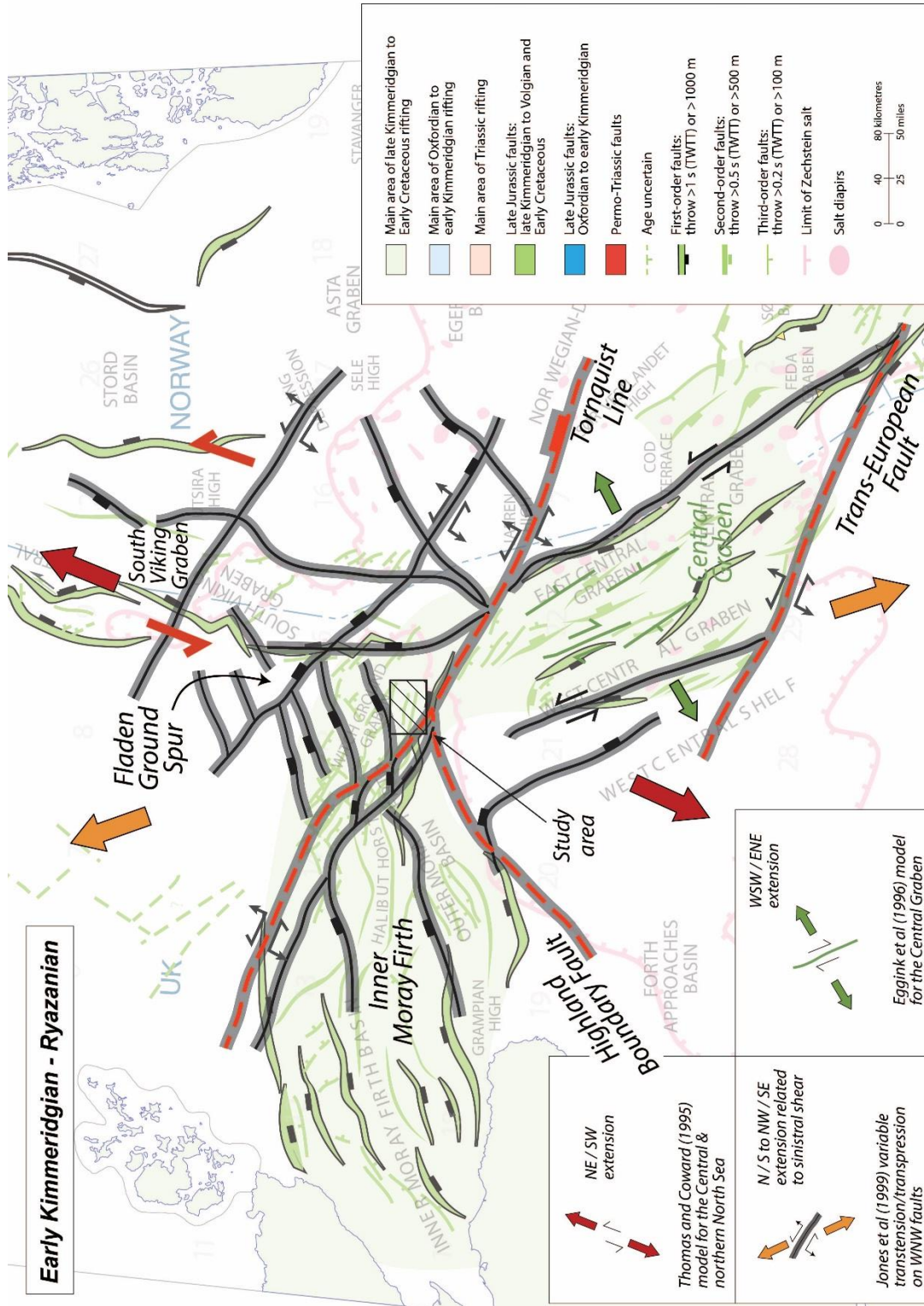


Fig. 3.2 – Summary and reconstruction of the structural state of the Central North Sea during the Lower Jurassic (after Jones et al., 1999 and reference therein). The Tornquist line can be recognised as a major structural feature during much of the post-Caledonian history of NW Europe.

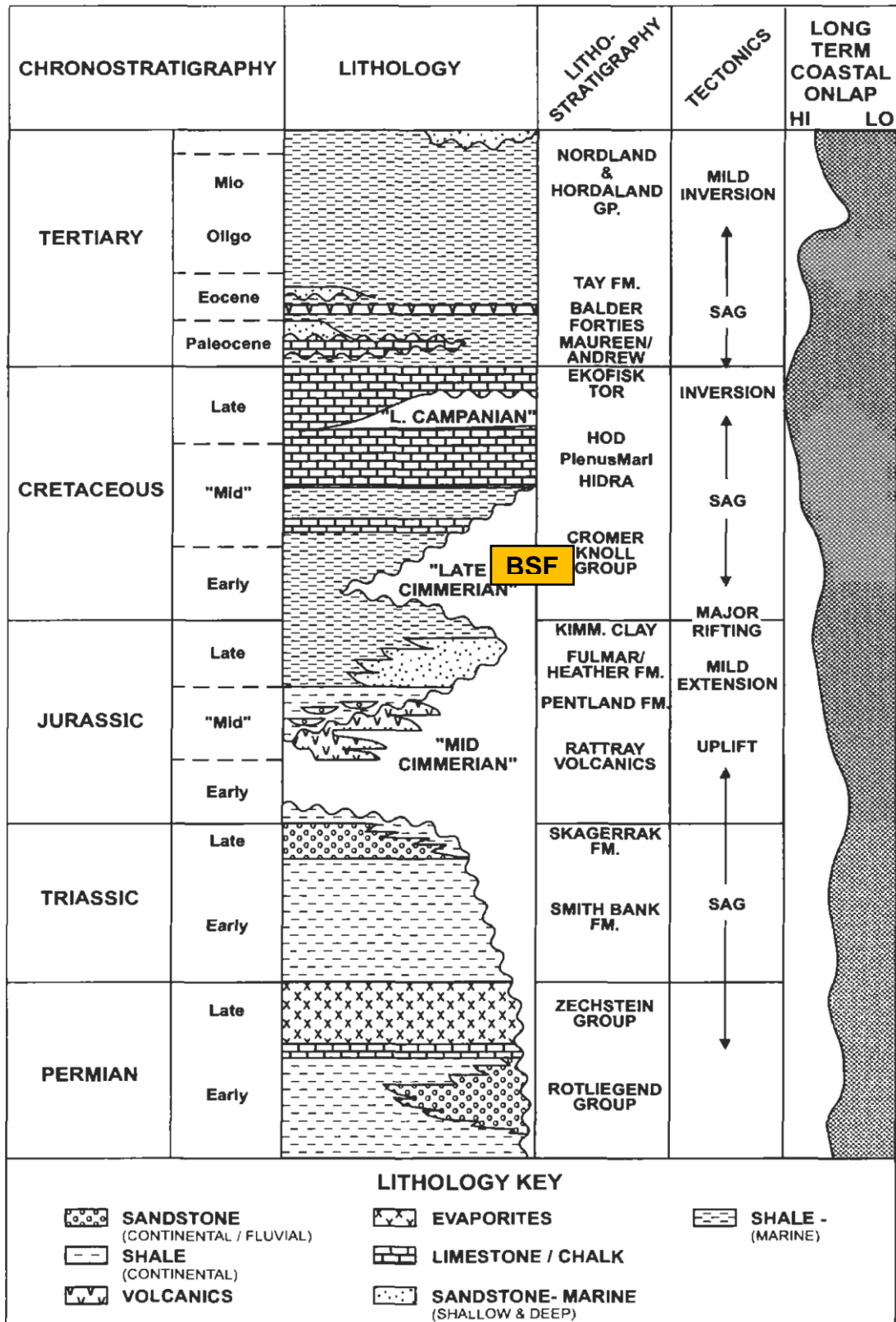


Fig. 3.3 – Summary stratigraphic column for the Central North Sea area (modified from Erratt et al., 1999; after Cayley, 1987).

3.2.1 Pre-rifting phase (Palaeozoic)

Only a few tens of wells penetrate basement rocks in the vicinity of the North Sea Graben. Drilling reached the Caledonian basement, consisting of intrusive igneous rocks and low- to high-grade metamorphic rocks, including metasedimentary sequences (Ziegler, 1990; Gautier, 2005). In the Middle Devonian, deposition of marine limestone and shale was largely confined to the current Central Graben, indicating its early structural configuration (Gautier, 2005; Downie, 2009). The evaporities from the Late Permian Zechstein basin cover much of the southern North Sea, whereas salt becomes scarce northward (Fig. 3.3).

3.2.2 Syn-rifting phase (Triassic)

Marine transgression of the North Sea Graben arose due to accelerating extension and subsidence in the latest Jurassic (Callovian) time (Fig. 3.3). The principal phase of extension occurred between Late Jurassic (Middle Oxfordian) and earliest Cretaceous (Berriasian) with basin deepening and associated retreat of the shoreline. A series of narrow, long and interconnected basins developed as a consequence of Late Jurassic to early Cretaceous extension, with deposition of fine grained mudstone, commonly laminated and rich in organic matter. During the Late Jurassic sedimentation became more rapid with over 2,000 metres thick of shales (Kimmeridgian shales) deposited in the western Viking Graben and 1,000 metres deposited in the Central Graben (Fig. 3.3). During deposition of the early Late Jurassic to earliest Cretaceous shales, coarse sandstones and conglomerates were generated by uplift and erosion of various structural blocks; these locally-derived coarse clastic sediments interfingered with the fine-grained, organic-rich shales of the Kimmeridge Clay (Cornford, 1998). Extensional tectonic shaped complex sets of half-graben, symmetrically oriented with respect to the basin axis such as the Viking Graben and the Moray Firth / Witch Ground Graben (Glennie and Underhill, 1998). Crustal doming started in the late Toarcian; emergence in the Bajocian was associated with a phase of intensive volcanism in the Bathonian/Callovian (encountered on the Rattray High, a local horst in the south Witch Ground Graben) (Erratt et al., 1999).

3.2.3 Post-rifting phase (Cretaceous)

The rifting phase in the North Sea ended in the Early Cretaceous time (Ziegler, 1990) with a gradual cooling and associated subsidence, especially where the thickness of post-rift sediments was greatest. Resulting from uplift of intra-basinal highs such as the Fladen Ground Spur, Halibut Horst and Forties-Montrose High coarse clastic sediment was dispersed through the Moray Firth/Witch Ground area; these sediments formed the reservoirs of fields such as Britannia, Captain, Scapa and North Claymore (Cornford, 1998, Garrett et al. 2000). Fine-grained pelagic carbonate (chalks) rocks dominate the Late Cretaceous to earliest Paleocene post-rift phase (Fig. 3.3). The topography was controlled by Cretaceous sedimentation together with ongoing regional subsidence during the early Tertiary, as the steep thermal gradient of the rift diminished; in the Viking Graben sediments reached 3000 m thickness, mainly composed of marine mudstone with submarine fans locally (Coward 1990) (Fig. 3.4).

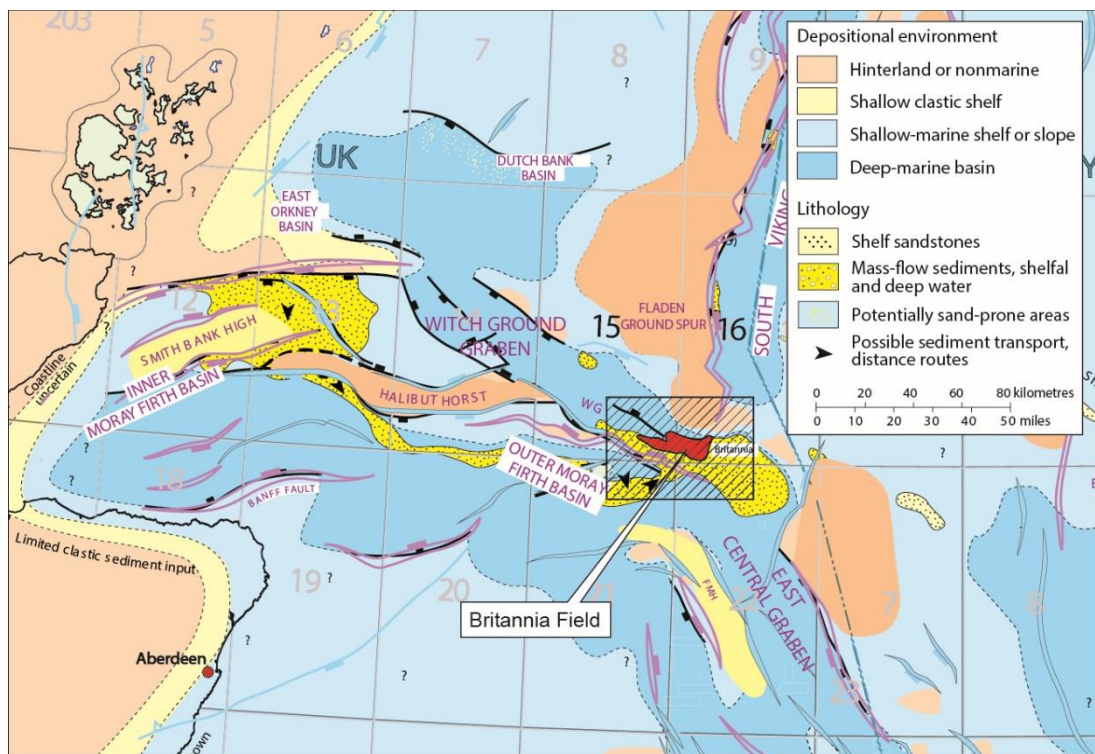


Fig. 3.4 – Regional palaeo-geography of the Aptian, Lower Cretaceous with sand fairway stretching from the Inner Moray Firth to the Outer Moray Firth, Central North Sea Triple Junction. Britannia Field is outlined by red area (from Copestake et al., 2003). Box with striped fill highlights area shown by Fig. 3.6.

The Lower Cretaceous sand fairway in the Moray Firth extends from the present day Scottish Coast eastwards and follows the southern margin of the Halibut Horst and the Renee Ridge highs. Jeremiah (2000) provided a sequence stratigraphic framework for the deep-water deposits of the Lower Cretaceous Moray Firth Basin,

placing the deposition of the sandstones in the Britannia area in his sequences K60-K80 (=K40; K45; K50 *sensu* Coperstake et al., 2003), with the main phase of activity in sequence K80, concurrent with the main phase of activity in the proximal Captain trend and the deposition of the Captain Sandstone Member (Fig. 3.5). The Britannia Sandstone Fm. is one of the principal sandstones of the Lower Cretaceous Cromer Knoll Group of the UK Central North Sea, and it is part of the Aptian-Albian play (Fig. 3.4 - Johnson and Lott, 1993; Coperstake et al., 2003; Milton-Worsell et al., 2006). The stratigraphy and the depositional model for the BSF are discussed in detail in Section 3.3, however, a brief description of the stratigraphic intervals from the Base Cretaceous to the Tertiary (Fig. 3.5) is presented below.

The Base Cretaceous Unconformity (BCU) in the Central North Sea is commonly taken as a major seismic reflector corresponding to top Humber Group / Kimmeridge Clay Formation within the UK sector (Coperstake et al., 2003; Erratt et al., 1999). This is an important horizon for defining the geometry of the fault array in the Witch Ground Graben/South Viking Graben. The seismic boundary represents a dramatic change in the regional tectonic style from transtension, which was dominant in the Jurassic to early Cretaceous transpression (Oakman and Partington, 1998; Oakman, 2005). Depth-converted seismic maps of the BCU are used to constrain the structural evolution during the Lower Cretaceous interval below the BSF and the effect of the post-rifting phase on the structural setting underneath the Britannia Field defining the geometry of the fault array in the Outer Moray Firth. Stratigraphically and sedimentologically this surface is the interface between high gamma, laminated organic mudstones of the Kimmeridge Clay and basal marls of the Valhalla Formation (Jeremiah, 2000). In the study area the thick interval between the BCU and the base of BSF is dominated by calcareous claystones, marls and limestones, and characterised by the absence of turbidite deposition that is instead recorded in other areas (e.g., North Halibut Basin). The passage to the base of BSF is marked by the presence of two distinct greyish black laminated organic-rich shales, the second of which representing the Fischechiefer bed (see Fig. 3.5). The BSF is described in Section 3.3 below, but in summary comprises a series of coarse clastic gravity flow deposits (turbidites and hybrid event beds) intercalated with mass transport deposits (MTDs).

The stratigraphy above the BSF comprises the shale-rich Middle Cretaceous Upper Cromer Knoll Group, which lies immediately on top of it, the Middle Cretaceous-Middle Palaeocene Chalk Group and a series of Tertiary shale- and sand-rich Groups of Tertiary age (Fig. 3.5).

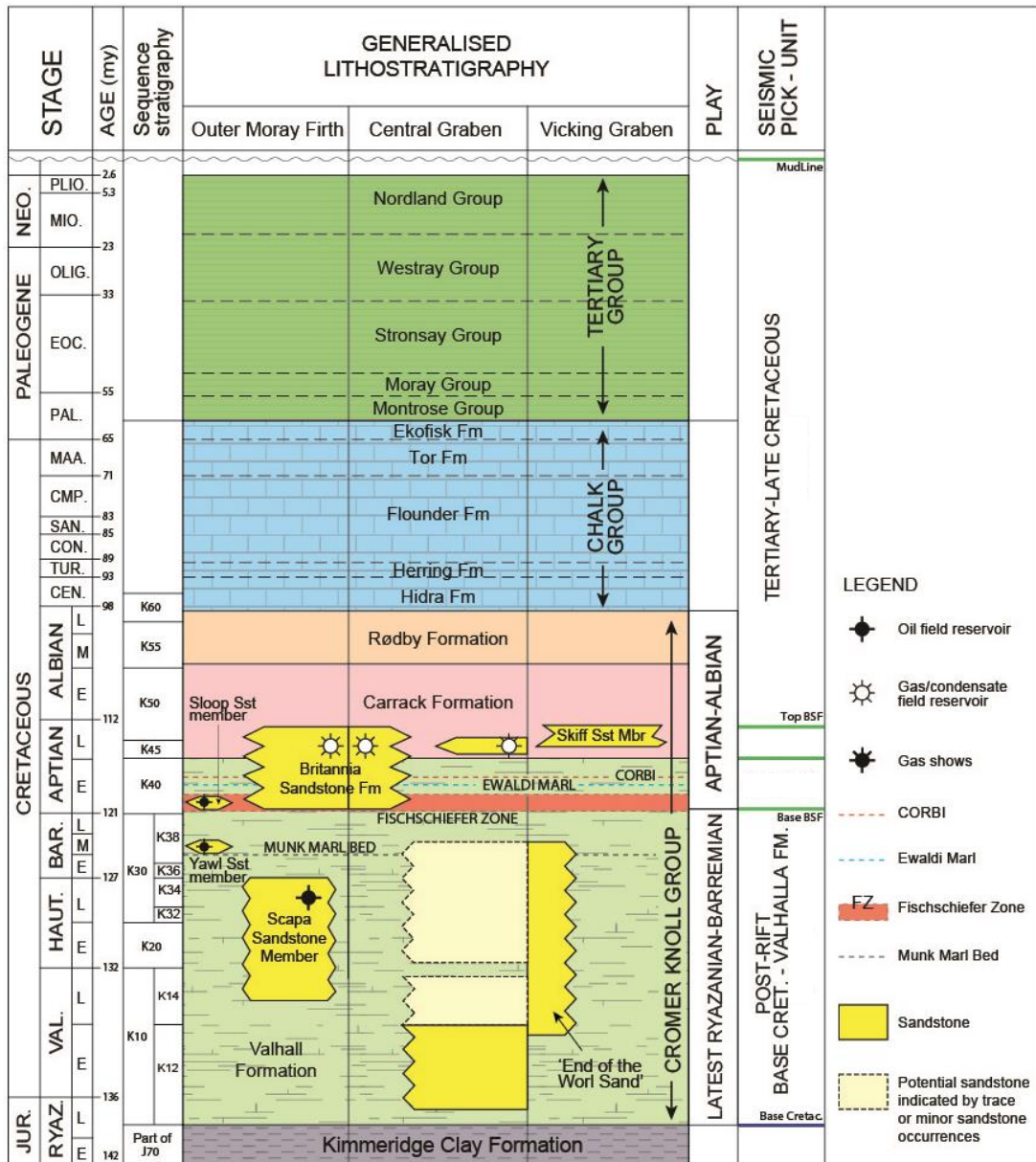


Fig. 3.5 – Stratigraphic summary chart of the UK Central North Sea in the Outer Moray Firth, Viking Graben and Central Graben (modified after Coperstake et al., 2003; Milton-Worsell et al., 2006). Britannia Sandstone depositional fairway was recognised in both Outer Moray Firth (mainly in the Witch Ground Graben) and in the Central Graben (as in the Fisher Bank Basin) (Coperstake et al., 2003). In the right column the main seismic pick units are shown within the post-rift Central North Sea stratigraphy.

3.3 Britannia Sandstone Formation

BSF consists of a series of turbiditic sand bodies set within shale-rich units, which can be correlated over wide areas of the Witch Ground Graben and surrounding basins (Law et al., 2000). Considerable variations exist in the sedimentary architecture across the formation, where the distribution of these deposits and hence the emplacement by different flow types (turbidity current versus slurry flow versus debris flow etc.) is still a matter of debate (e.g., Jones et al., 1999a).

The Britannia Sandstone Formation (BSF) has been extensively studied after the discovery of the Britannia Field in 1975 (Guy, 1992), a gas/condensate field located 225 km north/west of Aberdeen (Fig. 3.4) in the UK offshore. It is one of the largest hydrocarbon discoveries in the Lower Cretaceous sediments of the North Sea. Seismic imagery shows that the reservoir is a combination of 3-way dep closure and stratigraphic pinch-out trap (Fig. 3.10). Onlap of reservoir sandstones onto the Fladen Ground Spur provides closure to the north and structural closure characterises the southern trap. Closures to the east and west are not still firmly defined, however a hydrodynamic gradient seems to influence the dip of the hydrocarbon-water contact and hence the overall trapping geometry (Coperstake et al., 2003; Machell, 2003).

The BSF is characterised by a wide depositional fairway (Fig. 3.6), albeit segmented due to the structural features developed in the Outer Moray Firth – Witch Ground Graben during the rifting phase of the North Sea. However, the regional pathways of the flows that deposited the sandstones at the location of the Britannia field are disputed. Thus, it is not certain if and if so, to what extent the Britannia sands are sourced through the Captain fairway of the Moray Firth. Coperstake et al. (2003) were the first to indicate that the Britannia sands may form the distal end of this trend. Regardless, the Halibut Horst and Renee Ridge seem to have had a significant influence on the distribution of the BSF. These structural features partially confined sands within the Witch Ground Graben. However Britannia sands are also found on the south of these horsts (Machell, 2003; Aas et al., 2010). Hailwood and Ding (2000) suggest a further north-western point source of sediment coming off the Fladen Ground Spur, based on AMS grain fabric analysis. They consider a topographic high was located in the northern Britannia basin, representing the southern elongation of the Fladen Ground Spur, which separates the Witch Ground Graben on the east from the South Viking Graben on the west. The regional slope can be inferred from seismic data and rises to the N-NW in the area north of the Britannia Field. However the length scale and steepness of the Fladen Ground Spur is not known. Its structural presence since the pre-rifting phase is confirmed by Erratt, 1993 (Fig. 3.2).

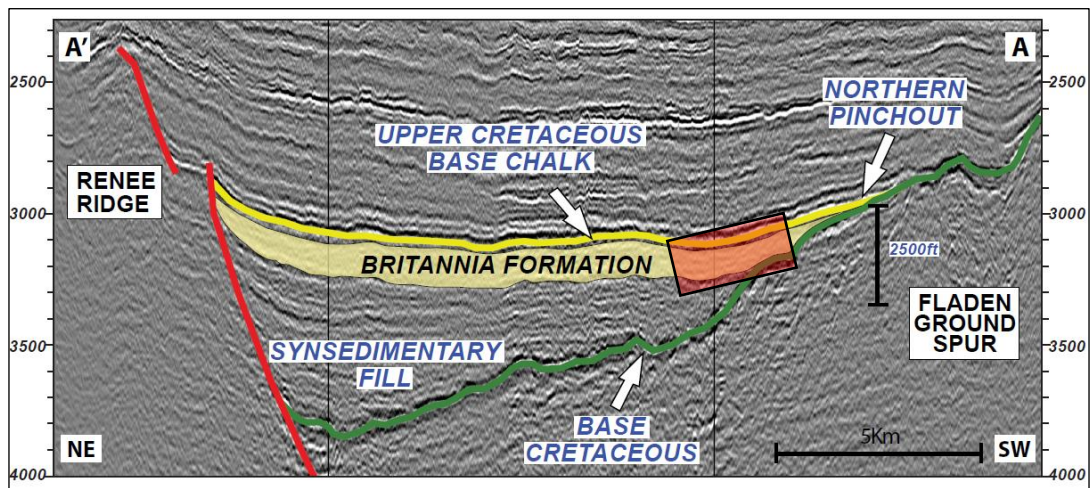
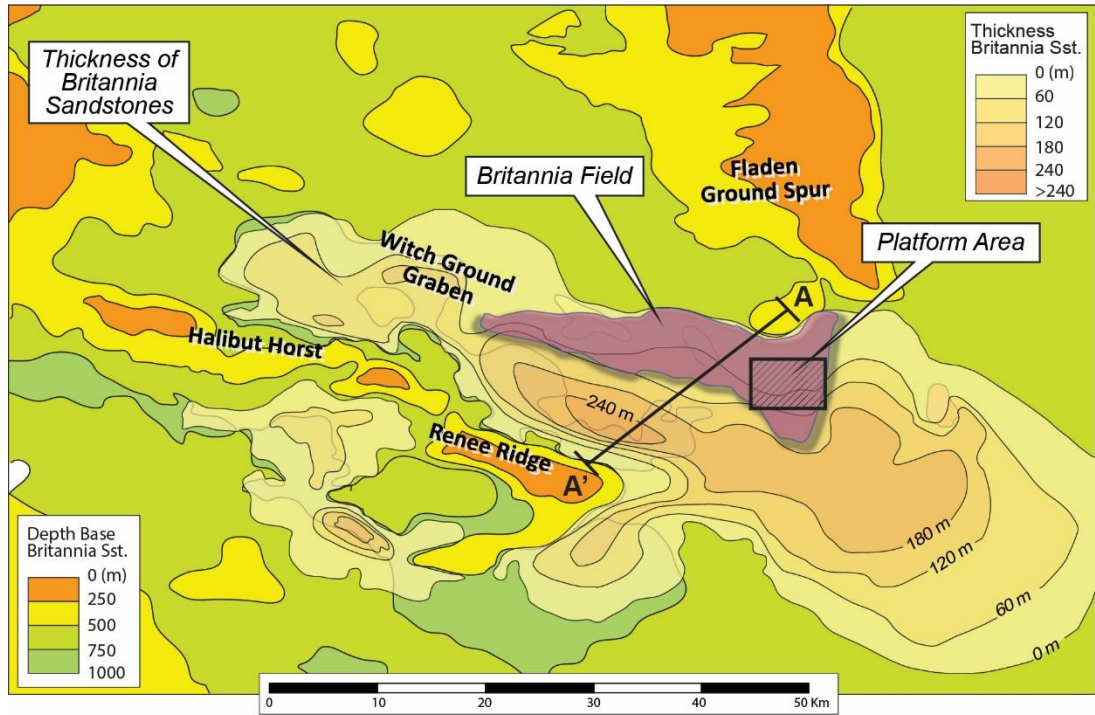


Fig. 3.6 – Principal structural features around the Britannia Field (for location see Fig. 3.4). Two sets of contour lines are shown: 1) the thickness distribution of the BSF (light orange) (modified after Machell A., 2003; Copestake et al., 2003) and 2) the present depth to the base of the formation. Seismic profile A-A' that shows the stratigraphic closure on the flank of the Fladen Ground Spur (north) and structural confinement due to the Renee Ridge (south) of the Britannia Sandstone Fm. The box on the seismic image shows the Platform Area.

The Britannia Field can be separated into two structural domains (Fig. 3.7), which are characterised by distinctive structural patterns: the western “subsea centre” and the eastern “Platform Area” (the focus of this study).

The development of the reservoir structure in western (subsea) Britannia area appears to be related to the topography of the basin during reservoir deposition. A steep slope to the south-southwest (off the axial high) led to the development of predominantly southwards throwing, west-northwest to east-southeast - trending faults, which reflect the general orientation of the Witch Ground Graben (Porter et al., 2000). The faults identified in this area were identified to be prone to detachment near the base of the reservoir, with rare linkage to deeper basement faults where the Valhall Formation is very thin (Porter et al., 2000; Hill and Palfrey, 2003). Seismically-resolvable thin detachment systems were identified to the south of faults mapped at top Britannia level with little evidence for significant inversion in the western part of the Britannia Field (Hill and Palfrey, 2003).

The eastern (Platform Area) part of Britannia Field is the most structurally complex, with numerous intersecting structural trends and a relatively high density of faults (Fig. 3.7). The Fladen Ground Spur promontory represents the principal structural feature in this part of the field. The main fault trends present in Block 16/26 (western part of the Platform Area) are east–west (Witch Ground Graben), northwest–southeast (Tornquist) and approximately north–south (Viking Graben) (Porter et al., 2000). Porter et al. (2000) identified a series of faults that downthrow the reservoir to the southwest off the flanks of the Fladen Ground Spur (Fig. 3.7). Most of the faults in Block 16/27 (eastern part of the Platform Area) are linked and form segments up to several kilometres long that tend to lie sub-parallel to the flanks of the Fladen Ground Spur. The reservoir is cut by a number of relatively steep, predominantly basement-linked faults, with a few faults detaching within the reservoir interval (Porter et al., 2000). Inversion-related deformation within this eastern area, associated with north–south (Viking Graben) trending structures was also recognised. This is thought to have developed during the Eocene and appears to be associated with oblique or strike-slip reactivation of basement structures (Porter et al., 2000).

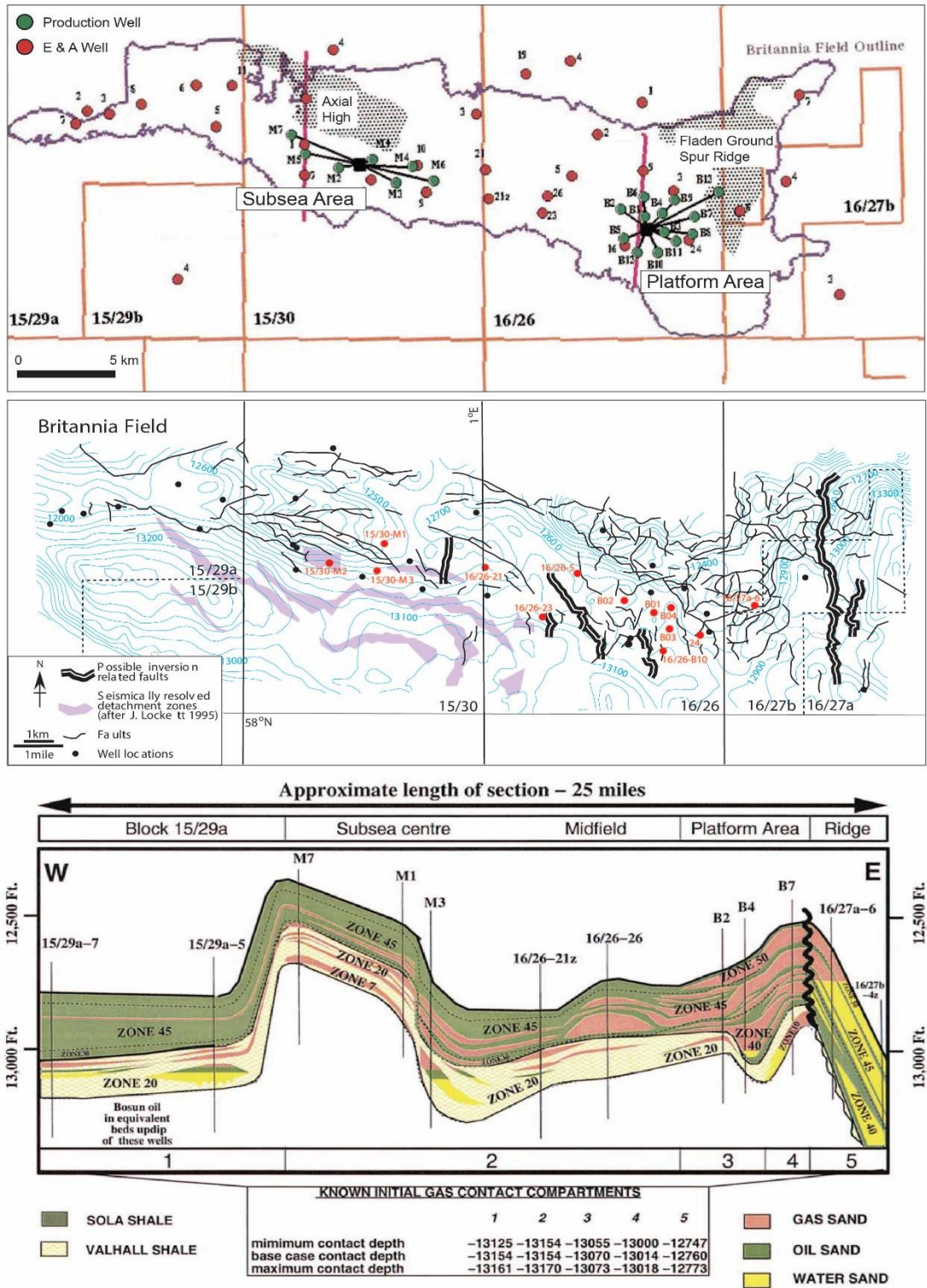


Fig. 3.7 – Series of maps and cross-section of the Britannia Field. On top: Britannia Field outline and well database (from Hill and Palfrey, 2003). In the middle: top Britannia reservoir depth structure map, which shows the difference in the seismically resolved fault patterns identified within the western (Subsea Area) and the eastern (Platform Area) parts of the field. At the bottom: reservoir cross-section and hydrocarbon contact variations of the Britannia Field (from Hill and Palfrey, 2003). The principal gas-bearing reservoir sands vary from west to east across the field in association with vertical and lateral facies heterogeneity. Some reservoir development is restricted, for instance Zone 7 in the Subsea Area and Zone 10 in the Platform Area. Zone 30 shales are developed in the west but are absent east of the Midfield Area.

3.3.1 Key stratigraphic intervals

The Britannia Sandstone Formation is divided into 7 principal Reservoir Zones (informally labelled 7, 10, 20, 30, 40, 45, 50 from base to top shown in Fig. 3.8 and Table 3.1) based primarily on biostratigraphic zonation in the Valhall Fm. and on more limited biostratigraphy coupled with lithostratigraphy in the Sola Fm. (Jones et al., 1999a; Ainsworth et al., 2000).

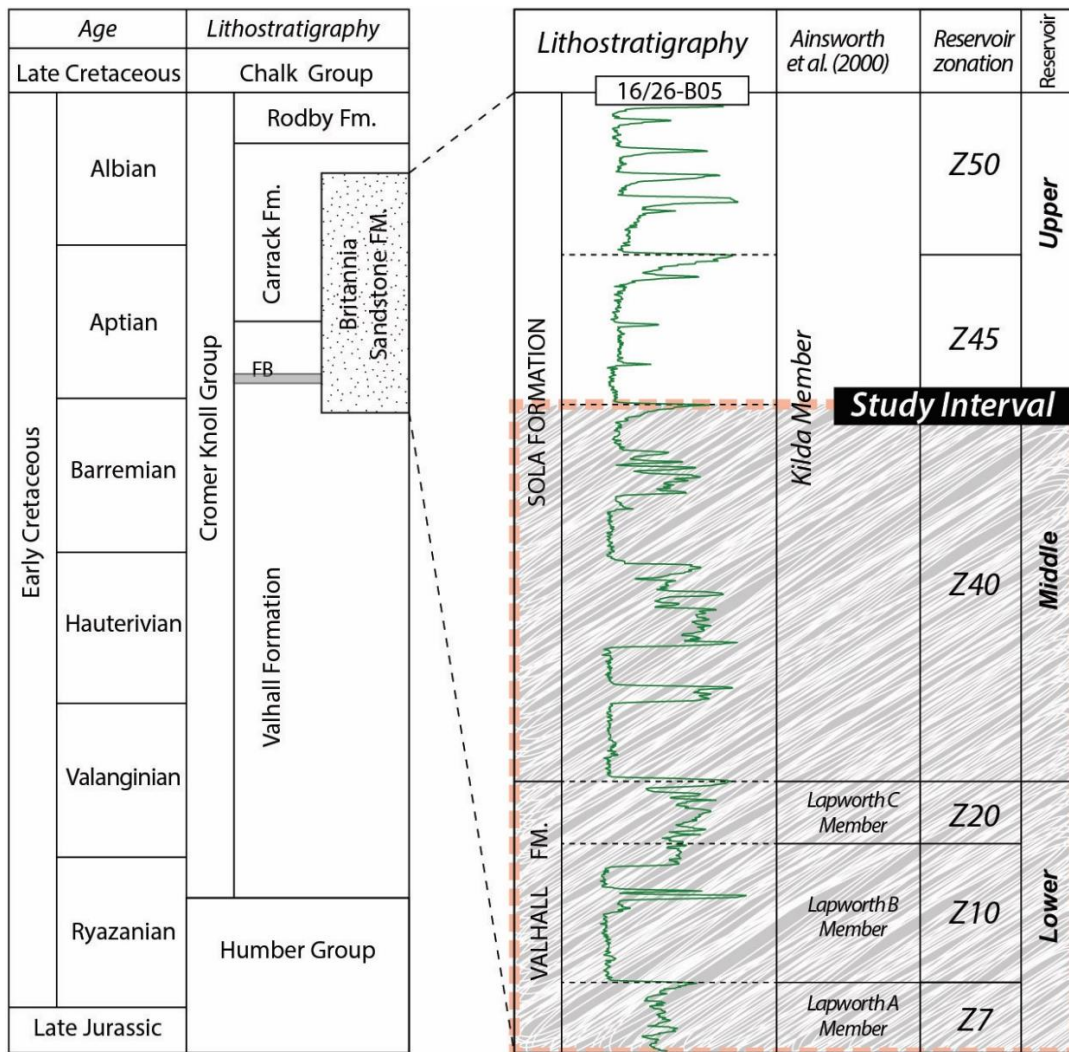


Fig. 3.8 – On the right the Britannia informal stratigraphic nomenclature and zonal calibration based on well 16/26-21 (modified after Jones et al., 1999a and Porter et al., 2000). On the left stratigraphic framework of the Britannia Sandstone Fm. within the Early Cretaceous Cromer Knoll Group (modified after Eggenhuisen et al., 2010).

Reservoir Zones are differently distributed in different parts of the Britannia Field: in the Subsea area the thicker sands are attributed the lower reservoir Zones (Z7, Z10 and Z20), whilst in the Platform Area the main reservoir sands are attributed to the middle (Z40) and upper (Z45 and Z50) Zones (Fig. 3.7). Zone 30 shales are developed in the west but are absent east of the Midfield Area (Fig. 3.7). In the

Platform Area the lower and middle Zones (Z7-Z40) tend to be geometrically complex and difficult to correlate (Eggenhuisen et al., 2010), whereas the upper units (Z45, Z50) have a more tabular geometry (Barker et al., 2008).

The reservoir zonation used to subdivide sandstone intervals in the Britannia reservoir represented in Figure 3.8 is used to indicate particular sandstone intervals in the remainder of this chapter. The lowest marker used for stratigraphic correlation purpose is the Munk Marl in the Valhalla Fm. (Ainsworth et al., 2000), which predates deposition of all sand in the Britannia area (Eggenhuisen et al., 2010). This unit has been described in onshore Germany and it is encountered across the North Sea subsurface (Ainsworth et al., 2000). Eggenhuisen et al. (2010) recognised the Munk Marl in the east of the Platform Area. The Fischeschiefer bed, which is recognised regionally in the northern North Sea and onshore Germany (Oakman and Partington, 1998; Ainsworth et al., 2000) is characterised by the common occurrence of phosphatic fish debris, an absence of bioturbation and by its dark colouration (Ainsworth et al., 2000). The Fischeschiefer bed is located in the lower part of Zone 10. Rather than being a timeline, the Fischeschiefer is a zone (Jeremiah, 2000). Thus, some Z10 sands are intra-Fischeschiefer, with Fischeschiefer occurring both above and below sandstone beds (Ainsworth et al., 2000, Garrett et al., 2000; Fig. 3.8 and Table 3.1). The Ewaldi Marl is another lithological unit that is recognised across the North Sea region and is used to delineate the top of reservoir Zone 10 (Hill and Palfrey, 2003; Sumner et al., 2005). Some prominent red shales are recognised in the outer Moray Firth (Jeremiah, 2000; Sumner et al., 2005). Eggenhuisen et al. (2010) proposed that the upper transition from reddish shales to greyish shales can be used as the boundary between the Valhall Formation and the Carrick Formation in the Britannia Field (Sumner et al., 2005). In the local zonal stratigraphic nomenclature this boundary represents the Z20-Z40 boundary that divides the Lower and Middle BSF. A prominent ash band occurs near the top of the BSF just above the top of the Z50 sand. This “Z50 ash” provides a robust correlation horizon due to its characteristic gamma-ray signature (Barker et al., 2008).

Eggenhuisen (2009) reviewed the zonation of the lower BSF in the Platform Area, based on the recognition of shale facies associated at different stratigraphic levels and with different interbedded sandstone intervals, which constitute a background sequence that is firmly tied to the stratigraphic framework. This enabled the correlation of a prominent sandstone interval and the recognition of two separate remobilisation phases. Accordingly, Eggenhuisen (2009) split the Z10 into two sub-members, Z10A and Z10B. Zone 10A is deposited within the Fischeschiefer Zone (Jeremiah, 2000; Eggenhuisen et al., 2010) whereas Z10B is deposited on top of

this anoxic mudstone interval. Following Ainsworth et al. (2000), Eggenhuisen et al. (2010) reinterpret Z30 as being a fully remobilised interval following a large-scale slope failure. For this reason in the Platform Area this interval is not present and it was not included in Table 3.1 (see Eggenhuisen et al., 2010).

Age	Formation	Reservoir	Zone	Lithological marker
Late Aptian	Lower Sola - Britannia Sandstone Fm.	Upper Reservoir	Zone 50	Top marked by an ash band (regional isochronous datum <i>sensu</i> Ainsworth 2000)
			Zone 45	Top marked by an ash horizon (Marker bed east <i>sensu</i> Ainsworth 2000)
		Middle Reservoir	Zone 40	Bed 58 (tabular bed)
Early Aptian-Late Barremian	Valhalla - Britannia Sandstone Fm.	Lower Reservoir	Zone 20	Top marked by the Reddish mudstone CORB (<i>sensu</i> Ainsworth 2000; Eggenhuisen 2010)
			Zone 10B	Top marked by the Ewaldi Marl (<i>sensu</i> Ainsworth 2000; Eggenhuisen 2010)
			Zone 10A	Encased by the Fischeschiefer Zone (<i>sensu</i> Ainsworth 2000; Eggenhuisen 2010)
			Zone 7	Encased by the Valhalla Shales (<i>sensu</i> Ainsworth 2000)

Table 3.1 – Summary of the revised Britannia reservoir zonation (after Eggenhuisen et al., 2010 and Ainsworth, 2000).

3.3.2 Sediment source and fairways

Sandy gravity flows that built the BSF reached the areas south of the Fladen Ground Spur during the Early Aptian (~120 Ma). The introduction of sandstones into the basin is widely interpreted as resulting from a series of tectonoeustatic events coupled with the reactivation of intrabasinal structures that led to a reconfiguration of the linkages between basins (Crittenden et al., 1997; Oakman and Partington, 1998; Jeremiah, 2000). The most pronounced influence of these events seems to be in the Outer Moray Firth Basin (Fig. 3.6). The East Shetland Platform clastic-sediment supply areas, active throughout the Early Cretaceous, appear to have been supplemented by additional source sand across the Fladen Ground Spur and, possibly, from Middle Jurassic volcanic-cored intrabasinal highs to the south (Fig. 2.8) (Bisewski, 1990; Guy 1992; Jones et al., 1999; Ainsworth et al. 2000; Blackbourn and Thomson, 2000; Hailwood and Ding, 2000, Copestake et al., 2003).

The increased gradients caused by these tectonic events are inferred to have caused slope failures (Porter et al., 2000). This is recorded by mass-wasting deposits in the

Britannia succession, as demonstrated by cores from the Britannia Field (Porter et al., 2000; Barker, 2005; Eggenhuisen, 2009). Blackburn and Thomson (2000) interpreted the mud fraction of the debris flows and the fine-grained components incorporated in the sandstone beds in the Britannia sequence as not derived from the same source. The mudstone analysis carried out by Blackburn and Thomson (2000), together with the model proposed by Eggenhuisen et al. (2010) suggest a northern provenance for the debris flows (Fig. 3.6). The sandy gravity flows show instead various palaeoflow directions, and hence, inferred source areas, ranging from north, from south and from west (Hailwood and Ding, 2000; Lowe and Guy, 2000; Barker, 2005; Moore et al., 2009 – see below and section 6.3.4 for detailed review). Thus, although the processes and *loci* of the mass failure events has been relatively well constrained, sand provenance is still a contentious topic (Blackburn and Thomson, 2000).

Inferring palaeoflow within the BSF has been problematical because of the rarity of primary traction-deposited sedimentary structures and erosional bed base features (Lowe and Guy, 2003). For the Lower and Middle sandstones, a westerly provenance was suggested by Moore et al. (2009), based on facies distribution trends; they proposed a prograding fan interpretation for Zones 10, 20, 30 and 40 (see section 6.3.4).

Within the upper reservoir sands (Zones 45 and 50) anisotropy of magnetic susceptibility (AMS) techniques were used to measure preferred grain alignment and infer sediment transport directions (Hailwood and Ding, 2000). A NW to SE trend was detected in the eastern part of the field, consistent with a Fladen Ground Spur source. Spatial grain size fining trends mapped by Lowe et al. (2003) were interpreted to be a proxy for palaeoflow direction, suggesting a N to S trend within Z50 (following a reversal from a S to N trend in the underlying Z45). However, textural analysis by Barker (2005) based on revised correlations of the Upper BSF did not detect a systematic change in grain size suggesting the method cannot be used as a palaeoflow indicator in the study area. Instead Barker (2005) inferred an W-E transport direction along the inferred basin axis, based on locations of maximum amalgamation and consistent on- to off-axis trends in deposit character (see also del Pino Sanchez, 2006).

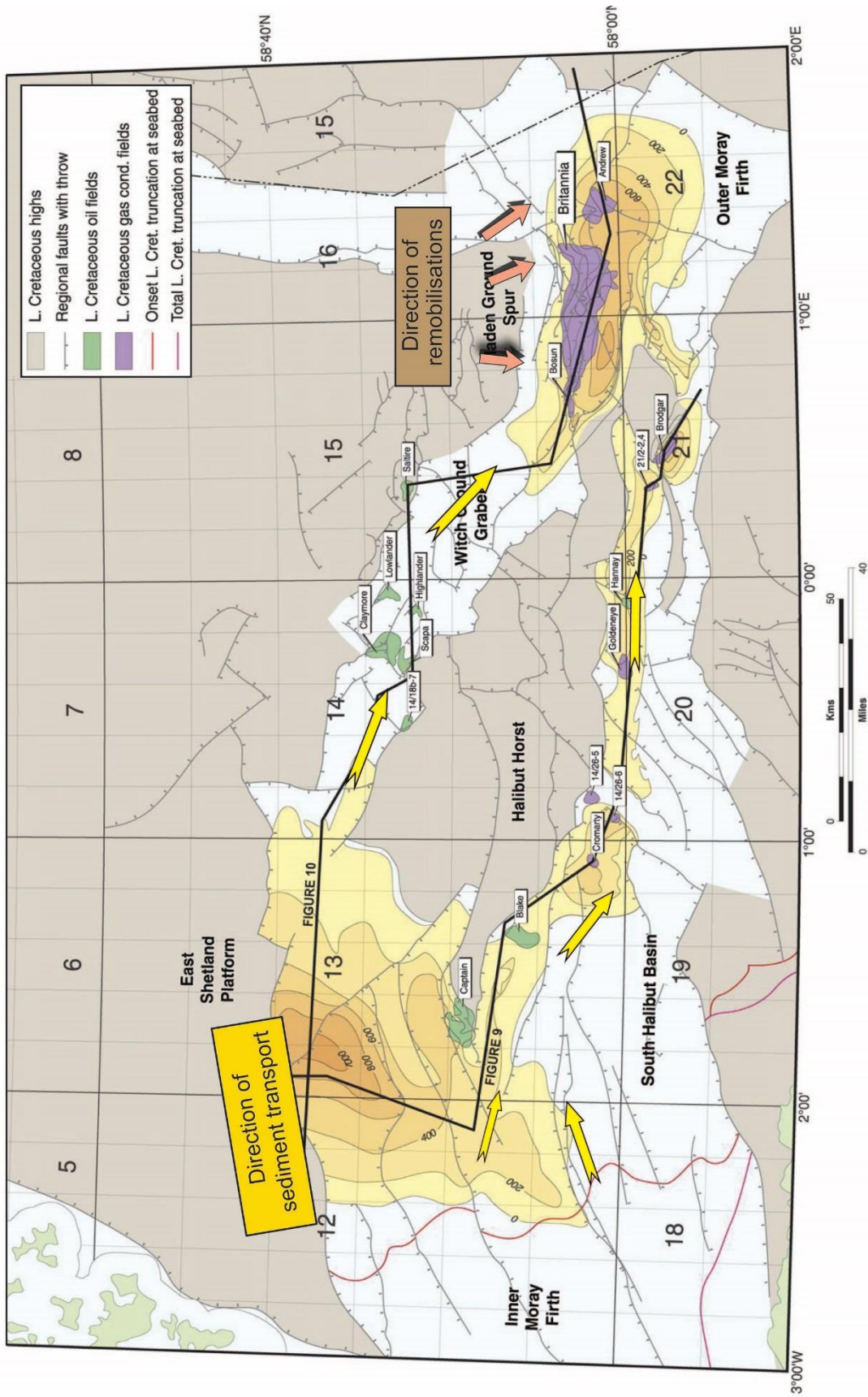


Fig. 3.9 – Provenance and direction of turbidity currents and debris flows (modified after Machell A., 2003).

3.3.3 Inherited facies scheme

A number of studies have focussed on the different deposits characterising the BSF, with particular focus on the wide range of sandstones recognised in cored wells of the Britannia Field. Several facies schemes have been proposed by different authors through time: Guy (1992), Lowe and Guy (2000), Barker et al., (2008) and Eggenhuisen et al., (2010). A summary of these is proposed in the table 3.2 below for guidance only (note: a comprehensive one-to-one facies correspondence is not implied).

Guy (2000) firstly developed a facies description for the Kopervick sand (later named Valhall and Sola Fm. - Table 3.1) where he identified six facies associated to various sediment gravity flows. Observations from core were integrated with gamma-ray and density/neutron logs. His facies scheme was clearly conditioned by the then limited number of cored wells (i.e., the muddier banded facies characteristic of many later Britannia field wells were not abundant). This scheme is mainly based on classic turbidite classifications (Bouma, 1962 and Lowe, 1982).

A significant evolution of the facies scheme for BSF was proposed by Lowe and Guy (2000), where the authors introduced 7 sedimentary structure division types (M1, M2, M3, M4, M5, M6, M7) to describe “slurry beds”, and debrite/mudstone (IMF). The suggested facies order aims to describe a recurrent motif observed in slurry beds on core, where intervals characterised by the presence of dewatering structures are part of these stacking pattern of facies. Lowe and Guy (2000) developed their facies scheme from the large amount of core data available by then; later they integrated additional data and interpretations (Lowe et al. 2003).

Barker et al. (2008) focused their attention in the Upper Reservoir Section where they present an updated correlative framework and a revised facies for this interval. They provided a further subdivision for M2 (banded division - *sensu* Lowe and Guy, 2000) and introduced the term “mixed slurried” for sheared internal fabric of contorted and folded sandy structures set in a dark, heterolithic sand, silt and mud matrix with various degrees of mixing, which substituted for the “mixed sandstone/mudstone” of Lowe and Guy, 2000. In addition, Barker et al. (2008) introduced the “heterolithic breccia” facies to describe a chaotic mixture of sandstone injections, deformed mudclasts and sandstone blocks, and the “green sandstones and siltstones” facies that comprises extra-formational lithologies of mudstones, shell fragments and glauconite clasts. Well mixed matrix of sand grains together with mudstone clasts and blocks set in mud matrix (debrites) takes the informal name of “starry night”. A further substantial change in the work of Barker et al. (2008) was the attempt to avoid

using dewatering structures (e.g., pipes, sheets, dishes and consolidation lamination) as primary descriptors of core facies.

The most facies scheme was proposed by Eggenhuisen et al. (2010) in a study that investigated the cored intervals of the Lower Reservoir Section in the Platform Area. The restructuring of the facies classification consisted of grouping the mixed slurried, heterolithic breccia and extra formational sand and mudclasts (Barker et al., 2008) into “sheared dewatering” facies and including the remaining sandstones with dewatering structures into a “dewatered sandstones” class. Also, they consider “sandstone injectite” as standalone facies. A significant novelty was the recognition of four types of mudstone, three of which represent stratigraphic markers, which can be used to aid well correlation in the Lower Reservoir Section.

Guy (1992)			Lowe and Guy (2000)			Barker et al. (2008)			Eggenhuisen et al. (2010)		
Name	Code	Description	Name	Code	Description	Name	Code	Description	Facies	Code	Description
High-density turbidite	HDT	Sandstones relatively free of detrital clay, moderately sorted. It occurs as thick stacked units where individual bed contacts are difficult to see. The most obvious and characteristic feature is the pervasive syn-depositional water escape dish and pillar structures.	Traction-structured and massive	M1	Current structured (large-scale cross-stratification, sweeping low-angle cross-stratification and flat lamination) and/or massive sandstones. These divisions lack water-escape structures and soft-sediment foundering features.	Massive	Ma	Clean, poorly-sorted sandstones, no primary structures; may be overprinted by dewatering fabrics.	Massive sandstone	Sma	Massive, clean, fine to medium grained sandstone. Usually structureless apart from occasional very indistinct cm-thick spaced laminations.
						Granule-rich	Gra	Coarse outsize quartz grains set in fine- to medium-grained sand matrix; mud rip-up clasts occasionally present; rare subtle lamination; basal 1-2 cm commonly inversely graded.	Granule-containing sandstone	Sgr	Granule-rich, clean, fine to medium grained sandstones. The host sandstone is usually massive-structureless but occasionally with some dewatering structures.
									Dewatered sandstone	Sdew	Clean fine to medium grained sandstones with abundant dewatering fabrics: straight horizontal consolidation laminations; dish structures and ruptured consolidation laminations.
Marginal sand		Stacked units of argillaceous and arenaceous couplets which range from centimetre- to decimetre-scale. Each couplet is normally graded and upward-cleaning profile, with the upper and lower contacts often stylolitized.	Banded	M2	Sandstones with cyclic, alternating light and dark bands or laminations. Individual dark-light band couplets range from a few millimetres to >50 cm in thickness. Three types of banded divisions are distinguished based on couplets thickness: M2a (mixed slurred and megabanded divisions)	Banded	Ba	Alternation between light and dark horizons. Dark bands form basal division of each light-dark couplet, display sharp bases and an intensely sheared fabric; light bands are lithologically cleaner, load into top of dark bands. Banding developed on a range of scales: macro, meso, and micro-banding.	Banded sandstone	Sba	Fine to very fine sandstones with couplets of intermediate dark grey and light yellowish brown bands. Dark divisions have a sheared fabric containing strung-out and folded lighter dewatering structures and lighter sheared sand globules. The light divisions are often faintly laminated, with laminations in the lower part of the division

Table 3.2 – Table showing a summary of the facies schemes proposed by different authors for the BSF. Guy (1992) firstly introduced a basic facies scheme to describe core facies from the early exploration phase of the Britannia Field. Lowe and Guy (2000) developed a facies scheme with the intent to better describe “slurry beds”. Barker et al., (2008) and Eggenhuisen et al., (2010) proposed new core facies schemes for the Upper and Lower BSF in the Platform Area, respectively. The comparison is acknowledges that there is not necessarily a comprehensive one-to-one correspondence between like facies (continued in the next page).

Guy (1992)			Lowe and Guy (2000)			Barker et al. (2008)			Eggenhuisen et al. (2010)		
Name	Code	Description	Name	Code	Description	Name	Code	Description	Facies	Code	Description
					band couplets that exceed 50 cm in thickness are termed megabanded divisions, where bands are present, and mixed slurried divisions, where they are composed exclusively of dark-band sediment; M2b (macrobanded) band couplets 10-50 cm thick; and M2c (mesobanded) couplets 1-10 cm thick.	Pseudo-banded	Ps	Low angle dish or consolidation-lamination, dewatering structures forming dark bands that alternate with light bands. Dark bands comprise clean, sandy matrix with dewatering structures; light bands comprise clean sandstone, massive fabric with no dewatering features.			affected by the loading into the underlying dark division. Banding occurs on a range of scales from micro-banding to mega-banding.
Laminated sand		Parallel laminated light-buff grey to light grey (due to an increase of detrital clay content) sandstones, often flecked by dewatering pillars. Typically they are fine grained and moderately to poorly sorted.	Wispy laminated	M3	Discontinuous, commonly crenulated layers and laminations. Dark, mud-rich zones from less than 1 mm to about 1 cm thick that commonly contain fine, sharp, anastomosing microstylolites are present. They are separated by thin layers and lenses of lighter coloured sandstone. Distinctive water-escape structures are recognised.	Wispy laminated	Wis	Thin, dark, discontinuous laminations of heterolitic sandstones within cleaner sandstone matrix. Typically pervasively dewatered.	Laminated sandstone	Sl _a	Finely laminated very fine sandstones and siltstones. Lamination is distinct due to the alterations between clean sandstone laminae with dark grey to black siltstone and mudstone laminations. Sand laminae are commonly associated with an erosive base cutting into underlying mudstone facies (M) or underlying Sl _a laminae.
Low-density turbidite	LDT	Flat parallel laminated fine- to very fine-grained sands to muds, occasionally starved ripples are observed. Bases of the units are sharp while the tops grade into hemipelagic shale.	Dish-structured	M4	Dewatering dish structures with sharp to wispy and nearly flat to strongly concave upwards.						
			Microbanded and flat-laminated	M5	Fine, even, cyclic microbands and flat laminations. They lie at the tops of thick slurry-flow beds and are rarely interstratified with divisions showing thicker band types.						

Table 3.3 – Continued.

Guy (1992)			Lowe and Guy (2000)			Barker et al. (2008)			Eggenhuisen et al. (2010)		
Name	Code	Description	Name	Code	Description	Name	Code	Description	Facies	Code	Description
Liquefied sand		Light grey, very argillaceous sand with a conspicuous lack of bedding contacts with random occurrence of clean, off-white streaks that are slumped, sheared or highly deformed.	Foundered and mixed sandstone/mudstone	M6	Contorted and deformed laminated sandstone, siltstone and mudstone.	Mixed slurried	MS	Pale-dark grey to brown in colour; highly sheared internal fabric of contorted, folded and sheared sandy structures set in a dark, heterolithic sand, silt and mud matrix which display various degrees of mixing.	Sheared dewatering	Ssd	Very fine to medium grained sandstone facies with a chaotic appearance of intermediate grey and light yellowish brown colours. Sheared darker parts contain sheared out lighter dewatering features and are occasionally cut by later generations of dewatering sheets.
	Masses of fine- to very fine-grained laminated sandstone sheared and mixed with dark-grey mudstone are foundered.				Heterolithic breccia			HB			
	Divisions structured by vertical water escape		M7	Sandstones dominated by vertical water-escape structures: well-developed vertical to steeply inclined dish structures and/or streaks, wisps and laminations.	Green sandstones and siltstones	Gre	Conglomeratic, sandstones and ash layers; pale green colour; clasts comprise extra-formational lithologies of pale mudrock, brown nodules, shell fragment, glauconite and shale clasts.				
									Sandstone injectite	Si	Very fine to medium sandstones in 1mm to 1.1 m thick intervals. Boundaries of the sandstone are often discordant with the bedding orientation of surrounding facies

Table 3.4 – Continued.

Guy (1992)			Lowe and Guy (2000)			Barker et al. (2008)			Eggenhuisen et al. (2010)		
Name	Code	Description	Name	Code	Description	Name	Code	Description	Facies	Code	Description
<i>Debrite</i>		Development of large clasts floating at any level, with a rudimentary shear and compaction-imposed lineation. Detrital sand grains can be seen floating in the abundant silty and muddy matrix which forms up to 40% of the rock.	<i>Interflow sedimentary layers</i>	IF		<i>Starry-night</i>	SN	Well-mixed matrix of rigid mineral grains set in mud matrix; mudstone clasts and blocks of various size set into matrix; clasts and blocks are generally aligned.	<i>Debrite matrix</i>	Dm	Dark grey mud and silt matrix containing floating very fine to medium sand grains. Light-coloured sand grains in the dark matrix give this facies an unmistakable "starry night" appearance. Occasional higher sand content, with sand apparently injected.
									<i>Debrite clast</i>	Dc	Clast thickness of unambiguously recognised clasts ranges from mm scale to 2.25 m. Small clasts that are less wide than core width are abundant and are surrounded by Dm.
			<i>Interflow sedimentary layers</i>	IMF	Variety of predominantly muddy layers that separate sandstones, including mudstones and claystones with highly carbonaceous claystones deposited under conditions of regional anoxia. Less carbonaceous and extremely cyclic interlayering of grey, brownish and greenish mudstones, showing fine bioturbation are recognised. Bright red oxidized claystone is also locally present.	<i>Shale</i>	Sh	Laminated clay; black to gray; common gray silty pseudonodules often present; occasional convolute near sand injections.	<i>Mudstone 1</i>	M1	Unbioturbated dark grey to black mudstone. Brown horizontally elongate nodules occur. Characteristic beige laminated bands form zones of 4-15 cm thickness.
		<i>Mudstone 2</i>							M2	Light grey to light green speckled mudstone. Lighter colours are cyclically alternated with darker divisions on 5-25 cm scale.	
		<i>Mudstone 3</i>							M3	Reddish speckled to completely red mudstone. Usually occurring in 10-30 cm thick bands. The background colour is intermediate dark grey where the shale is not red.	

Table 3.5 – Continued.

3.3.4 Platform Area correlations

The first published attempts to correlate the reservoir zones of the BSF in the Platform Area of the Britannia Field are by Guy (1992) and by G. Jones et al. (1999), who were followed by Lowe and Guy (2000) and by Lowe et al. (2003). More recently, Barker et al. (2008) and Eggenhuisen et al. (2010) revised the correlation framework for the Upper and Lower Reservoir Sections, respectively.

Original correlations were based on formal subdivision into seven chrono/lithostratigraphical zones. From oldest to youngest these includes: Zone 7, 10, 20, 30, 40 and 50 (Jones et al., 1999a). Zonal scheme were largely maintained during reservoir development however some changes were adopted across the three Britannia Reservoir Section.

Zone 50 in the Upper Reservoir Section (Sola Formation), firstly defined and correlated as a single zone, was subdivided in Zone 45 and 50 (Jones et al., 1999a), using sand lithostratigraphy, based on facies type, texture, log signature, and volcanic ash band markers. Subsequently these zones were revised by Lowe and Guy (2000) first, and Barker et al. (2008) secondly (see below).

If the Upper Reservoir shales are mostly turbiditic in origin and do not lend themselves to a reliable biostratigraphic correlation (Lowe and Guy, 2000), in the Lower Reservoir (Valhall Formation) a robust biostratigraphical scheme was established using palynology, micropalaeontology and calcareous nannoplankton from hemipelagic Valhall shales (Ainsworth et al., 2000). The boundary separating Zone 20 (Valhall Formation) from Zones 30 and 40 (Sola Formation) was defined by biostratigraphy and lithostratigraphy together and it represents a significant change in depositional style. However, some zones cannot be extended across the whole field as single chronostratigraphic events; for instance, Zone 30 is not defined in the east (see below), and Zone 40 is not defined in the west (Fig. 3.7). In the recent years, Barker (2005) erected a new correlation framework for the upper Britannia Sandstone Section in the Platform Area, which includes important revisions to previous and published correlation schemes (Lowe and Guy, 2000) with respect to the tracing of individual sandstone event beds, the total number of sandstone beds and the position of zonal boundaries at this level of the stratigraphy. The Upper Reservoir Section (thickness between 34 and 64 meters), made up of two sandy reservoir intervals (Z45 and Z50) separated by debritic deposits identified across the entire Platform Area (see Fig. 3.10), is bounded on top by the "Ash layer" and at the base by the "Boxcar Sandstone" package *sensu* Barker et al. (2008) (see Table 4.3. for explanation); the Boxcar Sandstone represents the boundary with the underneath

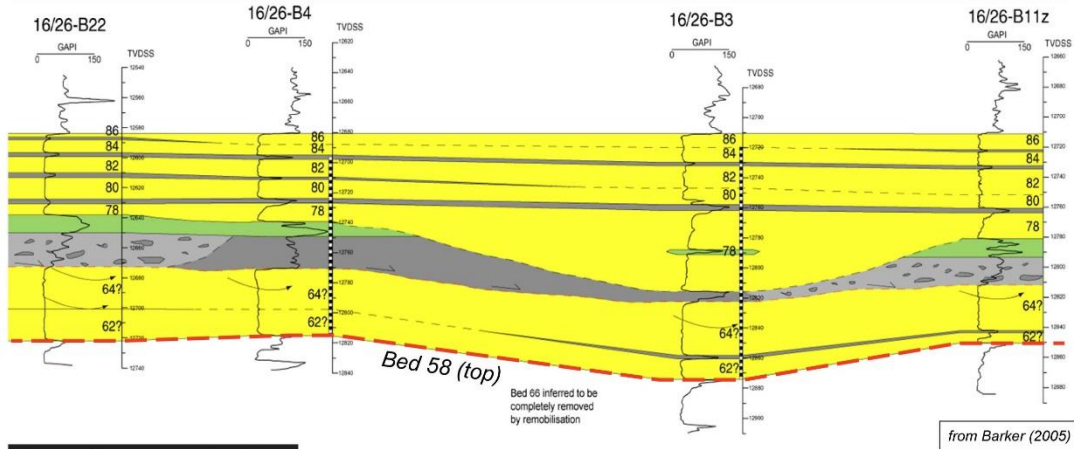
Middle-Lower Britannia (Ainsworth et al., 2000; Barker et al., 2008). The development of this thick interval of sandstones and the nearly complete absence of interleaved mudstone are interpreted to reflect sandstone bed duplication/excision due to post-depositional sliding of this portion of stratigraphy, without development of subsidiary debritic intervals. Zone 50 comprises 5 distinct depositional events or 'beds' (labelled 78, 80, 82, 84, 86 from base to top, Figure 3.10). Individual sand beds represent single sustained flow episodes, each representing infrequent catastrophic sand input into an otherwise sediment-starved basin (Barker et al., 2008). The beds within Zone 50 are interpreted as the deposits of unusually large-volume, axially dispersed turbidity currents close to their run-out limit (Barker 2005). Zone 50 (in particular Bed 78) was initially deposited onto complex seafloor bathymetry (Fig. 3.4) resulting from the action of large debris flows and associated olistostrome deposition of the Zone 45 Clay (Barker 2005). This bathymetry was largely healed by deposition of Bed 78, which displays significant thickness variation, while subsequent beds (80-86) have a relatively uniform thickness (Fig. 3.4). Defining the Upper Britannia deposit volume and discriminating it from the underlying unit is more straightforward than for higher intervals in well correlation across the study area, suggesting a different depositional style and likely geological evolution (see Barker, 2005; Barker et al., 2008).

More recently, Eggenhuisen et al. (2010) studied the Lower Reservoir Sections (Z7, Z10 and Z20), focussing on the stratigraphy from below the Britannia sands to the base of the "Zone 40" sandstone interval (Fig. 3.10). This interval is composed of interleaving of sandstones, hemipelagic mudstones and MTDs. A key conclusion of Eggenhuisen et al. (2010) was that just two significant mass flow events had affected this interval, and that the post-MTD bathymetry likely significantly affected subsequent deposition. This conclusion undermined confidence in the bespoke biostratigraphic correlation scheme previously in use (Ainsworth et al., 2000), which was concluded to have been in part based on analysis of remobilised clasts. Thus a second innovation by Eggenhuisen et al. (2010) was the considered use of the background shale stratigraphy as a correlation aid. The revision of the stratigraphic interval of the Lower Reservoir Sections proposed by Eggenhuisen et al. (2010) and based on zonal correlation of 11 cored wells, allowed them to identify two distinct components to the Z10 sandy reservoir interval, Zones 10A and 10B, based upon their lithological character and interleaved mudstone markers (Fig. 3.10 and table 3.1). To obtain a correlated geometry that was not biased by a priori assumptions made on vertical positions of beds (e.g., Z10 sand base/top is horizontal), Eggenhuisen et al. (2010) used the base-Zone 45 Bed 58 reference datum on which

to pin the sedimentary logs; it is present in most of the wells and shows relatively small and systematic variations in thickness and grainsize distribution (Barker et al., 2008), indicating that its substrate was essentially flat and horizontal over the area of interest (Eggenhuisen et al., 2010). This is important because it elevated an unreferenced stratigraphic correlation panel, in which depositional lobes could not be distinguished from incised units nor from compensating units filling substrate topography, to a dataset that could be used to analyse the relation between spatial thickness variations and bathymetry (Eggenhuisen et al., 2010). The Bed 58 datum is further exploited in the current work, albeit with the top, rather than the base of the bed being chosen as the actual datum horizon.

Correlations of the Britannia Sandstone Formation

Upper Reservoir Section



Lower Reservoir Section

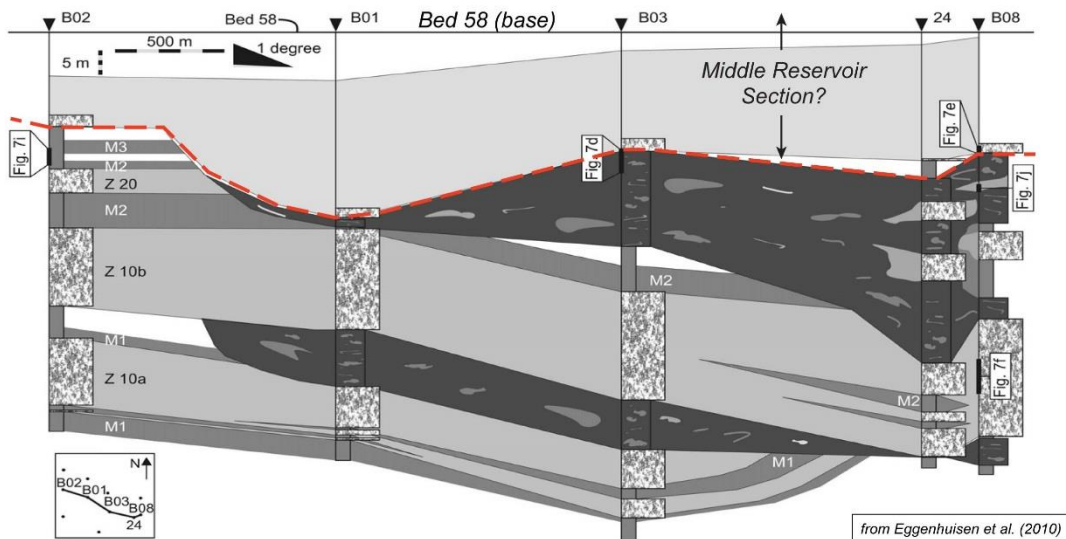


Fig. 3.10 – Correlations of the Upper and Lower-to-Middle Britannia Sandstone Formation in the Platform Area (from Barker, 2005 and Eggenhuisen et al., 2010, respectively). Correlations are both oriented NW-to-SE (see inset for well locations). Dashed red line represents the boundary of the Upper and Lower Reservoir Section with the Middle Reservoir Section. The Upper Britannia is correlated on a bed-by-bed base, whereas the Lower Section is based on correlation of reservoir zones. Dark-grey layers represent MTDs whereas greyish colour represents mudstones. Yellow (in the Upper Reservoir correlation) and light greyish colour (in the Lower Reservoir correlation) represents mainly sandstones.

4 A revised facies scheme and correlation framework of the Britannia Sandstone Formation in the Platform Area

This Chapter aims to integrate prior studies and new observations collected as part of this work to produce a revised facies scheme and correlation framework for the Lower and Middle Reservoir in the Platform Area of the Britannia Field. In detail this chapter aims to:

- describe the facies scheme used for a core-based investigation of the Lower and Middle Reservoir (Platform Area);
- present a new correlation framework and an improved informal bed and zonal numbering scheme for the Lower and Middle Reservoir (Platform Area) at both zonal and bed scale.

4.1 Introduction

Core, core photos, cuttings petrography (from Blackburn and Thomson, 2000) and wireline logs were used for the characterisation of the Middle Britannia reservoir architecture and to review the Lower Britannia reservoir (Eggenhuisen et al., 2010), in order to better support well correlations across the Platform Area.

A facies scheme (Table 4.1) is erected as a revised and simplified version of previous facies classifications (Guy, 1992; Lowe and Guy, 2000; Barker et al., 2008 and Eggenhuisen et al., 2010), and includes full descriptions and interpretations of the facies identified from the cored intervals of the Middle Reservoir Section, and from re-evaluation of core logs from the Lower Reservoir (originally collected by Eggenhuisen et al., 2010).

The revised reservoir correlation framework combines data from previous authors (Barker, 2005; del Pino Sanchez, 2006; Eggenhuisen, 2009) with new observations. Table 4.3 aims to summarise previous work and highlight the novelties of this study (e.g., internal divisions in Z40A).

Reservoir interval subdivision is based on the lithological character of the intervals; lithofacies distributions were also used to characterise and better identify reservoir intervals for the Lower and Middle stratigraphy, however these will be shown in the following Chapter 5 (MTDs) and Chapter 6 (Sandstones) together with descriptions and their associated flow process interpretations. The identification of these intervals is essential for a comprehensive reconstruction of the Britannia reservoir architecture

that in turn enables a better understanding of the evolution of the depositional system through time.

4.2 Data and methods

The Platform Area of the Britannia Field covers approximately 35 km² (Fig. 4.1) and has been the subject of intense exploration drilling (47 wells) and an extensive coring campaign with over 20,000 ft. (~6,000 metres) of core taken from both exploration and production wells (15 wells in total; Table 4.1). Wells are spaced between 200 and 1300 metres apart, to form an irregular grid that covers the entire study area. The high concentration of drilled wells in the Platform Area (47 wells across an area of 35 km²) makes this an excellent case study area, where the lack of good quality seismic image is compensated for by a high quality resolution well-dataset.

Detailed sedimentary analyses of ~3,500 ft. (~1,000 metres) of high quality resinated core slices from 14 wells were undertaken at 1:20 scale (Appendix B) at the Iron Mountain core store facility in Dyce, Aberdeen and provided by Britannia Operator Limited (BOL). Visual grain size estimation was made on core using a grain size comparator. Sedimentary structures, internal fabrics and colours were sketched, described and incorporated into the logs in order to determine different lithofacies.

High quality core photographs were also available for the majority of cored wells in the study area and they were used during follow-up investigations and for those cored intervals object of previous PhD projects (Barker, 2005; del Pino Sanchez, 2006, and Eggenhuisen, 2009). New photographs were taken by high-resolution camera and used to aid facies classification (Fig. 4.3).

Wireline log data, including gamma ray, combined neutron-density and sonic-logs, were analysed for all cored wells and for 25 uncored wells (Appendix A) contained in a database provided by BOL and available through ODMTM (Oilfield Data Manager) software. Core logs were corrected for the core shift and well deviation and uploaded into the ODMTM database in order to have zone and bed thickness identified on cored wells checked against the true vertical depth sub-sea scale (TVDSS) measured for the wireline log plots for each well.

The ODM software was used to visualise all available data (wireline, core, etc.) in the same environment, helping interpretation of the depths of base and top of each reservoir zone. The dataset output from ODM is shown in Figure 4.2. The same software was also used to record those depths and to produce correlation panels that were then edited in Illustrator to improve their graphic appearance (e.g., Fig. 4.7, 4.8 and 4.9). BOL internal reports produced by various internal geoscientists and external consultant companies containing data related to facies, lithologies,

zonal and bed-scale correlation models were available for scrutiny and comparison purposes with the present work. A database of cuttings petrography produced by Blackburn Geoconsultants for BOL was also available to support the correlation of uncored wells.

Wells	Core Log	Core Photos (quality)	Cuttings	Gamma-ray Log	Sonic Log
16/26-3	✓		✓	✓	✓
16/26-9			✓	✓	✓
16/26-16			✓	✓	✓
16/26-24	✓	poor	✓	✓	✓
16/27A-6		poor	✓	✓	✓
B01	✓	high	✓	✓	✓
B02	✓	high	✓	✓	✓
B03	✓	poor	✓	✓	✓
B04	✓	high	✓	✓	✓
B05	✓	poor	✓	✓	✓
B06	✓	high	✓	✓	✓
B07	✓	high	✓	✓	✓
B08	✓	poor	✓	✓	✓
B09Z			✓	✓	✓
B10	✓	poor	✓	✓	✓
B11z			✓	✓	✓
B12			✓	✓	✓
B13z	✓	poor	✓	✓	✓
B14			✓	✓	✓
B15			✓	✓	✓
B16			✓	✓	✓
B17			✓	✓	✓
B18			✓	✓	✓
B19			✓	✓	✓
B20			✓	✓	✓
B22			✓	✓	✓
B23z			✓	✓	✓
B24			✓	✓	✓
B27			✓	✓	✓
B28			✓	✓	✓
B29			✓	✓	✓
B30			✓	✓	✓
B31			✓	✓	✓
B32			✓	✓	✓
B33	✓	good	✓	✓	✓
B35			✓	✓	✓
B37			✓	✓	✓
B40z			✓	✓	✓
B43			✓	✓	✓

Table 4.1 – Dataset summary table for the Middle Reservoir Zone. Core and core photos were available for 14 wells whilst gamma-ray and sonic logs obtained from the boreholes were accessible for all the wells of the Platform Area. Well locations are displayed in Figure 4.1. Well depths across which each type of data were available are shown in Appendix A.

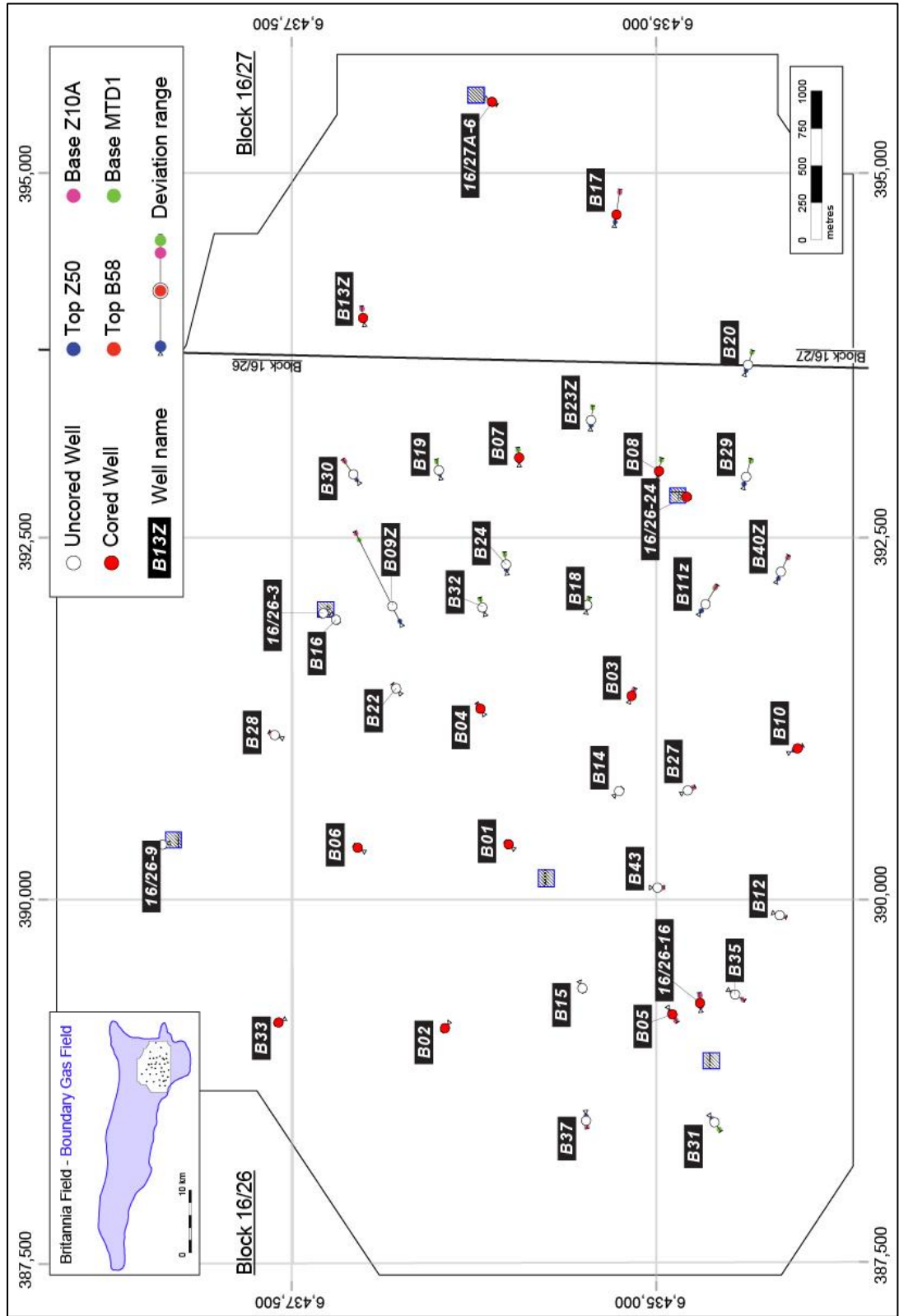


Fig. 4.1 – Platform Area of the Britannia Field. Red dots represent cored wells, whereas white dots correspond to uncored wells. Wells are projected at the intersection of the well with the bottom of Z45 (Bed 58), described in Chapter 3. Deviation range is also shown by the position at which the well intersect the top/base of the BSF (Z10A/MTD1 = base Britannia; Z50= top Britannia).

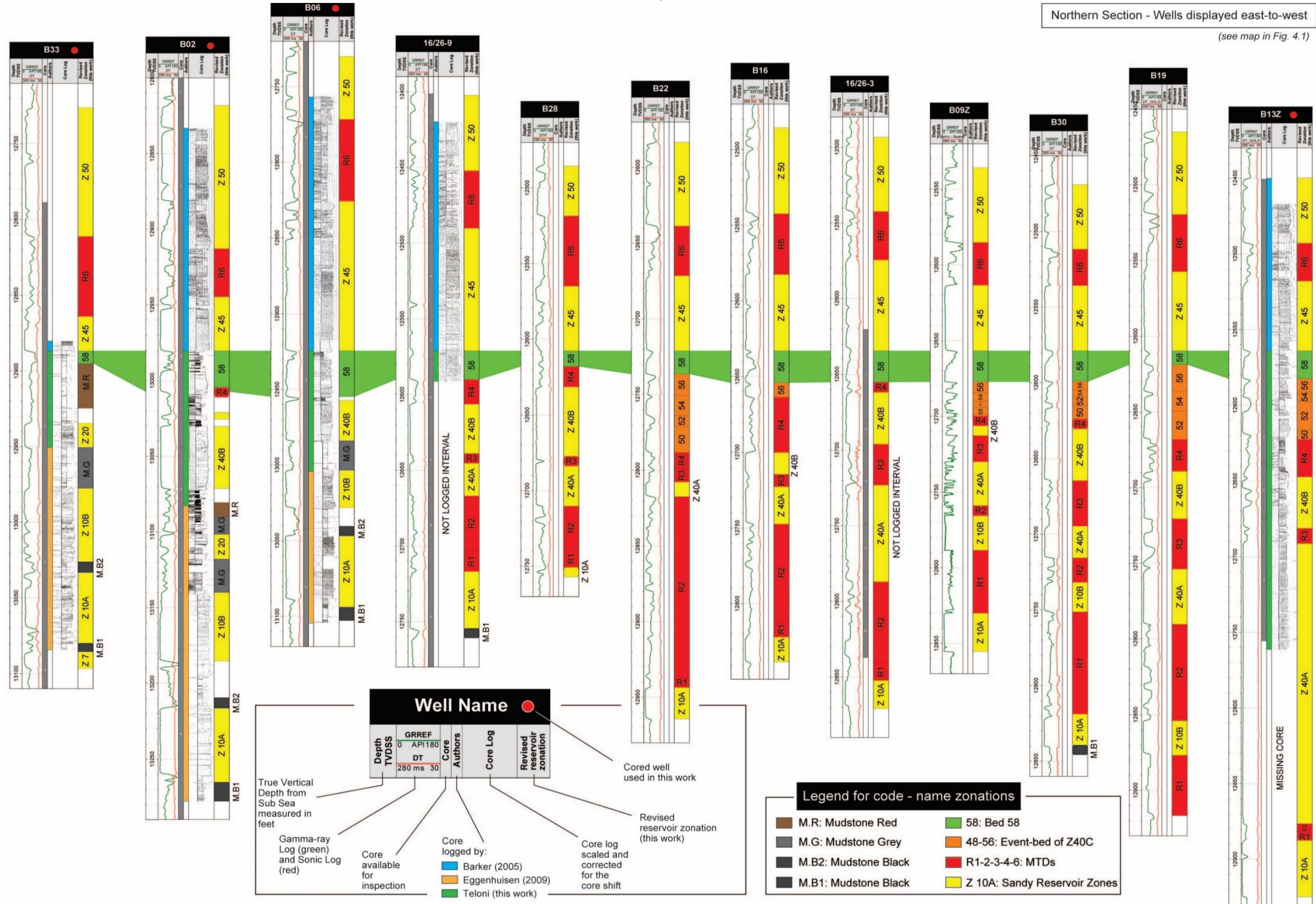
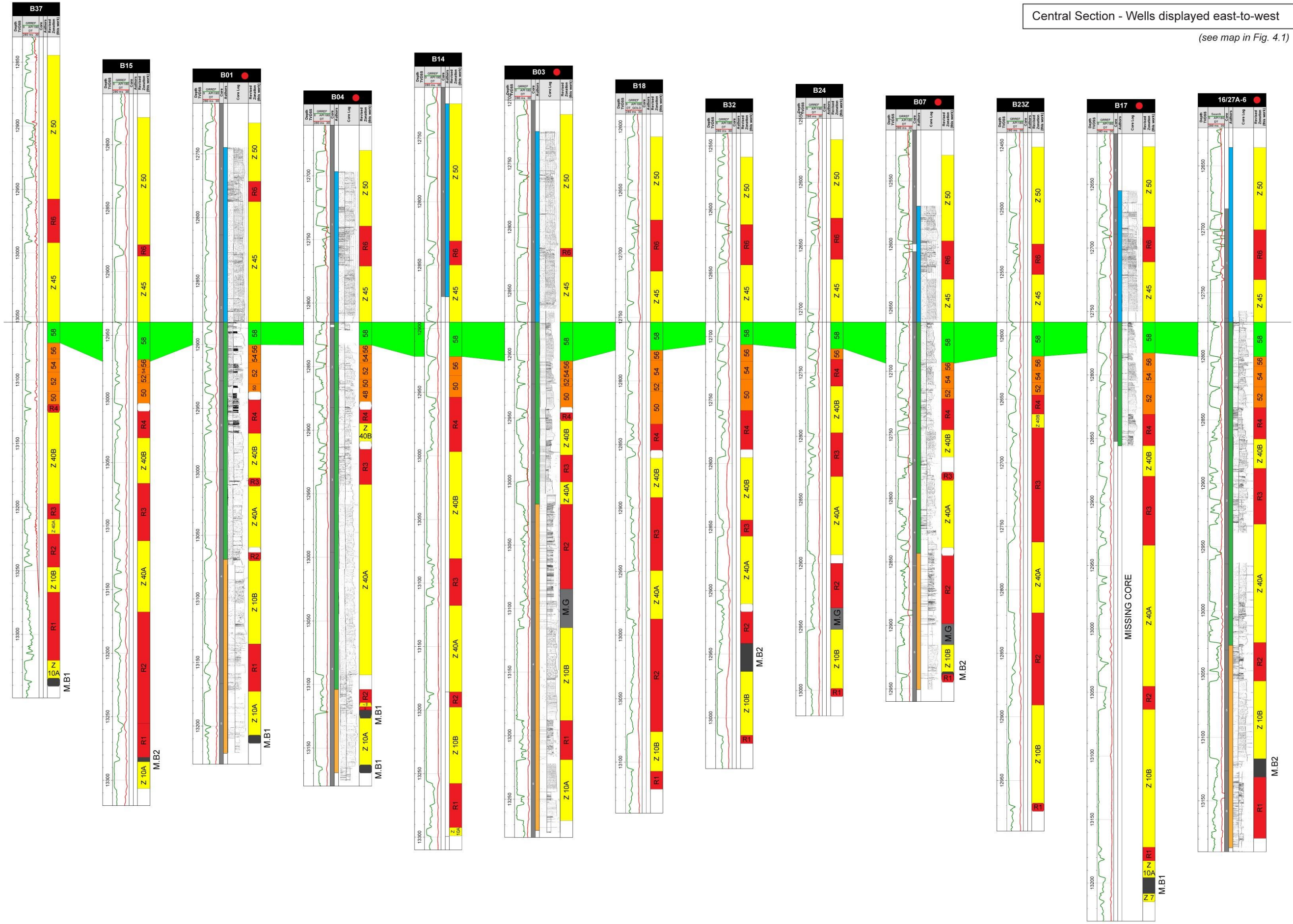
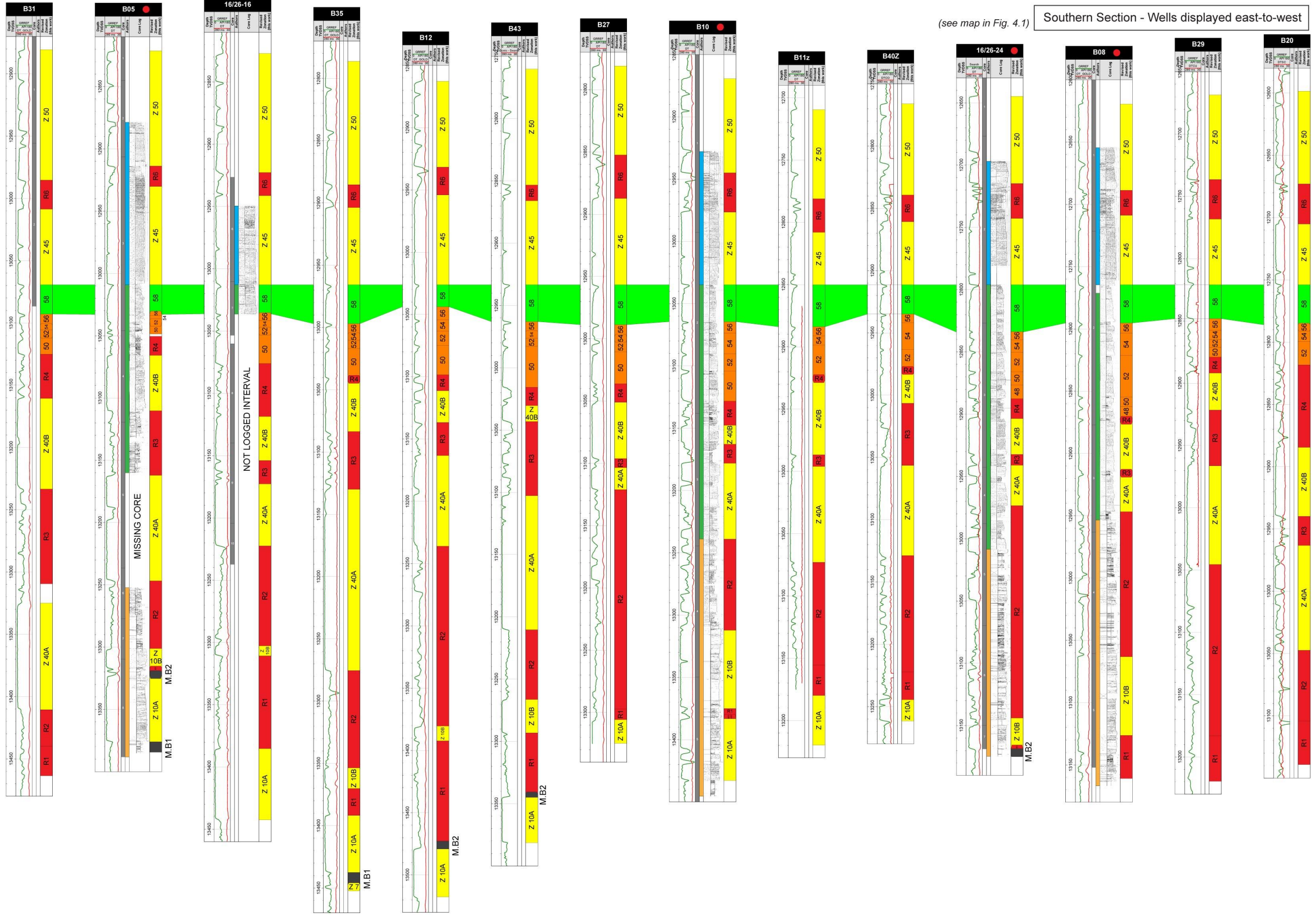


Fig. 4.2 – Dataset exported from ODM software. ODM allows to visualise all available data (wireline, core, etc.) in the same environment, helping interpretation of the depths of base and top of each interval for cored and uncored wells. Per each well depth, prephysical logs (gamma-ray Log and sonic logs), available core, author that investigated the interval and reservoir zonation are displayed. The same software was also used to produce correlation panels that cover all the available wells of the Platform Area (e.g., Fig. 4.6, Fig. 4.7 and Fig. 4.8). Further data (facies, lithologies, cuttings etc., that are not displayed in the above figures) are contained in the ODM database

Central Section - Wells displayed east-to-west

(see map in Fig. 4.1)





(see map in Fig. 4.1)

Southern Section - Wells displayed east-to-west

4.3 Revised facies scheme

The facies scheme proposed for this study (see Table 4.2) is based on the combination and partial simplification of the schemes proposed by Lowe and Guy (2000), Barker et al. (2008) and Eggenhuisen et al. (2010) previously summarised in Table 3.2 (see section 3.3.3). The changes aimed to overcome some of the limitations present in each of the schemes, as detailed below and at the same time to provide a comprehensive facies scheme that could describe the full range core facies observed in the BSF; significant variations are recognised vertically throughout the entire BSF in the PA, from the Lower, Middle and Upper Reservoir Section.

A first simplification consisted in subdividing the core facies into three main classes based upon their proportions of mud and sand, as sand-rich, mud-rich and mudstone (see Table 4.2), in order to identify the increase/decrease mud/sand content associated with core facies.

The clean sand (sand-rich) lithotype comprises clean, structureless, massive sandstones (here termed “massive” following the existing literature on Britannia core facies) and laminated sands (which consist of finely laminated very fine sandstones and siltstones; Fig. 4.3). The descriptions given in table 4.2 are in line with those by Lowe and Guy (2000), Barker et al. (2008) and Eggenhuisen et al. (2010); some of the earlier “granule-rich” and “granule-containing sandstone” facies introduced by Barker et al. (2008) and Eggenhuisen et al. (2010), respectively, are here included within the “massive sandstone” class given that outsized grains up to 4 mm large are hosted by the massive-structureless sandstones. In agreement with those previous papers, the sand-rich class is interpreted as being deposited from turbulent sandy gravity flows.

The classification of the clay-prone sandstone lithotype follows the nomenclature of Lowe & Guy (2000) and includes banded facies (also comprising pseudobanded and wispy laminated sandstones that were originally kept separate in the facies scheme proposed by Barker et al., 2008) in which darker and lighter bands form couplets, together with the mixed-slurried facies (a continuous facies resembling the darker bands of the banded facies - Barker et al., 2008). The complex nomenclature given by Lowe & Guy (2000) is here simplified and revised, given that in these deposits the authors included divisions characterised by dewatering features which are here considered ubiquitous structures within the Lower and Middle Reservoir Section.

These deposits are interpreted as being deposited from a continuum of sandy gravity flows in which increasing proportions of clay cause periodic suppression of turbulence (Baas et al., 2009) and the development of transitional types of flow

(Haughton et al., 2003; Talling et al., 2004; Kane and Pontén, 2012). The distribution of these facies and associated interpreted flow process are discussed in detail in Chapter 6.

The debrite facies is generally characterised by the presence of fine to medium sand grains floating in a dark grey mud-silt matrix which give the characteristic “starry-night” appearance. However, dark grey mud-silt matrix characterised by the absence of floating quartz grains in the matrix is also observed and differentiated. The distinction between “starry night” and “muddy” debrite facies is described in detail in Chapter 5. The matrix generally surrounds mudstone clasts and sandstone blocks of various sizes (from mm to cm scale) and generally orientated bed parallel. Barker et al. (2008) and Eggenhuisen et al. (2010) proposed two main facies for debrite deposits upon the concentration of clasts (e.g., “debrite matrix facies” and “debrite clast facies”), however, in this work clasts of various sizes are recognised within both starry night and muddy debrite facies.

The mudstone facies groups together distinctive mudstone lithotypes (e.g., Eggenhuisen et al., 2010) which can be used to support well correlation of the Lower Reservoir Section (see section 3.3.4) and undifferentiated mudstones. The distinctive mudstone lithotypes are interpreted to have been deposited through hemipelagic settling, while the undifferentiated mudstone is interpreted to be either hemipelagic or turbiditic in nature.

Following the approach taken by Barker (2008), dewatering has not been considered as a key criterion for facies classification given that dewatering features are ubiquitous across the sandstones of the sandy and muddy reservoir zones. In fact, the facies described above are often overprinted by a variety of dewatering fabrics that may have formed both syn- and post-depositionally. Such fabrics are formed by water escape upwards through the porous sediments, possibly entraining solid particles (elutriation) and deforming the sediment along its path or without displacing the grains. These structures are frequent in sands that accumulate quickly. Commonly “blind deformation” is observed in which water escape is associated with basal massive sands, but becomes less common higher in beds. This is explained by the more permeable sand at the beginning of deposition, massive facies being associated with rapid sedimentation; sedimentation rates decreases higher up in beds resulting in a decrease in permeability (Lowe, 1975). Consolidation laminations are mainly observed in massive and clean sandstones, whereas pipes and sheets are most common in banded sands (Fig. 4.5). Traction structures as ripples and cross

laminations are not recognised within the whole Lower and Middle Reservoir Sections in the Platform Area.

A summary of the facies classification used in this study to describe core from the Middle Reservoir Section (Z40) is provided in Table 4.2, with examples of individual facies shown in Figures 4.3, 4.4 and 4.5.

Lithol.	Divis.	Facies	Code	Description	Process Interpretation
Sand	Sand-rich	Massive Sandstones	SMa	Massive, clean, poorly sorted, fine to medium grained sandstone; no primary sedimentological structures, usually overprinted by dewatering fabric (dishes or consolidation laminations).	Associated with deposition from a high density turbulent flow; unsorted clean sandy material dropped out of suspension from the turbulent section of the flow.
Sand		Laminated Sandstones	SLa	Planar parallel laminated light-buff grey to light grey sand. Sand is fine-grained and moderately to poorly sorted. Detrital clay content is concentrated along dark planar laminations.	Laminated sands could represent Bouma's Tb and Lowe's S1 division as upper flow regime parallel lamination, or they could represent poorly developed shear laminations associated with incipient traction carpet formation or they could represent pervasive millimetres-scale dewatering dishes appearing as continuous crenulated laminae after pressure solution (Guy, 1992; Jones et al., 1999b).
Sand	Sand-rich	Banded Sandstones <i>(mega-banding, meso-banding and micro-banding)</i>	SBa	Fine to very fine sandstone with cyclic alternation between dark grey and light yellowish brown horizons ("bands"). Dark divisions have a sheared fabric containing strung-out and folded lighter dewatering structures and lighter sandy, sheared globules. The base of the dark divisions is generally horizontal, straight and sharp. Light horizons are cleaner with planar or slightly undulate laminations, commonly without consolidation laminations. Banding occurs on a different range of scales, mega-banding, meso-banding and micro-banding (<i>sensu</i> Guy and Lowe, 2000). Sheet dewatering features are often present and cross cut the dark horizons.	Deposition from sandy gravity currents in which the flow conditions at the bottom of the flow alternate from fully turbulent to cohesion-dominated shear layers or viscous sub-layers (dark band zones). Rapid fallout from suspension in less muddy flows results in the development of thin, short-lived viscous sublayers to form wispy-laminated divisions (Lowe and Guy, 2000). The absence of textural sorting within wispy divisions also suggests that deposition took place under conditions of high suspended-load fallout rates (Lowe and Guy, 2000).
		Pseudo-banded and Wispy Laminated		Thin, dark, discontinuous (laterally at < 10 cm scale) commonly crenulated layers and laminations of heterolithic sandstone ("wisps" <i>sensu</i> Barker et al., 2008) separated by thin layers and lenses of cleaner sandstone are also distinguishable. Wispy laminations form dark, mud rich zones from less than 1 mm to about 1 cm thick.	
Sand	Mud-rich	Mixed Slurried Sandstones	SMS	Very fine to medium grained sandstone, highly sheared internal fabric, with contorted, folded, and sheared, light, sandy blobs that sit in dark, heterolithic sand, silt, and mud matrix highlighting various degrees of mixing. Sheared dewatering facies may contain remnants of banded (Sba) and wispy-laminated facies as well as deformed massive (Sma) facies.	The various degrees of mixing are here interpreted as the result of three different processes: (i) primary deposition of "slurry flows" <i>sensu</i> Lowe and Guy (2000), where mixed slurried sandstone represents the following stage of the banded (micro- meso- mega- banding) sandstone; (ii) gravitational deformation, where the fabric is due to post-depositional translation down the slope of water rich sand and mud mixture (Barker et al., 2008) or (iii) due to the partitioning of shear strain into the substrate of turbidity currents during their emplacement (Butler et al., 2015)
Sand		Injected Sandstones	Slnj	Very fine to upper fine sandstones with thickness ranging between 1 mm and 1 m. Sandstone boundaries are irregular with a high angle of discordance with the underlying bedding orientation. Mud clasts float in the sandy injection matrix.	Post-depositional injection of a viscous sand-water mixture into the host lithologies.
Debrite		Sandy starry-night and muddy debrite	DSn	Fine to medium sand grains floating in a dark grey mud-silt matrix. The "starry-night" appearance is given by the light-coloured sand grains suspended in the dark matrix. Dark grey mud-silt matrix characterised by the absence of floating quartz grains in the matrix is also observed. Occasional mudstone clasts and sandstone blocks occur in the matrix, with various sizes (from mm to cm scale) and generally orientated bed parallel. Occasional higher sand content through sand injections.	Mudstone clasts and sandstone blocks set into the mud-silt matrix are the product of debris flow, characterised by en-masse deposition. The complete mixing of sand grains into the matrix indicates remobilisation of unconsolidated sandstone. Deposition from highly concentrated, highly viscous, sediment-fluid dispersions.
Mud	Mudstone	Undifferentiated Mudstone	Mds	Laminated dark-grey clay with slightly darker and lighter shades. Common silt constituent disseminated throughout. Sometimes partially bioturbated with occasional sand injections.	These mudstones are interpreted to represent the upper portion of sandstone beds which grade upward from laminated fine-grained sandstone to structureless mudstone, overlain by hemipelagic mudstone containing deep-water fossil assemblages.

Table 4.2 – Revised facies scheme used in this study for the cored wells of the Platform Area (partly based on Lowe and Guy, 2000; Barker et al., 2008; Eggenhuisen et al., 2010).

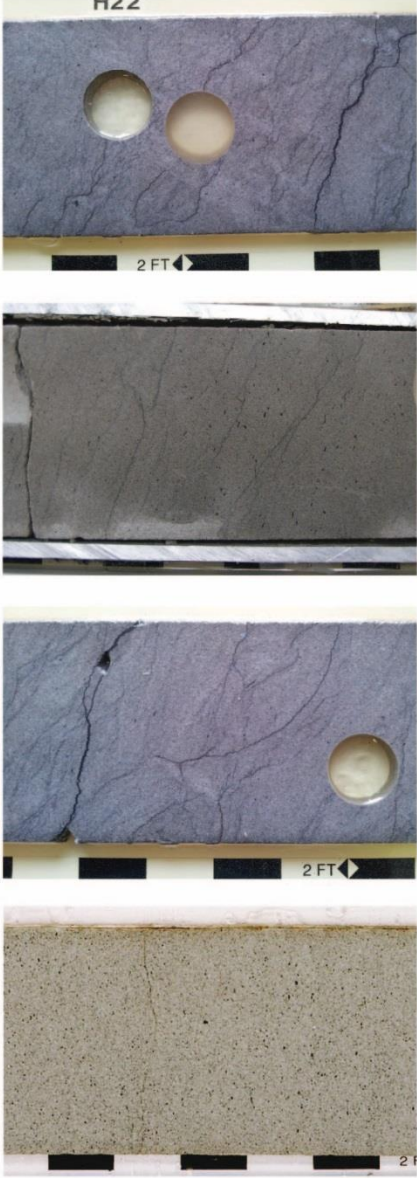
<p>ϕ - mD</p>	<p>Average porosity: 16% Average Permeability: 50-100 mD</p>	<p>Average porosity: 14-18% Average Permeability: 10-15 mD</p>
<p>CORE PHOTOS</p>		
<p>FACIES</p>	<p>MASSIVE SANDSTONE (SMa)</p>	<p>LAMINATED SANDSTONE (SLa)</p>

Fig. 4.3 – Facies core photograph of sandstones for sandy reservoir zones (as in the next two pages). Scale bar intervals are one tenth of a foot long.

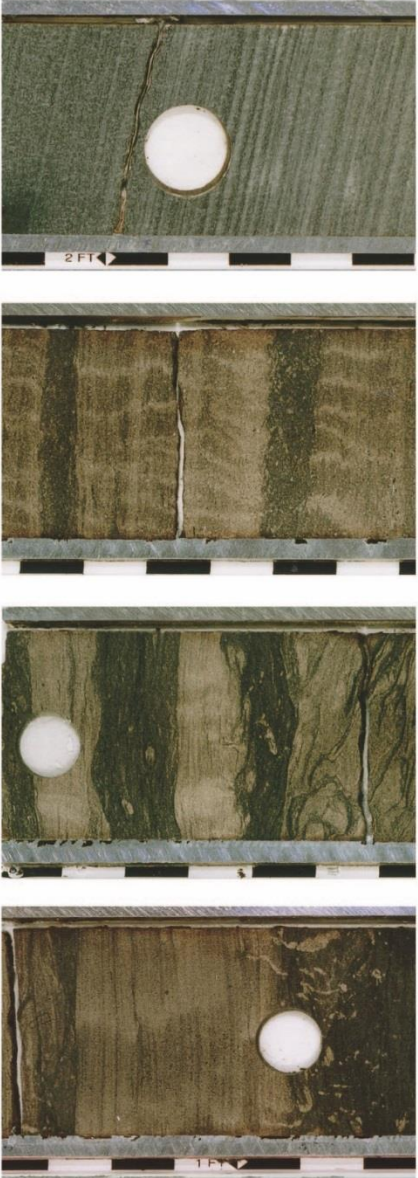
ϕ - mD	<p>Average porosity: 13% Average Permeability: 0.1-10 mD</p>	<p>Average porosity: 10-14% Average Permeability: <1 mD</p>
CORE PHOTOS		
FACIES	<p>BANDED SANDSTONE (SBa)</p>	<p>MIXED-SLURRIED SANDSTONE (SMs)</p>

Fig. 4.3 – continued

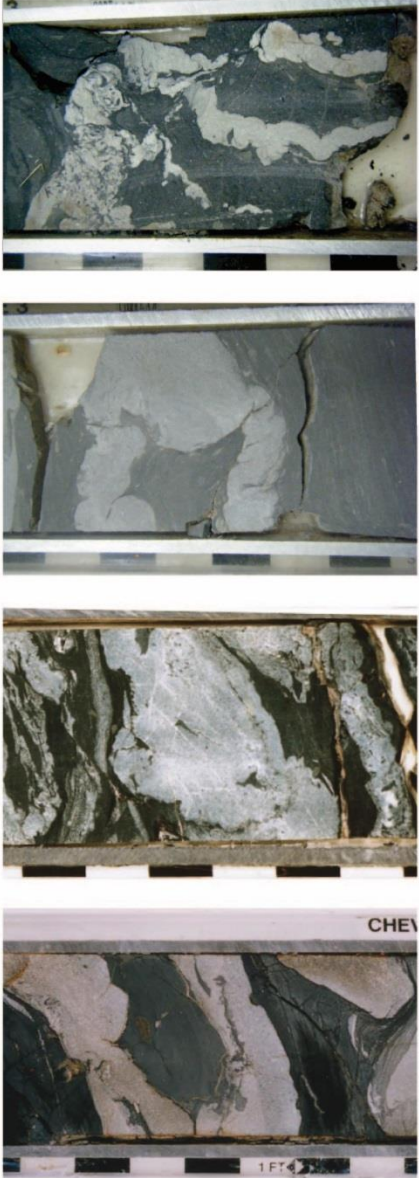
ϕ - mD	<p>Average porosity: 13% Average Permeability: 10-50 mD</p>
CORE PHOTOS	
FACIES	<p>INJECTED SANDSTONE (SInj)</p>

Fig. 4.3 – continued.

ϕ - mD	Average porosity: - % Average Permeability: - mD	Average porosity: - % Average Permeability: - mD
CORE PHOTOS		
FACIES	DEBRITE (DSn)	UNDIFFERENTIATED MUDSTONE (Mds)

Fig. 4.4 – Representative core photograph of facies for debritic deposits and mudstones identified within the sandstone reservoir zones. Scale bar intervals are one tenth of a foot long.

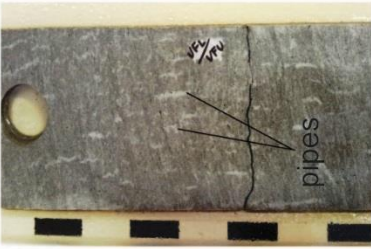
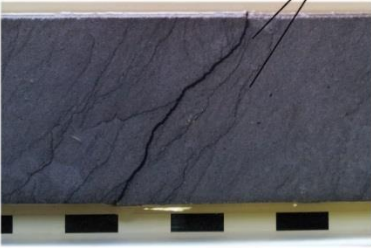
<p style="text-align: center;">DEWATERING (pipes, sheets, dishes, consolidation laminations)</p>	
<p>DISHES</p> <p>Dark convex down structures within a paler sandstone background. Generally lengths between 5 and 8 cm. Various intensity of distribution.</p>  <p style="text-align: right;">dishes</p>	<p>PILAR</p> <p>Vertical to sub-vertical features, subparallel lineation, between 2 and 50 cm in length and between 0.5 and 4 cm wide; light-colored relative to background sandstone; often calcite cemented; often sheared from vertical.</p>  <p style="text-align: right;">pillar structure</p>
<p>PIPES</p> <p>Vertical to sub-vertical features; vary in both size and density of distribution; lighter in colour relative to background sand; often calcite cemented; cross sections in core may be 1 to 10 cm in length, or spherical, circa 6 mm diameter, depending upon intersection of cut core surface with pipe length or pipe diameter generally both present in an interval which contains pipes and this helps</p>  <p style="text-align: right;">pipes</p>	<p>CONSOLIDATION LAMINATIONS</p> <p>Horizontal to low-angle dark laminations (crinkled); generally continuous across core width but often associated with dish structures.</p>  <p style="text-align: right;">consolidation lamination</p>

Fig. 4.5 – Core photographs of dewatering fabric recognised on sandstone facies. Scale bar intervals are one tenth of feet long.

4.4 Revised correlation framework

Distinctive log signatures for each zone (and internal beds, as appropriate) and the recurring stacking patterns across different wells, as described in the table 4.3, underpin the new zonal/bed correlations for the Lower and Middle Reservoir in the Platform Area. Various authors' reports, including Moore et al. (2009) and Blackburn and Thomson (2000) for Britannia Operator Limited and published papers including Guy (1992), Lowe and Guy (2000), Hill and Palfrey (2003) were also considered. Table 4.3 shows all the PA reservoir intervals, including Lower Britannia (Z10A, Z10B and Z20), previously studied by Eggenhuisen (2009), and Upper Britannia reservoir section (Z45 and Z50) investigated by both Barker (2005) and del Pino Sanchez (2006), together with the Middle Britannia (Z40) representing the main focus of this study.

4.4.1 Lower Reservoir

A new correlation framework for the Lower Reservoir Section was prepared by expanding the published correlation framework by Eggenhuisen (2009), which was based on 11 cored wells (and 6 uncored wells), up to the current dataset of 14 cored wells (and 26 uncored wells) (Table 4.1 and Fig. 4.2). The position of MTD-2 (Eggenhuisen, 2009) is reinterpreted in a number of wells thanks to the inspection of new cored wells (e.g., 16/27A-6) and the integration of wireline logs located in proximity to cored wells. A key example is shown in Fig. 4.8, where the MTD-2 in 16/27A-6 was previously recognised at the base of the BSF in this area, whereas further core investigation highlighted the presence of a small portion of black anoxic shales of the Fischschiefer bed underneath the Z10B, which is older than MTD-2, and difficult to recognise on wireline logs. Furthermore, the thickness of this reservoir zone is within the range of the surrounding cored wells, supporting the new interpretation of the MTD-2 and associated Z40A on top. Similar observations are then extended to uncored wells in the PA upon wireline logs. A detailed comparison between the actual revised correlations and previous correlation models of the Lower Reservoir proposed by Eggenhuisen et al. (2010) was not possible; this is because in the previous work, only a limited subset of uncored wells was used to test the correlation model erected on the basis of the cored wells.

4.4.2 Middle Reservoir

In this work, the stratigraphy of the Middle Reservoir Section (Zone 40) is entirely re-correlated at the zonal and bed-scale thanks to the identification of the deposits of two different large-scale failures, termed MTD-3 and MTD-4 (Fig. 4.8 and 4.7). These characteristic chaotic deposits can be recognised due to their prevalently muddy

matrix, which is different from the mainly “starry night” texture of the MTD-1 and MTD-2 matrices (see Chapter 5). MTD-3 and MTD-4 occur at different stratigraphic heights, interrupting the continuity of the Z40 sandstones. Therefore, the Z40 can be split into three intervals, informally named Z40A, Z40B and Z40C in ascending stratigraphic order (Fig. 4.7 and 4.8).

Individual beds could not be correlated within Zones 40A and B. However, the new core logging allowed identification of six individual beds that make up Z40C and their correlation across the PA (see full description in section 6.4.5).

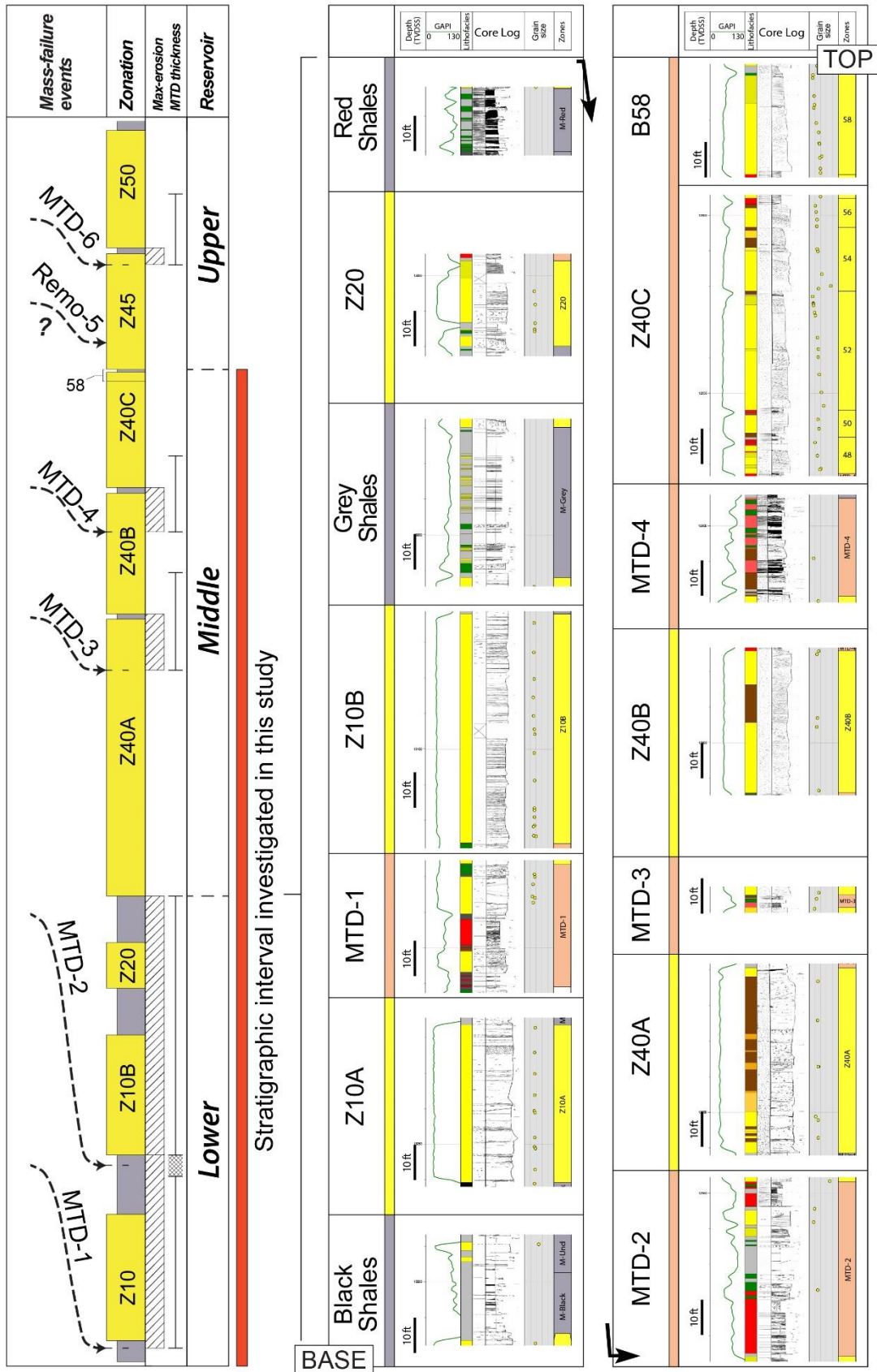


Fig. 4.6 – Stratigraphic chart summarising the revised Britannia Field zonation in the Platform Area after Eggenhuisen (2009) and this work. Columns on the right show detailed zone characterisation of the Lower and Middle reservoir section, including zonation, gamma-ray style, core log and grain size.

Reservoir Interval	Wireline description	Core description	Interpretation
MTD-2	"Jagged" GR log profile (but supplementary cuttings data required for confident interpretation).	MTD-2 is present across most of the Platform Area and shows thickness variations between 10 and 70 m. It is a debritic interval with an erosive base and an irregular upper topography.	This zone is associated with the occurrence of a slope failure that leave remobilised deposits behind.
RED SHALES	Increase in GR and decrease in sonic velocity.	Shales in the upper part of this zone are commonly stained red, due to the presence of hematite (observations from core logs of Eggenhuisen, 2009).	The red colour is interpreted to be analogous to other Cretaceous Oceanic Red Beds (CORB's) (Eggenhuisen et al., 2010). These mudstones are defined as "reddish sediments that were deposited in situ in marine environments" (Hu et al., 2005; Neuhuber and Wagreich, 2011)
Z20	Sharp lower boundary with blocky gamma ray log profile. The upper boundary is gradational to sharp.	Clean sands normally graded with little or no evidence of erosion sandwiched within hemipelagic shale (Reddish Shales and Bioturbated Shales respectively on top and base). In the Platform Area, Zone 20 is represented by only a few apparently isolated and uncorrelated sand bodies (observations from core logs of Eggenhuisen, 2009).	This interval may represent storage and re-working of sands on and around local highs to the north of the basin (Hill and Palfrey, 2003).
GREY SHALES	Characterised by an abrupt decrease in GR response and an increase in sonic velocity values (Ainsworth et al., 2000).	Bioturbated Shales (correlative to regional marker "Ewaldi Marls") are dominated by greyish marls/calcareous claystones (observations from core logs of Eggenhuisen, 2009).	This interval represents a quiescent period of low sedimentary input and it is used to define the top of Z10B (Eggenhuisen et al., 2010).
Z10B	Blocky GR log profile, i.e., with a very sharp base and well defined upper boundary.	Ungraded, massive, dewatered and banded sandstones with a minor component of mixed slurried sands. Grain size trends, core character and the absence of mud caps suggest amalgamated sandstones (observations from core logs of Eggenhuisen, 2009).	Second important influx of sand into the basin, thought to be primarily derived from the Fladen Ground Spur (Hill and Palfrey, 2003). It may represent deposition as lobes developed within localised depressions created by differential subsidence and/or by MTD-1 evacuation.
MTD-1	"Jagged" GR log profile (but supplementary cuttings data required for confident interpretation).	Characterised by a structureless, well-mixed siltstone and mudstone matrix which contains a variety of isolated mud and sand clasts up to several meters in scale (observations from core logs of Eggenhuisen, 2009).	This zone is characterised by debrite thickness variations between 10 and 50 m across the Platform Area. It has an erosive base and an irregular upper topography. It is interpreted to be emplaced after a slope failure.
Z10A	Blocky GR log profile, i.e., with a very sharp base and well defined upper boundary. Usually the GR top can be ambiguous due to the overlying MTD-1.	Usually dominated by clean massive sands and only occasionally by banded sandstones. These sands show either amalgamation or a non-erosive character but they are usually fine grained, conspicuously lacking a coarse component (observations from core logs of Eggenhuisen, 2009).	First major input of sands into the basin. Both amalgamated and banded sandstones are arranged in a proximal (west) to distal sense (east), and are well correlated across the length of the field, sitting on anoxic Black Shales.
BLACK SHALES	Abrupt increase in GR and decrease in sonic velocity (distinctive "viper tongue" sonic log motif; Ainsworth et al., 2000). This is recognised also on top of Z10A.	Dark mudstone with absence of bioturbation, generally black anoxic (observations from core logs of Eggenhuisen, 2009).	These shales are located in the lower part of the Zone 10A and represent a widespread Ocean Anoxic Event (OAE) (Eggenhuisen et al., 2010 and references therein).
Z7	GR lower boundary is very sharp, marked by an abrupt decrease in GR response coincides with the presence of sandstone.	Light grey, fine to medium grained, commonly well sorted with the presence of some gluconate. This zone contains only clean sandstones (observations from core logs of Eggenhuisen, 2009 and Ainsworth et al., 2000)	This interval is mainly present in the Western Sub Sea Britannia Field and is only identified in wells B02, B33, B35 located in the west sector of the Platform Area leading to the interpretation that it represents the farthest deposition of a Z7 distributary fan system (assuming an eastern provenance of the sands) (Ainsworth et al., 2000)

Table 4.3 – Table showing the reservoir intervals recognised in this work and those revised from previous PhD works. The table aims to characterise reservoir intervals providing wireline logs (gamma ray, sonic) and core description together with interpretation. Intervals are ordered from base (earlier) to top (younger) Britannia Field stratigraphy in the Platform Area. Colour codes represent data from different authors: orange from Eggenhuisen, 2009; green this work; blue from Barker, 2005.

Reservoir Interval	Wireline description	Core description	Interpretation
Z50	Lower and upper boundary are moderately sharp with increasing upwards wireline log motifs.	Five event beds making up this interval are recognised on core; they can be traced across the Platform Area. The lower bed displays marked thickness variation within the Platform Area, whereas the beds above are almost tabular (Barker, 2005).	This interval is deposited above MTD-6 and generally lacks evidence of significant remobilisation, although the basal Bed 78 shows compensational character due to the irregular MTD-6-related topography (Barker, 2005).
MTD-6	"Jagged" GR log profile that has to be supported by cuttings data for confident interpretation.	A mudstone-dominated interval separates Z45 and Z50. Debritic character is recognised on core, overlaid by ash layer (Barker, 2005).	Evidence for large-scale slope failure is present within this unit. Emplacement of debrite and olistostrome deposits is inferred to be associated with sliding processes (Barker, 2005).
Z45	Blocky GR log profile, i.e., with a very sharp base and well defined upper boundary that represent a thick sand package. The division is informally termed the "Boxcar Sandstone" due to its distinctive blocky gamma ray signature (Barker, 2005)	This interval is recognised on core as a sand package made up of three event beds (62, 64 and 66). These show repeated massive clean sand and banded facies (Barker, 2005).	Both bed preservation and overall thickness of this interval are interpreted to be highly variable due to widespread remobilisation (remobilisation = MTD-5). The thick interval and the absence of interleave mudstone are interpreted as sandstone bed duplication/excision due to sliding of portion of stratigraphy without any subsidiary debritic intervals left behind (Barker, 2005).
Bed58	Very sharp GR characterises the lower boundary between mudstones at the top of Z40C and the basal sand of this interval. The upper boundary is gradational, characterised by increasing mud content.	Clean/massive sand in the lower portion fining upward and characterised by an increase in mud content toward the top. This sandstone interval is recognised across the entire Platform Area, except in B33.	Due to its almost tabular character across the study area, it is interpreted that by the time of deposition of this bed, its substrate was essentially flat and horizontal over the area of interest. The Top Bed 58 – Base Bed 62 surface (see Barker, 2005) is used as datum for the well correlations of the Lower and Middle Reservoir.
Z40C	Lower boundary is moderately sharp with increasing upwards wireline log motifs.	Sandstones show strong normal grading and fine upwards into mud. Individual units may develop medium grain size at their base which is useful in sand-body correlations. Hybrid bed types dominate the entire Z40C.	Event beds in the upper part of this interval can be correlated over several kilometres representing widely extensive sheet-like deposits, whereas lower events are more influenced by the MTD-4-related topography and develop a compensational geometry.
MTD-4	"Jagged" GR log profile (but supplementary cuttings data required for confident interpretation).	Characterised by muddy matrix on core. This event incorporates clasts and injections.	MTD-4 is relatively small in comparison to the earlier MTDs, with thickness varying between 2 and 25 m.
Z40B	Characterised by either blocky or inter-fingered GR log profile representing amalgamated and individual beds respectively.	Upward fining units pass from clean massive into banded character which in turn passes into mixed slurried and debritic deposits (hybrid-like beds). This interval is defined purely on sedimentological criteria, occurring across the whole Platform Area and showing different character depending on well location.	Thickness variation together with sedimentological characters of this reservoir interval observed across the whole Platform Area suggests that deposition of these sands were under bathymetric control.
MTD-3	"Jagged" GR log profile that has to be supported by cuttings data for confident interpretation.	Muddy matrix with clasts and injections that sometimes change laterally into well-mixed sandy debritic matrix (starry night).	This interval is interpreted as a remobilisation event triggered up on the slope, in fact it incorporates large quantity of mud (without significant dispersed sand grains).
Z40A	Defined by blocky (northern Platform area) or inter-fingered (southern area) GR log profile with a sharp top.	Clean sands in the lower part of the interval which pass vertically to banded and slurried sandstones. Overall there is a subtle fining upward trend.	Significant thickness variations across the whole Platform Area suggest bathymetric confinement. Petrographic data suggest a southern source for the Zone 40A sands (Hill and Palfrey, 2003).

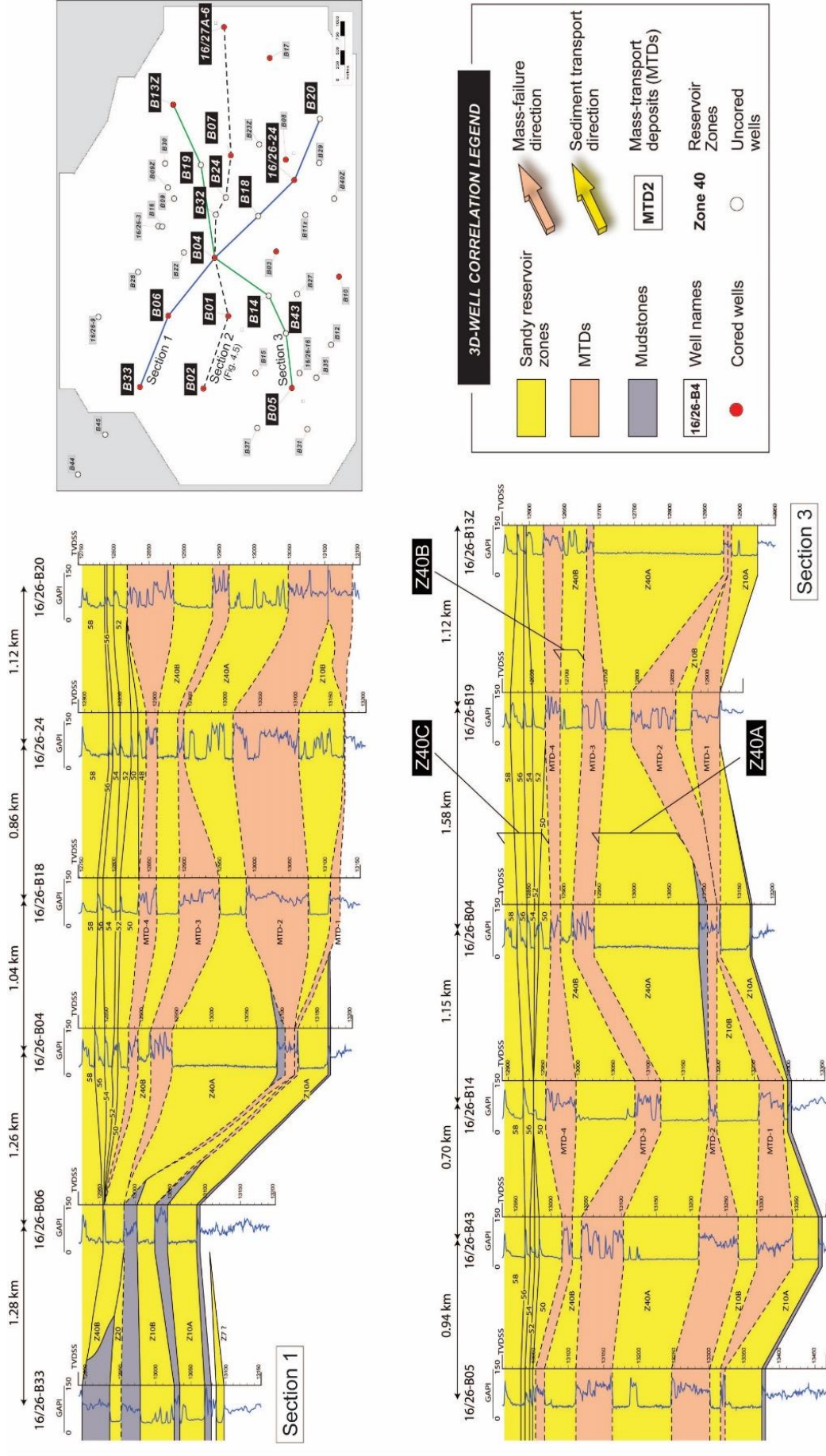


Fig. 4.7 – Correlations of the Lower and Middle Reservoir Section. Section lines and well positions are displayed on the map of the Platform Area (top right). Red dots represent cored wells, while white dots are un-cored wells. Section 1) North-to-south correlation panel. Section 3) West-to-east correlation panel.

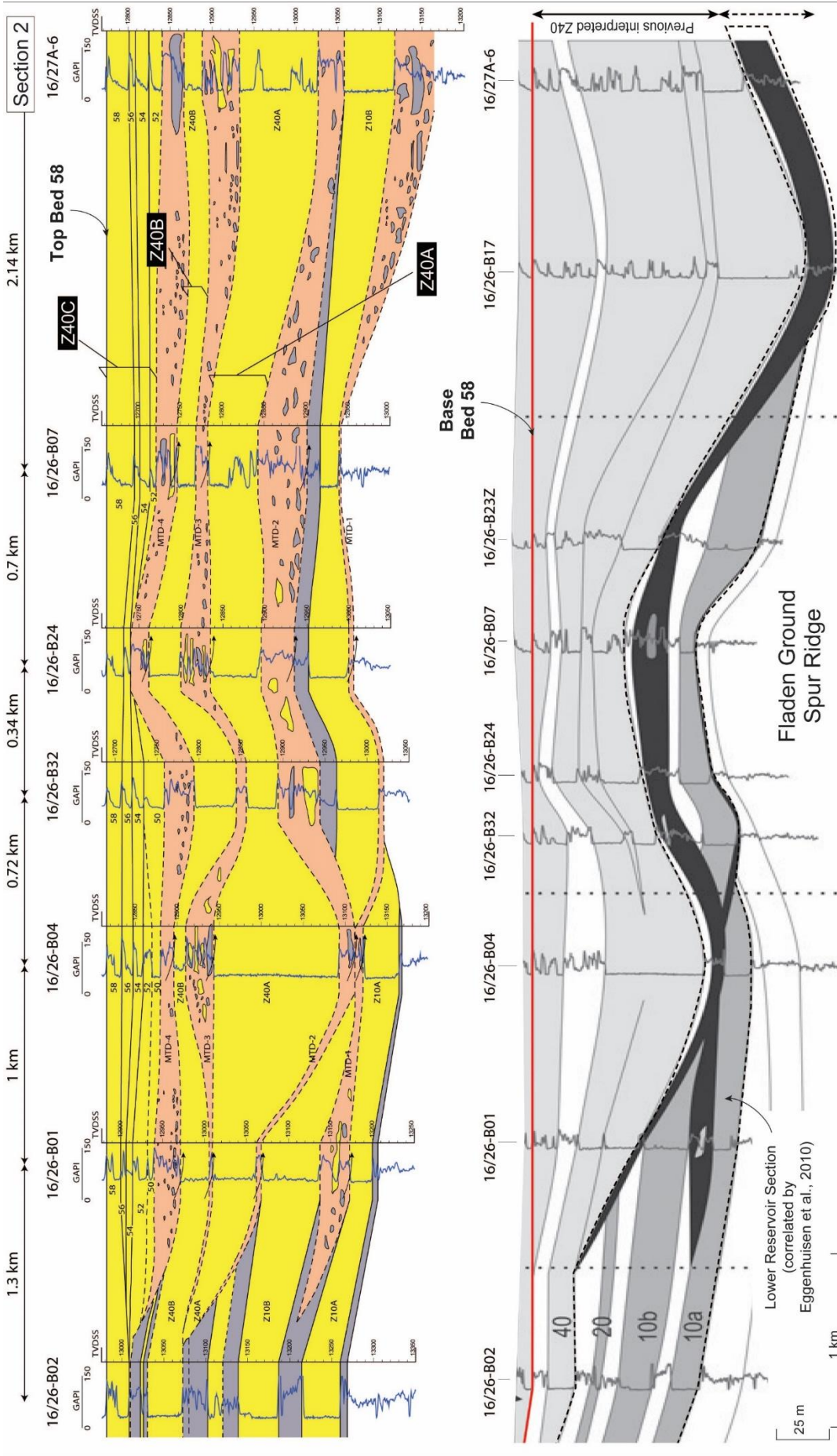


Fig. 4.8 – Comparison between earlier well correlation of the Lower-Middle Reservoir Section (below; Eggenhuisen et al., 2010), and new correlation (above; this work) along an east-to-west transect. The new analysis including all cored and uncored wells permitted to re-evaluate some of the correlations (e.g., well 16/27A-6). In addition, the identification and correlation of MTD-3 and MTD-4 allowed Z40 to be divided into three zones (Z40A-B-C), with the upper one being further divided into event beds. See map in Fig. 4.6 for the location of the section line.

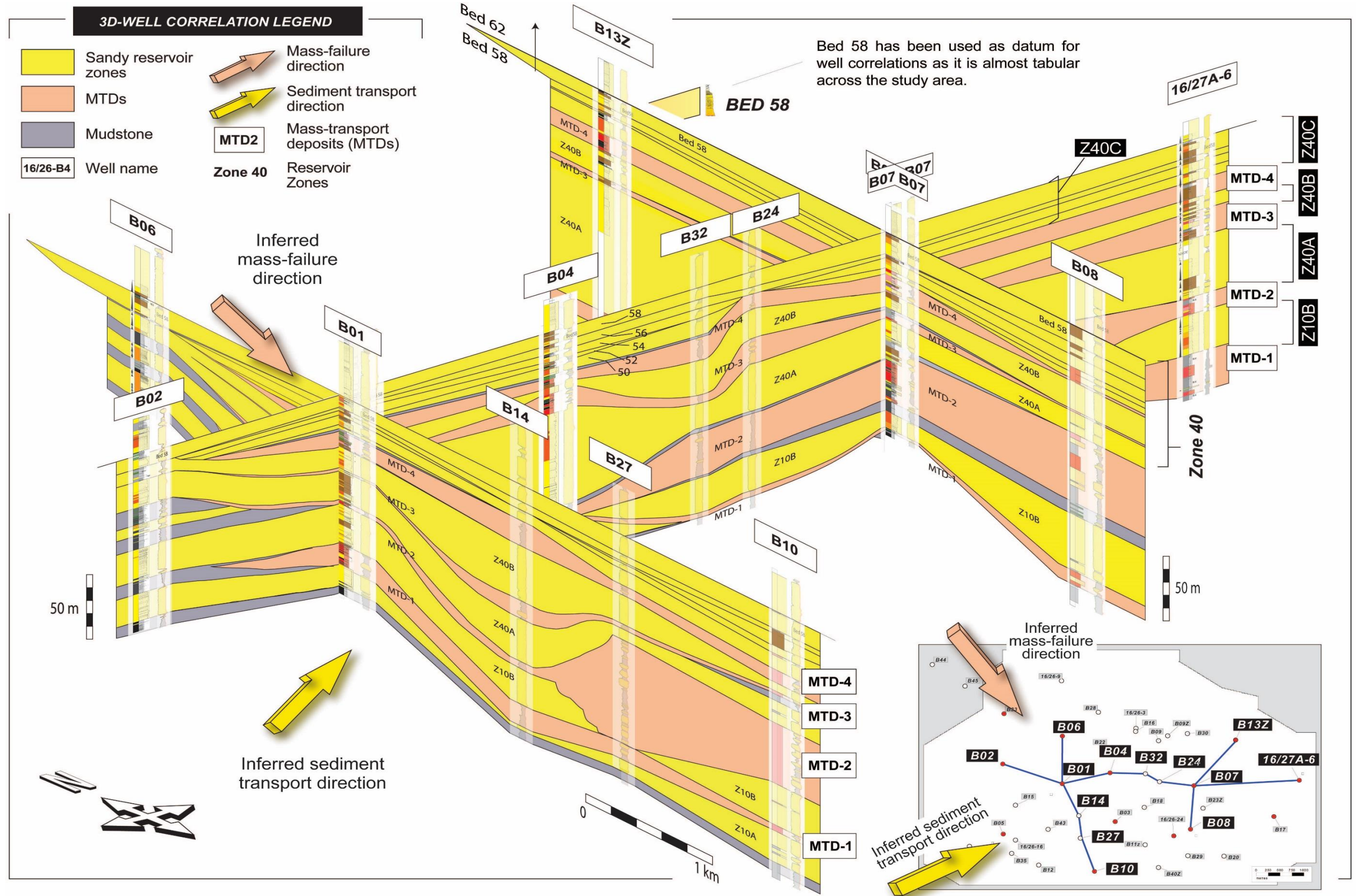


Fig. 4.9 - Fence diagram for the Lower and Middle Reservoir Section in the Platform Area. Section lines are shown on the inset map (bottom right). The diagram highlights the effects of large-scale remobilisation followed by the sandy infill of the evacuated topography. The Middle Reservoir Zone shows the highest degree of architectural complexity, characterised by units that are influenced by MTD-related bathymetry.

5 Architecture of the MTD-dominated BSF in the Platform Area

5.1 Introduction

Submarine landslides have been documented in many deep-water systems, thanks to improvements in seismic resolution (e.g., Eastern Mediterranean, Frey Martinez et al., 2005, Northwest European Atlantic, Evans et al., 2005; Brunei, McGilvery and Cook, 2003; Angola, Gee et al., 2006; Venezuela and Trinidad, Moscardelli et al., 2006). These deposits have been subject of intense study by the hydrocarbon exploration in recent years, because of their capacity to reshape the bathymetry of deep-water basins, creating new seascapes that can then influence the pathways taken by subsequent sediment gravity flows and the form of associated turbiditic reservoir sandstones (Brami et al., 2000; Armitage et al., 2009); such sandstone constitute the main exploration target for the oil industry (P Weimer and Slatt, 2006). Bathymetric features on the seafloor linked to the occurrence of large-scale failure events and the emplacement of associated mass-transport deposits (MTDs) might either trap or lead to enhanced bypass of sand-bearing gravity flows (Kneller et al., 2016). Thus, reconstruction of seafloor palaeobathymetries, as influenced by MTDs, is an important tool to investigate the link between large-scale failure and mass transport evolution, the resulting seascape morphology and prediction of the subsequent reservoir sandstone distribution. In subsurface studies, such reconstruction is best performed via a backstripping analysis of the deposits, which requires high resolution seismic data in order to reconstruct surfaces. Commonly, backstripping cannot be performed optimally due to low quality of seismic data, undermining the capacity to identify or interpret sand-bodies and/or hydrocarbon presence. In this case, alternative datasets (such as combinations of cored well and wireline log data) can be used. This is the case of the Aptian Britannia Sandstone deposits in the Central North Sea, whose evaluation necessitates a high dependence on the reconstruction of the geological model based on sedimentological characterisation to evaluate potential sweet spots within the play fairway (Hill and Palfrey, 2003; Sumner et al, 2005).

Palaeobathymetric surfaces corresponding to the base of BSF have been reconstructed by BOL (Britannia Operator Limited Internal Report) for the Britannia Field area and by Aas et al. (2010) for the Buchan Graben within the Outer Moray Firth, with the aim of studying the physiography of the basin before the emplacement

of sandstones in different areas, and the associated tectonic setting. Both studies were undertaken using a surface-based 3D model and stepwise backstripping, assuming 'Airy isostasy' or 'flexural Isostasy' of the post-Aptian overburden and removal of the post-depositional structural overprint based on gravity models. However, this methodology cannot be applied to the reconstruction of palaeobathymetric surfaces associated with several deformational processes, as recognised within the intra-BSF of the Platform Area (Guy, 1992; Lowe and Guy, 2000; Porter et al., 2000; Lowe et al., 2003; del Pino Sanchez, 2006; Barker, 2005; Eggenhuisen, 2009), compounded by the low seismic resolution at the reservoir scale (i.e. 10s - 100s of metres) (Sumner et al., 2005) and the limited area of study (~35 km²). Yet, this chapter aims to reconstruct palaeo-MTD-related topography using a core-based dataset from the Platform Area of the Britannia Field. Furthermore, the chapter attempts to map (through cored wells) and predict (at the inter-well scale) the distribution of mass-transport deposits (MTDs) and to identify the accommodation space that was available for turbidite reservoir sands, in order to better characterise reservoir properties.

The objectives of this study are:

- Identify key stratigraphic surfaces;
- Investigate the causes of internal reservoir heterogeneity through the choice of the appropriate modelling assumptions and by performing a decompaction and restoration analysis;
- Determine the gross evolution of the area in terms of the deformation style (regional sag vs. local tectonic effects);
- Constrain the scales of rugosity that may be developed on the upper surface of the MTDs;
- Relate the mass failure sequence to the associated reconstructed palaeobathymetry each failure left behind, and the associated form of the accommodation space for subsequent flows, and to
- Evaluate the implications of this areally-restricted study for the development of the BSF outside the Platform Area.

5.2 Geometry of the BSF in the Platform Area

Since the beginning of academic studies on the Britannia Field, correlated reservoir intervals have been documented and interpreted as having been structurally controlled (Jones et al., 1999b; Porter et al., 2000; Machell, 2003). Deformational processes analysed by Porter et al. (2000) presented the effects of large-scale remobilisation on core, but also identified fault sets across the Britannia Field, later confirmed by Hill and Palfrey (2003) using more recent seismic data (Fig. 5.2).

As introduced in Chapter 3, Eggenhuisen et al. (2010) showed that the Lower Reservoir Sections, Z10A, Z10B and Z20 (where preserved) are characterised by relatively constant thickness and hence represent a tabular architecture that was maintained until the emplacement of MTD-2. The same authors interpreted that these reservoir sandstones draped pre-existing basin topography (e.g., the Fladen Ground Spur), suggesting that sand was emplaced onto a subtle slope by very large flows in the early development of the system. However, northwest – southeast oriented correlation panels of the Lower and Middle Reservoir Section show that the top of the Middle Reservoir and the sands forming the base of the Lower Reservoir (Z10A and Z10B) are not parallel. When hanging the logs to the top of the Middle Reservoir (Bed 58), the Z10A and Z10B are deeper in wells that are located in the south of the study area (e.g., B01, B04 etc.) in comparison to those in the north (e.g., B33, B02, B06 etc.), implying that differential creation of accommodation space must have occurred during the deposition of the Lower and Middle Reservoir (Fig. 5.1). This created a characteristic wedge geometry, which thins towards the Fladen Ground Spur.

This Chapter applies several methodologies to investigate the wedge geometry of the BSF deposits and thus contribute to a better understanding of the BSF in the Platform Area, and on a broader scale in terms of stratigraphic and tectonic settings of the Central North Sea during the early Cretaceous.

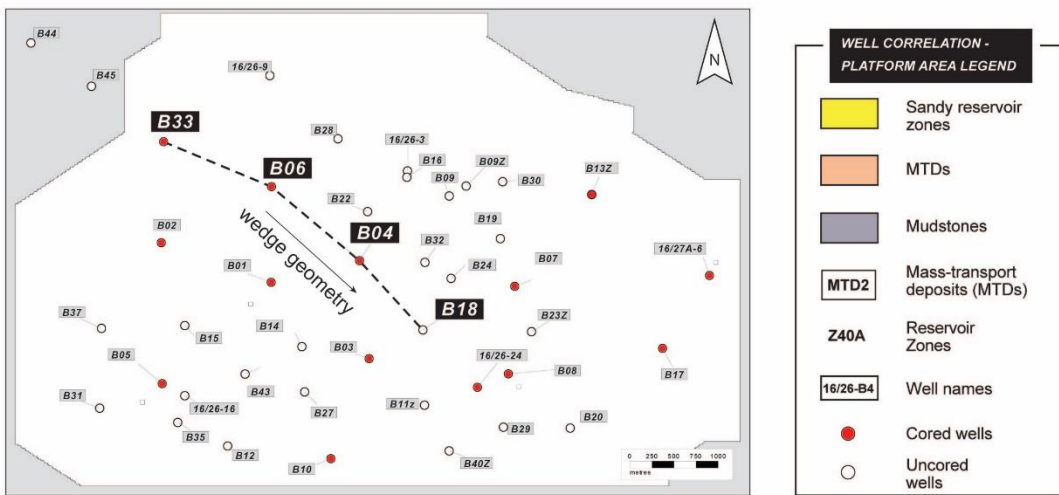
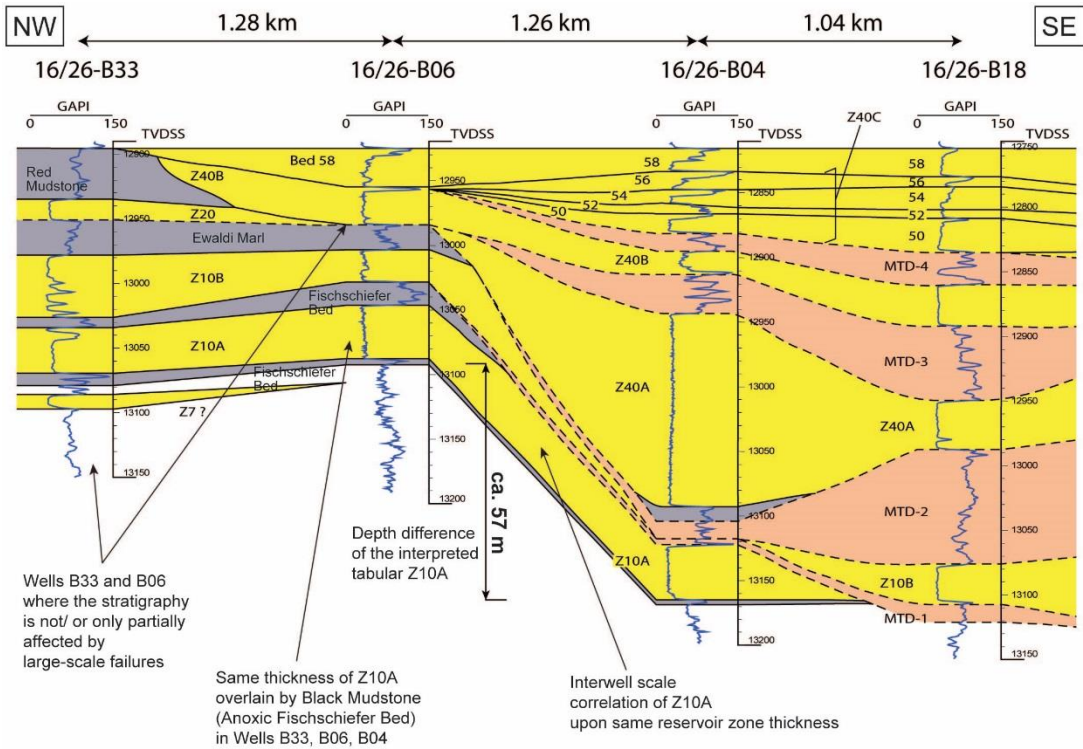


Fig. 5.1 – NW-SE – oriented cross section through the BSF in the Platform Area, showing the development of a wedge geometry that thins towards the north-west of the deposits of the Lower and Middle Reservoir Section.

5.3 Investigation of the origin of the wedge geometry

This section aims to evaluate causes of the wedge geometry that characterises the deposits of the Lower and Middle Reservoir Section, between the lowermost reservoir sandstones of Z10A and the assumed palaeo-horizontal datum Bed 58, as shown in Fig. 5.1. The role of sediment compaction within the above mentioned reservoir sections and below the BSF, within the underlying Valhall Shales will be investigated.

The hypothesis that differential compaction may have played a significant role in creating the wedge geometry thinning towards the north of the study area arose through recognition of the different lithologies in cored wells and, by inference, in wireline logs making up the Lower and Middle Reservoir Section (Tables 4.2 and 4.3). The main deposits recognised in this portion of the reservoir comprise sandstones (characterised by different matrix clay content), hemipelagic mudstones and MTDs (characterised by the presence of a muddy matrix, with or without floating sand grains). In addition, spatial variations in their relative distribution should be considered. In fact, relatively thick mudstone intervals are mainly recognised in the north of the study area, where wells B33, B02 and B06 show the complete lower and middle stratigraphic sequence of the BSF. Decompaction analysis on these deposits might explain their relatively reduced thickness in comparison with the thicker correlative reservoir sandstones in adjacent Wells B01 and B04. A priori, it is thought that the stratigraphy in the north of the study area might decompact to a thickness greater than a factor of two than the decompact thickness of the deposits of the central and south Platform Area. A further decompaction investigation will necessarily involve the deposits underlying the BSF down to the Base Cretaceous Unconformity (BCU), which are characterised by different interval thickness under the Platform Area. Although differential compaction may have influenced these deposits, it is unclear when the compaction took place and if it contributed to the development of the wedge geometry of the reservoir architecture of the BSF.

Finally, if sediment decompaction alone could not explain the wedge geometry, a mechanism involving active deformation during the deposition of the BSF, due to fault movement under the Platform Area, passive tilting at a larger scale, or both must be considered. Seismic data show that structural features were already present within the BSF under the study area (Fig. 5.3). However, it is not clear if these structures were active during BSF time so as to have played a major role in the creation of accommodation space across the PA.

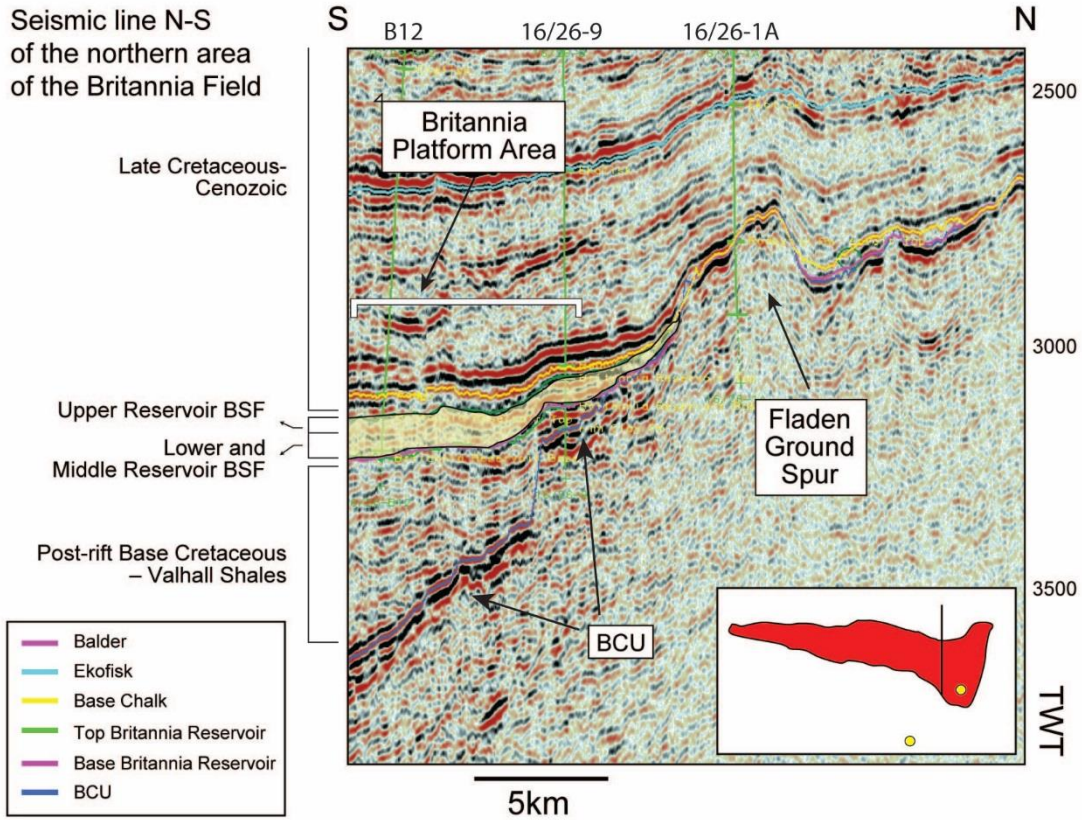


Fig. 5.2 – Seismic profile of the northern portion of the Witch Ground Graben across the Platform Area of the Britannia Field (seismic image from Wilson, 2009).

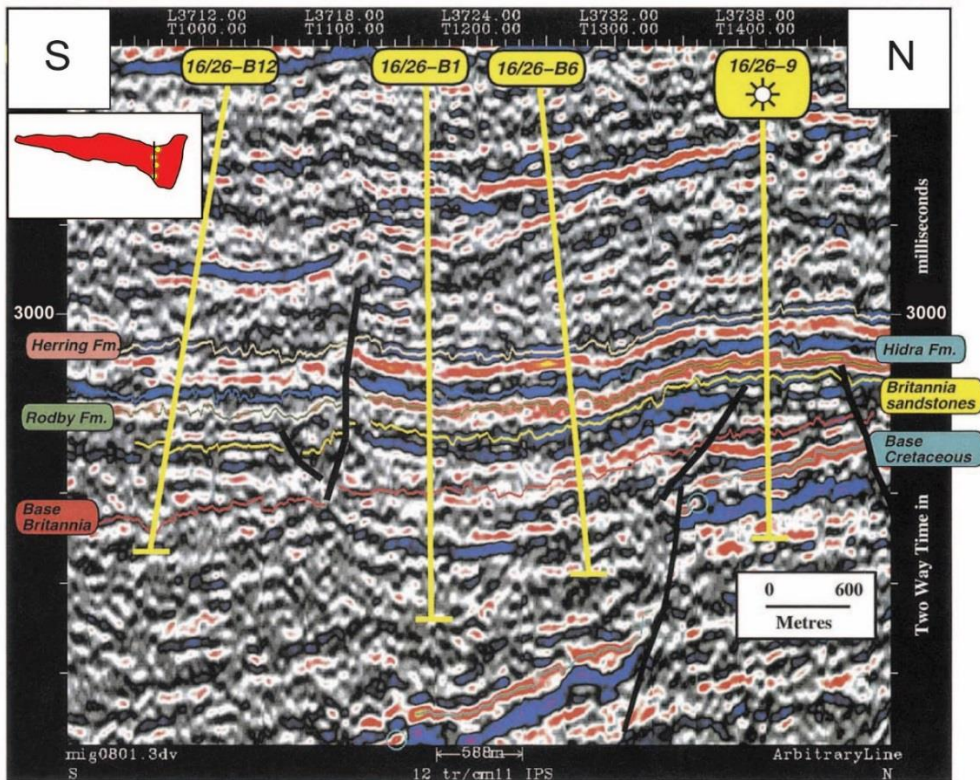


Fig. 5.3 – North-south seismic line across the flank of the Fladen Ground Spur under the Platform Area. The seismic data with dominant frequency of approx. 30 Hz limits vertical resolution to about 80 ft (Hill and Palfrey, 2003).

5.3.1 Assumptions and boundary conditions for palaeobathymetric modelling

Several mechanisms have been postulated to explain the high degree of subsidence characterising the syn- and post-rift phase of many extensional basins such as cooling following lithospheric thinning (thermal subsidence) and creeping of ductile lower crust (Bott, 1980). The latter is mostly associated with an advanced phase in the formation of oceanic crust and the unequal topographic loading across a passive margin. This is not the case in the Central North Sea, where the subsidence is mainly related to thermal relaxation of the lithosphere following upwelling of the asthenosphere, accompanied by extensive volcanisms and a subsequent cooling phase (McKenzie, 1978; Royden et al., 1980; Royden and Keen, 1980; Allen and Allen, 1990); this is recognised at the 'triple-junction' (White and Latin, 1993) and at the Fisher Bank Basin (Clark et al., 1993) where the Britannia Field lies (Chapter 3). Subsidence might also be caused by sediment loading, calculated by Bott (1980) as being on the order of roughly two to three times the initial water depth, although this mechanism alone is inadequate to explain the creation of deep accommodation space (Allen and Allen, 1990).

The aim of this work is to reconstruct the morphology of the seafloor shaped by the occurrence of large-failure events. In order to achieve this aim a series of considerations and assumptions to simplify the modelling approach are made:

- The Britannia Field is bounded at the base and top by two continuous tabular sand intervals: Z10A and Z50. These are interpreted to represent sand deposition upon an essentially flat basin floor and hence to be paleohorizontal datums. Of course, this assumption is reliable only over the relatively small study area.
- The Britannia Field contains horizons that represent time-stratigraphic markers (mudstones, sandstone beds and MTDs). They are used for well correlation and to differentiate three reservoir intervals in the Platform Area: the Lower and Middle Reservoir Sections (i.e., the main focus of this study), occurring up to the datum Bed 58 and the Upper Reservoir Section, above Bed 58, previously studied by Barker et al. (2008) and included in this study to enable a comprehensive analysis of the geological evolution of the Britannia Sandstone in the Platform Area.
- Debritic intervals are interpreted as deposits of large-scale mass failure events which occur episodically and are responsible for shaping the seafloor through erosion and deposition in the Platform Area. The sandstones on top of these debritic intervals are able to smooth and heal topographic rugosity associated with the MTDs, restoring sub-horizontal conditions on the seafloor.

5.3.2 Decompaction of the BSF to investigate differential compaction within the Lower-Middle Reservoir Section (Z10A-B58) in the PA

Decompaction analysis entails the calculation of each sedimentary unit's thickness at the time of deposition. Different lithologies commonly have different porosity, pore shapes, and mineral matrix compositions that may have different responses to burial. Lateral changes in lithology give rise to lateral changes in compaction, or simply "differential compaction", once buried. For this reason, surface maps created using undecompressed deposit thicknesses might not show their original geometries at time of deposition. Recognition of differential compaction effects is a key technique in modern seismic geomorphology (e.g., Chopra and Marfurt, 2012). In order to understand the creation of accommodation space that occurred between the deposition of the palaeo-horizontal datums Z10A and Bed 58 for the Lower and Middle reservoirs and for the base of Z45 and the ash layer capping the Z50 in the Upper reservoir and differentiate this from differential compaction effects, a decompaction analysis of the deposits is necessary. The workflow can be detailed as follow:

1st STEP – Choice and description of the formula to decompact reservoir intervals.

2nd STEP – Selection of the values for *initial porosity* (φ) and *compaction factor* (c) for sand and mud.

3th STEP – Determination of the intervals upon which to perform the analysis, and their present day (compacted) interval thicknesses.

4th STEP – Calculation of the net/gross of each of the selected intervals

5th STEP – Decompaction of the reservoir intervals for the average middle point of the total thickness of Britannia reservoir calculated for all wells of the Platform Area.

5.3.2.1 Decompaction equation (STEP 1)

Decompaction requires the variation of porosity with depth to be known. Porosity-depth curves of sandstone and mudstones observed from sonic logs show that there is an exponential relationship between porosity and depth (1) first noted by Athy (1930) for shales:

$$\varphi = \varphi_0 e^{-cy} \quad (1)$$

where φ is the porosity at any depth y , φ_0 is the surface porosity and c is a coefficient that is dependent on lithology and prescribes the rate at which the exponential decrease in porosity takes place with depth (Allen and Allen, 1990).

To calculate the thickness of a sediment layer at any time in the past, it is necessary to calculate where it may have been located along an appropriate porosity-depth

curve at that time. This is equivalent to sequentially removing overlying sediment layers and assessing the thickness of the layer of interest prior to the last phase of decompaction.

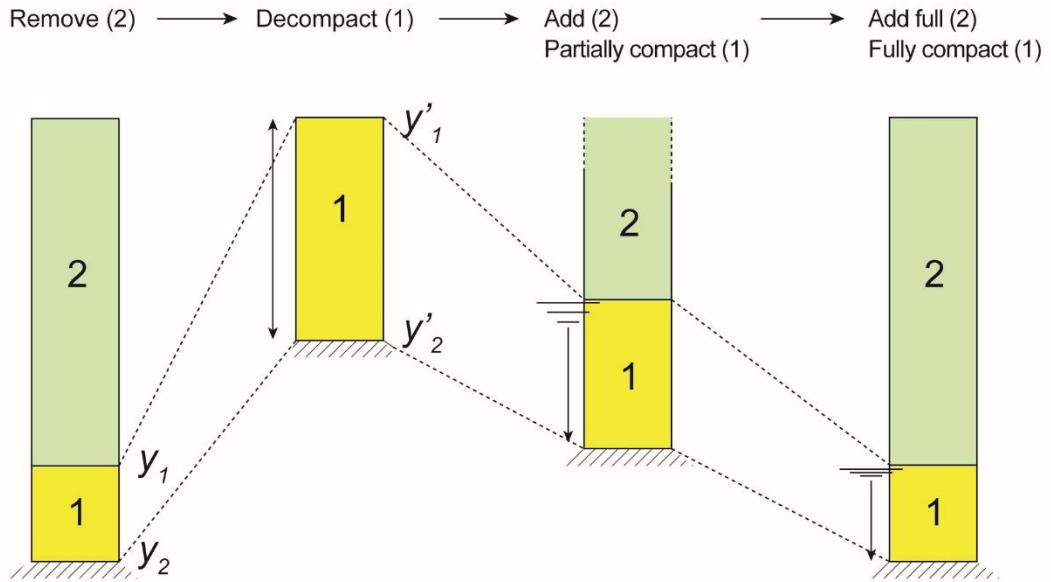


Fig. 5.4 – Concept of the successive stages in a decompaction exercise (modified after Allen and Allen, 1990).

To apply this methodology to compacted deposits the mass is assumed constant and only changes in volume (and therefore thickness) are considered. The total thickness of the sediment layer represents the volume due to pore-filling water and the volume of the sediment grains. On decompaction the sediment volume remains the same, only the volume of water expands. If a sediment layer at present depths of y_1 and y_2 (top and base) is moved vertically to new shallower depths y'_1 and y'_2 (Fig. 5.4), the decompacted thickness of the sediment layer is the sum of the thickness due to the sediment grains and that due to the water, which is calculated as

$$(y'_2 - y'_1) = (y_2 - y_1) - \frac{\varphi_0}{c} \{(\exp(-cy_1) - (\exp(-cy_2)))\} + \frac{\varphi_0}{c} \{(\exp(-cy'_1) - (\exp(-cy'_2)))\} \quad (2)$$

where the equation can be resolved as if $y'_1 = 0$

$$y'_2 = (y_2 - y_1) - \frac{\varphi_0}{c} \{(\exp(-cy_1) - (\exp(-cy_2)))\} + \frac{\varphi_0}{c} \{(1 - \exp(-cy'_2))\} \quad (3)$$

However, it should be noted that present-day thicknesses and depths of stratigraphic units are expressed in relation to a present-day datum, normally taken as the mean sea level. Thus, the depth of the sea, measured from the mean sea level and the

mudline on present seafloor, has to be subtracted from the absolute depths of the interval units measured in the wells.

5.3.2.2 Selection of the values for initial porosity (ϕ) and compaction factor (c) for sand and mud (STEP 2)

The decompaction equation is based on the compressibility of a rock volume during burial and hence is a function of initial porosity at the surface (ϕ_0) and a compaction factor (c) of the lithologies that make up the deposit. The lithologies used in the decompaction equation were differentiated into *sands* and *shales*, to which were assigned initial porosity (ϕ_0) and compaction factors (c).

The initial porosity (ϕ) and compaction factor (C_f) of *shales* were selected upon values of compaction of North Sea shales (Table 5.1) calculated by Sclater and Christie (1980) and based on a curve computed by taking the observed normal pressure sonic log plots of Schlumberger (1974) and the porosity/sonic log velocity relation of Magara (1976). This is based on the assumption that shales in the North Sea have a porosity of 63% near the surface (Schlumberger Limited, 1974). This value is also confirmed by Hansen (1996) who established the relationship between transit time and porosity for shales on the Norwegian Shelf.

Lithology	Shale	<i>Sandstone</i>
Initial porosity (ϕ)	0.63	0.49
Compaction factor (C_f)	0.51	0.271

Table 5.1 – Initial porosities and compaction factors used for various modelled lithologies in the North Sea basin, from Sclater and Chistie (1980).

The choice of initial porosity (ϕ_0) and compaction factor (c) for the *sands* requires more consideration. This is due to a higher concentration of observational data on the relation between porosity and depth: Maxwell (1964) and Selley (1978) suggest a linear relationship for the porosity and depth of sandstone whereas Atwater and Miller (1965) and Pryor (1973) describe an exponential decrease of porosity with depth. The exponential relation is also supported by Sclater and Christie's work (1980) which show an excellent match between their values based on Pryor's (1973) data at the surface and the mean porosity values published by Maxwell (1964). However, Pryor's initial porosity of 49% ($\phi=0.49$) for sands is considered too high for this study; such value might represent sand grains that are still suspended in water. Spheres of a single size in random close packing attain a maximum density of ~64% and hence a porosity of ~36%. When grains are deposited directly from suspension,

they may be in a "random loose packing" with higher porosities of c. 42%. However, sands deposited with such porosities will re-organise immediately after or even during deposition by pre-burial dewatering due to the weight of the sand grains on top of the bed (Butler et al., 2015); upper values for sand porosity in lab experiments may reach 42%, but such deposits liquefy, dewater, and compact immediately during the experiment. An alternative approach to constrain the choice of initial porosity (ϕ_0) for sands was proposed by Bear and Weyl (1973) who investigated the relationship between porosity, permeability and texture for artificially mixed and packed sands (comprising eight grain-size subclasses and six sorting groups). Following this methodology, the mean sorting/grain size of a compacted sand can be used to yield an appropriate near-surface porosity. Britannia sand values were derived following core-based visual grain size estimation using a grain size comparator, which established a grain size range from fine-upper (0.0177 - 0.025 cm) to medium-lower (0.025 - 0.035 cm) and sorting from moderately sorted (0.71 to 1.0 phi) to well sorted (0.35 to 0.50 phi). The investigated wells typically show a relationship between finer sand and better sorting, therefore two values for sands were selected from the Bear and Weyl's (1973) table of porosity of artificially mixed wet-packed sand (Table 5.2).

Sorting/ Grain size	<i>csU</i>	<i>csL</i>	<i>msU</i>	<i>msL</i>	<i>fsU</i>	<i>fsL</i>	<i>vfsU</i>	<i>vfsL</i>
<i>ews</i>	43.1	42.8	41.7	41.3	41.3	43.5	42.3	43.0
<i>vws</i>	40.8	41.5	40.2	40.2	39.8	40.8	41.2	41.8
<i>ws</i>	38.0	38.4	38.1	38.8	39.1	39.7	40.2	39.8
<i>ms</i>	32.4	33.3	34.2	34.9	33.9	34.3	35.6	33.1
<i>ps</i>	27.1	29.8	31.5	31.3	30.4	31.0	30.5	34.2
<i>vps</i>	28.6	25.2	25.8	23.4	28.5	29.0	30.1	32.6

Table 5.2 – Porosity (%) of artificially mixed wet-packed sand (after Bear and Weyl, 1973). Porosity is insensitive to grain size, but critically controlled by grain sorting. Sorting column: (*vps*) very poorly sorted; (*ps*) poorly sorted; (*ms*) medium sorted; (*ws*) well sorted; (*vws*) very well sorted; (*ews*) extremely well sorted. Grain size row: (*csU*) coarse sand upper; (*csL*) coarse sand lower; (*msU*) medium sand upper; (*msL*) medium sand lower; (*fsU*) fine sand upper; (*fsL*) fine sand lower; (*vfsU*) very fine sand upper; (*vfsL*) very fine sand lower.

5.3.2.3 Calculation of the reservoir interval thicknesses (STEP 3).

The thicknesses of the Britannia Field reservoir intervals (identified on cored-wells and wire line data for uncored-wells) were calculated upon the difference between the absolute depths of base and top of each interval (Appendix A). All the values contained in the Britannia Field database (provided by BOL) consist are in the form

TVDSS (True Vertical Depth Sub Sea), measured from mean sea level. These measurements have therefore been corrected for well-deviation; for simplicity these values were converted from feet (ft) into metres (m) (Appendix A).

5.3.2.4 Calculation of the net/gross for the reservoir intervals (STEP 4)

In order to calculate the net/gross of intervals the identification of the lithologies making up the BSF is required. Through core inspection five main lithologies were distinguished: sandstone, mixed sandstone/mudstone, sandy and muddy debrite and mudstone. Each of these lithotypes was assigned a value between 1 and 0, corresponding to their proportion of sand, in which sand and mud are 1 and 0, respectively (Table 5.3).

Lithology	Sandstone	Mixed Sand/ Mud	Sandy Debrite	Muddy Debrite	Mudstone
Sand proportion	1	0.7	0.3	0.1	0

Table 5.3 – Sand proportion assigned to the lithologies in the Britannia Field reservoir

The presence of both cored- and uncored-wells required the development of two different methodologies in order to calculate the net/gross of each reservoir interval.

These are based on the:

- i. Identification of the lithofacies making up each reservoir interval through core-inspection;
- ii. Investigation of gamma-ray logs for un-cored wells combined with cuttings data (see Chapter 4).

5.3.2.5 Decomposition of the reservoir intervals for the average middle point of the total thickness of Britannia reservoir calculated for all wells of the Platform Area (STEP 5)

The selected reservoir intervals identified in each Platform Area well, were multiplied by the appropriate sand and mud decompaction coefficients (shown in Appendix C) prior to decompaction using formula (3). Although decompaction analysis should be conducted layer-by-layer for the intervals making up the reservoir, in this case a simpler spreadsheet-based decompaction analysis using Equation 3 (above) was undertaken, which did not take into account any correction in the decompacted thickness due to sediment loading within the interval. However, the errors introduced are small; e.g., in well B04 the full decompacted thickness was overestimated by 5 metres (2.8%) (see Appendix C). Therefore, reservoir intervals were decompacted for the average middle point of the total thickness of the Britannia reservoir measured in all wells of the Platform Area.

5.3.3 Decompaction of Valhall Shales below BSF in the PA

The approach described above is used to decompact the deposits beneath the BSF of the Platform Area, and above the BCU, which consist of interbedded marls and shales of the Valhall Shales. This is because the compaction of these deposits of different thickness (Fig. 5.5) may have contributed to the creation of accommodation space which resulted in the wedge geometry that characterises the northern sector of the study area. The investigation of the role that differential compaction may have played in shaping the base of BSF is also useful to test some of the assumptions introduced in section 5.3.1. In fact, the tabular character of Z10A led to the inference that sands making up this interval were deposited over a sub-horizontal basin floor, characterised by only local bathymetric rugosity, and thus, significant compaction of the underlying Valhall Shales had to have already happened before the emplacement of Z10A. However, the deposits of the large flows interpreted to have characterised the early development of the BSF system might have increased the compaction of the underlying deposits leading to a further and constant creation of accommodation space in the study area.

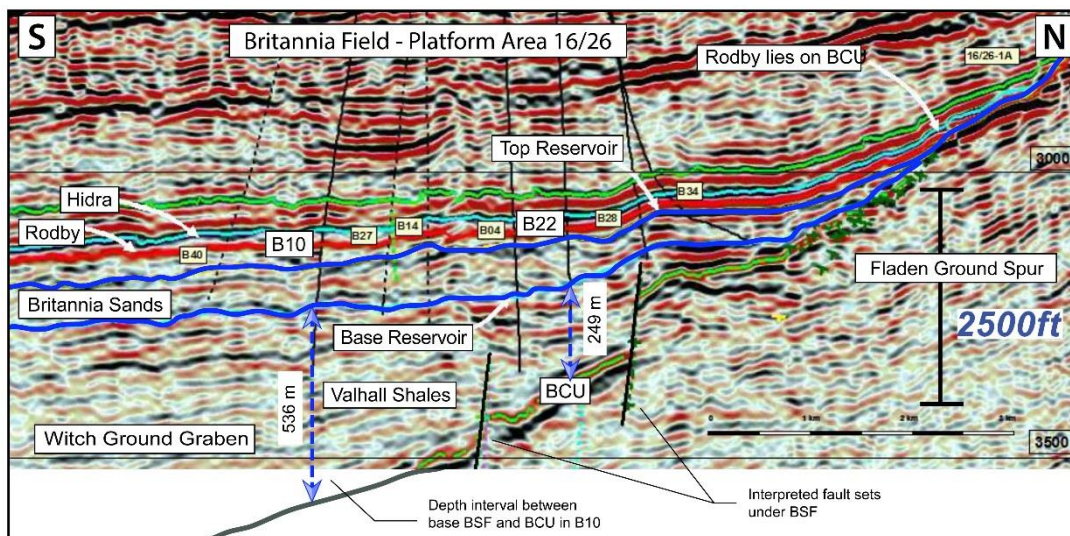


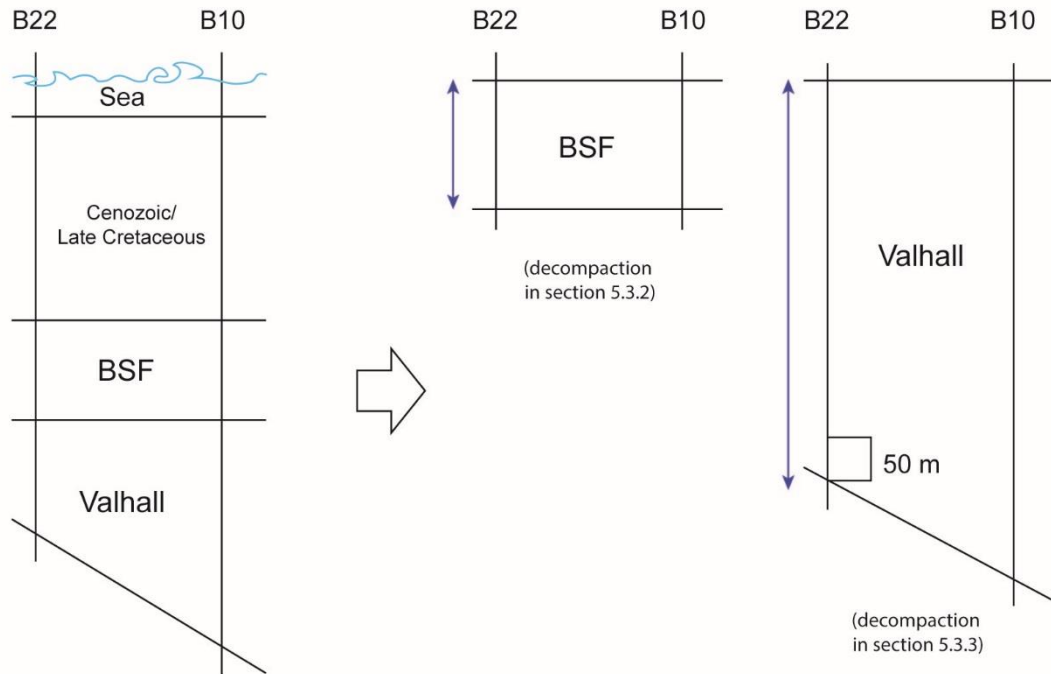
Fig. 5.5 – Seismic profile across the Platform Area calibrated with wells towards a north-to-south line. (seismic image from Archer, 2002). The BCU = the Base Cretaceous Unconformity.

A decompaction analysis to address this question was undertaken in two key wells, located respectively in the northern (B22) and in the southern (B10) portion of the study area. This allowed to calculate the differential creation of accommodation space between the north and south of the Platform Area (Fig. 5.5), related to the compaction of the deposits between the BCU and the base of BSF during the time of the Lower and Middle Britannia deposition. Direct measurements of the thickness of the Valhall Shales from wells was not possible in this interval as wells extend only a

few metres beneath the lowermost reservoir sandstones. The thickness of the Valhall Shales under wells B22 and B10 were thus calculated from seismic data (BOL database in ODM). The thickness interval between the BCU surface and the base of Z10A under B22 is ~249 metres, whereas the same interval under B10 is ~563 metres thick, confirming the current wedge geometry of these deposits.

Following the same methodology adopted to decompact BSF in the Platform Area, the Valhall Shales interval was decompact multiplying the selected interval thickness for the appropriate mud decompaction coefficient prior to decompaction using equation (3). The mud decompaction coefficient was calculated by using the inverse function of the decompaction equation (3) as described in the previous section for the deposits of the BSF (full explanation in Appendix C). In this case the specific decompaction coefficient for mud was calculated for the entire Valhall Shales interval.

Although decompaction analysis should be conducted layer-by-layer for the intervals, in this case a simpler spreadsheet-based decompaction analysis using Equation 3 (above) was undertaken, which did not take into account any correction in the decompact thickness due to sediment loading within the interval.



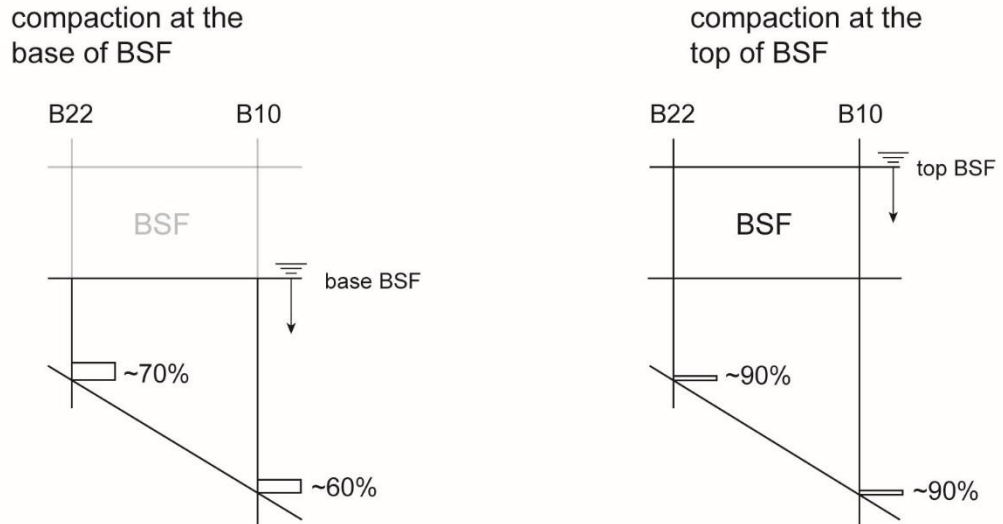
1. Decompaction

Fig. 5.6 – Sketch of the methodology used to decompact the Valhall Shales interval. The column on the left hand side shows the stratigraphic intervals above the Valhall Shales removed to fully decompact their deposits. On the right hand side the decompact BSF shown in section 5.3.2 and the Valhall Shales decompact in this section.

In order to better evaluate the role of differential compaction occurred in the deposits under the BSF during different time intervals, the Valhall Shales were decompacted respectively at the top and base of the BSF. This allowed to distinguish the amount of compaction that occurred prior deposition of the BSF from the compaction that occurred during deposition of the BSF. The calculation of the compaction of the Valhall Shales due to the load of the BSF requires a partial re-compaction of the previously decompacted shale deposits using the inverse function of the decompaction equation (3). The decompaction “window” was chosen to calculate an upper limit to the possible compaction that occurred during BSF time and corresponded to an interval of 50 metres at the bottom of the studied interval (Fig. 5.6 and 5.7). In fact, the choice of any other interval would have resulted in a smaller value for the calculated compaction. This method also assumes that compaction within the Valhall Shales did not take place before the emplacement of the BSF. This simplification also results in an upper limit for the differential compaction that occurred under the BSF (i.e. if the simplification was not applied, then the amount of compaction would be less).

The re-compaction exercise at the base of the BSF (i.e. highlighting compaction during the deposition of the Valhall Shales) shows that the thickness of the investigated “model” interval of 50 m thick was compacted to ~74% of its original thickness under B22 and to ~60% under B10. This are maximum values hence the actual values (and the difference between the two wells) was likely smaller.

In the second case, where compaction analysis was considered at the top of the BSF, both chosen “model” intervals of 50 metres placed at the bottom of the studied interval show compaction trends to around 90% of their original thickness (Fig. 5.7). The implications of this exercise are discussed in Section 5.3.4, below.



2. Partial-compaction

Fig. 5.7 – Models that show the partial re-compaction of Valhall Shales at the base of BSF, under its own weight (left hand side), and at the top of BSF (right hand side), due to the BSF load. Percentages represent compacted thickness of the investigated “model” interval of 50 metres thick, placed at the bottom of the Valhall Shales, under Wells B22 and B10, respectively after the deposition of the Valhall Shales (left hand side) and during BSF time (right hand side).

5.3.4 Causes of the creation of the wedge geometry of the Lower and Middle Reservoir in the PA

The decompaction analysis undertaken for the deposits of the BSF and for the Valhall Shales showed that the wedge geometry of the Lower and Middle Reservoir cannot be fully explained as a consequence of the differential compaction of the deposits making up these intervals. This is supported by the results of the decompaction exercise between two wells that were selected to compare deposits respectively for the north (B22) and south (B10) of the Platform Area (Fig. 5.8). In fact, the fully decompacted thickness difference between the two wells is ~75 metres, but only ~58 metres can be accounted to differential compaction during Valhall Shales and BSF time. It must be added that this value of 58 metres has been obtained through a series of approximations – all converging to produce a “maximum” value; hence the actual value must be smaller than that.

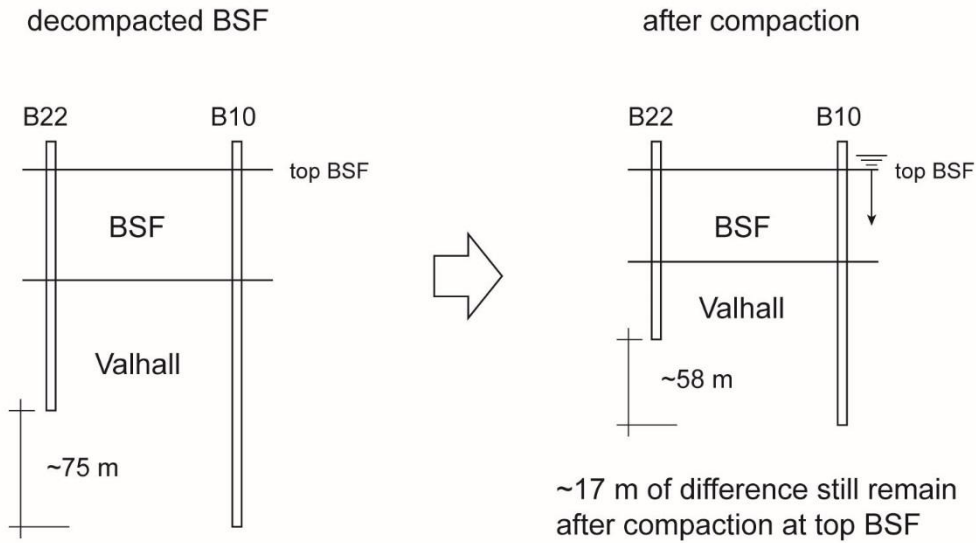


Fig. 5.8 – Comparison between fully decompacted deposits of the BSF and the Valhall Shales, and the partial compaction of sediments of the BSF and Valhall Shales at the top of the BSF. The difference between the fully decompacted intervals in B22 and B10 and the re-compacted deposits in the same wells is around ~17 metres that cannot be explained invoking differential compaction alone.

Although some uncertainty remains regarding the reliability of the reverse function of the formula (3) at shallow depths (see also Appendix C), if we assume a flat basin floor at Z10A and Bed 58 deposition time, it follows that a thickness difference of >17 metres between the two selected wells still needs to be accounted for as it cannot be fully explained by differential compaction of either the deposits of the BSF or the underlying deposits of the Valhall Shales (Fig. 5.9).

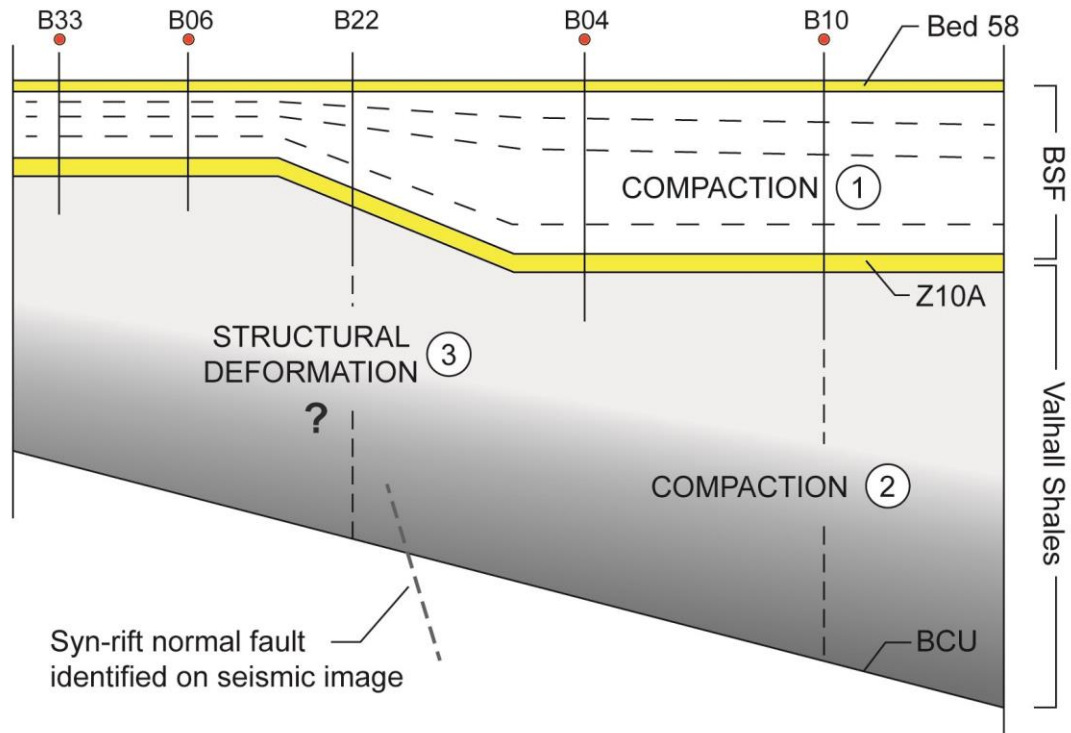


Fig. 5.9 – Schematic model showing the creation of accommodation space within the Lower and Middle Reservoir Section and the analysis undertaken to identify possible differential compaction effects. The decompaction analysis undertaken highlighted that structural deformation might have been active. The inferred fault segments across the study area were earlier noted by Porter et al., 2000 and by Hill and Palfrey, 2003 on seismic images.

Therefore, in addition to differential compaction of underlying or of recently deposited sediment, three different additional mechanisms can be invoked to be responsible for the creation of the space for sediment deposition in the Platform Area: type 0, subsidence at the sub-regional level during the rifting phase (i.e. Jackson and Larsen, 2008), which may be associated with local rotation and tectonic effects (type 1) and at a smaller scale with local evacuation due to MTD effects (type 2).

The partitioning of the structural deformation through time, from the Lower Cretaceous to the present day seafloor, in the Platform Area was not possible due to the lack of good quality seismic data for the Britannia Field interval. However, the decompacted and restored deposits of the Lower-Middle and Upper Reservoir, together with isopach maps of stratigraphic interval thicknesses above and below the BSF, are used to improve the understanding of the evolution of the BSF depositional system. The aim is to differentiate potential syn- and post-depositional structural deformations, drawing upon the broader area analysis of the Central North Sea and the Triple Junction (Fig. 5.10) as reviewed in Chapter 3. Four isopach maps (Fig. 5.10) of the four rock volumes identified in the stratigraphic interval of the Lower Cretaceous-Quaternary in the Platform Area (see Chapter 3), were contoured and

compared (Fig. 5.11). The structural maps of the units above and below the Britannia Field were made without decompacting the deposits, and considered as lithologically homogeneous and thus any potential lateral variation in lithofacies and hence compaction effects were ignored (further work would be difficult without more well data that could better constrain these deposits). In fact, decompaction analysis for these intervals can be ignored as it is assumed that the seafloor was flat at the time of the first Britannia sand input (Z10A) and during the last sandstone bed deposition (Bed 86 on top of Z50), confirmed by the regular thickness distribution of Z10A and Bed 86 across the Platform Area. Also, it is assumed that the highest rate of compaction is registered during deposition of the first few hundreds of meters of sediment although shale compaction may have continued after the deposition of the Z10A interval. These intervals are respectively the Late Cretaceous-Cenozoic deposits between the present-day basin floor and the top of the BSF (Fig. 5.11-D) and the Early Cretaceous (Ryazanian-Early Aptian) Valhall Shales, which is the interval between the Base Cretaceous Unconformity (BCU) and the base of BSF (Fig. 5.11-A). However, the Lower-Middle (Fig. 5.11-B) and Upper Reservoir Section of the Britannia deposits (Fig. 5.11-C), were contoured using decompacted reservoir intervals in order to differentiate structural from differential compaction effects. These stratigraphic intervals are separated using the palaeo-datum Bed 58 and Z10A and top Z50 (bed 86) where these bound the base and top of the BSF, with all the three datums representing sub-horizontal depositional conditions at different times during the emplacement of the BSF. Particular attention is given to the isopach map of the Lower-Middle Reservoir where four large-scale failure events (MTD-1 to 4) of the six MTDs recognised within the Britannia Field, are described and discussed below (see section 5.5).

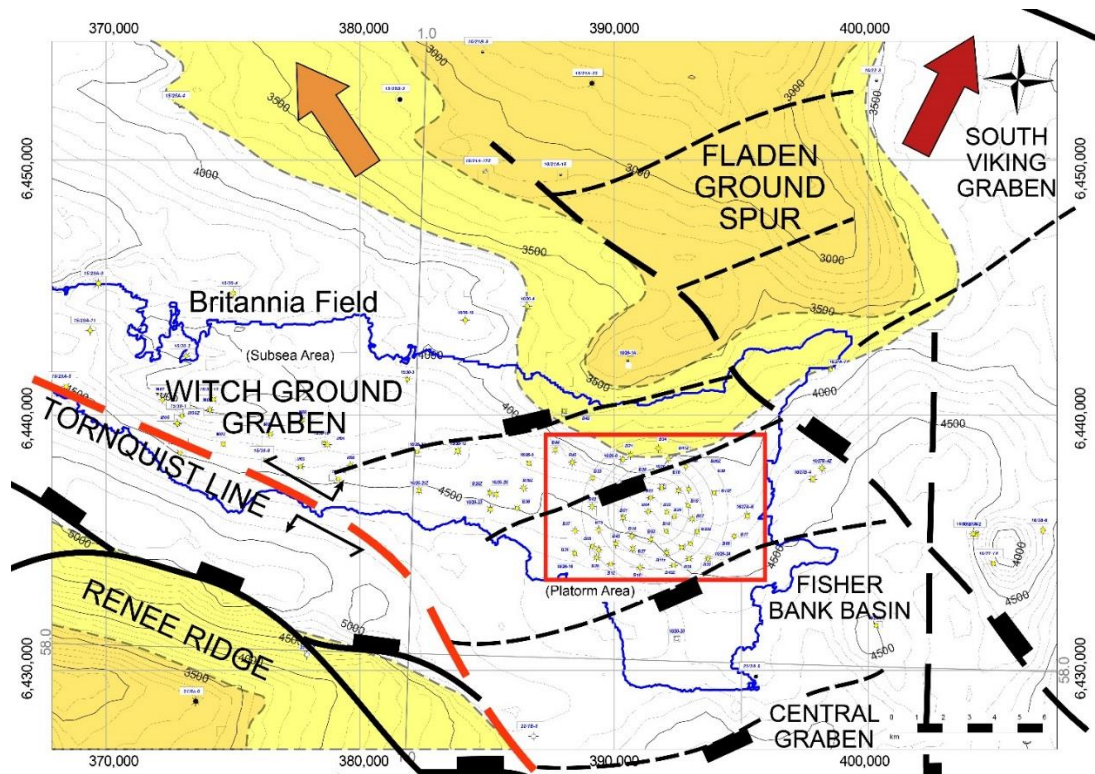


Fig. 5.10 – Isopach map showing the main structural features around the Platform Area. The red box represents the study area and contours show the Base Cretaceous Unconformity underneath the BSF (modified after Jones et al., 1999; Machell, 2003).

5.3.4.1 Early Cretaceous Valhall Shales - Under Britannia (Fig. 5.11-A)

Description (BCU-Base BSF)

The isopach map of Early Cretaceous Valhall Shales, underneath the Britannia Sandstone Fm., is contoured measuring the vertical depth between the BCU and the base of Z10A (Fig. 5.11-A). The values were calculated subtracting the basal depths of the Britannia reservoir to the seismically resolved BCU depth in the Platform Area included into the Britannia database provided by BOL. The distribution of the thickness of this interval shows a uniform thickening from north-east toward the south-western Platform Area. Thickness values range from ~80 to ~560 metres measured in wells 9 and B31, located respectively in the north and south-west of the study area. For the south-eastern area, characterised by the remobilisation of the basal portion of the BSF and highlighted by the darkish area in the isopach maps (Fig. 5.11-A), the interval was measured taking the basal surface of the recognised MTD-1, as described for contouring the isopach map of the Lower-Middle Britannia interval. The choice of reconstructing Z10A using the MTD-1 basal surface is validated by the affinity of values between *in situ* and reconstructed boundary depths.

Interpretation

The removal of the stratigraphic units above the Valhall Shales and contouring the map of the resultant thickness between the base of BSF and the seismically resolved BCU, enables the identification of the pre-Britannia structural features. In particular, those structures making up the BCU constrain the tectonic activity to a period prior to the emplacement of the BSF. This is possible assuming the base of BSF was flat at the time of the first sand input (Z10A). Therefore, the absolute depths measured on each well within the Platform Area were taken from the base of BSF in order to contour the map of the BCU structure at the time of the base of the BSF when the basin floor is interpreted to have been almost flat, as confirmed by the tabular Z10A, and identifying the tectonic features that might have remained active just before Britannia deposition. In fact, the thickness distribution of the Valhall Shales in the Platform Area confirms the larger scale structural features associated with the Jurassic rifting phase, like the Witch Ground Graben bounded by the Renee Ridge on the south with the related fault that tilts the BCU toward the south. Assuming that the shales filled the topography, at least within the study area, their different thickness could have either relate to differential compaction effects on the flank of the Fladen Ground Spur, after the deposition of the first Britannia sand input (Z10A) or to reactivation of a faulting mechanism associated with the rifting that continued during deposition of the Valhall Shales. Both hypotheses could be responsible for the creation of accommodation within the Lower-Middle Britannia interval, although differential compaction effects should have taken place just after the deposition of (the ~20 metres thick Z10A, whereas the tilting of the southern Platform Area seems to continue until the deposition of the palaeo-datum Bed 58. Therefore, differential compaction of the Valhall Shales cannot be considered as the exclusive mechanism for creation of accommodation in the study area; some faulting activity is invoked, as deduced from the isopach map of the Lower-Middle BSF and confirmed by the decompaction analysis undertaken on Valhall Shales (see above).

A comparison of thickness maps of the Valhall Shales and that of the Late Cretaceous-Cenozoic interval suggests that similar morphologies and dipping trends are observed in both, apparently confirming that creation of accommodation space for these intervals is analogous, contrasting with the trends described within the Lower-Middle and Upper BSF. However, this conclusion must be considered speculative given the relative small size of the study area.

5.3.4.2 Lower-Middle Britannia (Fig. 5.11-B)

Description (Base BSF-Base Bed 58)

The thickness map of the Lower-Middle reservoir section (Fig. 5.11-B) was prepared using the decompacted thickness values for each well (see section 5.3.2). It shows differences of about ~200 metres across the Platform Area, with the southern sector recording thicker deposits in comparison with the northern zone. Wells B28 and B06 in the north sector record the lowest thickness values (77 and 83 metres) for the interval between the base of the Z10A and the top of the Bed 58. The same interval is ~200 metres thicker in well B12 located in the south-west of the Platform Area, where it measures 281 metres (the thickest in the study area), representing the thickest interval in the study area. Adjacent wells show interval thicknesses between approximately 200 and 240 metres. In the south-east sector wells B29, B20 and B17 exhibit similar thicknesses (230-210 m) but with an uncertainty due to the erosion of Z10A by the MTD-1 (which might be partially resolved considering that this interval measures ~ 212 metres in well B17). Where Z10A is not present because of erosion by MTD-1 (highlighted by the darkish area in the isopach maps), the interval was measured from the basal surface of the recognised MTD-1. The increase of depth from the shallow north sector to the deeper southernmost area is marked by an abrupt change in thickness represented by relatively close thickness contour lines that separate the area represented by wells B28 - B06 - B33 - 9 (at ~90 metres) and that represented by wells B13Z - B30 - B04 - B01 - B37 - B02 (at ~150 metres). A less pronounced thickness increase is aligned with the wells of the central sector towards the south where the interval thickness varies between ~160 and ~190 metres (Fig. 5.11-B).

Interpretation

The Z10A-Bed 58 reservoir interval illustrates an increase in creation of accommodation space towards the southern sector of the Platform Area, constrained by the two palaeo-datums, which are interpreted flat at the time of their deposition. The different thickness between the north and south sector of this unit can be firstly explained by differential compaction effects. However, the difference between decompacted and compacted thickness deposits is not sufficient to explain the ~200 metres of accommodation space created during BSF time (see section 5.4.1.2). An additional factor may relate to tectonic activity during the emplacement of the Lower and Middle BSF. Furthermore, the contouring of the thickness of the Unit 2 highlights several structural features which are interpreted to correspond to the palaeo-highs in the north-east sector, that extend slightly toward the central area, and the topographic

lows located respectively in the south-west and south-east extremities of the study area, if the Bed 58 top is used as horizontal upper datum.

The described features might be interpreted as the result of faulting activity, which could have directly affected the deposits of Lower and Middle Britannia or the effect of the influence of underlying faults developed within the Valhall Shales as the result of either tectonic activity associated with the post-rifting phase or differential compaction of the shales after the deposition of Z10A.

The effects of these inferred faults can be identified by the abrupt changes in thickness of the Z10A to Bed 58 interval across the Platform Area and marked by relatively close thickness contour lines that separate the different areas. One of these inferred fault lines is bounded by wells B37 and B30 that are aligned along the contour 150 metres, with the strike of the interpreted fault measuring N70 with dip toward the S-SE. Here the contour lines indicate abrupt thickening towards the southern study area. A further set of faults are inferred to explain the two topographic lows measured in wells B12 and B29 which are separated by a shallow elongation of the high identified by the transect formed by wells B30, B07, 24 and B11z. This could represent the relay ramp between the two inferred overlapping fault segments with fault strike measuring N20 and dipping toward E-SE. However, fault presence must be considered speculative, as it is inferred based upon observing the isopach map of decompacted deposits of the Z10A-Bed 58 interval alone (given the challenge in recognising faults features on core and due to the lack of high quality seismic data for the BSF in the Platform Area).

5.3.4.3 Upper Britannia (Fig. 5.11-C)

Description (Top Bed 58-Top BSF)

The Upper Britannia stratigraphic interval (Fig. 5.11-C), bounded by the top of Bed 58 and the top of Z50 (which is also represented by Bed 86, *sensu* Barker et al., 2008), is thinner than the Lower-Middle reservoir in the Platform Area. The decompacted thickness of these deposits ranges from ~110 m in well B37 to ~54 m in well B30 with an average thickness of ~76 m. A systematic and uniform thickening is not observed in this interval; rather, groups of wells with similar thickness are distributed across the study area to characterise the Upper Britannia. Wells B06 and B37 record the thickest deposits with respectively ~104 and ~110 metres along a NE-SW transect and bounded by shallower deposits in the north-east sector where they measure about 50 metres.

Interpretation

Thickness distribution across the Platform Area is characterised by relatively limited variation in the isopach map of the stratigraphic interval Bed 58-Z50. However, the map of the thicknesses of this interval shows slightly higher creation of accommodation space in the northern sector than the southern area, which represents the opposite trend of that seen below, in the Z10A-Bed 58 stratigraphic interval. Bed 58 therefore marks a significant change in the pattern of accommodation. In fact, the thickness distribution of the Upper Britannia interval might represent the result of a minor tectonic inversion active during the emplacement of Z45 and Z50. The putative inversion recorded in the differential creation of accommodation space is highlighted by the comparison between the two palaeo-horizontal datums Bed 58, below Z45, and Bed 86 on top of Z50, both of which represent sub-horizontal depositional conditions in the study area at different times. In this stratigraphic interval, higher rate of creation of accommodation space is concentrated in the northern sector, mainly in those wells (B06-B02-B33) where the Lower-Middle interval shows thinner thickness deposits in this area.

5.3.4.4 Late Cretaceous-Cenozoic interval above Britannia (Fig. 5.11-D)

Description (Top BSF-present day seafloor)

The Late Cretaceous-Cenozoic isopach map was contoured measuring the depths between the present-day seafloor on the mudline and the top of the Britannia Sandstone Fm. (Fig. 5.11-D). The isopach map of the thickness of this interval shows a systematic and uniform thickening from the north-east toward the south-west Platform Area, with the thickness of the Late Cretaceous-Cenozoic interval approximately ranging from ~3780 metres, measured in well 16/26-9, and ~3926 metres in well B31, located respectively in the north and south-west of the study area. In the north-east sector contour lines highlight a slightly raised area corresponding to well B23z that is, in turn, bounded by wells B07, B08 and B17 that show thicker interval thickness.

Interpretation

The isopach map of the deposits above the BSF aims to identify relevant post-Britannia structural features in the Late Cretaceous-Cenozoic interval in order to distinguish and separate the post-Britannia tectonism from potential faulting mechanism active during the emplacement of Britannia deposits. The large thickness of this stratigraphic unit makes it difficult to recognise small scale effects due to the faulting. However, some morphological features can be highlighted by the irregular contouring of depth values such as the area delimited by wells B30, B09z, B22, B19 and B32, that could show either the influence of a fault on the sediments above

Britannia, with the fault strike measuring N130, or the effects of differential compaction on the deposits of this interval. Nonetheless, both hypotheses suggest that small-scale mechanisms of deformation were active after the deposition of the BSF, whereas the general dipping trend toward the south-west sector of the Britannia Field might be interpreted as the response to larger-scale thermal subsidence active during or after the deposition of Britannia sandstones.

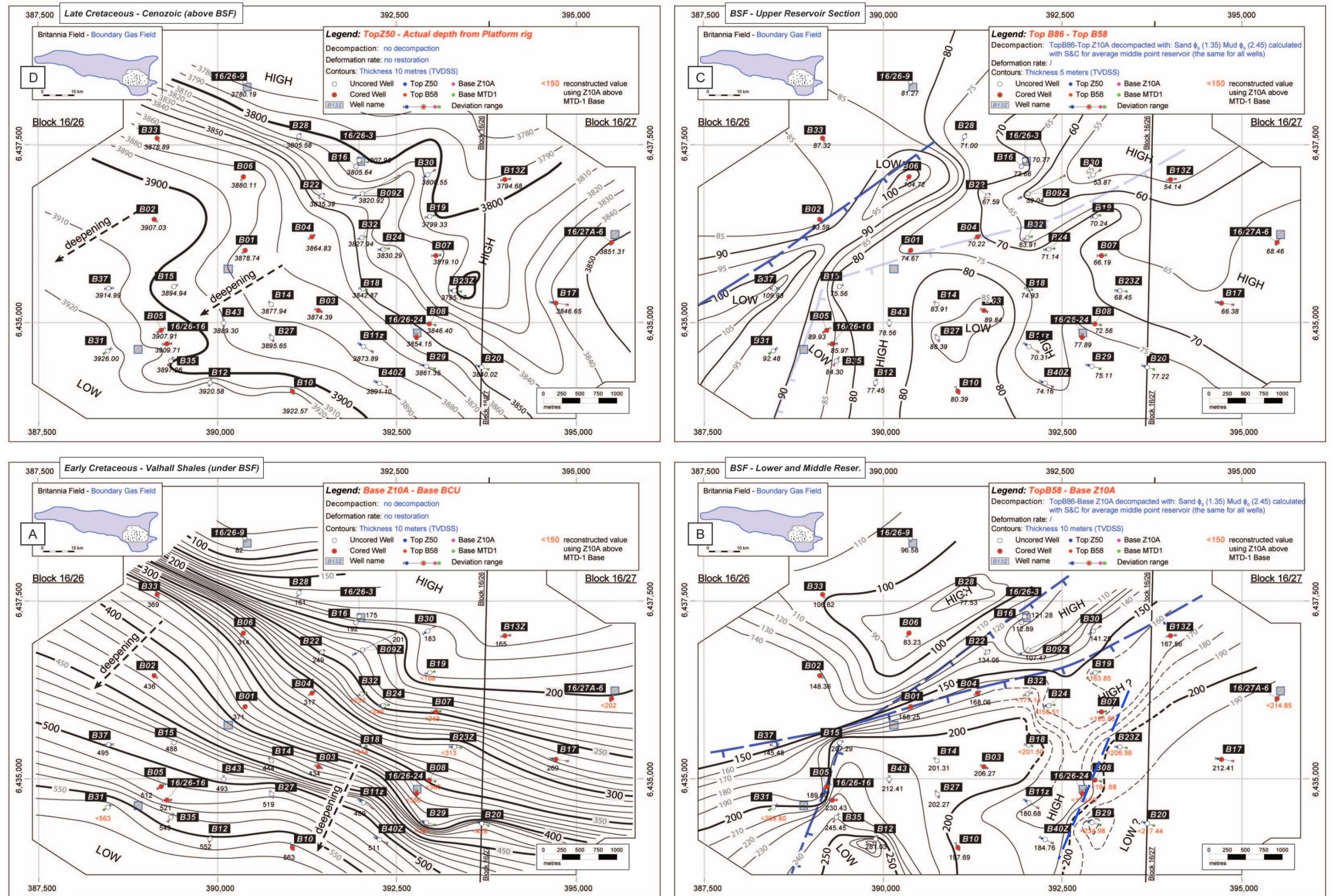


Fig. 5.11 – Isopach maps showing the Lower Cretaceous-Quaternary stratigraphic intervals identified in Chapter 4, contours in metres. (A) BCU-Base BSF thickness distribution; (B) Base BSF-Bed 58 thickness distribution with inferred fault sets; (C) Bed 58-Top BSF thickness distribution with inferred fault set; (D) Top BSF-present day seafloor thickness distribution. Note that B and C show decompacted thickness at the top of the respective intervals, while A and D represent present-day thickness.

5.4 Reconstruction of post-MTD palaeobathymetric surfaces

Reconstruction of contour maps of successive palaeobathymetric surfaces of the BSF in the Platform Area is an important tool to help interpret the evolution of the depositional system, through developing a better understanding of flow processes and pathways, the distribution of associated sediments and their facies variations. In order to create such maps a workflow consisting of two steps was devised: 1) decompaction of post-depositional overburden to yield sediment thicknesses at time of deposition and 2) restoration of syn- and post-depositional structural overprints. This workflow is usually associated with the backstripping technique which requires high quality seismic data combined with lithological information in order to have reliable reconstruction of the evolution of tectonic features of an area. Low subsurface image quality may reduce the applicability of the backstripping technique and consequently affect the reliability of reconstructed palaeo-surfaces and the deposits under investigation. This is the case of the Britannia Field in the North Sea, and specifically the Platform Area, where the data are poor due to the presence of highly reflective lithologies overlying the reservoir. However, the lack of good quality seismic data is largely compensated for by a high concentration of wells (47 wells in 35 km²) making this area an excellent laboratory for the study of MTDs and their spatial variability. In fact, a full and detailed decompaction and restoration analysis of the overburden deposits in the Britannia Platform Area can be conducted on high quality well-based dataset to create palaeobathymetric surfaces for chosen intervals within the Britannia stratigraphy, to facilitate an investigation of the depositional evolution of the BSF basin in the PA (study area, see Fig. 5.1). In particular, the markers identified through core and cuttings investigation and wireline study make the reservoir interval Z10A-Bed58 ideal for a decompaction-restoration well by well.

The workflow consists of the a) decompaction and creation of the isopach maps of the Britannia Field deposits and b) multi-surface restoration for each depositional time associated with large-scale failure events.

- a) Decompaction of the BSF volume and contouring of the thickness maps between the base and top of BSF allow the identification of early-Britannia structural features within the Upper Reservoir Section and the Lower-Middle reservoir in order to identify and calculate the accommodation space created during the Late Aptian-Early Albian time.
- b) The final step of the reconstruction of the five failure/healing cycles characterising the geological evolution of the Britannia Sandstones deposition consists of the restoration of palaeobathymetric surfaces shaped by large mass

failure events at each of those cycles, based upon identification of a palaeo-datum within the Britannia stratigraphy and a well-restoration model. Each restoration will consider a surface to be flattened (palaeo-datum) and the related surfaces to be restored (basal MTD surfaces).

The structural restoration of Britannia Field deposits aims to:

- Reconstruct and constrain possible deformational process active during the emplacement of the BSF in the post-rift Late Aptian to better understand the mechanisms and the influence of the geological structures on the sediment input and deposition within the Britannia Platform Area.
- Create contour maps of palaeobathymetric surfaces associated with the emplacement of large-mass failures in order to study the role of these catastrophic events on the evolution of the depositional system in the study area.
- Reconstruct the accommodation space created at each of the time intervals immediately following each of failures. Implicit in our discussion of the depositional process that follows is the concept that different mechanisms of accommodation space creation existed in the basin of BSF (see section 5.3.4).

5.4.1 Methodology of the restoration

Restoration involves taking 2D and 3D well-correlations and working back in time to progressively restore them, hence identifying possible features present on the palaeobathymetric surfaces at specific time intervals. Documented examples of restoration examples include both outcrop (Albertão et al., 2011; Moretti, 2008) and subsurface studies (Fernández et al., 2004). Each is based on a common workflow which consists of a) identification and interpretation of continuity (e.g., datum-like tabular beds, same-thickness sand intervals) and discontinuity surfaces (e.g., faults, failures, etc.), b) construction of a comprehensive geological model based on key horizons, faults and contacts among the surfaces (e.g., onlap, offlap, unconformities, etc.) and then c) multi-surface restoration in order to derive palaeo-topographies at selected times. Accordingly, the same approach was applied to the Britannia surfaces with a four step workflow:

1st STEP – Identification of continuity and discontinuity surfaces within the Britannia stratigraphy.

2nd STEP – Construction of a geometrical model that can be used to calculate the tectonic deformation.

3rd STEP – Calculation of restored surface depths and associated hand-contouring bathymetries.

5.4.1.1 Identification of the continuity and discontinuity surfaces (STEP 1)

The restoration of selected surfaces to re-create the palaeobathymetry of the seafloor at a certain time requires the choice of palaeo-datum that represented palaeo-horizontal conditions in the past in order to calculate the deformation that occurred in succeeding intervals. Layers are here differentiated according to their significance, with datum-like tabular beds (e.g., Bed 58) and same-thickness sand intervals (e.g., Z10A) considered as continuity surfaces whereas MTD-related topographies (i.e., the basal and upper MTD surfaces) represent discontinuity surfaces, whose original form is to be derived by the restoration. The identification of stratigraphic markers at local and regional scale, such as the hemipelagites described above (i.e. section 3.3.1), were also used as a high resolution constraint upon the creation of accommodation space. For instance, sandstones capped by hemipelagic mudstones might represent a palaeo-horizontal datum to use for restoration. All these key surfaces were identified by using well data such as core, cuttings and wire line logs, with the exception of local structural features that could have been present at the time of BSF deposition and that could be inferred based upon analysis of the isopach map of the decompacted interval between Z10A and Bed 58 (see Fig. 5.11).

5.4.1.2 Building the geometrical model to calculate the creation of accommodation space (STEP 2)

In order to identify a strategy for surface restoration, a comprehensive unscaled geological reconstruction of the depositional history of the basin in the study area is required using the available data. Once the geological history is considered reliable, the construction of a geometrical model enables most of the deformation to be quantified and the reconstruction of the palaeobathymetric surfaces corresponding to each time interval associated with the emplacement of MTDs. The model must include the identification of horizons and markers that enable the definition of stratigraphic geometries in order to distinguish the different reservoir intervals useful for the restoration. The modelling also requires a general description of the deformation possibilities explained by rotation, translation, flexural slip, simple shear or the combination of some of these based on a literature review of the tectonic setting of the Central North Sea (see section 3.2). The deformed sections and map can then be restored by applying reciprocal versions of the hypothesised deformations. Once a horizon is restored this can be used as a constraint for the construction of new horizons and so forth until all the identified palaeobathymetric surfaces are restored, reconstructing the geological evolution of the study area. A

conceptual model of the Z10A-Bed 58 representing the Lower and Middle Reservoir sections is gathered from the 2D and 3D well-correlations (Fig. 5.12).

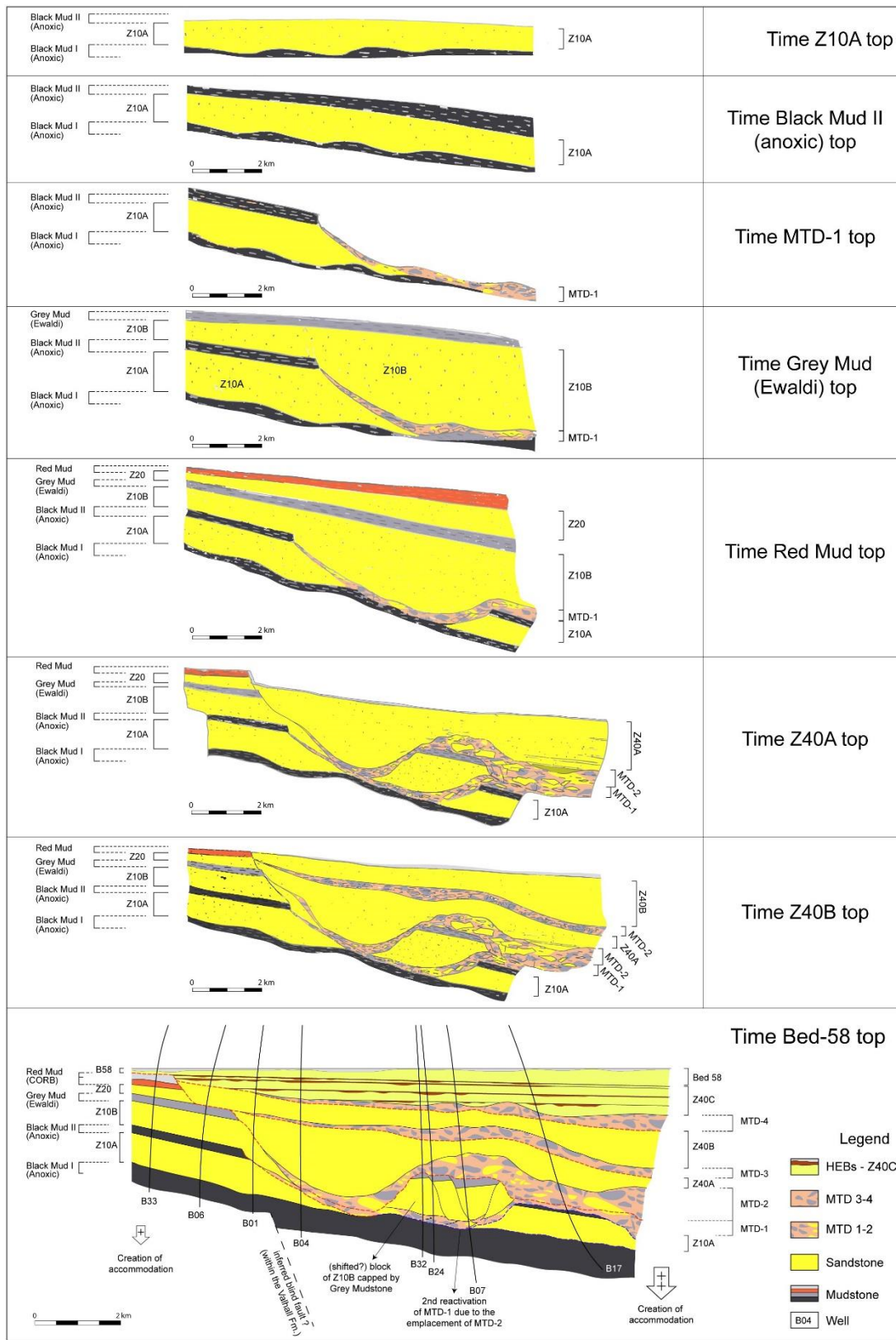


Fig. 5.12 – Hypothesised geological evolution of the stratigraphic interval Bed58-Z10A of the Britannia deposits, showing the emplacement of the different reservoir intervals and their interplay with the MTDs.

Stratigraphic datums such as the interpreted tabular sandstones and the continuous hemipelagic intervals with regional stratigraphic significance were used to constrain and identify the evolution through a coherent geological reconstruction of the stratigraphic surfaces of interest.

The model is based on the visualisation of wells of the Platform Area, in the sequence of progressively increasing thickness values of the decompacted interval Z10A-Bed58, hung on the top of Bed58 (Fig. 5.13). This is an original approach to data management in support of a restoration exercise. In this case the approach appears to show that the accommodation space developed between these two datums was not created equally across the Platform Area. Furthermore, the graph highlights a distinctive clustering of wells identifying two main sectors in the study area (Fig. 5.14), characterised by similar thickening trend of Z10A-Bed58. However, considering the geographic location and spatial distribution of the wells, four sectors can be identified: a) North-west sector, b) North-east sector, c) Central sector and d) Southern sector. The two relatively close sectors of the northern part of the Platform Area (a and b) are composed of respectively four (B28, B06, 9, B33) and five wells (B09z, B16, 3, B22, B30), which are split because they are characterised by different deformation trends, mainly in terms of creation of accommodation space. By way of contrast, the central and southern portions of the study area principally developed southwest-northeast trending deformation trends. Cored-wells B06 and B03, located on Northern and Southern Sectors, respectively, show a 3-fold difference in stratigraphic thickness between the palaeo-horizontal datums Z10A and Bed58 (Fig. 5.13), indicating significant differential creation of accommodation during this time interval.

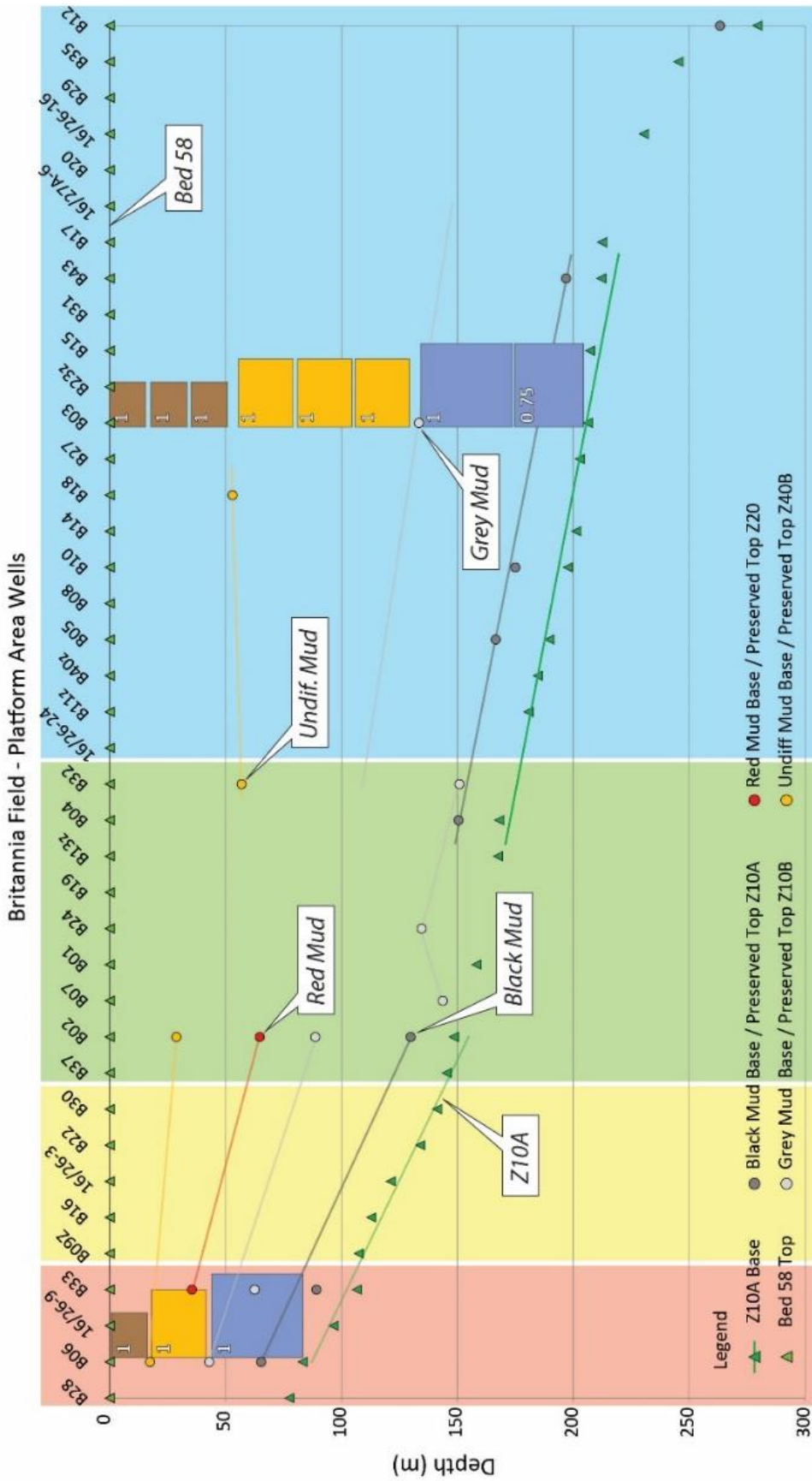


Fig. 5.13 – Simplified plot showing differential creation of accommodation space within the Platform Area, as evidenced by the stratigraphic interval thickness Bed58-Z10A (wells are sorted on this interval thickness). Wells are assigned to different sectors as indicated by the coloured background, which are shown in map view in Fig. 5.14.

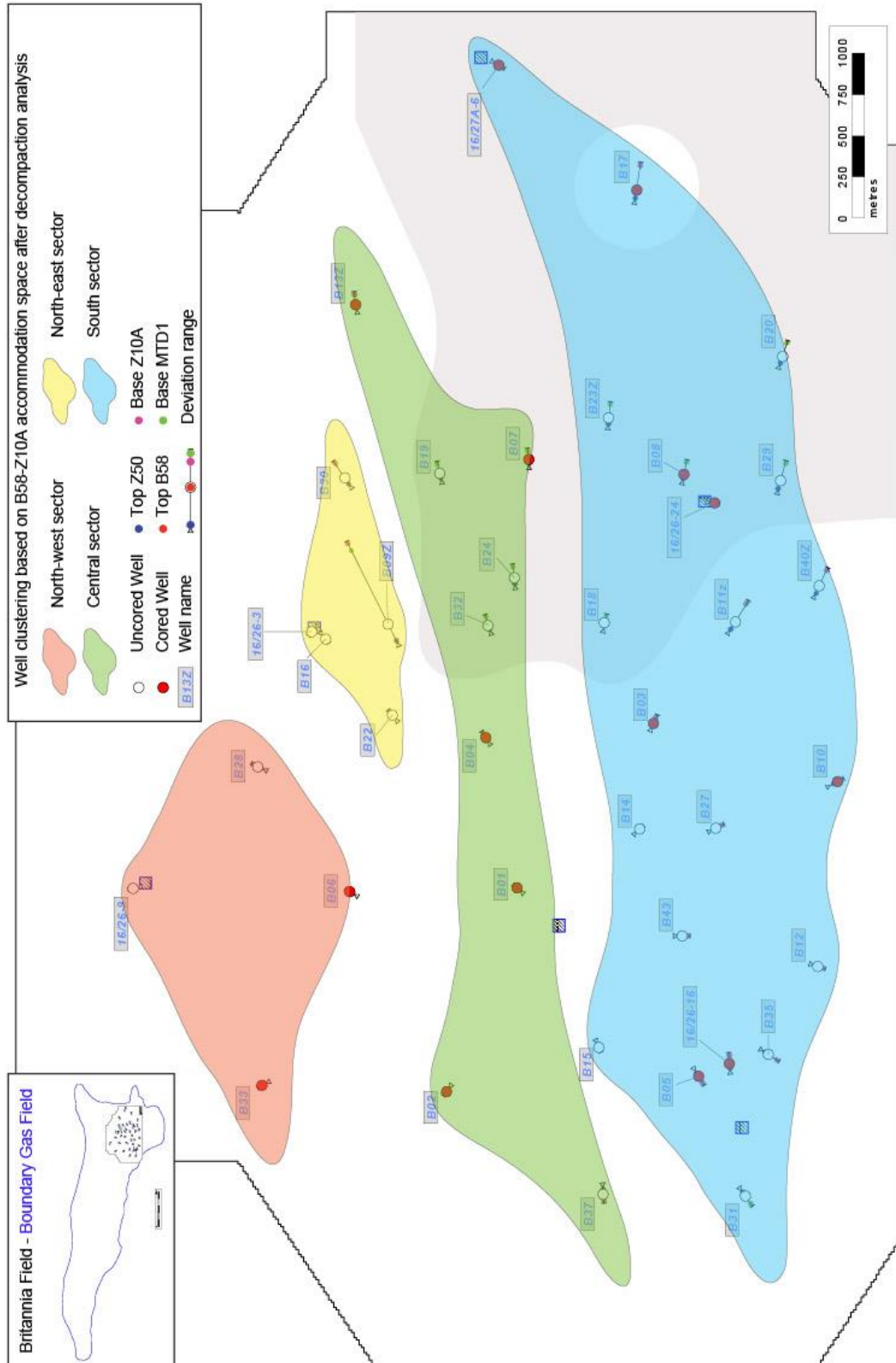


Fig. 5.14 – Map showing the sectors identified by the clustering character of wells based on the accommodation space created within the Z10A-BED58 interval: a) North-west sector, b) North-east sector, c) Central sector and d) Southern sector. The dark area in the SE represents the sector where the lower palaeo-datum Z10A is not recognised and reconstruction is done using the MTD-1 base (see section 5.5.1). Well deviation ranges are shown plotting depths of significant stratigraphic markers as: Z10A base, MTD-1 base, Bed 58 top and Z50 top.

Two non-exclusive models of creation of accommodation space during the BSF time, may have operated in the Platform Area. A model where the creation of accommodation space is considered “uniform” leads to the development of essentially similar reservoir interval thicknesses in each well across the study area, whereas a “rotating tilting” model leads to an asymmetric creation of accommodation space, increasing in proportion to the distance from a single or double fulcrum line.

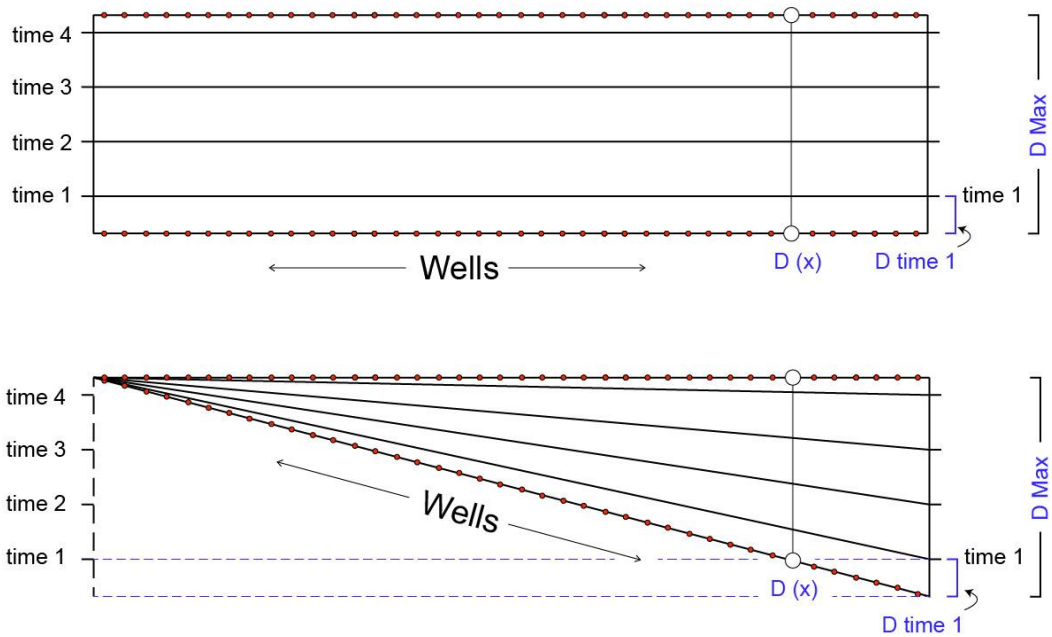


Fig. 5.15 – Scheme that shows how uniform/differential creation of accommodation was applied to wells (see text).

A combined model can be invoked (Fig. 5.16) that aims to integrate uniform sediment aggradation with the differential creation of accommodation space. By assigning an appropriate deformation index - from 0 (min deformation) to 1 (max deformation) - this geometric model aims to capture the differential deformation seen across the study areas (i.e., between the northernmost B33 and the southernmost B12 Platform Area wells).

sandstone beds, based on the possible interpretation that sandstones in Britannia Field generally heal topography, such that their tops represent conditions of sub-horizontal deposition as already shown by Eggenhuisen et al. (2010). Hemipelagites may also be used to constrain stratigraphic interpretations, however these deposits might not always represent sub-horizontal depositional conditions. In fact, hemipelagic sediment is usually considered to be draping rather than compensating, but when these deposits are identified on top of sandstone intervals, their basal surfaces can be interpreted as palaeo-horizontal, as can their upper surfaces, if not eroded. Some hemipelagites are distinctly recognisable and used as regional markers across the North Sea (see Chapter 3). When such sediments are in-situ, their recognition allows to underlying sands to be considered as having been preserved by potential erosional processes, like large-scale failures. In this case, preserved sandstone tops can be used for restoring palaeo-horizontal datums at the time of the emplacement of the failure event underneath. These enable the creation of palaeobathymetric surfaces corresponding respectively to 1) the décollement layer of large-scale failures, 2) the post- emplacement topography related to the MTDs and 3) surfaces associated with subsequent sand deposition; all are considered as having occurred in relatively short time and hence, being effectively time equivalent. This assumption can be considered reliable if compared with the hemipelagic deposition making up thick mudstones that are recognised on top of the succession described above (Fig. 5.17).

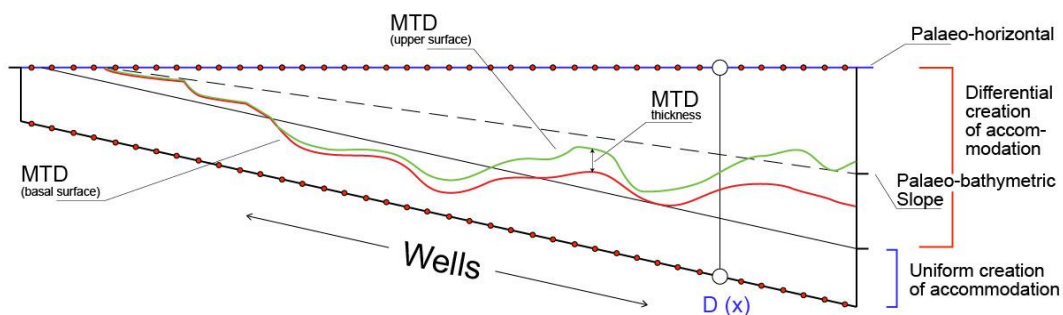


Fig. 5.17 – Model of the deformation applied to the well-dataset of the Platform Area in which the surfaces of interest are identified. These correspond to the basal and upper surfaced of MTD and related restored palaeo-datums, represented by the basal slope and palaeo-horizontal lines.

Computerised and hand-drawn approaches were compared for contouring thickness values between the reconstructed palaeo-horizontal datum and the restored surfaces, and revealed significant differences. A “bullseye” effect was seen when thickness values were assigned to each well of the Platform Area in ODM™ (Oilfield Data Manager) software and then contoured. This effect is thought to arise due to

gridding algorithms. Conversely, hand-drawn contoured plots were thought to be more realistic. However, this approach requires the user to attempt to be objective whilst retaining a geological perspective, including an awareness of the processes that produced the mapped surfaces to map. In the end the choice was made to adopt hand contouring, informed by, e.g., the geomorphology of MTDs-related topography from seismic (Posamentier and Kolla, 2003) and outcrop analogues (Armitage et al., 2009).

5.4.2 Choice of parameters, issues and associated uncertainties which arose when applying the methodology to the dataset

In order to best apply the chosen restoration approach to the BSF deposits in the Platform Area, a well visualisation method has been adopted in which the wells are placed laterally in order of increasing accommodation space, based on the decompacted reservoir interval thickness Z10A-Bed 58. This interval is divided vertically into discrete reservoir deposits bounded by hemipelagic stratigraphic markers recognised on cored-wells. On the basis of these correlations shown in Chapter 4, four failure/infill cycles are recognised in the Z10A-Bed58 interval (Lower and Middle Britannia). Restoration of the four MTD-related topographies at the point immediately after failure is achieved via restoration of associated palaeo-horizontal datums.

A range of deformation rates (comprising a proportion of the uniform and a proportion of the differential accommodation) were applied to the Z10A palaeo-datum depths to be restored through attempts, on an Excel worksheet (see Appendix C), until the restored Z10A values overlaid the depths of the inferred palaeo-horizontals (key surfaces) at each time of the occurrence of failure events (Fig. 5.19). A full reversed restoration of Z10A palaeo-datum is shown on the graph of Fig. 5.18 in order to describe the overall restoration of the four MTDs-related topography, within the Lower-Middle Britannia reservoir (Z10A-Bed 58) (see below).

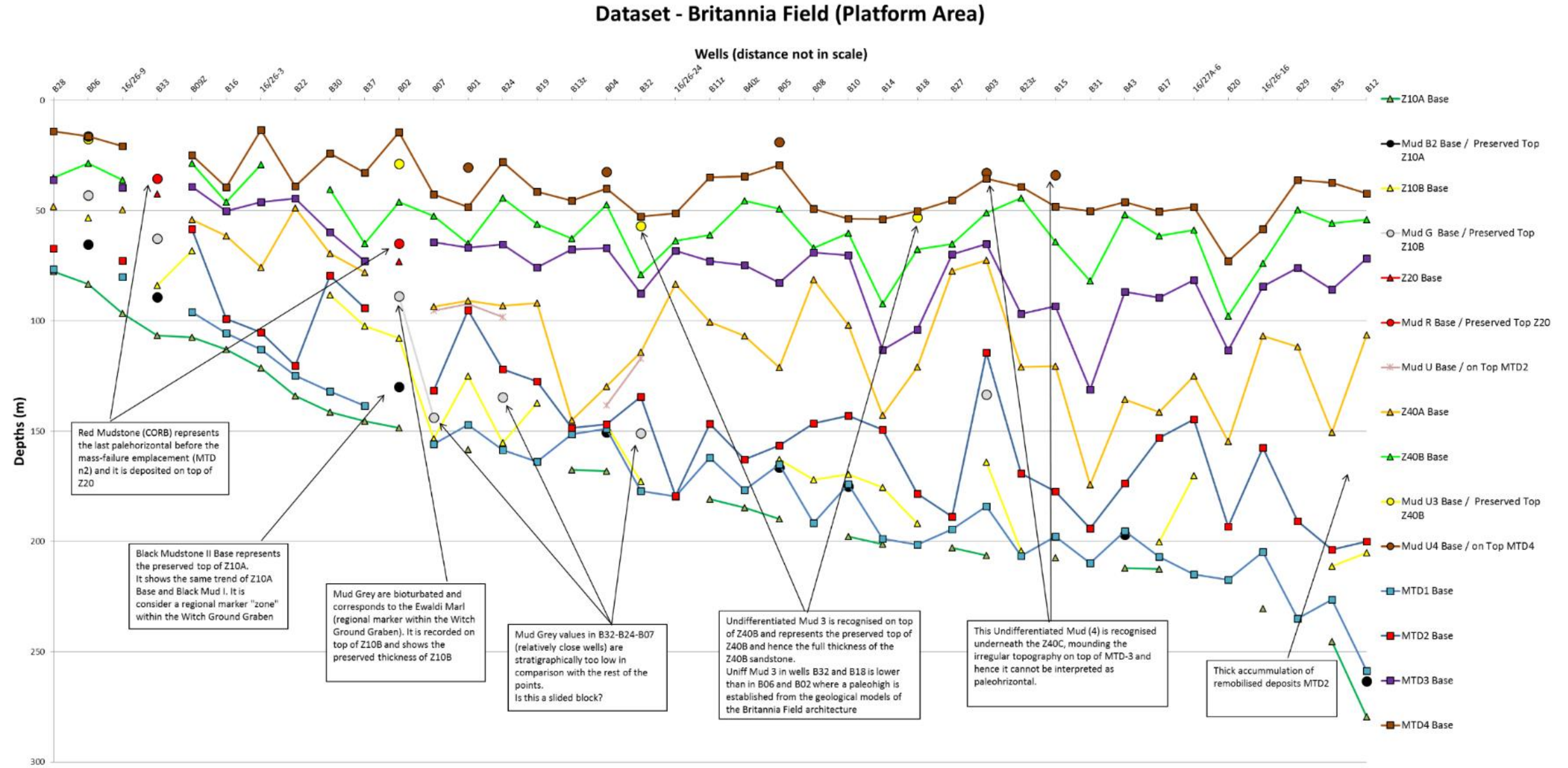


Fig. 5.18 – The Britannia Field (Platform Area) dataset in which wells are sorted on the depths of Z10A measured from the top of Bed 58. Thicknesses are decompacted. Bases of mudstone markers are displayed with dots, whereas triangles and squares represent respectively the bases of sandstone intervals and base of MTDs. The basal surface of the MTD-1 is used to reconstruct the depth values of Z10A in wells where this sand interval is not preserved because remobilised by the first large-mass failure and hence assuming the detachment surface occurring just underneath the base of Z10A, within anoxic mudstones.

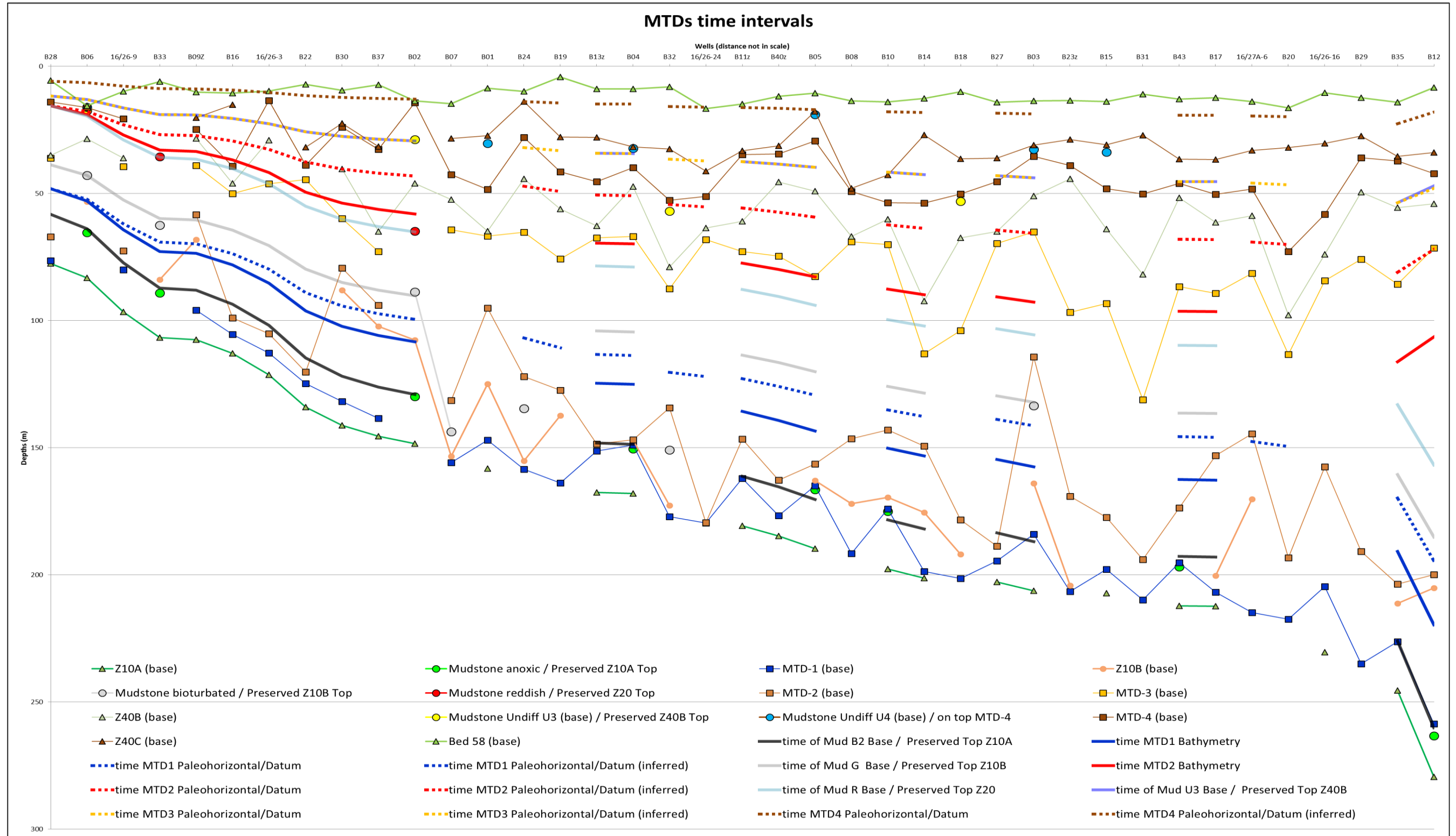


Fig. 5.19 – Palaeo-datum restoration through time. The diagram shows the full reversed creation of accommodation history of the Lower and Middle Britannia deposits (Z10A-Bed 58 stratigraphic interval) in the Platform Area and the step-wise restoration of the Z10A palaeo-datum at each depositional event. Green triangles at the bottom represent Z10A, whereas light-green triangles at the top represent the base of Bed 58. Solid lines represent the reconstruction of palaeo-slope at different times based on the restoration of palaeo-datum Z10A: black line = time anoxic hemipelagic mudstones (base); blue line = time MTD-1 (base); grey line = time bioturbated hemipelagic mudstone (base); light blue line = time reddish hemipelagic mudstone (base); red line = time MTD-2 (base). Dashed lines represent the reconstruction of palaeo-horizontal when this is different from the palaeo-slope as in the lower stratigraphic intervals until MTD-3 and MTD-4 times, when palaeo-horizontals corresponds with bathymetry of the seafloor (for a full description of the graph, see main text below).

5.4.2.1 Restoration of the palaeobathymetry at MTD-1 time

The creation of the palaeobathymetric surface associated with the first large-scale failure event is based upon the restoration of the Z10A palaeo-datum to the palaeo-horizontal at the time of MTD-1 which is represented by the top of Z10B sandstone interval. Z10B is interpreted as having healed the space left after MTD-1 and sandstones are considered to have been deposited just after the emplacement of the debritic deposits. These sands are considered *in situ* only if capped by hemipelagic mudstones corresponding with the greyish-bioturbated Ewaldi Marl. The recognition of these mudstones excludes any remobilisation of sandstone deposits allowing the restoration of the palaeo-horizontal at the time of MTD-1.

Where preserved (as in wells B06-B02-B03) the Z10B sandstone shows a thickening trend from the north toward the south-eastern sector of Platform Area. The top of Z10B is thought to represent a palaeo-horizontal surface developed during the sand infill of the MTD-1 related bathymetry, immediately after the failure.

The thickness interval between Z10A palaeo-datum and the top of Z10B can be split into a uniform component (representing 38% of the total between Z10A-Bed 58) and a differential creation of accommodation space (representing 27.5% of the total between Z10A-Bed58). The thickness between the Z10A paleo-datum and the base of the Z10B (when deposited on top of the *in situ* anoxic black mudstone marker) represents 15% of the total differential creation of accommodation space between Z10A-Bed 58. This value can be used to calculate the palaeo-slope of the basin at the time of MTD-1 (as MTD-1 is interpreted as occurring shortly before the Z10B deposition) due to the maximum thickness of the anoxic mudstone measured in wells.

It should be noted that not all the wells can be satisfactorily restored using this model. Wells B33, B07, B24 and B32 record the preserved Z10B top but do not fit the thickness trend observed for the other wells and in addition Z10B in these wells is now preserved at deeper depths than expected when compared to their neighbours. However, the peculiar depth of Z10B in these wells might represent the effect of large-scale failures (see section 5.5.2). A different history for these wells can be invoked, involving post-depositional remobilization of these deposits from the northern sector (i.e., they are not *in situ*). This idea is supported by the Z10B thicknesses of these wells, which are compatible with the accommodation space inferred for the northern sector (see section 5.5.2).

An additional complication is that this interpretation does not explain the Z10B thickness and depth in well B33, which might instead be possibly explained due to

the difficulty of picking up the base of the Z10B on core and gamma-ray log due to the presence of numerous injections (see Chapter 6, section 6.4.2).

5.4.2.2 Restoration of the palaeobathymetry at MTD-2 time

The second large-scale failure event occurred after the emplacement of a sequence comprising the Z10B sands, the bioturbated Grey hemipelagic mudstone, the Z20 sands and the reddish (hematitic) hemipelagite; this sequence was therefore deposited by alternations of periods of relatively quick sedimentation and of quiescence. A full *in situ* sequence is only preserved in wells B06 and B02; this is only partially recorded in other Platform Area wells due to the large-scale failure associated with MTD-2 that removed a large portion of these deposits.

The reddish mudstones overlying Z20 are used as stratigraphic marker to restore the palaeo-slope at the time of the emplacement of MTD-2, whereas the preserved top of Z10B sandstones might represent the palaeo-horizontal (see section 5.3.2). A value of 80% of the uniform creation of accommodation and 61% of differential creation of accommodation space are necessary to line up the Z10A palaeo-datum with the highest preserved sandstones making up Z40A recorded in the cored wells B03, B08 and B10. This sandstone package is capped by the debrites of the MTD-3 which might have eroded its top. Due to the shallow depth contact between the Z40A and MTD-3 in these wells a minimal erosion of the sand deposits is inferred.

Well B12 issue – Inversion trend on the creation of accommodation

Top of Z40A in B12 (which was probably partially eroded, given that no mud is recognised on top) is characterised by too high a depth in comparison with the Z10A underneath. In B12, the creation of accommodation seems reduced at “MTD-2 / Z40A-infill” time because of the high value depth of the preserved Z40A. Finally, a different creation of accommodation magnitude is required for time intervals MTD-2, -3, -4 (MTD-2: 72%; MTD-3: 82%; MTD-4: 94%).

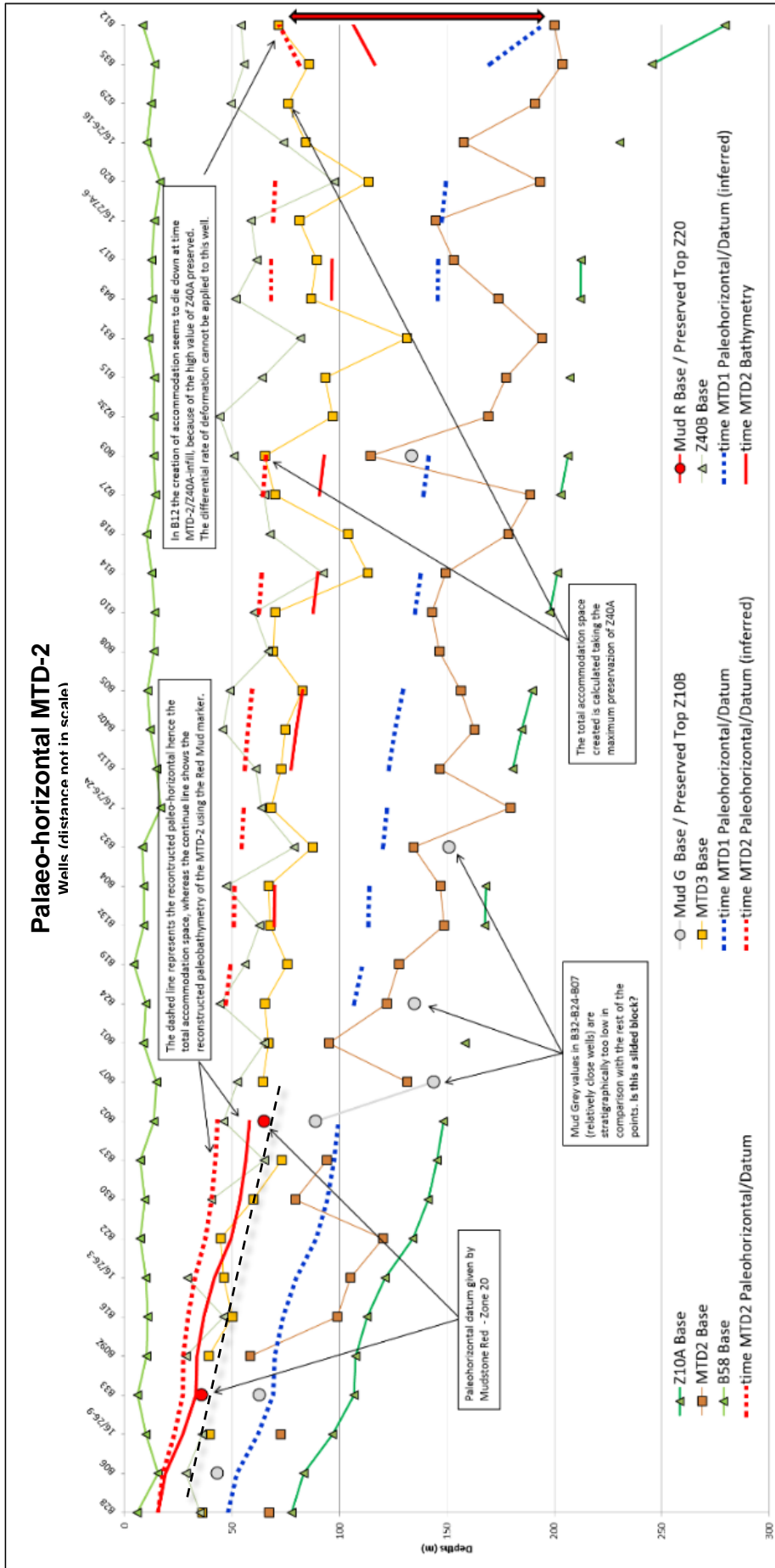


Fig. 5.21 – Restoration of the palaeobathymetry surface at the time of the MTD-2 (dashed red line). Red continuous line represents the reconstructed palaeo-slope using the preserved tops of the Zone 10B

5.4.2.3 Restoration of the palaeobathymetry at MTD-3 time

Restoration of palaeobathymetry at the time of MTD-3 is achieved through the reconstruction of the palaeo-horizontal datum using Z40B sand infill that overlies and heals the topography associated with MTD-3. A fully preserved Z40B interval is recognised in four wells (B06, B02, B32 and B18), where sandstones are capped by hemipelagic undifferentiated mudstone (Fig. 5.22). This sandstone interval is inferred as corresponding to the maximum accommodation space created at the time of the MTD-3. Thus, Z40B tops recognised in these four wells should represent the palaeo-horizontal, which can be used to reconstruct the associated bathymetry of the seafloor after the emplacement of MTD-3. Depths of Z40B tops in wells B06 and B02 seem to fit the tilting trends recorded by the previous hemipelagic markers. Wells B32 and B18 show interval depths of Z40B that are significantly lower than the values measured in B06 and B02. This could be interpreted as secondary movements of earlier shifted blocks associated with the emplacement of MTD-2 (see section 5.5.4).

Based on the restoration model (shown in section 5.4.1), 85% of the total uniform accommodation and 75% of the total differential creation of accommodation are applied to restore this surface.

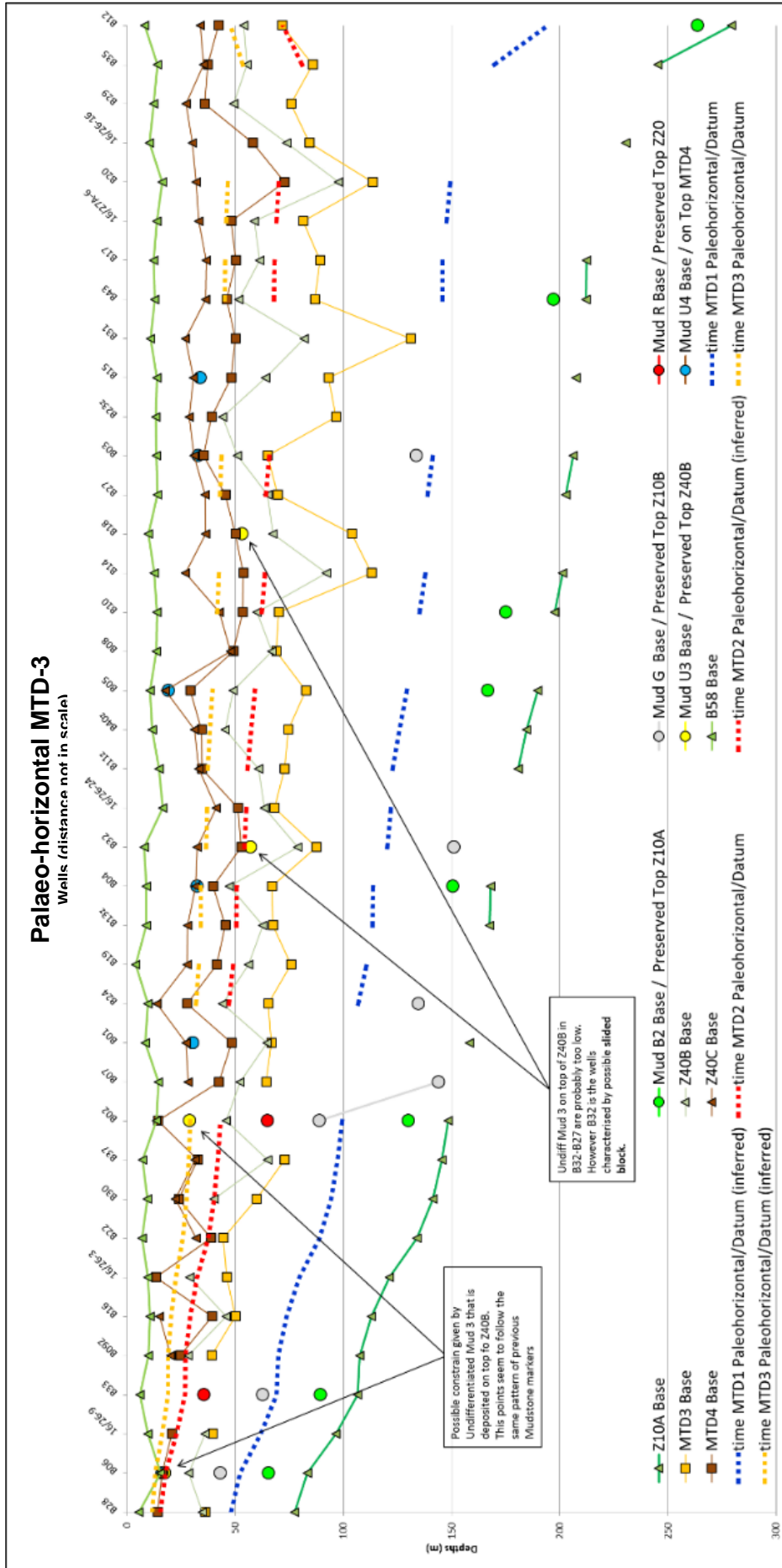


Fig. 5.22 – Restoration of the palaeobathymetric surface based on the reconstructed palaeo-horizontal at the time of the MTD-3 (yellow dashed line). Four yellow dots pointed out by the arrows represent the base of undifferentiated mudstones and hence the preserved top of Z40B sandstones package. Blue and red lines represent the previous reconstructed palaeo-bathymetries showing the creation of accommodation space across the wells of the Platform Area.

5.4.2.4 Restoration palaeobathymetry at MTD-3 time

The fourth palaeobathymetry, associated with the emplacement of MTD-4 is reconstructed by restoring the palaeo-horizontal at the boundary between the top of Z40C and the base of Bed 58, assuming the deposition of sands were relatively quick and hence, considered almost time equivalent to MTD-4 (Fig. 5.23). The upper topography of the MTD cannot be taken as a datum due to the rugosity usually associated with the debritic character of MTDs. In the absence of significant stratigraphic markers throughout the uppermost Britannia deposits, such as hemipelagic deposits, restoration on the basis of these assumptions represent the best estimate to calculate the creation of accommodation space that occurred before the emplacement of MTD-4. Values chosen on this basis are 92.5% of the total uniform deformation and 90% of the differential deformation.

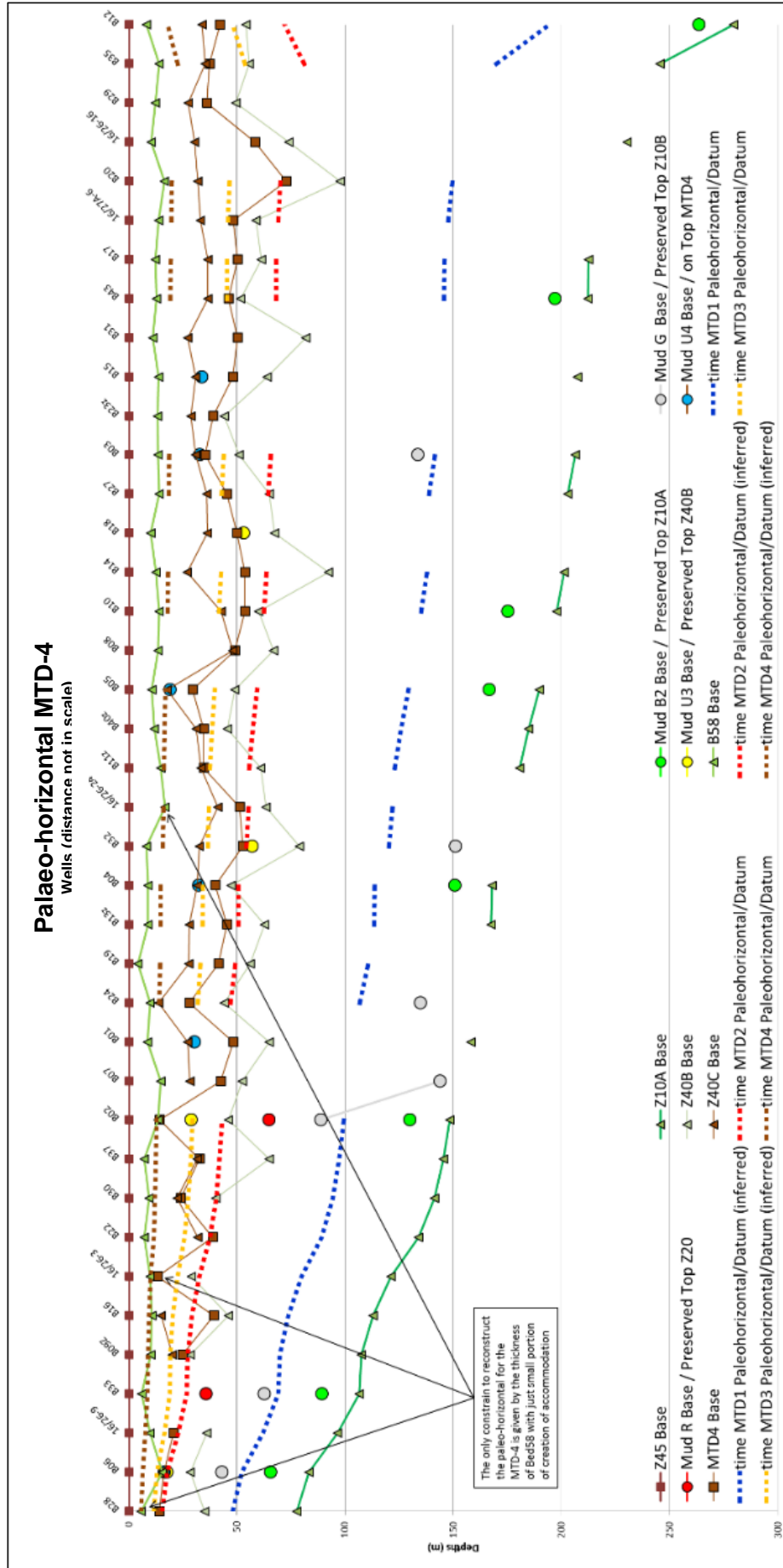


Fig. 5.23 – Restoration through time of the palaeo-horizontal datums (dashed lines) associated with the MTDs occurring within the Z10A-Bed 58 interval. The uppermost brown dashed line represents the reconstructed palaeo-horizontal datum at the time of MTD-4. Stratigraphic constrain to reconstruct this palaeo-datum is given by the boundary between the top Z40C and base Bed 58 (green triangles on top).

5.5 MTD-related palaeobathymetries

The evolution of the palaeo-seafloor during the Britannia Sandstone Formation emplacement is analysed below. Britannia deposit zonations and well correlations described in Chapter 4, together with the decompaction analysis and structural restoration of the reservoir intervals conducted in this Chapter (see section 5.2 and section 5.3) helped reconstruct the evolution of that portion of the depositional basin corresponding to the Platform Area of the Britannia Field. The investigation of the stratigraphic intervals above and below the BSF forms a necessary contribution to the spatially and temporally constraining of the study area including the creation of accommodation space during the Lower Cretaceous post-rift deposition of siliciclastic sediment.

In the Platform Area of the Britannia Field six failure/infill cycles can be recognised within the stratigraphy, characterised by large-scale sediment remobilisation deposits on the southernmost flank elongation of the Fladen Ground Spur, followed by subsequent sandstone deposition. Each of these remobilisation events marks a break in sedimentation combined with the removal of some portion of the Britannia stratigraphy, creating accommodation space for further sand deposition on the basin floor. Isopach maps of the MTD-related topography are drawn for each MTD top, reconstructed through the decompaction and structural restoration analysis described in the section 5.2 and 5.3 of this Chapter.

5.5.1 MTDs of the Lower-Middle reservoir in the Platform Area

MTD character (rheology, deposits, etc.), and evolution during the Lower-Middle BSF interval in the Platform Area are analysed below and tied to the inferred palaeo-topography. Following the methodology described in the section 5.4.1, maps of the basal and upper MTD surfaces are drawn and described (Figs. 5.28, 5.29, 5.32 and 5.33), starting with the lowermost MTD-1 and progressing systematically upward through the Lower-Middle reservoir interval, culminating with the uppermost MTD-4. Cross sections built with data from cored and uncored wells are also used to characterise the MTDs and to describe their influence on the seafloor in terms of erosional and constructional topography.

The Platform Area was previously subdivided by Eggenhuisen (2010) into three sectors based on core observations, distinguishing areas without any debrite facies (in-situ stratigraphy; northern sector), areas that show evidence of partial or completely eroded stratigraphic deposits (central sector) and sectors characterised by thick debrite as products of remobilised material (southern sector). The above

subdivision of the study area is here refined with the integration of uncored wells into the correlation panels and the interpretation of wireline logs (Fig. 5.24).

The northern area is characterised by three cored-wells (B33, B02 and B06) in which remobilisations (i.e. debritic deposits) are not recognised in core and which are hence considered in-situ. These wells record the “full” stratigraphy, which was used to build a template of in-situ sandstone intervals and interbedded mudstones facies with regional stratigraphic significance (Eggenhuisen et al., 2010) as described and reviewed in Chapter 4 (Fig. 5.25). The central sector corresponds to a group of 24 wells characterised by the partial evacuation of the lowermost Z10A sandstone (interval fully preserved in Wells B04, B05, B10, B12 and B43 as it is capped by black Anoxic shale as in B2). Based on this observation the central area can also be interpreted as a sector with moderate evacuation character with only Well B31 missing the lowermost sandstone interval in the south-west central area. On the contrary, the south-eastern sector comprises 12 wells where Z10A is not recognised and it is interpreted to have been fully evacuated by the failures. The exception is B17 where Z10A sandstones are recognised in core, as supported by the presence of the underlying Z7 and interbedded Black Anoxic shales which both mark the very basal Lower BSF (Fig. 5.24).

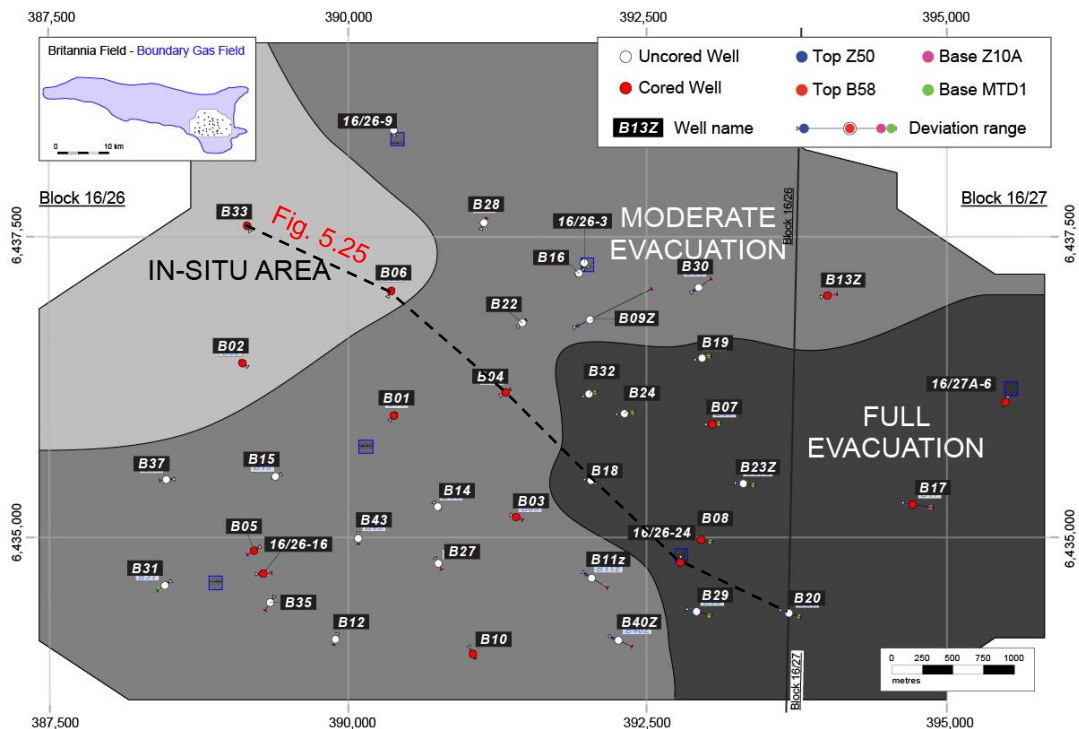


Fig. 5.24 – The three main sectors identified in the Platform Area based on different amounts of removal of the Britannia Sandstone stratigraphy.

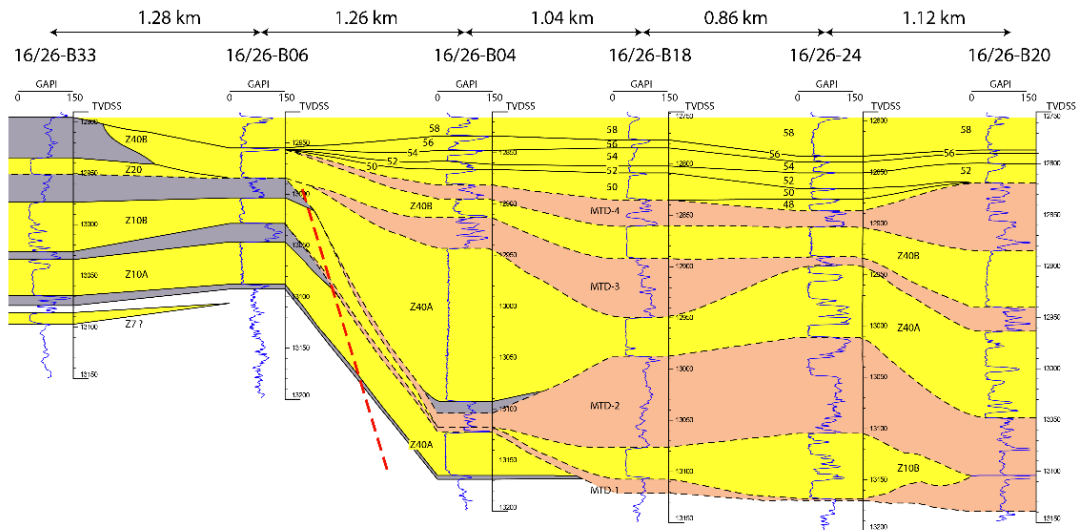


Fig. 5.25 – WE-SE section integrating cored and uncored wells (location in Fig. 5.24).

5.5.2 MTD character at different scales of observation

The partial or full erosion of reservoir intervals in the Platform Area has been interpreted as resulting from large-scale failure events (Eggenhuisen et al., 2010). Usually these events are well recognised at the outcrop scale (Lucente and Pini, 2003; 2008; Ogata, 2010; Van Der Merwe et al., 2011; Martín-Merino et al., 2014; Ogata et al., 2014b; Fukuda et al., 2015; Sharman et al., 2015) or on high quality seismic dataset (Frey-Martinez, 2010; Gamberi and Rovere, 2011; Olafiranye et al., 2013) and compared together (Armitage and Stright, 2010; King et al., 2011; Posamentier and Martinsen, 2011) in order to better recognise such events during 1D core log investigation (Cossey, 2011). Abrupt boundaries between different lithologies can be either interpreted as a change in the depositional character (e.g., composite lobe switching, see Deptuck et al., 2008), or interpreted as a characteristic feature of missing stratigraphy and hence evacuation of sediments due to erosion, whereas debritic deposits, folded layers and chaotic intervals are recognised as the product of remobilisation of previously deposited material. Eggenhuisen (2010) has already shown in his work how it can be difficult to distinguish in-situ stratigraphy from remobilised deposits (Chapter 3), but correlation panels of cored and uncored wells, constrained by regional stratigraphic markers may facilitate this differentiation (Fig. 5.27).

Sandy and silty debritic deposits are characterised in core by different concentrations of light-coloured sand grains suspended in the dark matrix (Table 5.4). This causes “starry night” texture, which slightly differs from this facies *sensu* Lowe and Guy, (2000). In addition, mudstone clasts and sandstone blocks of various sizes, from mm scale to 2 m, occur in the matrix and are generally orientated bed parallel (Fig. 5.26-

A i-ii). Muddy debrites are identified in core by dark grey mud-silt matrix without floating quartz grains in the matrix. Mudstone clasts and sandstones blocks are suspended into the muddy matrix with various sizes (from mm scale to 80 cm) and they are also generally orientated bed parallel (Fig. 5.26-B i-ii).

These debrite facies when recognised in core at different stratigraphic depths, interbedded with sandy reservoir intervals interpreted as in-situ, highlight the occurrence of failure events through time. They are nearly always identified in the wells of the study area with the exception of the northern sector (B33, B06 and B02). However, a systematic thickening of this type of deposits is observed from the central sector toward the south and east of the study area. The recognition and distinction between the two debrite facies also enables differentiation of the earliest and lowermost MTDs from the younger and upper deposits. Thus, sandy debrites (starry night) mainly characterise MTD-1 and MTD-2 whereas muddier debrites make up MTD-3 and MTD-4. The difference between the lowermost debrite encountered in the stratigraphy, MTD-1, and the second, MTD-2, is based on their thickness, although sometimes this could be misinterpreted, given that MTD-1 could have been eroded by later turbidity currents or by MTD-2 where MTD-1 and MTD-2 deposits are interpreted to be in contact in some wells (3, 16, 24, B13z, B15, B16, B20, B22, B27, B29, B31, B28, B40z, B43). In this case the boundary cannot be recognised in core. However the two MTDs can be partially distinguished on wireline logs on the basis of the material incorporated within their deposits. MTD-2 is characterised by a higher presence of sandstone clasts, which can be recognised on gamma ray logs, in comparison with MTD-1 that shows lower concentration of clasts. Finally, MTD-3 and MTD-4 show more similarities between each other, in terms of character and thickness distribution of remobilised deposits.

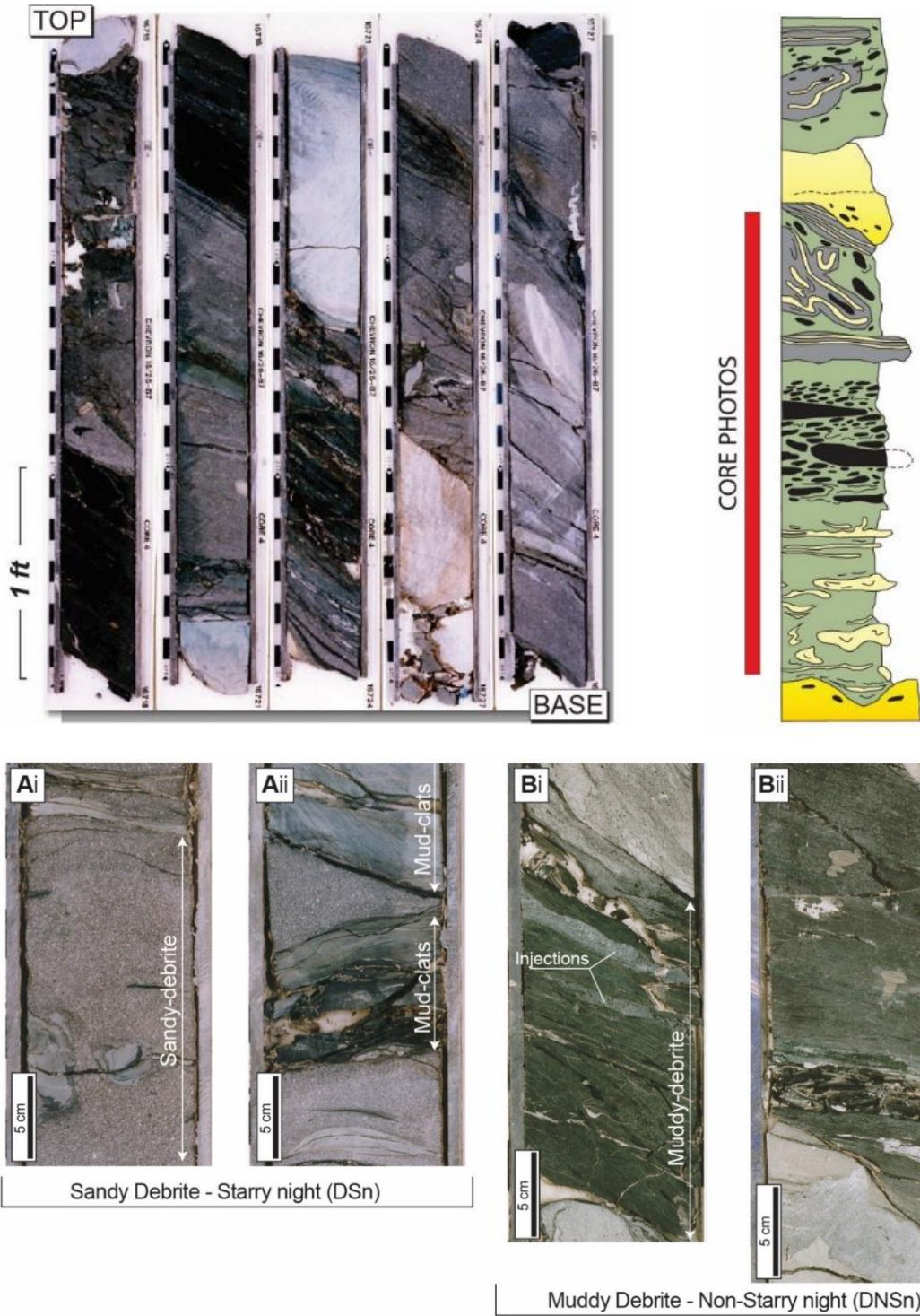


Fig. 5.26 – Representative core photos of the debris facies groups recognised in this work.

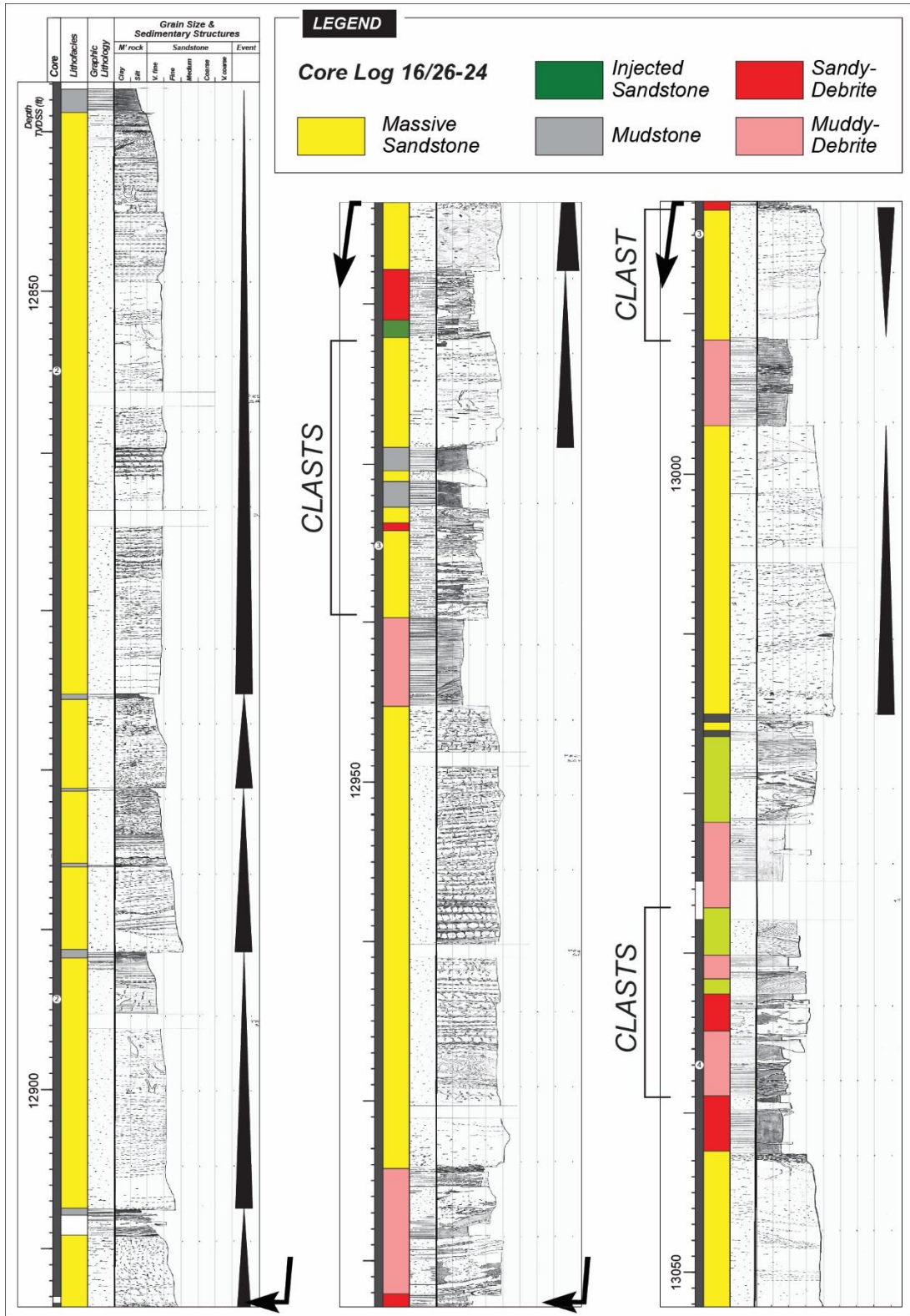


Fig. 5.27 – Representative core log (well: 16/26-24) showing a range of sand and mud clasts surrounded by the muddy matrix within the MTD-3 interval.

Mudclasts and sandstone blocks in a muddy-silty matrix with high percentage of floating quartz grains (up to 40%) represent the product of debris flow characterised by en-masse deposition making up “sandy debrites”. The complete mixing of sand grains into the matrix of the debrites suggests that the remobilised sandstones were apparently unconsolidated. “Muddy debrites” are interpreted as deposited by highly concentrated, viscous, sediment-fluid dispersions that move downslope under the influence of gravity. The absence of floating quartz grain in the matrix can either be explained by a different provenance compared to the starry night debrite deposits or can be associated with an early stage of disaggregation of sandstones clasts.

The facies described above are both interpreted as the products of debris flows associated with large-scale mass-failure events (Shanmugam et al., 1996; Talling et al., 2007c; Masson et al., 2008; Strachan, 2008; Ogata et al., 2011; Ogata et al., 2014; Qin et al., 2015). Although debris flows are also documented and interpreted as standalone events (e.g., Lastras et al., 2004; Talling et al., 2012), in the Britannia Field these processes seem to be linked with large-scale sliding events that involve large portions of in-situ stratigraphy. In fact, Britannia deposits could be interpreted either as the result of the rheological transformation of a laterally failed mass into a debris flow with the excision surfaces characterised by missing stratigraphy, representing failure planes, or as the products of largely bypassing mass flows sourced from upslope that left relatively thin debrite lag behind. In the first case, the initial failure might take place locally within the Platform Area, whereas in the second interpretation the failure occurred higher up on the northern slope of the Fladen Ground Spur (Eggenhuisen et al., 2010). Each of the MTDs recognised is associated with some reshaping of the seafloor in the Platform Area based on different magnitudes of remobilisation which characterise the basal erosive style and which also influence the development of constructional topography. Palaeobathymetric maps of the basal and upper topography of each of these MTDs are shown below.

Facies	Code	Description	Process Interpretation
<i>Debrite "Starry- night" matrix</i>	DSn	Well-mixed matrix of fine to medium sand grains and dark grey mud-silt matrix. The "starry-night" appearance is given by the light-coloured sand grains suspended in the dark matrix. Occasional mudstone clasts and sandstone blocks occur in the matrix, with various sizes (from mm scale to 2 m) and generally orientated bed parallel. Occasional higher sand content through sand injections.	Mud-clasts and sandstone blocks set into the mud-silt matrix characterised by high concentration of light-coloured sand grains are the product of debris flow, characterised by en-masse deposition. The complete mixing of sand grains into the matrix indicates remobilisation of unconsolidated sandstone. These deposits can be interpreted as either events linked to large-scale sliding process or standalone events.
<i>Debrite Non- starry night</i>	DNSn	Dark grey mud-silt matrix characterised by the absence of floating quartz grains in the matrix. Mudstone clasts and sandstones blocks of various sizes (from mm scale to 80 cm) are floating into the muddy matrix and are generally orientated bed parallel.	Deposition from highly concentrated, highly viscous, sediment-fluid dispersions that move downslope under the influence of gravity. The absence of floating quartz grain in the matrix can be explained with a different provenance compared to the starry night debrite deposits or to an early disaggregation stage.

Table 5.4 – Facies table for the MTDs from core logs.

5.5.3 MTD-1

Description

The first remobilisation phase (MTD-1) was recognised by Eggenhuisen et al. (2010) and it is characterised by the partial or full removal of the sand interval Z10A and of the Black Anoxic mudstone which encases it. Debritic and chaotic deposits are not recognised in the northern sector B33, B06 and B02 wells. In these wells, the Z10A and the overlying stratigraphy made up of the Z10B and Z20 sandstones, interbedded with the grey marl (Ewaldi Marl) and reddish mudstones (Red Mudstone) on their respective tops were interpreted as being in-situ by Eggenhuisen (2010), as the deposits were not affected by failure processes.

The map of the basal surface of the MTD-1 highlights three distinct areas based on the erosional character of this interval. The northern sector is the in-situ area, while the central and south-eastern sectors record the respectively partial or total evacuation of Z10A (Fig. 5.28-A). In the south-eastern area Z10A together with the black anoxic mudstone (approximately 5 metres of thickness measured from in-situ wells B33, B02 and B06; Eggenhuisen et al., 2010) are missing and the removed material is only partially replaced by a thin debrite. The remobilisation index, calculated by measuring the ratio between the thickness of the removed deposits and the reconstructed thickness of Z10A where it is not preserved, substantially increases from the central sector (35%) toward the south-eastern area (85%).

Various thicknesses of debritic intervals interpreted as linked to the first failure event are recognised in 36 wells across the Platform Area ranging from ~2 m to ~53 m (Fig. 5.28-C). Fifteen of these wells (3, 9, 6, 24, B11z, B13z, B15, B16, B22, B27, B28, B29, B31, B40z and B43) were not included in this calculation because MTD-1 and MTD-2 deposits are juxtaposed and hence their common boundary cannot be distinguished (e.g., Le Friant et al., 2015). However, given the different times of MTD-1 and MTD-2, they cannot be considered a mass-transport complex (MTC), which is defined as the occurrence of juxtaposed multiple events. Thin debritic intervals are recognised in wells over the central sector where these deposits sit on preserved (B05 and B10), or partially eroded Z10A sandstones as in B27 and B17. The latter is the only well of the otherwise fully removed south-eastern area where the Z10A is partially preserved. In this central sector, thin debrites cluster over an area of 4.5 km². Thicker debrite intervals are non-uniformly present across the study area with the thicker remobilised deposits found in wells B30 and 27A-6 located on the north-eastern sector and in the group of B01, B14, B03 and B12 which sit over a thick Z10A (likely fully preserved interval, although the capping mudstone on top of Z10A is not

recognised). In B37, ~36 m of debrite are deposited over a thin, partially eroded Z10A.

Interpretation

The first remobilisation that occurred after the deposition of Z10A and the overlying anoxic hemipelagic mudstone did not affect the Z10B sandstone and the associated Ewaldi Marl mudstone, and therefore must have occurred just before the deposition of the Z10B sand interval (Eggenhuisen et al., 2010) (Fig. 5.28-D). The décollement surface could be identified within the anoxic hemipelagic mudstone which might constitute a weak layer. In fact, Urlaub et al. (2015) noted that layers that are extremely rich in organic matter or that undergo a rapid porosity decline, are a potential weak plane for generating slope failure when sediment accumulation is the only pressure source.

A trend of increasing erosional character can be observed from northwest to southeast, with the first remobilisation partially eroding Z10A and related Ewaldi Marl interval in the central Platform Area and fully removing the south-eastern sector of the study area. This is also highlighted by the substantial increase of the rate of remobilisation in the same direction. The reconstruction of Z10A is possible given the distinctive tabular character of the sandstones making up this interval (see Chapter 4) that measure ~12 metres (max = ~16 m; min = ~10 m). The wide area of missing stratigraphy in the south-eastern sector is likely the result of the erosion associated with a remobilization which acted as a slide, as supported by the small debrite thickness overlying the erosion surface. The topographic lows developed due to the partial and full removal of Z10A and of the anoxic mudstone show a gradually steepening connection between the shallower and un-remobilised north-west sector and the central sector. This gentle morphology can be associated with an extensive slide of the lowermost Britannia stratigraphic intervals that should have measured ~33 metres in thickness (as the reconstruction based on B33, B06 and B02) and covering most of the Platform Area.

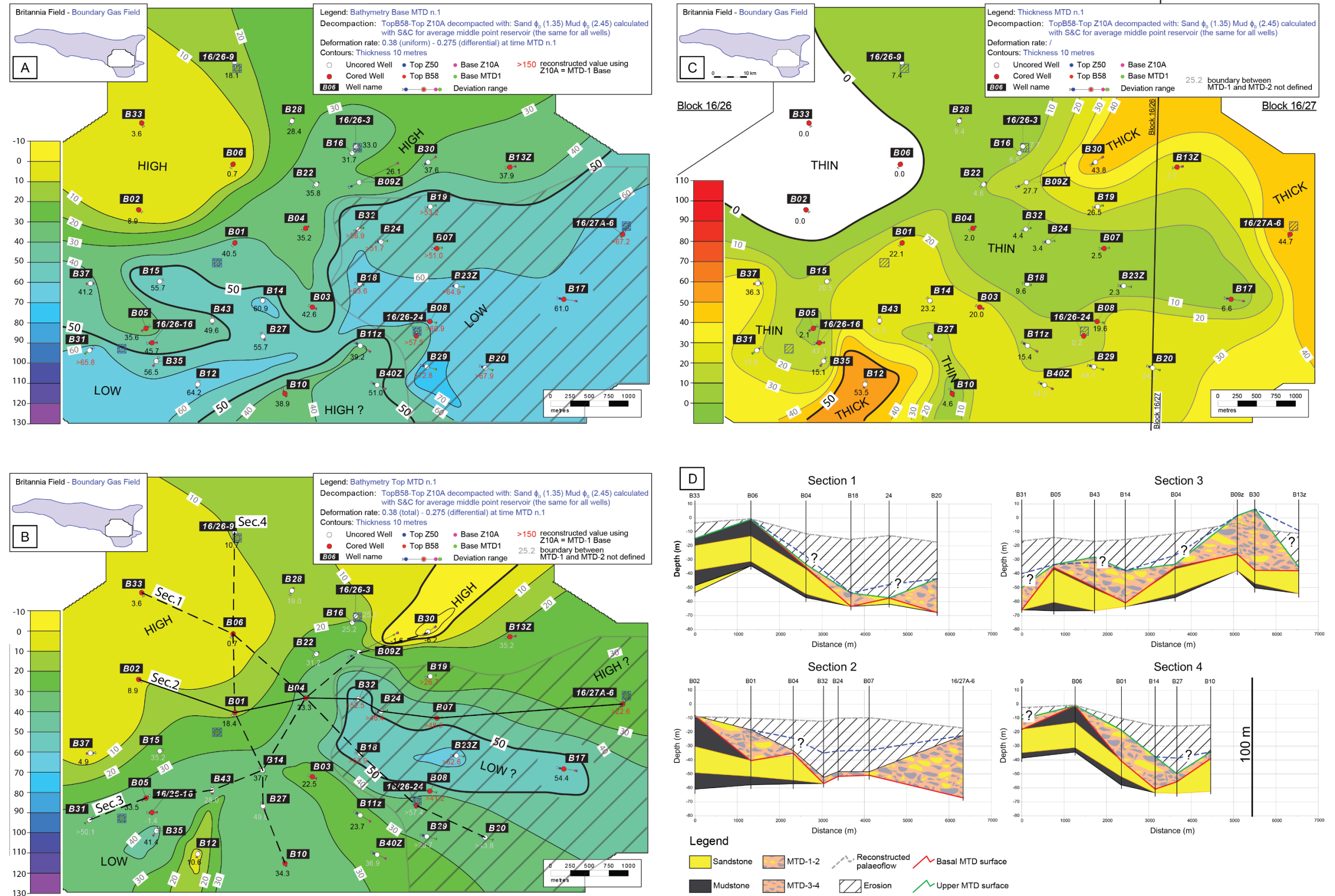


Fig. 5.28 – A-B) Palaeobathymetric maps of the basal-upper topography associated with MTD-1, for reconstructed MTD1-time. Contours in metres: blue = deep; orange = shallow. Dashed area represents reconstructed Z10A depths values. C) MTD-1 Thickness map; D) Geological sections showing 2D deposits distribution. Question marks and dashed blue line represent an interpretation of MTD-1 distribution in absence of erosion due to the second slope-failure (MTD-2) (see text for description).

5.5.4 MTD-2

Description

The second remobilisation, MTD-2, affects the sandstones deposited above the first remobilisation and its timing is restricted to a period just before input of the Z40 sands. A comparison with the thickness of in-situ stratigraphy in wells in the northern area (B02-B33) yields a reconstructed ~111-115 metres of decompacted stratigraphy (Figs. 5.25, 5.29-D) that was remobilised by the MTD-2 (Eggenhuisen et al. 2010 and this work). Also for the second phase of remobilisation, the stratigraphy in the south-eastern area results is more deeply eroded than in the north-western area, with a widening of the erosion surface that moves backwards in the central sector of the study area up to the edge of the topographic high represented by wells B33, B02 and B06 (Fig. 5.29-A). The deepest topographic low is located around wells B35 and B12 in the south-western sector with the base of MTD-2 identified at ~127 metres below the reconstructed palaeo-horizontal datum. The basal surface of the second remobilisation does not permit a full and comprehensive understanding of the central sector which is represented by Wells B03, B07, B18, B23z, B24 and B32 and marked by the dashed area on Fig. 5.29-A. This is due to the difficulties in the recognition of the remobilised vs in-situ portion of stratigraphy in core and thus further analysis and a detailed interpretation for this area are required (see interpretation below). In fact, Fig. 5.29-A shows a deeply eroded area in B18 and B23z (~100 metres), juxtaposed with 30.5 metres of interpreted in-situ Z10B (it is capped by ~19 metres of hemipelagic mudstone of the Ewaldi Marl), leading to some doubts as to the real history of the coupled sandstones-mudstone intervals in B03. This uncertainty certainly affects the contouring of the isopach maps of the basal surface of MTD-2 and the thickness distribution of its deposits (Fig. 5.29-C) but it does not influence the reconstructed morphology associated with the top of MTD-2 (Fig. 5.29-B), which also represents the palaeo-seafloor after the second remobilisation event. The palaeobathymetry shaped by the emplacement of MTD-2 is characterised by a deep trough developed on the flank of the in-situ sector and delimited by the topographic high shaped by debritic deposits associated with the remobilisation event recognised in wells B27, B03, 24 and B08. Both topographic features are oriented SW-NE, parallel to the edge of the in-situ area of the north-west sector. The irregular topography over the seafloor associated with MTD-2 is highlighted by the geological sections across the study area (Fig. 5.29-D). The elongate depression corresponds with the partial or full remobilisation of the stratigraphic intervals composed of Z10B, Ewaldi Marl, Z20 and Reddish mudstone, as shown by the geological sections n.1,

2, 3 and 4. These sections also highlight the tilting of the lowermost intervals between the north-west and the central sector.

Interpretation

The isopach map of the palaeobathymetric surface after the second large remobilisation event represents the décollement surface of MTD-2. This is characterised by a flat surface over the southernmost and central sector, by a headwall scarp alongside wells B37, B15, B01 and just below B09z and B30, and by two discontinuous edges identified in B02-B33 and B09z-B30, likely corresponding to the MTD-2back-scarp. These morphological features are often observed over the depletion zone of a landslide (e.g., Sawyer et al., 2009; Watt et al., 2012b) which also is interpreted being the proximal area of an MTD. The interpreted headwall-scar is interrupted in the proximity of wells B04, B22, B16, 3 and B28 where erosion moves back towards the north. This depression is filled by debritic deposits as product of subsidiary debris flows associated with larger scale sliding mechanism that shows a NW-SE movement direction. The inferred sliding process can explain the described headwall-scar morphology recognised in the north sector of the study area. However, recognition of shifted blocks associated with sliding mechanisms is difficult in core; in fact, intact large blocks of remobilised material can move downdip maintaining bed parallel orientation (see “shifted blocks model” below) and hence concealing remobilisation features, especially in core and well logs.

Thick debritic deposits recognised in the south-eastern sector are juxtaposed with the discontinuous headwall scar shaping the seafloor with an elongated ridge that constrains the trough on the north. This morphological feature represents re-deposition of translated and disaggregated blocks that moved down from the up-slope evacuated topography that corresponds with the elongated trough identified in the central sector of the study area. Sandy debrites (“starry night” texture) recognised in this area are interpreted as the result of disaggregation of large portions of stratigraphy over 1.5 km. In fact these deposits are characterised by high concentrations of sandstone- and mudstone-clasts of various size (from mm scale to 2 m).

Finally, the highly irregular rugosity identified over the reconstructed palaeobathymetric seafloor after the emplacement of MTD-2 is thought to be the result of remobilisation and subsequent re-deposition of the disaggregated lower portion of the Britannia stratigraphy, associated with sliding processes that laterally transformed into more fluid debris flows, likely due to the entrainment of water. However, the debritic deposits recognised within the depression that interrupts the

back-scar and extends toward the north might be interpreted as the product of debris flows coming from higher up the Fladen Ground Spur, given the minor concentration of sand-clasts.

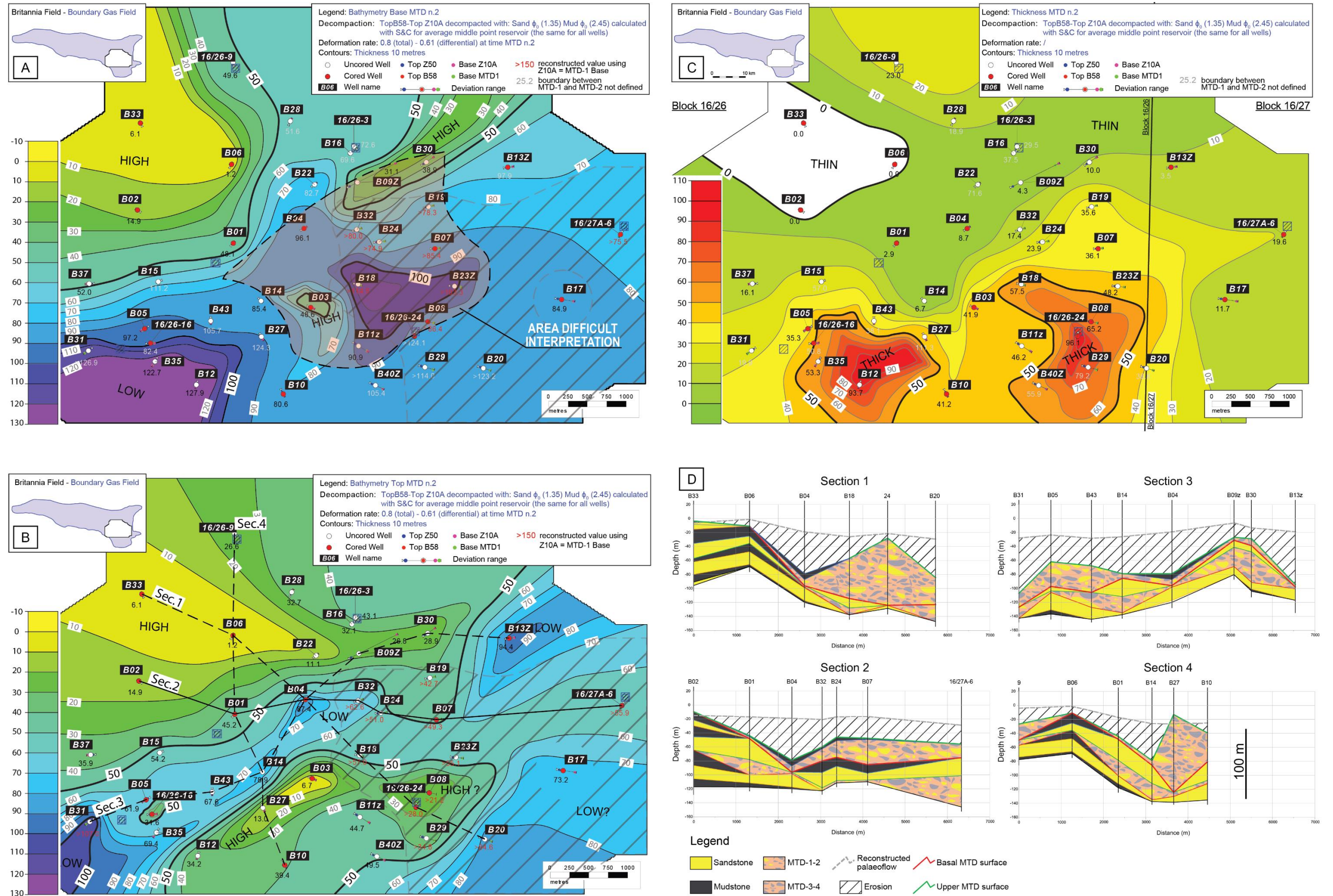


Fig. 5.29 – A-B) Palaeobathymetric maps of the basal-upper topography associated to MTD-2, for reconstructed MTD-2-time. Contours in metres: blue=deep; orange=shallow. Dark area marked by dashed line on isopach map A represents the area of difficult interpretation. Dashed area on isopach map B represents reconstructed Z10A depths values. C) MTD-2 Thickness map; D) Geological sections showing 2D deposits distribution.

MTD-2 slid blocks model

The area of difficult interpretation, marked by the dashed zone in Fig. 5.29-A, is here investigated with a detailed analysis undertaken on Z10B and overlying stratigraphy, in order to constrain the uncertainties due to the difficult distinction of in-situ vs. remobilised large blocks of the lower portion of Britannia deposits over the basal surface of the MTD-2.

After initial slope failure, fragmentation and movement of large blocks are associated with sliding processes (Masson et al., 1998; Masson et al., 2006); the translation of large portion of stratigraphic intervals can occur together with rotational and rolling mechanisms (Ilstad et al., 2004; Gee et al., 2005; Lourenço et al., 2006) or without substantial tilting of the blocks (Bull et al., 2009). The recognition and characterisation of large rafted blocks is possible on outcrops (e.g., Lucente and Pini, 2003; Sobiesiak et al., 2013, 2016; Strachan et al., 2013; Alves, 2015) or through good quality seismic dataset (e.g., Jackson, 2011; Watt et al., 2012a; Omosanya and Alves, 2013; Crutchley et al., 2013; Gamboa and Alves, 2015), whereas it is extremely difficult investigating just cored wells, given the large size of the blocks (e.g., Cossey, 2011) and the lack of dip meter data.

In the Platform Area, the area encompassing wells B22, B16, 3, B09z, B30, B04, B32, B24, B19, B07, B03 and B18, characterised by ambiguous contouring of the décollement surfaces associated with the MTD-2 (see Fig. 5.29-A) is investigated by studying the relationship between the reconstructed palaeobathymetric surface associated with the emplacement of MTD-1 and the subsequent Z10B sandstone infill. Observing the thickness distribution of Z10B across this area, it seems that the reservoir intervals in these wells are displaced and shifted south from where they were deposited. This hypothesis is supported by comparison of the thickness of fully preserved Z10B, and hence capped by bioturbated mudstone of the Ewaldi Marl (B03, B32, B24 and B07), with the bathymetry reconstructed at MTD-1-time. Assuming that Z10B sandstones healed the rugose palaeo-seafloor after the emplacement of MTD-1 (see section 5.4.2.2), as demonstrated by wells B06 and B02 (Fig. 5.30), Z10B sandstones capped by hemipelagic mudstone in B32, B24 and B07 do not seem to fully fill the bathymetry in this area (Fig. 5.30). Z10B in wells B07, B24 and B32 represents less than 50% of the space available for deposition.

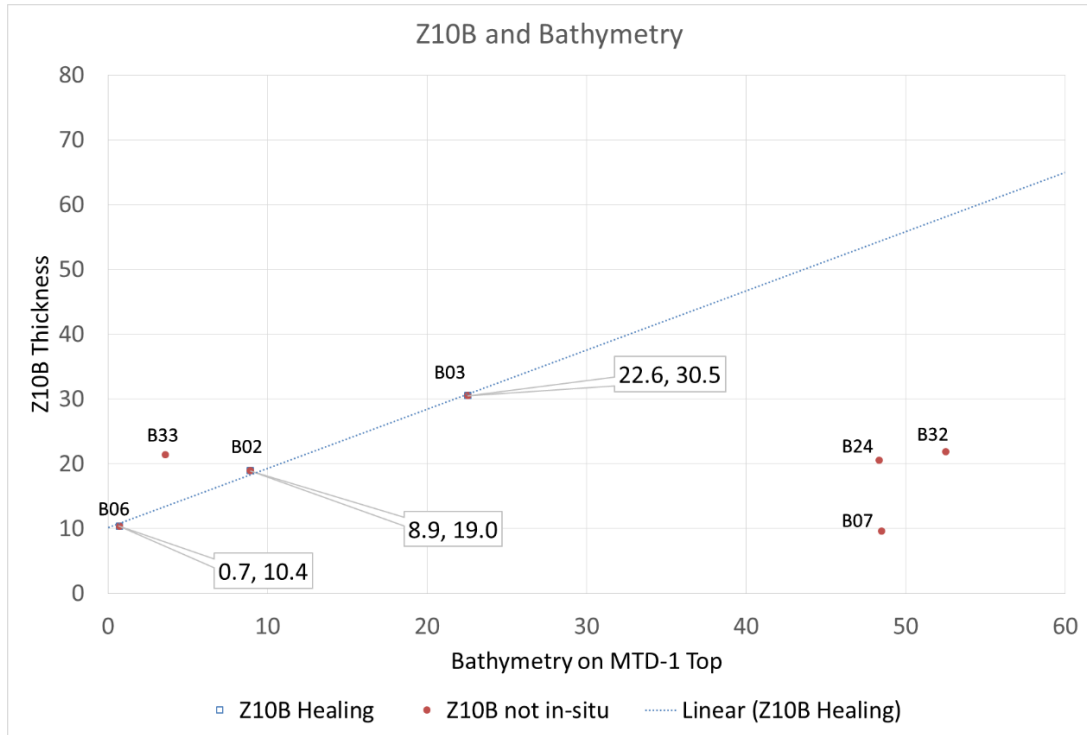


Fig. 5.30 – Relationship between the Z10B thickness in wells with preserved tops and reconstructed palaeobathymetric surface associated with MTD-1 in order to recognise remobilised stratigraphic intervals. The relationship shows that the accommodation space created by MTD-1 is filled by Z10B in wells B06, B33, B02 and B03, whereas B07, B24 and B32 seem deposited in topographic lows without Z10B filling the accommodation space. Z10B thickness in well B33 is characterised by high concentration of injections, giving a misleading impression of the real thickness of the sandy reservoir zone in this well.

The sandstone thickness measured in B07, B24 and B32 is instead compatible with a shallower bathymetry located on the north of the inferred remobilised area. Figure 5.31-A aims to reconstruct the location of the shifted blocks (dashed red boxes in the Fig. 5.31-A).

Geological sections drawn across the area of interest (Fig. 5.31-D) show that the blocks inferred to have been shifted are bounded by debritic deposits of MTD-1 below and MTD-2 on top. Considering the deposition of Z10B occurred after the emplacement of MTD-1, block translation is the result of sliding processes associated with the MTD-2. In this case, large portions of lower Britannia Stratigraphy moved over a décollement surface that corresponds to the presumably unconsolidated and water-rich debritic deposits of MTD-1. The overpressure due to the emplacement of Z10B and overlying intervals (Ewaldi Marl, Z20 and Reddish mudstones) together with the MTD-2 could have triggered the sliding of these large blocks, which were deposited bed parallel (e.g., Ogata et al., 2014a).

The inferred slid blocks cover an area of 250 km²; the basal surface of the MTD-2 is deeper, shaping a deep topographic low of ~110 metres (Fig. 5.31-B). The reconstructed isopach map of the thickness distribution of MTD-2, incorporated the slide block model for the central sector, highlights a continuous edge formed by both debrite and slide blocks, oriented SW-NE and hence parallel to the headwall scar on the edge of the in-situ area (B02-B33), where the initial slope failure likely triggered.

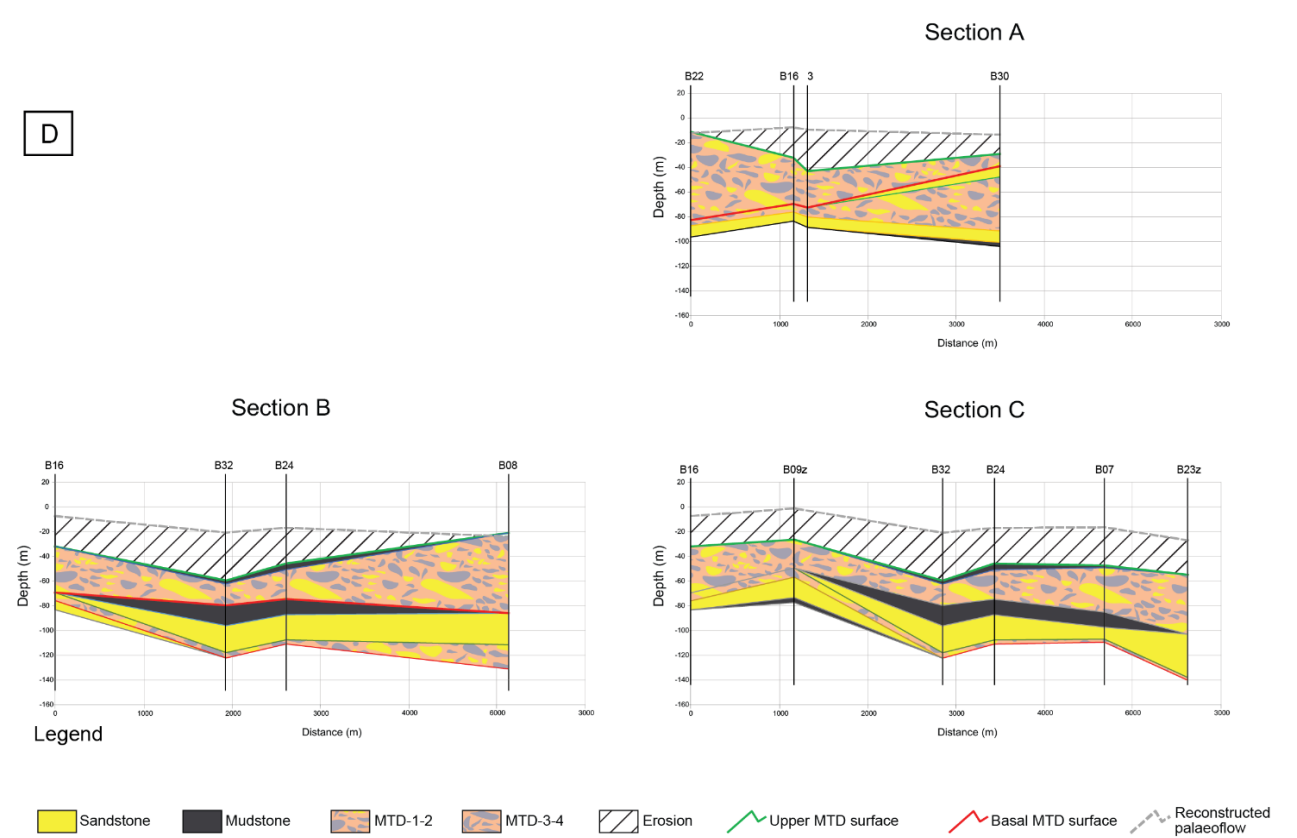
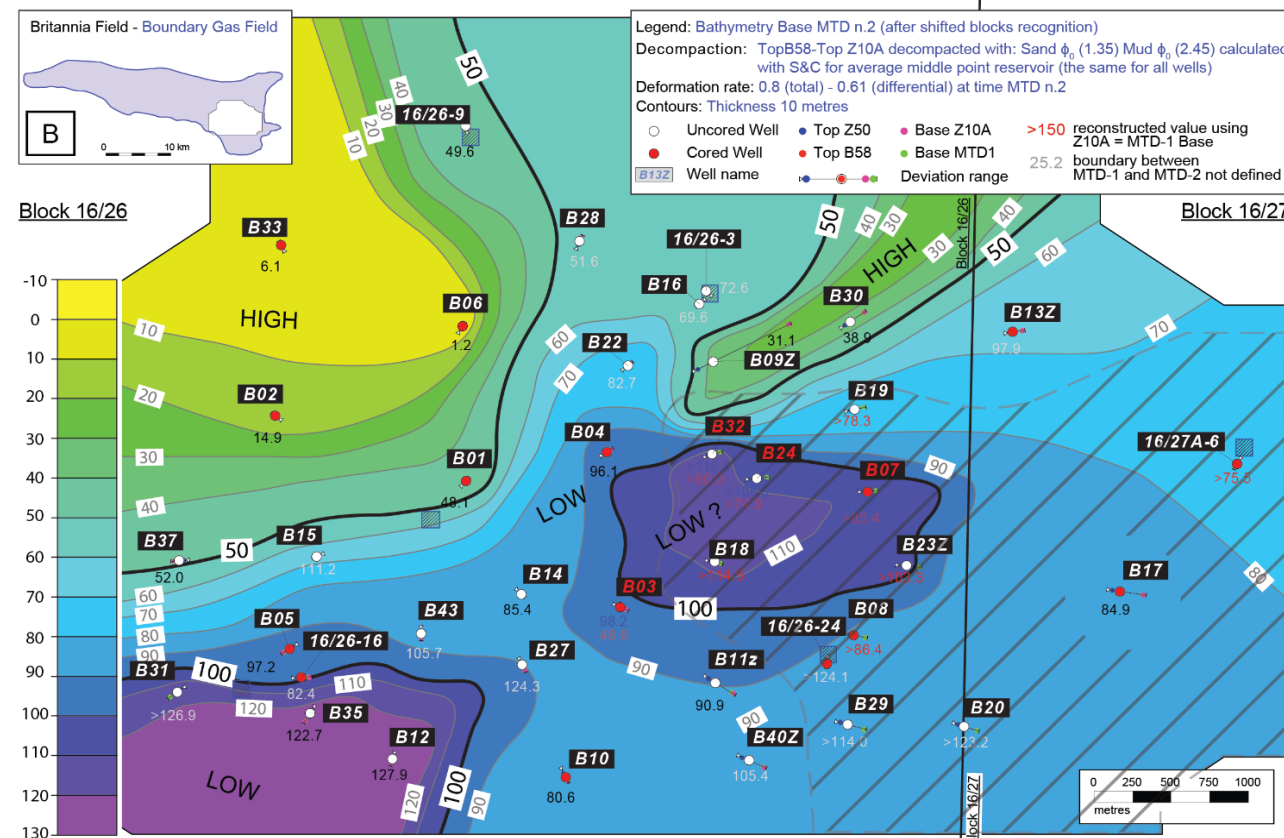
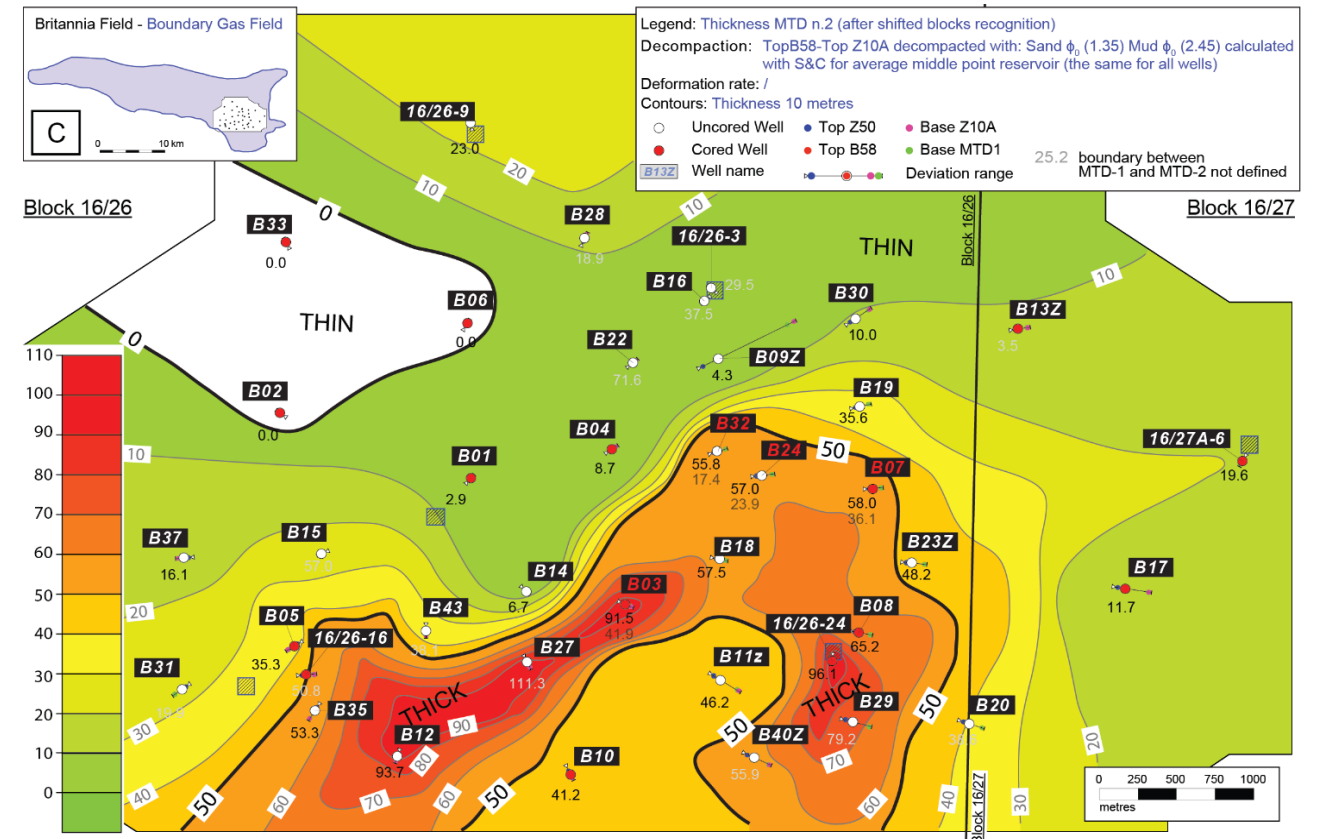
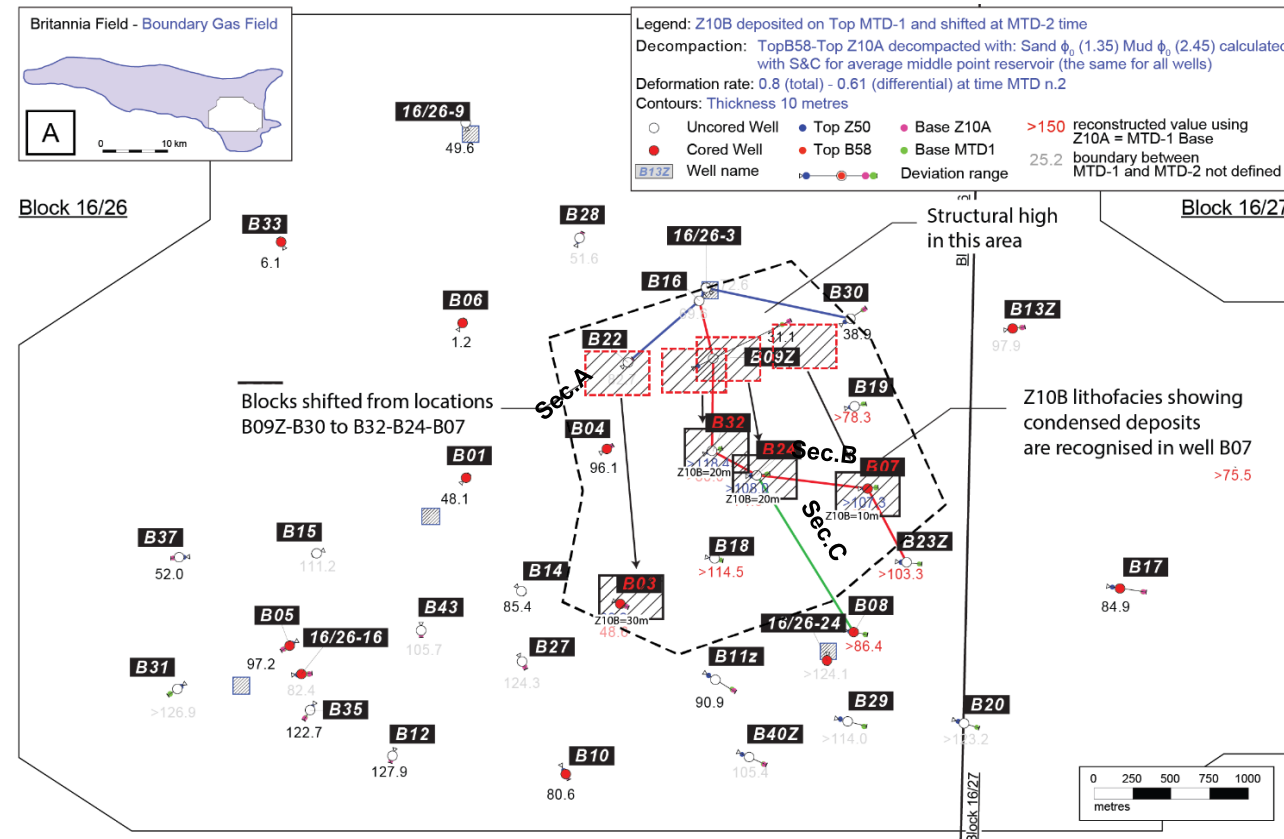


Fig. 5.31 – A-B) Palaeobathymetric maps of the basal topography associated to MTD-2, for reconstructed MTD-2-time. Contours in metres: blue=deep; orange=shallow. Dashed area on isopach map B represents reconstructed Z10A depths values. C) MTD-2 Thickness map including shifted blocks; D) Geological sections showing: Sec A) inferred source area of the slid blocks; Sec B-C) shifted large blocks of Z10B-Bioturbated mudstone interval above MTD-1.

5.5.5 MTD-3

Description

In the upper part of the Lower-Middle BSF the third phase of remobilisation occurs after the deposition of Z40A, which is partially eroded by the failure itself. Debritic intervals are recognised across the wider Platform Area with the exception of well B33 and B02 where the stratigraphy is interpreted as being in-situ and Z40A is followed by the Z40B. In well B06, the Z10B sandstone and Grey Ewald Marl are followed by the Z40B; the couplet Z20-reddish mudstone and the Z40A are not recorded. As in the lower MTD1 and -2 the area of deepest evacuation is in the south-east sector, where the erosion results in the development of up to 50 metres of accommodation space. Topographic lows are highlighted on the contour map of the basal surface of the MTD-3 (Fig. 5.32-A), which form a long and continuous SW-NE topographic low with the deepest area represented by B31, where the basal surface is over ~90 m deep. In the south-eastern area B20 and B23z record a depression which is approximately 50 metres deep.

The upper MTD-3 topography, which represents the seafloor after the deposition of the remobilised material (Fig. 5.32-B), almost retraces the morphology of the basal MTD surface, the only difference being in depth. Deeply eroded areas (~60-70 m) are infilled for 1/3 of the total depth, with ~20-30 metres of debrites, leaving ~30-40 of accommodation space (Fig. 5.32-C). Debrite deposits are almost uniformly distributed along the SW-NE trough associated with the partial erosion of Z40B whose top is not preserved in any well of the study area. However, different MTD-3 thicknesses are recorded along the NW-SE Sec.1 (Fig. 5.32-D).

The south-eastern corner of the study area remains underfilled only in B20 with just ~15 m of debrite deposited in the evacuated area (~65) resulting in a topographic low 50 metres deep, whereas the depocentre created by the failure in B23z is completely healed with ~50 m of debritic deposits (Fig. 5.32-C). This leaves a positive relief that separates the elongated SW-NE transect from the SE area.

Interpretation

The timing of the third MTD is difficult to constrain because of the lack of hemipelagic deposits directly above the MTD-3. In fact MTD-3 is overlain by the sandstones of Z40B which infill the accommodation space developed on the MTD's upper topography. In the northern sector the absence of Z40A might be due to slope-failure process associated with the MTD-3, whereas the missing stratigraphic interval composed of Z20 capped by the reddish hemipelagic mudstones might be related to the second remobilisation phase. Thus, it might be speculated that this area

represents the source area of the debris flow associated with the emplacement of MTD-3. The steep gradient of the MTD basal surface that links the deep SW-NE trough to the shallow and in-situ north-west area could represent the scarp of the failure or lateral margin. Juxtaposed with the scarp, the underfilled area corresponds to the erosive area of the slope failure, morphologically represented by the SW-NE trending trough developed that follows the same displacement trends observed above the décollement surface associated with MTD-2. Debride deposits are aligned to the trough, as shown on the geological sections Sec.4 and Sec.3 (Fig. 5.32-D).

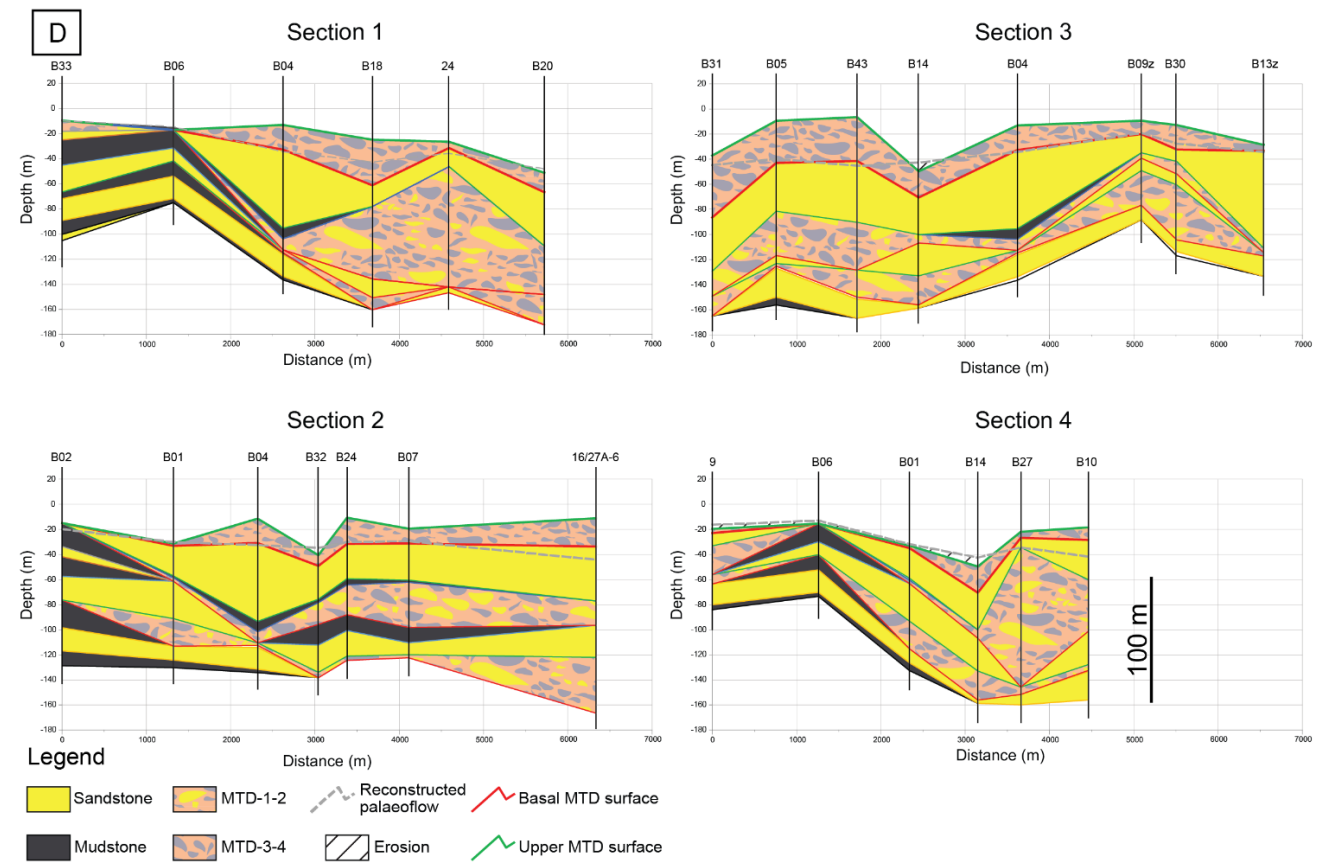
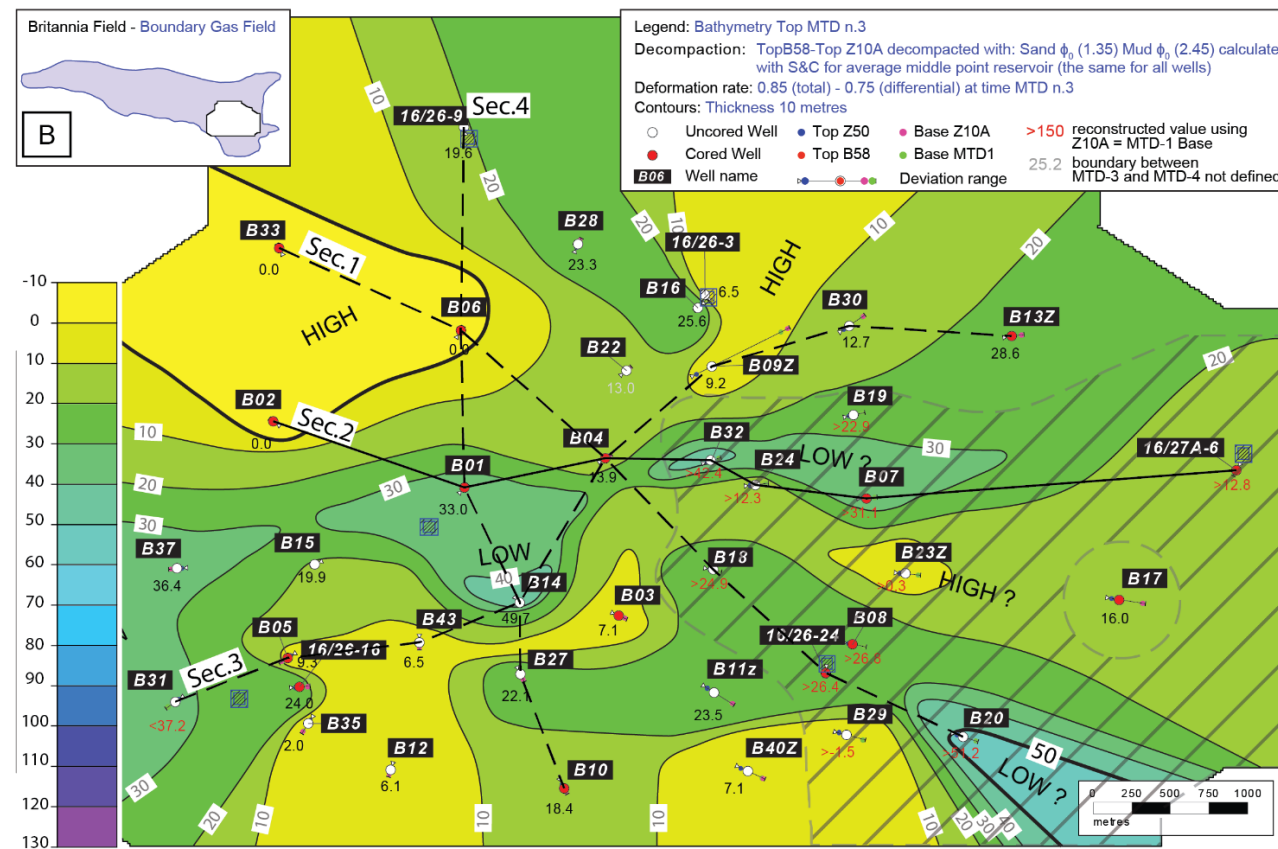
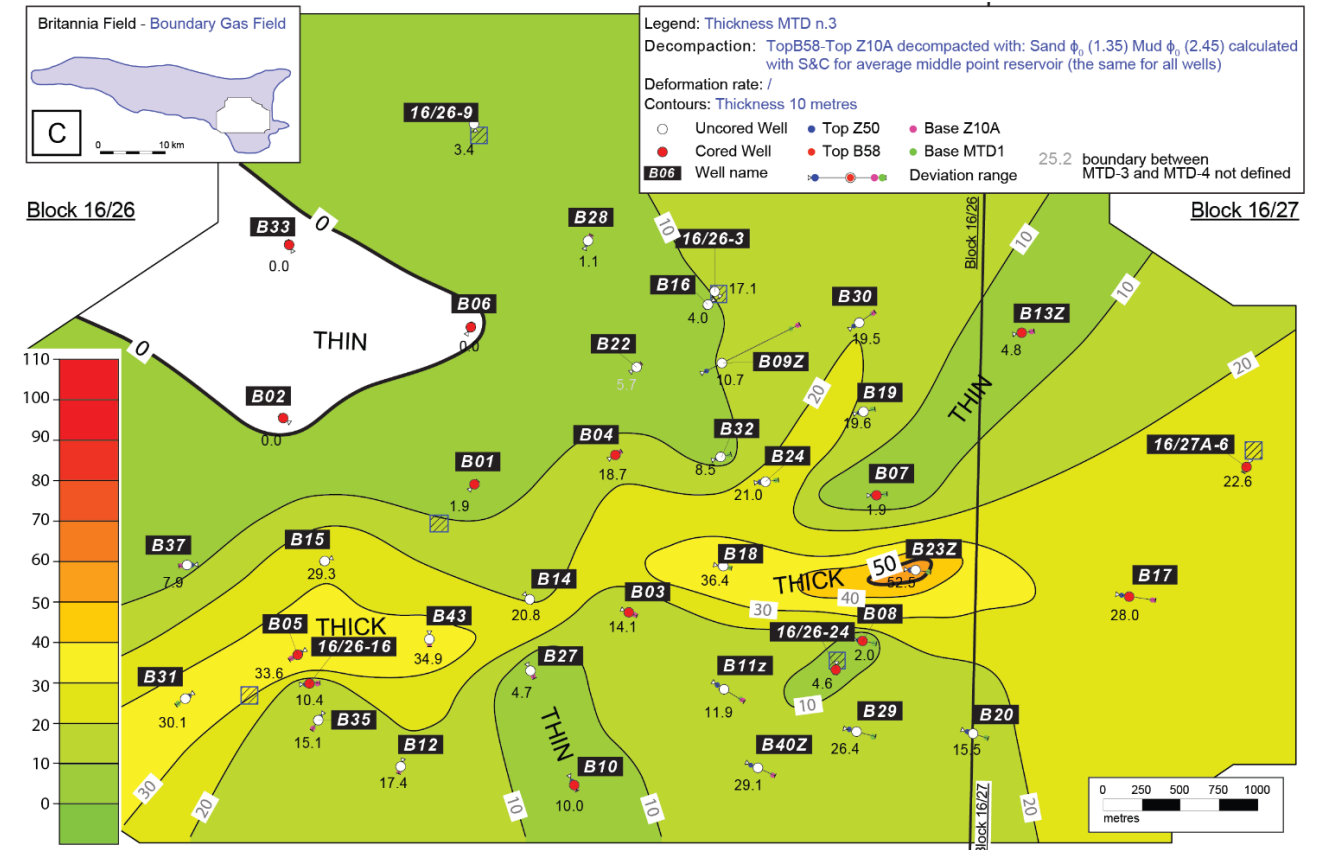
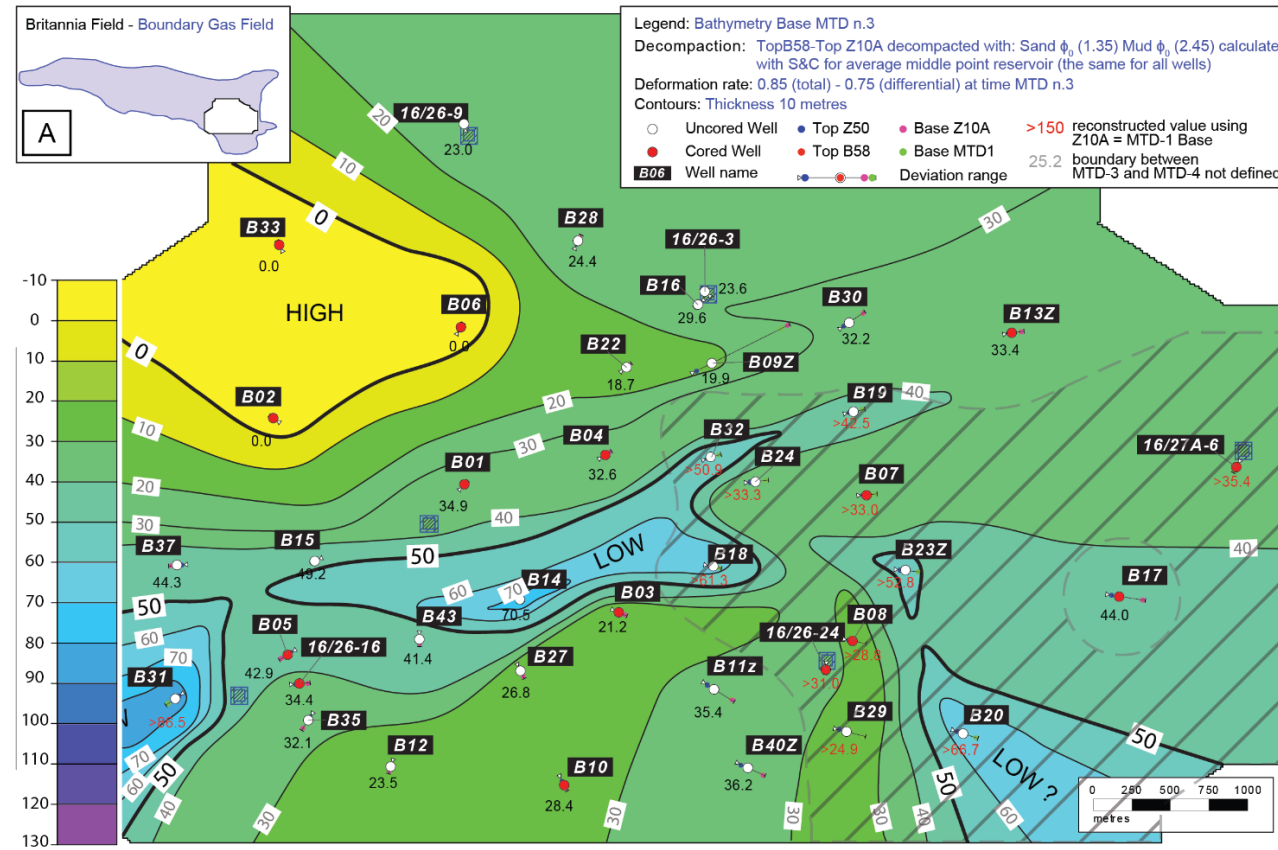


Fig. 5.32 – A-B) Palaeobathymetric maps of the basal-upper topography associated with MTD-3, for reconstructed MTD-3-time. Contours in metres: blue = deep; orange = shallow. Dashed area on isopach map B represents reconstructed Z10A depths values. C) MTD-3 Thickness map; D) Geological sections showing 2D deposit distribution.

5.5.6 MTD-4

Description

The last remobilisation event in the Lower-Middle interval is characterised as MTD-4; it covers all the study area with a range of thickness that varies between 10 m (B06) and ~40 m (B20), except for the northern in-situ area that is only represented by B33 and where a debritic interval was not recognised in core. Very thin debrites are identified in B02 and B06 with a gradual thickening towards the south-eastern sector of the Platform Area. Three thicker deposits are also recognised in 16, B14 and B32 (Fig. 5.33-C-D). The contour map of the MTD-4 basal surface highlights a similar erosion pattern to those described for the MTD-2 and -3, with a SW-NE trough that is slightly shifted toward the NW sector (Fig. 5.33-A). The upper MTD-4 topography shows the seafloor after the emplacement of the remobilised material (Fig. 5.33-B). This is the result of re-deposition of remobilised stratigraphy after the occurrence of the failure. The morphology of the seafloor is characterised by a series of positive features that form two narrow topographic highs with SW-NE orientation. The orientation of these structures is parallel to the cut-edge of the in-situ area on the north-western sector, bounding at least two depressed areas. These valleys, which were initially wrongly interpreted as channels (Sumner et al., 2005), are respectively ~15 and ~25 metres deep with the deepest area located in the south-eastern sector. Geological sections oriented NW-SE (Fig. 5.33-D - Sec. 1, 2 and 4) highlight topographic lows and highs associated with MTD-4

Interpretation

Despite the small size of MTD-4 (i.e., it has a relatively low thickness across the study area), shallower depth of erosion and limited rugosity on its top, the seafloor after the emplacement of the MTD-4 shows topographic features typical of a failure event with an evacuation and a deposition area, both interpreted as part of the proximal zone of depletion (Frey Martinez et al., 2005). This interpretation is supported by the presence of a trough developed along the previously inferred scarp morphology that in this case is slightly moved backwards onto the in-situ sector. The remobilised deposits are also aligned following the SW-NE trend which constitute the transverse edges to the interpreted axial failure direction (Twichell et al., 2009; Joanne et al., 2010; Rovere et al., 2013), which is interpreted to confirm the movement direction from NW to SE of the previous slope failures.

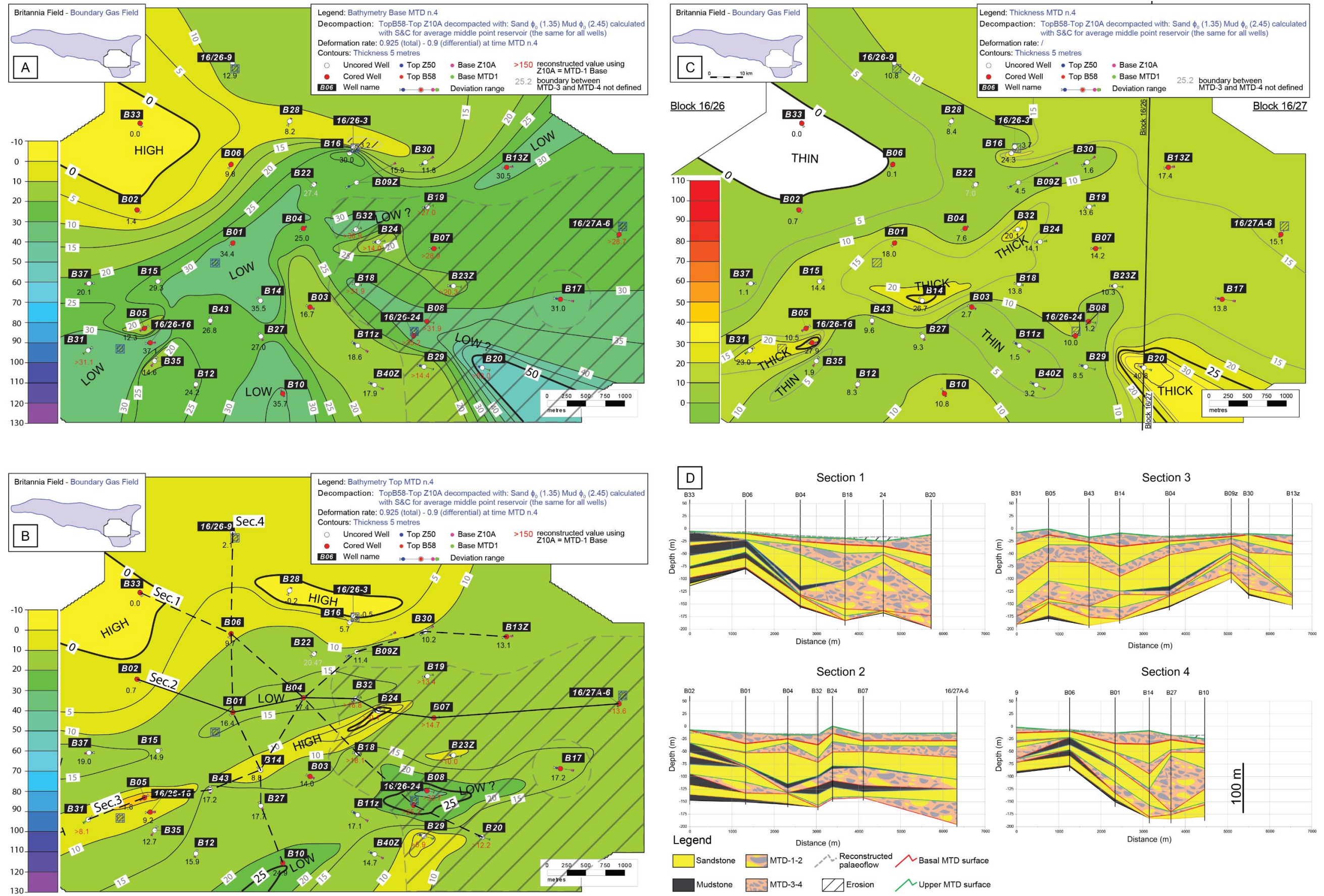


Fig. 5.33 – A-B) Palaeobathymetric maps of the basal-upper topography associated to MTD-4, for reconstructed MTD-4-time. Contours in metres: blue = deep; orange = shallow. Dashed area on isopach map B represents reconstructed Z10A depths values. C) MTD-4 Thickness map; D) Geological sections showing 2D deposits distribution.

5.5.7 Creation of accommodation space associated with MTD emplacement

The palaeobathymetric maps shown are based on the restoration using palaeo-horizontal datums that are inferred to represent the situation at the time of each MTD. For a better analysis and characterisation of these deposits a detailed study of the mechanisms of creation of accommodation in the Platform Area is performed. In the Britannia Field the accommodation space, defined as the space available for potential sediment accumulation (Jervey, 1988), may be either interpreted as being created by local rotation of the palaeo-seafloor or as consequence of sea-level rise (see section 5.4.1). In addition, erosion of substrate due to MTDs is also responsible for creation of accommodation space in the study area. These two mechanisms are distinguished as the space from the equilibrium depositional surface (seafloor-slope) up to the palaeo-horizontal line (parallel at the water line surface) likely due to tectonism, and as the space created between the existing equilibrium sediment surface (palaeo-slope) and the rugose topography formed by the emplacement of MTDs (Fig. 5.34) (Armitage et al., 2009; Armitage and Jackson, 2010; Olafiranye et al., 2013; Kneller et al., 2016).

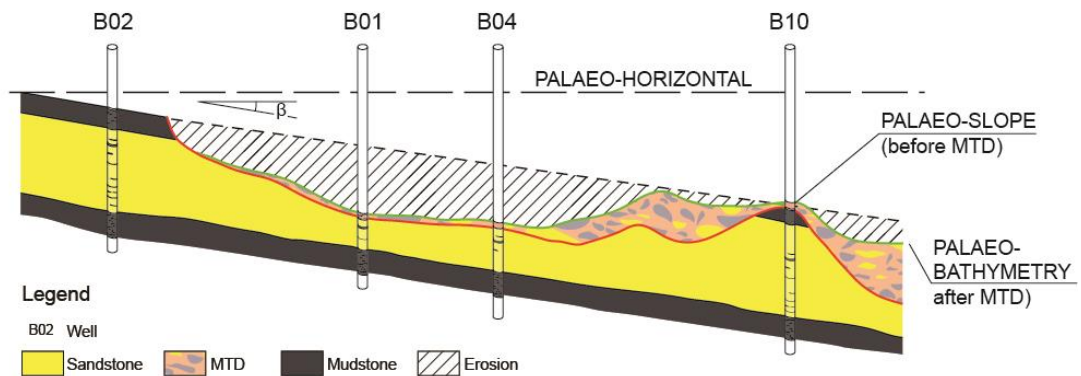


Fig. 5.34 – Schematic NW-SE section to show the accommodation space at the sub-regional scale Platform Area.

As shown in section 5.4.1, the palaeo-slope in the Platform Area was reconstructed by assuming that the remobilisation and the subsequent sand infill were almost time equivalent. This is supported by the assumption that most of the time in the Lower-Middle Britannia stratigraphy is recorded by hemipelagic deposition that occurred before each of the MTDs (see Chapter 3). The modelling of the palaeo-slope at each MTD-time enables measurement of the amount of erosion associated with remobilisations. Therefore, a better understanding of the magnitude of the MTDs in the Lower-Middle Britannia reservoir is possible in terms of maximum erosion on the seafloor, maximum thickness of MTD and maximum positive topography associated

with re-deposited material (Fig. 5.35) on the same modelled seafloor. Figure 5.35 shows that MTDs in the Z10A-Bed 58 interval possess similar thickness with the exception of MTD-2 that recorded double the thickness of the other MTDs (~50 m vs 110 m). MTD thickness mainly ties to the associated volume of multiple headward failures of previously deposited sediments. In fact, the maximum erosion measured for the four MTDs shows similar trends of the maximum thickness but from different wells. Usually, highly remobilised areas updip are juxtaposed with zones characterised by deposition of remobilised material downdip (Fig. 5.36). This relationship is confirmed by MTD-2 that recorded the most similar maximum erosion (~100 metres) and maximum thickness (~110 metres), among the four MTDs. Positive relief is recorded mainly in the re-deposition area (Fig. 5.36) where debrites are deposited on top of preserved or partially evacuated Britannia material, making up to ~20 metres of positive topography above the seafloor. The rugosity formed by topographic highs and lows associated with MTD emplacement is an important as it contributes to the evolution of the depositional system, through obstructing and trapping subsequent turbidity currents. The calculation of erosion for each MTD of the Lower-Middle Reservoir is also shown on the geological section of Figures 5.28, 5.29, 5.32 and 5.33-D.

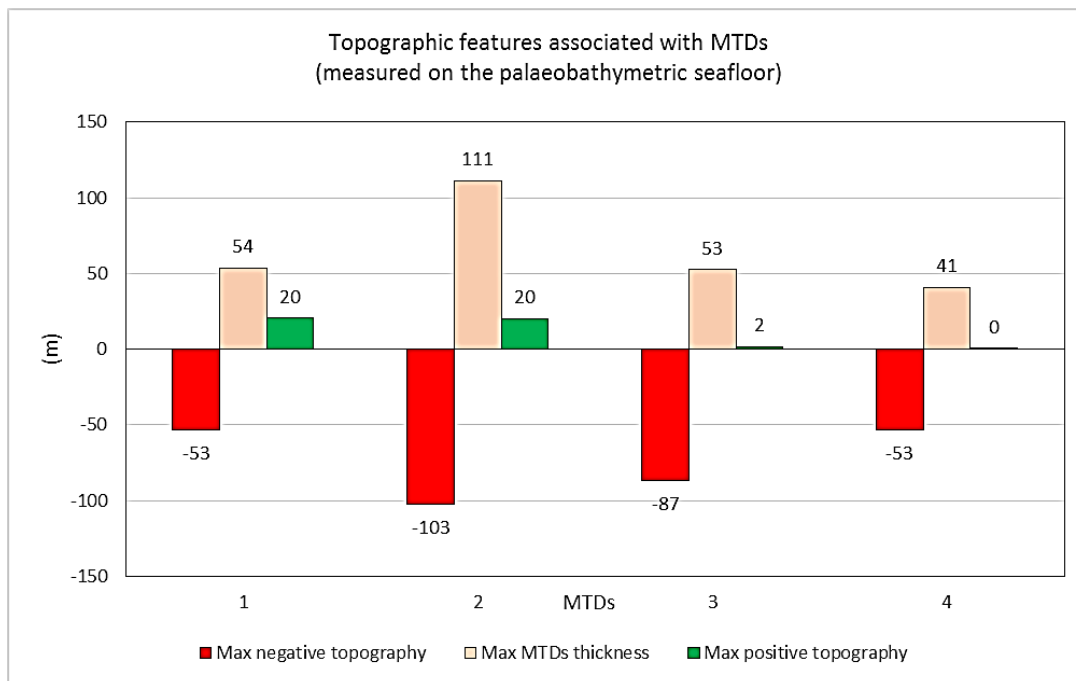


Fig. 5.35 – Graph showing the topographic features associated with the large mass-transport and related deposits in terms of max evacuation, max MTD thickness and max positive topography on the reconstructed palaeo-slope.

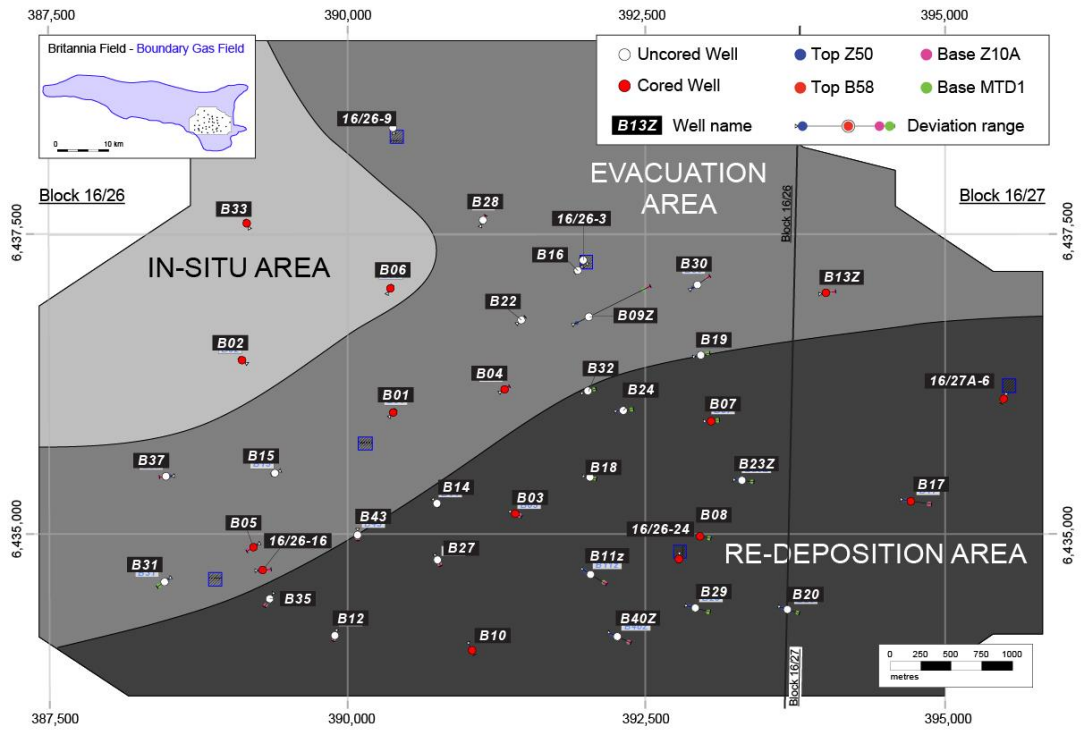


Fig. 5.36 – Map showing the three main sectors identified in the Platform Area based on remobilisation area map.

5.6 Discussion

The overarching aim of the research undertaken in this Chapter was to investigate the relationship between the creation of accommodation space, the occurrence and possible triggers of large-scale failure, the effects on the shape of the seafloor and the development of the BSF depositional system. This section aims to integrate key results from the different approaches that were adopted to address subsurface uncertainties in the interpretation of the BSF

5.6.1 Discussion on the workflow to build palaeobathymetries

In the Platform Area the wedge geometry recognised from well correlations and hence the associated differential creation of accommodation space depicted by the tilted Z10A and Bed 58 datums and characterised by the internal heterogeneity of reservoir sandstones, were investigated in order to identify and hence differentiate the roles that differential compaction, structural deformation and occurrence of large-scale failures may have played in shaping the bathymetry of the study area.

A comparison between three palaeobathymetric maps built using the investigative approaches described earlier was undertaken in order to test the impact of applying decompaction and structural restoration on the interval isopach obtained and hence on the resulting bathymetric reconstruction. The surface chosen for this comparison is the upper surface of MTD-2. Thus, the present-day map of this surface (1) was compared respectively against the map of the simple decompacted interval depths (2) and the map of fully decompacted and restored interval depths (3).

The present-day isopach map of the upper surface of MTD-2 was obtained measuring the thickness interval between the identified top of MTD-2 and Bed 58 (Fig. 5.37), whereas the same thickness interval were firstly decompacted (Fig. 5.38) and then restored to produce palaeobathymetric maps of such surfaces (Fig. 5.39).

The first conclusion after comparing the three maps is that the gross trends in dip and surface morphologies are quite similar. However, large difference in bathymetric values are observed. This is evident in the map of decompacted deposits where the top of MTD-2 is generally between 10 and 50 metres lower in comparison with the isopach map of the present-day MTD-2/Bed 58 thickness interval (Fig. 5.38). This result further shows that decompaction of the deposits of this stratigraphic interval do not fully resolve the tilted wedge geometry identified in the correlations. Initially, the thick mudstone deposits recognised in the wells that were not subject to failing processes in the north of the study area, were thought to have played an important role in producing differential compaction and hence in the creation of the wedge

geometry across the study area. However, the analysis shows that the MTDs within the reservoir architecture of the BSF are subject of high degrees of compaction and hence the cumulative volume of accommodation space between the Z10A and Bed 58 datums across the study area should have been significantly larger than the present-day thickness. Furthermore, the decompacted interval shows significant dips at the top of MTD-2 towards the south of the study area, likely unreliably high at $\sim 4^\circ$, where underlying surfaces identified with the top of tabular reservoir sandstone were substantial sub-horizontal.

The restoration analysis aims hence to resolve this issue reconstructing palaeobathymetric map of the same top of MTD-2 using stratigraphic markers as the contacts between sandstones and the overlying hemipelagic deposits. In fact, early BSF sands demonstrated that to first order the system was able to heal up to 50 metres of differential topography to build the characteristic tabular architecture of the reservoir sequence within the Lower Britannia Section (Eggenhuisen et al., 2010). Thus, preserved tops of sandstones represent potential sub-horizontal surfaces to use in the restoration analysis described in section 5.4. Significant differences between the decompacted-restored map and the present-day isopach map of the MTD-2 top are mainly observed in association with remobilised deposits. Thus the decompacted-restored palaeobathymetry shows a subtle dipping trend which is thought to be more reliable.

Decompacted-restored palaeobathymetries seem to better constrain the successive development of key stratigraphic surfaces (e.g., post-MTD bathymetries) within the BSF basin in comparison with the simple decompacted map and the present-day isopach map, with likely positive effects on the further reconstruction of the BSF depositional system in the Platform Area.

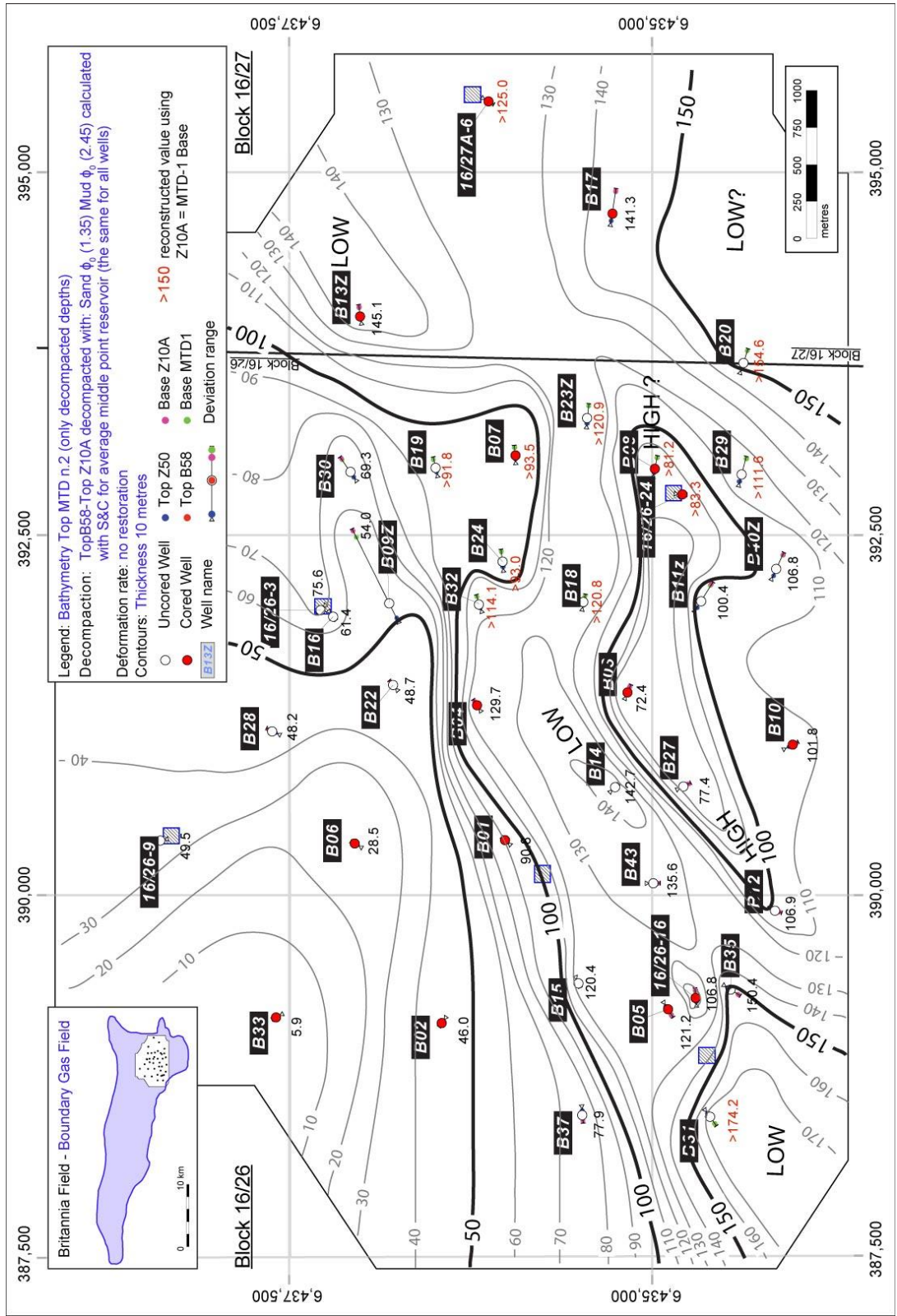


Fig. 5.38 – Bathymetry of the Upper surface of MTD-2 after decompaction of the BSF deposits.

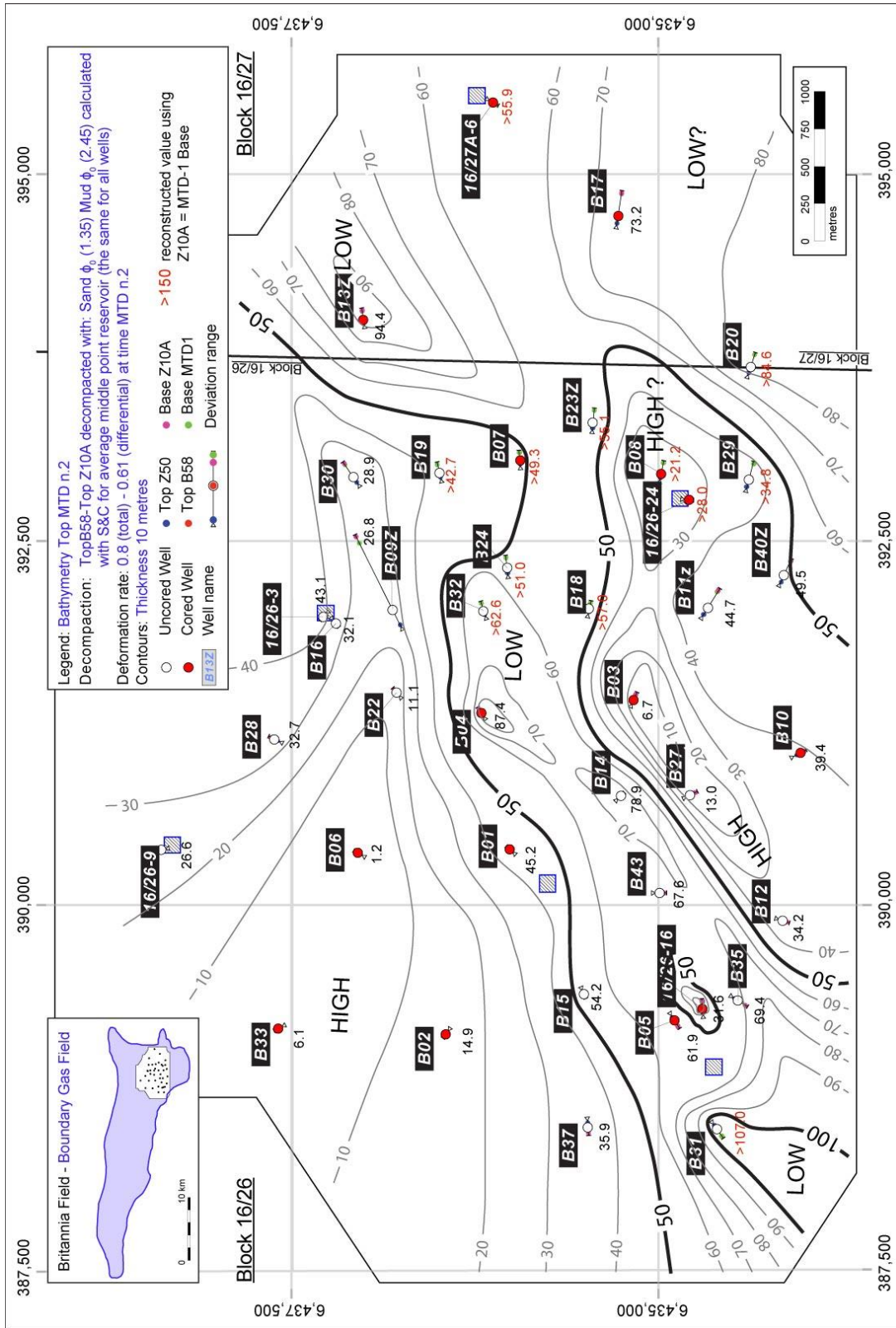


Fig. 5.39 – Palaeobathymetry of the upper surface of the MTD-2 after decompaction of the BSF deposits and restoration at MTD-2 time, so after the emplacement of the hemipelagic Reddish Mudstones.

5.6.2 Deformation during the Lower-Middle reservoir time and its relationship with the MTDs

The mapped horizons and inferred structural features are here interpreted to represent important elements in understanding of the local geology of the Z10A-Bed 58 stratigraphic interval. Moreover, the structurally restored surfaces provided additional criteria for the interpretation of large-scale mass failure events and their possible relationship with local deformation, as well as the characterisation of palaeo-bathymetries developed on top of the MTDs. Deformation in the Platform Area is thought to be associated with the creation of accommodation space mainly during intervals of hemipelagic sedimentation, given the slow deposition rate of these sediments and their thicknesses identified from both core and wireline logs. The creation of accommodation space can be measured using stratigraphic markers, which constrain the restoration of palaeo-horizontal datums. The overall deformation is therefore subdivided between uniform creation of accommodation space (assigned uniformly to all wells of the study area) and the differential creation of accommodation space (assigned individually for each well according to its location within the study area, as described in section 5.4.2). This distinction is necessary after having observed the thickness of the sandstone intervals (as Z10A, Z10B and Z20) capped by hemipelagic deposits (as Black Anoxic Shales, Ewaldi Marls and Reddish Mudstones), which recorded different creation of accommodation space across the study area, likely associated with large scale rotation of the basin floor centred on the Fladen Ground Spur. In addition, it is also useful to specify that the interpreted uniform creation of accommodation space could be interpreted as also the result of just aggradation of the sediment pile, although it is difficult to differentiate these mechanisms over the limited area of the Platform Area.

Values between 0 (absent of deformation) and 1 (significant deformation) were assigned for each MTD-time and hemipelagic marker deposition, proportional to the space between the two palaeo-datums Z10A and Bed 58 (Table 5.5). Values are directly in relation to the time of sediment emplacement, noting that the deposition of mudstone is usually associated with long periods of time in comparison to the emplacement of sandstones and MTDs, which are interpreted as quasi-instantaneous events.

Events	Uniform deformation	Differential deformation	Sequential Uni. Def.	Sequential Diff. def.
Bed 58	1	1	0.075	0.1
time MTD-4 (base)	0.925	0.9	0.1	0.15
time of Base Undiff. Mud / Top Z40B	0.825	0.75	0.025	0
time MTD-3 (base)	0.8	0.75	0	0.14
time MTD-2 (base)	0.8	0.61	0	0.31
time of Base Reddish Mud / Top Z20	0.8	0.3	0.3	0.025
time of Base Bioturbate Mud / Top Z10B	0.5	0.275	0.12	0
time MTD-1 (base)	0.38	0.275	0.13	0.275
time of Base Anoxic Mud / Top Z10A	0.25	0	0.25	0
Z10A	0	0	0	0

Table 5.5 - Summary of the uniform and differential deformation rate assigned to each stratigraphic time event represented by hemipelagic markers and MTDs identified in the Z10A-Bed 58 interval (see section 5.4.1)

Table 5.5 aims to show the sequential uniform and differential creation of accommodation rate calculated by subtracting each rate at a specific time interval with the previous one in order to measure the exact creation of accommodation space that occurred between two events/times. The sequence of both differential and uniform creation of accommodation might be interpreted as pulses of respectively basin scale passive tilting and/or local faulting/rotation of the palaeo-seafloor across the Platform Area, vs. or sea-level rise, during the Lower-Middle Britannia sandstone emplacement, even if sea level changes have not been well constrained in the literature of the BSF. In this regard, Jeremiah (2000) states that the compiled BSF inferred sea level curve primarily reflects tectonism, with little calibration to eustatic sea-level change, and that mudstone intervals overlying turbidites are interpreted representing the temporary cessation of tectonism.

Figure 5.40 aims to show the relationship between the uniform and differential creation of accommodation space plotting the percentage of the total Z10A-Bed 58 accommodation space occurred between Z10A and Bed 58 on the y-axis and the percentage of the Z10A-Bed58 interval tilting between Z10A and Bed 58 on the x-axis. The chart shows that uniform creation of space can be inferred as the main result of the relatively quick aggradation of sands, whereas the differential creation of accommodation space mainly grows during hemipelagic sedimentation until the triggering of the MTDs, as in the case of the MTD-1 and MTD-2. A linear relationship is only observable after the emplacement of the MTD-3, where the aggradation is combined with the inferred tilting of the basin floor.

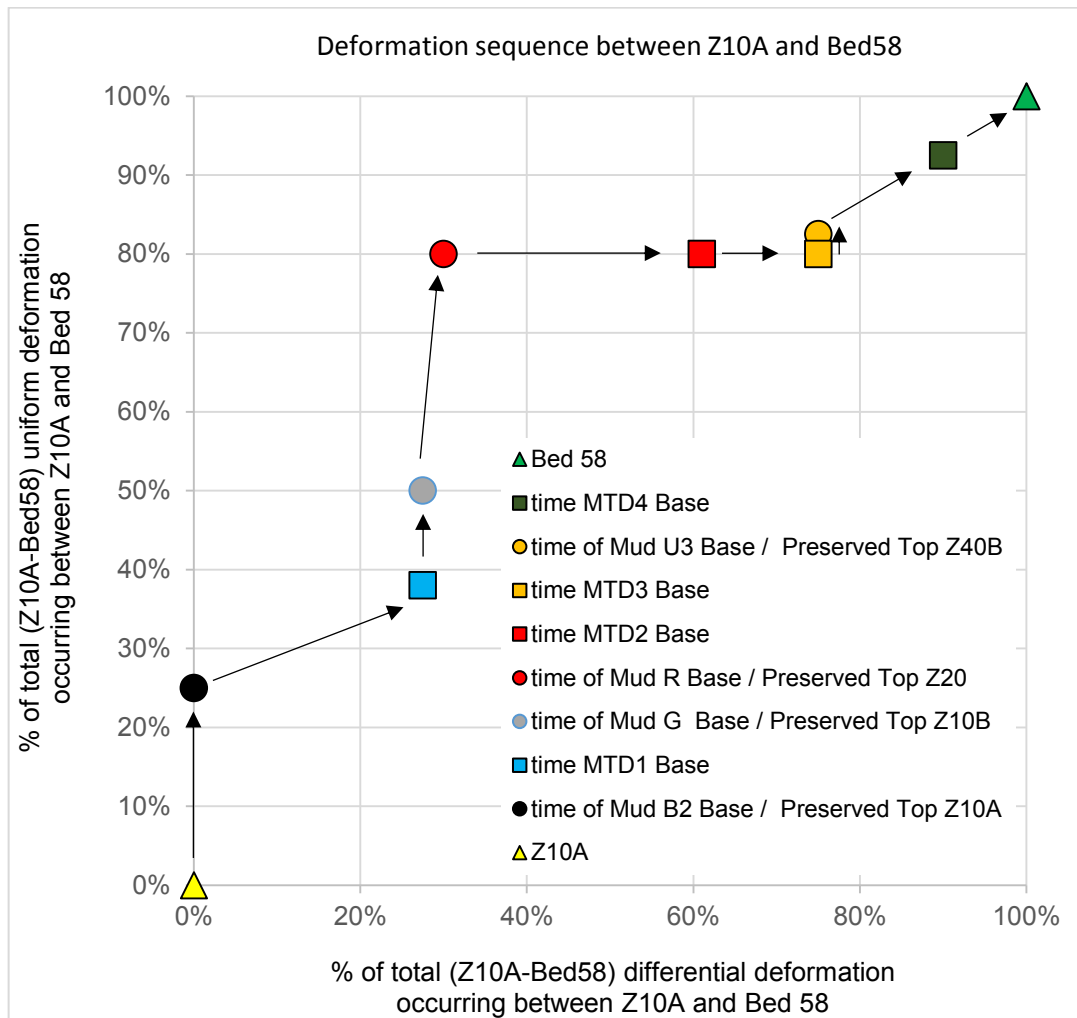


Fig. 5.40 – Deformation sequence between Z10A and Bed 58. The uniform deformation pulses are recorded by the hemipelagic mudstones whereas the differential deformation is mainly highlighted by MTDs (square symbols) both occurred between Z10A and Bed 58 in terms of percentage of Z10A-Bed 58 interval.

The magnitude of large failure events can be measured in different ways and in this section the relationship between the erosive character of MTDs and the steepening of the slope gradient is investigated by plotting the maximum erosion measured on the seafloor and the differential deformation associated with the tilting in the chart below (Fig. 5.41). The highest evacuation character (127 metres) is recorded at the basal surface of the second MTD which also marks the main differential deformation at the time of the MTD-2 (31%). However, the other MTDs show similar smaller erosive trends (MTD-1: ~72 m; MTD-3; ~86 m; MTD-4: ~53 m) combined with lower differential deformation rates of between 14% and 27.5% as measured between the timings of failure events.

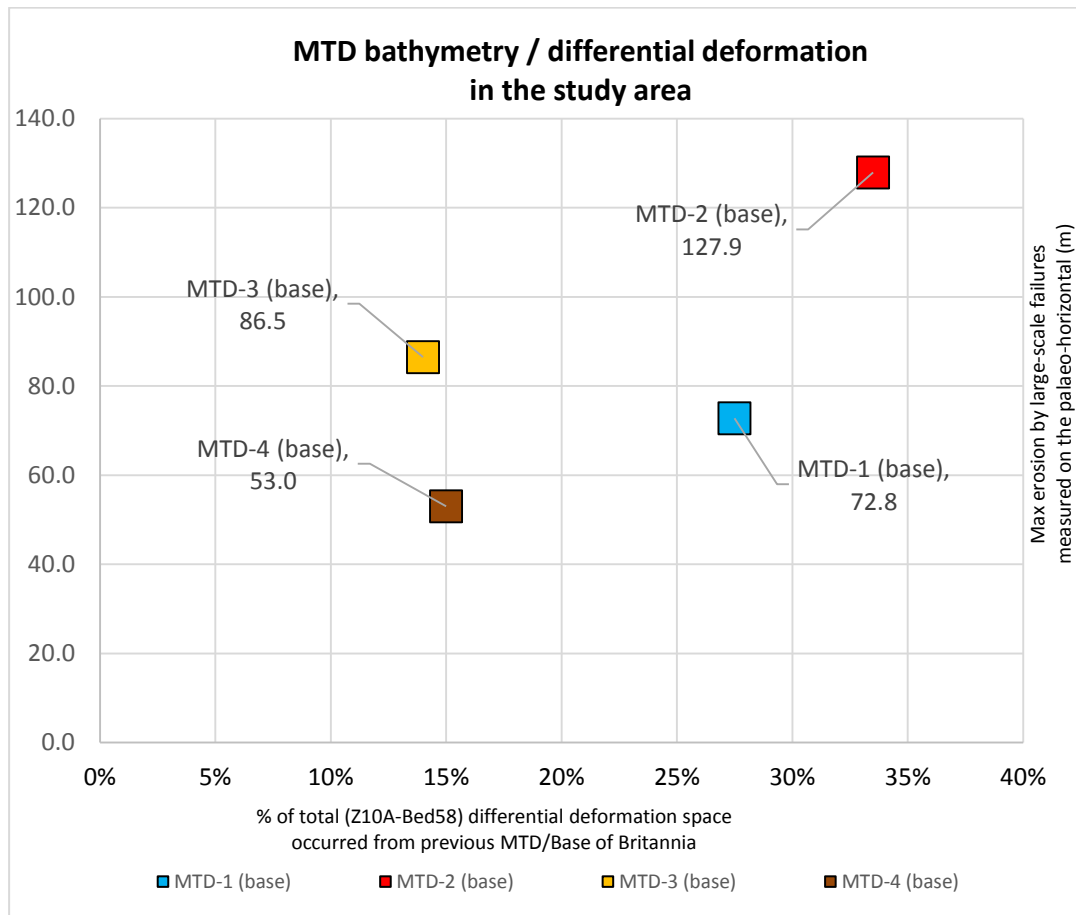


Fig. 5.41 – Relationship between bathymetry created by MTDs and differential creation of accommodation space recorded by the stratigraphic event (hemipelagic deposition and MTDs). Larger creation of accommodation space, in relation to the Z10A-Bed58 interval, are associated with more erosive failures.

The steepening of low gradient slopes together with major earthquakes related to an underneath fault system, are often considered the main triggers of large-scale mass failures (e.g., Wynn et al., 2000; Strasser et al., 2007; Basilone et al., 2016). The size of these events and the volume of remobilised sediments also show some relationship with the time that elapses between two successive mass-failures (e.g., Nelson et al., 2011; Hunt et al., 2014 - see below).

5.6.2.1 *Palaeo-slope modelling in the Platform Area*

Identification of palaeo-horizontal datums at different stages enables insight into the likely slope gradient in the Platform Area. This is calculated between key wells located in different sectors of the study area. At the time just before each MTD different slope gradients can be identified.

Wells used for the gradient / restoration time	NW-SW	NW-SE	N-S	N-S
	B28 – B35	B28 – B17	B28 – B22	B28 – B04
time MTD-1	0.3°	0.2°	0.4°	0.4°
time MTD-2	0.5°	0.4°	0.7°	0.8
time MTD-3	0.6°	0.4°	0.9°	0.9°
time MTD-4	0.2°	0.1°	0.4°	0.4°

Table 5.6 - Slope gradients measured between wells across the Platform Area and representing different times associated with the emplacement of the MTDs during the Lower and Middle Britannia Members. This calculation is based on the modelled evolution of Britannia deposits associated with the restoration analysis (see section 5.4.2). B28 is considered as the reference well because is the “highest point” in the study area whereas the other wells (B35-B17-B12-B22-B04) represent “low points”.

The wells used to reconstruct the palaeo-slope gradient were selected in order to study the slope angle between the most elevated area in the north (represented by B28) toward both the south-western and south-eastern sectors, as represented by wells B35 and B17, respectively. The gradients prior to each MTD-emplacement indicated progressive slope steepening up to MTD-3 time, with a decrease in pre-failure slope angle prior to the MTD-4 failure (Table 5.6). This difference could be interpreted as being tectonically related, due to either a less faulting activity on the study area scale or tilting on the basin scale, or might be due to a shorter time interval between MTD-3 and MTD-4. These two possibilities are not necessarily mutually exclusive. In fact acceleration in slope steepening could be the reason for higher frequency MTD-occurrence. Therefore, the slope steepening, interpreted as the result of an underlying fault system (as inferred by the decompacted isopach map of the Z10A-Bed 58 - see section 5.3.4), could have triggered the instability in the northern sector of the Platform Area, where a headwall morphology was identified and supported by observations on the basal surfaces of MTD-2, 3 and 4 (see section 5.5.3).

5.6.3 Clastic rate input associated with MTD emplacement

The Lower Cretaceous BSF is characterised by the interplay of a turbidite system, a mass transport-system and hemipelagic deposition with different pulses of sand deposition forming the turbidite system. Figure 5.42 shows that in the study area sandstone deposition was not steady through the time. The amount of sand comprising BSF reservoir zones, including the Upper Section, was calculated by adding together the sand recognised for each zone from both cored and uncored wells of the Platform Area. The net/gross of the reservoir zones allows an estimation of the thickness of sand for each interval, inferred to represent different pulses of sand deposition. Of course, the BSF is not a geographically or stratigraphically closed turbidite system, which makes this interpretation reliable only within the study area.

The first sand input identified in the study area corresponds with Z7 as recognised in wells B02, B33 and B35. These wells are located in the west sector of the Platform Area and they might have recorded the farthest deposition of a Z7 distributary fan system (assuming a western provenance of the sands – see Chapter 3).

The Z10A and Z10B intervals mark an increase in sand volume. The presence of stratigraphic markers (i.e. the black anoxic mudstone at the base and top of Z10A and the bioturbated Ewald Marl mudstone on top of Z10B) constrains the two different pulses of sand deposition. The sand volumes of these intervals are also influenced by two large remobilisation event associated with the emplacement of MTD-1 and MTD-2. Regardless of the late evacuation of large portion of sediments by the failure events, Z10A and Z10B mark a significant rise in the amount of sand deposition within the study area.

Zone 20, which is recognised in small volumes in B02, 06 and B33 only, is inferred to be largely remobilised by the second remobilisation phase that occurred after the deposition of the reddish hemipelagic mudstone. The deposition of the mudstone on top of the Z20 indicates the cessation of sand deposition just before the emplacement of MTD-2.

A substantial and significant increase of the sand volumes associated with Z40A marks a change in the sandstone deposit style and the character of the associated reservoir intervals, which are doubled in thickness in comparison to the zones of the Lower Britannia stratigraphy. The significant sandstone deposition of Z40A is associated with the pronounced topography left by the MTD-2. Topographic lows and positive relief areas, as shown in Fig. 5.29-B might have obstructed and trapped a larger proportion of sand in the Platform Area .

The smaller volumes of sands represented by Z40B and Z40C may be associated with their emplacement over the relatively subdued rugose topography associated with MTD-3 and MTD-4 respectively. Z40C is also characterised by hybrid-like sandstone deposition (*sensu* Haughton et al., 2003) which is described in Chapter 4; it is capped the thick Bed 58, that healed the topography and restored sub-horizontal conditions on the seafloor.

The Upper Britannia section shows different trends from the underlying Lower-Middle reservoir, in fact high volumes of sands making up Z45 and Z50 are identified across the study area (Barker et al., 2008) marking a less clear relationship between scale of rugosity associated with the MTD-related topography and the deposition of sand.

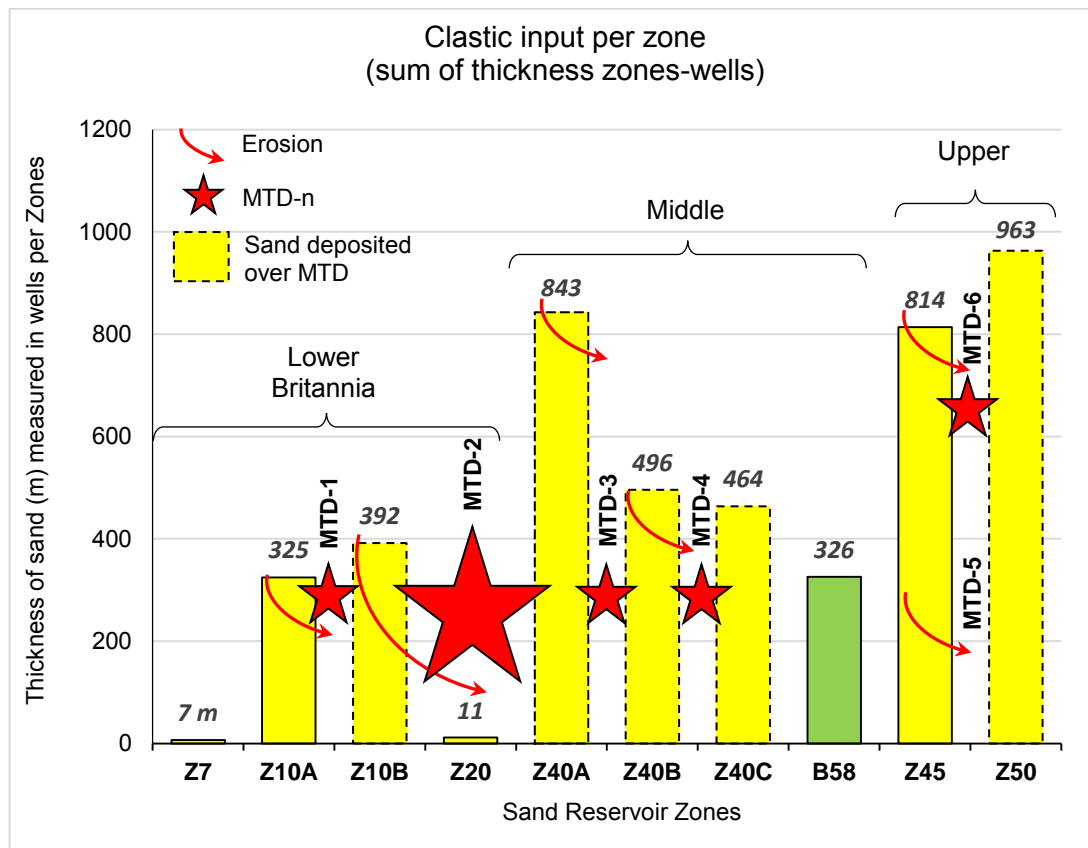


Fig. 5.42 – Clastic input measured on wells per each zone (columns) of the Britannia stratigraphy grouped per reservoir section (Lower, Middle and Upper). The green column represents the event Bed 58 that is used as palaeo-datum and to differentiate the Lower-Middle from the Upper reservoir section. The red arrows represent the occurrence of failure events whereas the dashed columns represent the cumulative thickness of sandstones deposited on top of the MTDs (marked with a star).

The amount of sandstone deposited in the platform area appears to positively correlate with the scale of rugosity developed on top of the MTD, with associated sequestration of sand from the turbidite-system. However, the timing and ultimate

cause of the different pulses that characterise the sand deposition are unclear. These could be associated with tectonic events that occurred during the Lower Cretaceous and associated with the post-rifting phase in the Witch Ground Graben (i.e. outside the study area). In fact, the Britannia Subsea Area, showed in Fig. 5.17, has a different tectonic configuration to the Platform Area, with a W-E fault system (Chapter 3) that could have led the reactivation of intrabasinal structures and reconfiguration of the linkages between basins (Crittenden et al., 1997; Oakman and Partington, 1998; Jeremiah, 2000). Furthermore, provenance work (Jones et al., 1999a; Blackbourn and Thomson, 2000; Hailwood and Ding, 2000; Milton-Worsell et al., 2006) suggest different inputs of large portions of reworked sandstones from different entry points to the basin, with the depositional system switching from east for the Lower and Middle reservoir section, to the west of the field (Chapter 3) for deposits of the Upper reservoir interval.

The combination of loading by the pulses of sandstone deposition and increased slope gradient associated with tectonic events is thought to have led to the initiation of failure events along the basin flank on the Fladen Ground Spur with the emplacement of MTDs which facilitated the sequestration of sandstone in the study area.

5.6.4 Implications outside the Platform Area

The new results and interpretations arising from this work may contribute to a re-evaluation of the BSF outside the study area, i.e., contributing to the characterisation of the wider depositional fairway of the Britannia sands within the Witch Ground Graben and the Fischeschiefer Basin in the Central North Sea. Firstly, the distribution, morphology (rugosity) and character of the MTDs in the Platform Area described in this chapter may give insight into their development outside the study area with implications for general understanding and for hydrocarbon exploration. Secondly, the inferred trapping of sand during the healing phase of MTD-induced topography, and its bypass during post-healing episodes may have implications for the timing and volume of downstream sediment dispersal.

A principal component of this study was to build reliable palaeobathymetric maps associated with the upper surface of the MTDs in order to characterise morphologies and rugosity of these deposits. The presence of MTDs in deep-water reservoirs is generally linked with architectural uncertainties related to the high heterogeneity that these deposits may create, in terms of reservoir sandstone correlations and facies distribution. In this case, the morphology of the four MTDs within the Lower and

Middle Reservoir Sections shows a wide range of rugose features that may indicate transport direction of the large-scale failures and the run-out of these events, which confirm earlier work (e.g., Eggenhuisen et al., 2010) concluding that unconsolidated material deposited on the flank of the Fladen Ground Spur moves downslope across the Platform Area and is re-deposited downdip towards the south.

A case that might support this theory is the identification of a headwall scarp formed by the earliest event and marked by the subsequent failures, with the maximum size associated with MTD-2. The orientation of the scarp is SW-NE, adjacent to a deep trough that has the same orientation. Furthermore, MTD-2 showed possible translation of large blocks, whose removal was likely responsible for the development of deep topographic lows beneath the headwall scarp. The orientation of these features might indicate a relatively local source of the failures, which henceforth inferred to have originated just to the north of the study area (e.g., north of wells B02, B06 and B33). This also leads to the prediction that the bulk of the remobilised deposits might be found in the southern area of the BSF basin, outside the Platform Area. At the same time, the character of the MTDs differs, with the main difference being that the muddy matrix is either pervaded by floating sand grains (MTDs 1 and 2) or just contains sand and mud clasts. This difference might be explained by the run out distance that mass-wasting flows have travelled and by their source updip. In fact, MTD-3 and MTD-4 are characterised the total absence of floating sand grains which can be explained by a completely muddy source such as the hemipelagic mud deposited on slopes (perhaps above the limit of where sandstone were deposited) or by transportation of less disaggregated / more consolidated sandstones, that may have been incorporated into the mass flow once it reached areas of earlier-deposited Britannia sandstone of the Platform Area. In both cases the bulk of remobilised deposits is expected to lie to the south of the Platform Area.

In terms of sandstone distribution, as noted above, MTD-associated rugosity may have led to the relative retention of sand in MTD-prone areas, whereas smoother, post-healing phase pathways may have allowed more efficient sand bypass (although through-going lows might have accelerated flow preventing sand retention during the healing phase). In addition, MTDs south of the Platform Area might could have deflected flows into the study area, where topographic lows are oriented parallel to the estimated turbidity current flow direction (see Chapter 3), either augmenting the rates of sand retention, of possibly aiding its bypass. Further considerations on the relationship between MTD-related topography and turbidites are investigated in Chapter 6.

5.7 Conclusion

This Chapter documents a reconstruction of the palaeobathymetric seafloor evolution of the 35 km² area around the Britannia Platform Area (see Fig. 5.43). The reconstruction is based on revised correlation panels of the Lower Reservoir Section (after Eggenhuisen, 2009 - see Chapter 4) and on correlations of newly cored intervals and of uncored wells from the Middle Reservoir Section. Core facies analysis combined with the investigation of cutting and gamma-ray data for the uncored wells aided the evaluation of the evolution of the Lower and Middle Reservoir Section, which is characterised by periodic episodes of large-scale remobilisation, and subsequent healing of the post MTD bathymetry by sandy gravity flows.

- Creation of accommodation space was investigated by undertaking decompaction analysis on the BSF and on the underlying Valhall Shales under the Platform Area. Results from this analysis, combined with stratigraphic assumptions (e.g., tabular Z10A and Bed 58 datums edging the Lower and Middle Reservoir Section) established that differential compaction only partially contributed to the differential creation of accommodation space in the study area.
- Creation of contour maps of palaeobathymetric surfaces that were affected by strong post-depositional overprint has been achieved through restoration analysis of the decompacted Z10A-Bed 58 stratigraphic interval, which might demonstrate either the role of passive tilting (large scale – wider basin) or the reactivation of normal faults (local scale – Platform Area) across the study area, or both of them, during the Lower and Middle Reservoir Section as related to the post-rifting phase in the Central North Sea Basin.
- Thus, the inferred syn-sedimentary passive tilting of the larger basin as well as inferred locally active faults are interpreted to have contributed to the creation of accommodation space in the central and southern sector of the Platform Area with particular influence on the differential creation of accommodation. On the contrary, differential compaction effects were interpreted to have been either insignificant or of second order importance during the period of sedimentation, along with regional subsidence.
- In the study area, debrite deposits are differentiated according to their sedimentological characteristics as resulting from either sandy or muddy debris flows. These are interpreted as being either subsidiary events to a larger scale slope failure process, which largely bypassed (MTD-1 and MTD-2), or standalone

remobilisation events of unconsolidated deposits (MTD-3 and MTD-4). Sandy debrites transporting sand and mudclasts of various sizes, from cm to tens of m scale, characterising MTD-1 and MTD-2 in the lower portion of the stratigraphy, are interpreted as the result of disaggregation of large blocks from proximal debris slides. Identification of large slide blocks within MTD-2, covering an area of >2.5 km², is an entirely new result of this study. The blocks represent the result of a block sliding mechanism associated with large-scale slope failure in which large portions of intact stratigraphy were laterally translated. This translation is interpreted to have been responsible of the creation of a series of deep troughs, with the largest measuring 80 metres in depth and 4 km in max width; they extend parallel to the lateral slope strike (likely influenced by inferred blind faults) and orthogonal to the main transport direction of the MTD, shaping a high rugose bathymetry on the seafloor. Muddy debrites characterised by sand and mudclasts from cm to m scale in a “non-starry-night” texture, are recognised across most of the study area making up MTD-3 and MTD-4. Smaller scale rugosity associated with these deposits shows up to 40 m of amplitude over a ~1 km width. The sedimentological character of MTD-3 and MTD-4 together with the size of the debritic intervals allows them to be interpreted as the product of either an early disaggregation stage of remobilised stratigraphy from upslope deposits of debris flows with different provenance in comparison with earlier “starry-night” – matrix MTDs.

- Creation of accommodation due to slope failures was also calculated by modelling the palaeo-slope at the time of the emplacement of each MTD, through the recognition of preserved tops of sandstones deposited above the MTDs. Erosion on the seafloor associated with the remobilisation phases was between ~50 and ~100 metres, with the largest evacuation recorded at the base of MTD-2. Topographic lows were usually partially infilled by the remobilised material itself, however ~50-70 metres of unfilled depression were still recognised along the headwall. Preserved portions of Britannia stratigraphy underneath the main scarp constitute the ramp of the detachment surface where remobilised material was deposited en-masse, creating ~20m positive relief after the lower MTD-1 and MTD-2 emplacement.
- Basin floor deformation is inferred to have occurred principally during periods of hemipelagic sedimentation. The deposition of interleaved sandstone in the Lower and Middle Britannia reservoirs was modelled in order to better understand the evolution of the basin in the Platform Area. Episodes of uniform and differential deformation can be interpreted as resulting from pulses of basin scale tilting and

local faulting/rotation, respectively. Periods of significant differential deformation seem to be related to the MTD's erosive character calculated on the reconstructed palaeo-seafloor: larger erosive failures (MTD-2 and MTD-3) are associated with high percentage of differential deformation, whereas smaller erosive events (MTD-1 and MTD-4) are related to shallower tilting.

- Palaeo-slope gradients were modelled for each MTD-time, showing a steepening of the slope toward the southern area, with an increase of the palaeo-slope angle up to $\sim 0.7^\circ$ prior to emplacement of MTD-2, reaching a maximum angle at MTD-3 time ($\sim 0.9^\circ$) and decreasing prior to triggering and emplacement of MTD-4. The steepening of low gradient slopes is interpreted as a principal trigger for large-scale mass failure in the Platform Area.
- The morphological features recognised on top of the MTDs, such as the orientation of a headwall scarp formed by the earliest event (and modified by subsequent failures), a deep trough underneath the scarp and the possible translation of blocks jointly suggest that failures might have been locally generated (on the southern flank of the Fladen Ground Spur) and then moved towards SE. It follows that the bulk of remobilised deposits might be found in the southern area of the BSF basin, outside the Platform Area, contributing to the creation of topographic highs that might have confined higher reservoir sandstones (e.g., Z40) in the study area.
- The inferred trapping of sand during the healing phase of MTD-induced topography, and its bypass during post-healing episodes may have implications for the timing and volume of downstream sediment dispersal.

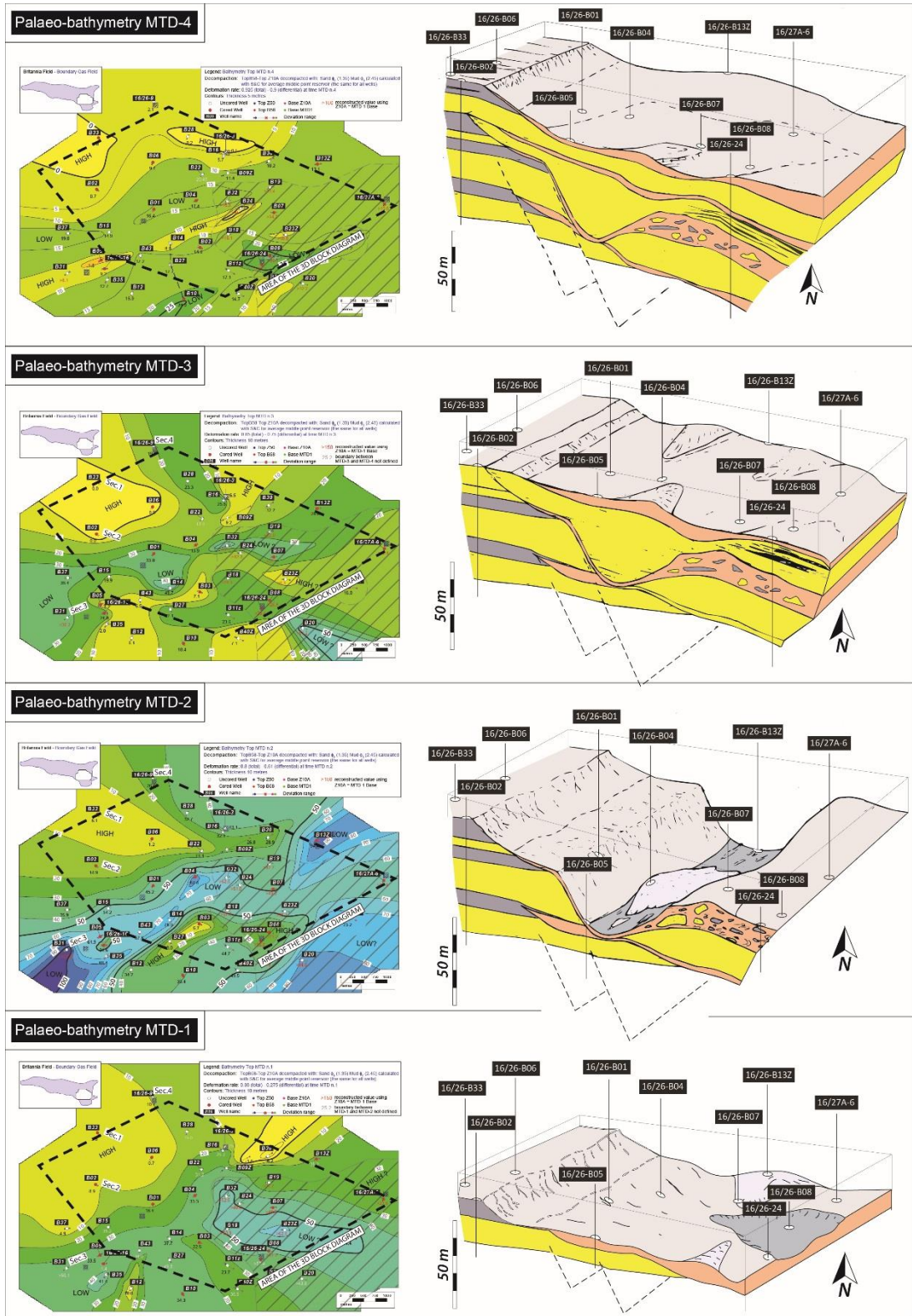


Fig. 5.43 – Reconstruction of the palaeobathymetric evolution of the Platform Area after the emplacement of MTD-1, 2, 3, 4. On the right side, 3D block diagrams representing the seafloor of the study area after the emplacement of each MTD together with tilting due to inferred fault set system.

6 Sandstone deposition associated with MTDs-related topography: vertical and lateral sandstone lithofacies distribution influenced by pronounced vs subtle seafloor morphology shaped by large landslides in the Britannia Field

Abstract

Sandy gravity flows often exhibit variation in depositional character over relatively short length scales (< 1 km) when travelling over a rugose topography such as the upper surface of mass-transport deposits (MTDs). The latter can create new seascapes which then influence the pathways taken by subsequent sediment gravity flows, with flow constriction and expansion points dictating the dispersal patterns and deposit heterogeneity of the ensuing deposits.

The Aptian deep-water Britannia Sandstone Formation, North Sea, provides an opportunity to study a succession of sand-body reservoirs deposited above a series of MTDs, in a densely drilled area around the Britannia Platform. The work is based on integration of well-data from 47 wells from the 35 km² Platform Area of the Britannia Field and detailed sedimentary analyses of 3720 ft. (~1130 m) of high quality core from 14 of those wells. This dataset provides a unique subsurface example of the influence that different scales of MTD depositional relief may have on later turbidite deposition. In the study area, sandy gravity currents interacted with four transversely emplaced MTDs with surface rugosity on each MTD ranging from 5 to 60 metres in height. Topographic lows were infilled, then fully buried by sandstone deposits, with evidence for changes of thickness, facies development and inferred flow type in the sandstone deposits over length scales of up to 8 km. Sharp-based, medium to fine-grained, clean, amalgamated turbidite sandstones were deposited onto deep topographic lows (some 5 km long and up to 60 m deep). In contrast, less pronounced topography was infilled by muddier sandstone beds, including those with banded sandstone facies, and subsidiary hybrid event beds (HEBs) that pinch out and lap onto the relatively subtle confining slopes (5-10 m high relief); these facies may indicate partial lateral confinement .

The documented spatial variation in sandy lithofacies and interpreted flow types on these MTD influenced setting are studied to better understand how flows adjust to

different scales of rugosity. Depositional trends are discussed in terms of the interaction of a range of flow sizes with a range of scales of local seafloor topography. This work illustrates how facies distribution in MTD-prone settings differs from conventional architectural and facies models. In the Platform Area of the Britannia field, thick clean sandstones seem to be deposited within the largest topographic lows (100s m to km length, 10s m depth), whereas muddier deposits are interpreted to be associated with the partial surmounting of small-scale relief (m to 10s m) by the uppermost fraction of a turbidity current. These insights aid linkage of seismic scale reservoir architecture to facies distributions.

6.1 Introduction

Sandy gravity flows are often influenced by change in the gradient over the seafloor (Fig. 6.1). Topographic rugosity on the seafloor can be associated with multiple causes such as a) tectonic control (e.g., faults, subsidence, etc.), b) mobile substrate (e.g., halokinesis), or c) erosion by gravity flows, such as turbidity currents and mass-failure processes. The latter have been identified as the main mechanism responsible for reshaping the seafloor in the study area, through erosion and accumulation of remobilisation deposits following large-scale landslides (see Chapter 5). Numerous studies have demonstrated that seafloor topography can be a significant control on sediment gravity flow behaviour (Fig. 6.1 - Fisher, 1990; Thornburg et al., 1990; Kneller, 1995; Kneller and McCaffrey, 1999). However, only a few studies have focused specifically on the interaction between sandy gravity flows and topographic features developed after the emplacement of mass-failure (Cronin et al., 1998; Paul Weimer and Slatt, 2006; Armitage et al., 2009; Kneller et al., 2016; Sobiesiak et al., 2016; Fallgatter et al., 2016).

The results of this research should contribute to an ongoing effort to better understand the role of mass-transport deposits (MTDs) in influencing the evolution of stratigraphic architecture in deep-water settings. This chapter uses insights into how the emplacement of MTDs altered the topography of the seafloor in the Platform Area of the Britannia Field (described in Chapter 5) to investigate controls on subsequent sediment gravity flows that run across the study area and hence distribution of reservoir sandstones. The study may have practical implications for the prediction, characterisation and development of hydrocarbon reservoirs in other deep-water systems influenced by the presence of MTDs.

Much of the older part of the BSF succession is characterised by a high degree of heterogeneity in terms of vertical and lateral extension of sandstones. This

succession comprises a range of “enigmatic facies”, characteristic of the BSF (Guy, 1992; Lowe and Guy, 2000; Lowe et al., 2003; Barker et al., 2008; Eggenhuisen et al., 2010 - see Chapter 3 for definition), that have become pivotal in the study of hybrid sandstone deposition (Haughton et al., 2003; Haughton et al., 2009; Davis et al., 2009).

In this study, the Middle Section of the BSF is analysed using core and well data from the densely-drilled Platform Area of the Britannia Field (Fig. 6.2), together with the re-assessed wireline data and core logs from the Lower Section that were previously used to erect the models for large-scale remobilisation (see Eggenhuisen et al., 2010).

The interplay between gravity-induced slope failure and sand deposition was explored in Chapter 5 by tracking the evolution of the inferred seafloor morphology associated with each phase of slope instability. Gravity-driven deformation during and after deposition of the sandstones has had a demonstrable impact on the spatial patterns of facies, grain size distribution, sandstone thickness and inter-well correlation. These factors all have a bearing on interpretations of the spatio-temporal evolution of flow events, palaeoflow, the origin, distribution and character of the different facies, and on the wider significance of this succession for the interpretation of other deep water deposits elsewhere.

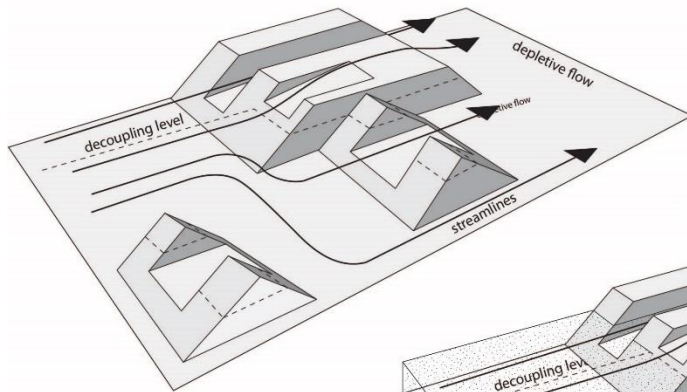
The overall purpose of this chapter is to investigate the sedimentology of the Lower and Middle BSF, in order to develop an understanding of the spatial distribution and process significance of sandstones deposited above the MTDs, integrating existing models for the Lower Britannia with new well correlations from the Middle Reservoir Section. Particular emphasis is placed on understanding flow behaviour, spatio-temporal evolution of individual flow events and processes of sandstone deposition. In detail, the main objectives of this chapter are:

- To undertake a core-based investigation and interpretation of reservoir Zones 10A, 10B, 20, 40A, 40B, 40C within the Platform Area of the Britannia Field. Core sedimentological logs, core photos and cuttings analysis provide the principal dataset used in this study. The results obtained through core description have also been integrated with other available datasets as wireline data and petrographic information (cuttings).
- To map bed thickness variation across the study area. Following the detailed correlation of the stratigraphy of reservoir zones (see Chapter 4) at both zonal and bed scales, the thickness of individual zones and beds will be determined at each well (datapoint) position detailing sand distribution patterns.

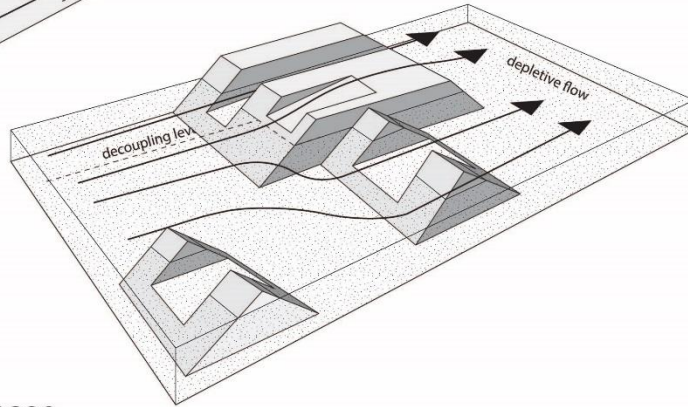
- To map sandstone facies across the study area. This analysis will also rely upon the detailed correlations and will help determine spatial patterns in facies distribution that may provide further insights into flow hydrodynamics when associated with MTD-related bathymetry (Fig. 6.1).
- To define the vertical sandstone facies organisation within individual wells by documenting the distribution of primary depositional fabrics, categorising deposition styles and interpreting their modes of emplacement over different magnitudes of MTD rugosity (see Chapter 5).
- To re-construct the evolution of the Lower and Middle Britannia turbidite-system through time, investigating the range of sandstone deposition styles with respect to the inferred spatial and temporal changes in basin morphology (both regional and local – see Chapter 5)

This work package should help aid the assessment of the impact of geological reservoir heterogeneity on fluid flow in production wells and of stratigraphic controls on reservoir compartmentalisation.

stage 1 - flow decoupling



stage 2 - infill topography



stage 3 - post-healing phase

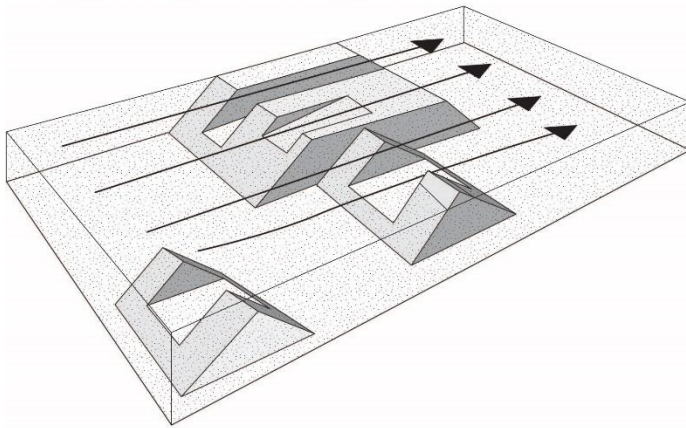


Fig. 6.1 – Schematic illustration showing the effects of different degrees of confinement (1. large; 2. small; 3. no confinement) and the dividing streamline given by the internal Froude number criterion (Fi). For small values of Fi the denser, lower regions of the flow, below the dividing streamline, are unable to converge or overcome topography and are therefore deflected around it, whilst the upper flow is able to move over topography and is 'stripped' from lower flow. Where the topography is sufficiently large, flow is unable to surmount it regardless of Fi and is effectively blocked (modified after de Leeuw, 2012, from Kneller and McCaffrey, 1999).

6.2 Dataset

The dataset used is described in detail in Chapter 4, but to recap, high quality resinated core slices provided by Britannia Operators Limited (BOL) were investigated and described in detail for each of the sandy reservoir intervals. Core description of 3720 ft (3125 m) of core (see Table 6.1) at 1:20 scale (see Appendix B) from 14 wells in the Platform Area (Fig. 6.2) was the principal source of data for this study. Visual grain size estimates were calculated using a grain size comparator. Sketches of all sedimentary structures and internal fabrics were incorporated into the graphic logs; gross lithologies were determined on the basis of sandstone colour and internal fabric during the core logging. Additional grain size measurements were also available for all the cored wells and for some of the uncored wells (Blackbourn and Thomson, 2000). Wireline log data, including gamma ray and combined neutron-density logs, were analysed for all cored wells and for a further fourteen uncored wells (Appendix B).

Core logs from the Middle Reservoir Britannia Member (this study) were integrated with 2025 ft (617 m) of core logs from the Lower Britannia investigated by Eggenhuisen et al. (2010) together with core photos, which were available for the majority of cored sections in the Lower reservoir.

This study focussed on Zones 10A, 10B, 40A, 40B, 40C with Bed 58 used as a correlation datum. Detailed work was also undertaken on Z40C where six stacked sandstone events are recognised. Bed and zone thickness data were derived from the cored wells, corrected for well deviation and then checked against the true vertical depth sub-sea scale (TVDSS) on the wireline log plots for each well. Thickness data were derived from uncored wells using the TVDSS scale on the wireline log plots, corrected for well deviation using ODMTM software (Oilfield Data Manager).

Wells	Core Data	Lower Reservoir Zone (from Eggenhuisen, 2009)		Thickness logged (feet)	Middle Reservoir Zone (This study)		Thickness logged (feet)
16/26-24	C	13225	13015	210	13030	12830	200
16/27A-6	C	-	-	-	13350	12870	480
B01	C	13410	13240	170	13260	12973	287
B02	C	14128	13910	218	13992	13827	165
B03	C	14280	14013	267	14030	13840	190
B04	C	14005	13913	92	14004	13600	404
B05	PC	14248	14101	147	14120	13730	390
B06	C	13995	13864	131	13872	13842	30
B07	C	16827	16691	136	16660	16490	170
B08	C	17085	16816	269	16830	16600	230
B10	C	15520	15345	175	15370	15070	300
B13Z	PC	-	-	-	19564	19325	239
B17	PC	-	-	-	21100	20780	320
B33	PC	15270	15060	210	15280	14965	315
TOT				2025			3720

Table 6.1 – Dataset summary table. Legend: C = core available; PC = partial core available. Depths are available in the Appendix A.

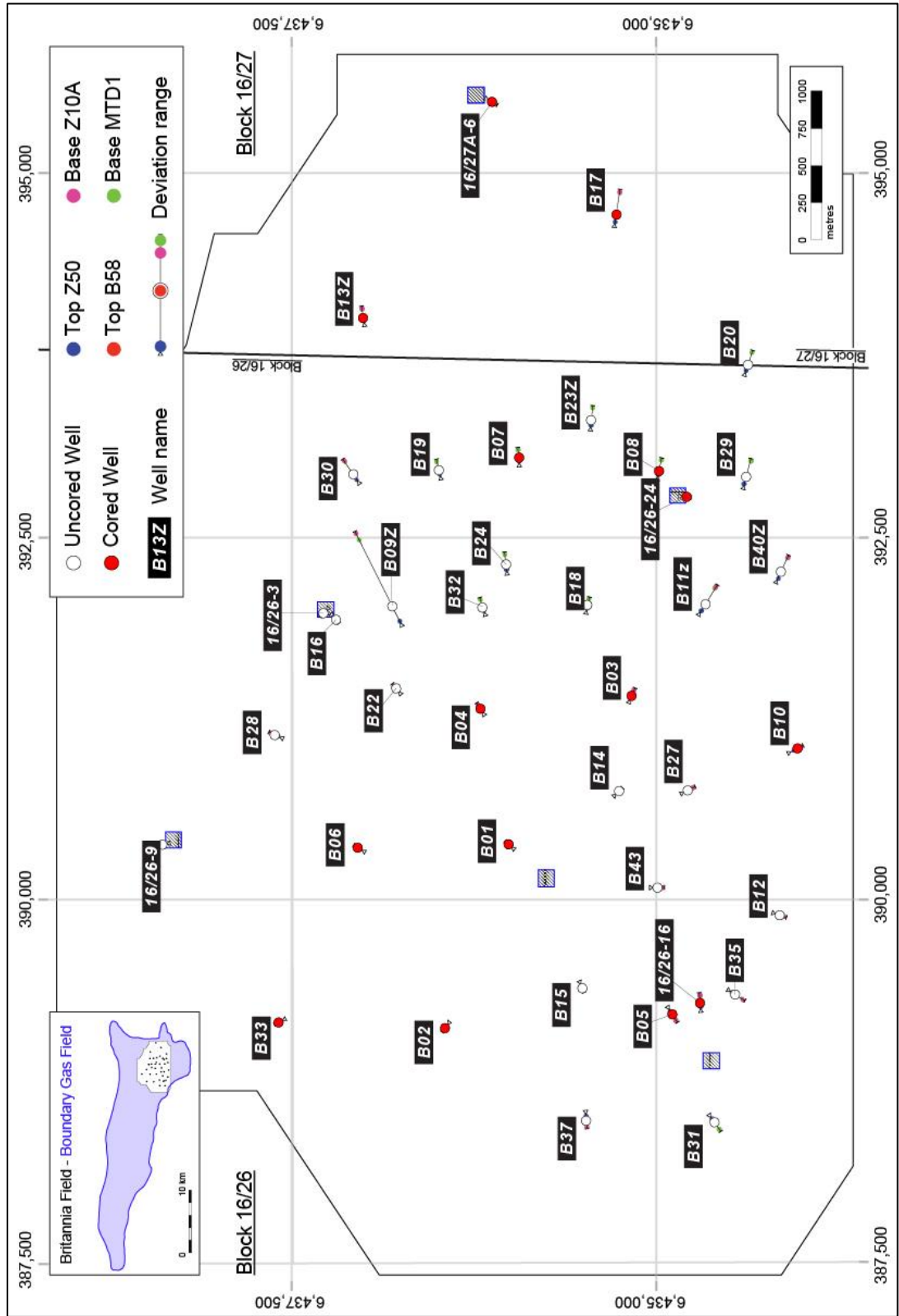


Fig. 6.2 - Platform Area of the Britannia Field. Red dots represent cored wells, while white dots represent uncored wells; their position is shown at the intersection of the well with datum 'Bed 58'. Well deviation range is shown by the pink, green and blue dots that represent the projection of the well intersection with key horizons at the base (pink/green) and at the top (blue) of the reservoir interval.

A summary of the sandstone Reservoir Sections and Zones investigated in this study in ascending stratigraphic order is shown below (see also section 4.4):

Lower Reservoir Section

- i. Zone 10A - forming the base of Britannia Sandstone Formation and the basal interval of this study.
- ii. Zone 10B - overlying Z10A from which it is separated by the Anoxic Shales.
- iii. Zone 20 - sandwiched within hemipelagic shale (Reddish Shales and Bioturbated Shales respectively above and below), it is recorded only in wells B02 and B33; the limited amount of data makes the investigation of sandstone lithofacies distribution difficult and hence this reservoir zone is not further considered in this chapter.

Middle Reservoir Section

- iv. Zone 40A – representing the lower portion of the Middle Reservoir and overlies the MTD-2. This forms the main sand package within the Middle Reservoir and has the most pronounced thickness variation within the study area together with the highest heterogeneity in lithofacies distribution.
- v. Zone 40B – lying in the middle part of the Middle Reservoir and bounded by MTD-2 and MTD-3. This interval is defined on purely sedimentological criteria, occurring across the whole Platform Area and showing different depositional character (e.g., amalgamation vs non-erosion trends) depending on well location.
- vi. Zone 40C – forming the upper portion of this study, it is bounded above by the datum Bed 58 which can be correlated over several kilometres, and below by the top of MTD-3. This interval is characterised by widely extensive sheet-like deposition.

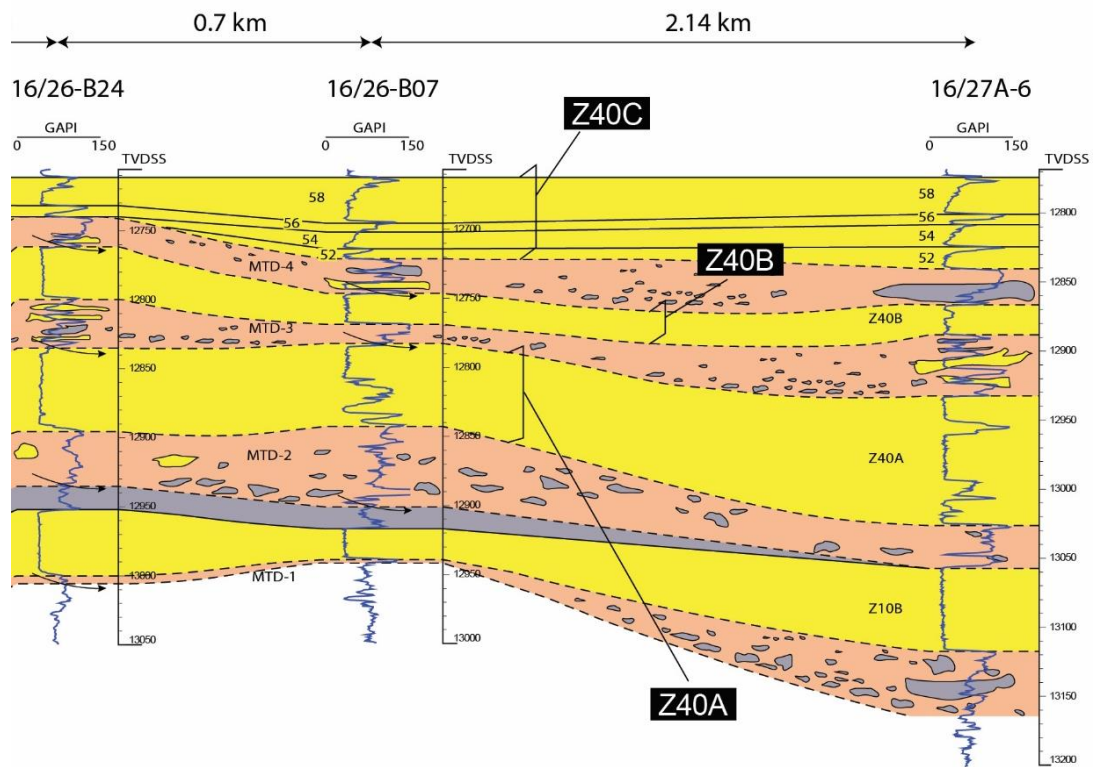


Fig. 6.3 – Correlation of the Lower and Middle Britannia Sandstone Member (cropped from Fig.4.7; a full suite of panels are shown in Chapter 4). The figure also shows the bed-by-bed correlation of Zone 40C.

6.3 Core facies

The use of core, core photos, cuttings analysis and wireline logs was the basis for the characterisation of the reservoir architecture, and the development of well correlations across the Platform Area (Chapter 4). In the following section, a detailed review of the core facies identified is undertaken as an introduction to the data regarding their vertical and spatial distribution, which constitute the main result of this Chapter.

6.3.1 Lithology

Four main classes are used to classify the deposits of the Lower and Middle Reservoir Section: clean and dirty sandstones, debrites and mudstones (see Chapter 4).

The clean sandstone lithotypes (containing ~2-15% of clay; Lowe & Guy, 2000) is characterised by pale grey to pale yellow colour with a matrix grain size ranging from fine (~62-88 µm) to lower medium (~250-350 µm). Toward bed bases, floating quartz

grains (~1400 µm in size) set within the main sandstone matrix are also common. These have been interpreted as high-density turbidites by Lowe & Guy (2000).

Sandstones with higher clay content (15-35% clay; Lowe & Guy, 2000) have similar character to the clean sand lithotypes, but tend to be darker in colour, typically dark grey to grey, or yellowy brown. Grain size is typically finer-grained than the clean sandstone lithotype, ranging from very fine (~62-88 µm) to lower medium (~250-350 µm) and clay content is inferred to be >35%. These are classified as 'slurry' facies after Lowe & Guy (2000).

Mud-silty matrix characterised by either the presence or absence of floating quartz grains is interpreted to represent the debrite class. In terms of colour, these deposits are typically grey to very dark grey. Clay content is inferred to be >50%. Clasts and coarser grains comprise various exotic lithologies including pale brown and white marly mudrock, brown nodules, shell fragments, glauconite (from shelf) and shale clasts.

Mudstones are black to dark grey in colour and although grain size is dominated by clay grade sediment, most contain a subordinate population of silt.

6.3.2 Facies descriptions and interpretations

Seven main lithofacies have been recognised, superimposed upon the classes described above: i) massive sandstone ii) laminated sandstones iii) banded sandstones, iv) mixed slurried sandstones v) injected sandstones, vi) debrites and vii) mudstones.

A summary of the facies identified in this study with related description was provided in Table 4.2 with examples of individual facies shown in Figures 4.3 and 4.4 (see section 4.3). The facies scheme represents a revised and simplified version of the inherited facies classifications sequentially proposed by Lowe and Guy (2000), Barker et al. (2008) and Eggenhuisen et al. (2010) summarised in Table 3.2 (see section 3.3.3).

Facies	Massive Sandstone	Laminated Sandstone	Banded Sandstone	Mixed Slurried Sandstone	Injected Sandstone	Debrite	Mudstone
Code	Sma	Sla	Sba	SMs	Sinj	DSn	Mds

Table 6.2 – List of the core facies (and associated codes) identified in the BSF in the PA. The full description and interpretation of these facies is shown in Table 4.2

6.3.3 Bed/Zone thickness and internal organisation

The sandstone reservoir zones of the Lower and Middle BSF across the Platform Area are characterised by highly variable thickness, with Zone 40A ranging between 2 and 60 metres. This also results in challenges when correlating individual beds and in some cases even zones. As shown in Chapter 4, five reservoir intervals are recognised and correlated using stratigraphic markers (such as hemipelagic intervals) and sedimentological observations (grain size, texture) of the sandstones.

Sandstone beds recognised in Z40C are exceptionally thick when compared to other deep-water systems, with individual beds reaching 11 metres locally as in the case of Bed 58 (Fig. 6.17). The large sandstone thickness variation within the study area is a consequence of the presence of large MTDs that were able to shape the seafloor, eroding previously deposited sandstones and building up different scales of rugosity that trapped and deviated gravity flows (see Chapter 5). The number of individual beds is difficult to recognise, but it is generally low, especially if compared with other turbidite systems. The typical organisation of facies within the Lower and Middle Reservoir Sections is illustrated in the graphic logs of Figure 6.5 that shows different depositional characteristics identified in core.

The sandstones tend to display sharp, planar bases, generally lacking evidence for small scale erosional topography. Bed bases are typically dominated by a granule-rich massive sandstone facies that ranges from 5 to 20 cm in thickness. Similar granule-rich sandstone divisions are observed to form bed bases across the study area in most instances. Overlying this basal facies, a stacked vertical sequence of primary banded and slurried facies, overprinted by dewatering structures (e.g., sheets, pipes and dishes superimposed upon primary facies) forms the main sand-rich section of these beds. Toward the tops of the beds, a relatively thin division of the mixed slurried facies is usually present (Fig. 6.5). Beds are typically capped by comparatively thin silty-mudstones, suggesting that only a limited portion of the muddy suspension cloud carried by the flows evolving down-dip was deposited in this part of the slope/basin. When preserved, a thin, 1-3 cm, layer of hemipelagic mudstone may also be present at the very top of the capping mudstone unit. Generally, mudstone caps are absent, due to subsequent erosion and sand bed amalgamation (e.g., Fig. 6.4). The vertical grain size profiles of beds generally show a grading signature, although “pulsed” divisions of coarser and finer sand intervals around 10-30 cm in thickness are sometimes apparent (see graphic log summary diagrams in Fig. 6.4, and graphic logs in Appendix B).

Very few sedimentary structures indicative of sediment traction (e.g., ripple-lamination or cross-bedding) are observed in the thick sandstone beds of the Middle Reservoir Section, which therefore lack a potential palaeoflow indicator. The lack of traction structures in conjunction with the poorly-sorted texture of the sands, pervasive dewatering and exceptional thicknesses exhibited by Britannia sandstone beds provides strong evidence for high suspended-load fallout rates during deposition, likely driven by the change in slope-gradient or related to bathymetric irregularities (Lowe, 1975, 1982; Arnott and Hand, 1989; Kneller and Branney, 1995; Kneller & McCaffrey, 1999; Lowe & Guy 2000).

The organisation of facies discussed above is significantly different from standard facies models (see Chapter 1) such as the Bouma sequence (Bouma, 1962) and the high-density turbidite sequence of Lowe (1982). The inferred transition within Britannia beds from sand-rich deposition by dominantly turbulent flow to mud-rich sandstone deposition by cohesive laminar flow with an increase of flow concentration during run-out, are not predicted by either of these models which shows progressive flow dilution in the case of the Bouma sequence and flow dilution once deposition from the main sand-rich portion of flows had ceased in the Lowe (1982) model. Progressive flow dilution controls the down-dip transformation of various types of gravity flow (e.g., Hampton, 1972; Fisher, 1983; Mulder et al., 1997; Piper et al., 1999; Waltham, 2004). However, recent studies (Haughton et al., 2003; Talling et al., 2004; Haughton et al., 2009;) have recognised deposits in which individual beds show a sharp upward transition from massive and dewatered sandstones into chaotic, highly sheared, clast-rich sandy mudstones and muddy sandstones. Haughton et al. (2003, 2009) termed these deposits 'Hybrid event beds' (HEBs) and inferred that they represent the deposits of co-genetic turbidity currents and debris flows that evolved spatially and temporally from dominantly turbulent flows to high-concentration laminar flows (see Chapter 1 for detailed review). In this respect, the Britannia slurry beds appear to evolve in a similar fashion spatially and temporally to turbidites with linked debrites, but the contact between the sand-rich division (turbulent flow) and the mud-rich division (laminar flow) is much more gradational.

Britannia beds show local evidence of transient cyclic flow transformations between laminar and turbulent flow regimes (e.g., banded facies) up to slurry flow (mixed-slurried facies). Banding horizons have been reported within the sandstone divisions of HEBs (Haughton et al., 2003) but is not uniformly developed or as extensive as in the Lower and Middle Britannia Sections. One exception is the Z40C, where 6 stacked HEBs are less banding-dominated and show a facies arrangement more similar to Haughton's scheme.

Other studies that have reported the deposition of slurry beds (e.g., Wood and Smith, 1958b; Burne, 1970, 1995; Ricci Lucchi and Valmori, 1980) do not report the range of fabrics observed in the Britannia Sandstone Fm. Furthermore, as discussed in later sections, the more enigmatic Britannia fabrics are only developed in certain parts of the study area and are laterally equivalent to more conventional structureless and dewatered sandstones (cf. Barker et al., 2008).

Lower/Middle Reservoir Section (Zone 10B-40A): typical bed/facies organisation

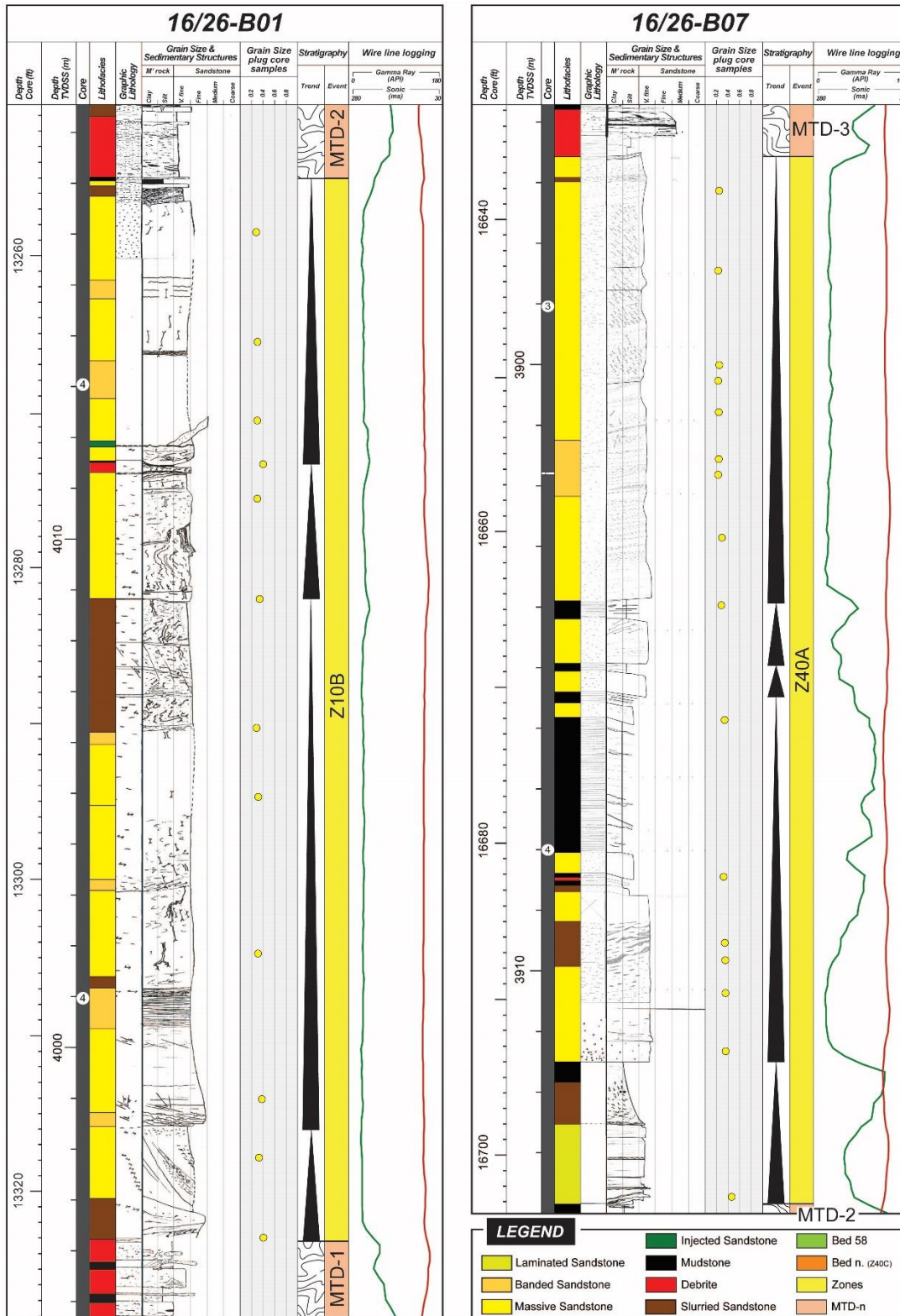


Fig. 6.4 – Example logs of typical beds encountered in the Middle Britannia Formation. Facies codes and log symbols are shown in key on diagram.

Middle Britannia Reservoir Section (Zone 40C): typical bed/facies organisation

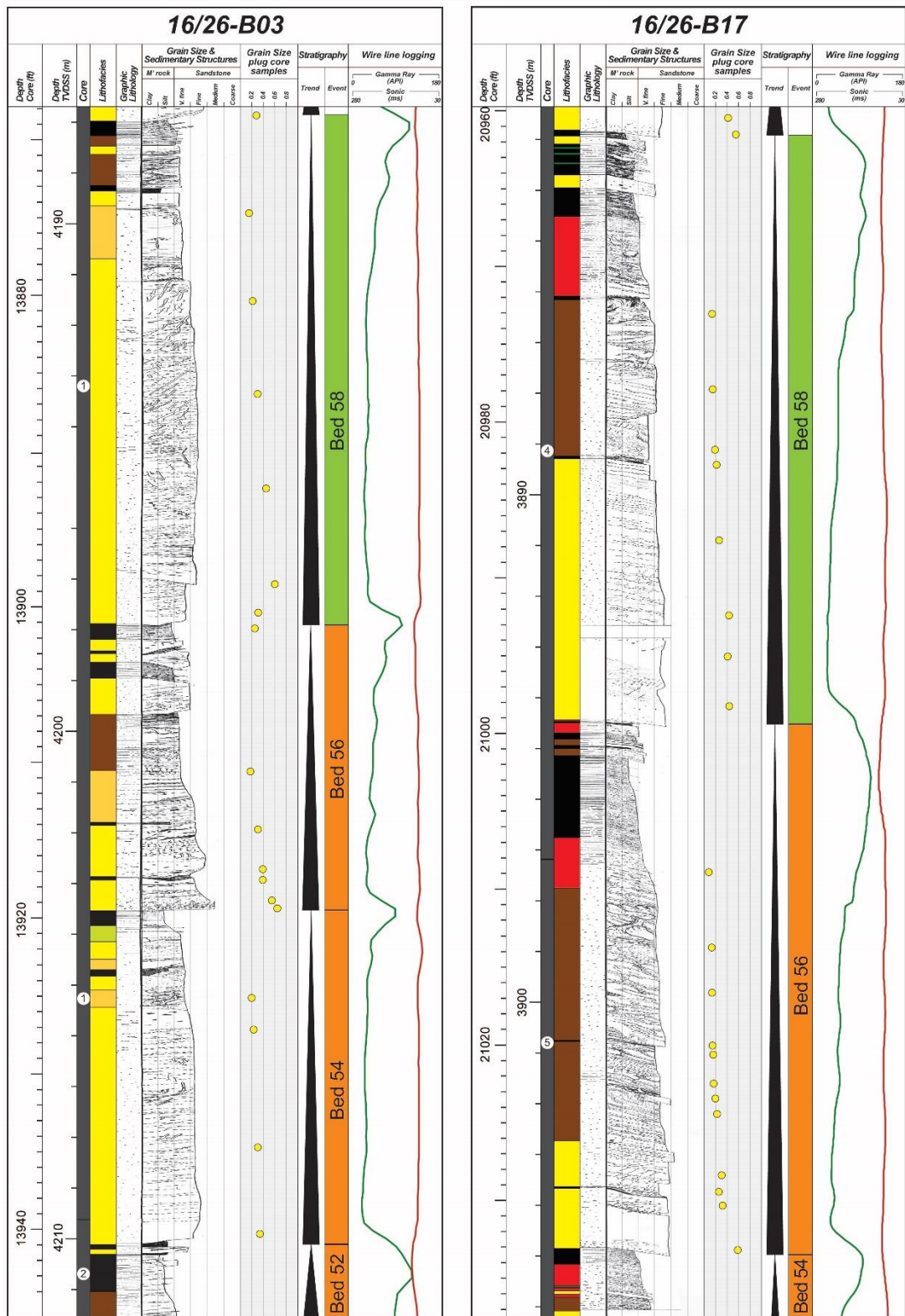


Fig. 6.5 – Graphic sedimentary logs (wells B01, B07, 16/26-24 and B17) summarising typical zone/bed organisation and internal character of different reservoir units. Facies codes and log symbols are shown in key on diagram. For well locations and the positioning of core taken from this well, refer to Fig. 6.1 and 6.2, respectively.

6.3.4 Complicating factors

The study of vertical and spatial sandstone facies variation is complicated by a number of factors that make facies analysis and flow process interpretation more difficult. These factors are:

- Amalgamation – Individual beds cannot be easily recognised due to their depositional character. In fact, lower reservoir zones (Zones 10A-10B and 40A-40B) are characterised by widespread sandstone bed amalgamation, whereas preservation of intra-bed shale horizons is only common within the upper reservoir zone (Zone 40C).
- Thickness/facies variations – Correlating individual beds/units between wells is problematic where thickness and facies vary over short distances. Some beds show large differences in thickness, grain size and sedimentary character between closely spaced wells (i.e., beds of Z40C).
- Transitional character – although facies divisions are quite distinctive, the transitional character of these events can complicate their discrimination. Some facies intervals may grade into one other and transitional facies may be difficult to classify.
- Determination of mud content – quantitative analysis of the mud content undertaken by Lowe and Guy (2000) by using thin sections was problematic. This is due to the presence of dewatering zones that show less mud than surrounding sediment, and compaction, stylolite formation and laminations that reduced the volumetric mud content of beds and within individual thin sections showing pressure solution effects (Lowe et al., 2003).
- Remobilisation – The presence of remobilisation features such as slides (Boxcar Sandstone, *sensu* Barker et al., 2008), slumps and debris flows make biostratigraphic correlation difficult, in fact over half the mudstone intervals between reservoir zones might be interpreted as deposited by mass-wasting processes or creep (Lowe et al., 2003; Barker et al., 2008; Eggenhuisen et al., 2010 and Chapter 5 of this thesis). The upper parts of reservoir zones are in many cases removed by these large failures, with truncated beds lacking some of the original divisions and therefore complicating any facies analysis.

6.3.5 Grain size distribution and palaeoflow

The lack of both traction-deposited primary sedimentary structures and erosional features such as flutes (which are, in any case, difficult to identify in core) have consequences for reconstructing the palaeo-flow direction, with a significant

uncertainty in developing models to explain the origin of the Britannia sandstones and their complex character.

The petrography and origin of BSF have been studied in detail by several authors (Blackbourn and Thomson, 2000; Garrett et al., 2000; Hailwood & Ding, 2000; Lowe and Guy, 2000; Barker et al., 2008) in order to try to constrain the provenance of the sediments deposited within the Britannia Field (see Chapter 3).

As noted in Chapter 3 (section 3.3.2), the Fladen Ground Spur and East Shetland platform to the north and northwest of the Outer Witch Ground Graben are source areas identified by Guy (1992) and Jones et al., (1999), with flows inferred to have flowed into the basin toward the south/southeast as confirmed by Hailwood & Ding, (2000). Using zircon dating, Machell (2003) and Moore (2009) suggest the east Shetland platform - west Scotland as the main sediment source, with sediments travelling from the west, along the southern edge of the Halibut Horst to pinch out against the Fladen Ground Spur (see bottom of Fig. 6.6-G).

Grain size distribution had been investigated in detail by Lowe et al., (2003) and subsequently by Barker et al. (2008) in order to gain insights into the palaeoflow direction of the sand-depositing events. Lowe et al. (2003) mapped the distribution of grain size between wells within inferred time-equivalent horizons deposited by single event beds. They interpreted the spatial grain size fining trends to be a proxy for palaeoflow direction resulting in an interpreted South to North trend and a reversed North to South trend for Zones 45 and 50, respectively, in the Upper Reservoir Section. However, a systematic change in grain size was not detected by Barker et al., (2008) who undertook textural analysis on event beds of revised correlation within the same reservoir intervals, and concluded that the method could not be used as a palaeoflow indicator for the Upper Britannia Section. Instead they used maximum amalgamation trends and consistent on- to off- axis trends in deposit character to estimate the orientation of the basin axis and thus to infer a West to East direction of transport.

The Lower and Middle Reservoir Section has a different depositional style in that reservoir zones are fully amalgamated in the Platform Area. The only exception is Z40C, where individual event beds can be traced across the study area. Because these intervals show different characteristics to those investigated by Lowe and Guy (2000) and Barker et al. (2008), an attempt to estimate palaeoflow directions for the Lower and Middle Reservoir Section was undertaken. The uniform vertical grain size trends observed in many wells of the Lower and Middle Britannia Sections (Z10A, Z10B, Z40A and Z40B) might validate Lowe and Guys' method of assessing spatial

patterns of grain size variation to determine palaeoflow for those zones characterised by fully amalgamated intervals. Figures 6.4 and 6.5 show the difference in reservoir character of the Lower Britannia Z10A and Z10B (and also Z40A and Z40B, not shown) and the upper part of Middle Britannia Z40C: in the first figure a uniform grain size trend is recognised throughout the entire sandstone interval, whereas in the second figure individual event beds are normally graded. Grain size values shown in the figures and used in this study were produced by Lowe and Guy (2000) and represent the mean grain size, calculated measuring and averaging the longest grain dimension of 300 (for E&A wells) or 100 (for predrill wells) quarts and feldspar grains for each sample. Lowe and Guy (2000) also conducted measurements termed 'max5', which consist of measuring the 'a' and 'b' intercepts (representing respectively the longest grain dimension and the second longest dimension perpendicular to the first) for each grain, averaged for each section.

In the work of Lowe and Guy (2000) the mean grain size dataset was evaluated by plotting the average of the mean values measured within inferred time-equivalent reservoir zones in each well of the study area. This helped to identify potential lateral grain size fining trends as a proxy for palaeoflow. Plotting average mean grain size for intervals should avoid misleading results that might arise due to a) uncertainty in investigating same inferred time-equivalent horizons, b) irregular spacing of samples within beds in individual wells (Lowe et al., 2003), and c) possible influence of topographic rugosity on abrupt changes of grain size within individual event beds (Barker et al., 2008).

Contour maps of grain size for Z10A, Z10B, Z40A and Z40B show a possible fining trend toward East/North-East and South. Average mean grain size in these intervals ranges between 0.40 and 0.11 mm, with values generally decreasing from West to East, with very few cases where the average grain size of an interval measured in a well does not fit the trend (i.e. wells B01 and B07 in Z10B and Z40A, and well B04 in Z40B). Furthermore, the map of grain size distribution of Z40A appears to highlight the deep conduit formed by MTD-2 (see Chapter 5), such that coarser grain sizes are deposited along the transect formed by wells B05, B04 and B13z (Fig. 6.6-A, -B, -C, -D).

The different reservoir architecture characterising Z40C makes the method described above (calculation of average grain size for each zone) less reliable for estimating palaeoflow directions within this zone. The reason is that Z40C is characterised by six well-recognised event beds with only modest signs of amalgamation and erosion, given the presence of mud-rich layers on top of most of these event beds. This is

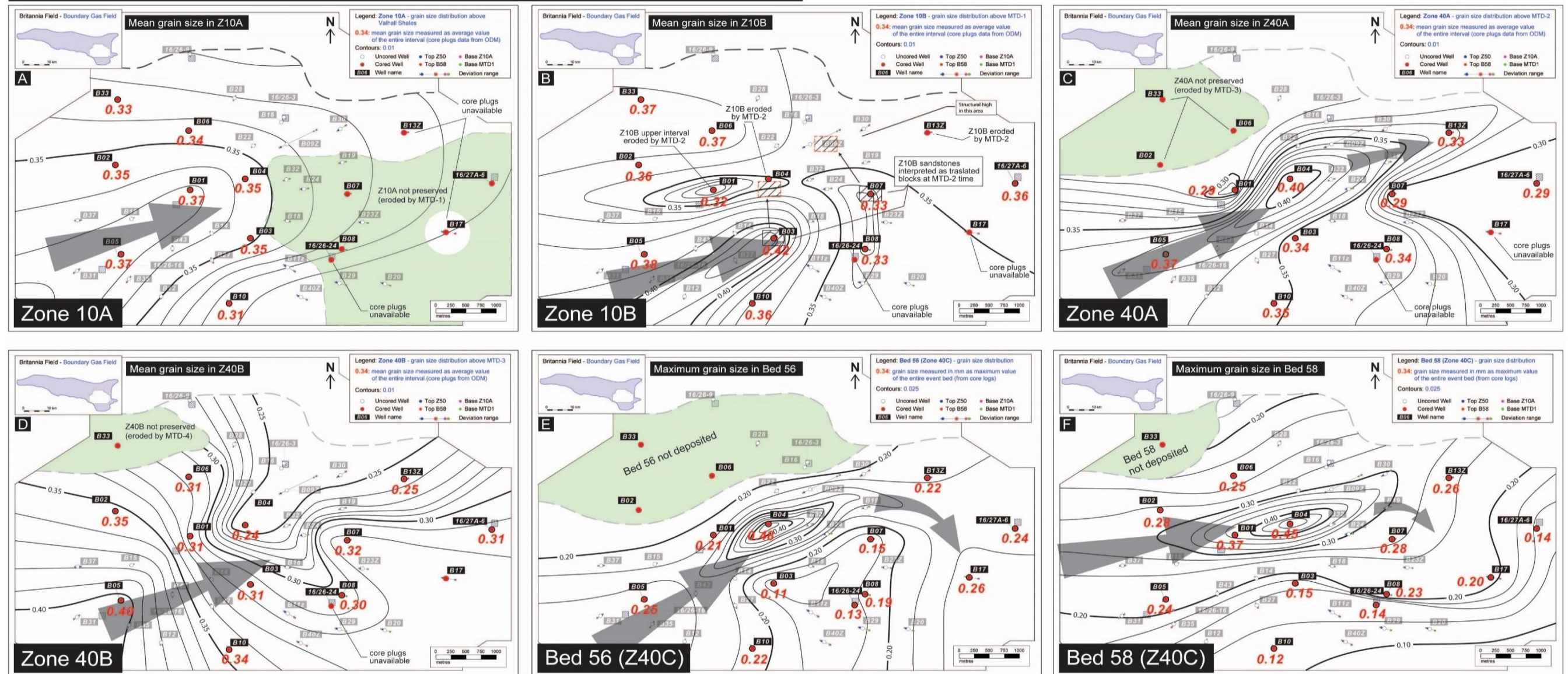
coupled with the irregular spacing of samples with grain size data within beds in individual wells, prevented calculation of a meaningful mean grain size for each bed (see Fig. 4.8 showing Z40C event beds). Lowe and Guy's (2003) attempted to resolve this issue by calculating the averaged values of mean and 'max5' at 25%, 50% and 75% of the distance from the base to the top of some beds and evaluating the consistency of these measures with the graphically estimated mean and 'max5' at the midpoint of each bed (Lowe et al., 2003). However, uncertainties linked to these methods likely arise caused by a) the position of samples along the thickness of the event bed, b) the lack of preservation of the full thickness of each event bed. In order to address such issues and to provide an estimate of palaeoflow direction within Z40C, maximum grain size for the two uppermost event beds was measured from graphic core logs (Fig. 6.6-E, -F). Both maps of Bed 56 and Bed 58 show grain size fining toward the eastern sector of the study area. Bed 56 may also show a slight deflection towards the south in well B17. The coarser sands in this bed are concentrated in well B04, in the central study area, where flows were likely confined by a palaeo-slope on the northern area (where this event is not deposited) and by earlier sandstone deposits which were in turn influenced by relict topography inherited by MTD-4 underneath.

Higher up in the stratigraphy Bed 58 is identified across the whole Platform Area with the exception of well B33, and shows a west to east grain size fining trend. Coarser grain sizes are encountered in well B04 which presumably might represent the axial flow. Of course, this method to estimate palaeoflow direction should be used with care due the uncertainties listed above. Palaeoflow trends for the lower event beds within Z40C are not shown because of their higher degree of uncertainty, linked to the proximity of MTD-4 related topography which might have a major role in spatial grain size distribution.

The palaeoflow direction estimated through the grain size trends across the Platform Area align with those of previous interpretations (Lowe et al., 2003; Moore et al., 2009) which include a larger dataset with well data from the Subsea Area and broader Britannia Sandstone (Fig. 6.6-G). Moore et al. (2009) have attempted to build a facies model distribution for each reservoir zone of the Britannia Reservoir based on facies associations and palaeoflow directions from core, and their relationship to modern submarine fan morphology of deep-water depositional system (Mutti and Ricci Lucchi, 1972; Mutti and Normark, 1987, 1991; Mutti et al., 2009a). However, the authors also define a) the degree of thickness variability between close wells; b) the lateral and longitudinal extent of depo-centres, and c) the facies distribution outside the Platform Area as key uncertainties that could not be achieved in their work. In

conclusion, spatial grain size trends identified by this and previous work suggests that currents in the Britannia Field area travelled parallel to the Fladen Ground Spur slope and were thus potentially sourced 100s of km to the west/northwest.

Sandstone grain size distribution across the Platform Area



Depositional pathways of the Lower and Middle Britannia Sandstones (modified after Moore et al., 2009)

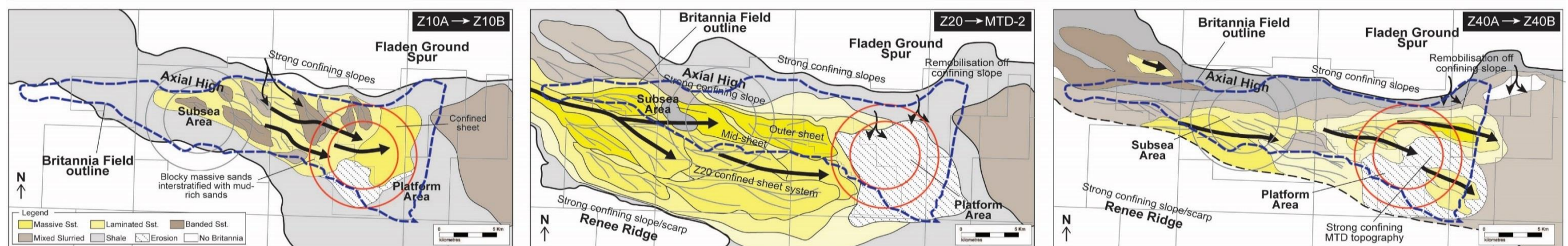


Fig. 6.6 – A-F) Contour maps showing average (A-D) and max (E-F) grain size for four reservoir intervals and two event beds across the Platform Area. Maps A-D are drawn using average mean grain size referring to the entire investigated interval, calculated from a database of grain size values measured from core plugs by Blackburn and Thomson 2000 and Lowe and Guy, 2000. Grain size distribution could represent a reliable palaeoflow indicator in absence of other data to estimate gravity flow directions. However, the role of topography on grain size partition is also known so this should be exercised with care. The six maps (A-F) show grain size trends suggesting flows from west to east. At the bottom (G) a redrawn reconstruction of the large scale Britannia depositional fairways for the Lower and Middle Reservoir Section proposed by Moore et al. (2009).

6.4 Sandstone deposition in the Lower and Middle Reservoir

Sandstone deposits emplaced above MTDs are here investigated in terms of lateral facies trends for each of the reservoir intervals identified in Chapter 4. Sandstone beds are generally characterised by high degree of thickness variability and lithofacies heterogeneity, which makes their correlation across the Platform Area difficult, with the exception of Z40C where individual event beds can be traced and correlated across most of the study area with confidence (Fig. 6.7).

Lithofacies for the Britannia Field are plotted by stratigraphic interval in younging order and by relative proportion on pie-charts to investigate their spatial distribution across the Platform Area. Both approaches are important for studying the influence of topography on the distribution of lithofacies and may be predictive in terms of facies distributions in similar settings.

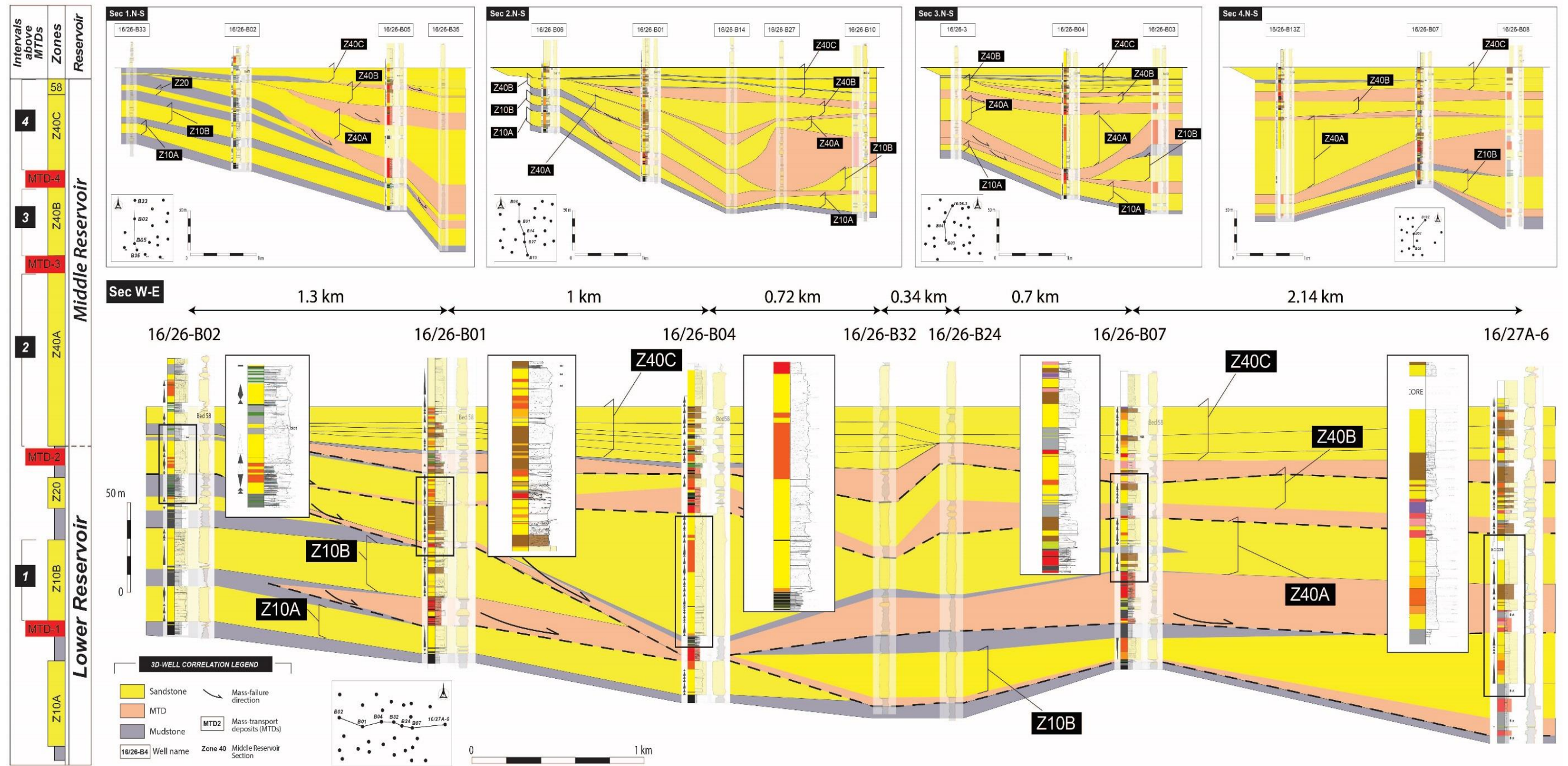


Fig. 6.7 – Well correlation panels of cored and uncored wells of the Lower and Middle Reservoir Section across the Platform Area. Spatial and vertical distribution of sandstone lithofacies is also shown for cored wells. Sections N-S across the study area, shown at the top of the figure, describe the stratigraphy between the in-situ area (north-west) and the remobilised sectors (south-east). Section W-E shows the geometry of the reservoir intervals and the lithofacies heterogeneity encountered in cored wells. A stratigraphic column with the identified sandstone reservoir intervals and MTDs is shown on the left hand of the figure. Reservoir intervals 1 - 4 are associated with deposition on MTDs-related topographies.

6.4.1 Zone 10A

Zone 10A represents the first extensive and well-recognised sand-body reservoir within the Platform Area. This sand interval is deposited above the Valhall Shales on a slightly sloping surface (Fig. 6.7 – 6.9) and it is stratigraphically bound at the base and top by anoxic shales of the Fischeschiefer Bed (see Chapter 3), with anoxic mudstone recognised on both cored wells and wire line logs. Data from this reservoir interval were collected by previous workers (Lowe and Guy, 2000; Eggenhuisen et al., 2010) and are here re-evaluated to better constrain and integrate this interval with the new identified reservoir zones of the Middle BSF.

Sandstone core facies distribution are displayed on pie charts above the reconstructed palaeobathymetric map (Fig. 6.8; see also Chapter 5). Z10A intervals are present only in the west-side of the study area because in the eastern-side Z10A was later removed by MTD-1. In addition, Z10A in wells B01 and B03 does not have its top preserved (pie-charts with red borderlines in Fig. 6.11), whereas only wells B33, B06, B02, B04, B05, and B10 preserve the entire Z10A as shown by them being capped by thick anoxic mudstones representing the higher portion of the Fischeschiefer Bed (marked by black borderlines). Geological sections also show the reconstructed fully eroded (Fig. 6.8; Sec.1) and partially remobilised sector (Fig. 6.8; Sec. 2-3) due to the emplacement of MTD-1 in the Platform Area. Within the remobilised area (dashed area in Fig. 6.8), only B17 recorded ~4 metres of Z10A sandstones deposited above anoxic mudstones as recognised from wire line data, but core was not available for investigation.

Pie charts are expressed in terms of percentage calculated on the entire thickness of the investigated intervals. In addition, radii of the pie charts are proportional to the thickness of the sand-body intervals. This shows that Z10A represents an interval of relatively constant thickness, with the exception of the wells B01 and B03 where this is eroded. However, lithofacies percentages highlight a slight difference between the southern and the northern sectors of the Platform Area. In fact, the large proportions of massive clean sand (SMa) that characterise the central and southern study area decrease toward the north from ~90% to 36%. The Z10A becomes progressively muddier and develops banded sandstones (SBa) in B04 and B06 (respectively 3% and 41%), and mixed slurried intervals (SMs) in B04 (1%), B06 (12%) and B33, where significant portions of mixed slurried sandstones are recorded (23%). Relatively small intervals of laminated sands (Sla) are also recognised in B06 and B01 (respectively 6% and 4%). Mudstones are recorded in all wells with the exception of B04, with an average percentage between 6% and 25%.

The character of Z10A is summarised in Figure 6.9. These logs were measured by Eggenhuisen (2008) and in this study they are revised in order to study the vertical distribution of facies within the sand packages.

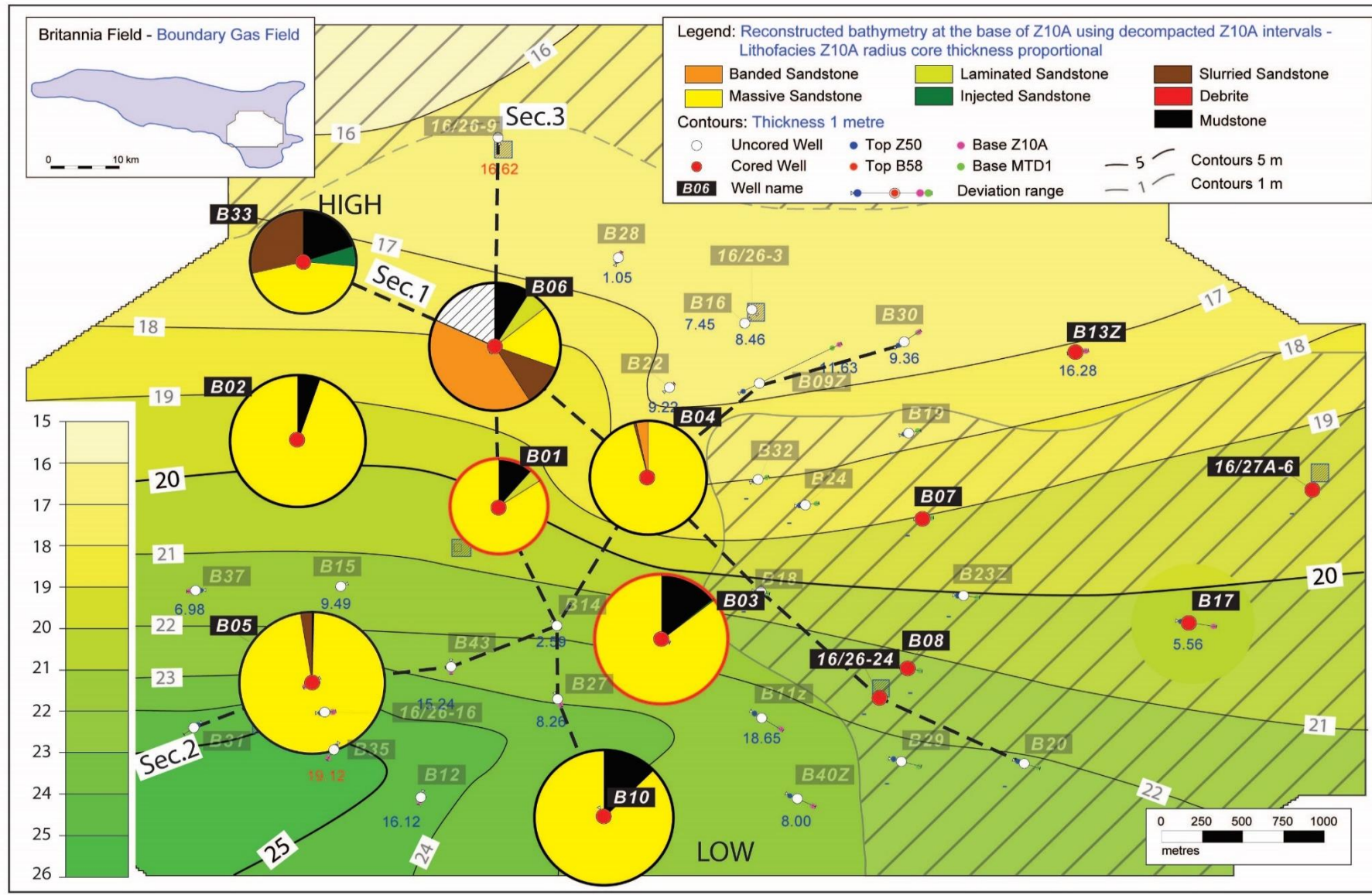
This sand interval is mainly made up of amalgamated sandstones which may be considered to represent a distinctive character, similar to the Boxcar Sandstone Division (*sensu* Barker et al., 2008) identified in Z45 in the Upper Reservoir Section. The extensive amalgamation features observed in this interval across the Platform Area (where not remobilised by MTD-1) are confirmed by an ungraded character, with grain size not showing any fining/coarsening trends (the same grain size character is recognised for Z10B, see Fig. 6.6). Locally, some rare clay smears are seen. Thicker mudstone intervals are recognised within the very basal portions of wells B33, B06, B02 and B01, capping 0.5 to 1 metre thick sandstones that can be traced between these wells (Fig. 6.9). These may represent the first extensive sand input in the Platform Area within the Lower Britannia (older Z7 sands are recognised only in B33 and B35). Two of these beds can be identified confidently in the northern study area (B33, B06, B02, B01 and B04), whereas amalgamation makes their correlation difficult in wells that are located in the slightly deeper southern Platform Area (B05, B03 and B10) (Fig. 6.9). The very basal event bed, ranging between 0.5 and 1 metres thick, thickens toward the centre of the study area and records a significant lateral facies variability characterised by massive clean sands in B04, where it is thick, to laminated in B06 and passing to mixed slurried character in B33 towards the north of the study area.

In the southern sector of the study area, amalgamation results in development of a continuous sandstone interval in B05, whereas a calcareous laminated mudstone interval ranging between 1.5 and 2 metres, breaks the monolithic sand columns in B03 and B10. Different features are observed in the mudstone capping the basal ~4.5 metres of sands in B10, whose composition has a higher percentage of silt.

The higher proportion of mudstones shown by the pie charts of wells in the northern sector of the study area coincides with the abundance of banded and mixed-slurried facies. These intervals are observable on graphic logs of wells B06 and B33 (Fig. 6.9). In well B06, 0.5 to 1 metre banded sandstones are interleaved with 0.2-0.7 metre-thick laminated sandstone intervals and mixed slurried sandstones comprising the remaining lower portion of Z10A. These latter intervals seem better developed in B33 where they are interleaved with massive sandstones and include several injected sandstones. Dewatering features such as dishes and consolidation laminations pervade the entire sandstone interval. Pipes are also recognised and tends to overprint the internal fabric, cross-cutting previous structures.

Z10A sandstone distribution

- B33**
Thickness: 11.67 m
20% - Mudstone
29% - Mixed Slurried S.
6% - Injected Sandstone
45% - Massive Sandstone
- B02**
Thickness: 14.87 m
5% - Mudstone
95% - Massive Sandstone
- B06**
Thickness: 14.39 m
9% - Mudstone
12% - Mixed Slurried S.
41% - Banded Sandstone
6% - Laminated Sandstone
14% - Massive Sandstone
- B01**
Thickness: 10.74 m
11% - Mudstone
5% - Laminated Sandstone
84% - Massive Sandstone
- B03**
Thickness: 14.62 m
14% - Mudstone
1% - Injected Sandstone
85% - Massive Sandstone
- B05**
Thickness: 15.50 m
1% - Mudstone
3% - Injected Sandstone
96% - Massive Sandstone



- B04**
Thickness: 12.77 m
3% - Banded Sandstone
1% - Mixed Slurried S.
96% - Massive Sandstone
- B07**
Thickness: 0 m
ERODED by MTD-1
- B13z**
Thickness: 11.40 m
CORE not preserved
- 16/27A-6**
Thickness: 0 m
ERODED by MTD-1
- B17**
Thickness: 4.05 m
CORE not preserved
- 16/26-24**
Thickness: 0 m
ERODED by MTD-1
- B08**
Thickness: 0 m
ERODED by MTD-1
- B10**
Thickness: 15.01 m
12% - Madstone
1% - Injected Sandstone
87% - Massive Sandstone

Geological sections

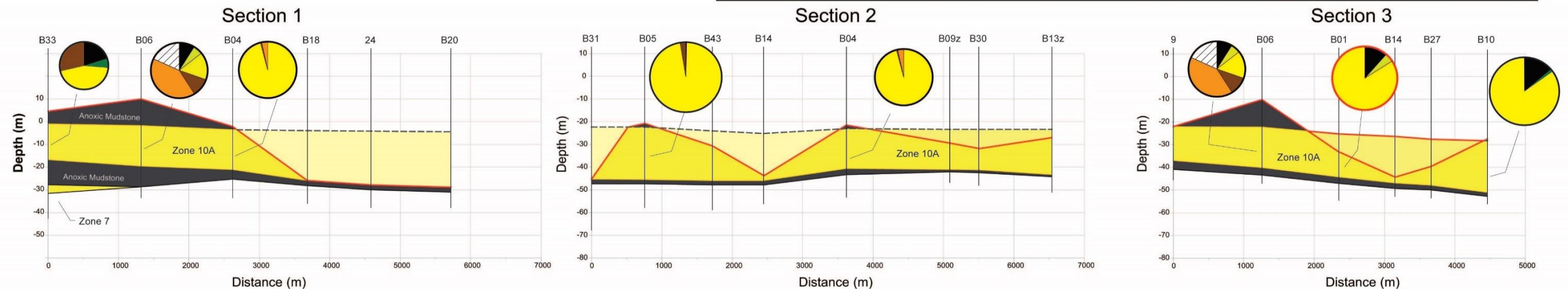


Fig. 6.8 – Palaeobathymetric map of the BSF in the Platform Area representing the basal surface of Zone 10A (for decompacted deposits and reconstructed Z10A time). Pie charts show proportion of lithofacies identified within Z10A in cored wells (red dots). Map: contours in metres (blue = deep; yellow = shallow). Dashed area represents reconstructed Z10A depths values. Lithofacies: pie charts radius represent proportional thickness of the reservoir interval. Red and black borderlines of the pie charts represent eroded and preserved top intervals. Quantitative analysis of the sandstone lithofacies are displayed at the map sides. Geological sections at the bottom: 2D deposits distribution are shown using decompacted intervals.

Z10A lithofacies distribution

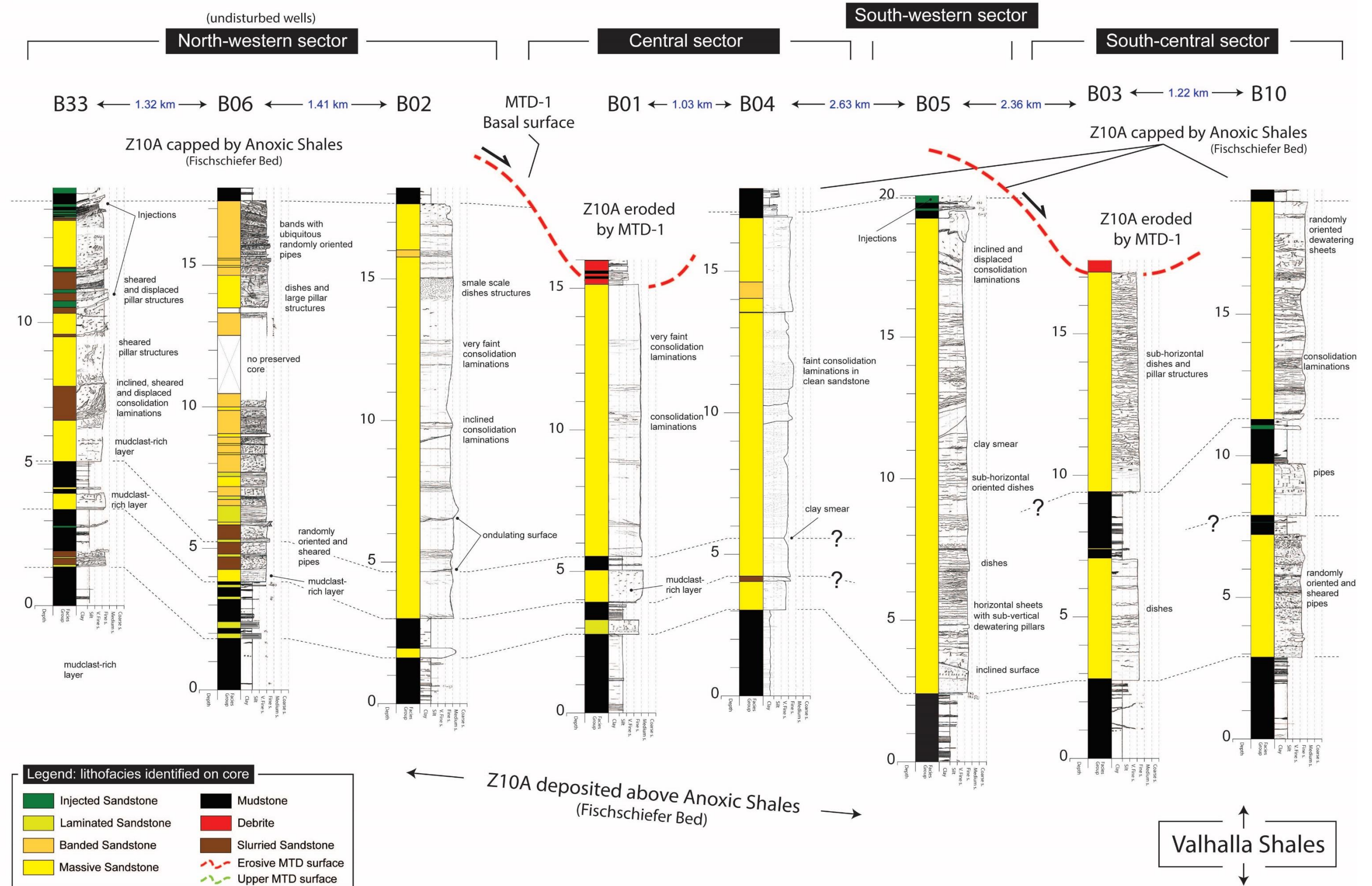


Fig. 6.9 – Graphic sedimentary logs summarising facies and bed organisation of Zone 10A. The reservoir interval is bounded at the bottom and on top by Anoxic Shales. Wells B01 and B03 show an erosional truncation at their top related to the emplacement of MTD-1, whereas the rest of the investigated wells exhibit preserved tops. Relatively clean, massive sandstones tend to dominate this interval, with the exception of well B06 where sandstones are characterised by an extensive banded texture and a high content of mud within the mixed slurried sands at the bottom.

6.4.2 Zone 10B (above MTD-1)

Zone 10B represents the second important input of sandy-gravity flows into the Platform Area with sandstone deposits identified in all cored wells with the exception of wells B04, B13z and 16/26-24, where this interval is interpreted as being eroded by MTD-2 (Fig. 6.10). Z10B is stratigraphically deposited above the anoxic mudstones of the Fischschiefer Bed on the north-west area where wells B33, B02 and B06 are interpreted as lacking any remobilisation features. On the contrary, in the south-eastern sector of the Platform Area, Z10B rests above MTD-1, across the area where the associated mass-failure evacuated Z10A (see Chapter 5 for better description of the geological model of the study area).

The size of pie charts for Z10B reservoir interval varies widely across the study area with the thickness of this sandy interval ranging between 7.5 metres in B06 in the north to ~22 metres in the central sector and thus some considerations to describe thickness trends are necessary. Wells B33, B02, B06, B03 and B07 are interpreted having their total Z10B thicknesses preserved, with the sand interval being capped by bioturbated mudstones attributed to the Ewaldi Marls (see Chapter 3). The rest of the wells show sandstone intervals between ~18 and ~20 metres thick, but they are overlain by remobilised deposits associated with MTD-2 and lack the bioturbated muds, probably due to later erosion. A significant amount of erosion is thought to have occurred in B05 where the sandstone package measures just 4.6 metres thick within a relatively deep topographic low (Fig. 6.10).

The thickness of Z10B measured across the study area also reflects the palaeobathymetry of the Platform Area restored at the time of MTD-2 emplacement. Thick sandstone intervals are recorded in locations where more accommodation space was available. An exception to this trend is well B07 where a relatively thin Z10B (6.97 metres) characterised by banded sandstones is deposited in proximity to the deepest area of the Platform Area. In this case, erosion by later flows was excluded as a cause, because of the presence of bioturbated mudstones on top of the interval (an important stratigraphic marker that bounds the Z10B sand-body). These deposits are hence interpreted to have been deposited in different location (e.g., on a topographic high in the northern sector) and to have been moved to their present location by later mass-wasting processes (see Chapter 5). This would also account for their banded appearance, suggesting flow thinning above a lateral slope (Barker et al., 2008)

The facies distribution map (Fig. 6.10) shows that sandstones developed various facies in the Platform Area. Massive-clean sands represent the predominant facies,

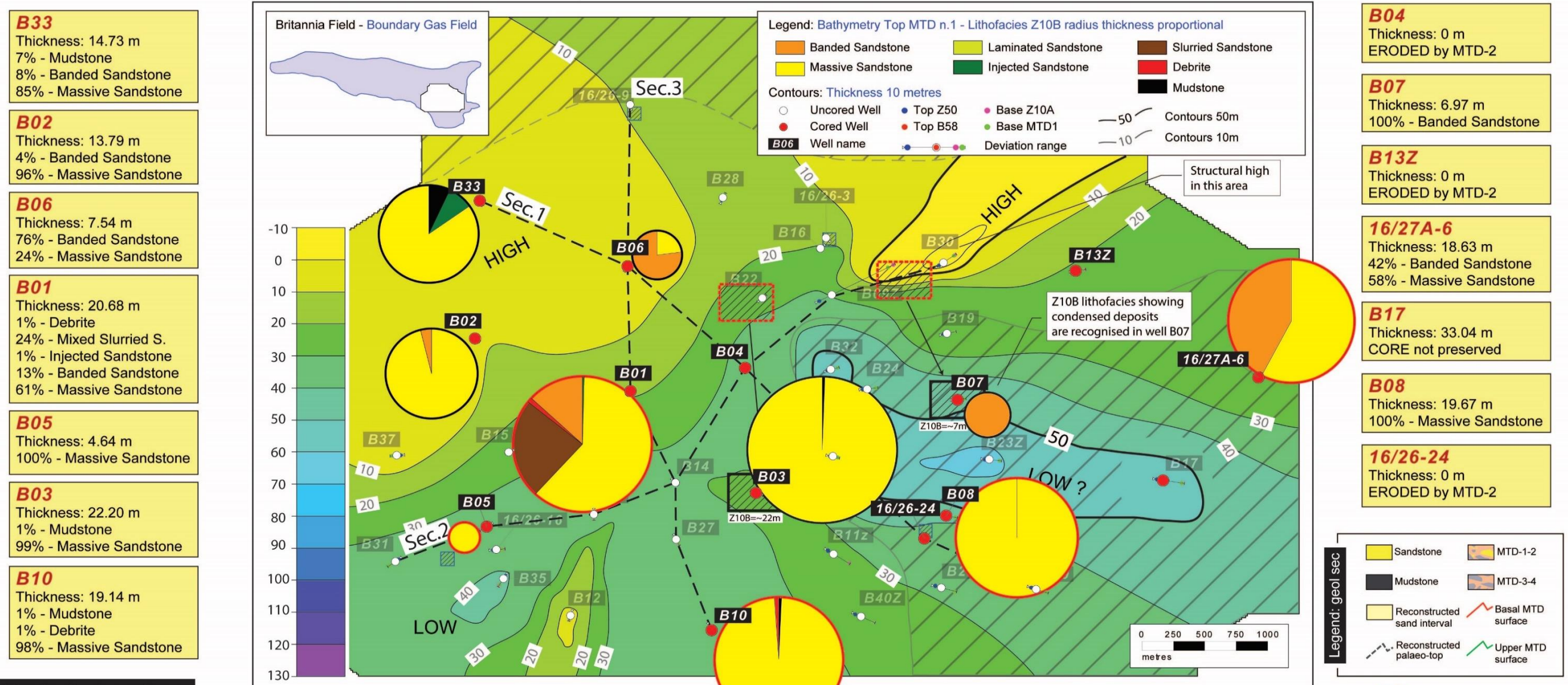
being ~72% of the total thickness of Z10B intervals from cored wells. They are combined with banded sands that in turn represent ~24% of the total thickness. While massive-clean sands are encountered in all cored-wells in the study area, banded sands are recognised in B02, B06, B01, B07 and 27A-6 forming between 4% and 100% of the thickness of each well. In this regard, sedimentary features in B06 and B07 are relatively similar, with the banded sandstones accounting for the same proportion of Z10B, likely a primary similarity, given that the presence of in situ hemipelagic mudstone at top of Z10B in both wells (Fig. 6.11), which appears to rule out later modification of facies proportions by erosion. However, the similar facies and thickness trends recognised in B06 and B07 are recorded at different bathymetric depth, with B06 deposited over a relatively topographic high whilst B07 about 30 metres deeper (see Fig. 6.10). This led to the interpretation that sediments in B07 were probably remobilised, and translated as part of the mass-failure event that emplaced MTD-2, from a topographic high that was supposed to be at the same depth of the base of Z10B in B06, in the northern area. These observations might support the interpretation of slide blocks in the same area, earlier introduced in Chapter 5, where stratigraphic intervals in B03, B24, B32, if compared with the reconstructed accommodation space, were recognised at unusual depths (see Chapter 5 for further explanation). A similar mechanism is inferred for deposits of B03, where massive-clean sands are interpreted as having been originally emplaced some ~1.5 km to the north of the actual location, before being translated in the present site. The thickness of Z10B in B03 is ~22 metres (no erosion is observed as it is capped by bioturbated mudstones), which is thought to be indicative of the palaeobathymetric of the location from where the translated block might have sourced, whereas these deposits are encountered in a deeper area where the depth is ~30 metres (see also Chapter 5).

Minor facies components include mixed slurried sands, debritic and mudstone intervals, jointly representing <4% of the total. These are mainly present as relatively thin layers within B33 and B01, with mixed slurried sands ranging between 0.2 and ~2 metres thickness in B01 and mudstone horizons interleaved with sandstone intervals in B33 and at the basal portion of B02, as shown on the sedimentary graphic logs of Figure 6.10. Z10B across the study area shows the development of extensive, amalgamated thick sandstone intervals that are mostly ungraded. However, small differences in grain size are observed in core and they likely represent the contact between cryptic amalgamated event beds (Fig. 6.11).

Event beds are recognised at the base of the Z10B in B02 and B33 thanks to the presence of mudstone layers capping massive clean sands. However, contacts

between event beds cannot be easily recognised toward the eastern and the southern sector, which are characterised by thickened sections with multiple inclined surfaces and internal bed deformation (i.e. lower portion of wells B08 and B10). Mud-rich intervals are frequently encountered in well B01 with significant portions of mixed-slurried and banded sand intervals. Relatively thin debrite layers are identified in B01 and B10, likely due to pervading shear. An interesting feature observed in these intervals is the relatively constant grain size of the sand, which remains similar to those measured in massive-clean sands within the same reservoir zone. The difference is the mud content, with clay and silt increasing considerably in the banded and even more so in the mixed-slurried sands. Dewatering features such as consolidation laminations, dishes, pillar structures and pipes pervade all the Z10B cored wells as highlighted by the graphic logs of Figure 6.11, but are preferentially concentrated within banded and mixed-slurried sandstones.

Z10B sandstone distribution above MTD-1



- B33**
Thickness: 14.73 m
7% - Mudstone
8% - Banded Sandstone
85% - Massive Sandstone
- B02**
Thickness: 13.79 m
4% - Banded Sandstone
96% - Massive Sandstone
- B06**
Thickness: 7.54 m
76% - Banded Sandstone
24% - Massive Sandstone
- B01**
Thickness: 20.68 m
1% - Debrite
24% - Mixed Slurried S.
1% - Injected Sandstone
13% - Banded Sandstone
61% - Massive Sandstone
- B05**
Thickness: 4.64 m
100% - Massive Sandstone
- B03**
Thickness: 22.20 m
1% - Mudstone
99% - Massive Sandstone
- B10**
Thickness: 19.14 m
1% - Mudstone
1% - Debrite
98% - Massive Sandstone

- B04**
Thickness: 0 m
ERODED by MTD-2
- B07**
Thickness: 6.97 m
100% - Banded Sandstone
- B13Z**
Thickness: 0 m
ERODED by MTD-2
- 16/27A-6**
Thickness: 18.63 m
42% - Banded Sandstone
58% - Massive Sandstone
- B17**
Thickness: 33.04 m
CORE not preserved
- B08**
Thickness: 19.67 m
100% - Massive Sandstone
- 16/26-24**
Thickness: 0 m
ERODED by MTD-2

Geological sections

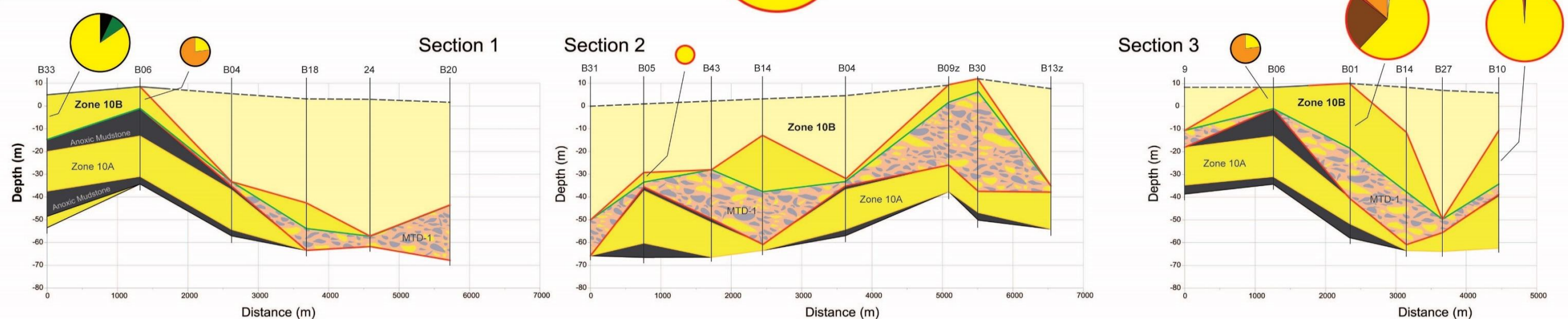


Fig. 6.10 – Palaeobathymetric map of the upper topography associated with MTD-1 (for decompacted deposits and reconstructed MTD-1 time) with pie charts showing proportion of lithofacies identified within Zone 10B in cored wells (red dots). Map: contours in metres (blue = deep; yellow = shallow). Dashed area represents reconstructed Z10A depths values. Lithofacies: pie charts radius represent proportional thickness of the reservoir interval. Red and black borderlines of the pie charts represent eroded and preserved top intervals. Geological sections at the bottom: 2D deposits distribution are shown using decompacted intervals.

Z10B lithofacies distribution above MTD-1

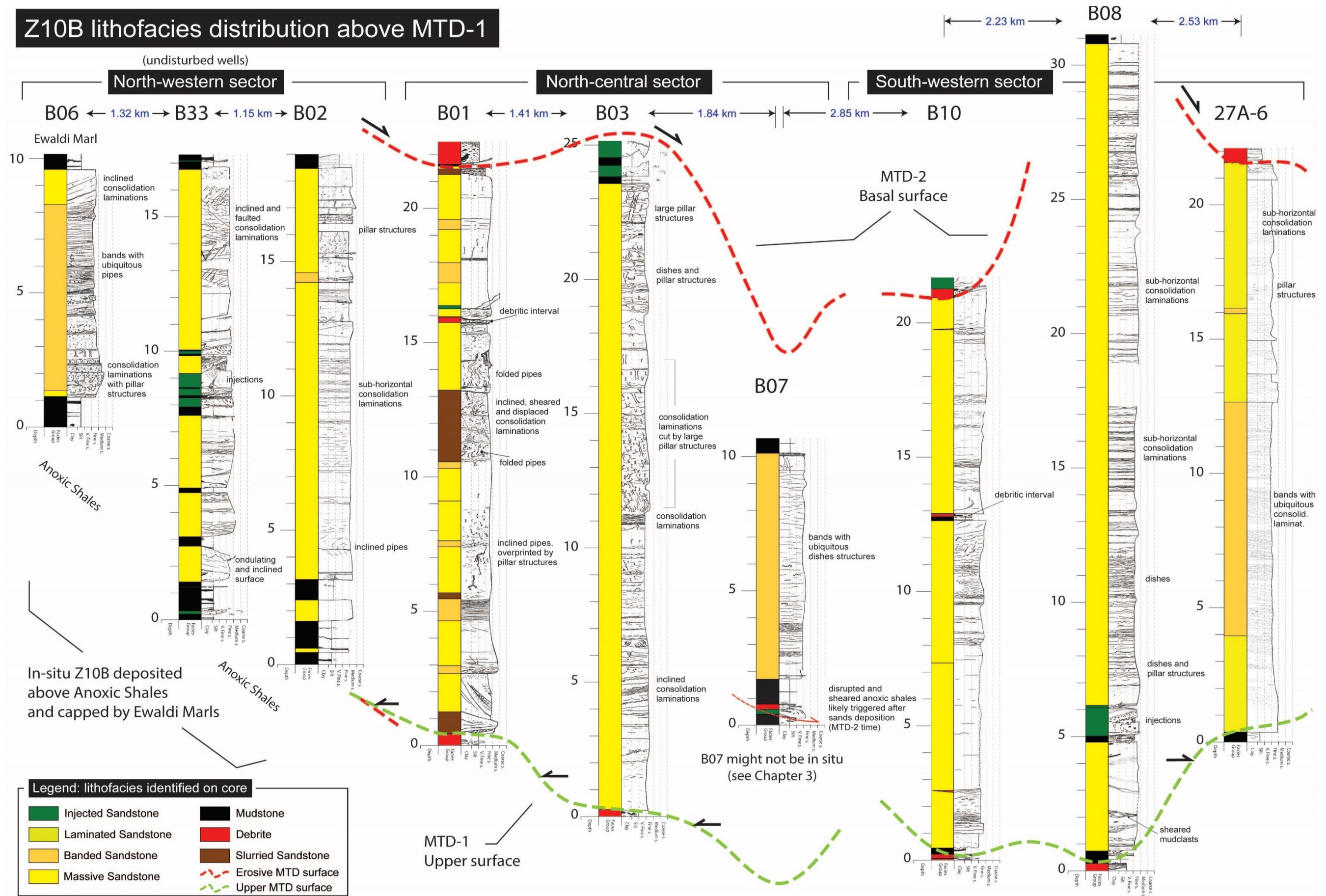


Fig. 6.11 – Graphic sedimentary logs summarising facies and bed organisation present within Zone 10B. This sandstone reservoir interval is bounded by Anoxic Shales at the bottom and by Ewaldi Marls on top. The latter mudstones are recognised on top of Z10B interval in wells located in the north-western area (B06, B33 and B02) only. Well B07 shows relatively short thickness in comparison with the wells from the same area (north-central sector) and was interpreted as remobilised by MTD-1 (see Chapter 3). The rest of the wells show erosion features at their top which are related to the emplacement of MTD-1.

6.4.3 Zone 40A (above MTD-2)

Within the Platform Area, the Zone 40A sandstone package represents the first sand-body of the three making up the Middle Reservoir Section. This interval sits in between the remobilised deposits of MTD-2 and MTD-3, which makes correlation of these sands problematic. The correlation of this unit between wells of the study area shown in Fig. 6.7 represents the current best estimate of the stratigraphic relationships within the field (see Chapter 4). The thickness of Z40A sand-body is variable, with sandstone packages ranging between 5 and 56 metres, likely due to multiple factors as the highly pronounced bathymetry shaped by MTD-2 (Fig. 6.12) and the subsequent erosion associated with the emplacement of MTD-3 suggested by the fact that the sandstones are in apparent continuous contact with the overlying remobilised deposits (Fig. 6.13). At the same time, some observations regarding the relationship between Z40A thickness and the underlying topography can be made: thicker sandstone packages are recorded where the seafloor shaped by MTD-2 was locally deeper. This is the case for the narrow SW-NE aligned trough where wells B05, B04 and B13z are located (Fig. 6.12). A high proportion of massive clean sands of Z40A (>70%) is observed within the wells located along the trough (B05, B04 and B13z) and those wells in its proximity (27A-6). In some of these wells a smaller percentage of muddier sands is also present with banded features developed in B04 (32%) and mixed slurried structures recognised in 27/A-6 (21%). Mudstone is present in the above wells and also in B05, ranging between ~10 and ~20% compacted thickness. A significantly smaller percentage is seen in B04 (1%) and it is totally absent in B13z. This latter well is composed of clean massive sands. A different situation is recorded in sandstones of B07, which are deposited in a relatively deep topographic low but show a limited thickness of sand (51% of clean massive sandstones) and a high percentage of muddier sands.

The Zone 40A sand interval identified in wells B01, B03, B08, 24 and B10 is made up of thinner deposits, likely due to the combined effect of higher seafloor topography and top-down erosion by MTD-3. In these wells, thickness is between ~15 and ~21 metres with an even thinner Z40A characterising B03 (5.34 m), B08 (8.9 m) and 24 (9.89 m). The relatively small thickness of Z40A in the latter wells is likely related to the presence of topographic relief shaped by remobilised deposits associated with MTD-2 as shown in the geological section at the bottom of Figure 6.12. Facies analysis of wells B03, B08 and 24 highlights a high proportion of massive sandstones, however the unpreserved tops suggest prudence in extrapolating information from these wells.

Among sandstones that are deposited above or on the side of topographic relief a decrease in the massive clean sand proportion (<50%) and an increase in concentration of muddier sands with slurried facies (between 20% and 60%) are observed in B01, B10, 24 (see geological sections on the bottom of Fig. 6.12). Debritic textures are also recognised within the Z40A in well 24.

Geological sections also show the inferred original palaeo-top of Z40A sandstone interval reconstructed using the restoration model developed for the study area (Chapter 5). Wells B33, B02 and B06, located in the northern sector are not shown on the maps because Z40A was not recognised on core, an absence ascribed to non-deposition of the sandstones or their erosion by MTD-3.

The vertical arrangement of facies shows a distinctive concentration of massive-clean sands within deep topographic lows (i.e. wells B04 and B13z in Fig. 6.13). Sandstone intervals deposited over higher topographic relief are characterised by the presence of thick mud-rich divisions, mainly mixed-slurried sands. Higher presence of mudstones is observed in wells where Z40A is interpreted to have been deposited above subtler irregular topography developed on the upper surface of a thick MTD that made up topography highs (i.e. wells B10, B07 and 27A-6). In these wells, up to 7 m thick event beds with thick capping mudstone (up to 4 m) are recognised. The characteristic facies stacking patterns and the relatively similar reconstructed deposition depths allow the inference that these deposits could be mapped across these locations.

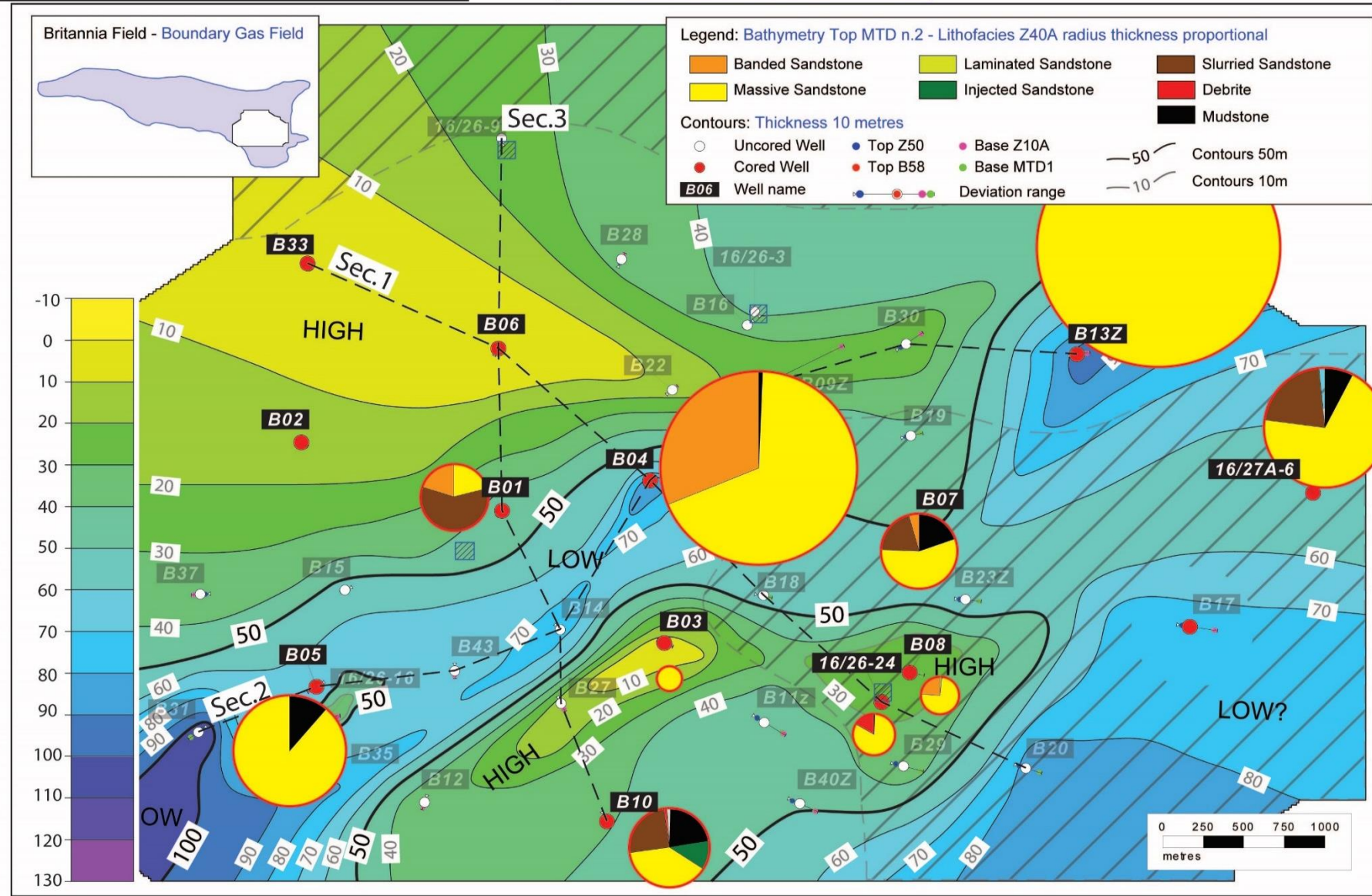
Although Z40A is characterised by a high degree of amalgamation, a single sandstone bed is recognised and traced across wells B03, B10, 24, B08 and B07, on the upper portion of this reservoir sandstone (Fig. 6.13). The bed is marked by a characteristic basal granule-rich layer, which is not largely common in sandstones making up Z40A, and by a debrite interval that represents the upper portion of the bed. This is a particular case where a single event bed can be defined as laterally traceable and so with a relatively uniform characteristic that is distinguishable from rock above (MTD-3) and below (amalgamated sandstones) (McKee and Weir, 1953), over a highly pronounced bathymetry.

Z40A sandstone distribution above MTD-2

- B33**
Thickness: 0 m
ERODED by MTD-3 (?)
- B02**
Thickness: 0 m
ERODED by MTD-3 (?)
- B01**
Thickness: 15.87 m
59% - Mixed Slurried S.
20% - Banded Sandstone
21% - Massive Sandstone
- B04**
Thickness: 45.66 m
1% - Mudstone
32% - Banded Sandstone
68% - Massive Sandstone
- B03**
Thickness: 5.34 m
100% - Massive Sandstone
- B05**
Thickness: 25.81 m
11% - Mudstone
89% - Massive Sandstone
- B10**
Thickness: 19.39 m
23% - Mudstone
2% - Debrite
24% - Mixed Slurried S.
12% - Injected Sandstone
1% - Laminated Sandstone
39% - Massive Sandstone

B06
Thickness: 0 m
ERODED by MTD-3 (?)

- B13Z**
Thickness: 56.41 m
100% - Massive Sandstone
- 16/27A-6**
Thickness: 28.38 m
8% - Mudstone
2% - Debrite
21% - Mixed Slurried S.
70% - Massive Sandstone
- B07**
Thickness: 17.29 m
20% - Mudstone
20% - Mixed Slurried S.
5% - Laminated Sandstone
4% - Banded Sandstone
51% - Massive Sandstone
- B17**
Thickness: 33.83 m
CORE not preserved
- B08**
Thickness: 8.90 m
2% - Laminated Sandstone
24% - Banded Sandstone
75% - Massive Sandstone
- 16/26-24**
Thickness: 9.89 m
1% - Mudstone
16% - Debrite
83% - Massive Sandstone



Geological sections

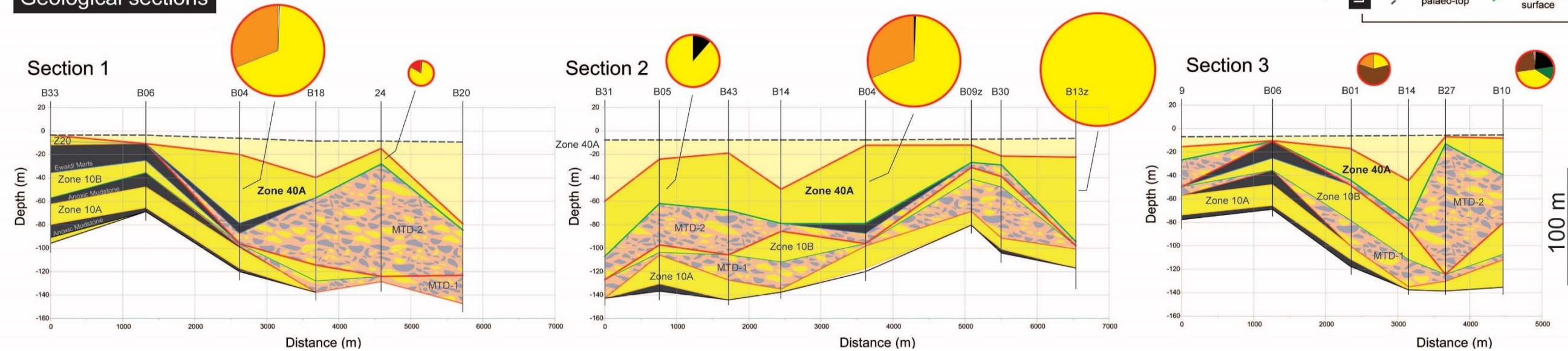


Fig. 6.12 – Palaeobathymetric map of the upper topography associated to MTD-2 (for decompacted deposits at MTD-2 time) with pie charts showing proportion of lithofacies identified within Zone 40A in cored wells (red dots). Map: contours in metres (blue = deep; yellow = shallow). Dashed area represents missing lower datum (reconstructed Z10A depths). Lithofacies: pie charts radii are proportional to the thickness of the reservoir interval. Red and black borderlines of the pie charts indicate eroded and preserved top intervals. Quantitative analysis of the sandstone lithofacies are displayed at the map sides. Geological sections at the bottom: 2D deposits distribution are shown using decompacted intervals.

Z40A lithofacies distribution above MTD-2

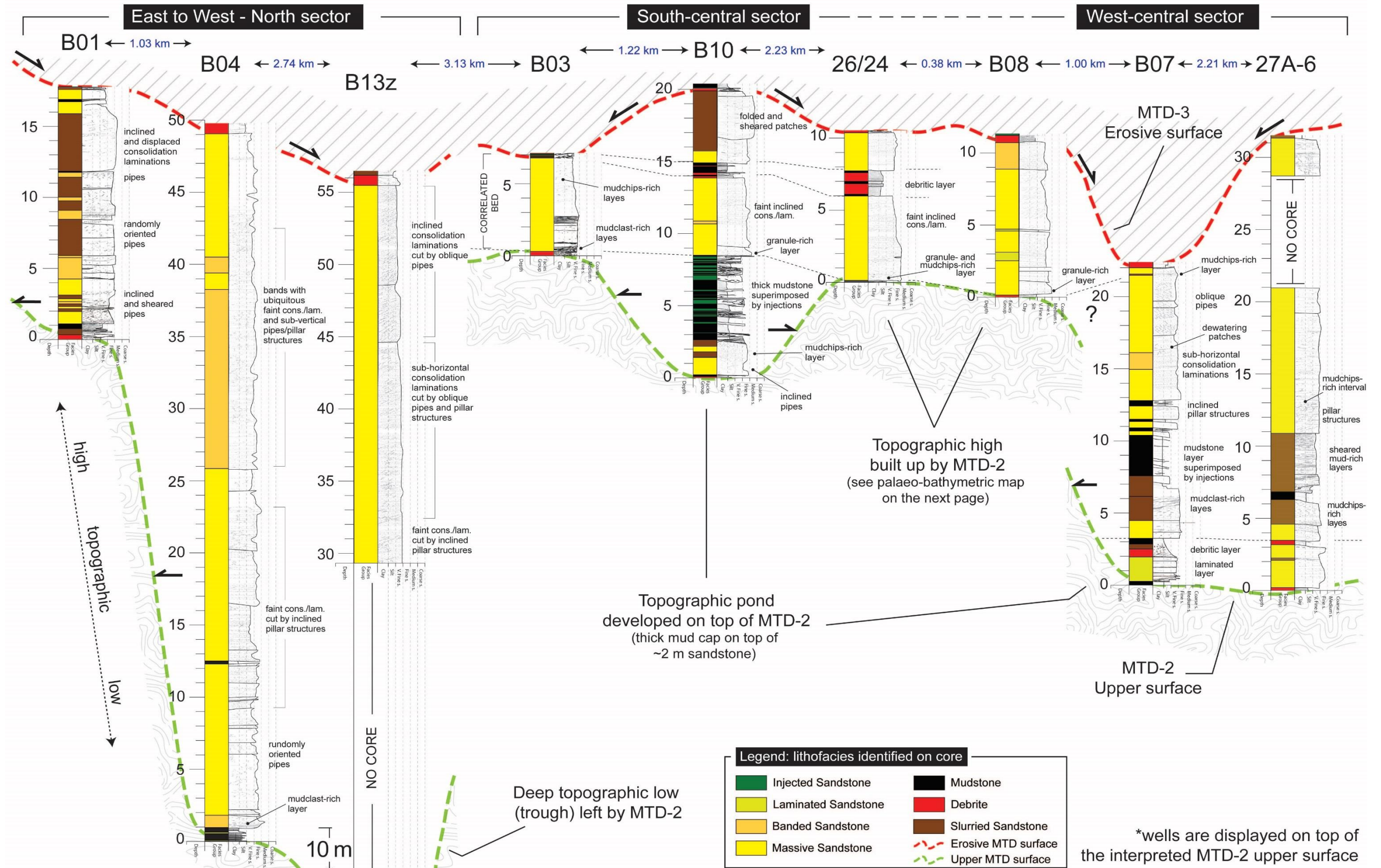


Fig. 6.13 – Graphic sedimentary logs summarising facies and bed organisation of Zone 40A. The reservoir interval is bounded at the bottom and on top by MTD-2 and MTD-3 respectively. The thickness variability of this interval represents a primary consequence of the sandstone emplacement above the pronounced topography associated with MTD-2 upper boundary. The north-western area is influenced by large evacuation with sandstones that are not preserved. Wells B01, B04 and B13z are located in the north sector following a west to east direction. The rest of the wells are displayed on a south to east direction. Wells are positioned vertically according to the MTD-2-related topography.

6.4.4 Zone 40B (above MTD-3)

Remobilised deposits of MTD-3 and MTD-4 define the base and top of the Z40B and allow correlation of this sandy reservoir unit within the Middle Reservoir. The overall thickness is generally less variable than the underlying and overlying Z40A and Z40C sand-units, with sandstone packages ranging between ~5 and ~12 metres in thickness among the cored wells in the study area. The palaeobathymetric map of the Platform Area restored at the time of the emplacement of MTD-3 is characterised by two main areas with lows up to ~40 metres deep (Fig. 6.14). In contrast to what observed for Z40A, the thickness of Z40B does not seem to be related to the underlying topography, possibly because the erosion associated with the MTD-4 above might have been important (see Chapter 5). In fact, comparing the thickness of this unit in the cored wells with the reconstructed palaeobathymetry highlights that the accommodation space after the deposition of Z40B sands on top of MTD-3 was unfilled.

The red dashed line in Figure 6.15 highlights extensive erosion on top of this sand interval, reducing the overall thickness of the identified Z40B. The maximum erosion is seen in B33, where Z40B is not recognised. A different trend is observed in wells B02 and B06 where sandstones have their tops preserved, capped by greyish hemipelagic mudstone. Sandstone packages identified in these wells are respectively 12.53 m and 8.09 m thick. Cross sections also show the reconstructed eroded portion of sands, likely remobilised by MTD-4 and mainly active in the southern sector of the Platform Area (Fig. 6.14).

Facies analysis undertaken in this sandstone interval shows a full range of massive-clean, banded and slurried sands but no debritic intervals. Massive-clean sands represent 45% of the total facies encountered in Z40B cores, whereas banded sands represent 32%. The other 33% is composed of slurried (18%) and laminated sands (1%), and mudstones (4%).

Massive-clean sands are encountered in all wells with the exception of B04 (which is thought to be largely eroded by the overlying MTD-4; see Section 2 on Fig. 6.14 and Fig. 6.15). High proportions of clean-massive sands are present in wells B02, B06, B07, B08 and B13z where they are >60% in each cored-well. In other wells (e.g., B05, B01, B04, 24 and 27A-6), lower proportions of clean-massive sands are compensated by an increase in banded facies ranging between 69% and 53%. An increase in mud content is also observed along Section 2 on Fig. 6.14 and in the southern study area, with slurried sand proportions between 12% (B10) and 36% (B03, B07).

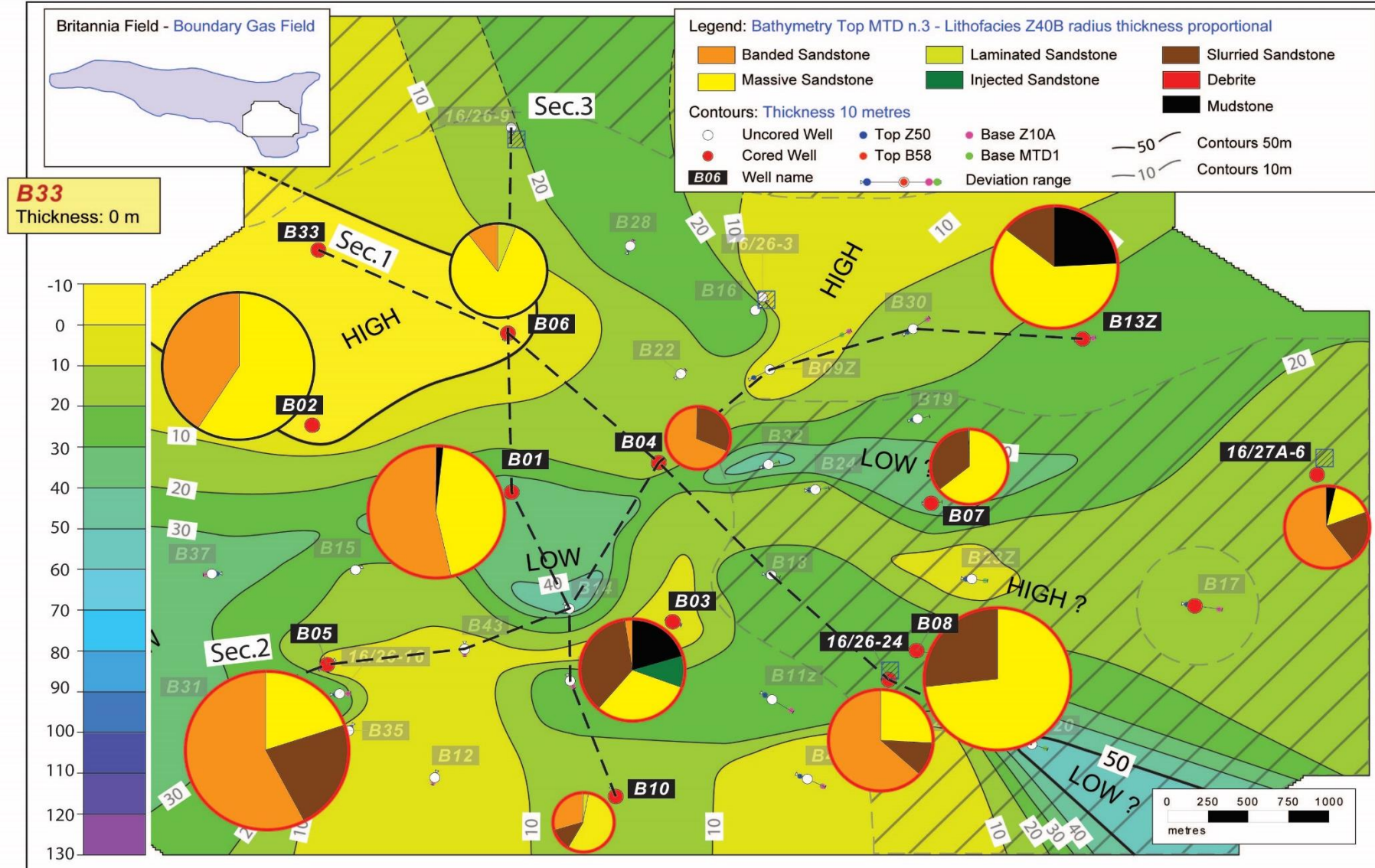
Intra-Z40B mudstone intervals comprise a small proportion of just a few wells within the study area; in the eastern sector B13z and 27A-6 record respectively 4% and 24% of mud, whereas in the central area, mudstone intervals are present in B03 (20%) and in B01 (1%).

The vertical arrangement of lithofacies does not show a repetitive stacking pattern, making flow process reconstruction difficult. However, whilst banded sands are recognised in all cored wells of the study area, and sometimes interleaved with clean-massive sandstones, mud-rich mixed-slurried sands are generally concentrated in the higher part of the Z10B stratigraphy. They are absent in the wells located in the norther sector.

No clear grain size trends can be observed, with the exception of wells B13z and B03 where a relatively thick interval of mudstone interrupts the usual uniform sandy grain size. Graphic sedimentary logs (Fig. 6.15) highlight the ungraded and amalgamated style typical of the sandstones that characterise the basal reservoir zones Z10A and Z10B.

Z40B sandstone distribution above MTD-3

- B06**
Thickness: 8.09 m
6% - Laminated Sandstone
10% - Banded Sandstone
84% - Massive Sandstone
- B02**
Thickness: 12.53 m
41% - Banded Sandstone
59% - Massive Sandstone
- B01**
Thickness: 11.29 m
2% - Mudstone
53% - Banded Sandstone
45% - Massive Sandstone
- B03**
Thickness: 8.79 m
20% - Mudstone
36% - Mixed Slurried S.
10% - Injected Sandstone
3% - Banded Sandstone
31% - Massive Sandstone
- B05**
Thickness: 13.55 m
22% - Mixed Slurried S.
58% - Banded Sandstone
20% - Massive Sandstone
- B10**
Thickness: 4.61 m
12% - Mixed Slurried S.
3% - Laminated Sandstone
29% - Banded Sandstone
56% - Massive Sandstone



- B04**
Thickness: 5.03 m
31% - Mixed Slurried S.
69% - Banded Sandstone
- B13Z**
Thickness: 10.35 m
24% - Mudstone
15% - Mixed Slurried S.
61% - Massive Sandstone
- B07**
Thickness: 6.49 m
36% - Mixed Slurried S.
64% - Massive Sandstone
- 16/27A-6**
Thickness: 7.02 m
5% - Mudstone
20% - Mixed Slurried S.
61% - Banded Sandstone
16% - Massive Sandstone
- B17**
Thickness: 7.03 m
CORE not preserved
- B08**
Thickness: 12.15 m
27% - Mixed Slurried S.
73% - Massive Sandstone
- 16/26-24**
Thickness: 8.76 m
11% - Mixed Slurried S.
63% - Banded Sandstone
26% - Massive Sandstone

Geological sections

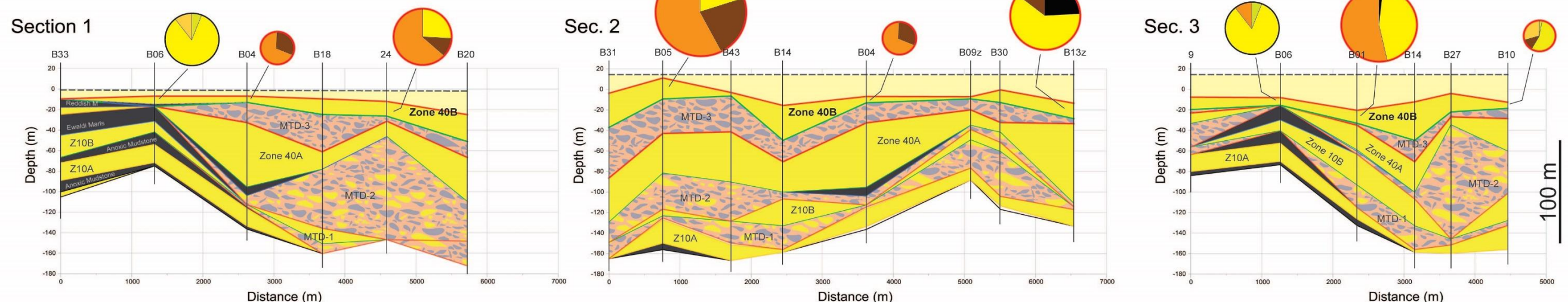


Fig. 6.14 – Palaeobathymetric map of the upper topography associated to MTD-3 (for decompacted deposits at MTD-3 time) with pie charts showing proportion of lithofacies identified within Zone 40B in cored wells (red dots). Map: contours in metres (blue = deep; yellow = shallow). Dashed area represents missing lower datum (reconstructed Z10A depths). Lithofacies: pie charts radii are proportional to the thickness of the reservoir interval. Red and black borderlines of the pie charts indicate eroded and preserved top intervals. Quantitative analysis of the sandstone lithofacies are displayed at the map sides. Geological sections at the bottom: 2D deposits distribution are shown using decompacted intervals.

Z40B lithofacies distribution above MTD-3

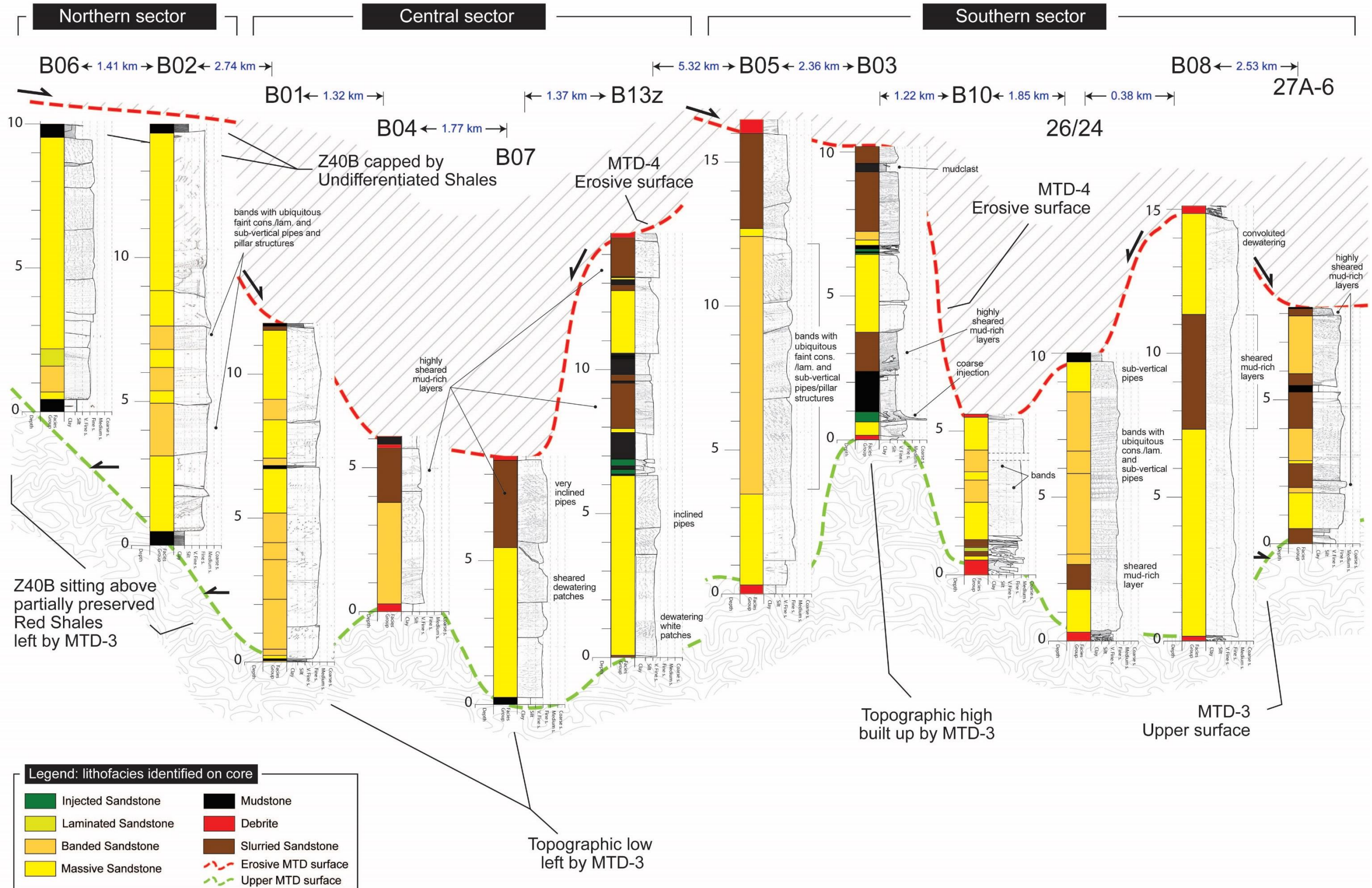


Fig. 6.15 – Graphic sedimentary logs summarising facies and bed organisation of Zone 40B. The reservoir interval is bounded at the bottom and on top by MTD-2 underneath and MTD-3 erosive surface on top. Wells are vertically displayed in relationship to MTD-3-related topography and grouped according to their locations.

6.4.5 Zone 40C (above MTD-4)

Zone 40C represents the upper portion of the Middle Reservoir Section and the top of the study interval. This zone is characterised by a relatively robust well correlation in the Platform Area, facilitated by the widespread presence of MTD-4 at the bottom, recognised by the sharp upward lithological transition from debritic deposits of the MTD, to sandstones of Z40C.

In this zone individual sandstone event beds can be identified and traced across the Platform Area with relatively high confidence, in a similar manner to the recognition of beds in the Upper Reservoir Section (Zones 45 and 50) undertaken by Lowe and Guy (2000) and subsequently revised by Barker et al. (2008). Six sheet sandstone beds stratigraphically numbered 48, 50, 52, 54, 56 and 58 are interpreted in each well of the study area (Fig. 6.17). The upper Bed 58 provides a robust marker horizon for the younger beds of the Upper Reservoir Section, above, and for the older stratigraphy below (Middle and Lower Reservoir Section) (Lowe et al., 2003; Barker et al., 2008; Eggenhuisen et al., 2010), where together with Z10A, it was also used for the restoration analysis undertaken in the Platform Area (see Chapter 5 and Appendix C). Bed 58, which sits beneath the Boxcar Sandstone Division (Barker et al., 2008), was previously interpreted as the result of two depositional events, apparently on the basis of lithology, where the mud-rich division was distinguished from the underlying sand-rich division and respectively termed Bed 60 and Bed 58 (Guy and Lowe, 2000). However, Barker et al. (2008) and also this study interpreted the two divisions to represent a single depositional event.

Intra-bed mudstone horizons are widespread, although instances of sandstone bed amalgamation are also identified. Vertical grain size profiles are also used to support correlations, consisting of base-to-top normally graded trends within individual sandstone event beds. However, sometimes thickness variations and amalgamation increase uncertainty in bed-to-bed correlation. Detailed graphic sedimentary logs and bed organisation are shown in Fig. 6.17.

The six event beds identified in each well were vertically grouped in order to study the spatial lithofacies distribution within the Platform Area (Fig. 6.16). The cumulative thickness of mudstone intervals between sandstone beds increases as a percentage of the entire interval in the north-eastern area. This may be interpreted as being caused by deposition of thinner sandstone intervals that pinch out against positive relief created by the top of the MTD-4.

Banded sandstones are common within Z40C; the highest proportion of banded facies (up to 60% of cumulative thickness in individual wells) is seen at the northern

part of the Platform Area. Analysis of the cumulative spatial distribution of lithofacies making up Z40C shows that massive-clean sand intervals are more abundant (up to 75% of the thickness) where more accommodation space was left by the MTD-4 suggesting a possible confinement effect on sand deposition.

A series of SW-NE oriented well-correlation panels is shown in Fig. 6.18 in a 3D fence diagram, in order to better constrain the lithofacies distribution in the study area. The section located in the northern Platform Area, against the slope of the Fladen Ground Spur shows a high lithofacies heterogeneity within the upper Z40C with beds 50-52 compensating each other over a large change in thickness toward the north-eastern area, until Bed 58 healed the remain accommodation space in the Platform Area.

In the central sector, Beds 50 and 52 still vary in thickness, whereas thickness becomes more uniform toward east. In the most south-easterly section, lithofacies are more uniformly distributed, although an evident pattern is not recognised. Bed thickness is still heterogeneous at the base of the Z40C (Beds 48 and 50).

Pie charts of the cumulative lithofacies expressed as percentage of the entire interval in each well enable the identification of three main areas: i) the southern area, where massive-clean sands intervals are more abundant and larger accommodation space was built by the MTD-4; ii) the northern border of the study area, where banded sandstones may represent up to 60% of cumulative bed thickness in individual wells; iii) the north-eastern area, where the cumulative thickness of mudstone intervals between sandstone beds increases as a percentage of the entire interval.

The vertical arrangement of facies within each event bed shows a tri-partite stacking pattern consisting of i) basal sand-rich division, typically composed of massive-clean and laminated sands, that grades upward into ii) mud-rich division characterised by banded and mixed slurried sands, and iii) laminated silt-rich mudstones representing the capping division. Debrite intervals forming part of co-genetic event beds (linked-debrite *sensu* Haughton et al., 2003) are also recognised in core and distinguished from debrite related to the remobilised material (MTD) by their relatively subdued thicknesses sandwiched by mixed-slurried and capping mudstones within the upper finer grained portion of an event beds. These are mainly observed within wells located in the southern sector (e.g., bed 56 in well B17; Fig. 6.17).

Z40C sandstone distribution above MTD-4

- B01**
Thickness: 17.03 m
15% - Mudstone
16% - Mixed Slurried S.
46% - Banded Sandstone
23% - Massive Sandstone
- B04**
Thickness: 19.96 m
11% - Mudstone
1% - Debrite
26% - Mixed Slurried S.
4% - Laminated Sandstone
29% - Banded Sandstone
29% - Massive Sandstone
- B03**
Thickness: 20.70 m
7% - Mudstone
9% - Mixed Slurried S.
1% - Laminated Sandstone
12% - Banded Sandstone
71% - Massive Sandstone
- B05**
Thickness: 12.24 m
5% - Mudstone
15% - Mixed Slurried S.
3% - Injected Sandstone
31% - Banded Sandstone
46% - Massive Sandstone
- B10**
Thickness: 28.45 m
3% - Mudstone
4% - Debrite
21% - Mixed Slurried S.
1% - Laminated Sandstone
10% - Banded Sandstone
61% - Massive Sandstone

B33
Thickness: 0 m

B02
Thickness: 8.21m
26% - Mudstone
23% - Injected S. 52% Massive S.

B06
Thickness: 9.22m
17% - Mudstone 38% - Mixed Slur.
2% - Injected S. 43% - Massive S.

B13Z
Thickness: 16.97 m
19% - Mudstone
19% - Mixed Slurried S.
3% - Laminated Sandstone
30% - Banded Sandstone
29% - Massive Sandstone

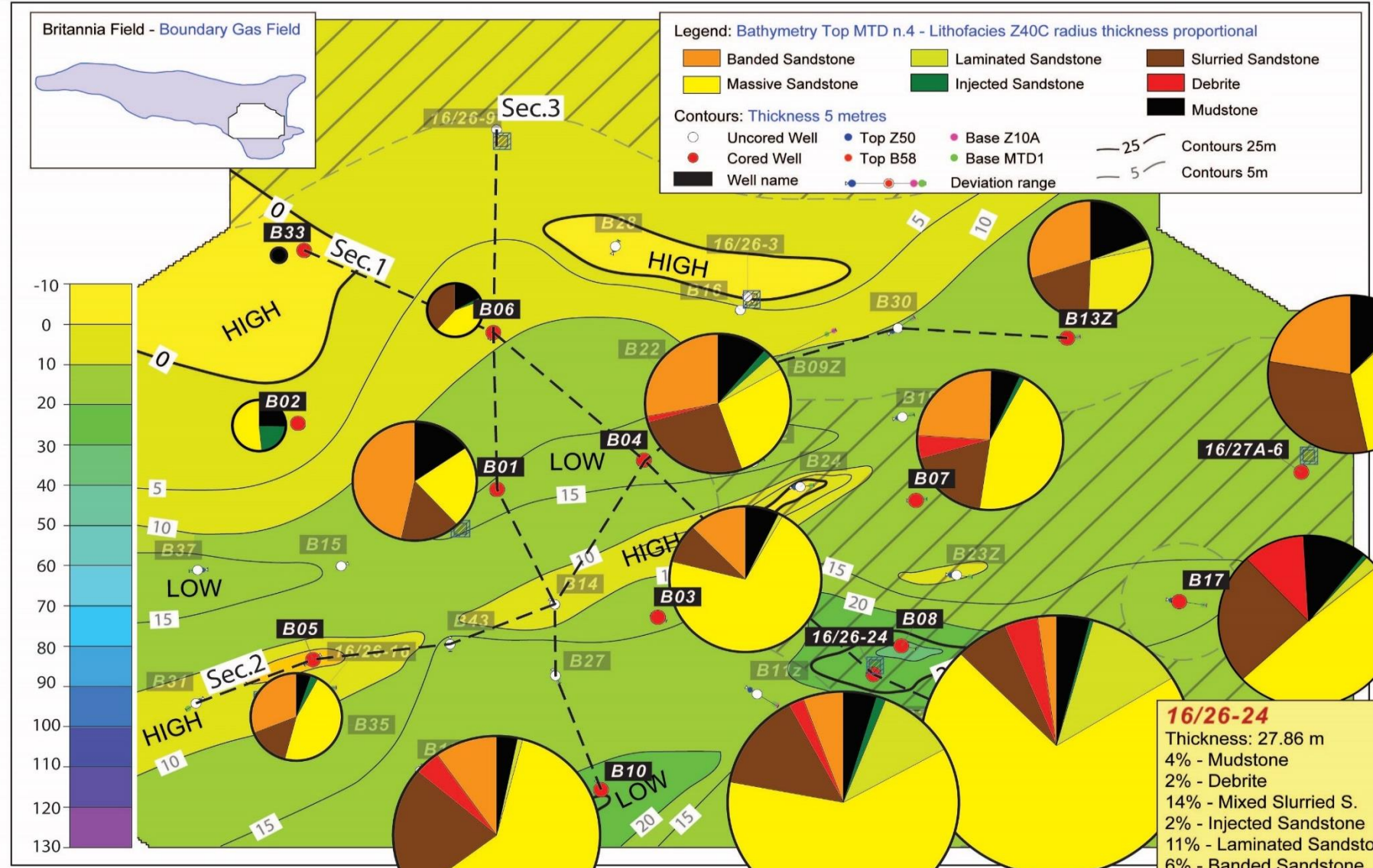
B07
Thickness: 18.38 m
7% - Mudstone
5% - Debrite
18% - Mixed Slurried S.
1% - Injected Sandstone
24% - Banded Sandstone
45% - Massive Sandstone

16/27A-6
Thickness: 20.52 m
12% - Mudstone
31% - Mixed Slurried S.
1% - Laminated Sandstone
22% - Banded Sandstone
34% - Massive Sandstone

B17
Thickness: 22.11 m
11% - Mudstone
11% - Debrite
25% - Mixed Slurried S.
1% - Injected Sandstone
3% - Laminated Sandstone
49% - Massive Sandstone

16/26-24
Thickness: 27.86 m
4% - Mudstone
2% - Debrite
14% - Mixed Slurried S.
2% - Injected Sandstone
11% - Laminated Sandstone
6% - Banded Sandstone
61% - Massive Sandstone

B08
Thickness: 32.89 m
4% - Mudstone
4% - Debrite
6% - Mixed Slurried S.
1% - Injected Sandstone
12% - Laminated Sandstone
2% - Banded Sandstone
71% - Massive Sandstone



Geological sections

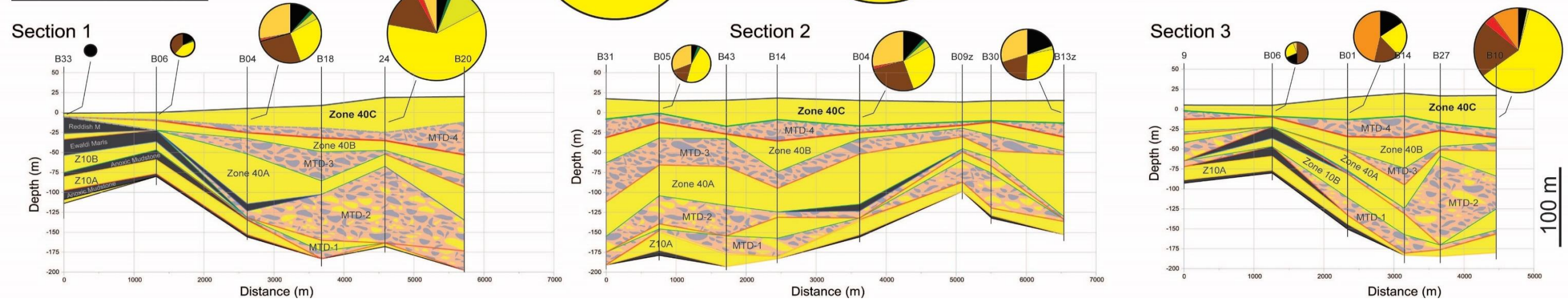


Fig. 6.16 – Palaeobathymetric map of the upper topography associated to MTD-4 (for decompacted deposits at MTD-4 time) with pie charts showing proportion of lithofacies identified within Zone 40C in cored wells (red dots). Map: contours in metres (blue = deep; yellow = shallow). Dashed area represents missing lower datum (reconstructed Z10A depths). Lithofacies: pie charts radii are proportional to the thickness of the reservoir interval. Red and black borderlines of the pie charts indicate eroded and preserved top intervals. Quantitative analysis of the sandstone lithofacies are displayed at the map sides. Geological sections at the bottom: 2D deposits distribution are shown using decompacted intervals.

Z40C lithofacies distribution above MTD-4

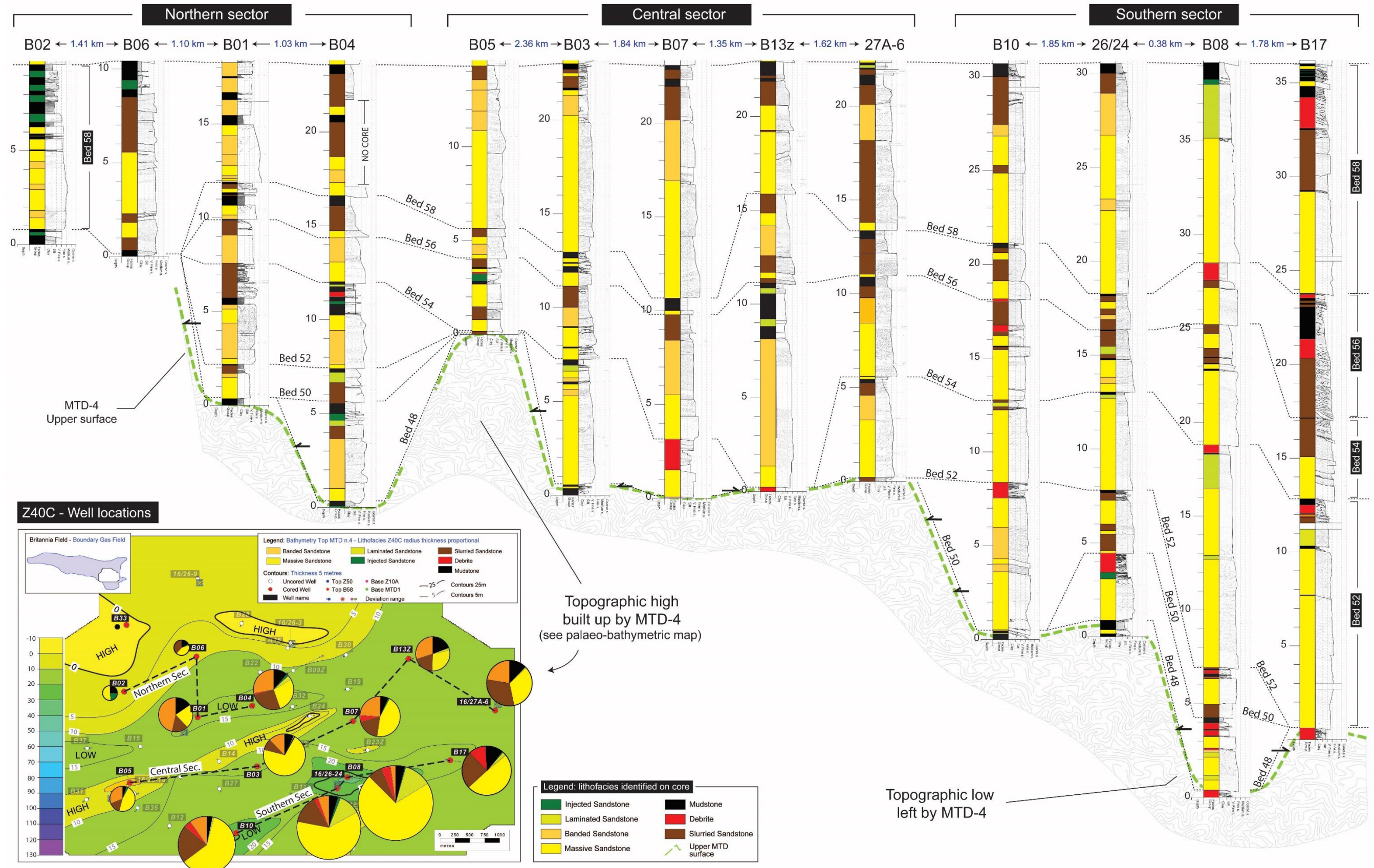


Fig. 6.17 – Graphic sedimentary logs of cored wells summarising facies and bed organisation of Zone 40C. Six event beds (Bed 48-50-52-54-56-58) are recognised that can be traced across most of the Platform study area (35 km²).

Z40C Bed-by-bed spatial and vertical lithofacies distributon above MTD-4

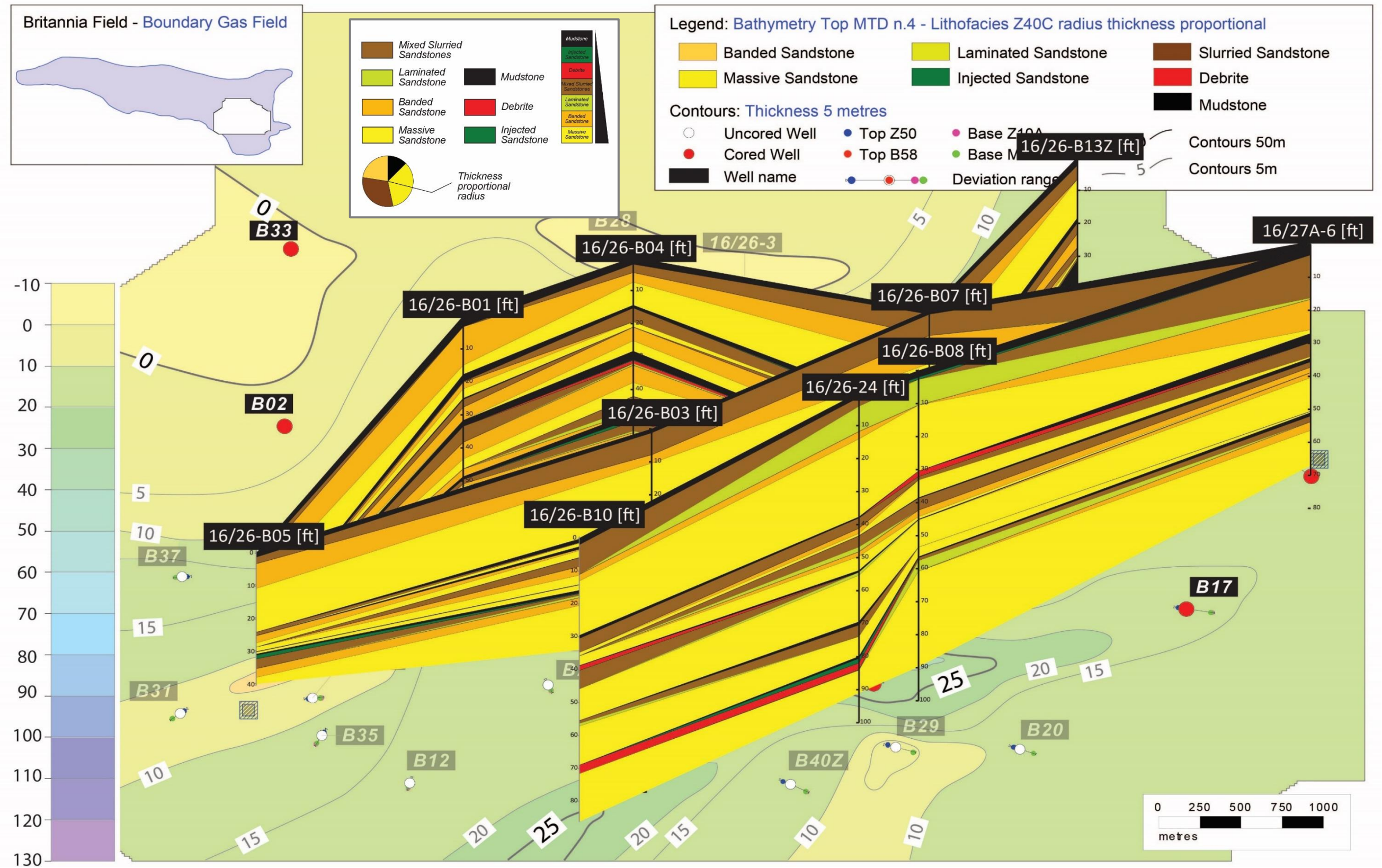


Fig. 6.18 – Contour map showing the MTD-4-related topography and fence diagram of Zone 40C with related sandstone lithofacies distributions on top of the MTD. The six event beds (Bed 48-50-52-54-56-58) recognised in core can be traced across most of the Platform study area (35 km²). Lithofacies can occur at multiple vertical positions in a single event bed, but often they follow an ordered stacking pattern as represented in the legend. The northernmost section located against the slope of the Fladen Ground Spur shows a high thickness and facies variability, with lower beds compensating each other, changing in thickness toward the north-eastern area. Toward the south-eastern Platform Area facies are less variable, with higher proportion of massive-clean sandstones; however, bed thickness is still variable in the lower portion of the interval (Beds 48 and 50).

6.5 Effects of MTD deposition upon subsequent sandstone emplacement

Mass-transport deposits were episodically emplaced throughout deposition of the BSF, (see Chapter 3), shaping the seafloor, with different resultant scales of rugosity developed over their upper surfaces, and in association with MTD-related erosion (see Chapter 5). A resulting question is the degree to which such rugosity might have influenced localised facies and internal sandstone character within reservoir zones as described in the previous section. A particular focus is to assess the processes responsible for the development and distribution of banded and mixed slurried sandstones within the Platform Area of the Britannia Field, which form unusually thick intervals compared to other documented subsurface case studies (Lowe and Guy, 2000; Lowe et al., 2003; Barker et al., 2008; Haughton et al., 2009). A related question is whether the impact of MTDs on the basin floor can fully explain the broadest, basin-wide trends in facies distribution within the Lower and Middle Britannia Reservoir Section.

To explain the lateral and vertical distribution of facies between wells an analysis is undertaken that exploits the new well correlation scheme (Chapter 4), the reconstruction of palaeobathymetric evolution associated with the emplacement of MTDs through time (Chapter 5) and the refined palaeo-flow analysis and better understanding of sandstone architecture within each reservoir interval (this chapter). This analysis is intended to cover the scale range from single depositional events to the entire BSF. Comparing and combining the all available scales of observations could also help differentiating allogenic factors (i.e. tectonics, hinterland geology, climate and sea-level) from autogenic processes inherent to the sedimentary system (Gardner et al., 2008). The focus is primarily upon reservoir zones Z10A, Z10B, Z40A and Z40B, analysed as sand packages in which general facies trends are observed, whereas Z40C facilitates a relatively more detailed facies analysis on a bed-by-bed scale.

6.5.1 Lower and Middle Britannia Sandstone architecture

The lateral and vertical lithofacies distribution of the Lower and Middle Britannia Section described above permits a reconstruction of the reservoir architecture and its evolution through time (Fig. 6.19). In ascending order:

Zone 10A – This interval is dominated by clean massive sands with only occasional development of the banded facies. These sands show either amalgamation or a non-erosive character and they are typically fine grained, conspicuously lacking a coarse

component. They are interpreted as the first major input of sands into the study area and their deposition is not influenced by an MTD-topography, as their emplacement precedes the first observed large failure (MTD-1).

Zone 10B – This interval is mainly composed of ungraded, massive, dewatered and banded sandstones with a minor component of mixed-slurried sands. Grain size trends, core character and the absence of mud caps highlight the amalgamated character of these sandstones, corresponding with the second important influx of sand into the basin. This zone may represent deposition of lobes developed within localised depressions created by differential subsidence and/or by MTD-1 evacuation.

Zone 40A – This zone forms the main sand package within the Middle Reservoir and shows the most pronounced thickness variation within the study area together with the highest heterogeneity in lithofacies distribution. Clean sands in the lower part of the interval pass vertically to banded and slurried sandstones. Overall, there is a subtle fining upwards trend. Significant thickness variations across the whole Platform Area suggest bathymetric confinement.

Zone 40B – This interval is characterised by a lower part dominated by clean massive sandstones that pass upwards into banded sandstones and in turn pass into mixed slurried and debritic deposits (hybrid-like beds) towards the top. Thickness variations together with the heterogeneous sedimentological character of this interval observed across the whole Platform Area suggest that these sands were deposited under the influence of a bathymetric control. It is also inferred that the shearing features characterising the mixed slurried deposits might have been caused by the stress associated with the emplacement of MTD-3 (e.g., overpressure, loading, liquefactions).

Zone 40C – This reservoir zone is composed of six stacked sandstone event beds, with the top one being correlation datum for the Lower and Middle Reservoir (Bed 58). Individual event beds show strong normal grading and grade normally into mudstones. They may develop medium grain size at their base with granule-rich layers that can be used to support some bed correlation. Hybrid bed types dominate the entire Z40C. Event beds towards the top of the investigated interval can be correlated over several kilometres representing extensive sheet-like deposits, whereas lower events show a mutual thickness compensation as a result of stronger influence of the MTD-4-related topography. Facies arrangement in each event bed show the typical HEB character (Fonnesu et al., 2016), but marked by a distinctively thick banded division (Barker et al., 2008; Haughton et al., 2009). The abundance of

the banded facies might be related to the position in the lateral or distal margins of a fan succession (Barker et al., 2008; Haughton et al., 2009).

A similar evolution trend is also observed in the Upper Reservoir Section, where the depositional character of the Upper Britannia Sandstone Member was earlier studied by Lowe and Guy (2000) and subsequently refined by Barker et al. (2008), with the latter providing a temporal reconstruction of the depositional evolution. In these stratigraphic models, amalgamated clean-massive sands (Z45), interpreted as the result of bed excision and duplication by downslope remobilisation processes, are followed by deposition of the Z45 clay interval (debrite deposition) and succeeded by widespread hemipelagic shale deposition, which represented a break in sandstone deposition. The inherited topography developed on the seafloor after the emplacement of the MTD induced significant lateral thickness and facies variation in the above Bed 78, which largely healed the antecedent bathymetry restoring palaeo-horizontal conditions for the more hybrid-prone sandstone beds 82, 84 and 86 (Barker et al., 2008).

Analysing the overall reservoir architecture development three possible sets of controls can be proposed:

- 1) Largest scale. Evolution of the depositional system through time, with axial-lobe clean-massive sandstone deposition within basal Z10A and Z10B and fringe mud-rich prone sedimentation upward in the stratigraphy (Z40A, Z40B and Z40C), invoking allogenic factors (i.e. climate and sea-level change) that might have controlled the evolution of the depositional system and related facies distribution through time, via system backstepping.
- 2) Intermediate scale. Active tectonic faulting outside of the study area during Britannia time may have played a role both in initiating remobilisation of sediment into deeper water, and in dictating flow pathways (through conduits, relay ramps or fault segments obstructing topography). This control would have affected sandstone deposition across the entire Britannia Sandstone Fm. with direct influence on the depositional evolution within the Platform Area.
- 3) Smaller scale. Tectonic deformation within the study area might have triggered large-scale remobilisation events which in turn were responsible for shaping the seafloor and building up rugose topography. The largest failures took place during breaks in sandstone deposition and after the emplacement of thick volumes of hemipelagic shales (MTD-1 and MTD-2), as shown in Chapter 3. Different scales of rugosity developed on the seafloor would have dictated the non-uniformity of

subsequent gravity flows (i.e., turbidity currents and hybrid flows). Haughton et al. (2003, 2009) describe how specific basin conditions may lead to a dominance of hybrid beds over conventional turbidites by facilitating flow partitioning and development of cohesive behaviour in sedimentary currents.

A combination of these models may account for the apparent reservoir character transition between the Lower and Middle Reservoir Section; further work is required to try and better distinguish the interplay between these mechanisms to account for the full heterogeneity of the Britannia depositional system.

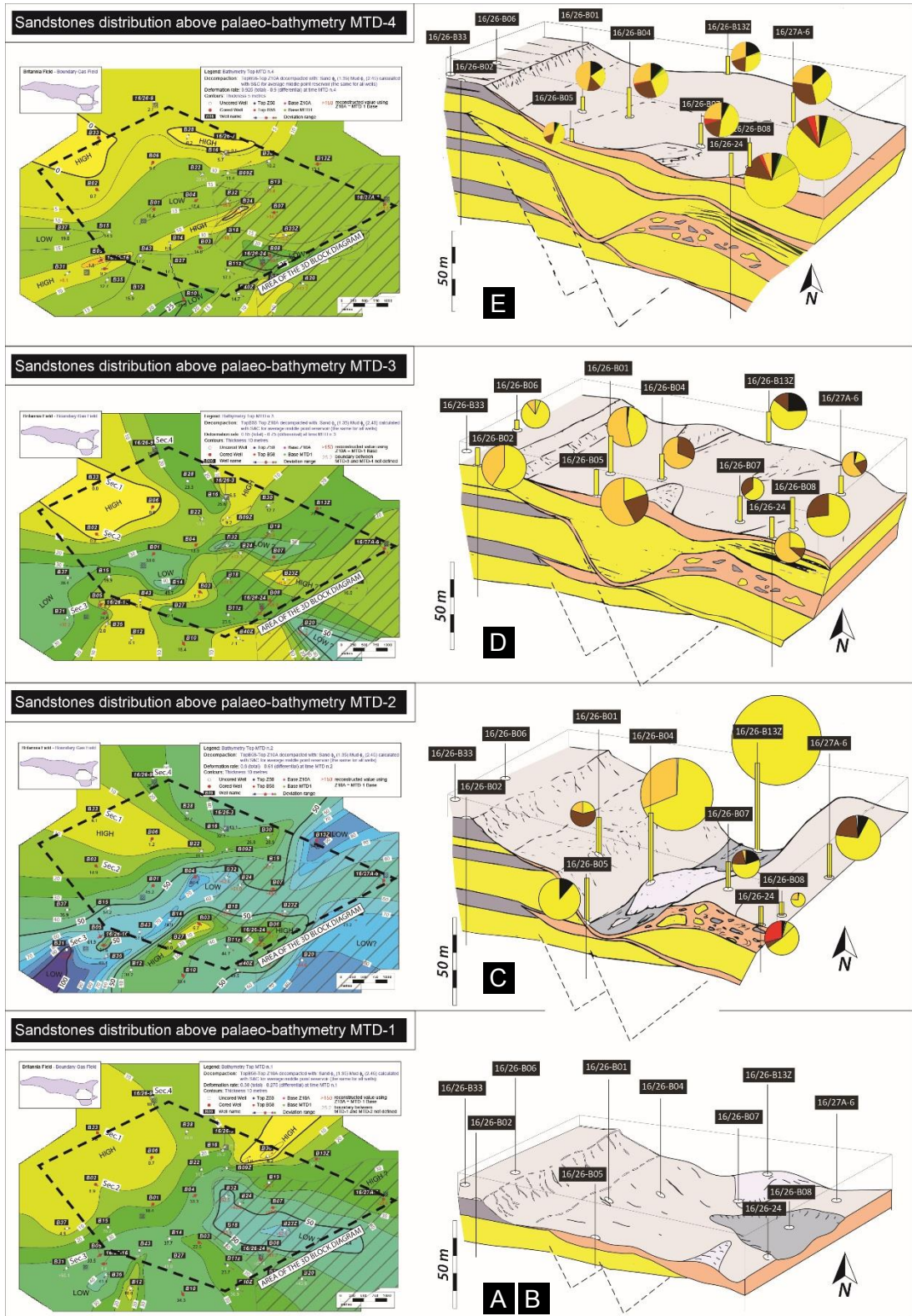


Fig. 6.19 – Reconstruction of the depositional history of the Lower and Middle Britannia Reservoir in the Platform Area. From the bottom, A-B) Z10B is deposited upon a relatively shallow palaeo-slope thinning toward the northern basin margin due to tectonism (direct faulting) and small-scale rugosity (<40 m) associated to a remobilisation event (MTD-1) which overlies Z10A. C) Z40A is deposited over a highly pronounced topography (>80 m) developed on the palaeo-seafloor after the joint effect of faulting and collapsing movement associated with MTD-2. D) Z40B is characterised by heterogeneous sand deposition with increased portions of mixed-slurried facies onto a palaeo-seafloor with significant

bathymetric variation (~30 m) formed through continuing tectonism and a large-scale remobilisation (MTD-3). E) Z40C is characterised by hybrid-prone deposition over a relatively small-scale rugosity (<15 m) related to the emplacement of MTD-4. Note that intervals representing the deposition of reservoir zones Z10A and Z20 are not included in this reconstruction as separate time steps, but these sandy deposits are sketched in the block diagrams. Lower Reservoir sands (Z10A, Z10B and Z20) are sandwiched by thick intervals of hemipelagic shales which marked abrupt and long breaks in sandstone deposition. In contrast, sandstone deposits of Z40A, Z40B and Z40C (Middle Reservoir) are interrupted by the occurrence of large-scale remobilisation events (MTD-3, MTD-4).

6.5.2 Interpretation of flow character based on vertical facies evolution within beds

The new core description undertaken as part of this study can be integrated with earlier core investigations (Eggenhuisen, 2009; Eggenhuisen et al., 2010) and flow interpretations (Lowe and Guy, 2000; Barker, 2005; Barker et al., 2008) to build a model of the depositional processes that played a role in the Britannia depositional system across the Platform Area.

Common facies stacking patterns were determined for the Upper Reservoir Section by Lowe and Guy (2000) using Markov chain statistical analysis in order to identify five common slurry bed types representing different depositional processes and flow evolution (Lowe et al., 2003). Unfortunately, applying bed type analysis to the Lower Reservoir intervals is difficult due to widespread amalgamation which makes the identification and correlation of individual beds problematic.

A broad tri-partite division consisting of sand-rich facies, mud-rich facies and mudstone facies was recognised by Barker et al., (2005, 2008) aimed at simplifying the Lowe and Guy (2003) model for the same reservoir units. This simpler model of facies and of their vertical stacking pattern can be broadly applied to the Lower and Middle Reservoir Sections which were the object of this study. Distinctions between these divisions can be essentially made on the basis of the mud content of each facies which varies from as little as 2% by volume of some dewatered sandstones (part of the sand-rich group of facies) to 10-35% of mixed slurried sands (part of the mud-rich group of facies) as reported by Lowe and Guy (2000); Table 6.3.

	Sand-rich facies		Mud-rich facies		
Facies	Massive-Clean	Laminated	Banded	Mixed Slurried	Debrite
Mud content (mean)	<2%	>2%	~20%	<35%	>40%

Table 6.3 – Mud content within facies division (data from Lowe and Guy, 2000).

The sand-rich facies group (Fig. 6.20) comprises massive clean sands and parallel laminated sands (interpreted as deposited by classical turbidity currents), whereas banded, mixed slurried and debrite facies comprise the mud-rich facies group (interpreted as deposited by a range of transitional flows, see Fig. 6.20). Finally, the mudstone facies is thought to represent deposition by the muddy tails of gravity flows and hemipelagic suspension. When observed in vertical association, the three facies groups are here interpreted as the result of longitudinal variations in rheology, due to the transition from high-concentration turbulent flow to laminar behaviour (decreasing

Reynold number) as function of runout distance (e.g., Haughton et al. 2009, Kane and Pontén, 2012).

Poorly-sorted and extensively dewatered massive-clean and laminated facies composing the sand-rich division are interpreted as the result of high sediment fallout from high concentration flow (Lowe, 1982; Guy, 1992; Mutti, 1992; Kneller and Branney, 1995; Jones et al., 1999; Lowe and Guy, 2000; Barker et al., 2008).

The mud-rich sandstone facies group comprises clay-rich facies in sand-prone event beds (such as banded and mixed slurried sands, see Fig. 6.20) interpreted as the result of transitional flow regime, alternating between non-cohesive and cohesive behaviour during deposition (Haughton et al., 2003, 2009; Kane and Pontén, 2012). Barker et al. (2008) interpreted these facies as being deposited by the waning fines-enriched tail of the flow. These authors also pointed out that the absence of traction-related features might be due to rapid deposition, passing from suspension to cohesive freezing deposition as mud content increased towards the back of the tail, developing mixed-slurried sands, which are characterised by ubiquitous shear features within their deposits (see also Butler et al., 2015). The presence of genetically-linked debrite deposits upwards within beds (i.e., Beds 52, 56 and 58 in well B17 - see Fig. 6.17) also suggests that the tail end of the flow was highly concentrated, with en-masse deposition (Kneller and Branney, 1995; Lowe and Guy, 2000; Haughton et al., 2003; Amy and Talling, 2006; Haughton et al., 2009). Mudstone facies group are interpreted as the collapsing suspension cloud from the rearmost portions of the tail end of flows and are mainly found as the capping division in event beds. In contrast, pure mudstone intervals are rare (with the exception of the hemipelagic sedimentation interleaved to reservoir zones – Lower Reservoir Section) and mainly observed as thin mud caps above the beds of Z40C (see Fig. 6.17).

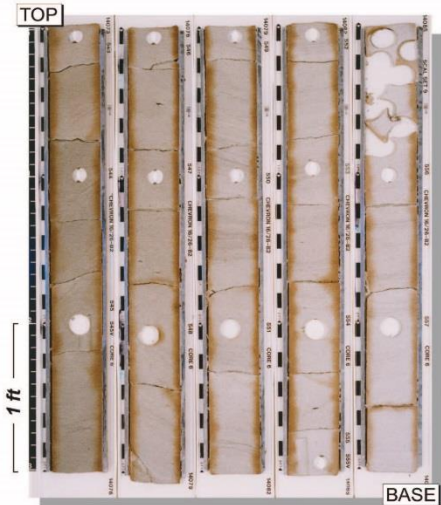
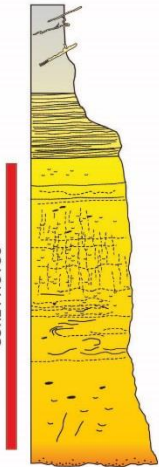
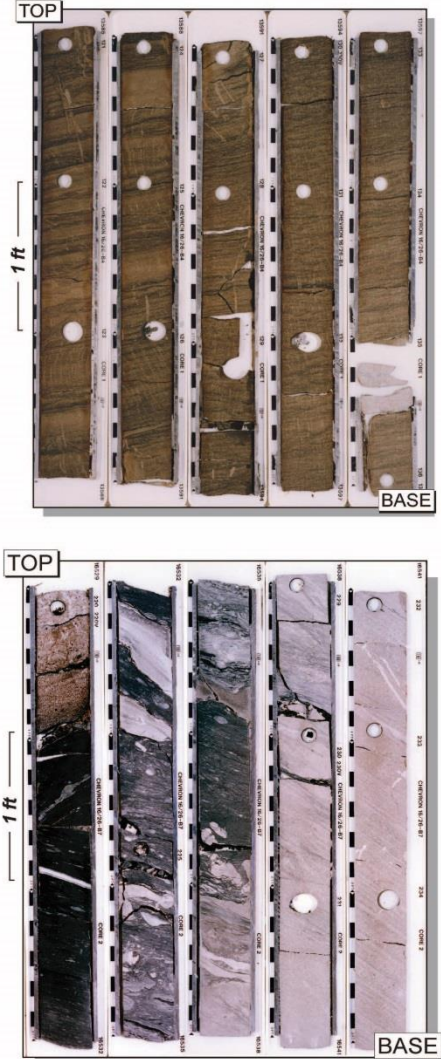
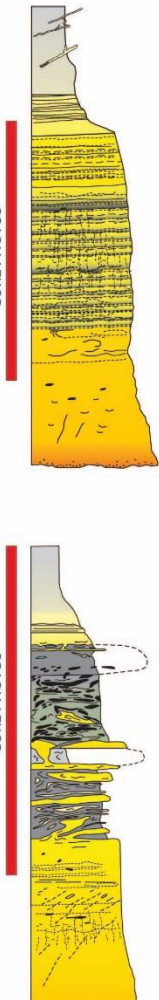
DIVISION	FACIES	CORE PHOTOS	DEPOSIT STYLE
<u>SAND-RICH</u>	MASSIVE-CLEAN (SMa) & LAMINATED SANDSTONE (SLa)	 <p>Core photos showing massive and laminated sandstone facies. A 1 ft scale bar is provided. The photos are labeled 'TOP' and 'BASE'.</p>	 <p style="text-align: center;">CORE PHOTOS</p> <p style="text-align: center;">HIGH-DENSITY TURBIDITE</p>
<u>MUD-RICH</u>	BANDED SANDSTONE (SBa) MIXED-SLURRIED SANDSTONE (SMs) & DEBRITE	 <p>Core photos showing banded sandstone and mixed-slurried sandstone with debris. A 1 ft scale bar is provided. The photos are labeled 'TOP' and 'BASE'.</p>	 <p style="text-align: center;">CORE PHOTOS</p> <p style="text-align: center;">COMPOSITE / CO-GENETIC HEBs</p>

Fig. 6.20 – Core examples of sand-rich HDT and mud-rich HEB recognised in the Lower and Middle BSF in the PA. A) Core interval of clean-massive sandstone-dominated bed in Well 16/26-B02 (14073-14088 ft) ; B) banded texture developed in cleaner sandstone facies in Well 16/26-B04 (13585-13600 ft); C) debritic interval of very fine grained matrix with floating grains and angular clasts of sandstone, and injections near the top of the bed in Well 16/26-B07 (16529-16544 ft). Note depths are in feet.

6.5.3 Interpretation of lateral facies variations

Lateral sandstone facies variation in the Platform Area of the Upper Reservoir Section was investigated by Lowe and Guy (2000) and subsequently revised by Barker et al. (2008) based on relatively robust well correlations, with individual beds traced with confidence. However, while well correlations are difficult to establish with confidence in the Lower and Middle Reservoir (apart from within Z40C), the reconstructed evolution of the basin floor (see Chapter 5) provides a constraint to study the facies distribution in relation to the reconstructed palaeobathymetric surfaces associated with the MTDs, in association with a palaeoflow analysis.

In each interval of the Lower and Middle Reservoir, a general sand-cleaning trend is observed from north to south across the study area, usually combined with the palaeobathymetric deepening trend. Clean-massive sands generally dominate the southern sector of the study area, which is interpreted to represent the axis of the system with respect to basin configuration (see Fig. 6.6-G). Sandstones with a high abundance of mud-rich facies (e.g., banded and mixed-slurried intervals) are mainly recognised in the northern sector of the study area which is interpreted to represent the off-axis/fringe portion of the system (Fig. 6.22). This trend is also observed in the Upper Britannia Reservoir where Barker et al. (2008) recognised an off- to basin-axis relationship on the distribution of mud proportions within the depositional system. In their model, sediments deposited across the southern sector of the Platform Area have an overall lower mud content in comparison with the northern sector, due to an inferred process of fractionation within the flow transverse to the palaeo-flow direction, from basin-axial to basin-marginal positions. Barker et al (2008) speculate that this is due to higher rates of sand deposition closer to the slope, combined with a lateral flow thickness-related reduction in turbulence. This model can be applied to the deposits of the Lower and Middle Reservoir Section where similar off- to basin-axis relationships are recognised (see Figs. 6.22-A, 6.23).

However, the lateral distribution of sand-rich versus mud-rich facies for each of the reservoir zones within the study area is not always so straightforward. Considering the new correlations to be reliable, the transition between these sands seems to occur locally, taking place at the inter-well scale. This scale of variation shows that there are limitations to the simple off- to basin-axis model.

The observed distribution of clean and mud-rich sandstone facies could also be related to the presence of local palaeobathymetric lows present at different times across the study area. It has been shown before that negative topographies in the Platform Area were likely the combined result of tectonic and remobilisation

processes as described in Chapter 5. A relationship between cleaner sandstone facies and topographic lows appears strong in the Z40A (Fig. 6.21), where a relatively high percentage of clean massive sandstones is recorded over the central sector (slightly laterally up dip from the southern area), which is dominated by a deep depression representing the morphological expression of the translation of MTD-2 towards the SE (see Fig. 6.22-B).

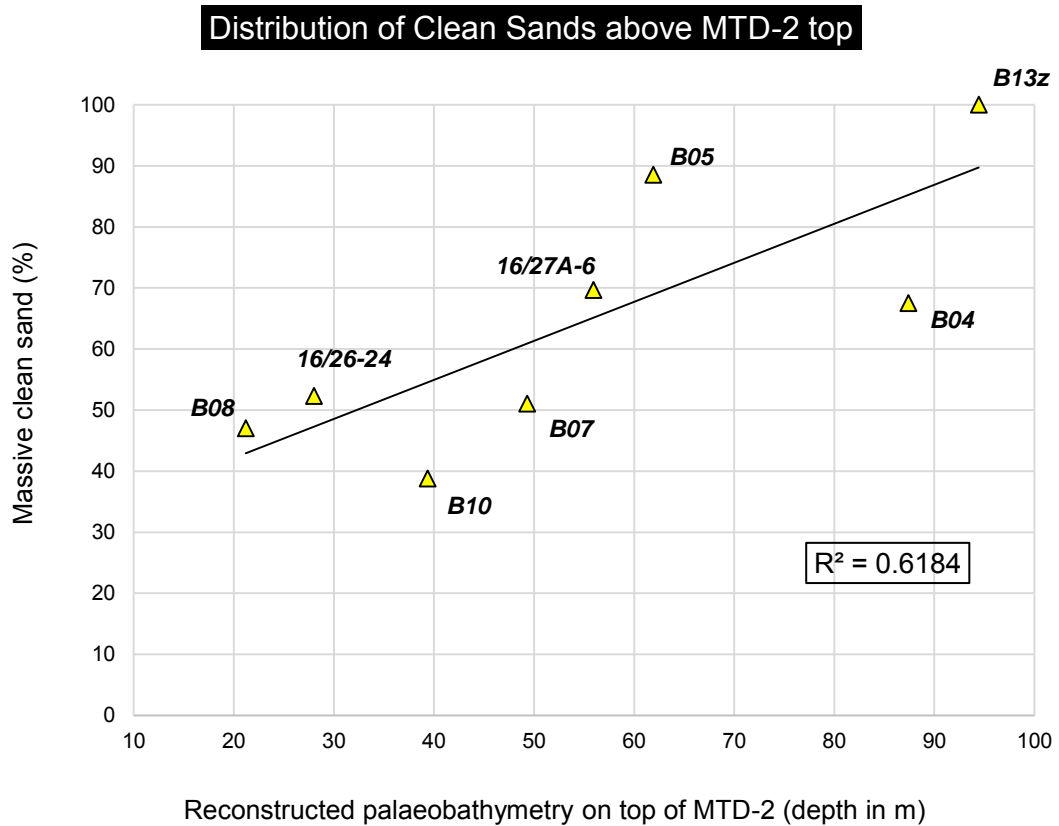


Fig. 6.21 – Diagram showing the spatial relationship between the distributions of clean massive sands (expressed in percentage of the total preserved thickness of Z40A) and the reconstructed relative bathymetric depth (referenced to the non-failed basin floor) associated with the upper surfaces of MTD-2.

In this case, it is inferred that the topography controls flow behaviour, and thus the distribution of lithofacies, over a relatively short distance. In particular, the confining topography developed along the head scarp of the MTD may represent the morphological shape of a conduit which could have effectively channelized flow (Fig. 6.22-B). In this scenario, the topographic constraint might have resulted in increased flow velocity together with increased turbulence strength, likely favouring erosion that would lead to vertical amalgamation of deposits, if not bypass. In fact, experimental studies conducted by Mohrig and Buttles (2007) show that a turbidity current is effectively “confined” within a conduit when the channel depth is greater than the height of the vertical velocity maximum. Furthermore, de Leeuw et al. (2016) show

that spatial and temporal variations of flow velocity and associated deposition may lead to the autogenic confinement of flow, with increases in axial velocity in the confined flow. In the case of Z40A, the speeding up of the flow due to the confining topography could be responsible for the bypass of the finer component leading to the deposition of medium sand grain size (Fig. 6.22-B). This could explain the larger sandstone thicknesses measured in wells B05, B04 and B13z within Z40A (see Fig. 6.12). In this case, however, the confinement is thought to have been eventually smoothed by deposition. Reduction in confinement would have led to the development of mud-rich intervals as shown by the vertical and spatial facies distribution of Z40A above areas of positive relief (Fig. 6.22-B).

However, this model of confinement and infill cannot be applied to the intervals above Z40A. In fact, Z40B and Z40C show different vertical and spatial facies organisations, likely as the result of a smaller scale of rugosity developed as consequence of the emplacement of MTD-3 and MTD-4. It is thought that a more evenly distributed pattern of rugosity might have caused a broad pattern of changes in flow behaviours over relatively short distances. An example of this phenomenon is Bed 78 in the Upper Reservoir (Barker et al., 2008). In this case, a single flow is thought to have healed the palaeo-topography introduced by the remobilisation at the Z45/Z50 boundary, resulting in a deposit (Bed 78) characterised by significant lateral thickness and facies variation and a wide range of slurry facies (*sensu* Lowe and Guy, 2000). In this case, Barker et al. (2008) inferred that flow behaviour was not uniform at the time of deposition because of the off- to on-axis variations in sediment entrainment and deposition, and because of the topography associated with the MTD.

The non-uniform distribution of mixed-slurried facies across the study area necessitates extra care when developing models to explain their presence, especially in distinguishing their mode of formation, by primary depositional (cohesive freezing – Lowe and Guy, 2000; syn-depositional shear strain – Butler et al., 2015) or by secondary processes (remobilisation, gravity-induced deformation – Barker et al., 2008).

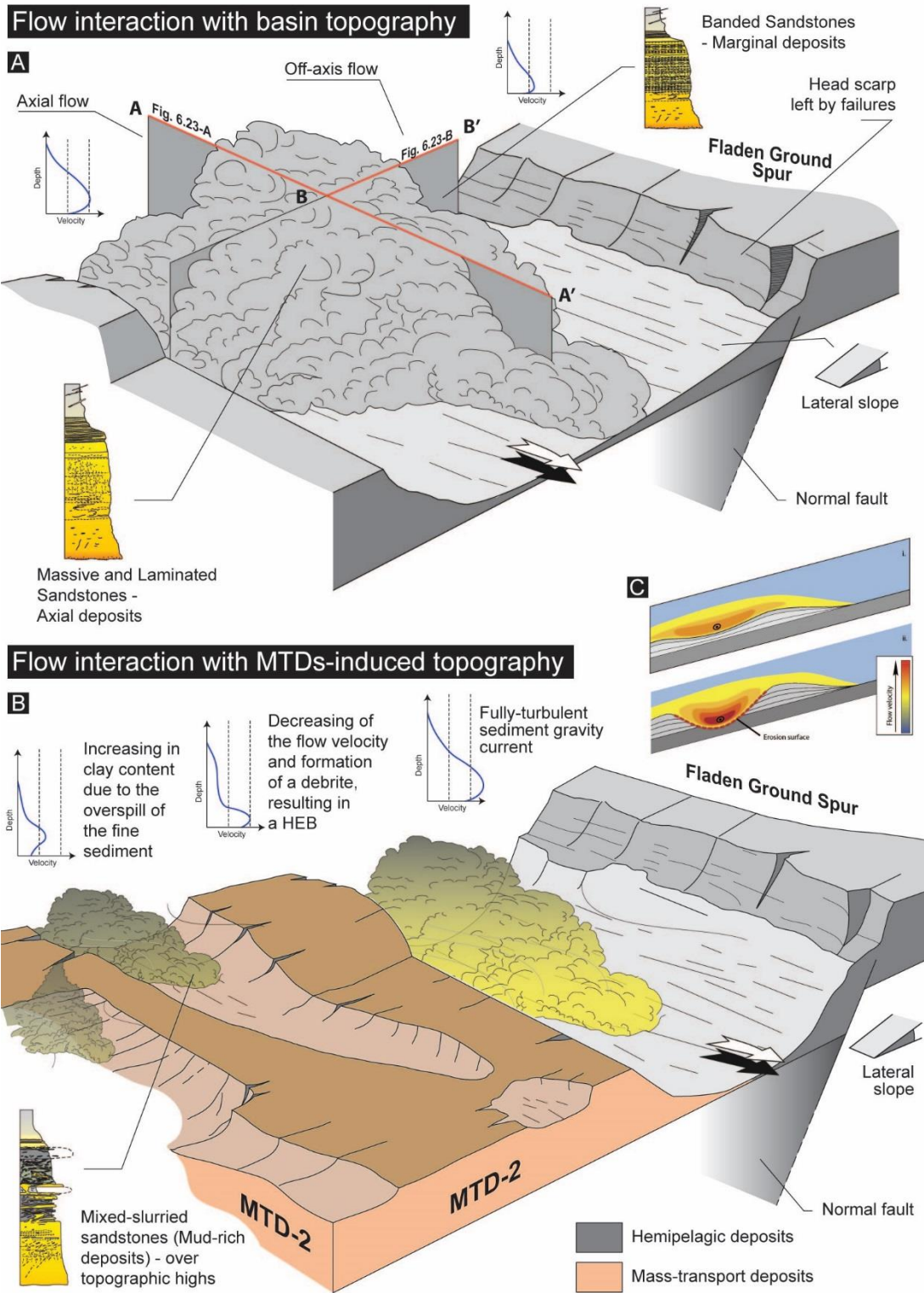
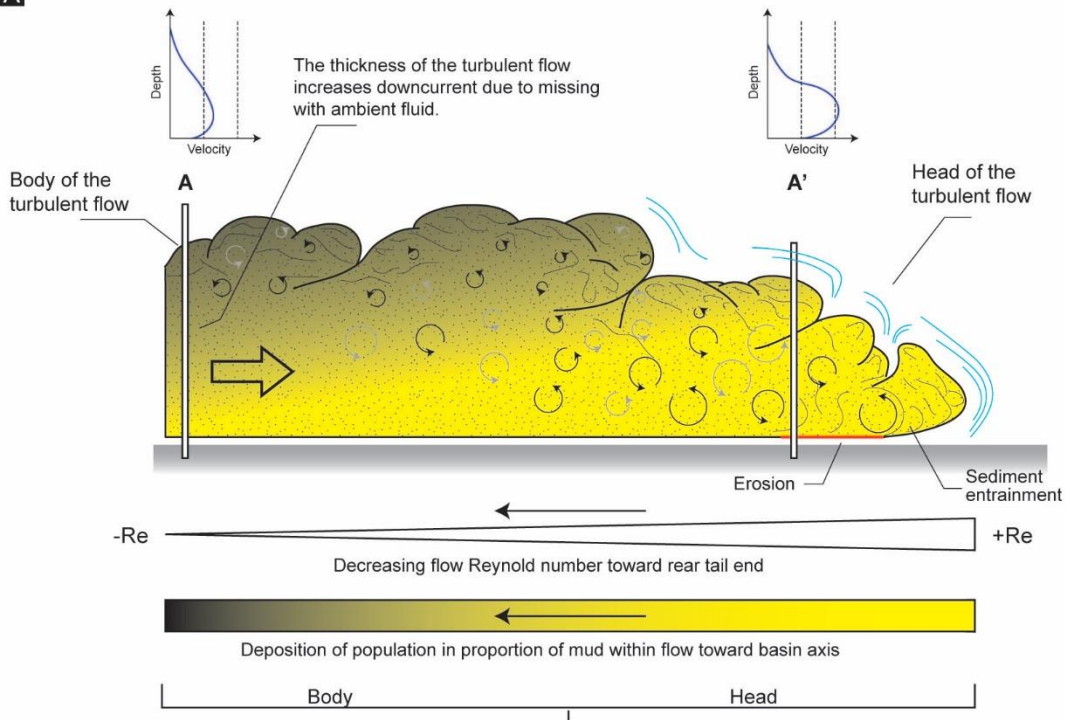


Fig. 6.22 – Two conceptual sketches illustrating flow-topography interactions in the Lower and Middle Britannia within the Platform Area. A) Deposition over a relatively simple palaeo-seafloor with flow thinning off-axis toward the northern basin margin (Fladen Ground Spur) (inspired by Barker et al., 2008); B) Reconstructed palaeo-seafloor after the emplacement of MTD-2 with strong confinement toward the northern sector of the study area and secondary rugosity developed in the southern sector. C) On the right side, two experimental models showing changes in velocity profiles from broad and weakly confined flows (above) and rapid increase in the confinement relief (below) (from de Leeuw et al., 2016).

Longitudinal flow structure - Sec A-A'

A



Orthogonal flow structure - Sec B-B'

B

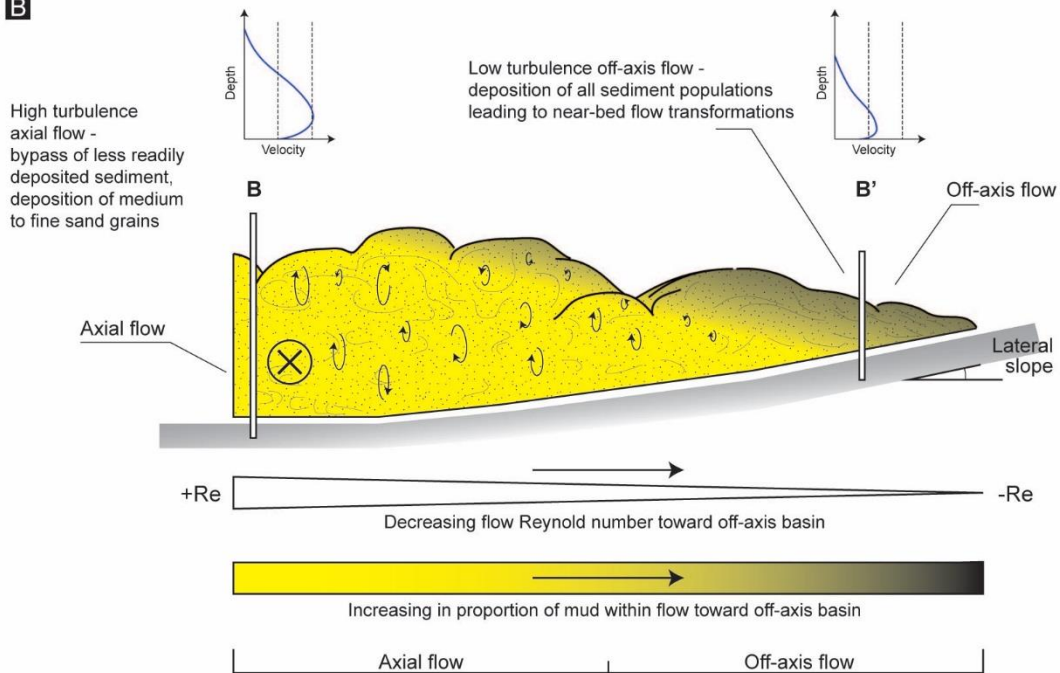


Fig. 6.23 – Vertical profile sections of gravity flow portioning axially and orthogonal to flow direction (see Fig. 6.22-A). A) A-A' section showing axial and longitudinal variation in flow volume in mud aggregate and change in flow turbulence as a model to explain inferred flow segregation of clay, mud and clasts with suppression of the fluid turbulence; B) B-B' section showing spatial variation in flow volume in mud aggregate and change in flow turbulence as a model to explain inferred axial to off-axis variation (inspired by Barker et al., 2008).

6.6 Conclusions

The investigation of new data from cored intervals of the Middle Britannia Reservoir, integrated with earlier core investigation, enable the reconstruction of the Lower and Middle BSF reservoir architecture. This reconstruction entails significant revision and re-interpretation of earlier work, in order to test previous depositional models upon the new palaeobathymetric maps of the Platform Area.

- Five main sandstone reservoir zones (Z10A, Z10B, Z40A, Z40B, and Z40C) were identified and correlated across the study area, four of which are interpreted as having been deposited above a palaeo-seafloor shaped by large-scale remobilisation events and related mass-transport deposits (MTDs).
- Contour maps of the mean grain size for each reservoir zone were built using published data from core thin sections in order to investigate spatial grain size trends as potential indicator for palaeo-flow direction. Z10A, Z10B, Z40A and Z40B showed a grain size fining trend toward East/North-East and South, suggesting a SW-NE palaeo-flow direction. A different approach was used for Z40C, where contour maps of the basal grain size for individual event beds (based on new graphic core logs) could be drawn. These maps confirmed the spatial grain size fining trends toward the eastern sector of the study area supporting the SW-NE palaeo-flow direction.
- Reservoir zones from the Middle Reservoir (Z40A, Z40B and Z40C) show significant local thickness and facies variation. This is linked to a rugose palaeo-seafloor, related to mass flow processes and related MTD emplacement and that is inferred to have influenced sandstone deposition. Despite the inferred wide scale range over which such effects are seen, some spatial facies trends are recognised. A linear relationship between the proportion of sand-rich clean-massive sandstones and relative paleo-depth is observed in topographic lows. Mud-rich divisions are preferentially encountered in enclosed topographic ponds that are likely responsible of the retention of the tail end of flows.
- The gross distribution and the vertical stacking pattern of sand-rich to mud-rich facies highlight the non-uniform behaviour of the flow during deposition. This non-uniformity is inferred to have modulated the temporal (sometimes cyclical) transition from fully turbulent character to a more cohesive behaviour that commonly occurs in association with the waning of flow.
- Several mechanisms may have acted in tandem to dictate the variable distribution of facies within each reservoir zone, and are summarised below. However, a

common motif is the development of an off- to on-axis variation in deposit character. The model invoked to explain this is based on the inferred predisposition of flow to develop a more cohesive behaviour along the off-axis flow area and a more turbulent nature over the axial part of the flow. This is inferred to be controlled in turn by i) the lateral (orthogonal to the flow direction) segregation of fine-grained sediment toward the outer flow margins, and associated early lateral sedimentation of sand, which led to deposition of mud-rich divisions, ii) a possible preferred lateral entrainment of fine sediments within the flow, and iii) the spatial change in flow Reynolds number from axial to off axial position related to the flow direction (Fig. 6.22). This last model may explain the broad character of sandstone deposits across the study area for each reservoir zone.

A general change in the vertical reservoir architecture through time is also observed, with clean-massive amalgamated sand deposition (Z10A and Z10B) passing to the more hybrid event bed - prone Z40C; the middle reservoir intervals (Z40A and Z40B) are interpreted to represent the transition between the two reservoir types. The recorded evolution might be explained invoking: i) allogenic factors that might have controlled the evolution of the depositional system and related facies distribution through time; ii) the role of active normal faulting that might have blocked or favoured preferential pathways for sandstone deposition; iii) different scales of rugosity developed on the seafloor by the emplacement of MTDs, dictating the flow non-uniformity of turbidity currents which may have developed hybrid-prone deposition instead of classic turbidite deposits. However, any one or possibly a combination of these models may account for the apparent reservoir character transition within the Lower and Middle Reservoir Section and further work is required to try and better distinguish the mechanisms operating in the Britannia depositional system.

7 Turbidite emplacement upon the irregular topography left by a large-scale MTD: the Casaglia MTD, Middle-Miocene Marnoso-arenacea, Central Italy

Abstract

Mass-transport deposits (MTDs) commonly display rugose top surfaces with considerable relief that influences the distribution of subsequent sand deposition. Such MTD-related topography can only partly be imaged in petroleum industry seismic-reflection data due to resolution limitations. Hydrocarbon reservoir characterisation commonly utilises outcrop analogues in order to constrain physical geological properties that are commonly under the scale of seismic scale resolution, such as bed thickness, surface continuity and lithofacies distribution, in order to reduce subsurface uncertainty.

The Middle Miocene Marnoso-arenacea Fm., Central Italy, provide spectacular outcrops to investigate geological processes at different scales, ranging from the depositional mechanisms of individual beds to the evolution of the larger depositional system. The basin is characterised by the occurrence of large-scale submarine landslides during the sandstone accumulation in the depocentre area which allows the study of the influence of MTD-related topography on the geometry of later sandstone deposits. Key issues are: i) the different scales of seafloor rugosity created by the presence of the MTD and ii) the effect of such topographies upon sandstone facies distribution and lateral termination geometries.

The work is based on integration of eighteen graphic sedimentary logs taken along two intersecting orthogonal transects, 3 and 9 km long, where axial gravity currents interacted with the older, transversely-emplaced Casaglia MTD. The resulting MTD-related topography was infilled then fully buried by turbidite sandstones, with evidence for changes of thickness, facies and overall depositional style over different length scales. Massive or traction-structured sands are recognised deposited over and around subtle topography (1-5 m high relief), whereas thick sandstone beds characterised by thick mud caps are encountered in ponded topographic lows (5-30 m). Very muddy successions are observed in topographic highs situated in superelevated positions with respect to the basin floor. This dataset provides an exceptional opportunity to document well-exposed depositional relationships between an MTD and the overlying turbidite sandstone deposits.

7.1 Introduction

The influence of MTD-related topography on sandstone distribution is an important factor that should be considered in the reconstruction of the geological models and in reservoir characterisation of deep-water settings, particularly when MTDs underlie the reservoir. In fact, the topography commonly developed on the upper surface of MTDs is usually on the order of several tens of metres in both the lateral and vertical dimensions, relative to the local elevation (M. Dykstra, 2005; Armitage et al., 2009; Dykstra et al., 2011; Kneller et al., 2016), that may lead to primary compartmentalisation of sandstone. However, the study of these deposits in the subsurface is difficult when the reservoir is thin relative to the scale of the topography and/or when it cannot be resolved at low seismic-reflection frequencies (Paul Weimer and Slatt, 2006). Armitage and Stright (2010) show that the resolvability of thick (up to 70 metres) sandstone packages is challenging when they are encased in MTDs of at least equivalent thickness, leading to uncertainties in the interpretation of lithofacies distribution and depositional geometries.

Reservoir facies are easily identified in cored wells; however interpretation of their distribution is usually difficult to extend away from the wells, because of the complicated depositional environments and the limited number of cored wells. Outcrop analogues are commonly used to constrain physical geological properties of the MTDs, such as their internal heterogeneity and surface continuity, and of the overlying sandstones, in terms of bed thickness variations and lithofacies distribution, in order to reduce subsurface uncertainty and aid reservoir performance prediction by eliminating unlikely scenarios (e.g., Slatt, 2000; Sullivan et al., 2000). MTD studies based on outcrop data aim to enhance hydrocarbon exploration and production by optimising interpretation of low resolution seismic-reflection profiles gathered across reservoirs, through the study of MTD distribution, morphology, sedimentology and depositional processes at outcrop, which provide good insight into seismic facies recognised on subsurface datasets.

This chapter aims to contribute to an ongoing effort to better understand the role of MTDs in influencing the evolution of stratigraphic architecture in deep-water settings. The focus of this chapter is a relatively thin stratigraphic portion of the Marnoso-arenacea Fm., Fiorenzuola system, Unit V (*sensu* Muzzi Magalhaes and Tinterri, 2010) overlying the Casaglia MTD (Lucente et al., 2006). The aim is to use sedimentary logs in order to establish the topographic control on the depositional style of turbidity currents above the MTD, with particular emphasis placed on better understanding the types of deposits associated with different scale of rugosity. The

results may have practical implications for the prediction, characterisation and development of hydrocarbon reservoirs in other deep-water systems influenced by the presence of MTDs.

In detail, the main objectives of this chapter are:

- To undertake an outcrop characterisation based on investigation and interpretation of the sandstones immediately overlying the Casaglia MTD (Marnoso-arenacea, Fiorenzuola system, Unit V *sensu* Muzzi Magalhaes and Tinterri, 2010). Sedimentary logs represent the principal data set used in this study. The results obtained in the field can be framed in the wider context of the Marnoso-arenacea Basin along the Apennine Foredeep, by comparison with previous work in the study area (e.g., Muzzi Magalhaes and Tinterri, 2010);
- To reconstruct of the irregular topography of the Casaglia MTD through the correlation of sedimentological logs, in order to identify and define scales of rugosity associated with the upper surface of the MTD;
- To analyse net-to-gross (i.e., sand proportion) and sandstone facies character in selected portions of the sedimentological logs. This dataset is used to determine spatial patterns in facies that may provide insights into the topographic controls on sandstone deposition.
- To document the small scale geometries of sandstones immediately above the MTD that contribute to sandstone heterogeneity (e.g., pinch-out, onlap, loading, etc.)

7.2 The Marnoso-arenacea Formation

Among foredeep turbidites, the Marnoso-arenacea Fm. (MAF) is probably one of the most well studied, best exposed and least structurally deformed, due to its relatively external position within the Apenninic orogeny. The MAF (Langhian-Tortonian) was deposited in an elongate, NW-stretched foredeep basin formed in front of the growing Northern Apennines orogenic wedge (Ricci Lucchi, 1978, 1981, 1986; Ricci Lucchi and Valmori, 1980). The basin, in which the MAF deposition occurred, is well represented in Fig. 7.1-A, which shows the simplified palaeogeographic map of the Proto-Adriatic basin introduced by Di Biase and Mutti (2002).

The main flows that deposited the MAF were turbidity currents with siliciclastic composition. They were sourced from Alpine fluvio-deltaic systems to the north-west (see also Ricci Lucchi, 1978, 1981, 1986; Gandolfi et al., 1983, 2007; Zattin and Zuffa, 2004) and deposited a great part of their sediment load in an elongate, southern NW-SE-stretched foredeep formed in front of the growing Apennine

orogenic wedge (Fig. 7.1-B). Minor sources were also located in the southern and south-eastern margins characterised by carbonate (“Colombine”) and hybrid (mixed siliciclastic and carbonate; “Contessa-like”) turbidity currents flowing in the opposite direction (i.e. towards the NW); the beds deposited by such flows form very important markers for high-resolution stratigraphic correlations.

In order to explain deposition within the MAF, Mutti et al. (2003) show that sedimentation of a foreland region usually takes place in three distinct and coeval basins including: a) wedge-top basins, characterised by alluvial, deltaic and mixed depositional systems; b) a foredeep basin, characteristically in-filled with deep-water basinal turbidites; c) an outer and shallower ramp developed on the passive foreland plate (Fig. 7.1-C).

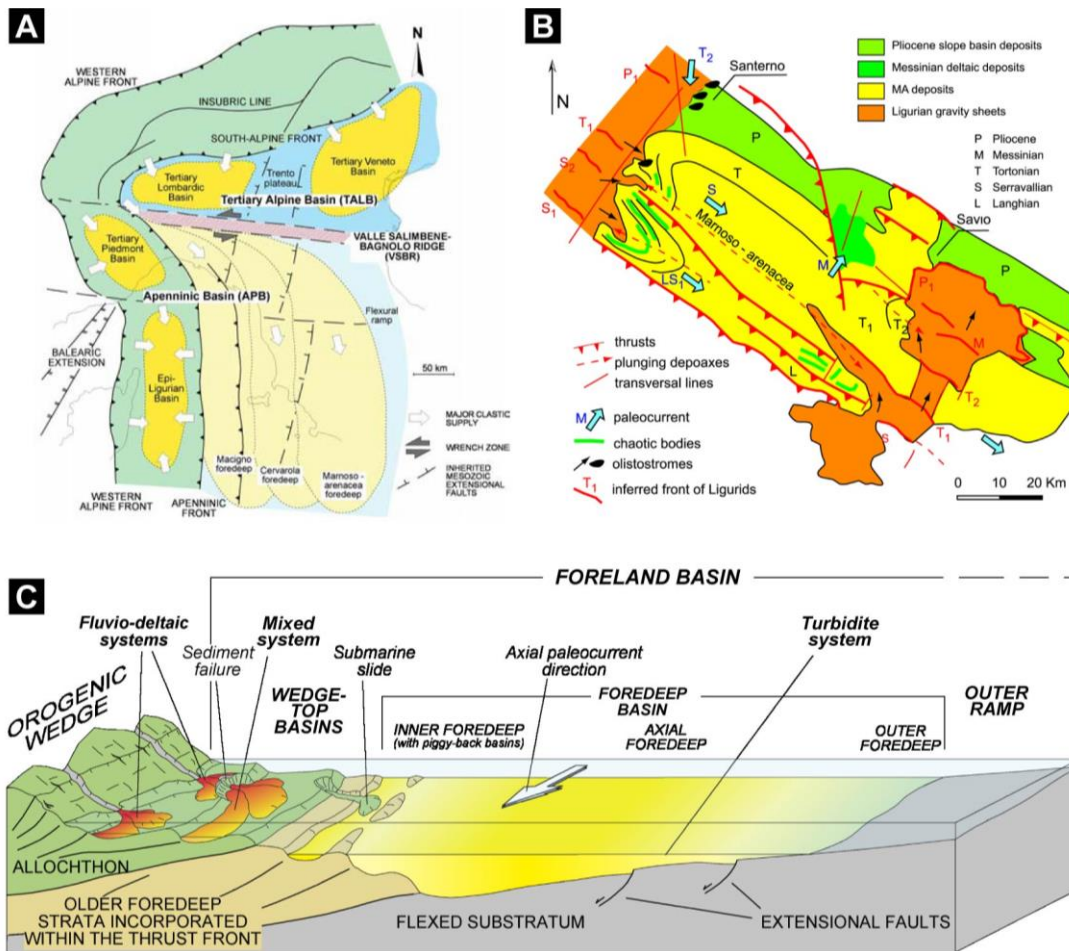


Fig. 7.1 – A) Simplified palaeogeographic reconstruction of the areal distribution of the main Tertiary basins developed within the Alps-Apennine orogenic system (modified by Mutti et al., 2002, after Di Biase and Mutti, 2002). B) Simplified sketch of the Romagna Apennine illustrating the progressive migration of the thrust front and main depocentres toward NE (modified by Mutti et al., 2002, after Ricci Lucchi and Ori, 1985) C) Scheme showing the main elements of a foreland basin and the relationships between a growing orogenic wedge and the outer flexed board (from Mutti et al., 2003).

7.2.1 Geological setting and stratigraphic setting

The Apennines foredeep basin is one of the classic examples of deep-water turbidite basins associated with the development of an orogenic wedge (e.g., Ricci Lucchi, 1986 with references therein). The MAF foredeep can be considered a complex foredeep (sensu Ricci Lucchi, 1986) characterised by syn-sedimentary structural highs and depocentres related to the main thrust fronts, which controlled the lateral and vertical distribution of turbidite facies (see Muzzi Magalhaes and Tinterri, 2010; Tinterri and Muzzi Magalhaes, 2011).

The MAF is a wedge-shaped sedimentary body deposited in an elongate, northwest-southeast trending foredeep that migrated progressively towards the northeast in response to migration of the Apenninic thrust-front in the same direction (Ricci Lucchi, 1986). This foredeep was bounded to the west and south by tectonically active slopes, to the east by a submarine rise that received mainly pelagic sediments but also formed local carbonate platforms, and to the north by a foreland ramp bounded by the Alpine chain and adjacent shelf (Fontana et al., 1986; Ricci Lucchi, 1986).

The MAF locally reaches a thickness of 4000 metres (Fig. 7.2-A) and crops out in a northwest-southeast direction, over an area that is approximately 180 km long and 40 km wide in the Umbria-Romagna fold and thrust belt (Fig. 7.2-B - Ricci Lucchi, 1983; Ricci Lucchi and Valmori, 1980; Boccaletti et al., 1990). Deposition of the MAF began in the Late Burdigalian overlying the Schlier Formation and continued until the Tortonian, followed by deposition of evaporites and euxinic shales of the Gessoso-Solfifera Formation (Fig. 7.3-A - Maxwell, 1959; Ricci Lucchi, 1986).

Turbidites of the MAF consist of intermittent turbiditic deposits that can be subdivided into two distinct depositional stages (Ricci Lucchi, 1983). Inner stage deposits form the northwest (i.e. inner basin) part of the outcrop belt while outer stage deposits form the northeast (i.e. outer basin) part of the outcrop area (Ricci Lucchi, 1986). The first stage is characterised by deep water high efficiency basin floor turbidites, while the second one consists of low-efficiency mixed turbidites in a shallower and more confined basin. The transition from the older inner stage to the younger outer stage occurs at the Serravallian-Tortonian boundary and is marked by an increase in the sand/mud ratio and a significant decrease in clastic carbonate input (Ricci Lucchi, 1986). The passage between inner and outer stages is also marked by an important tectonic phase (upper Serravallian in age) characterising the basal part of Unit V of Muzzi Magalhaes and Tinterri, 2010), which is time equivalent to the Fiorenzuola and Paretaio systems (Fig. 7.3-A).

Over the years, several authors have stressed the importance of syn-sedimentary tectonic activity (Fig. 7.3-B) affecting the Marnoso-arenacea deposits (Ricci Lucchi, 1986; Mutti et al., 2002; Lucente, 2004). They recognised the growth of two major structures (M. Castellaccio Thrust and Verghereto High; Tinterri and Tagliaferri, 2015) associated with the transition phase between the inner and the outer basin (Muzzi Magalhaes and Tinterri, 2010). This transition is the result of the progressive shifting of the basin depocentre towards the northeast due to thrust-front migration, mainly recorded in the Fiorenzuola turbidite system (Tagliaferri and Tinterri, 2016) which includes the strata investigated in this chapter. Various studies have shown that the structural deformation that exerted control over basin geometry is also associated with the presence of large volume mass transport complexes (MTCs) (Ricci Lucchi, 1986; Argnani and Lucchi, 2001; Conti, 2001; Mutti et al., 2002; Roveri et al., 2002; Lucente, 2004; Tinterri et al., 2009, 2011; Muzzi Magalhaes & Tinterri, 2010).

The MAF stratigraphic succession, therefore, can be described in three stages characterised by three different facies associations related to the progressive increase, over time, of the structural control and the associated morphologic confinement: 1) a Langhian-Serravallian inner basin; 2) an Upper Serravallian phase that records the transition between inner and outer basins and 3) a Tortonian outer basin (see Fig. 7.2).

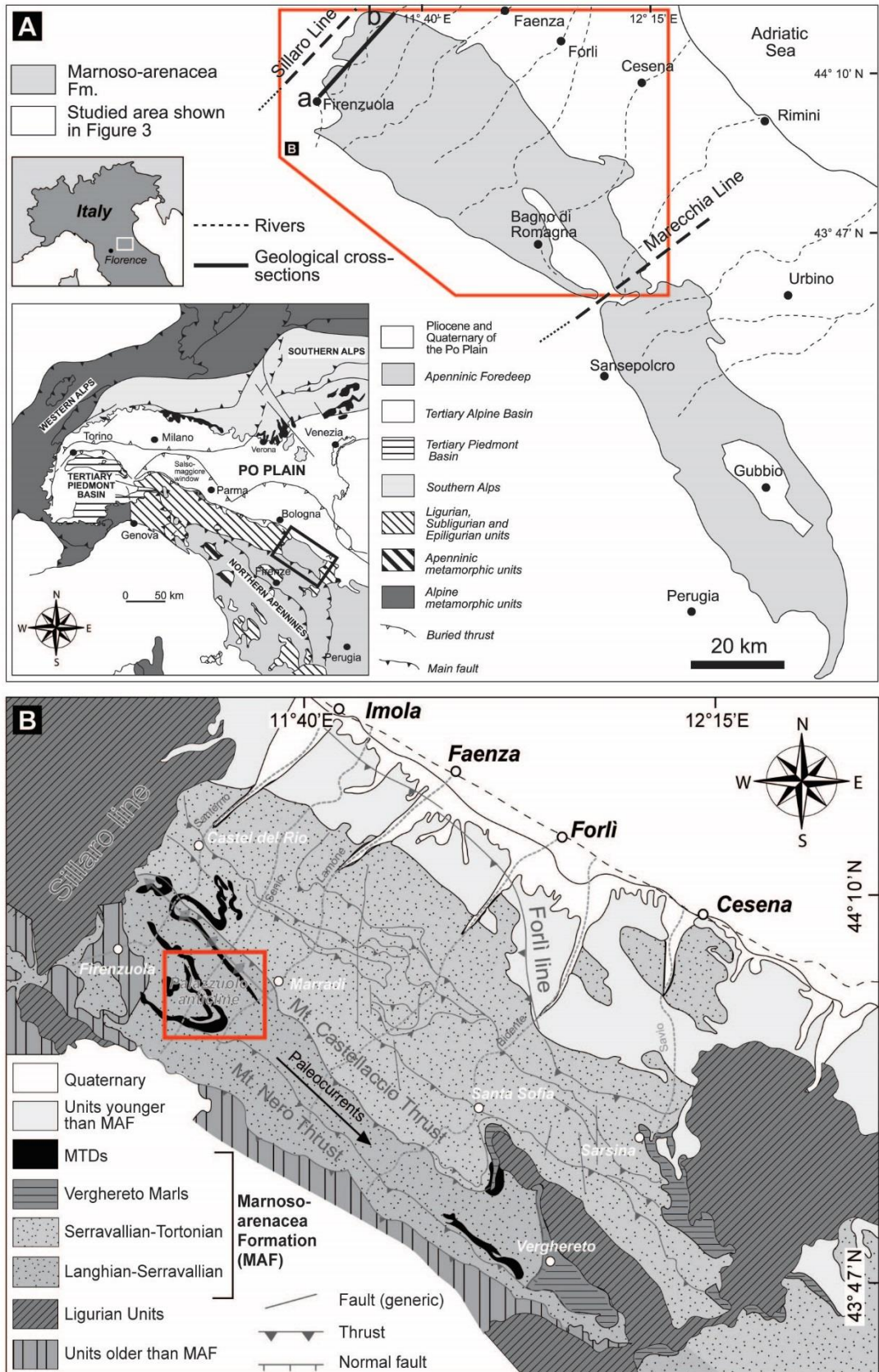


Fig. 7.2 – A) MAF cross out in the northern Apennines (from Muzzi Magalhaes and Tinterri, 2010). B) Schematic geological map of the north-western sector of the Romagna Apennines (location shown in the inset map by the red polygon – from Ogata et al., 2017). Red box represents the study area of this work shown in Fig. 5.4.

7.2.2 Fiorenzuola System

The Fiorenzuola turbidite System (Unit V of Muzzi Magalhaes and Tinterri, 2010) is an important stratigraphic interval within the MAF because it represents the phase of transition between inner and outer basin, caused by the growth of the major structures of the M. Castellaccio Thrust and the Verghereto High (Tinterri and Tagliaferri, 2015). The Fiorenzuola System was studied by Tinterri and Tagliaferri (2015) and Tagliaferri and Tinterri (2016) in order to document the progressive closure and isolation of the inner portion of the foredeep, as well as the beginning of a coeval shifting of the main depocentre to the outer basin.

The main phases of thrust propagation are marked by MTC emplacement and by thinning and fining of the stratigraphic succession over the syn-sedimentary structural highs (Argnani and Lucchi, 2001; Roveri et al., 2002; Lucente, 2004; Muzzi Magalhaes and Tinterri, 2010). The large-scale events are important markers that have been used to divide the Langhian to Serravallian interval into five stratigraphic units (I, II, III, IV, V), which indicate structurally-induced changes in basin physiography (Muzzi Magalhaes and Tinterri, 2010; Tinterri and Muzzi Magalhaes, 2011). In particular, Lucente (2004) focused his study on a limited stratigraphic interval below the Casaglia MTD (Fig. 7.3-A - upper part of Unit IV). On the basis of the structural analysis of the main MTDs and of a simplified stratigraphic analysis focusing on the correlation of some key beds, this author proposes a palaeogeographic scheme highlighting that, at this specific time, the foredeep was influenced by the M. Castellaccio Thrust and its south-eastern propagation represented by the Biserno and Verghereto Highs (see Fig. 7.2-A).

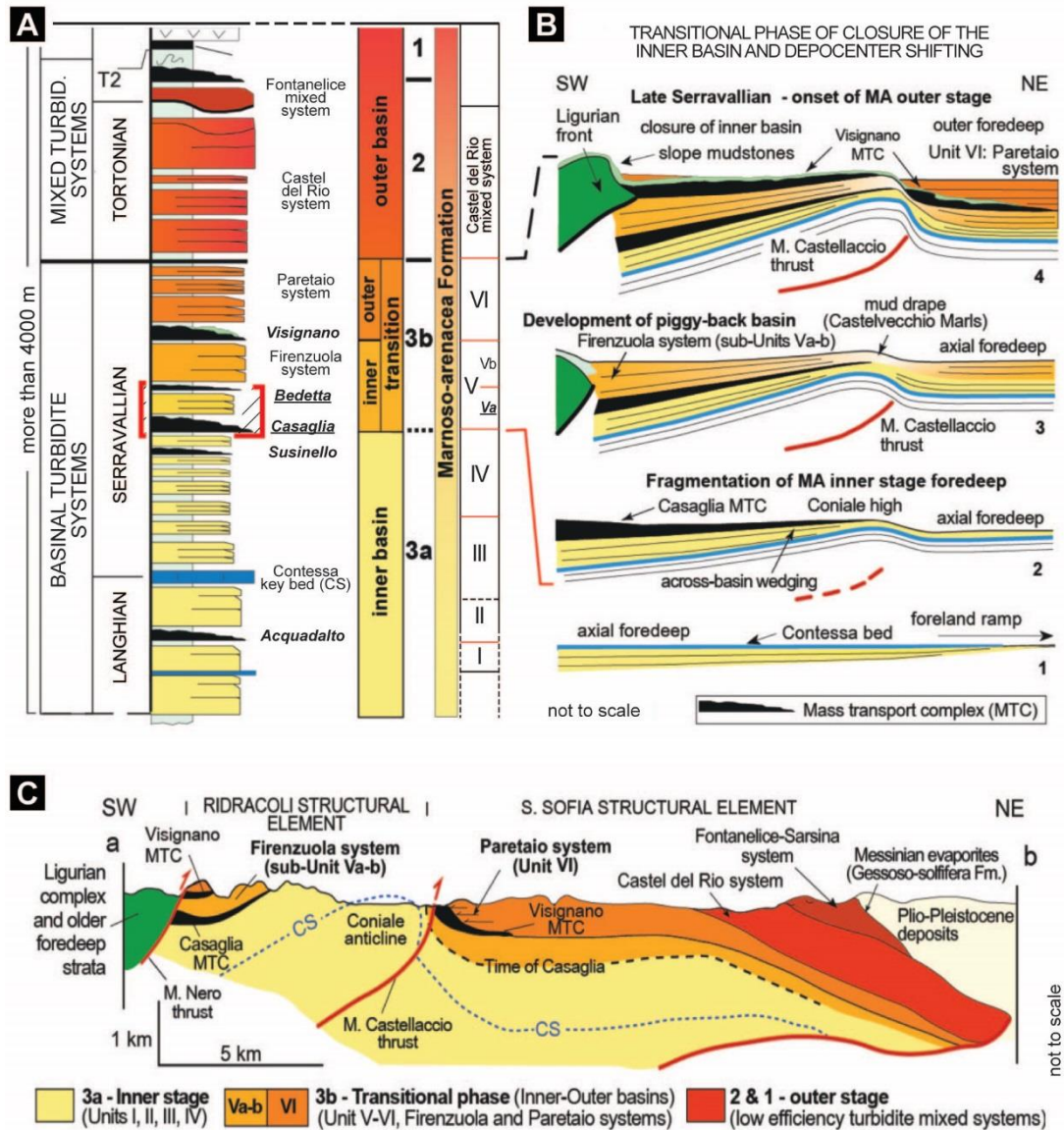


Fig. 7.3 – Schematic stratigraphic log of the MAF deposits (modified from Muzzi Magalhaes and Tinterri, 2010 and Mutti et al., 2002). Units I, II, III, IV, Va, Vb and VI were introduced by Muzzi Magalhaes and Tinterri (2010) and Tinterri and Tagliaferri (2015). On the right, diagram showing the structural evolution of the M. Castellaccio, thrust-related fold from early to late Serravallian recording the passage between inner, transition and outer basins or stages, *sensu* Ricci Lucchi, (1986). The time equivalent deposits of Unit VI (Paretaio system) in the inner basin are also shown (modified from Tagliaferri and Tinterri, 2016, after Roveri et al., 2002; see also de Jager, 1979 and Fig.18 by Tinterri and Tagliaferri, 2015).

7.3 The Casaglia MTD

The Casaglia MTD is one of the thickest and best exposed examples of ancient submarine mass-transport deposits and the most extensive in the Marnoso-arenacea Fm. (Lucente and Pini, 2003). It was deposited during the inner stage of Marnoso-arenacea deposition (Serravallian) and after the deposition of the Contessa marker bed (Fig. 7.3-A) and it crops out in the northernmost sector of the Romagna Apennines between the valleys of Santerno and Lamone rivers (Fig. 7.4). The area of the MTD was estimated to be at least 15×10^9 square metres of remobilised deposits (Lucente, 2002), which includes both intrabasinal and extrabasinal sediments, covering an area of approximately 350 km² (Lucente and Pini, 2003). Intrabasinal sediments are mainly composed of “basin plain” lithofacies, including thick and thin turbidites with a preponderance of Bouma Ta-e and Tc-e divisions and “slope” sediments characterised by hemipelagic mudstones and rare, thin turbidites. Extrabasinal input is confirmed by the presence of an olistostrome complex, an ordered aggregate of large slabs derived from the palaeo-Apennine accretionary wedge moving towards the NE that incorporates older Ligurian, Subligurian, Tuscan, and Epiligurian successions (Lucente and Pini, 2003). The olistostrome crops out in two lenses in the southwestern portion of the MTD body (Fig. 7.4).

Transport directions for the Casaglia MTD were determined by Lucente and Pini (2003), based on fold vergence and fold axes from deformed horizons in the MTD (Fig. 7.4). The orientation of slump fold axes is consistent for each sector and it is in agreement with the sense of fold vergence and with the palaeo-slope strike (Fig. 7.4). The vergence of folds in the deformed intrabasinal component of the MTD is partially consistent with two ramp directions (Lucente, 2002), indicating movement towards the NE in the sector south of the Senio river and toward NW in the northern sector.

An additional complication is that on the northern side of the Campanara sector the fold vergence shows two distinct and very different directions (towards N and towards W). According to Lucente (2002), the W-verging folds could be interpreted as a ponding effect against a plane dipping to west. The author also argues the existence of a local zone of failure in an “outer” basin margin, which may be due to the presence of a gentle intra-basin high, possibly related to syn-sedimentary tectonics. Finally, in the Santerno Valley the fold vergence is consistent with the ramp and the progressive decrease of slide thickness.

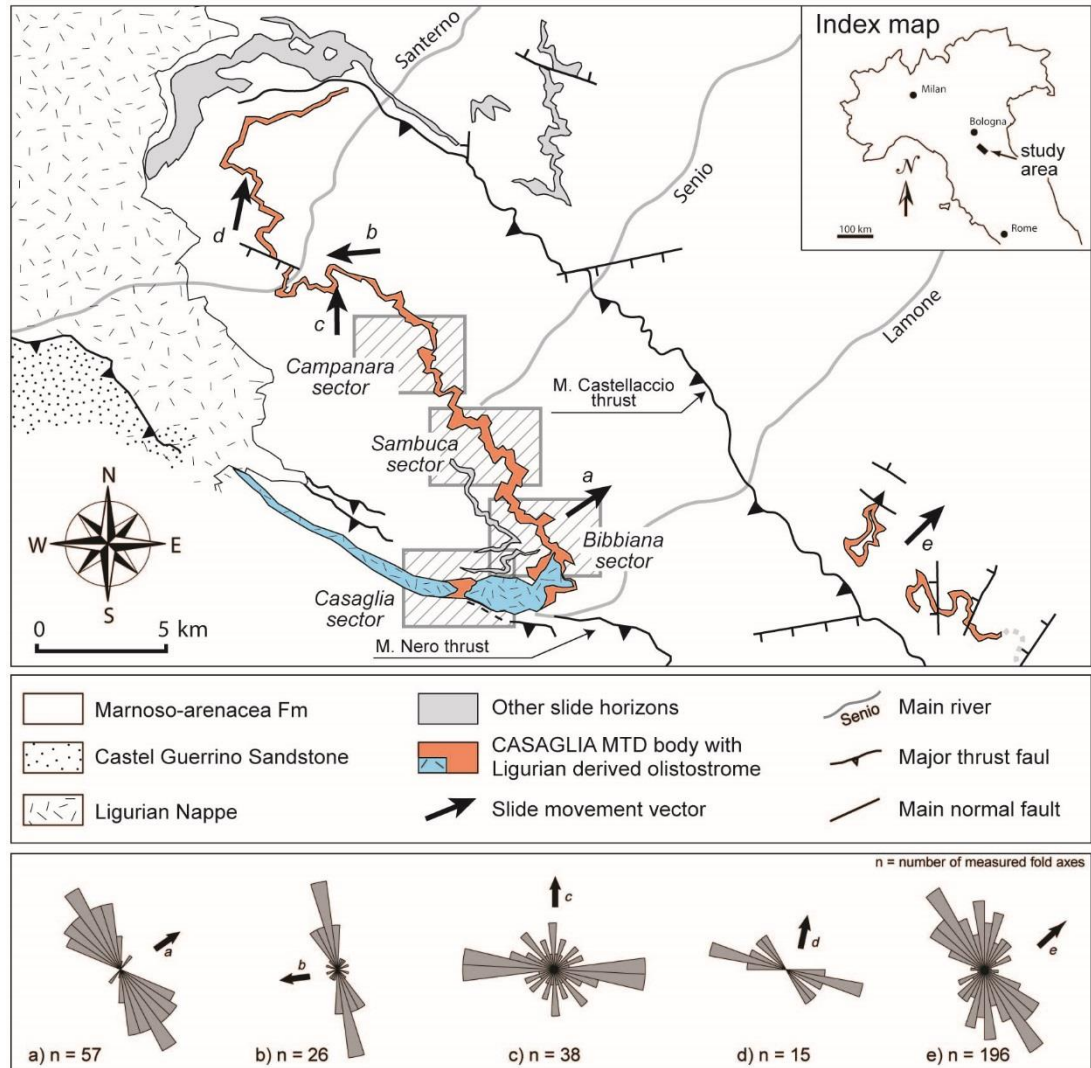


Fig. 7.4 – Geologic map of the field area, showing the outcropping portion of the Casaglia MTD, main stratigraphic and structural elements, and investigated sector of study (Casaglia, Bibbiana, Sambuca and Campanara). Slide movement vectors are shown by the dark arrows (in the map) and by the related rose diagrams (below) based on the measurement of fold vergence. Notice the large olistostrome that dominates the Casaglia sector and in part the Bibbiana sector (modified after Lucente, 2002 and Lucente and Pini, 2003).

7.4 Dataset

7.4.1 Methodology

The purpose of this study was achieved by measuring and correlating 18 highly detailed sedimentary logs with lengths of 50-120 metres covering the stratigraphic interval immediately overlying the Casaglia MTD (Table 7.1). In particular the data collected consist of:

- Bed thickness measurements using a Jacob's staff with a laser sighting device (Patacci, 2016);
- Estimation of the grain size of each bed with the aid of a grain-size comparator and a hand lens (20x magnification);
- Palaeocurrent measurement of the sole casts and recording of the beds sedimentary structures;
- Correlation of the sedimentary graphic logs;
- GPS measurements of the position of the contact between the upper surface of the Casaglia MTD and the overlying sandstones.

Geological mapping of the study area did not represent one of the main aims of this work. However, a preliminary overview of the study area was undertaken before the logging by using geological maps produced by the Toscana Geological Survey at a scale of 1:10000 (Regione Emilia Romagna Geological, 1994), in order to investigate the position and accessibility of the sandstone interval overlying the upper surface of the Casaglia MTD. When observed, the contact between the upper surface of the Casaglia MTD and the overlying sandstones was measured with a GPS receiver in order to integrate these data with the measured sedimentary logs.

Deposit grain size was measured with the aid of a grain-size comparator - an approach that in previous work (Talling et al., 2004) showed a skew measurement to the coarsest 10% of grains within a sandstone interval and measurement errors estimated at <5% in a 30 metres interval study undertaken in the MAF by Amy and Talling (2006).

Outcrops usually show a resistant weathering profile, which highlights potential changes in fabric and makes the description of outcropping deposits easier. The main uncertainty in measuring sandstone bed thickness is in defining the transition where sandstone grades into siltstone. Difficulties were also frequently encountered when differentiating between turbidite mudstone and hemipelagite. In all the sedimentary logs particular attention was paid to the fine-grained intervals between turbidite beds

which are described in detail in the facies table (Table 7.2) and on the measured logs (see correlation panel in Appendix D).

7.4.2 Location of the sedimentary logs

The study area is located in the Northern Apennines between the Santerno and Lamone rivers near the boundary of the Italian regions of Tuscany and Emilia-Romagna (Fig. 7.5). The outcrops used in this study lie south of the Mt. Castellaccio Thrust within the Casaglia Sector of the Casaglia MTD (Fig. 7.4). In this area, the MTD crops out in a narrow belt that trends northwest-southeast, roughly paralleling the Mt. Castellaccio Thrust (Fig. 7.4). The deposits of the Casaglia MTD located to the north of the Mt. Castellaccio Thrust (Fig. 7.4) were not included in this work because of the difficulty in correlating the sandstones overlying the Casaglia MTD across the thrust.

Sedimentological logs for the turbidite succession immediately overlying the Casaglia MTD can be grouped in four sectors (Casaglia, Bibbiana, Sambuca and Campanara) (Fig. 7.5 and Table 7.1).

Sectors	<i>Casaglia</i>	<i>Bibbiana</i>	<i>Sambuca</i>	<i>Campanara</i>
Number of logs	n. 2	n. 6	n. 4	n. 8
Names of sedimentary logs	- CAS-1 - CAS-2	- BIB-1 - BIB-2 - BIB-2A - BIB-2B (~15 m) - BIB-3 - BIB-4	- SAM-1 - SAM-2 - SAM-3 - SAM-4	- CAM-1 - CAM-2 - CAM-3 - CAM-4 - CAM-5 - CAM-6 - CAM-7 - CAM-8 (~5 m)

Table 7.1 – Summary of the sedimentary logs of the sandstone interval overlying the Casaglia MTD. Note that the numbers associated with the names of the logs follow the measurement sequence undertaken during the field work, not a geographical progression.

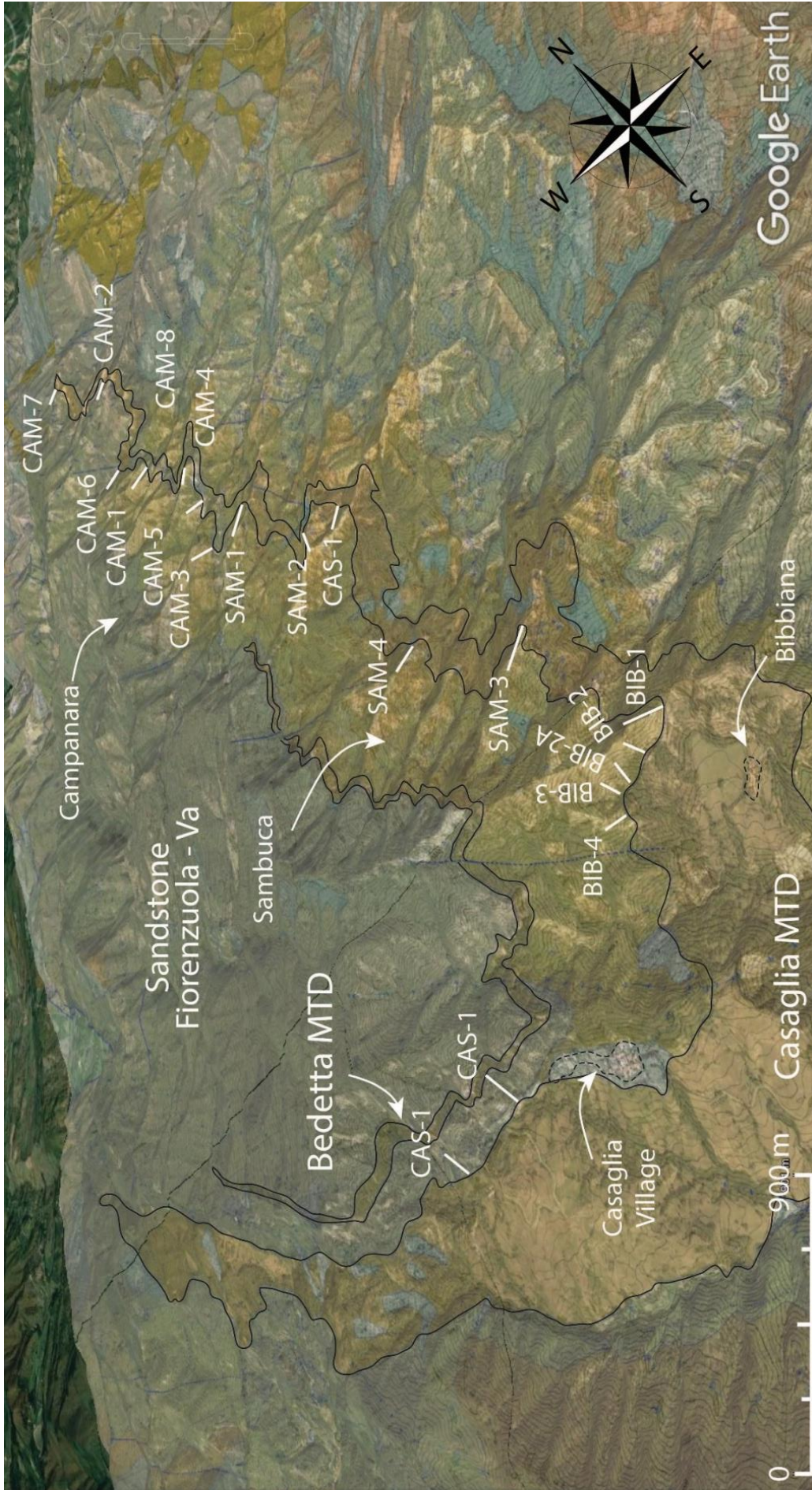


Fig. 7.5 – Satellite view of the study area. In yellow the locations of the measured sedimentary logs along the upper top of the Casaglia MTD.

7.4.3 Lithology and lithofacies

The main lithologies recognised in the study area consist of 1) sandstones and silty mudstones representing the stratigraphic succession overlying the Casaglia MTD, and 2) folded and deformed sandstones and mudstones, characterising the MTD itself. These two categories are described as follow:

- Detailed facies description of the sandstones overlying the MTD (section 7.4.3 - Table 7.2);
- Brief description of the Casaglia MTD character (section 7.5).

7.4.4 Sandstones overlying the Casaglia MTD

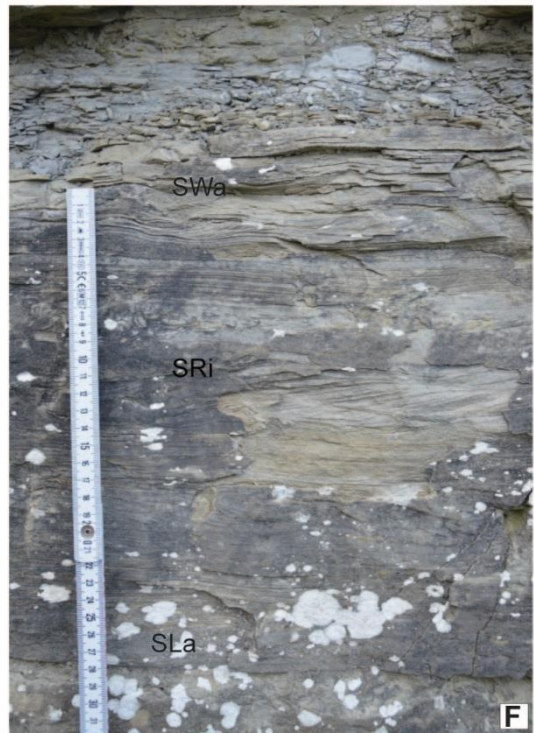
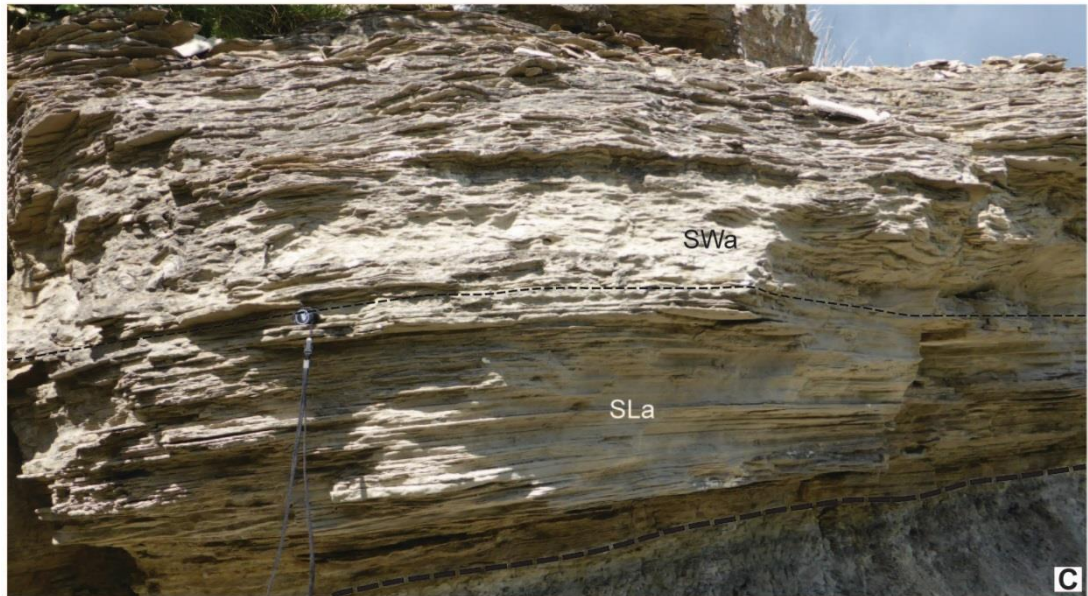
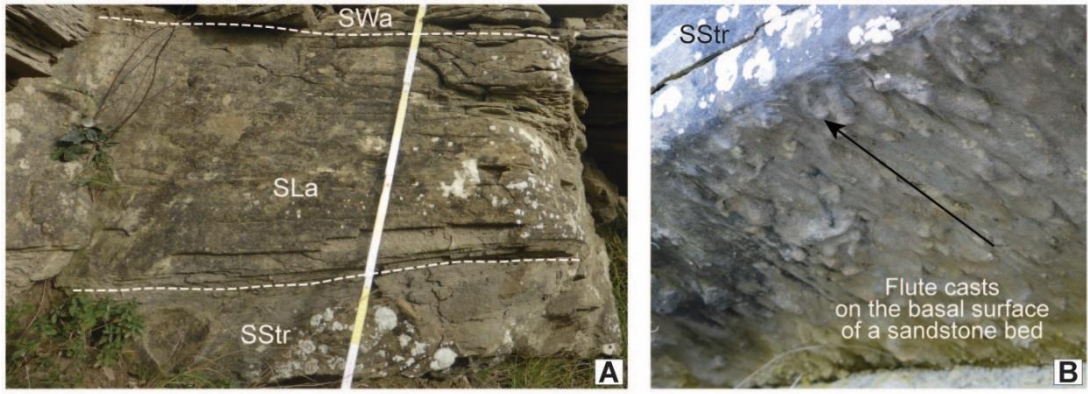
The facies belonging to the succession above the Casaglia MTD are grouped in: i) sand-rich, ii) silt-rich and iii) mudstone facies (Fig. 7.6). The sand-rich group includes structureless, ungraded, parallel, wavy and ripple laminated sands. Debritic siltstones and clean siltstones constitute the silt-rich group. Finally, two different types of mudstone are identified: clastic (darker colour) and calcareous (lighter colour) mudstones.

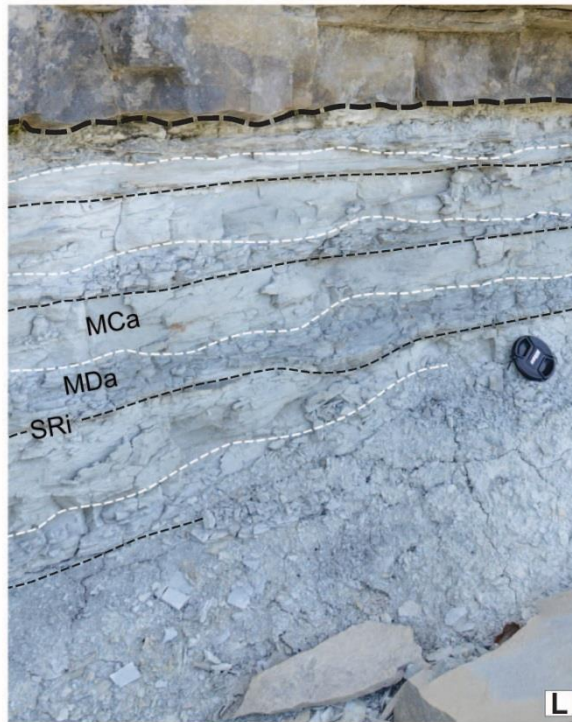
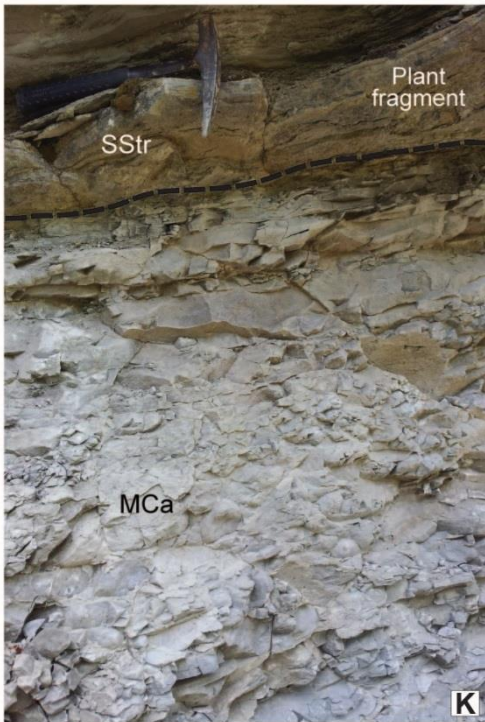
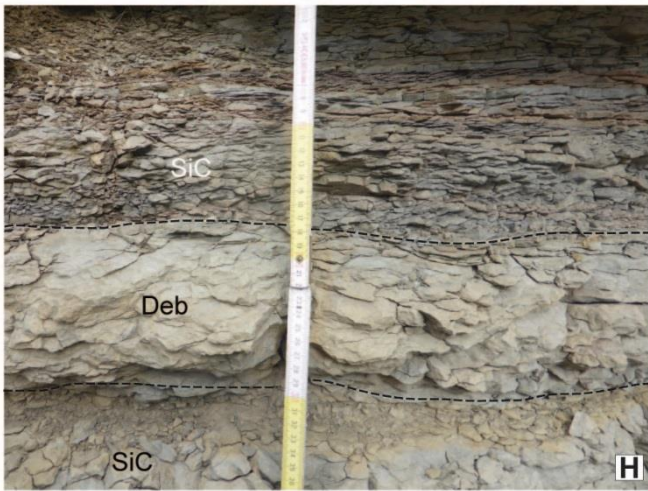
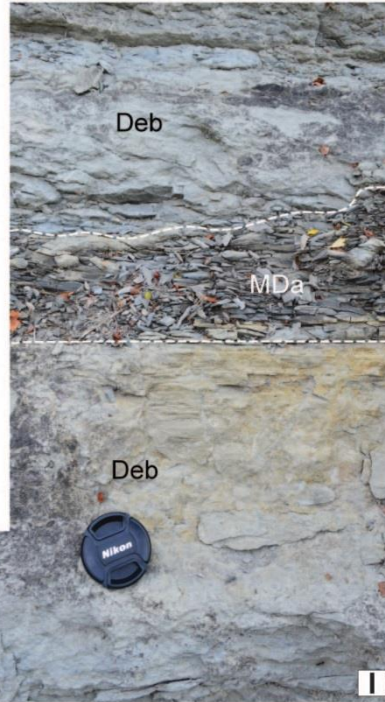
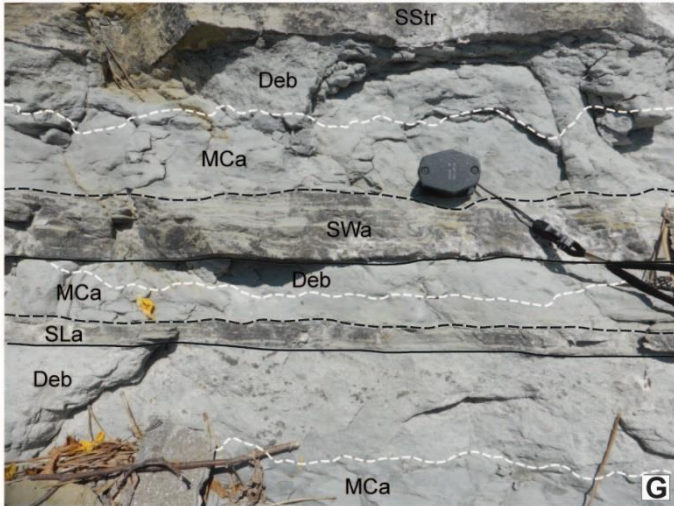
Debritic siltstones represent an unusual facies in this study area; these are typically less than 30 cm in thickness, silty, poorly sorted, and extremely heavily bioturbated. They are generally structureless, with the exception of abundant biogenic sedimentary structures across the four sectors.

The sandstones commonly contain abundant micas and lithic fragments. Grain size is generally lower medium to fine at the base and grade upward to silt. Thick beds (> 50 cm) are consistently medium-grained at the base. Coarse-grained sandstones are extremely rare.

Lithol.	Group	Facies	Code	Description (Photos in Fig. 7.6)	Process Interpretation
Sand		Structureless ungraded	St	Sharp-based structureless, clean, moderately to poorly sorted, medium- to fine-grained sandstones. The bottom layer (2-5 cm) of thick (>100 cm) sandstone beds can be up to coarse grain size. Devoid of primary sedimentological structures. Grading is usually weak or absent. When present, grading is subtle (<1 phi) and only toward the top of the interval. Usually grey to light-grey due to the presence of muscovite. Plant fragments are usually found in the basal portion of thick (>100 cm) coarse sand beds, preferentially concentrated and aligned within relatively thin layers. Sole marks as groove and flute casts of mm to cm scale are usually recorded on the lower bedding surface of thick beds (>50 cm). Dewatering fabric (dishes) is present, but difficult to recognise in outcrop.	Rapid deposition or en-masse freezing of unsorted clean sand dropped out of suspension from the turbulent section a relatively high density turbidity current (HDT). The basal flow boundary is dominated by grain interactions and/or hindered settling. Equivalent to Bouma Ta (Bouma, 1962). The presence of groove marks may indicate deposition from a traction-dominated flow under high sediment load fall-out rates, probably during the upper stage flow regime.
Sand	Sand-rich	Parallel laminated	SLa	Sub-horizontal parallel laminae (<3 mm) occurring in moderately to poorly sorted, medium- to fine-grained thin sand intervals (<15-20 cm). Sometimes detrital clay is concentrated along darker planar laminations. Grading is subtle or absent. This facies is only present within thicker sandstone beds (>50 cm) and at times it substitutes the structureless sand interval.	Deposition from steady traction-dominated flow-boundary beneath a dilute and turbulent current. Equivalent to Bouma Tb (Bouma, 1962).
Sand		Wavy laminated	SWa	Relatively thick (1-2 mm) wavy to sinusoidal laminae occurring in poorly sorted, medium- to fine-grained sandstones exhibiting weak grading. Low-angle wavy surface or truncations, usually overlying parallel laminated intervals. Convolutions and fluid escape features (pillar structures and pipes) are common.	Deposition from a traction-dominated flow-boundary zone where the current was sufficiently dilute to form bed forms as dune-scale cross-lamination (Ricci Lucchi and Valmori, 1980). The high water content and the continue deposition may be responsible for the pervasive convolutions due to vertical fluid escaping.
Sand		Ripple laminated	SRI	Fine-, very fine-grained sandstones to coarse siltstone, moderately sorted with thin sets of rippled laminae (<2 mm) making up relatively thin intervals (2-20 cm). These can be climbing ripples, mainly in thick sandstone beds (>50 cm). Sets of ripples are used to measure palaeoflow direction. Subtle grading is observed at the passage to the upper interval.	The ripple-laminated division is thought to represent the waning tail of low-density turbidity currents. Complex ripple laminae internal structures suggest highly unsteady conditions during the waning stage of the flow (Mutti et al., 2002). Equivalent to Bouma Tc (Bouma, 1962).
Silt	Silt-rich	Debritic siltstone	Deb	Light-grey to light-green, to yellowish well-mixed matrix of fine- to very fine-grained sands floating into a muddy siltstone matrix. Occasional misleading matrix with high sand content, similar to massive sands. Usually the lower contact is irregular, overlying muddy siltstone intervals, whereas the top is normally flat, overlaid by very thin clean rippled sandstones (0.5-3 cm). <i>Ophiomorpha</i> -type burrows are abundant.	These deposits may invoke a double interpretation, difficult to resolve in outcrop. The mud-silt matrix may be the product of i) debris flow, characterised by en-masse deposition from highly concentrated and viscous sediment-fluid dispersions. ii) The complete mixing of fine- to very fine-sand grains into the matrix may also be associated to pervasive and intense bioturbation (Uchman, 1995)
Silt		Clean siltstone	SiC	Graded interval of either finely horizontally-laminated or structureless siltstone usually occurring between very-fine sand and mud in the upper portion of sandstone beds, with gradual grading at its upper contact. Often contains millimetre-sized platelets of mica.	Deposition from i) traction-dominated flow boundary zone beneath a dilute and turbulent current, or from ii) suspension fall-out under waning conditions; equivalent to Bouma Td (Bouma, 1962).
Mud	Mudstone	Darker mudstone (clastic)	MDa	Dark grey colour shales, devoid of structures or grading that break into thin chips with roughly parallel tops and bottoms, characterised by the presence of distinct sub-vertical <i>Ophiomorpha</i> -type burrows. Siliciclastic composition.	Suspension fall-out from a static or slow-moving mud cloud, probably involving a fluid mud layer. Final deposition from a sediment gravity flow event. Equivalent to Bouma Te division (Bouma, 1962).
Mud		Lighter mudstone (marl)	MCa	Light grey, bluish, massive, speckled appearance that break into blocky pieces. Calcareous composition.	These mudstones may be interpreted in three different ways: they could represent: i) the settling of suspension clouds produced by fading turbidity currents ("hemiturbidites" <i>sensu</i> Stow and Wetzel, 1990); ii) muddy contourites deposited from semipermanent bottom currents flowing parallel to the basin axis (Dall'Olio et al., 2013); iii) the settling of hemipelagic particles from the overlying water column.

Table 7.2 – Facies scheme used in the study of the succession above the Casaglia MTD.





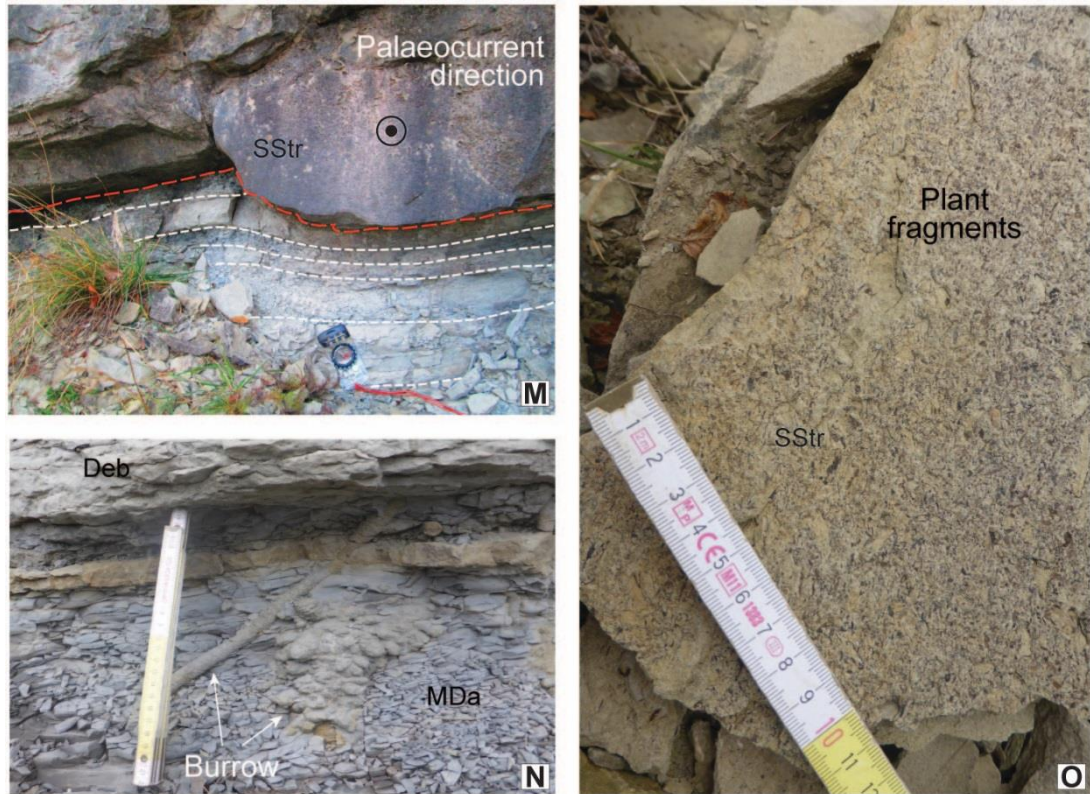


Fig. 7.6 – Example of lithofacies defined in Table 7.2. Folding wooden ruler (23.8 cm long), compass (10 cm long), hammer (28 cm long), hand lens (3 cm) and lens cap (5 cm) for scale. A-F) Sand-rich sandstones lithofacies; G-I) Silt-rich lithofacies; J-L) mud-rich lithofacies. Vertical sequence of structureless, planar parallel-laminated and wavy-laminated intervals characterising medium-thick (>50 cm) graded sandstone beds (A). Sole marks (e.g., flute and groove marks) often recognised on the bases of these medium-thick sandstone beds (B). Sometimes the basal clean and structureless sand interval may be absent and substituted by parallel laminated- (C) and wavy-laminated sands (D) with the latter that can reach the size of dunes. Convolutions are mainly developed within wavy-laminated intervals, where fluid escapes are also recognised (E). Ripples (and rare climbing ripples) are commonly recognised on top of wavy-laminated sands, but sometimes are also sandwiched between parallel- and wavy-laminated sand intervals (F). G-I) Silt-rich divisions can be found either on top of sandstone intervals as part of a normally graded bed, or as stand-alone event beds. Debritic siltstones are often recognised on top of sandstone beds, or interleaved with clean siltstones (H). Sometimes, debritic intervals may be also identified as part of tripartite beds (<20 cm thick), on top of basal structureless, wavy-laminated and frequently convoluted sandstones, and massive dark (rarely calcareous) mudstone intervals (G). The surface between dark mudstones and debritic siltstones is commonly irregular (I). Light-greyish massive calcareous mudstone intervals are generally thick (<50 cm). Silt-rich divisions can sometimes be substituted by dark mudstones (J). J-L) Mud-rich divisions. Typical thin-bedded section composed of very thin sandstones (>2 cm), relatively dark coloured mudstones and lighter coloured calcareous mudstones (L). Shallow elongated scours filled by structureless sands are typically at the base of thick (>50 cm) event beds that can deform underlying thin-bedded package (M). Bioturbation is common in mudstone intervals, with long burrows usually developed vertically or obliquely connecting different sandstone beds (N). Plant fragments, when present, are usually concentrated along distinct planar surfaces, in the lower portion of thick sandstone beds (O).

7.4.5 Palaeocurrent data

Flute, ripple, and tool mark orientations were collected to reconstruct palaeocurrents and are indicated on the sedimentological logs (Fig. 7.12 - see Appendix D). The palaeocurrent measurements were taken after visual restoration to correct for the structural orientation of bedding (around 20 degrees). The data collected in the field were then analysed for three stratigraphic intervals (T1; T2; T3 – see section 7.6.1)

From a general point of view, palaeocurrent directions are consistent with those reported in the earlier published literature (Ricci Lucchi and Valmori, 1980; Amy and Talling, 2006; Amy and Talling, 2007; Talling et al., 2007a; Tagliaferri and Tinterri, 2016). However, significant variations in mean palaeocurrent direction are observed between the four sectors identified for this work. Within interval T1, mean palaeocurrent directions in the Campanara sector (furthest from MTD source) have a more easterly orientation, with values ranging between N 105° and N 110°, whereas palaeocurrents in the intermediate Sambuca sector appear deviated by 30° to the south, with values of approximately N 140°, mainly measured on flute and groove marks. Ripples show a N 035° direction, which might represent flow reflection (Tinterri, 2011; Tinterri et al., 2016), likely due to the underlying MTD topography. Mean palaeocurrent directions in the sectors closer to the MTD source (Casaglia and Bibbiana) have again a more easterly orientation, with values of N 115°. However, flutes, but mainly current ripple lamination, show a wider range of palaeoflow directions and variations in palaeocurrent directions within a single bed at a single outcrop location have also been documented.

Within interval T2, mean palaeocurrent directions from the different sectors show less variation, ranging between N 125° and N 130° in the distal Campanara and proximal Bibbiana sector, respectively. However, slightly deviated palaeocurrent directions are still measured in the intermediate Sambuca sector.

The analysis of interval T3 palaeocurrents is difficult, due to the very different number of measurements for each log, given their different length (not all logs reach the same upper stratigraphic level). However, a preliminary analysis suggests the presence of a large-scale deflection in the early flows which seems to be less significant within the T3 interval.

7.5 MTD character

MTDs usually can be divided into a proximal extensional zone (detachment) at the head and a contractional zone (accumulation) at the toe, separated by a translational zone (Fig. 7.7). In the case of the Casaglia MTD the extensional head zone is not preserved. The outcrop includes a contractional ramp zone, characterised by a system of duplex, thrusts, and folds, followed by a zone of sediment transfer, where layer parallel gliding is observed, and by the distal toe portion of the MTD where material accumulated (Lucente and Pini, 2003; Fig. 7.7).

The Casaglia MTD has an irregular wedge shape caused by the presence of an additional contractional ramp zone in the Casaglia sector, below a large olistostrome (Fig. 7.8) which was responsible for the displacement of slide material leading to the formation of antiformal duplexes and steeply inclined folds; in fact, in this area, the ramp is recognised to cut off over 200 metres of footwall strata across 2 km, building up to 300 m of MTD thickness (Lucente and Pini, 2003). In the less proximal Bibbiana sector (in comparison to the Casaglia sector which is considered the most proximal area), on the northern side of the contractional ramp zone, the MTD reaches 250 metres in thickness. This thickness decreases significantly through the intermediate Sambuca sector and the MTD thins out to approximately 20 metres in the most distal Campanara sector.

7.5.1 Casaglia sector (Sector A)

The outcrops in the Casaglia sector show exposures of the olistostrome, consisting of deformed Subligurian calcareous shelfal and basinal sediments, (Fig. 7.8-A) which were deposited updip against the remobilised “basin plain” material pushed by the emplacement of the olistostrome itself. The olistostrome is highly folded and cut by a large number of faults, some of which cut the bedding at an angle, and some of which are bedding parallel (Fig. 7.8-B). It exhibits an increasing topographic relief to the E-NE (Lucente and Pini, 2003), creating topographic lows updip of it, on which mudstones are interpreted to have been ponded, but without completely filling the topography (Walker, 2008). Cleavage is present along the slide surfaces that are welded (no fill) or have highly boudinaged sandstones lining them (slide horizon) (Dykstra et al., 2006).

7.5.2 Bibbiana sector (Sector B)

The internal MTD character observed in the Bibbiana sector (Fig. 7.9) shows that probably the greatest amount of strain was accommodated in this area (Lucente, 2002), although a fair amount of slip must also have occurred in the external zone

(Lucente and Pini, 2003). The outcrops in this sector expose a succession of tilted and folded beds underneath large, gently folded, internally coherent slide blocks (Fig. 7.9-C-D). The transport direction for the rafted blocks and the underlying deformed sandstones was approximately toward NE.

7.5.3 Sambuca sector (Sector C)

A series of outcrops in the Sambuca sector allow a good transect through the entire thickness of the Casaglia MTD in the intermediate sector (Fig. 7.10). Compression dominates in the lower part of the MTD (Fig. 7.10-C-D), while extension dominates the upper portion, although compression is locally present underneath extensional sheets and blocks. Strata are commonly coherently deformed (Fig. 7.10-B) in slide sheets, between which zones of deformation are present (Fig. 7.10-D), showing that the deformation was localised along discrete zones, and was not penetrative (Dykstra et al., 2006).

Campanara sector (Sector D)

The Campanara sector is interpreted to correspond to the distal accumulation area of the Casaglia MTD (Fig. 7.11), although this area seems dominantly extensional, characterised by vertical thinning and horizontal stretching by listric normal faults and boudinage structures (Fig. 7.11-B). The outcrops consist primarily of remobilised “slope” sediments, which are much finer-grained overall than the ‘basin plain’ sediments observed in the proximal and intermediate areas (Bibbiana, Sambuca), although some basin-plain sediments are still present in the basal portion of the MTD. Cleavage is extensively recognised in the facies making up the MTD in this area and this is interpreted to be a function of the predominant clay-rich facies (Dykstra et al., 2006) (Figs. 7.11-C).

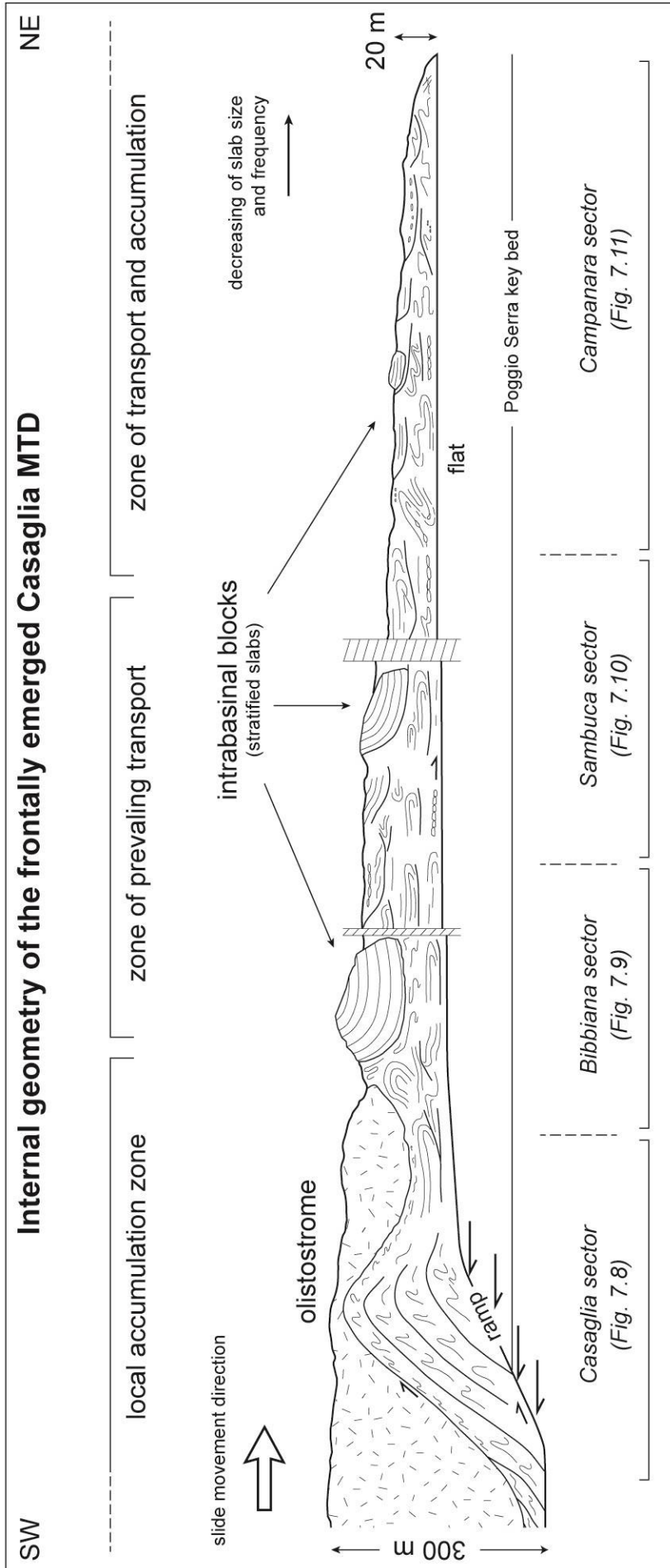


Fig. 7.7 – Idealised cross-section of the Casaglia MTD, parallel to the SE-NW direction of the mass-failure movement, showing the external geometry (irregular upper surface) and internal distribution of structures based on Lucente and Pini (2003) and adapted to the field observations in the investigated sectors. The sketch outlines the idealised segments (Casaglia, Bibbiana, Sambuca, Campanara) used to differentiate portions of the MTD based on overall geometry, type and distribution of structures and showed bellows (modified from Lucente and Pini, 2003).

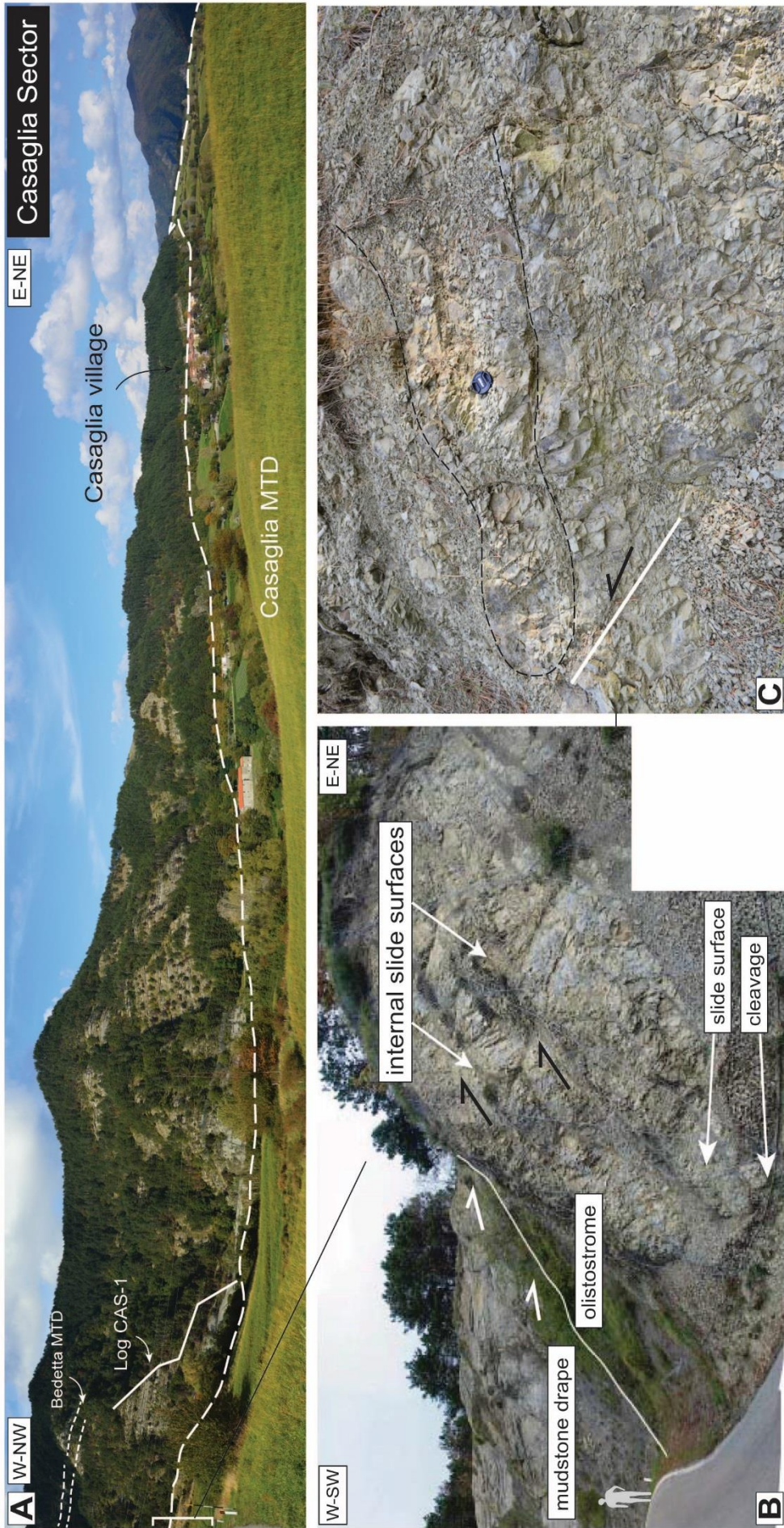


Fig. 7.8 – A) Photomosaic of the Casaglia MTD near the Casaglia village, characterised by the presence of the olistostrome overlain by a mudstone drape (shown by the onlap arrows). The internal slide surfaces exhibit thrust-type displacement. Cleavage is common in the bedding above and below the slide surfaces (photo by Dykstra, 2005c). C) Close up of a portion of the olistolith made up of calcareous material, likely derived by the Ligurian Nappe.

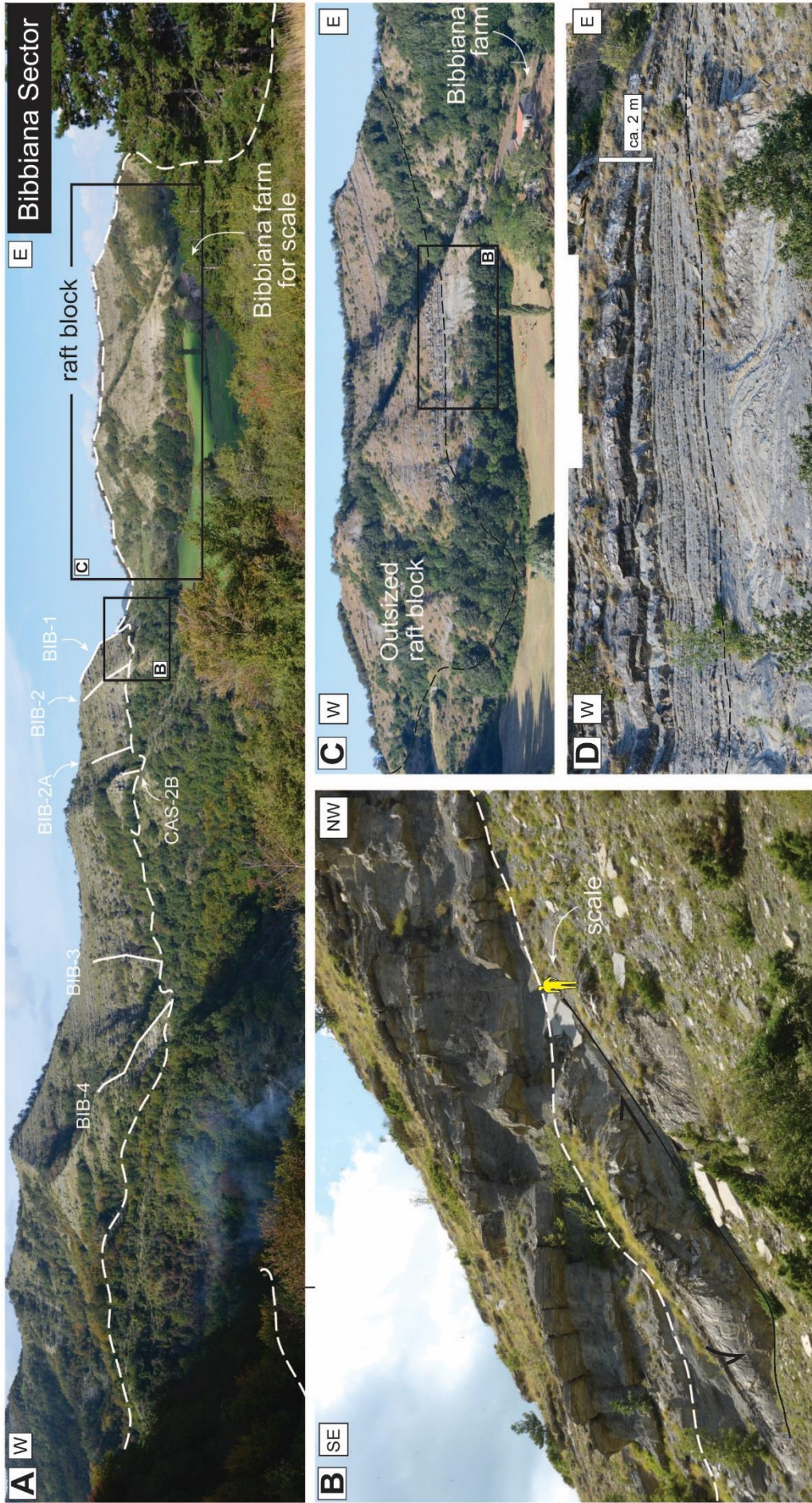


Fig. 7.9 – A) Overview of the outcrops in the Bibbiana sector, showing some of the major elements. B) Large fault-propagation fold overlying a thrust fault near the top of the MTD. This overlies the steepest part of the ramp (Fig. 7.6), where the largest compressional forces would be expected. The fold was created during the original movement of the mass-failure, the compressional orientation of which is shown by the arrows. C) View of an outsized rafted block. D) View from just below the rafted block showing the internal bedding. It comprised the accommodation horizon for movement of the overlying rafted block.

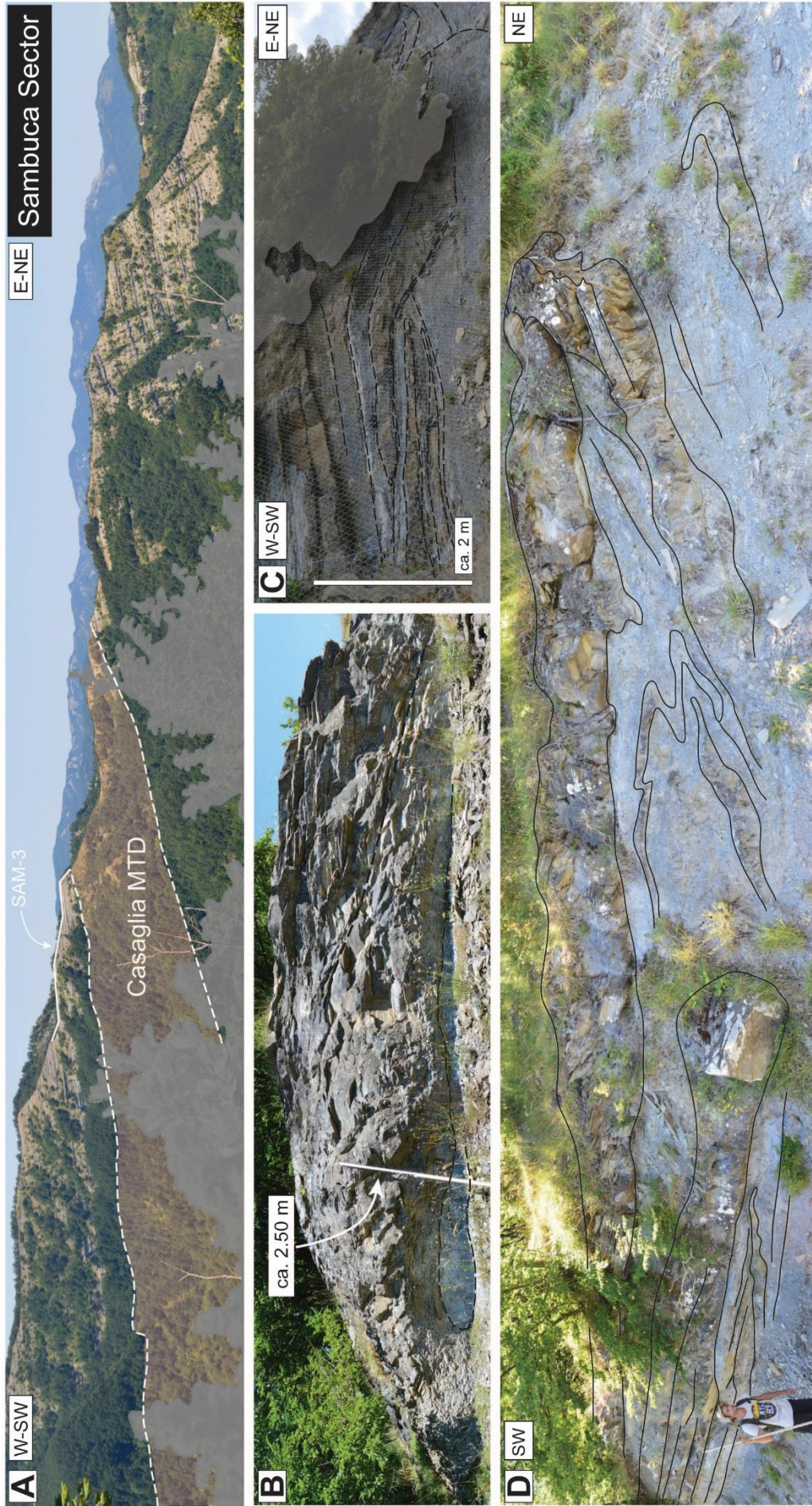


Fig. 7.10 – A) Photomosaic of the top and base of the Casaglia MTD in the Sambuca sector. B) Large remobilised basin plain deposits ripped up by the mass-failure due to the olistostrome emplacement. C) Road cut showing extensional bed thinning and stacking toward the direction of transport. Unfortunately the outcrop is covered by rockfall net barrier. D) Multiple thrust faults and sand injections within the MTD.



Fig. 7.11 – A) Photomosaic of the Campanara outcrops. B) Remobilised fine-grained “slope” sediments consisting of folded muddy succession with rare sandstones thin beds. C) Close up of the folds and boudinage structures characterising the area (Jacob’s staff is 2.1 m long).

7.6 Reconstruction of the topography left by the Casaglia MTD

The topography of the Casaglia MTD, defined as the relative elevation of features on the MTD surface, has been reconstructed using a number of key stratigraphic horizons which aided correlation of the 18 sedimentary logs measured above the MTD. These horizons are:

- The top of the Casaglia MTD;
- The uppermost identified event bed that can be traced across the four sectors of the study area (Bed 544 Muzzi Magalhaes and Tinterri, 2010);
- The base of the Bedetta MTD (a younger MTD above the Casaglia MTD).

One of the main issues in correlating the stratigraphic succession overlying the Casaglia MTD is related to its limited continuous vertical exposure. The recent landscape, made of alternations of cliffs, gullies and flat steps can make outcrops sometimes inaccessible, especially above the top of the MTD. Muzzi Magalhaes and Tinterri (2010) (see also Muzzi Magalhaes, 2009 and Tinterri and Muzzi Magalhaes, 2011) presented a stratigraphic framework of the Langhian to Serravallian portion of the Marnoso-arenacea (~250 metres), which includes the area and the stratigraphic interval described in this Chapter. However, their main focus was the syn-sedimentary tectonic control on the Marnoso-arenacea deposition. In contrast, the work presented in this Chapter focussed on a more accurate reconstruction of the rugosity of the top of the Casaglia MTD. Therefore, shorter sedimentary logs (~60 metres) were measured, but logging was performed at a very high resolution using a high precision Jacob's staff (Patacci, 2016).

The uppermost event bed that can be identified and correlated within the investigated interval is used to correlate the Bibbiana, Sambuca and Campanara sectors. However, this event cannot be recognised in the Casaglia sector due to the presence of a topographic high (Walker, 2008) that separates the Casaglia sector from the other sectors. In order to address this problem the base of the younger Bedetta MTD is used as the stratigraphic datum for flattening the Casaglia and Bibbiana sectors obtaining a continuous correlation panel for the study area. This solution is reliable given that the Bedetta MTD is characterised by only limited thickness variations and in the study area can be considered as a tabular feature (geological map of the area at 1:10,000 - Regione Emilia Romagna Geological, 1994).

In addition, the upper surface of the Casaglia MTD was locally mapped in the field with the use of a GPS where the contact between the MTD and the overlying sandstone succession was accessible.

7.6.1 Log correlation panel

The correlation panel is built upon the eighteen sedimentary logs across the four identified sectors, forming two hinged orthogonal transects, 2.5 km and 9 km long. The shorter transect is oriented W-E and correlates logs from Casaglia (CAS-1 and CAS-2) to the southernmost log in Bibbiana sector (BIB-4). The longer transect is oriented SE-NW and it correlates the logs from the Bibbiana, Sambuca and Campanara sector (Fig. 7.12) along the main transport direction of the Casaglia mass-failure event. This also represents the main turbidite transport direction, albeit the flows travelled in the opposite direction, from the north towards the south.

Logs were correlated first by establishing correlation of the main stratigraphic markers, then individual turbidite beds were correlated based on empirical matching of bedding patterns. Furthermore, for a better identification of the correlated beds, these were also numbered following the larger scale Muzzi Magalhaes and Tinterri (2010) bed correlation of the Langhian to Serravallian portion of the Marnoso-arenacea which includes the Casaglia MTD and related overlying deposits of the Fiorenzuola system (Unit Va - Tagliaferri and Tinterri, 2016).

Bed 544 of Muzzi Magalhaes and Tinterri (2010) was identified and used to correlate the 16 logs of the SE-NW 9 km long transect. In the Bibbiana sector many of the intervening beds have been traced and walked-out between the measured logs, in order to correlate beds as thin as 5 cm with confidence and hence, obtain more accurate information on the irregular top of the MTD. In fact, early sandstone beds deposited in different but adjacent topographic lows are difficult to correlate (e.g., because they pinch-out against the MTD) and it is therefore difficult to establish if they represent deposits of the same flow or if they represent different event beds. In this area bedding patterns indicative of stratigraphic growth are recognised at the scale of the correlation panel (Fig. 7.12) and in the field at the outcrop scale.

Both transects of the main correlation panel were subdivided into three vertical intervals (T1, T2, T3) defined by marker beds, to better characterise variation in thickness across the stratigraphy overlying the MTD (Fig. 7.12). In the SE-NW transect, T1 represents the interval immediately above the upper surface of the MTD during whose deposition most of topography along this transect seems to be healed by turbidite deposition. In the Casaglia sector, the T1 represents a mainly muddy succession that passes into a sand prone succession during the T2.

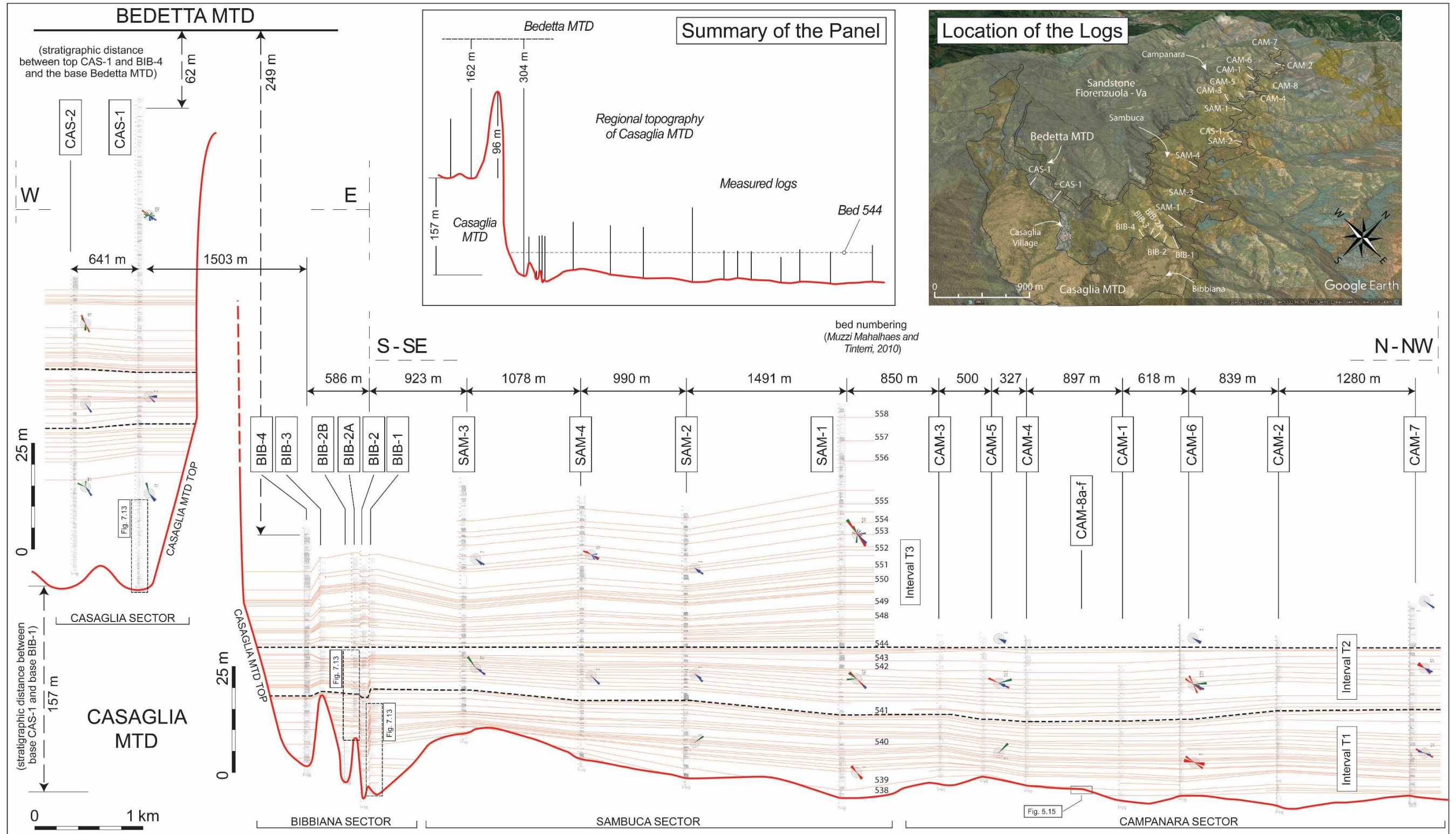


Fig. 7.12 – Stratigraphic correlation panels of sedimentary logs of the sandstones overlying the Casaglia MTD showing the spatial and vertical distribution of sandstone character (a high resolution version of this panel is provided as Appendix D). The small box illustrates the actual relationship between different sectors (not in scale in the main panel). Location of the measured sections is shown on the digital elevation model of the study area.

7.6.2 Scales of topographic rugosity left by MTDs

In many subsurface and field examples, the magnitude of surface rugosity is commonly associated with the sizes of the rafted blocks incorporated and transported by large-scale mass-failures (e.g., Moscardelli et al., 2006; Armitage et al., 2009).

The Casaglia MTD upper surface is characterised by an irregular geometry arising from local muddy mounds and rafted blocks and highlighted by the overlying, onlapping sandstone units (see Section 7.7.1). The scale of the morphological features building up the rugosity of the top of the Casaglia MTD can be considered in the framework of the three morphological tiers recognised by Armitage et al. (2009) in the Upper Cretaceous Tres Pasos Fm., southern Chile. These tiers are defined by the maximum values of the vertical (y) and the horizontal (x) dimensions of the topography relative to local elevation and each tier of the hierarchy is distinguished from the next by approximately one order of magnitude difference in both dimensions.

In the Casaglia MTD similar rugosity scales can be observed:

- subtle topography (y=1-5 m; x=10-25 m): identified in several outcrops across the intermediate Sambuca and distal Campanara sector (Figs. 7.14, 7.15) is ascribed to the presence of a thin linked cohesive debris flow recognised on top of the MTD;
- jagged topography (y=5-30 m; x=50-100 m) observed in the Bibbiana sector (Figs. 7.13) is a result of rafted sandstone blocks near or at the top of the chaotic deposits;
- large-scale topography (y=>30 m; x=500-1000 m) recognised between the Casaglia and Bibbiana sectors (Fig. 7.12), it is interpreted to be the result of the large scale architecture of the MTD, such as the presence of outsized rafted blocks and olistrostromes.

7.7 Turbidite character above the different scales of MTD-related topography

The turbidite systems of the Marnoso-arenacea Fm. are characterised by a significant tectonic control shaping the basin topography and resulting in characteristic facies trends and architectures (Muzzi Magalhaes and Tinterri, 2010; Tinterri et al., 2016 and Tagliaferri and Tinterri, 2016). However, the influence of the emplacement of large MTDs associated with this tectonic activity on the sandstone facies and architecture has not been studied in detail. As described in the previous section, the upper surface of the Casaglia MTD shows different scales of topographic rugosity, consisting of topographic lows and positive relief (Fig. 7.12). The topographic effects associated with the rugose upper surface of the MTD are investigated in this section by providing a sedimentological description and interpretation of the turbidite sandstones deposited above different topographic features, in terms of the large-scale healing character and small-scale bed geometry terminations. However, differentiating and quantifying the extent to which sediment gravity flows are influenced by the MTD-related topography from the effect of tectonics, basin morphology or autogenic factors is difficult. In this work a further detailed analysis on the sandstone character juxtaposed with the Casaglia MTD is attempted.

7.7.1 100s metres scale rugosity and sandstone infill (large-scale topography)

At the large scale, sand deposited above different morphological features of the Casaglia MTD show distinctive depositional styles that differ in terms of facies distributions and net-to-gross ratio. Three stratigraphic logs of the first 15 metres overlying the MTD were selected in the Casaglia (CAS-1) and Bibbiana sectors (BIB-1 and BIB-2A) to show the early topographic healing character in different locations above the MTD.

Topographically, the CAS-1 log is located at the west side of the 150 metres relief identified behind the Casaglia Village (Walker, 2008), and 1500 metres west of BIB-1 and BIB-2A. The latter logs are about 130 metres apart, with the log BIB-1 located in a topographic low compared with the log BIB-2A that sits over a mounded topography, ~15 metres above the base of log BIB-1 (see the topographic reconstruction in Fig. 7.12). These two logs can also be correlated, with Bed 538 (of Muzzi Magalhaes and Tinterri 2010) representing the uppermost and lowermost bed of the investigated logs BIB-1 and BIB-2A, respectively (Fig. 7.13).

When compared, the three logs show different amounts of fine-grained sediments, ranging from the muddy stratigraphy of CAS-1 (low net-to-gross), to the moderately sandier BIB-1 (medium net-to-gross), to the sandy BIB-2A (high net-to-gross).

The fine-grained CAS-1 log (Fig. 7.13-A) consists of a monotonous alternation of thin (~1 cm) layers of clastic or calcareous mud separating thicker “debrite” layers (~5-30 cm thick). The “debrites” comprise a well-mixed matrix of sand grains floating in a muddy siltstone (see Table 7.2) and are often highly bioturbated by the widespread presence of Ophiomorpha-type burrows (Uchman, 1995; Tinterri and Tagliaferri, 2015), especially in the lower ~6 metres of the investigated interval. Rare, thin sandstone beds (0.5-2 cm) are also present, mainly characterised by wavy-ripple laminations and occasionally with weakly erosive base. About 9 metres above the base of the log, a slumped horizon made up of deformed and folded thin bedded sandstones can be observed, followed by a ~40 cm fine-grained sandstone bed.

In the Bibbiana sector, both BIB-1 and BIB-2A logs are generally sandier than the one in the Casaglia Sector, however these logs slightly differ between each other in terms of sand proportion and mud cap character of the thicker sandstone beds (Fig. 7.13-B-C). Some 70% of the mud-rich intervals in BIB-1 (Fig. 7.13-B), which generally range between 50 and 100 cm, overlying medium-thick sandstone beds (80-100 cm), are mainly composed of clean dark mudstone, and for the remaining 30% by calcareous mudstones. On the other hand, BIB-2A log (Fig. 7.13-C) is characterised by clean mudstone caps rarely distinguishable from the more calcareous intervals and generally represents an overall statistically smaller percentage in comparison with BIB-1.

Silt-rich layers can be made of pure siltstone or including dispersed sand grains (“debritic” character) and they represent a relatively small proportion of the investigated BIB-1 log, with intense bioturbation only recognised in the intervals of the upper part of the same log, mainly within the debritic layers. In BIB-2A, silt-rich debritic intervals replace the clean siltstone layers and mud-caps that characterise the BIB-1 log, directly overlying both thin (0.5-2 cm) and medium-thick sandstone beds (5-100cm).

In both investigated portions of BIB-1 and BIB-2A logs, thicker sandstone beds are characterised by parallel to wavy lamination, while the thinner ones by cross ripple lamination. Wavy-laminated sandstones often include highly convoluted intervals. The substantial higher net-to-gross in the investigated BIB-2A (compared to BIB-1) represents an increase in the number of sandstone beds, which are overall thinner

but separated by thinner silt- and mud-rich intervals when compared with the sandstone events of BIB-1 (Fig. 7.13-B-C).

The three selected sedimentary logs described above document three styles of sandstone infill above different topographic features associated with the upper surface of the Casaglia MTD, and possibly providing three different examples of topographic control on the character of the sandstone deposits. The most significant difference in sedimentary architecture and facies distribution is observed comparing the muddy stratigraphy of CAS-1 in the Casaglia sector with the sandier successions BIB-1 and BIB-2 of the Bibbiana sector. The net-to-gross sandstone increases from 10% at CAS-1 to 33% and 60% at BIB-1 and BIB-2A respectively. Mean bed thickness increases from ~5 cm in CAS-1 to ~40 cm in BIB-2A and ~87 cm at BIB-1. However, while the change in mean bed thickness and net-to-gross between the section in the Casaglia sector and those in the Bibbiana sector is quite straightforward and linear, a significant discrepancy between the net-to-gross values and the mean beds thickness of the two investigated portions of Bibbiana logs is observed. In fact, net-to-gross ratio in BIB-2A is higher than the one calculated in BIB-1, although beds are overall thinner in the first log in comparison with the beds measured in the latter log. This is mainly explained by the thick mud caps overlying sandstone beds in BIB-1, which are not observed in BIB-2A. In the first case the deposition of thick mud caps might be associated with ponded or semi-ponded sedimentation (Haughton, 2000; Felletti, 2002; Southern et al., 2015), where the very dilute and fine-grained portion of the flow remains confined within the topographic pond (Kneller et al., 2016) favouring the deposition of fine particles. The thinner mud caps together with thinner sandstone beds measured in BIB-2A may be interpreted as a decrease in ponding control on turbidity flows (Sinclair and Tomasso, 2002; Marini et al., 2016b).

The above interpretation might be confirmed by the reconstructed topography of the Bibbiana sector, where the correlation of five sedimentary logs constrain the 10s of metres scale rugosity of the Casaglia MTD in this area, across a distance of approximately 580 metres. Based on this reconstruction, BIB-1 is located within a topographic low, whereas the investigated portion of BIB-2A sits over a mounded topography, approximately 15 metres above BIB-1. However, the presence of wavy-laminated sandstones as a common feature in both logs of the Bibbiana sector is interpreted to result from local confinement and focusing of flows by local topographic features (Tinterri, 2011; Tinterri et al., 2015), invoking the likely existence of other morphological features in the Bibbiana area, such as the mapped topographic high between the Casaglia and Bibbiana sectors (Walker, 2008). This latter structural feature might have induced the significant differences in stratigraphic architecture

between the Casaglia and Bibbiana sectors. In fact, the characteristic succession of CAS-1 may represent deposits of flow stripping resulting in deposition of thin and dirty sands by the part of the flow able to overcome the obstacle. Furthermore, the intense bioturbation recognised in these deposits also supports this hypothesis of a low-energy environment.

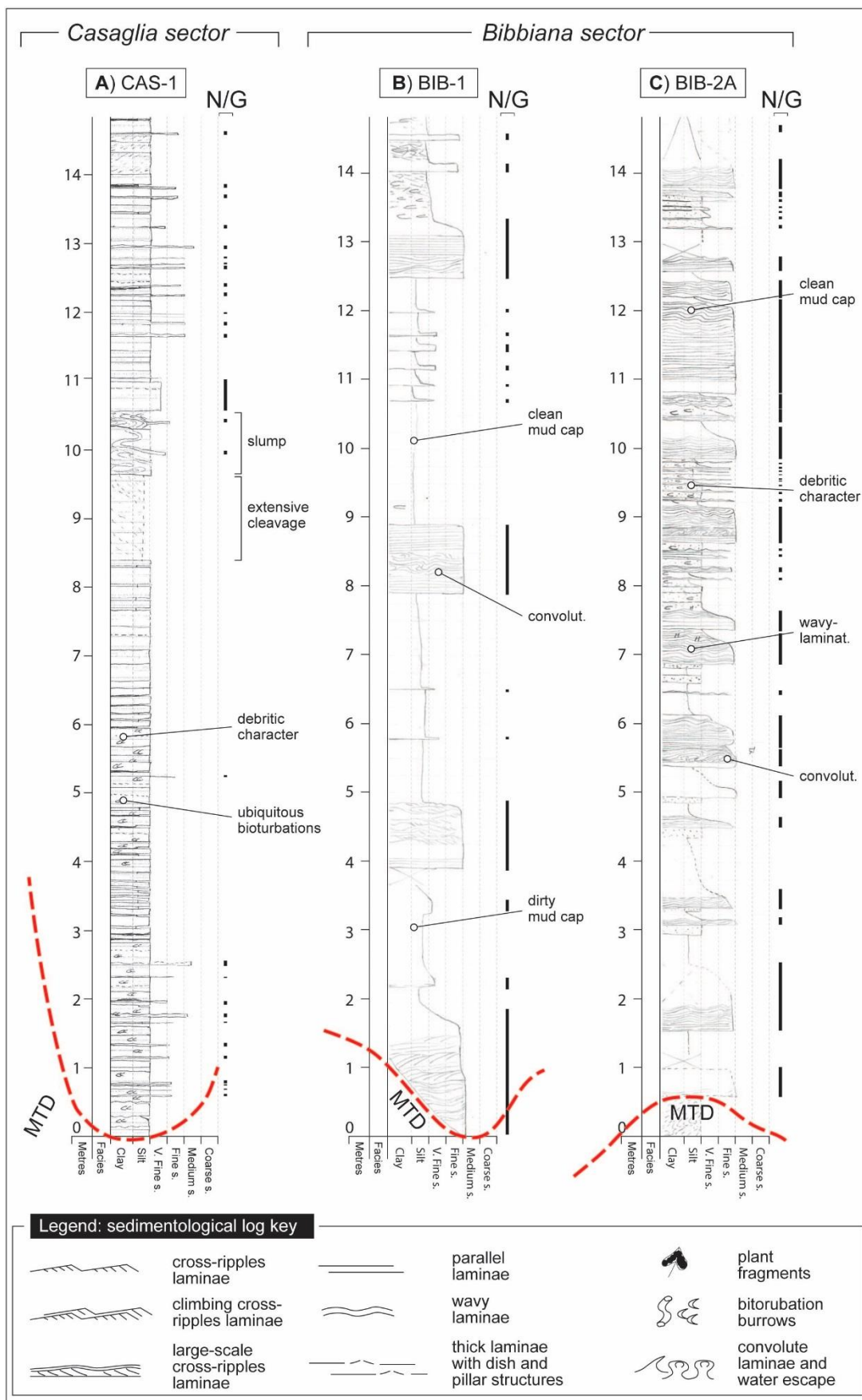


Fig. 7.13 – Sedimentary logs illustrating variability of the character of the deposits overlying the Casaglia MTD in different locations. Location of the logs is shown on the correlation panel (Fig. 5.12).

7.7.2 Sandstone geometries related to 10s metres scale rugosity (local topography)

The study of the relationship between small scale irregularities on top of the MTD and the first sandstone beds, in terms of facies variation and bed termination geometries (i.e. onlap, pinch-out, etc.) is important as this variability is usually under the minimum resolvable resolution of petroleum-industry seismic-reflection data (e.g., approximately 30 metres vertical, Armitage and Stright, 2010).

The Casaglia MTD allows direct observation of sandstone beds onlapping the topographic morphologies associated with the upper surface of the MTD. However, this is often possible only for limited portion of outcrops in comparison with the overall length of the deposits, due to the extent of vegetation and steepness of cliffs related to the highly erosive material that usually characterises muddy outcrops.

Three well exposed outcrops were selected in the Bibbiana, Sambuca and Campanara sectors (Figs. 7.14, 7.15) to undertake investigation of the influence of local topography on the overlying sandstones, characterising the geometrical features developed at the contact between the MTD and the sandstone beds. One outcrop is characterised in detail with six sedimentary logs (Fig. 7.14), while the other two are described with the aid of photo-panels (Fig. 7.15). In all three cases, outcrop sections are approximately oriented W-E, on south-facing slopes, where vegetation seems less dense in comparison with north facing slopes. This allows the observations of the rugosity along the W-E direction, but prevents description of any S-N features, parallel to the mass-failure emplacement direction (see Section 7.3). Palaeoflow direction is instead orthogonal to the outcrop orientation, aiding the description of lateral changes within the flow, but unfortunately preventing down-current observations.

7.7.2.1 Example I: Bibbiana outcrop

Terminations of strata in the Bibbiana outcrop (Fig. 7.14-A) are characterised by an abrupt contact of three sandstone beds between 1 and 2.5 metres thick against a topographic high. This mound measures ~40 and ~15 metres in horizontal and vertical dimensions respectively and it is made up of oversized blocks of folded medium- and thick-bedded turbidites ripped-up from the basin plain during the emplacement of the Casaglia mass-failure. It is overlain by a thin continuous layer of debritic calcareous mudstone. The sandstone beds (~1-1.5 m thick) are characterised by thick mudstone caps (~1 m) and by tractional structures, mainly parallel and wavy-laminations. The first two sandstone beds above the MTD can be recognised on both sides of the topographic high, whereas the third bed can be

traced across the mounded rugosity, with the sandstone thinning over the edge, but not the mud cap. Unfortunately, the limited lateral exposure of the top of the MTD in the Bibbiana sector prevent tracing sandstone beds over its irregular topography, which is shown by the correlation of relatively close sedimentary logs (BIB-1, BIB-2A, BIB-2B, BIB-3 and BIB-4), measured over an overall distance of ~580 metres.

7.7.2.2 Example II: Sambuca outcrop

A road cut outcrop located in proximity of SAM-1 log (see Fig. 7.12) provides another example of local topography developed over the Casaglia MTD (Fig. 7.14-B). In this case the topography is lower relief, with a mound measuring 20 and 2 metres, in horizontal and vertical dimensions, respectively. However, the orientation of the outcrop is slightly oblique to the mass-failure emplacement direction. The outcropping portion of the MTD is composed of folded and thrusting thin- to medium-sandstone beds packages, overlain by an irregular and discontinuous thin layer of debritic calcareous mudstone. Sandstone beds gently onlap onto the MTD, with the first three beds pinching-out over the highest portion of the recognised mounded topography. The basal bed is characterised by an irregular base and comprises dirty sand, rather than the usual clean sand.

7.7.2.3 Example III: Campanara outcrop

Six short sedimentary logs (4-8 metres each) were measured in the Campanara sector between logs CAM-4 and CAM-1 (Fig. 7.15 - CAM-8a,-b,-c,-d,-e,-f), across a distance of approximately 25 metres. The outcrop in the Campanara sector shows that the facies distribution seem to be controlled by the 25 metres horizontal and 5 metres vertical topography identified in this distal portion of the Casaglia MTD. The sandstone stratigraphy directly overlying the MTD is correlated across the length of the outcrop thanks to a 20 cm thick traction-structured sandstone bed. This is the first bed above the MTD with almost the same thickness measured in all the sedimentary logs, making it the first event where topographic control is not recognised at the outcrop scale. However, facies changes within this sandstone bed are observed. On the east side of the mounded topography it is characterised by convoluted and wavy laminations (CAM-8a,-b) which become parallel laminations over the topographic high (CAM-8c,-d,-e) before passing to a structureless, parallel, wavy and ripple laminated sands that are vertically organised within the same bed to the west of the high (CAM-8f). The stratigraphy below this local datum records abrupt changes in sandstone thicknesses and a high heterogeneity in facies distribution. The first two sandstone beds above the MTD show a pronounced thinning toward the mounded

topography, with the thicker one at the bottom climbing the slopes of the local topography, whereas the thinner one above pinching-out against the sandstone below. Furthermore, the lower sandstone is characterised by a clear partition of the structureless sands from the more traction-structured sands, respectively deposited on the west and east side of the high. Another difference between the two inferred topographic lows flanking the mounded topography is given by the different healing styles, characterised by sub-horizontal sandstone and siltstone deposits on the east side and by more drape-like sandstones followed by debritic intervals on the west. Considering that the turbidity flows are interpreted to travel perpendicular to the outcrop orientation, it is possible that the morphology of the rugose top outside of the plane of observation may have resulted in a different flow behaviour on each side of the mounded top.

Progressive differential compaction of the heterogeneous material incorporated within the MTD (Armitage et al., 2009; Alves, 2010), could also help explain the observed geometries that characterise the stratigraphy above the MTD. However, the two-dimensional section and the lack of additional evidence due to the limited lateral exposure of the outcrop make eventual topographic controls difficult to discriminate from intrinsic autogenic flow transformation.



Fig. 7.14 – A) Photomosaic showing sandstone bed onlap against the irregular top of the Casaglia MTD in the Bibbiana sector. B) Photomosaic of a road cut in the Sambuca sector showing subtle topography over the top of the MTD with beds pinching-out. (See Fig. 7.12 for locations).

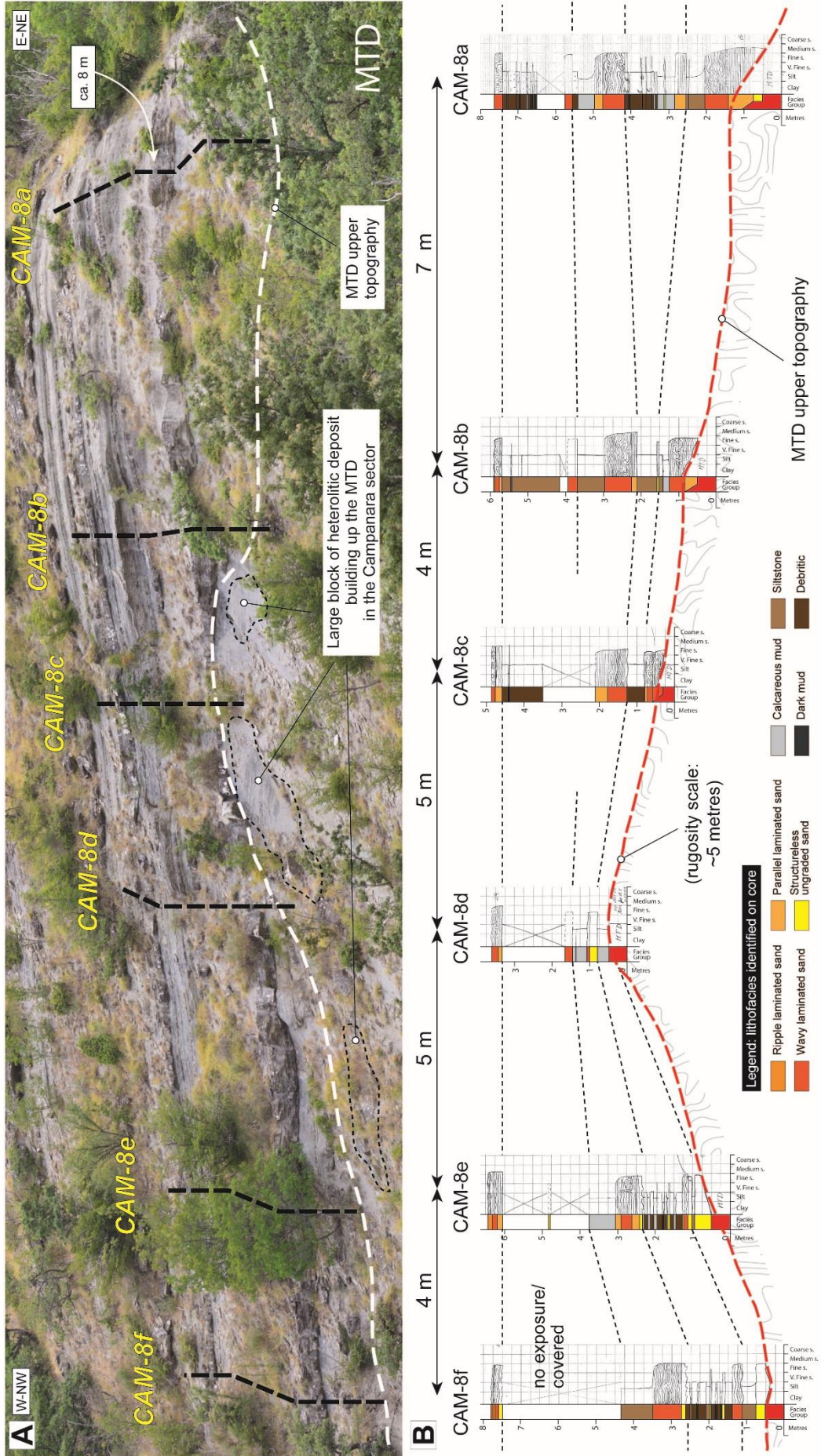


Fig. 7.15 – A) Small scale rugosity developed on the upper surface of the Casaglia MTD in the Campanara sector and location of measured sections. B) Correlation panel showing the pinching-out of sandstone beds against a 4 metres high mounded topography (see Fig. 7.12 for location).

7.7.3 Very small scale of rugosity (<1 m)

The smallest scale of rugosity identified on the Casaglia MTD top is made up of 10 cm deep and 40 cm wide depressions. This scale of rugosity is commonly observed across the four sectors of the study area. The physically walked-out MTD surface on accessible outcrops allowed observation of the compensation style of the first event that is commonly made by dirty structureless sands (Fig. 7.16-C), together with an undulating and likely non-erosive base (Fig. 7.16-B).

These dirty structureless sands are sometimes difficult to distinguish from the underlying debritic calcareous mudstone that usually blankets the MTD, making it hard to establish if the early sedimentary gravity flows had an erosive character. These geometries and bed character tend to be restricted to the first bed only, although some of the small scale topographic effects can be also noticed in the second bed (Fig. 7.16-D). Regular, "normal" sandstone deposition is restored by the immediately following event that compensates underlying deposit rugosity and recovers sub-horizontal depositional conditions. However, these flows may be successively controlled by the larger 10s of metres scale rugosity.

7.7.4 Loading

The contact between the upper surface of the Casaglia MTD and the first sandstone beds can also be characterised by the loading of turbidite sandstones into the underlying MTD, leading to sandstone thickness variations over short distances. These features are well documented in the more basinward outcrops of the Campanara sector. Domed sand bodies (~2 metres in depth) are observed intruded into the upper debritic calcareous layer blanketing the MTD (Fig. 7.17-A). The intrusion of the sandstones into the underlying MTD is marked by a concave-down shaped base combined with large (2 metres long) vertical muddy flame (Fig. 7.17-B). Loading features in this area are commonly characterised by the local thickening (Fig. 7.17-B) or thinning (Fig. 7.17-C) of the sandstones. These sands are usually traction-structured, with parallel and wavy laminations regularly preserved (Fig. 7.17-B).

Loading of turbidite sandstones into underlying MTDs are well documented in outcrop (Butler and McCaffrey, 2010; Van Der Merwe et al., 2011; de Leeuw, 2012) although interpretations can vary. Owen (2003) describes the loading as a process driven by a density contrast between sediment layers, while more recent studies (Butler and McCaffrey, 2010; Posamentier and Martinsen, 2011) showed that loading can also be driven by continued deformation of strata into which loading occurs, leading to the formation of sandstones with laminations that display a growth-fault geometry (Butler

and McCaffrey, 2010; Butler et al., 2015). These latter structures are not recognised in the study area leading to the interpretation of the described features as normal gravity driven load structures. This conclusion is also supported by the fact that loading is mainly observed over the distal portion of the Casaglia MTD (e.g., Casaglia sector), where the MTD is largely characterised by disaggregated muddy blocks which are blanketed by a debritic calcareous matrix layer, favouring loading mechanisms.

7.7.5 Growth strata

Spatial variations in thickness of the same stratigraphic interval across relatively short distances as shown in the Bibbiana and Campanara sectors (Fig. 7.16-A) may be attributed to stratigraphic growth caused by differential compaction rates in the Casaglia MTD during their deposition. These intervals are characterised by changes in total thickness without significant variation in the thickness of the turbidite sandstone beds (see Fig. 7.12). The overall change in thickness is related mainly to differences in thickness of the siltstones and mudstones. In order to establish if growth strata may have a control on the thickness or facies of subsequent turbidite deposits and causing flow confinement or ponding, further analysis is required. A relationship may exist between the development of growth intervals and the topographic framework of the Casaglia MTD. Areas of differential rates of MTD compaction and formation of growth intervals appear to be preferentially developed in the proximal sectors (Bibbiana and partially Sambuca).

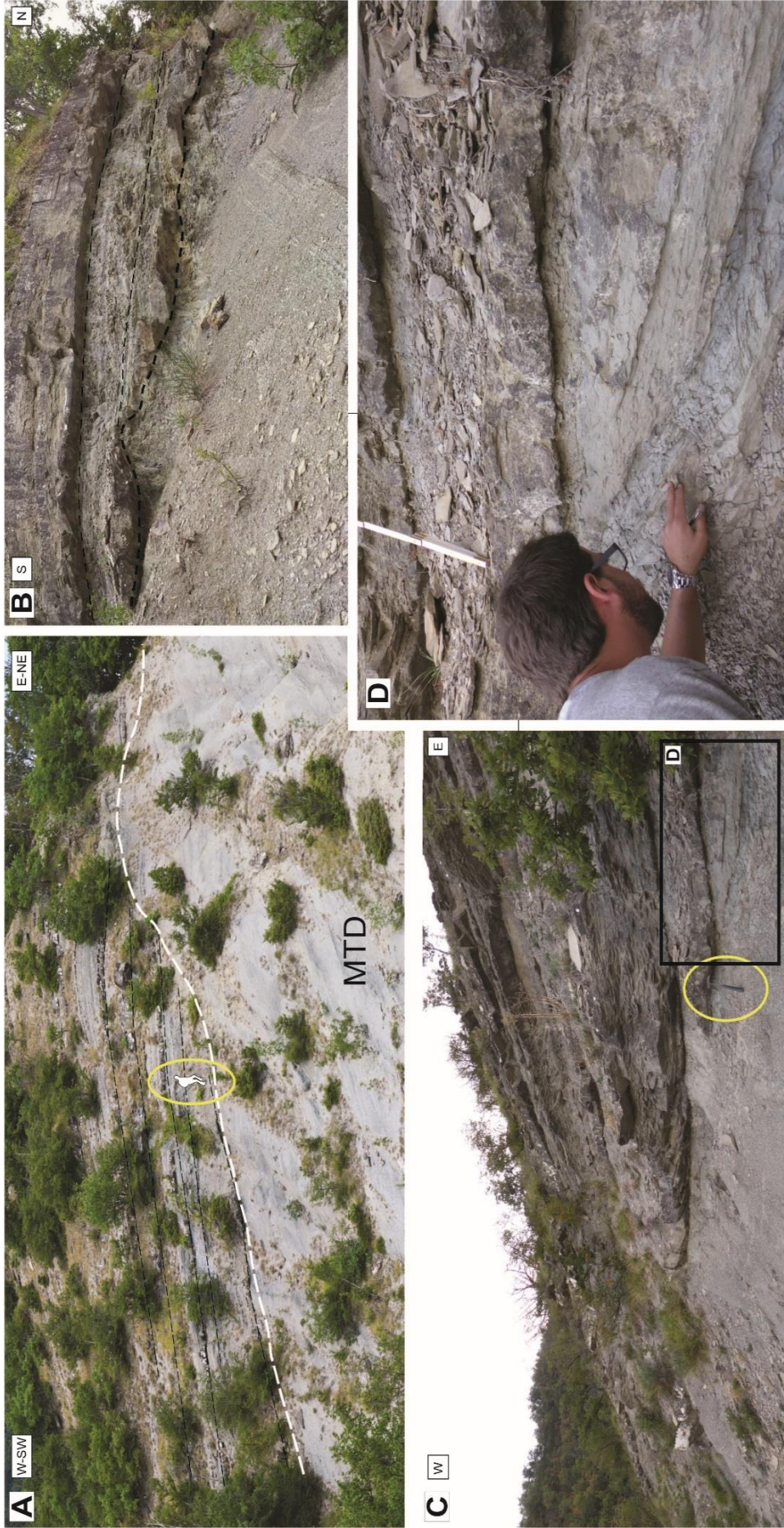


Fig. 7.16 – Outcrops of the MTD top in the Campanara sector. A) Irregular MTD top with beds onlapping the mounded topography. B) Irregular sandstone base characterised by dirty sands healing the very subtle rugosity ($y = \sim 0.5$ m; $x = 1$ m). C) Onlap and pinch-out bed geometries. D) Close-up of the dirty character of the first event bed onlapping the top surface of the MTD. The light greyish interval represents a calcareous layers that is interpreted to have blanketed the MTD after its emplacement on the basin floor. This layer is recognised in several other outcrops across the study area.

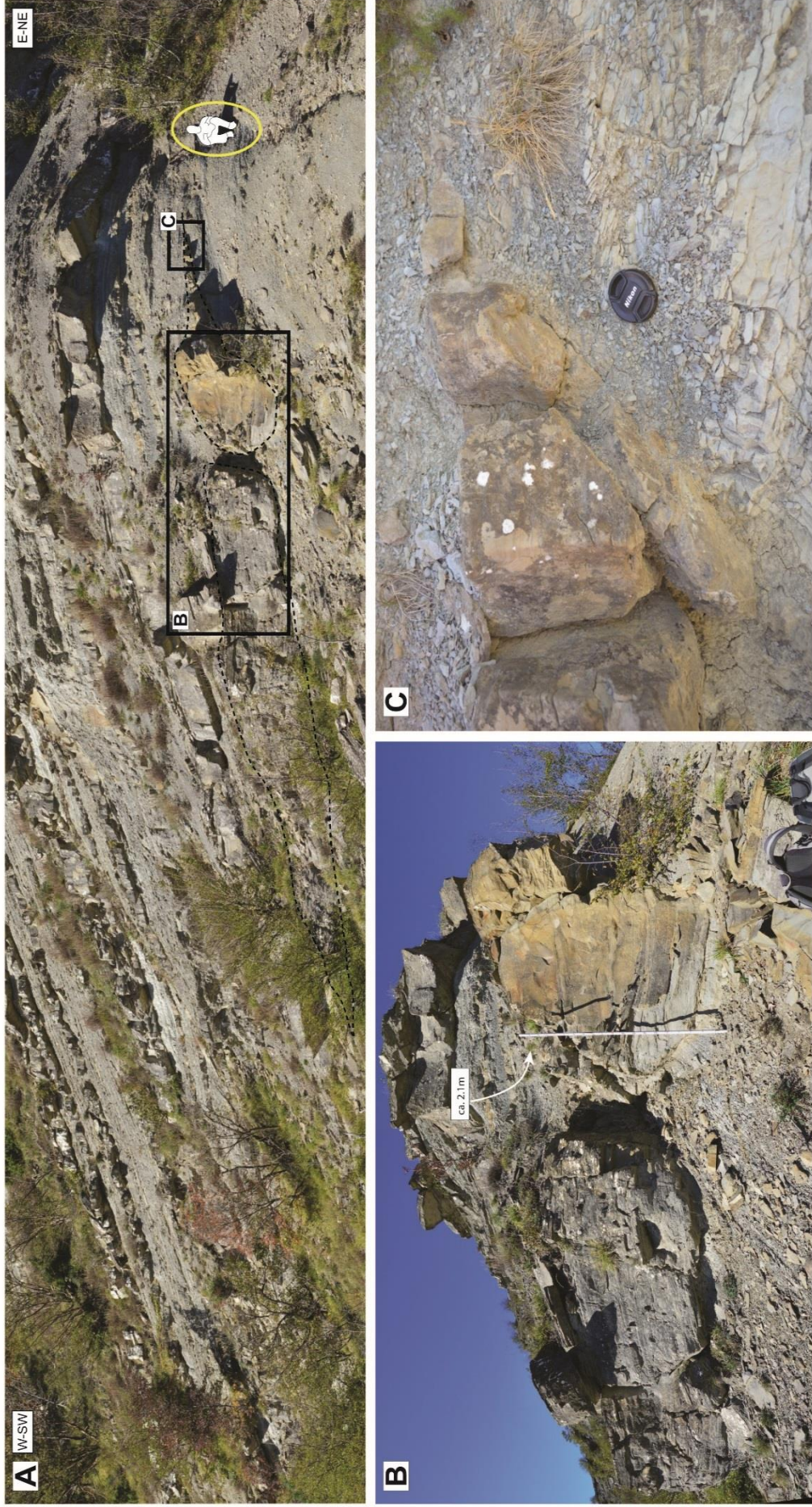


Fig. 7.17 – A) Top of the Casaglia MTD in the Campanara sector (CAM-2 – see Fig. 5.12 for location), characterised by metre-scale topography and by the presence of loading structures of the first sandstone bed above the MTD. B) Detail of loading of the first sandstone bed, with debritic material making up the MTD intruding into the sandstones. C) Close up of the loading termination with sand pinching-out against the top of the MTD.

7.8 Controls on turbidite character above MTD topography

The emplacement of the Casaglia MTD resulted in a substantial modification of the bathymetry of the basin plain over a large area. The Casaglia MTD formed a positive topographic feature on the seafloor upon which was superimposed local rugose topography relief resulting from internal complexity in the mass-failure deposit. A large diversity of deformational styles and resultant topographic profiles are observed in this area. The amount of local topographic relief exhibits a strong correlation with the type of internal material and deformation style of the MTD (Lucente and Pini, 2003). As introduced in section 7.5, the ramp zone (Bibbiana sector) is characterised by stacked thrusts and is more heavily deformed than the flat zone (Campanara sector). The size of rafted blocks of olistostrome, which may cause topographic variations on the upper surface of the MTD, is also greatest in the ramp zone and decreases toward the flat zone. In addition to forming topographic highs, olistoliths may also contribute to greater rates of compaction due to differential loading (Lucente and Pini, 2008).

The location of the study area with respect to the margin of the basin toward the orogen is an important consideration in the interpretation of the field data collected in this study. The headwall of the Casaglia MTD has not been preserved. However, previously published stratigraphic correlations in the interval below the Casaglia MTD (Lucente, 2004) provided estimations of the distance of the Casaglia MTD from the basin margin, showing that the portion of the MTD investigated in this work was located on the basin plain rather than immediately adjacent to the basin margin (Fig. 7.18). The recognised stratal terminations against the Casaglia MTD show similar characteristics to the bed thinning and terminations against other MTDs in the Marnoso-arenacea Basin (Tinterri and Tagliaferri, 2015). Tinterri and Tagliaferri (2015) show the effects of the emplacement of the Visignato MTD on turbidite deposition. However, they investigate the confinement control within a larger-scale syn-tectonic evolution, overlooking the possible small-scale controls that the MTD might have exerted on turbidite sedimentation.

The abrupt and instantaneous change of the seafloor bathymetry could have represented a dramatic impact on the flow pathways within the basin, with flows forced to adjust to the new basin floor morphology. Tinterri and Muzzi Magalhaes (2011) show that these flows were confined at the largest scale by the margins of the basin, however, the Casaglia MTD provided additional confining topography to the sediment gravity flows. Early flows were slightly deviated around the mounding MTD at the regional scale as shown by the comparison of palaeocurrent data for the

interval T1 at the Campanara and Bibbiana sectors. Smaller and more local topographic features (10s of metres scale) might have confined subsequent flows, changing their behaviour over a relatively short distance, as documented in section 7.7.2. It is difficult to draw conclusions about flow confinement and ponding in these areas without a three-dimensional morphological reconstruction of the structures in these sectors. More reliable conclusions may be deduced studying the vertical facies stacking patterns of the sandstones overlying the Casaglia MTD within the measured sedimentary logs. In fact, when limited portions of sedimentary logs sitting on different morphological features of the MTD are selected for comparison, significant differences in the style of deposition are recognised (see section 7.7.1). In the Bibbiana sector, while three-dimensional ponding cannot be demonstrated, the concentration of dune cross bedded and wavy laminated sandstones may indicate deflection and reflection of flows by topographic highs (Tinterri et al., 2015), in this case associated with the MTD. This hypothesis might be confirmed by the presence of thick mud caps overlying traction-structured sands (Haughton, 2000; Southern et al., 2015; Tinterri and Tagliaferri, 2015; Marini et al., 2016a) as shown in the section 7.7.1.

Palaeocurrent data from interval T2 show that the capacity of the MTD to influence flow pathways may have decreased as the height of the confining topography was reduced because of sediment infilling. This is well documented on selected portions of sedimentary logs just above topographic highs in the Bibbiana sector, marked by a clear decrease in mud caps thickness (e.g., fine grained sediments escape the basin due to bypassing) coupled with an increase in net-to-gross stratigraphically upwards (see also Brunt et al., 2004; Amy and Talling, 2007; Marini et al., 2016b). However, larger scale structures, such as the mounded topography between the Casaglia and Bibbiana sector (Walker, 2008), would have continued to divert the lower denser parts of sediment gravity flows and to force decoupling of the upper lower-concentration and finer-grained part of the flow (Fig. 7.19). This resulted in fine-grained sediment supply to the Casaglia area, confirmed by a large variation in net-to-gross over a distance of ~1.5 km as documented in section 7.7.1.

These observations confirm: 1) the ability of part of the large volume flows to undergo stripping when the height of the confining topography is in the order of a few tens of metres (BIB-1); 2) the transitional nature of the passage from an almost fully-ponded condition (e.g., BIB-1 thick mud caps) to a confined but non-ponded deposit character as the height of the topography is reduced (e.g., BIB-2A thinner mud caps and a deficiency in thicker beds); 3) the ability of the muddy component of large volume flows to undergo partial flow stripping even in the initial phase of deposition within a

confined-ponded basin (CAS-1). This suggests that important considerations for predicting the influence of MTD-related topography on subsequent turbidite deposition include: i) the extent and distribution of topographic relief on the surface of the MTD, ii) the volumes of sediment gravity flows that encounter the topographic features, and iii) the orientation of topographic features relative to flow direction.

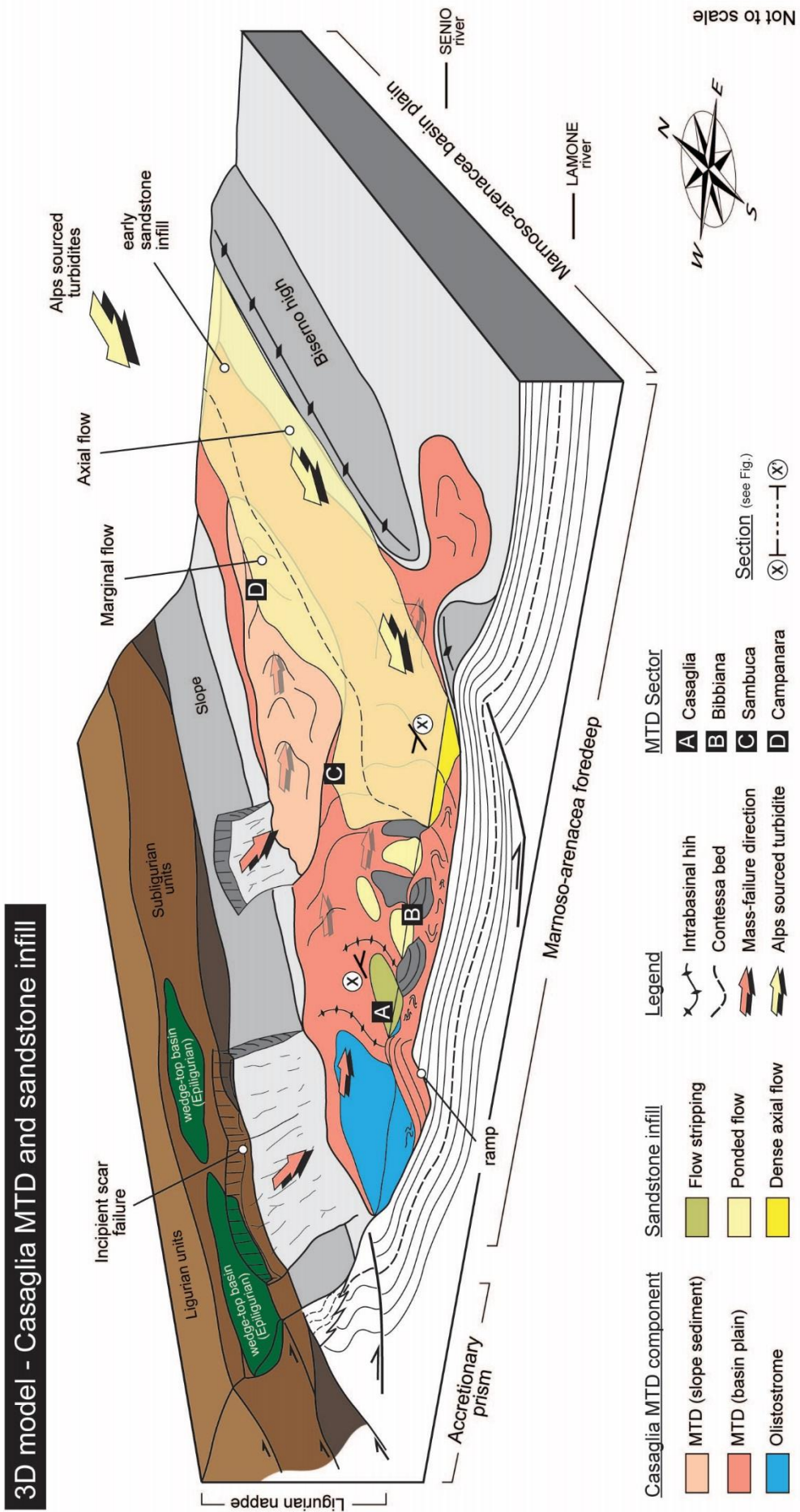


Fig. 7.18 – Interpretative palinspastic block diagram of the Casaglia MTD emplacement and subsequent turbidite sandstone emplacement (inspired by Lucente and Pini, 2008, after Lucente and Pini, 2003).

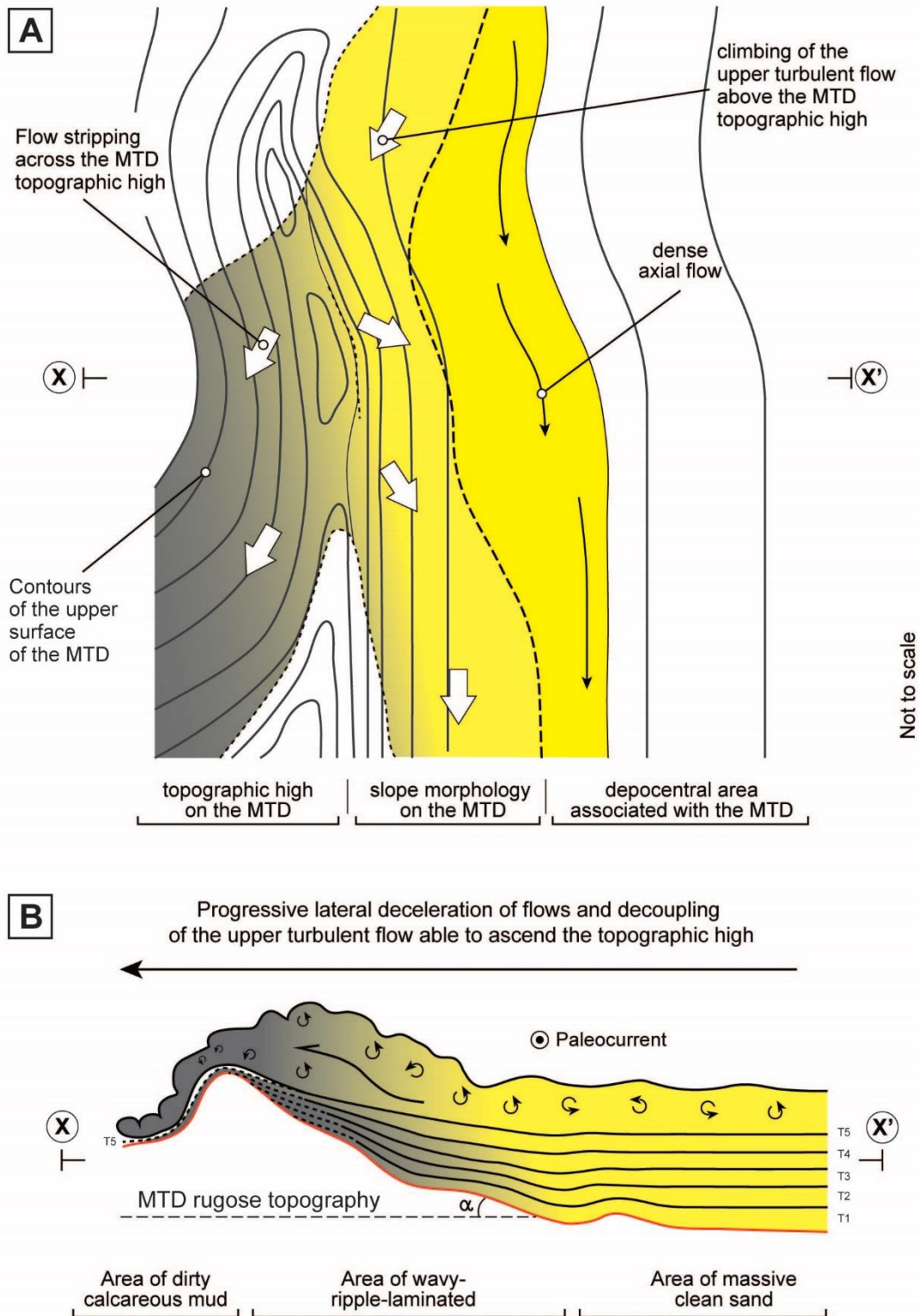


Fig. 7.19 – Sketch at a basinal scale illustrating how MTD-related topography can force the progressive down-current detachment of the upper turbulent flow from the lower axial dense part of a turbidity current. A) plan view; B) section (model inspired by earlier concepts outlined by Mutti et al., 2002; Muzzi Magalhaes and Tinterri, 2010; Tinterri et al., 2012; Tinterri and Tagliaferri, 2015; Tinterri et al., 2016).

7.9 Conclusions

The work undertaken on the Casaglia MTD, within the Fiorenzuola System (Unit V-a), provided the reconstruction of the sandstone architecture immediately overlying an MTD on outcrop, in order to document the influence of the irregular upper surface of the MTD on the subsequent sandstone deposits, which are often under the seismic scale resolution.

This included a revision of previous works undertaken in the study area (Lucente, 2002; Lucente and Pini, 2003; Walker, 2008) and integration of new data in order to test earlier basin scale depositional models and refine the reconstruction of the irregular Casaglia topography. The results of this study demonstrate that in addition to the control on the sandstone deposition at basin scale induced by 1) thrust-generated topography (Mutti et al., 2002; Muzzi Magalhaes and Tinterri, 2010; Tinterri et al., 2012; Tagliaferri and Tinterri, 2016) and by 2) the substantial change of seafloor configuration related to the emplacement of the Casaglia MTD (Lucente, 2002; Lucente and Pini, 2003; Walker, 2008), the irregular topography associated with the top of the MTD may have played a further important role in the control of local sandstone distribution during the early depositional stage of the Fiorenzuola system (Unit Va), within the Marnoso-arenacea Basin.

In detail this chapter shows that:

- Three different scales of rugosity based on their vertical (y) and horizontal dimensions (x), characterise the upper surface of the Casaglia MTD, across the study area: subtle topography ($y=1-5$ m; $x=10-25$ m); jagged topography ($y=5-30$ m; $x=50-100$ m); large-scale topography ($y=>30$ m; $x=500-1000$ m).
- A recurrent relationship has been demonstrated between the scales of rugosity and their development above the different portions of the MTD displacement, that in turn are linked to mass-failure development that emplaced the Casaglia MTD: subtle topography was mainly recognised in the distal area (zone of translation and accumulation), whereas jagged topography and large-scale topography were diagnosed toward the proximal zones of the MTD. This relationship is also likely linked to the degree of disaggregation of the remobilised material within the MTD, during its emplacement; in fact the muddy character of distal portion of the MTD is able to create shallow rugosity, whereas un-disaggregated remobilised deposits (e.g., ripped-up blocks from the basin plain) and oversized rafted blocks and olistostromes, making up the more proximal sectors, are able to form respectively one and two orders higher magnitudes of rugosity.

- The investigated stratigraphic succession immediately overlying the Casaglia MTD shows that turbidity currents were initially diverted as deduced by the mean palaeocurrent directions measured within the early T1 interval, which show a difference of 30° toward the south between locations on the distal MTD (Campanara) and the more proximal MTD sector (Bibbiana). However, it is unclear if this shift in flow direction is due to topographic relief or a different, extrinsic control.
- Spatial trends in the sandstone distribution have been documented on top of the Casaglia MTD, mainly associated with different morphological features developed on the upper surface of the MTD. Turbidity currents seem to interact with the topography which likely induced changes in flow behaviour over short distances. This is observed over the three scales of rugosity: facies and bed thickness change show that rugosity may have induced: 1) deposition of structureless or more traction-structured sands over subtle topography (e.g., at a single outcrop scale); 2) deposition of thick sandstone beds characterised by thick mud cap or turbidite succession characterised by both thinner beds with relatively thin mud caps; 3) deposition of entire muddy successions. These depositional characteristics highlight the relationship between scale of rugosity and flow size. In fact, in the first case the subtle topography was able to control facies deposition, whereas the second case shows that jagged topography might have created partial ponding effects on turbidite deposition that ceased once the topographic lows were healed, and in the third case, the large scale topography was able to deviate the dense axial flow and let the dilute portion of the flow climb the mounded topography.
- Consequently, percentage of sand within the turbidites changes significantly across the three documented healing-rugosity styles, with an increasing net-to-gross ratio observed from the interpreted fully-ponded to semi-ponded deposits.
- The interpretation of the observed growth intervals on the correlation panel requires further analysis, however, this might be associated with local increased subsidence due to differential compaction of the underlying Casaglia MTD. In fact, topographic lows might have initially received more sediment than surrounding areas, as demonstrated by loading features within topographic depressions.

Finally, this work shows that careful reconstruction of the MTD-related topography may aid prediction of gradients in reservoir properties in deep-water settings where turbidite sandstones are interleaved with MTDs. The documented onlap of turbidites

onto the upper surface of the MTD, which was able to form positive features on the earlier low-gradient basin plain, may indicate a manner of potential stratigraphic trap development for hydrocarbon accumulations that would not have been visible on seismic images. However, caution should be used when applying the results of this study to other deep-water settings: MTDs within a single basin may exhibit an extremely wide range of topographic expressions, and hence, not all MTDs should be expected to have sufficient relief to influence later sedimentation.

8 Integration of subsurface and outcrop studies to investigate the influence of MTDs on subsequent turbidite deposition at different scales

Previous chapters have documented how the emplacement of MTDs can influence the subsequent deposition of sands in deep-water settings. A key characteristic of the present study has been its capacity to constrain this relationship by integrating subsurface data from the Britannia Field in the Central North Sea (Chapters 4, 5, 6) with data from an outcrop analogue study of the Middle Miocene Casaglia MTD, in the Marnoso-arenacea Fm. (MAF), Central Italy (Chapter 7). In both cases, a reconstruction of MTD-related topography was undertaken, and the overlying sandstones investigated in terms of their thickness and facies distribution in relation to the rugose morphology that may characterise the upper surface of the MTDs. Developing a better understanding of such relationships represents an important academic research goal but may also have significant impact on hydrocarbon industry workflows.

In detail, this chapters aims to:

- i. constrain the impact of large-scale mass-failures on shaping the seafloor bathymetry (e.g., morphology, creation of accommodation space);
- ii. constrain the influence of MTD-related topography on turbidite emplacement, from sandstone facies distribution to flow process interpretation;
- iii. assess industrial applications of the work (principally with respect to hydrocarbon exploration and reservoir characterisation).

8.1 The role of MTDs in shaping seafloor bathymetry

Seafloor topography can be shaped by a multitude of processes (e.g., tectonic, gravity-driven remobilisation etc.) among which large-scale slope failures represent one of the main factors. A wide range of scales of both erosion and development of constructional topography are commonly associated with the passage of mass flows, and the emplacement of MTDs. In the subsurface, large-scale MTD-related morphology can be usually detected in high resolution seismic data. However, the recognition of these deposits in subsurface is not always accurate and reliable (Armitage and Stright, 2010; King et al., 2011; Stright et al., 2013; Kneller et al., 2016); smaller scales may never be directly detectable (Moscardelli and Wood, 2016; Sobiesiak et al., 2017). Some large and extensive exposures of outcropping MTDs

have provided the chance to document the rugose topography that is commonly developed on the upper surface of the remobilised deposits, which may range from just a few metres up to tens of metres (Armitage et al., 2009; Armitage and Jackson, 2010; Moscardelli and Wood, 2016; Kneller et al., 2016). However, three-dimensional exposures of MTDs in outcrop are relatively rare, limiting observations of the spatial distribution of the rugosity on top of these deposits. Therefore, the combination of subsurface datasets and outcrop studies may provide critical information regarding the role of MTDs in shaping the seafloor in deep-water basins.

8.1.1 MTD-related topography from subsurface and outcrop datasets: size, geometry and wavelength of the rugosity over the upper surface of an MTD

Different types of rugosity associated with the emplacement of MTDs were observed in both subsurface and outcrop datasets presented in this thesis. The size of the study areas of the Platform Area in the Britannia Field and of the Casaglia MTD in the MAF are relatively similar, measuring 35 km² and 24 km² respectively. However, the results from each case study permit evaluation of different aspects of the surface rugosity associated with the MTDs. For instance, the subsurface dataset provides the chance to reconstruct a three-dimensional MTD-related topography, whereas the outcrop study allows a two-dimensional characterisation of the top of an MTD at high resolution, overcoming the uncertainties and lower resolution arising due to well correlation. Furthermore, the Casaglia MTD can be followed for 9 km along its run out distance providing insight into MTDs changes in character along dip.

The reconstruction of palaeobathymetric maps after the occurrence of four large-scale mass-failures in the Platform Area of the Britannia Field, allows the characterisation of the rugosity at the hundreds of metres to kilometre scale horizontally, as depicted by the spatial distribution of topographic lows and highs across the study area (Chapter 5). Furthermore, the relationship between the thickness of the MTDs and their immediately post-depositional seafloor expression was also investigated. Morphological features such as a) a headwall scarp in the north of the study area, b) a zone dominated by translation of large blocks and c) an accumulation area in the south of the study area are interpreted as a result of the combination of erosion and accumulation of remobilised deposits.

Two principal low areas are identified across the Platform Area, which persist during the evolution of the Middle Reservoir Section, starting with the palaeobathymetry related to MTD-2. The deepest depression (up to 80 metres deep and up to 1 km wide) is located in the north of the study area, and it is interpreted as the foot of the

headwall scarp, given the elongated shape and the SW-NE orientation, perpendicular to the modelled dip of the local slope which represents the extension of the Fladen Ground Spur towards the south, extending beneath the BSF in the Platform Area. The downdip translation of sliding blocks is interpreted to have been responsible for the creation of this deep trough on the palaeobathymetry shaped by the MTD-2, with the main transport direction of the mass-failure orientated towards NW-SE. Similar morphological features are often observed over the depletion zone of submarine landslides (e.g., Sawyer et al., 2009; Watt et al., 2012b). The second low area is recognised in the south-eastern portion of the study area, with depths that are generally deeper than the ones developed in the north. These morphological features are approximately ~1 km wide and ~8 km long, separated by topographic highs that are ~1-2 km wide and follow the same trends developed by the elongated topographic lows.

Large-scale topographic rugosity is also observed in outcrop; the reconstructed upper surface of the Casaglia MTD, in the MAF, is characterised by morphological features that are ~50 metres deep and ~750 metres wide, separated by a topographic high that is ~1.5 km wide. However, the correlation panel does not allow the estimation of the three-dimensional distribution of such features to be extended into 3D. This can only be speculated at by looking at the geometry of the contact between the MTD and the overlying sandstone beds in outcrop, combined with observations of the internal deformation of the Casaglia MTD provided by Lucente and Pini (2003). The 18 sedimentary logs used to build the correlation panel shown in Fig. 7.12 form two almost orthogonal transects oriented respectively SW-NE and SE-NW and that are both interpreted to be parallel to the direction of the mass-failure in the proximal and distal areas, respectively (see section 7.3). Thus, the Casaglia MTD is interpreted to have travelled towards east/north-east in the proximal area, and towards the north/north-west in the middle and distal portion of its run out. Therefore, deep topographic lows in the proximal area might represent elongated troughs developed perpendicular to the interpreted transport direction of the mass-failure, similarly to what is seen in the Britannia Field and with the W-E transect of the correlation panel intersecting only the two relatively close topographic margins of the identified lows. The same idealised model might also apply to the second SE-NW - oriented transect, with the development of troughs perpendicular to the transport direction; note that large-scale topographic lows are not, though, identified in the distal portion of the Casaglia MTD. In fact, large-scale rugosity is only recognised in the proximal zones of the Casaglia MTD, which is likely linked to the degree of disaggregation of the remobilised material within the MTD, which is thought to

increase during its emplacement. Furthermore, the underlying basal surface of the MTD is characterised by an up-slope-facing ramp above which remobilised material was deposited en-mass, creating more than 100 metres of positive relief, contributing to the overall development of large-scale rugosity.

The distribution of the remobilised material within an MTD above its basal décollement surface is another aspect to consider when calculating the accommodation space for subsequent sediment deposition. In fact, if erosion associated with slope failures is usually a cause of creation of accommodation space, the emplacement of remobilised deposits commonly represents an element of reduction of accommodation space. This is observed in the Britannia Field, where topographic lows in the southern study area are partially filled by debritic deposits product of subsidiary debris flows associated with the large-scale mass-wasting events. Therefore, the accommodation space created by sliding and erosion of the early deposits can also be partially destroyed by the bulk of same remobilised deposits. However, irregularities in the distribution of the remobilised material may locally enhance erosional topography, as is seen in both case studies, or create additional accommodation independently of that created by failure erosion, albeit with likely smaller characteristic horizontal and vertical scales; the present study does not give insight into differences in the spatial continuity of the accommodation so created.

8.1.2 Investigation of the small-scale MTD top rugosity of the Casaglia MTD to reduce inter-well uncertainty in the Britannia Field

Inter-well correlation is generally a source of subsurface interpretational uncertainty, with well spacing commonly constraining whether correlations can be made, and their accuracy if so. This uncertainty increases when there is a high degree of variability between wells and when the chosen correlation surface is not regular, as is commonly that case with the upper topography of an MTD; such uncertainties may lead to errors in hydrocarbon reservoir modelling. This issue affects well correlation in the Platform Area, because of the presence of large MTDs interleaved with sandstone deposits. As noted above, outcrop analogues can be used to study MTD-related topography, including the range of rugosity scales developed on their upper surfaces and the geometry of the contact between MTDs and the overlying deposits. In fact, the interplay of MTDs and turbidites is well recognised in deep-water settings (Nelson et al., 2011)

The detailed characterisation of the upper surface of the Casaglia MTD, built upon the correlation of sedimentary logs and direct observation of the contact between the upper surface of the MTD with the overlying sandstones, enabled the identification of

two types of relatively small-scale rugosity. Both represent rugosity that is developed at the inter-well scale in most cases (e.g., the well spacing is 300-1000 metres in the Britannia Field). The characteristic scales of these two types of rugosity are $y=1-5$ m, $x=10-25$ m and $y=5-30$ m, $x=50-100$ m ('subtle' and 'jagged' topography, respectively, *sensu* Chapter 7). The horizontal spacing of the latter would entail its repetition as a sequence of three linked topographic lows and highs to cover the distance between the closest wells of the Platform Area.

When seeking to apply insight from an analogue study (e.g., the Casaglia MTD study) to the subsurface (e.g., the Britannia MTDs), it is clearly good practice to assess which aspects of the depositional settings of the respective study areas are sufficiently similar to permit the comparison. For example, the development of the rugosity must be evaluated as a function of the rheology, character and run out direction of the mass-failure. The Casaglia MTD includes intrabasinal material mainly composed of folded turbidite beds and large, gently-folded, internally coherent slide blocks of intrabasinal sandstones and mudstones, together with extrabasinal sediments in the form of an olistostrome complex which comprises an ordered aggregate of large slabs derived from the palaeo-Apennine accretionary wedge. The MTDs in the Britannia Field are mainly comprise intrabasinal sandy and silty debritic deposits, characterised by different concentrations of sand grains suspended in a muddy matrix; mudstone clasts and sandstone blocks of various sizes, from mm scale to 2 m scale are recognised within the matrix and are generally orientated bed parallel. Muddy debrites are also identified in core, with mudstone clasts and sandstones blocks of various sizes (from mm scale to 80 cm scale) suspended into the muddy matrix and generally orientated bed parallel. Although very large clasts are generally absent, large slide blocks are recognised in MTD-2. It may be concluded that in general the more coherent and less disaggregated material incorporated within the Casaglia MTD might contribute to the creation of a wider range of scales of rugosity than the less disaggregated material characterising the debritic deposits of the MTDs within the BSF, which might therefore have more subtle MTD-related rugosity on the inter-well scale. However, the large slide block recognised within MTD-2 of the BSF and the olistostrome within the Casaglia MTD, are responsible for the creation of large-scale rugosity. Deeper topographic lows are thought to be characteristic of the slope failures source areas (although a headwall scar is recognised only in the Britannia Field; none are preserved in the Casaglia MTD in the MAF).

In terms of run out distance and direction, the Casaglia MTD can be followed on outcrop for a distance of at least 10 km down-dip. The remobilised deposits are

deviated north-westwards by a frontal structural high, with the deposit thickness progressively thinning in that direction. In the Britannia field, the identified headwall scarp developed with SW-NE strike, adjacent to a deep trough of the same orientation. This suggests that the source areas of the failures were located just to the north of the study area, with the associated mass flows travelling towards the south-eastern area of the study area. This also leads to the prediction that the bulk of remobilised deposits might be found in the southern area of the BSF basin, outside the Platform Area; without further data it cannot be established whether these deposits show a deviation along the basin axis, or whether they are restricted to the area immediately outboard of the study area.

8.2 Emplacement of turbidites above MTD-related bathymetry, with consideration of how turbidity currents adjust to different scales of rugosity

Recently, examples of large failures affecting deep-sea turbidite systems have been documented, for example along North America margin (Tripsanas et al., 2008), in the Espirito Santo Basin, offshore Brazil (Alves and Cartwright, 2010), in the Nile deep-sea turbidite system (Rouillard, 2010) and elsewhere. Kneller et al. (2016) presented a review to illustrate the range of accommodation styles associated with MTD-related topography and their influence on subsequent turbidite deposition, detailed in Chapter 2 of this thesis, which has informed the following interpretations.

8.2.1 Nature of the substrate on subsequent flow transformation

MTDs can incorporate a broad range of remobilised material which can vary in terms of lithology, coherency and disaggregation rate. Variability in these characteristics may influence behaviour of subsequent turbidity currents, through the resultant rugosity of the substrate and its effect on flow, but also through the nature of eroded material and its effect upon subsequent flow development. These characteristics may influence the depositional character of turbidity currents (e.g., deposition of clean sands versus muddier sands, their relative volumes and their preferred locations of deposition).

In the Platform Area of the Britannia Field, reservoir sandstones that overlay MTDs of the Lower and Middle Reservoir Section developed a broad range of facies that varies both spatially and vertically. Chapter 6 shows that higher proportions of clean sandstones are recorded within the Lower Reservoir Zones, whereas an increasing percentage of mud is observed within the reservoir sandstone zones of the Middle

Reservoir. This change also is associated with the transformation in character recognised between MTDs 1 and 2 and MTDs 3 and 4. Cleaner sandstones reflecting deposition by classic high-density turbidity currents are mainly found above the lower MTDs, which are characterised by a high percentage of sand grains floating in the muddy-silty matrix. More hybrid-like beds are instead recognised on top of muddier MTD-3 and 4, developing characteristic facies such as mixed-slurried sandstone within Z40B and more classic HEBs within Z40C on top of MTD-4. Mixed-slurried sandstones in Z40B are mainly identified in wells located at the central and southern sector of the study area, whereas they are absent in the wells located in the north. The origin of these sandstones is debated. Early studies interpreted the slurried texture as primary, and controlled by flow dynamics, especially when slurried intervals cap sandstones beds (Lowe and Guy, 2000). However, the mixing character may wholly or in part reflects gravity-induced deformation, after deposition, driven by local seafloor gradients (Barker et al., 2008). A further hypothesis may be considered for the mixed-slurried sandstones of Z40B. As noted above, these are mainly recognised in the southern part of the Platform Area, where post-depositional overpressuring was likely induced by the emplacement of remobilised materials now preserved in Zone 45 (Barker et al., 2008). These intervals are interleaved with mudstones which may have led to water retention in underlying cleaner sands, increasing the likelihood of their remobilisation under shear.

In the Middle reservoir zone of the BSF, most of the mixed-sandstones are observed within the upper part of Z40B, in contact with the MTD. In outcrop, however, this trend is not observed; HEBs are not recognised within the turbidite succession overlying the Casaglia MTD. However, dirtier sandstones are found immediately on top of a mudstone layer that drapes the upper surface of the MTD, interpreted as hemipelagite deposited subsequent to emplacement of the Casaglia MTD. The first sandstone bed overlying the hemipelagites is usually composed of dirty sand, characterised by irregular base, and thicknesses between few cm and 50 cm and a relatively thick mudcap.

8.2.2 Character of MTD rugosity on facies patterns

Both flow and associated deposit character can be modified by interaction with seafloor topography. Where sediment gravity flows propagate through topographically complex settings, their potential run-out distance can be either reduced or increased compared to where the seafloor topography is relatively simple. MTDs in deep-water settings may generate such complex seafloor topographies,

affecting the properties of overpassing sedimentary gravity flows and that of their deposits, as described in both the subsurface (Chapter 6) and outcrop (Chapter 7) components of this study.

The analysis of sandstone distribution within the Lower and Middle Reservoir of the Britannia Field (Chapter 6) showed the relationship between the scale of rugosity and the associated facies pattern. Topographic lows in the Platform Area show a broad range of shapes that exert different control on flow behaviour, and thus on the distribution of sedimentary facies, over a relatively short distance.

The concentration of clean and amalgamated sandstone of Z40A along a trough identified at the foot of the interpreted headwall scarp of the associated MTD-2, may represent the confining effects of the scarp, which might act as a conduit that could have effectively channelised the flows. In this scenario, the topographic constraint might have resulted in increased flow velocity together with increased turbulence, likely favouring erosion and leading to increased sand amalgamation. Furthermore, the speeding up of the flow due to the confining topography could be responsible for the bypass of the finer component leading to the deposition of medium sand grain size. This interpretation might find confirmation in experimental studies conducted by de Leeuw et al. (2016), where it is shown that spatial and temporal variations of flow velocity and associated deposition lead to the autogenic confinement of flow that has a main consequence that the axial velocity of the flow is increased. At the same time, reduction in confinement might lead to the slowing down of flows and deposition of sands upstream, updip of topographic reliefs, with the development of muddier intervals as demonstrated by the vertical and spatial facies distribution of Z40A above areas of positive relief. The same effect is recognised in the upper reservoir sandstones Z40B and Z40C, where vertical and spatial facies organisations are interpreted as the result of muddier and less turbulent flows that were able to climb topographic reliefs and travel over a smaller scale of rugosity developed as a consequence of the emplacement of smaller MTD-3 and MTD-4. It is thought that a more evenly distributed pattern of rugosity might have caused a broad pattern of changes in flow behaviours over relatively short distances as observed within sandstones of Z40C.

The turbidite succession overlying the Casaglia MTD records the abrupt and instantaneous change of the seafloor bathymetry, which strongly impacted on the flow pathways in the basin, with flows being forced to adjust to the new basin floor morphology. The sediment gravity flows, which were already confined at large scale by the margins of the basin, were thus further confined by the Casaglia MTD. Early

flows were slightly deviated around the mounding MTD at the regional scale as depicted by the comparison of palaeocurrent data for the lower interval along different sectors of the Casaglia MTD. Smaller and more local topographic features (10s of metres) are inferred to have confined subsequent flows, changing their behaviour over a relatively short distance as documented in Chapter 7. However, it is difficult to draw conclusions about flow confinement and ponding without a three-dimensional morphological reconstruction of the structures in these sectors. More reliable conclusions may be deduced studying the vertical facies stacking patterns of the sandstones overlying the Casaglia MTD, where limited portions of sedimentary logs sitting on different morphological features of the MTD show significant differences in the style of deposition.

Although three-dimensional ponding cannot be demonstrated, the concentration of dune cross bedded and wavy laminated sandstones are interpreted by Tinterri et al. (2015) to indicate deflection and reflection of flows by topographic highs, albeit here interpreted to be associated with the MTD. This hypothesis might be confirmed by the presence of thick mud caps overlying traction-structured sands (Haughton, 2000; Southern et al., 2015; Tinterri and Tagliaferri, 2015; Marini et al., 2016a).

Selected portions of sedimentary logs just above topographic highs in the proximal-middle sector of the MTD document the decreased capacity of the MTD to influence flow pathways as the height of the confining topography was reduced because of sediment infilling, marked by a clear decrease in mud caps thickness (e.g., fine grained sediments escape the basin bypassing) coupled with an increase in net-to-gross stratigraphically upwards. However, because larger scale structures, such as the mounded topography, take longer to infill, they may have continued to divert the lower denser parts of sediment gravity flows, and to force decoupling of the upper lower-concentration and finer-grained part of the flow. Overspill from such decoupling may have resulted in fine-grained sediment supply to ponded accommodation in the proximal area of the Casaglia MTD, which was isolated from sand input; this interpretation is consistent with the large variation in net-to-gross seen over a distance of ~1.5 km (Chapter 7).

In conclusion, the Casaglia MTD outcrop study shows that large volume flows undergo stripping when the height of the confining topography is in the order of a few tens of metres, whereas when the height of the topography is reduced, flows record the transitional nature of the passage from an almost fully-ponded condition to a confined but non-ponded deposit character. Furthermore, thin and muddy turbidites observed on top of the topography high in the proximal area show that muddy

component of large volume flows can undergo partial flow stripping even in the initial phase of deposition within a confined-ponded basin.

Predicting the influence of MTD-related topography on subsequent turbidite deposition requires knowing the extent and distribution of topographic relief on the surface of the MTD, the volumes of sediment gravity flows that encounter the topographic features and the orientation of topographic features relative to flow direction (Fig. 8.1).

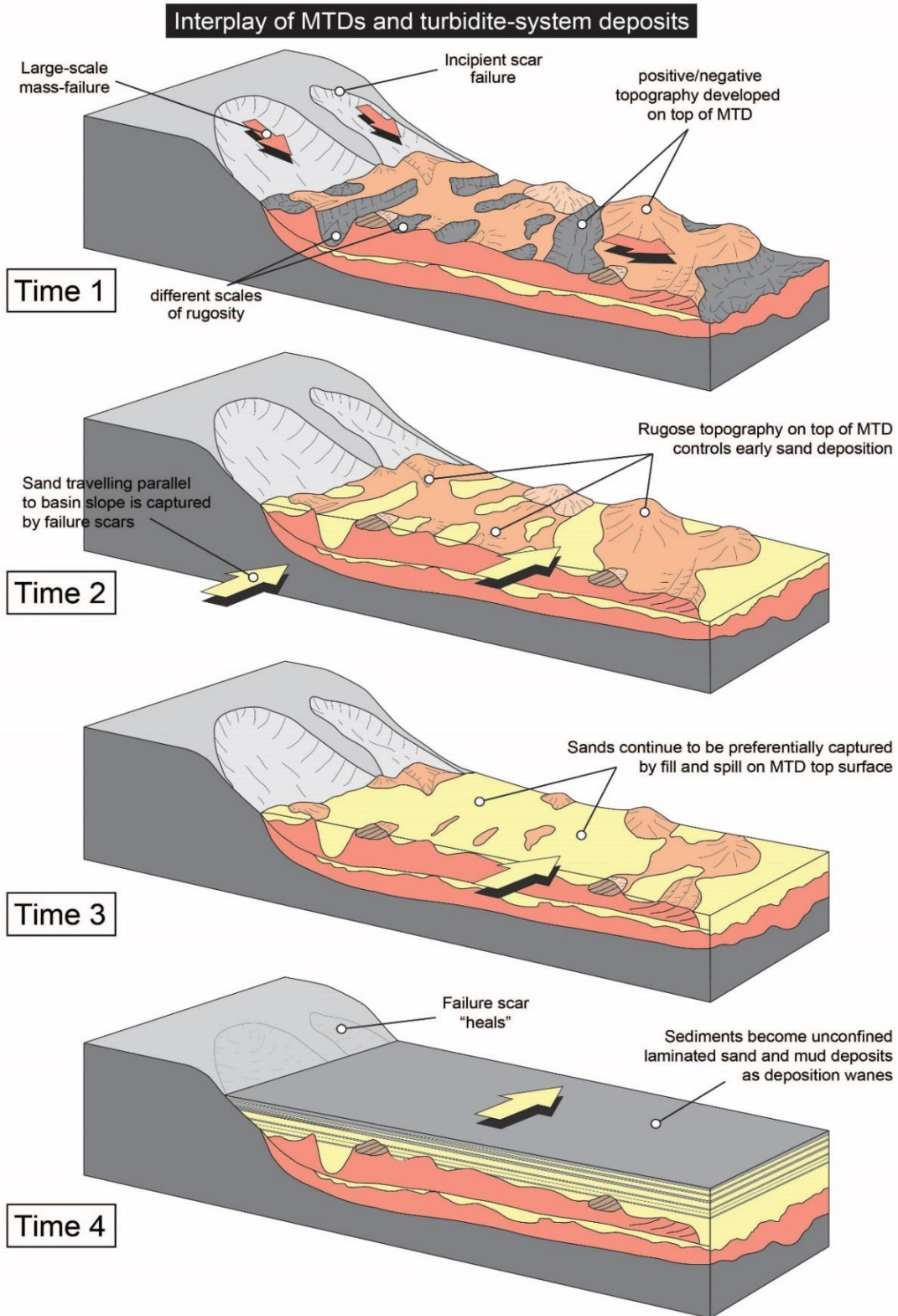


Fig. 8.1 – Block diagrams showing the interaction between MTDs (pink) and sandstone deposits (yellow). The emplacement of the MTD (T1) creates an irregular topography over the seafloor, with large and elongated troughs, ponds and positive reliefs, which influence subsequent turbidites (T2). Initially, there is little interconnectivity of the sands, but as soon as topography becomes subtler (T3), interconnectivity of sands increases until the topography is infilled (T4). Details of this scale of process are under the seismic resolution (model inspired by Algar et al., 2011).

8.3 MTDs in deep-water settings: an important aspect for hydrocarbon exploration and reservoir characterisation

The increasing number of oil and gas discoveries around the world in which reservoir sandstones are interleaved with MTDs has increased awareness of the role that MTDs may play in both hydrocarbon exploration and reservoir development (Frey-Martinez, 2007; Armitage et al., 2009; Jackson and Johnson, 2009; Algar et al., 2011; Armitage and Jackson, 2010; Gamboa, 2011; Lu and Shipp, 2011; Jackson, 2012; Nelson et al., 2012; Kneller et al., 2016; Sobiesiak et al., 2016; Fallgatter et al., 2016; Sobiesiak et al., 2017). Therefore, reducing uncertainties in distribution of reservoir quality associated with the presence of MTDs is an important aspect of the study of the relationship between MTDs and turbidites.

As noted in Chapter 2, MTD-related topography can be an important factor in hydrocarbon exploration in part because the rugose upper surface of these deposits may influence the distribution of subsequent sand deposition, or at least compartmentalise the basal parts of overlying sandstone units (Shor and Piper, 1989; Cronin et al., 1998; Pickering and Corregidor, 2000; Shultz et al., 2005; Armitage et al., 2009; Kneller et al., 2016).

The work detailed in this thesis may have applications in subsurface settings where challenges in reservoir characterisation of deep-water deposits arise due to the presence of MTDs. Such challenges commonly occur where morphological features associated with MTDs are under the scale of seismic resolution. In such circumstances, where the reconstruction of the sandstone architectures overlying the MTDs is problematic, the results from both subsurface and outcrop studies such as those detailed in this research can be used to constrain interpretations.

The extensive Britannia Field database, comprising core, cutting and wire line data, permits an accurate decompaction and restoration analysis to reconstruct the palaeobathymetric maps of the seafloor after the emplacement of large-scale mass-failure – related deposits. These maps provide new insights into the creation of accommodation space over rugose MTD-related topography, enabling characterisation of thickness and reservoir facies variations across the study area, and, by extension, in subsurface scenarios of similar character. However, the reconstruction of facies architecture at scales of rugosity smaller than the inter-well scale (between ~200 m and 1 km horizontally) remains a source of uncertainty. The work undertaken on outcrop (Casaglia MTD, Marnoso-arenacea) allowed identification of smaller scales of rugosity (y=1-5 m, x=10-25 m; y=5-30 m; x=50-100 m) that could be present at the inter-well scale, and of associated facies variations.

It is recommended that subsurface workflows accommodate the possible presence of facies and facies architecture variations at this scale.

In addition, both outcrop and subsurface studies show how knowledge of the transport direction of large-scale mass-failures and that of later turbidity currents might be used to guide prediction of reservoir properties of the sandstone architecture overlying MTDs. The relationship between scale of rugosity and sandstone distribution might be generalised to explain the heterogeneity that characterises reservoir sandstone above MTDs in relation to the shape, size, elevation, and most of all, orientation of the morphological features associated with MTDs, and in particular with regard to preferential linkage to high vs. low net-to-gross ratios in the overlying reservoirs. Thus, a significant relationship was observed between the orientation of the morphological features and the direction of transport of the failures. In the Britannia Field study area large, deep troughs are oriented orthogonally to the MTD emplacement direction (probably in association with orientation of the inferred fault underneath). Within these features, large volumes of amalgamated clean-structureless sandstone with good reservoir properties were recognised. At the same time, shallower or pond-like features seem to be associated with facies characterised by higher percentages of mud-rich facies, such as hybrid-event beds (e.g., Britannia, Z40C and Z50). Such facies distribution variations will influence the distribution of reservoir properties, and thus hydrocarbon fluid-flow.

Existing reservoir models investigating the influence of MTDs on hydrocarbon-fluid flow should incorporate the spectrum of morphological features and related turbidite depositional character recognised in the case studies documented in this thesis and also those in the wider literature (e.g., Gee et al., 2007; Armitage et al., 2009; Alves, 2010; Alves and Cartwright, 2010; Armitage and Jackson, 2010; Algar et al., 2011; Fairweather, 2014; Kneller et al., 2016). The documented range of reservoir types and the inferred spectrum of morphological features (e.g., local bypass vs. deposition) suggest that associated flow evolution may be expressed over relatively short distances. Thus, the size, shape and character of depositional elements may vary over MTDs-related topography on the reservoir scale.

Differences in system size, geometry, distributions and proportions of reservoir quality may be seen between those systems dominated by structural-tectonic features and those influenced by large MTDs; current understanding of such potential variation remains limited. Similarly, misinterpretation of the morphological features associated with MTDs and those related to depositional elements (e.g., channels vs. conduits) has significant implications for the prediction of facies and reservoir quality

distribution. In fact, a conduit like a trough created by the sliding of translated blocks and bordered by the headwall scarp, may act as bypassing zone, whose axial continuity may enable the flows to traverse different connected areas.

In the Britannia Field, the emplacement of large MTDs may have obstructed or deviated turbidity currents. In the first case, the bulk of the sediment transported by the flows, interpreted as being emplaced in a direction perpendicular to the mass-failure transport direction, may have been deposited to the west of the study area. In the second scenario, sediments may have been deviated and maybe confined in deep narrow depositional fairways (such as the trough identified at the north of the study area) and may have bypassed the study area, depositing sand to the east of the Platform Area. Effects of this type may occur in sequence, with up-dip trapping of sandy lobes up dip of an MTD being progressively succeeded by bypass through and over it, and eventually by deposition of sandy lobes in downdip locations.

In the BSF case study, the orientation of the headwall scarp and the development of topographic lows, together with the identification of slide blocks, suggest that the main transport direction of the MTDs was towards the south-east in agreement with earlier studies of slope deformation undertaken by Del Pino Sanchez (2006). This suggests that the bulk of remobilised material transported by the large-scale mass-failures might be located to the southeast of the Platform Area, unless it was diverted axially. In the case where MTD accumulation occurred principally outboard and to the southeast of the study area, good reservoir potential within the Lower and Middle Reservoir Section might preferentially be developed in the northern part of the Britannia basin, towards the flank of the Fladen Ground Spur. In the case where mass flow was diverted axially, the presence of good quality sands might depend upon how effectively the resultant MTD was able to block axially-dispersing turbidity currents.

9 Conclusions and future work

As outlined in Chapter 2, the overarching aim of the research described in this thesis was to investigate the relationship between the bathymetry left by large-scale mass-failure processes and subsequent sedimentary gravity flow deposits. Chapters 5-7 provided data and analysis to address some of the key questions related to the presence of MTDs in deep-water deposits, their effects on the basin floor and their influence on the distribution of subsequent sandstones.

9.1 Results from subsurface and outcrop datasets

The subsurface dataset of the Platform Area of the Britannia Field in the Central North Sea allowed a core based case study of the interplay of MTDs and turbidites across a 35 km² area. In Chapter 4, new reservoir sandstone zones (Z40A, Z40B, and Z40C) from the Middle Britannia Sandstone Formation (BSF) are recognised, correlated and integrated with earlier-defined reservoir zones (Z10A, Z10B, and Z20) of the Lower BSF, across the Platform Area (PA). The identification and correlation of new reservoir zones in the Middle Reservoir Section was supported by the recognition of different types of MTD. The reconstructed reservoir architecture underpinned Chapters 5 and 6, which investigated the relationship between MTDs and turbidites.

Chapter 5 analysed the sources of differential creation of accommodation space during BSF in the PA, as indicated by different thicknesses of reservoir sandstone zones that form a wedge-like geometry tapering towards the north of the study area. The key complication in the BSF is that the deposits are also characterised by periodic episodes of large-scale remobilisation which may have contributed to the creation of accommodation space. Accordingly, the palaeobathymetric evolution of the seafloor within the 35 km² area around the PA was investigated through decompaction and restoration analysis of the deposits of the Lower and Middle Reservoir Section. This was preceded by the investigation of the role of differential compaction and basin deformation in the study area, testing and calculating the contribution of each of these processes and concluding that differential compaction effects within the underlying shales and contemporaneously-deposited turbidites cannot explain the evolution of seafloor bathymetry in isolation; other effects must play a role. Syn-sedimentary (tectonic) basin deformation was identified in the central and southern sector of the Platform Area. This is interpreted to have contributed to

the differential creation of accommodation space across the study area, possibly associated with the post-rifting phase of the Central North Sea Basin evolution.

New palaeobathymetric maps of the seafloor reconstructed after each of the four large-scale mass-failure events combined with thickness maps of each MTD highlight erosional and depositional character of the mass-wasting processes. Larger failures with highly erosive character seem to occur after periods of relatively limited clastic input which resulted in fine grained deposition draping the seafloor. It is inferred that related palaeo-slope steepening during the extended time periods represented by deposition of fine-grained sediments preconditioned the slopes for failure; it is unknown whether autogenic (e.g., over-steepening) or allogenic (seismic) triggers ultimately released the mass flows.

Erosion on the seafloor associated with each of the remobilisation phases was between ~50 and ~100 metres, with the largest erosion recorded at the base of MTD-2. MTD-related topographic lows were usually partially infilled by the remobilised material itself. However, ~50-70 metres of unfilled depression were left along the headwall of the largest failure (MTD-2). Preserved portions of Britannia stratigraphy underneath the detachment surface constitute an up-slope – facing ramp above which remobilised material was deposited en-mass, creating an additional ~20 m positive relief after MTD-1 and MTD-2 emplacement. Large slide blocks (>2.5 km²) were identified as part of MTD-2 and interpreted to be the result of sliding associated with large-scale slope failure in which large portions of intact stratigraphy were laterally translated. These blocks are interpreted to have slid along a weak surface in the stratigraphy that may correspond to a previous remobilised and re-sedimented interval (MTD-1). The translation of sliding blocks is interpreted to have been responsible for the creation of a series of deep troughs in the bathymetry left by MTD-2, the largest of which (80 metres deep and up to 1 km wide) is orthogonal to the lateral slope dip direction and hence, to the main transport direction of the mass-failure.

In Chapter 6, the investigation of cored intervals enabled the characterisation of the infill of MTD-related topography of the Lower and Middle Reservoir architecture. This reconstruction entailed significant revision and re-interpretation of earlier work, in order to build new depositional models upon the new palaeobathymetric maps of the Platform Area. The distribution of sandstone facies above the reconstructed seafloor bathymetry after the emplacement of each MTD across the study area highlights significant local thickness and facies variation associated with the rugose palaeo-seafloor depicted by the combined effects of mass flow processes, syn-sedimentary

basin deformation and the SW-NE palaeo-flow direction of turbidity currents. A direct relationship between the proportion of sand-rich clean and amalgamated sandstones and palaeo-depth is observed within elongated topographic lows that may have acted as conduits. By way of contrast, muddier deposits are more abundant in enclosed topographic features. Furthermore, a common motif is an off- to on-axis variation in deposit character (off-axis banded and mixed-slurried sandstone facies vs clean and on-axis structureless sandstone facies). This motif invokes the idea that flows develop a more cohesive behaviour off-axis and a more turbulent character axially (cf. Barker et al., 2008). A general vertical change in reservoir architecture is also observed, with deposition of predominantly clean, structureless and amalgamated sand (Z10A and Z10B) passing to the more hybrid event bed - prone Z40C. The intervening reservoir intervals (Z40A and Z40B) are interpreted to represent the transition between the two reservoir facies types. The vertical trend of facies evolution in the Britannia Field might be explained invoking: i) allogenic factors that might have controlled the evolution of the depositional system and related facies distribution through time; ii) the role of active normal faulting that might have blocked or favoured preferential pathways for sandstone deposition; iii) different scales of rugosity developed on the seafloor by the emplacement of MTDs, dictating the behaviour of turbidity currents which may have developed hybrid-prone deposition instead of classic turbidite deposits. A combination of these factors may account for the character of the Lower and Middle Reservoir. Further work is required to try and better distinguish the mechanisms operating in the Britannia depositional system (see below). Factors thought to influence flow interaction with MTD-related bathymetry and resultant variation in facies distribution include: i) the lateral (orthogonal-to-flow-direction) segregation of fine-grained sediment toward the outer flow margins, and associated early lateral sedimentation of sand, leading to deposition of mud-rich divisions downstream, ii) a possible preferred lateral entrainment of fine-grained sediments within the flow, and iii) the spatial change in flow Reynolds number from axial to off axial position related to the flow direction. This last model may explain the broad character of sandstone deposits across the study area for each reservoir zone (see also Barker et al., 2008).

The study of sandstone architecture immediately overlying the Casaglia MTD in the Marnoso-arenacea Fm. (MAF) shown in Chapter 7 documents the relationship between the irregular upper surface of the MTD and the succeeding deposits at outcrop, at a scale generally below the resolution of most current 3D seismic datasets acquired for hydrocarbon exploration. The reconstruction of the upper surface of the Casaglia MTD across the study area highlights three scales of rugosity based on

vertical (y) and horizontal dimensions (x) and classified as subtle topography ($y=1-5$ m; $x=10-25$ m), jagged topography ($y=5-30$ m; $x=50-100$ m) and large-scale topography ($y>50$ m; $x=500-1000$ m). The areal distribution of these scales of rugosity is in relationship with the position relative to the mass-failure run-out path: subtle topography predominates in the distal area (zone of translation and accumulation), whereas jagged topography and large-scale topography predominate in the proximal zones of the emplaced MTD. This relationship is likely linked to the degree of disaggregation of the remobilised material within the MTD during its emplacement.

Palaeocurrent indicators suggest that turbidity currents flowing above the Casaglia MTD were diverted by the MTD, with rotation of the palaeoflow indicators (up to 30°) in proximity to the higher MTD relief. Furthermore, sandstone deposits also show the effects that different scales of rugosity have on sand deposition. In fact, structureless or more traction-structured sandstones with thin mud caps are generally associated with turbidites emplaced over subtle topography, whereas thick sandstone beds characterised by thick mud caps that pass vertically to thinner beds with relatively thin mud caps represent a typical turbidite succession encountered over a jagged topography. These variations are interpreted as partial ponding effects on turbidite deposition that ceased once the topographic lows were healed. Muddy successions found in super-elevated positions above the MTD represent deposition of the dilute portion of the flow that climbed the mounded topography and the deviation of the dense axial part of the turbidity current towards deeper areas on top of the MTD. In terms of sandstone net-to-gross, the percentage of sand was observed to increase from the interpreted fully-ponded to semi-ponded conditions.

Evidence of minor stratigraphic growth within the turbidite succession is observed and thought to relate to locally increased subsidence due to differential compaction within the underlying Casaglia MTD.

9.2 Main outcomes

The results of the previous chapters indicate that significant variations in sandstone depositional character may occur where deep-water settings are influenced by large-scale slope instability processes. In combination, the outcomes from the Britannia Field study and the Casaglia MTD study indicate that a range of MTD-related controls upon vertical and longitudinal variations in flow dynamics exists, which in turn govern sedimentation above MTDs. These controls are:

- A. The shape of morphological features identified on the upper surface of an MTD (e.g., bowl-shaped vs conduit-shaped) and their orientation with respect to the flow direction (Fig. 9.1-A);
- B. The depth and size of the morphological features on the top of MTD in relationship to the volume of the flows (fully contained vs non-contained flows) (Fig. 9.1-B);
- C. The elevation of the morphological features on the top of MTD above the seafloor bathymetry in relationship to the thickness of the flows (Fig. 9.1-C).

In both the Britannia Field and the Casaglia MTD case studies, the resulting heterogeneity in deposits is expressed by lateral thickness and facies changes across relatively small distances. Both studies provide insight as to how the combination of the controls outlined above might have influenced the behaviour of flows depositing supradjacent sandstones. In summary:

- Relatively large and deep conduits aligned in the direction of palaeoflow are filled by amalgamated, clean and structureless sandstones (Britannia, Z40A in wells B04, B05, and B13z).
- Relatively large but shallow features of various shapes are filled by HEB-prone deposits (Britannia, Z40C).
- Small and shallow bowl-shaped features are filled by medium-thick sandstones with thin mud caps (Casaglia, in logs BIB-2, CAM-8).
- Deep features situated above MTD relief (i.e. elevated with respect to basin floor) and laterally with respect to the sediment main provenance source area are filled by mud-rich successions, characterised by bioturbated mudstone and debritic facies (Casaglia MTD, in logs CAS-1, CAS-2).
- Bowl-shaped features, moderately elevated on top of large mounded areas, are filled by clean sands with thick mud caps (Britannia, Z40A in wells B07, B10, 16/27A-6; Casaglia, in logs BIB-1, BIB-3).

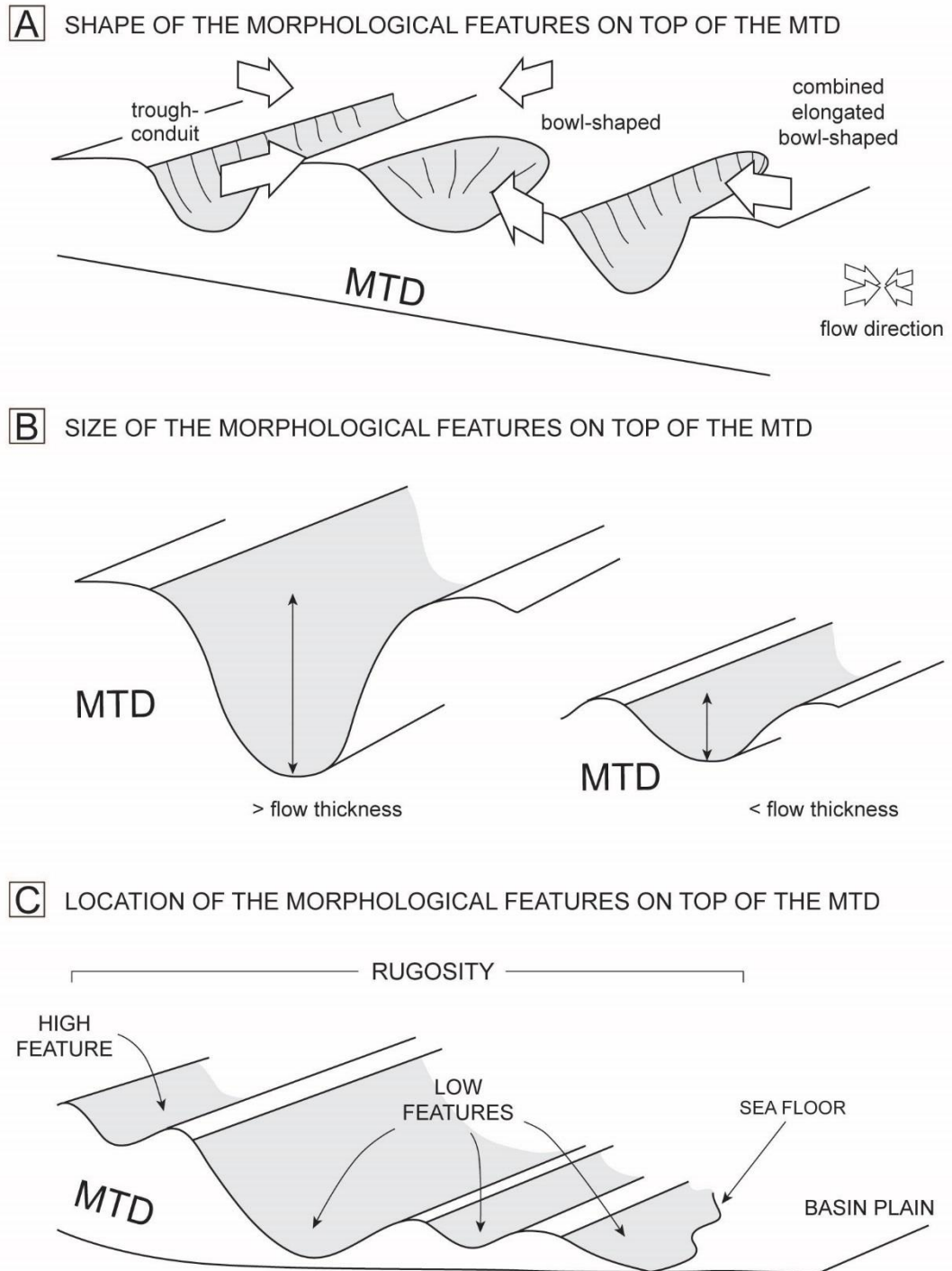


Fig. 9.1 – Schematic representation of the MTD-related controls on turbidite deposition. A) Shape of morphological features identified on the top of MTD (e.g., bowl-shaped vs conduit-shaped) and their relationship to the flow direction. B) Depth and size of the morphological features on the top of MTD in relationship to the volume of the flow (fully contained vs non-contained flow). C) Elevation of the morphological features on the top of MTD above the seafloor bathymetry in relationship to the thickness of the flow.

9.3 Recommendations for further work

This thesis has focused on the interaction between turbidity currents and the topography associated with large mass-failure events. Many interesting topics of work remain open for future pursuit in this area. Recommendations for possible follow-up work are here suggested.

The review of the geological framework of the study area within the Britannia Field together with revision of the well correlation, decompaction and restoration of the deposits of the Lower and Middle Reservoir Section in the Platform Area highlighted the role of basin deformation associated with inferred reactivation of structural features alongside differential compaction effects. Particular attention was paid to the methodology used to decompact and restore deposits of the BSF in light of the assumptions and boundary conditions chosen to run the analysis. However, further investigation on the reliability of the decompaction equations used at shallow depths is recommended. Testing and refining the decompaction and associated restoration analysis might contribute to a better defined role of differential compaction versus basin deformation. Furthermore, the activity of structural features, such as the ones inferred to have been active across the north of the Platform Area, would ideally be dated, to better constrain their possible influence on mass-failure occurrence and the impact on turbidity current pathways. In addition, the role of such the longer-range impact of such faults on the initiation of sediment remobilisation into deeper water by turbidity currents could be investigated.

The wavelength and amplitude of the rugosity associated with the upper surface of MTDs was investigated using the Casaglia MTD outcrop analogue. However, development of such rugosity on sub-seismic scales is likely to remain an issue in subsurface workflows. Although further analogue work in general has a role to play, the current study suggest that one particular area to focus upon could be the distribution of the clasts incorporated within the remobilised material. In the BSF itself, a more detailed evaluation of the broad range of internal features that seem to characterise the MTDs in the Platform Area is recommended, including the different degrees of disaggregation recognised within the remobilised material, the presence of “starry night” matrix material and of the floating clasts of varying size and lithology. Furthermore, the heterogeneous character of MTDs might influence the way hosting successions compact - a factor that might be taken into account in decompaction analysis.

More generally, it should be noted that the current study was restricted to the deposits of the Britannia Field across the Platform Area. Further investigation beyond these geographical limits is needed in order to better understand the development of different scales of rugose morphologies and the processes controlling mass-failures in terms of provenance, emplacement direction and prediction of the run-out of the remobilised material, both outside the Platform Area but, by analogy, also in other deep-water settings.

The distribution and character of Z40B sandstones above the MTD-3 shows how the sandstones associated with MTDs can be various and heterogeneous, hindering interpretation of the related depositional processes. An aspect that is not fully investigated in this thesis is the role of the overpressure induced by mass-failure during the emplacement of the MTDs. Thus, emplacement of MTD-3 might have contributed to the heterogeneity of the internal character of the underlying Z40B; associated remobilisation could have overprinted the original depositional fabrics and hence the original facies distributions. The characteristic distribution of mixed-slurried facies may not therefore be primarily controlled by flow dynamics, but instead reflect later deformation, although perhaps combined with the presence of mechanically weaker banded fabrics that would have been prone to deformation. Further investigation of the shearing features could be undertaken through SEM analysis on the morphological and compositional nature of the “detrital mud aggregate grains” (following earlier work by Barker, 2005) in order to differentiate primary features from syn-depositional deformation (Butler et al., 2015) and those arising from post-depositional remobilisation.

Another important aspect of the relationship between turbidites and MTDs is the vertical extent of the effects that MTD-related topography may have on the overlying sand deposition. To this regard, the sandstone interval overlying the Casaglia MTD might offer the chance to explore the vertical extent of the influence of subtle scales of rugosity above an MTD. The correlation panel shows stratigraphic growth that could be further investigated; this growth locally increases the thickness of the sandstone interval above the Casaglia MTD, especially in the proximal (Bibbiana) and intermediate (Sambuca) sectors. In this area, it may also be possible to obtain more insights into the relationship linking the scale of rugosity to the heterogeneous character of the MTDs.

Although new insights into the sandstone deposition above MTD-related topography have been gained with respect to some combinations of controls outlined in Section 9.2 and summarised in Fig. 9.1, not all possible permutations could be considered in

this study. Further insights could be obtained from new fieldwork in different systems where the role of some controls or combination of controls not considered in this thesis could be addressed. A possibility is the Pindos basin, in northern Greece, where a pilot study (not reported on herein) was conducted during an early stage of the research. In this area, several MTDs have been mapped and investigated by previous authors (Alexander et al., 1990; Leigh and Hartley, 1992; Avramidis et al., 2000; Avramidis and Zelilidis, 2001). However, the relationship between these MTDs and overlying turbidite sandstones is not well studied. Field mapping should be first carried out in order to investigate the spatial distribution of MTDs in the basin and better understand the process that controlled their emplacement. Small scale analysis could then be undertaken on relatively well exposed outcrops to document the form of the upper MTD surface, the internal character of the MTD, and that of the overlying sandstone deposits.

Reference list

- Aas, T.E., Howell, J.A., Janocko, M., Midtkandal, I., 2010. Re-created Early Oligocene seabed bathymetry and process-based simulations of the Peira Cava turbidite system. *J. Geol. Soc. London*. 167, 857–875. doi:10.1144/0016-76492009-005
- Ainsworth, N.R., Riley, L.A., Gallagher, L.T., 2000. An Early Cretaceous lithostratigraphic and biostratigraphic framework for the Britannia Field reservoir (Late Barremian-Late Aptian), UK North Sea. *Pet. Geosci.* 6, 345–367. doi:10.1144/petgeo.6.4.345
- Al Ja'Aidi, O.S., McCaffrey, W.D., Kneller, B.C., 2004. Factors influencing the deposit geometry of experimental turbidity currents: implications for sand-body architecture in confined basins. *Geol. Soc. London, Spec. Publ.* 222, 45–58. doi:10.1144/GSL.SP.2004.222.01.04
- Albertão, G.A., Mulder, T., Eschard, R., 2011. Impact of salt-related palaeotopography on the distribution of turbidite reservoirs: Evidence from well-seismic analyses and structural restorations in the Brazilian offshore. *Mar. Pet. Geol.* 28, 1023–1046. doi:10.1016/j.marpetgeo.2010.09.009
- Alexander, J., Nichols, G.J., Leigh, S., 1990. The origins of marine conglomerates in the Pindus foreland basin, Greece. *Sediment. Geol.* 66, 243–254. doi:10.1016/0037-0738(90)90062-X
- Algar, S., Milton, C., Upshall, H., Roestenburg, J., Crevello, P.D., 2011. Mass-transport deposits of the deep-water northwestern Borneo margin (Malaysia); characterization from seismic reflection, borehole, and core data with implications for hydrocarbon exploration and exploitation. *Mass-Transport Depos. Deep. Settings* 96, 351–366. doi:-
- Allen, P.A., Allen, J.R., 1990. Basin Analysis—Principles and Applications., 1990. Forw. Model. heat flow Invers. Vit. reflectance data Investig. Tert. Invers. events 449.
- Allen, J.R.L., 1991. Origin of Bouma Division A_Allen_1991.pdf, *Journal of Sedimentary Petrology*. doi:10.1306/D42676F4-2B26-11D7-8648000102C1865D
- Altinakar, M.S., Graf, W.H., Hopfinger, E.J., 1996. Flow structure in turbidity currents. *J. Hydraul. Res.* 34, 713–718.
- Alves, T.M., 2010. 3D Seismic examples of differential compaction in mass-transport deposits and their effect on post-failure strata. *Mar. Geol.* 271, 212–224. doi:10.1016/j.margeo.2010.02.014

- Alves, T.M., Cartwright, J.A., 2010. The effect of mass-transport deposits on the younger slope morphology, offshore Brazil. *Mar. Pet. Geol.* 27, 2027–2036. doi:10.1016/j.marpetgeo.2010.05.006
- Alves, T.M., Lourenço, S.D.N., 2010. Geomorphologic features related to gravitational collapse: Submarine landsliding to lateral spreading on a Late Miocene-Quaternary slope (SE Crete, eastern Mediterranean). *Geomorphology* 123, 13–33. doi:10.1016/j.geomorph.2010.04.030
- Alves, T.M., Kurtev, K., Moore, G.F., Strasser, M., 2014. Assessing the internal character, reservoir potential, and seal competence of mass-transport deposits using seismic texture: A geophysical and petrophysical approach. *Am. Assoc. Pet. Geol. Bull.* 98, 793–824. doi:10.1306/09121313117
- Alves, T.M., 2015. Submarine slide blocks and associated soft-sediment deformation in deep-water basins: A review. *Mar. Pet. Geol.* 67, 262–285. doi:10.1016/j.marpetgeo.2015.05.010
- Amerman, R., Trudgill, B., Nelson, E.P., Pyles, D.R., 2010. 4-D Distribution of Deepwater Mass-Transport Deposits (Late Cretaceous Upper Gosau Subgroup , Muttekopf Area , Northern Calcareous Alps , Austria): Implications for Syn depositional Structural Reconstruction. Group 30108.
- Amy, L.A., Talling, P.J., 2006. Anatomy of turbidites and linked debrites based on long distance (120 x 30 km) bed correlation, Marnoso Arenacea Formation, Northern Apennines, Italy. *Sedimentology* 53, 161–212. doi:10.1111/j.1365-3091.2005.00756.x
- Amy, L.A., Talling, P.J., 2007. Basin-plain deposits of the Marnoso Arenacea Formation, Italy. *Atlas Deep. Outcrops* 215–217. doi:-
- Archer, S.G., 2002. Britannia Field - Multicontractor meeting, Internal Report.
- Argnani, A., Lucchi, F.R., 2001. Tertiary silicoclastic turbidite systems of the Northern Apennines, in: *Anatomy of an Orogen: The Apennines and Adjacent Mediterranean Basins*. Springer, pp. 327–349.
- Armitage, D.A., Romans, B.W., Covault, J.A., Graham, S.A., 2009. The Influence of Mass-Transport-Deposit Surface Topography on the Evolution of Turbidite Architecture: The Sierra Contreras, Tres Pasos Formation (Cretaceous), Southern Chile. *J. Sediment. Res.* 79, 287–301. doi:10.2110/jsr.2009.035
- Armitage, D.A., Jackson, C.A.L., 2010. Role of Mass-Transport Deposit (MTD) Related Topography on Turbidite Deposition and Reservoir Architecture : A Comparative Study of the Tres Pasos Formation (Cretaceous), Southern Chile and Temburong Formation (Miocene), NW Borneo *. *Search Discov.* 30121.
- Armitage, D.A., Stright, L., 2010. Modeling and interpreting the seismic-reflection

- expression of sandstone in an ancient mass-transport deposit dominated deep-water slope environment. *Mar. Pet. Geol.* 27, 1–12. doi:10.1016/j.marpetgeo.2009.08.013
- Arnott, R.W.C., Hand, B.M., 1989. Bedforms, primary structures and grain fabric in the presence of suspended sediment rain. *J. Sediment. Res.* 59.
- Athy, L.F., 1930. Density, porosity, and compaction of sedimentary rocks. *Am. Assoc. Pet. Geol. Bull.* 14, 1–24.
- Atwater, G.I., Miller, E.E., 1965. The Effect of Decrease in Porosity with Depth on Future Development of Oil and Gas Reserves in South Louisiana: ABSTRACT. *Am. Assoc. Pet. Geol. Bull.* 49, 334.
- Avramidis, P., Zeligidis, A., Kontopoulos, N., 2000. Thrust dissection control of deep water clastic dispersal patterns in Klematia-Paramythia foreland basin, western Greece. *Geol. Mag.* 137, 667–685.
- Avramidis, P., Zeligidis, A., 2001. The nature of deep-marine sedimentation and palaeocurrent trends as evidence of Pindos foreland basin fill conditions. *Episodes* 24, 252–256.
- Baas, J.H., Best, J.L., 2002. Turbulence modulation in clay-rich sediment-laden flows and some implications for sediment deposition. *J. Sediment. Res.* 72, 336–340.
- Baas, J.H., McCaffrey, W.D., Haughton, P.D.W., Choux, C., 2005. Coupling between suspended sediment distribution and turbulence structure in a laboratory turbidity current. *J. Geophys. Res. Ocean.* 110, 1–20. doi:10.1029/2004JC002668
- Baas, J.H., Best, J.L., Peakall, J., Wang, M., 2009. A Phase Diagram for Turbulent, Transitional, and Laminar Clay Suspension Flows. *J. Sediment. Res.* 79, 162–183. doi:10.2110/jsr.2009.025
- Baas, J.H., Best, J.L., Peakall, J., 2011. Depositional processes, bedform development and hybrid bed formation in rapidly decelerated cohesive (mud-sand) sediment flows. *Sedimentology* 58, 1953–1987. doi:10.1111/j.1365-3091.2011.01247.x
- Bagnold, R.A., 1962. Auto-Suspension of Transported Sediment; Turbidity Currents. *Proc. R. Soc. Lond. A. Math. Phys. Sci.* 265, 315–319.
- Barker, S.P., 2005. Spatial and Temporal Evolution of Deep- Marine Particulate Gravity Currents: an Experimental, Subsurface and Outcrop Investigation. PhD Thesis. University College Dublin.
- Barker, S.P., Haughton, P.D.W., McCaffrey, W.D., Archer, S.G., Hakes, B., 2008. Development of Rheological Heterogeneity in Clay-Rich High-Density Turbidity Currents: Aptian Britannia Sandstone Member, U.K. Continental Shelf. *J.*

- Sediment. Res. 78, 45–68. doi:10.2110/jsr.2008.014
- Barley, B., 1999. Deepwater problems around the world. *Lead. Edge* 18, 488–493. doi:10.1190/1.1438319
- Basilone, L., Sulli, A., Gasparo Morticelli, M., 2016. The relationships between soft-sediment deformation structures and synsedimentary extensional tectonics in Upper Triassic deep-water carbonate succession (Southern Tethyan rifted continental margin ??? Central Sicily). *Sediment. Geol.* 344, 310–322. doi:10.1016/j.sedgeo.2016.01.010
- Beard, D.C., Weyl, P.K., Bear, D.C., Weyl, P.K., 1973. Influence of texture on porosity and permeability of unconsolidated sands. *Am. Assoc. Pet. Geol. Bull.* 57, 349–369. doi:10.1306/819A4272-16C5-11D7-8645000102C1865D
- Beaubouef, R.T., Friedmann, S.J., 2000. High resolution seismic/sequence stratigraphic framework for the evolution of the Pleistocene intra slope basins, Western Gulf of Mexico: depositional models and reservoir analogs. GCSSEPM Found. 20th Annu. Res. Conf. Deep. Reserv. World.
- Beaubouef, R.T., Abreu, V., 2010. MTCs of the Brazos-Trinity Slope System; Thoughts on the Sequence Stratigraphy of MTCs and Their Possible Roles in Shaping Hydrocarbon Traps, in: *Submarine Mass Movements and Their Consequences*. Springer Netherlands, Dordrecht, pp. 475–490. doi:10.1007/978-90-481-3071-9_39
- Bernhardt, A., Stright, L., Lowe, D.R., 2012. Channelized debris-flow deposits and their impact on turbidity currents: The Puchkirchen axial channel belt in the Austrian Molasse Basin. *Sedimentology* 59, 2042–2070. doi:10.1111/j.1365-3091.2012.01334.x
- Bisewski, H., 1990. Occurrence and depositional environment of the Lower Cretaceous sands in the southern Witch Ground Graben. *Geol. Soc. London, Spec. Publ.* 55, 325–338.
- Blackbourn, G.A., Thomson, M.E., 2000. Britannia Field, UK North Sea: petrographic constraints on Lower Cretaceous provenance, facies and the origin of slurry-flow deposits. *Pet. Geosci.* 6, 329–343. doi:10.1144/petgeo.6.4.329
- Boccaletti, M., Calamita, F., Deiana, G., Gelati, R., Massari, F., Moratti, G., Ricci Lucchi, F., 1990. Migrating foredeep-thrust belt systems in the northern Apennines and southern Alps. *Palaeogeogr. Palaeoclimatol. Palaeoecol.* 77, 3–14. doi:10.1016/0031-0182(90)90095-O
- Bøe, R., Hovland, M., Instanes, A., Rise, L., Vasshus, S., 2000. Submarine slide scars and mass movements in Karmsundet and Skudenesfjorden, southwestern Norway: morphology and evolution. *Mar. Geol.* 167, 147–165.

doi:10.1016/S0025-3227(00)00017-7

- Bott, M.H.P., 1980. Mechanisms of subsidence at passive continental margins. *Dyn. plate Inter.* 27–35.
- Bouma, A.H., 1962. *Sedimentology of some Flysch deposits; a graphic approach to facies interpretation.* Amsterdam, Elsevier 168.
- Bouma, A.H., 2004. Key controls on the characteristics of turbidite systems. *Geol. Soc. London, Spec. Publ.* 222, 9–22. doi:10.1144/GSL.SP.2004.222.01.02
- Bouriak, S., Vanneste, M., Saoutkine, A., 2000. Inferred gas hydrates and clay diapirs near the Storegga Slide on the southern edge of the Vøring Plateau, offshore Norway. *Mar. Geol.* 163, 125–148.
- Brami, T.R., Pirmez, C., Archie, C., Heeralal, S., Holman, K.L., 2000. Late Pleistocene Deep-Water Stratigraphy and Depositional Processes, Offshore Trinidad and Tobago, in: *Deep-Water Reservoirs of the World: 20th Annual. SOCIETY OF ECONOMIC PALEONTOLOGISTS AND MINERALOGISTS*, pp. 104–115. doi:10.5724/gcs.00.15.0104
- Branney, M.J., Kokelaar, B.P., 2002. *Pyroclastic density currents and the sedimentation of ignimbrites.* Geological Society of London.
- Brunden, D., Prior, D.B., 1984. *Slope Instability*, Wiley. Toronto.
- Brunt, R.L., McAffrey, W.D., Kneller, B.C., 2004. Experimental Modeling of the Spatial Distribution of Grain Size Developed in a Fill-and-Spill Mini-Basin Setting. *J. Sediment. Res.* 74, 438–446. doi:10.1306/093003740438
- Bryn, P., Berg, K., Forsberg, C.F., Solheim, A., Kvalstad, T.J., 2005. Explaining the Storegga Slide. *Mar. Pet. Geol.* 22, 11–19. doi:10.1016/j.marpetgeo.2004.12.003
- Buckee, C., Kneller, B., Peakall, J., 2001. Turbulence Structure in Steady, Solute-Driven Gravity Currents, in: *Particulate Gravity Currents.* Blackwell Publishing Ltd., Oxford, UK, pp. 173–187. doi:10.1002/9781444304275.ch13
- Bugge, T., Befring, S., Belderson, R.H., Eidvin, T., Jansen, E., Kenyon, N.H., Holtedahl, H., Sejrup, H.P., 1987. A giant three-stage submarine slide off Norway. *Geo-marine Lett.* 7, 191–198.
- Bull, S., Cartwright, J., Huuse, M., 2009. A review of kinematic indicators from mass-transport complexes using 3D seismic data. *Mar. Pet. Geol.* 26, 1132–1151. doi:10.1016/j.marpetgeo.2008.09.011
- Burne, R. V., 1970. The origin and significance of sand volcanoes in the Bude Formation (Cornwall). *Sedimentology* 15, 211–228.
- Burne, R. V., 1998. The return of “The Fan That Never Was” : Westphalian turbidite systems in the Variscan Culm Basin: Bude Formation (southwest England).

- Sedimentology 45, 961–975. doi:10.1046/j.1365-3091.1998.00184.x
- Butler, R.W.H., McCaffrey, W.D., 2010. Structural evolution and sediment entrainment in mass-transport complexes: outcrop studies from Italy. *J. Geol. Soc. London*. 167, 617–631. doi:10.1144/0016-76492009-041
- Butler, R.W.H., Turner, J.P., 2010. Gravitational collapse at continental margins: products and processes; an introduction. *J. Geol. Soc. London*. 167, 569–570. doi:10.1144/0016-76492010-003
- Butler, R.W.H., Eggenhuisen, J.T., Haughton, P., McCaffrey, W.D., 2015. Interpreting syndepositional sediment remobilization and deformation beneath submarine gravity flows; a kinematic boundary layer approach. *J. Geol. Soc. London*. 2014–150. doi:10.1144/jgs2014-150
- Canals, M., Lastras, G., Urgeles, R., Casamor, J.L., Mienert, J., Cattaneo, A., De Batist, M., Hafliadon, H., Imbo, Y., Laberg, J.S., Locat, J., Long, D., Longva, O., Masson, D.G., Sultan, N., Trincardi, F., Bryn, P., 2004. Slope failure dynamics and impacts from seafloor and shallow sub-seafloor geophysical data: Case studies from the COSTA project. *Mar. Geol.* 213, 9–72. doi:10.1016/j.margeo.2004.10.001
- Cardona, S., Wood, L.J., Day-Stirrat, R.J., Moscardelli, L., 2016. Fabric development and pore-throat reduction in a mass-transport deposit in the Jubilee Gas Field, Eastern Gulf of Mexico: consequences for the sealing capacity of MTDs, in: *Submarine Mass Movements and Their Consequences*. Springer, pp. 27–37.
- Carter, R.M., 1975. A Discussion and Classification of Subaqueous. *Earth-Science Rev.* 11, 145–177.
- Cayley, G.T., 1987. Hydrocarbon migration in the central North Sea. *Pet. Geol. northwest Eur.* London, Graham Trotman 549–555.
- Chopra, S., Marfurt, K.J., 2012. Seismic attribute expression of differential compaction. *SEG Tech. Progr. Expand. Abstr.* 2012 1–5. doi:10.1190/segam2012-1323.1
- Choux, C.M., Druitt, T.H., 2002. Analogue study of particle segregation in pyroclastic density currents, with implications for the emplacement mechanisms of large ignimbrites. *Sedimentology* 49, 907–928.
- Choux, C., Druitt, T., Thomas, N., 2004. Stratification and particle segregation in flowing polydisperse suspensions, with applications to the transport and sedimentation of pyroclastic density currents. *J. Volcanol. Geotherm. Res.* 138, 223–241. doi:10.1016/j.jvolgeores.2004.07.004
- Clark, D.N., Riley, L.A., Ainsworth, N.R., 1993. Stratigraphic, structural and depositional history of the Jurassic in the Fisher Bank Basin, UK North Sea. *Pet.*

- Geol. Conf. Proc. 4, 415–424. doi:10.1144/0040415
- Clark, I.R., Cartwright, J.A., 2009. Interactions between submarine channel systems and deformation in deepwater fold belts: Examples from the Levant Basin, Eastern Mediterranean sea. *Mar. Pet. Geol.* 26, 1465–1482.
- Conti, S., 2001. Gli intervalli pelitici della Formazione Marnoso-arenacea del Mugello (Miocene medio): relazioni fra tettonica, fluidi freddi e instabilità sedimentaria. *Boll. della Soc. Geol. Ital.* 120, 125–138.
- Coperstake, P., Sims, A., Crittenden, S., Hamar, G., Ineson, J., Rose, P., Tringham, M., 2003. Lower Cretaceous, in: Evans, D., Graham, C., Armour, A. and Bathurst, P. (Eds). (Ed.), *The Millennium Atlas: Petroleum Geology of the Central and Northern North Sea*. The Geological Society of London, London, pp. 191–211.
- Cornford, C., 1998. Source rocks and hydrocarbons of the North Sea. *Pet. Geol. North Sea Basic Concepts Recent Adv. Fourth Ed.* 376–462.
- Cossey, S.P.J., 2011. Mass-transport deposits in the upper Paleocene Chicotepec Formation, Mexico. *Mass-Transport Depos. Deep. Settings* 96, 269–277. doi:-
- Coward, M.P., 1990. The Precambrian, Caledonian and Variscan framework to NW Europe. *Geol. Soc. London, Spec. Publ.* 55, 1–34. doi:10.1144/GSL.SP.1990.055.01.01
- Crittenden, S., Cole, J.M., Kirk, M.J., 1997. The distribution of Aptian sandstone in the Central and Northern North Sea (UK Sector): a lowstand systems tract “play.” *J. Pet. Geol.* 20, 3–25. doi:10.1111/j.1747-5457.1997.tb00753.x
- Cronin, B.T., Owen, D., Hartley, A.J., Kneller, B.C., 1998. Slumps, debris flows and sandy deep-water channel systems: implications for the application of sequence stratigraphy to deep water clastic sediments. *J. Geol. Soc. London.* 155, 429–432. doi:10.1144/gsjgs.155.3.0429
- Crutchley, G.J., Karstens, J., Berndt, C., Talling, P.J., Watt, S.F.L., Vardy, M.E., Hühnerbach, V., Urlaub, M., Sarkar, S., Klaeschen, D., Paulatto, M., Le Friant, A., Lebas, E., Maeno, F., 2013. Insights into the emplacement dynamics of volcanic landslides from high-resolution 3D seismic data acquired offshore Montserrat, Lesser Antilles. *Mar. Geol.* 335, 1–15. doi:10.1016/j.margeo.2012.10.004
- Dall’Olio, E., Felletti, F., Muttoni, G., 2013. Magnetic-Fabric Analysis As A Tool To Constrain Mechanisms of Deep-Water Mudstone Deposition In the Marnoso Arenacea Formation (Miocene, Italy). *J. Sediment. Res.* 83, 170–182. doi:10.2110/jsr.2013.12
- Damuth, J.E., 1978. Echo character of the Norwegian—Greenland Sea: relationship

- to Quaternary sedimentation. *Mar. Geol.* 28, 1–36.
- Davis, C., Haughton, P., McCaffrey, W.D., Scott, E., Hogg, N., Kitching, D., 2009. Character and distribution of hybrid sediment gravity flow deposits from the outer Forties Fan, Palaeocene Central North Sea, UKCS. *Mar. Pet. Geol.* 26, 1919–1939. doi:10.1016/j.marpetgeo.2009.02.015
- de Jager, J., 1979. The relation between tectonics and sedimentary along the “Sillaro Line” (Northern Appennines, Italy). PhD Thesis. Utrecht University.
- de Leeuw, J., 2012. Controls on the architecture of turbidite sandstone in MTD dominated settings; the Vocontian paleomargin, SE France. MSc Thesis.
- de Leeuw, J., Eggenhuisen, J.T., Cartigny, M.J.B., 2016. Morphodynamics of submarine channel inception revealed by new experimental approach. *Nat. Commun.* 7, 10886. doi:10.1038/ncomms10886
- del Pino Sanchez, A., 2006. The kinematic significance of small-scale remobilisation fabrics in deep-water sediments: implications for facies architecture in slope-adjacent settings. PhD Thesis. University of Leeds.
- Deptuck, M.E., Piper, D.J.W., Savoye, B., Gervais, A., 2008. Dimensions and architecture of late Pleistocene submarine lobes off the northern margin of East Corsica. *Sedimentology* 55, 869–898. doi:10.1111/j.1365-3091.2007.00926.x
- Di Biase, D., Mutti, E., 2002. The “proto adriatic basin,” in: *Revisiting Turbidites of the Marnoso Arenacea Formation and Their Basin-Margin Equivalents: Problems with Classic Models: Excursion Guidebook*, 64 Th European Association of Geoscientists and Engineers Conference and Exhibition. pp. 1–4.
- Dorrell, R.M., Darby, S.E., Peakall, J., Sumner, E.J., Parsons, D.R., Wynn, R.B., 2013. Superelevation and overspill control secondary flow dynamics in submarine channels. *J. Geophys. Res. Ocean.* 118, 3895–3915. doi:10.1002/jgrc.20277
- Dott, R.H., 1963. Dynamics of Subaqueous Gravity Depositional Processes. *Am. Assoc. Pet. Geol. Bull.* 47, 104–128. doi:10.1306/BC743973-16BE-11D7-8645000102C1865D
- Downie, R.A., 2009. *Devonian. Pet. Geol. North Sea Basic Concepts Recent Adv.* Fourth Ed. 85–103.
- Duperret, A., Bourgois, J., Lagabrielle, Y., Suess, E., 1995. Slope instabilities at an active continental margin: Large-scale polyphase submarine slides along the northern Peruvian margin, between 5 S and 6 S. *Mar. Geol.* 122, 303–328.
- Dykstra, M., 2005. Review of mass-transport: processes and products.
- Dykstra, M., 2005. Dynamics of Submarine Sediment Mass-Transport, from the Shelf to the Deep Sea. PhD Thesis. University of California - Santa Barbara.

- Dykstra, M., Kneller, B., Gardner, M., Gamberi, F., 2006. A field guide to accompany the “Stratigraphic development of large-scale turbidite slope systems: rules for reservoir modeling and prediction” research consortium annual meeting, Bologna, Italy, 2006, in: Field Guide. pp. 1–17.
- Dykstra, M., Garyfalou, K., Kertznus, V., Kneller, B., Milana, J.P., Molinaro, M., Szuman, M., Thompson, P., 2011. Mass-Transport Deposits: Combining Outcrop Studies and Seismic Forward Modeling to Understand Lithofacies Distributions, Deformation, and their Seismic Stratigraphic Expression, in: Mass-Transport Deposits in Deepwater Settings. SEPM (Society for Sedimentary Geology), pp. 293–310. doi:10.2110/sepmsp.096.293
- Edwards, D.A., Leeder, M.R., Best, J.L., Pantin, H.M., 1994. On experimental reflected density currents and the interpretation of certain turbidites. *Sedimentology* 41, 437–461.
- Egawa, K., Furukawa, T., Saeki, T., Suzuki, K., Narita, H., 2013. Three-dimensional paleomorphologic reconstruction and turbidite distribution prediction revealing a Pleistocene confined basin system in the northeast Nankai Trough area. *Am. Assoc. Pet. Geol. Bull.* 97, 781–798. doi:10.1306/10161212014
- Eggenhuisen, J.T., 2009. The interaction between substrate evolution and turbidity current development. PhD Thesis. University of Leeds.
- Eggenhuisen, J.T., McCaffrey, W.D., Haughton, P.D.W., Butler, R.W.H., Moore, I., Jarvie, A., Hakes, W.G., 2010. Reconstructing large-scale remobilisation of deep-water deposits and its impact on sand-body architecture from cored wells: The Lower Cretaceous Britannia Sandstone Formation, UK North Sea. *Mar. Pet. Geol.* 27, 1595–1615. doi:10.1016/j.marpetgeo.2010.04.005
- Elmore, R.D., Pilkey, O.H., Cleary, W.J., Curran, H.A., 1979. Black Shell turbidite, Hatteras Abyssal Plain, western Atlantic Ocean. *Bull. Geol. Soc. Am.* 90, 1165–1176. doi:10.1130/0016-7606(1979)90<1165:BSTHAP>2.0.CO;2
- Embley, R.W., 1976. New evidence for occurrence of debris flow deposits in the deep sea. *Geology* 4, 371. doi:10.1130/0091-7613(1976)4<371:NEFOOD>2.0.CO;2
- Ercilla, G., Alonso, B., Wynn, R.B., Baraza, J., 2002. Turbidity current sediment waves on irregular slopes: observations from the Orinoco sediment–wave field. *Mar. Geol.* 192, 171–187. doi:10.1016/S0025-3227(02)00554-6
- Erratt, D., Thomas, G.M., Wall, G.R.T., 1999. The evolution of the Central North Sea Rift, in: *Petroleum Geology of Northwest Europe: Proceedings of the 5th Conference*. Geological Society of London, pp. 63–82. doi:10.1144/0050063
- Evans, D., King, E.L., Kenyon, N.H., Brett, C., Wallis, D., 1996. Evidence for long-term instability in the Storegga Slide region off western Norway. *Mar. Geol.* 130,

281–292.

- Evans, D., Harrison, Z., Shannon, P.M., Laberg, J.S., Nielsen, T., Ayers, S., Holmes, R., Hoults, R.J., Lindberg, B., Hafliðason, H., 2005. Palaeoslides and other mass failures of Pliocene to Pleistocene age along the Atlantic continental margin of NW Europe. *Mar. Pet. Geol.* 22, 1131–1148.
- Fairweather, L., 2014. Mechanisms of supra MTD topography generation and the interaction of turbidity currents with such deposits. PhD Thesis. University of Aberdeen.
- Fallgatter, C., Kneller, B., Paim, P.S.G., Milana, J.P., 2016. Transformation, partitioning and flow-deposit interactions during the run-out of megaflores. *Int. Assoc. Sedimentol. Spec. Publ.* 359–387. doi:10.1111/sed.12307
- Felletti, F., 2002. Complex bedding geometries and facies associations of the turbiditic fill of a confined basin in a transpressive setting (Castagnola Fm., Tertiary Piedmont Basin, NW Italy). *Sedimentology* 49, 645–667. doi:10.1046/j.1365-3091.2002.00467.x
- Fernández, O., Muñoz, J.A., Arbués, P., Falivene, O., Marzo, M., 2004. Three-dimensional reconstruction of geological surfaces: An example of growth strata and turbidite systems from the Ainsa basin (Pyrenees, Spain). *Am. Assoc. Pet. Geol. Bull.* 88, 1049–1068. doi:10.1306/02260403062
- Fisher, R., 1983. Flow transformations in sediment gravity flows. *Geology* 11, 273–274. doi:10.1130/0091-7613(1983)11
- Fisher, R. V., 1990. Transport and deposition of a pyroclastic surge across an area of high relief: the 18 May 1980 eruption of Mount St. Helens, Washington. *Geol. Soc. Am. Bull.* 102, 1038–1054.
- Fonnesu, M., Haughton, P.D.W., Felletti, F., McCaffrey, W.D., 2015. Short length-scale variability of hybrid event beds and its applied significance. *Mar. Pet. Geol.* 67, 583–603. doi:10.1016/j.marpetgeo.2015.03.028
- Fonnesu, M., Patacci, M., Haughton, P.D.W., Felletti, F., McCaffrey, W.D., 2016. Hybrid Event Beds Generated By Local Substrate Delamination on a Confined-Basin Floor. *J. Sediment. Res.* 929–943. doi:10.2110/jsr.2016.58
- Fontana, D., McBride, E.F., Kugler, R., 1986. Diagenesis and porosity evolution of submarine-fan and basin-plain sandstones, Marnoso-Arenacea Formation, northern Apennines, Italy. *Bull. Can. Pet. Geol.* 34, 313–328.
- Frey Martinez, J., Cartwright, J., Hall, B., 2005. 3D seismic interpretation of slump complexes: examples from the continental margin of Israel. *Basin Res.* 17, 83–108. doi:10.1111/j.1365-2117.2005.00255.x
- Frey-Martínez, J., Cartwright, J., James, D., 2006. Frontally confined versus frontally

- emergent submarine landslides: A 3D seismic characterisation. *Mar. Pet. Geol.* 23, 585–604. doi:10.1016/j.marpetgeo.2006.04.002
- Frey-Martinez, J., 2007. 3D Seismic Interpretation of Mass Transport Deposits: Implications for Basin Analysis and Geohazard Evaluation. *Submar. Mass Movements Their Consequences* 28, 553–568. doi:10.1007/978-90-481-3071-9
- Frey-Martinez, J., 2010. *Submarine Mass Movements and Their Consequences*, Submarine Mass Movements and Their Consequences. Springer Netherlands, Dordrecht. doi:10.1007/978-90-481-3071-9
- Fukuda, K., Suzuki, M., Ito, M., 2015. The origin and internal structures of submarine-slide deposits in a lower Pleistocene outer-fan succession in the Kazusa Forearc Basin On The Boso Peninsula of Japan. *Sediment. Geol.* 321, 70–85. doi:10.1016/j.sedgeo.2015.03.009
- Gamberi, F., 2010. Subsurface sediment remobilization as an indicator of regional-scale defluidization within the upper Tortonian Marnoso-arenacea formation (Apenninic foredeep, northern Italy). *Basin Res.* 22, 562–577. doi:10.1111/j.1365-2117.2010.00470.x
- Gamberi, F., Rovere, M., 2011. Architecture of a modern transient slope fan (Villafranca fan, Gioia basin-Southeastern Tyrrhenian Sea). *Sediment. Geol.* 236, 211–225. doi:10.1016/j.sedgeo.2011.01.007
- Gamberi, F., Rovere, M., Marani, M., 2011. Mass-transport complex evolution in a tectonically active margin (Gioia Basin, Southeastern Tyrrhenian Sea). *Mar. Geol.* 279, 98–110. doi:10.1016/j.margeo.2010.10.015
- Gamboa, D.A., 2011. An integrated seismic-scale analysis of reservoir compartmentalisation on continental margins: the Espirito Santo Basin, SE Brazil. PhD Thesis. doi:10.1144/gsjgs.135.1.0025
- Gamboa, D., Alves, T.M., 2015. Spatial and dimensional relationships of submarine slope architectural elements: A seismic-scale analysis from the Espirito Santo Basin (SEBrazil). *Mar. Pet. Geol.* 64, 43–57. doi:10.1016/j.marpetgeo.2015.02.035
- Gandolfi, G., Paganelli, L., Zuffa, G.G., 1983. Petrology and dispersal pattern in the Marnoso-arenacea Formation (Miocene, Northern Apennines). *J. Sediment. Res.* 53, 493–507.
- Gandolfi, G., Paganelli, L., Cavazza, W., 2007. Heavy-mineral associations as tracers of limited compositional mixing during turbiditic sedimentation of the Marnoso-Arenacea Formation (Miocene, Northern Apennines, Italy). *Dev. Sedimentol.* 58, 621–645.

- Garcia, M., Parker, G., 1989. Experiments on hydraulic jumps in turbidity currents near a canyon-fan transition. *Science* (80-.). 245, 393–396. doi:10.1126/science.245.4916.393
- Garcia, M., Parker, G., 1993. Experiments on the entrainment of sediment into suspension by a dense bottom current. *J. Geophys. Res. Ser.* 98, 4793.
- Garcia, M.H., 1994. Depositional Turbidity Currents Laden with Poorly Sorted Sediment. *J. Hydraul. Eng.* 120, 1240–1263. doi:10.1061/(ASCE)0733-9429(1994)120:11(1240)
- Gardner, J. V., Prior, D.B., Field, M.E., 1999. Humboldt Slide — a large shear-dominated retrogressive slope failure. *Mar. Geol.* 154, 323–338. doi:10.1016/S0025-3227(98)00121-2
- Gardner, M.H., Borer, J.M., Romans, B.W., Baptista, N., Kling, E.K., Hanggoro, D., Melick, J.J., Wagerle, R.M., Dechesne, M., Carr, M.M., Amerman, R., Atan, S., 2008. Stratigraphic Models for Deep-Water Sedimentary Systems, in: *Answering the Challenges of Production from Deep-Water Reservoirs: Analogues and Case Histories to Aid a New Generation: 28th Annual. SOCIETY OF ECONOMIC PALEONTOLOGISTS AND MINERALOGISTS*, pp. 77–175. doi:10.5724/gcs.08.28.0077
- Garrett, S.W., Atherton, T., Hurst, A., 2000. Lower Cretaceous deep-water sandstone reservoirs of the UK Central North Sea. *Pet. Geosci.* 6, 231–240. doi:10.1144/petgeo.6.3.231
- Gary L. Peterson, 1965. Implications of Two Cretaceous Mass Transport Deposits, Sacramento Valley, California. *SEPM J. Sediment. Res. Vol.* 35. doi:10.1306/74D7128A-2B21-11D7-8648000102C1865D
- Garyfalou, K., 2014. Integrated analysis of mass- transport deposits: Outcrop, 3D seismic interpretation and fast fourier transform. PhD Thesis. University of Aberdeen.
- Gautier, D.L., 2005. Kimmeridgian Shales Total Petroleum System of the North Sea Graben Province. *U.S. Geol. Surv. Bull.* 2204–C, 29.
- Gawthorpe, R.L., Clemmey, H., 1985. Geometry of submarine slides in the Bowland Basin (Dinantian) and their relation to debris flows. *J. Geol. Soc. London.* 142, 555–565. doi:10.1144/gsjgs.142.3.0555
- Gee, M.J.R., Masson, D.G., Watts, A.B., Allen, P.A., 1999. The Saharan debris flow: An insight into the mechanics of long runout submarine debris flows. *Sedimentology* 46, 317–335. doi:10.1046/j.1365-3091.1999.00215.x
- Gee, M.J.R., Uglas, D.O., Sson, G.M. a, Watts, a B., Mitchell, N.C., 2001. Passage of debris flows and turbidity currents through a topographic constriction : sea

- oor erosion and de-fection of-ow pathways. *Sedimentology* 3.
- Gee, M.J.R., Gawthorpe, R.L., Friedmann, J.S., 2005. Giant striations at the base of a submarine landslide. *Mar. Geol.* 214, 287–294. doi:10.1016/j.margeo.2004.09.003
- Gee, M.J.R., Gawthorpe, R.L., Friedmann, S.J., 2006. Triggering and Evolution of a Giant Submarine Landslide, Offshore Angola, Revealed by 3D Seismic Stratigraphy and Geomorphology. *J. Sediment. Res.* 76, 9–19. doi:10.2110/jsr.2006.02
- Gee, M.J.R., Gawthorpe, R.L., 2007. Early evolution of submarine channels offshore Angola revealed by three-dimensional seismic data. *Geol. Soc. London, Spec. Publ.* 277, 223–235.
- Gee, M.J.R., Uy, H.S., Warren, J., Morley, C.K., Lambiase, J.J., 2007. The Brunei slide: A giant submarine landslide on the North West Borneo Margin revealed by 3D seismic data. *Mar. Geol.* 246, 9–23. doi:10.1016/j.margeo.2007.07.009
- Ghibaudo, G., 1992. Subaqueous sediment gravity flow deposits: practical criteria for their field description and classification. *Sedimentology* 39, 423–454. doi:10.1111/j.1365-3091.1992.tb02126.x
- Glennie, K.W., Underhill, J.R., 1998. Origin, development and evolution of structural styles. *Pet. Geol. North Sea Basic Concepts Recent Adv. Fourth Ed.* 42–84.
- Goldfinger, C., Kulm, L.D., McNeill, L.C., Watts, P., 2000. Super-scale failure of the southern Oregon Cascadia margin. *Pure Appl. Geophys.* 157, 1189–1226.
- Grando, G., McClay, K., 2004. Structural evolution of the Frampton growth fold system, Atwater Valley-Southern Green Canyon area, deep water Gulf of Mexico. *Mar. Pet. Geol.* 21, 889–910.
- Greene, H.G., Murai, L.Y., Watts, P., Maher, N. a., Fisher, M. a., Paull, C.E., Eichhubl, P., 2006. Submarine landslides in the Santa Barbara Channel as potential tsunami sources. *Nat. Hazards Earth Syst. Sci.* 6, 63–88. doi:10.5194/nhess-6-63-2006
- Gupta, S., Underbill, J.R., Sharp, I.R., Gawthorpe, R.L., 1999. Role of fault interactions in controlling synrift sediment dispersal patterns: Miocene, Abu Alaqa Group, Suez Rift, Sinai, Egypt. *Basin Res.* 11, 167–189. doi:10.1046/j.1365-2117.1999.00300.x
- Guy, M., 1992. Facies analysis of the Kopervik sand interval interval, Kilda Field, Block 16/26, UK North Sea. *Geol. Soc. Spec. Publ.* 67, 187–220. doi:10.1144/GSL.SP.1992.067.01.08
- Haflidason, H., Sejrup, H.P., Bryn, P., Lien, R., Masson, D., Jacobs, C., Huehnerbach, V., Berg, K., 2002. The architecture and slide mechanism of the

- Storegga Slide, Mid Norwegian margin, in: NGF Abstracts and Proceedings, Annual Meeting in Trondheim, Norwegian Petroleum Society, Stavanger. pp. 80–81.
- Hafliðason, H., Sejrup, H.P., Nygård, A., Mienert, J., Bryn, P., Lien, R., Forsberg, C.F., Berg, K., Masson, D., 2004. The Storegga Slide: architecture, geometry and slide development. *Mar. Geol.* 213, 201–234. doi:10.1016/j.margeo.2004.10.007
- Hailwood, E., Ding, F., 2000. Sediment transport and dispersal pathways in the Lower Cretaceous sands of the Britannia Field, derived from magnetic anisotropy. *Pet. Geosci.* 6, 369–379. doi:10.1144/petgeo.6.4.369
- Hampton, M.A., 1972. The role of subaqueous debris flow in generating turbidity currents. *J. Sediment. Res.* 42.
- Hampton, M.A., 1975. Competence of fine-grained debris flows. *J. Sediment. Res.* 45.
- Hampton, M. a., Lee, H.J., Locat, J., 1996. Submarine landslides. *Rev. Geophys.* 34, 33–59. doi:10.1029/95RG03287
- Hand, B.M., 1997. Inverse Grading Resulting from Coarse-sediment Transport Lag. *SEPM J. Sediment. Res. Vol. 67.* doi:10.1306/D426850E-2B26-11D7-8648000102C1865D
- Hansen, J., Laciš, A., Rind, D., Russell, G., Stone, P., Fung, I., Ruedy, R., Lerner, J., 1984. Climate sensitivity: Analysis of feedback mechanisms. *Clim. Process. Clim. Sensit.* 130–163.
- Hansen, S., 1996. A compaction trend for Cretaceous and Tertiary shales on the Norwegian shelf based on sonic transit times. *Pet. Geosci.* 2, 159–166. doi:10.1144/petgeo.2.2.159
- Haq, B.U., 1995. Growth and decay of gas hydrates: a forcing mechanism for abrupt climate change and sediment wasting on ocean margins? *K. Akad. van Wet. Verh. Afd. Natuurkd.* 44, 191–203.
- Haq, B.U., 2009. Deep-sea response to eustatic change and significance of gas hydrates for continental margin stratigraphy. *Seq. Stratigr. Facies Assoc. (Special Publ. 18 IAS)* 100, 93.
- Haughton, P., 1994. Deposits of deflected and ponded turbidity currents, Sorbas Basin, Southeast Spain. *J. Sediment. Res.* 64, 233–246. doi:10.1306/D4267D6B-2B26-11D7-8648000102C1865D
- Haughton, P.D.W., 2000. Evolving turbidite systems on a deforming basin floor, Tabernas, SE Spain. *Sedimentology* 47, 497–518. doi:10.1046/j.1365-3091.2000.00293.x

- Haughton, P.D., Barker, S.P., McCaffrey, W.D., 2003. "Linked" debrites in sand-rich turbidite systems - Origin and significance. *Sedimentology* 50, 459–482. doi:10.1046/j.1365-3091.2003.00560.x
- Haughton, P.D.W., Davis, C., McCaffrey, W.D., Barker, S.P., 2009. Hybrid sediment gravity flow deposits - Classification, origin and significance. *Mar. Pet. Geol.* 26, 1900–1918. doi:10.1016/j.marpetgeo.2009.02.012
- Heiniö, P., Davies, R.J., 2006. Degradation of compressional fold belts: Deep-water Niger Delta. *Am. Assoc. Pet. Geol. Bull.* 90, 753–770. doi:10.1306/11210505090
- Hill, P.J., Palfrey, A.J., 2003. The Britannia Field, Blocks 15/29a, 15/30, 16/26, 16/27a, 16/27b, UK North Sea. *Geol. Soc. London, Mem.* 20, 415–429. doi:10.1144/gsl.mem.2003.020.01.34
- Hjelstuen, B.O., Sejrup, H.P., Haflidason, H., Berg, K., Bryn, P., 2004. Neogene and Quaternary depositional environments on the Norwegian continental margin, 62°N–68°N. *Mar. Geol.* 213, 257–276. doi:10.1016/j.margeo.2004.10.009
- Hjelstuen, B.O., Eldholm, O., Faleide, J.I., 2007. Recurrent Pleistocene mega-failures on the SW Barents Sea margin. *Earth Planet. Sci. Lett.* 258, 605–618. doi:10.1016/j.epsl.2007.04.025
- Hodgson, D.M., 2009. Distribution and origin of hybrid beds in sand-rich submarine fans of the Tanqua depocentre, Karoo Basin, South Africa. *Mar. Pet. Geol.* 26, 1940–1956.
- Homza, T.X., 2004. A structural interpretation of the Fish Creek slide (Lower Cretaceous), northern Alaska. *Am. Assoc. Pet. Geol. Bull.* 88, 265–278. doi:10.1306/10270303029
- Hu, X., Jansa, L., Wang, C., Sarti, M., Bak, K., Wagreich, M., Michalik, J., Sotak, J., 2005. Upper Cretaceous oceanic red beds (CORBs) in the Tethys: occurrences, lithofacies, age, and environments. *Cretac. Res.* 26, 3–20.
- Hüeneke, H., Mulder, T., 2011. *Deep-Sea Sediments, Developments in Sedimentology.*
- Hühnerbach, V., Masson, D.G., 2004. Landslides in the North Atlantic and its adjacent seas: an analysis of their morphology, setting and behaviour. *Mar. Geol.* 213, 343–362. doi:10.1016/j.margeo.2004.10.013
- Hunt, J.E., Talling, P.J., Clare, M.A., Jarvis, I., Wynn, R.B., 2014. Long-term (17 Ma) turbidite record of the timing and frequency of large flank collapses of the Canary Islands. *Geochemistry, Geophys. Geosystems* 15, 3322–3345. doi:10.1002/2014GC005232
- Huyghe, P., Foata, M., Deville, E., Mascle, G., Cagna, R., Callec, Y., Desaubliaux,

- G., Ellouz, N., Griboulard, R., Guerlais, S.H., Lallemand, S., Lebrun, F., Mascle, A., Mugnier, J.L., Padron, C., Prinzhofer, A., Schmitz, J., Wendenbaum, E., 2004. Channel profiles through the active thrust front of the southern Barbados prism. *Geology* 32, 429–432. doi:10.1130/G20000.1
- Ilstad, T., De Blasio, F. V., Elverhøi, A., Harbitz, C.B., Engvik, L., Longva, O., Marr, J.G., 2004. On the frontal dynamics and morphology of submarine debris flows. *Mar. Geol.* 213, 481–497. doi:10.1016/j.margeo.2004.10.020
- Iverson, R.M., 1997. The physics of debris flows. *Rev. Geophys.* 35, 245–296.
- Jackson, C.A.L., Larsen, E., 2008. Temporal constraints on basin inversion provided by 3D seismic and well data: A case study from the South Viking Graben, offshore Norway. *Basin Res.* 20, 397–417. doi:10.1111/j.1365-2117.2008.00359.x
- Jackson, C.A.L., Johnson, H.D., 2009. Sustained turbidity currents and their interaction with debrite-related topography; Labuan Island, offshore NW Borneo, Malaysia. *Sediment. Geol.* 219, 77–96. doi:10.1016/j.sedgeo.2009.04.008
- Jackson, C.A.L., 2011. Three-dimensional seismic analysis of megaclast deformation within a mass transport deposit; Implications for debris flow kinematics. *Geology* 39, 203–206. doi:10.1130/G31767.1
- Jackson, C.A.L., 2012. The initiation of submarine slope failure and the emplacement of mass transport complexes in salt-related minibasins: A three-dimensional seismic-reflection case study from the Santos Basin, offshore Brazil. *Bull. Geol. Soc. Am.* 124, 746–761. doi:10.1130/B30554.1
- Jeremiah, J.M., 2000. Lower Cretaceous turbidites of the Moray Firth: sequence stratigraphical framework and reservoir distribution. *Pet. Geosci.* 6, 309–328. doi:10.1144/petgeo.6.4.309
- Jervey, M.T., 1988. Quantitative geological modeling of siliciclastic rock sequence and their expression, in: *Sea-Level Changes*. SEPM (Society for Sedimentary Geology), pp. 47–69. doi:10.2110/pec.88.01.0047
- Joanne, C., Collot, J.Y., Lamarche, G., Migeon, S., 2010. Continental slope reconstruction after a giant mass failure, the example of the Matakaoa Margin, New Zealand. *Mar. Geol.* 268, 67–84. doi:10.1016/j.margeo.2009.10.013
- Johnson, A.M., 1970. *Physical processes in geology: A method for interpretation of natural phenomena; intrusions in igneous rocks, fractures, and folds, flow of debris and ice*. Freeman, Cooper.
- Johnson, D.A., 1984. The Vema Channel: Physiography, structure, and sediment—Current interactions. *Mar. Geol.* 58, 1–34. doi:10.1016/0025-3227(84)90114-2
- Johnson, H., Lott, G.K., 1993. Lithostratigraphic nomenclature of the UK North Sea.

Cretaceous of the Central North Sea.

- Jones, Garrett, S.W., Macleod, M., Guy, M., Condon, P.J., Notman, L., 1999a. Britannia Field, UK Central North Sea: modelling heterogeneity in unusual deep-water deposits. *Pet. Geol. Northwest Eur. Proc. 5th Conf.* 5, 1115–1124. doi:10.1144/0051115
- Jones, Rorison, P., Frost, R.E., Knipe, R., Colleran, J., 1999b. Tectonostratigraphic development of the southern part of UKCS Quadrant 15 (eastern Witch Ground Graben): implications for the Mesozoic-Tertiary evolution of the Central North Sea Basin. *Pet. Geol. Northwest Eur. Proc. 5th Conf. Pet. Geol. Northwest Eur.* 1, 133–152. doi:10.1144/0050133
- Kane, I.A., Pontén, A.S.M., 2012. Submarine transitional flow deposits in the Paleogene Gulf of Mexico. *Geology* 40, 1119–1122. doi:10.1130/G33410.1
- Kendrick, J.W., 2000. Turbidite Reservoir Architecture in the Northern Gulf of Mexico Deepwater: Insights from the Development of Auger, Tahoe, and Ram/Powell Fields, in: *Deep-Water Reservoirs of the World: 20th Annual. SOCIETY OF ECONOMIC PALEONTOLOGISTS AND MINERALOGISTS*, pp. 450–468. doi:10.5724/gcs.00.15.0450
- King, P.R., Ilg, B.R., Arnot, M., Browne, G.H., Strachan, L.J., Crundwell, M., Helle, K., 2011. Outcrop and seismic examples of mass-transport deposits from a Late Miocene deep-water succession, Taranaki basin, New Zealand, in: *Mass-Transport Deposits in Deepwater Settings*. pp. 311–348.
- Kleverlaan, K., 1987. Gordo megabed: a possible seismite in a tortonian submarine fan, tabernas basin, province almeria, southeast spain. *Sediment. Geol.* 51, 165–180. doi:10.1016/0037-0738(87)90047-9
- Kneller, B., Edwards, D., McCaffrey, W., Moore, R., 1991. Oblique reflection of turbidity currents. *Geology* 19, 250. doi:10.1130/0091-7613(1991)019<0250:OROTC>2.3.CO;2
- Kneller, B., 1995. Beyond the turbidite paradigm: physical models for deposition of turbidites and their implications for reservoir prediction. *Geol. Soc. London, Spec. Publ.* 94, 31–49. doi:10.1144/GSL.SP.1995.094.01.04
- Kneller, B.C., Branney, M.J., 1995. Sustained high-density turbidity currents and the deposition of thick massive sands. *Sedimentology* 42, 607–616. doi:10.1111/j.1365-3091.1995.tb00395.x
- Kneller, B.C., McCaffrey, W.D., 1995. Modelling the effects of salt-induced topography on deposition from turbidity currents, in: *Salt, Sediment and Hydrocarbons: Gulf Coast Section SEPM. SEPM*, pp. 137–145.
- Kneller, B.C., Bennett, S.J., McCaffrey, W.D., 1997. Velocity and turbulence structure

- of density currents and internal solitary waves: potential sediment transport and the formation of wave ripples in deep water. *Sediment. Geol.* 112, 235–250. doi:10.1016/S0037-0738(97)00031-6
- Kneller, B.C., McCaffrey, W.D., 1999. Depositional effects of flow nonuniformity and stratification within turbidity currents approaching a bounding slope; deflection, reflection, and facies variation. *J. Sediment. Res.* 69, 980–991. doi:10.2110/jsr.69.980
- Kneller, B., Buckee, C., 2000. The structure and fluid mechanics of turbidity currents: a review of some recent studies and their geological implications. *Sedimentology* 47, 62–94. doi:10.1046/j.1365-3091.2000.047s1062.x
- Kneller, B.C., McCaffrey, W.D., 2003. The Interpretation of Vertical Sequences in Turbidite Beds: The Influence of Longitudinal Flow Structure. *J. Sediment. Res.* 73, 706–713. doi:10.1306/031103730706
- Kneller, B., Dykstra, M., Fairweather, L., Milana, J.P., 2016. Mass-transport and slope accommodation: Implications for turbidite sandstone reservoirs. *Am. Assoc. Pet. Geol. Bull.* 100, 213–235. doi:10.1306/09011514210
- Krastel, S., Schmincke, H., Jacobs, C.L., Rihm, R., Le Bas, T.P., Alibés, B., 2001. Submarine landslides around the Canary Islands. *J. Geophys. Res. Solid Earth* 106, 3977–3997.
- Krause, F.F., Collins, H.N., Nelson, D.A., Machermer, S.D., French, P.R., 1987. Multiscale anatomy of a reservoir: geological characterization of Pembina-Cardium pool, west-central Alberta, Canada. *Am. Assoc. Pet. Geol. Bull.* 71, 1233–1260.
- Kruit, C., Brouwer, J., Ealey, P., 1976. A deep-water sand fan in the Eocene Bay of Biscay. *Submar. canyons Deep. fans; Mod. ancient.* 240, 383–387. doi:10.1038/physci240059a0
- Kuenen, P.H., Menard, H.W., 1952. Turbidity currents, graded and non-graded deposits. *J. Sediment. Res.* 22.
- Kuenen, P.H., Migliorini, C.I., 1950. Turbidity Currents as a Cause of Graded Bedding. *J. Geol.* 58, 91–127. doi:10.1086/625710
- Kvenvolden, K.A., 1993. Gas hydrates - geological perspective and global change. *Rev. Geophys.* 31, 173–187. doi:10.1029/93RG00268
- Labazuy, P., 1996. Recurrent landslides events on the submarine flank of Piton de la Fournaise volcano (Reunion Island). *Geol. Soc. London, Spec. Publ.* 110, 295–306.
- Laberg, J., Vorren, T.O., Mienert, J., Bryn, P., Lien, R., 2002. The Trænadjupet Slide: a large slope failure affecting the continental margin of Norway 4,000 years ago.

Geo-Marine Lett. 22, 19–24.

- Ladd, G.E., 1935. Landslides, subsidences and rock-falls. American Railway Engineering Association.
- Lamarche, G., Joanne, C., Collot, J.Y., 2008. Successive, large mass-transport deposits in the south Kermadec fore-arc basin, New Zealand: The matakaoa submarine instability complex. *Geochemistry, Geophys. Geosystems* 9. doi:10.1029/2007GC001843
- Lamb, M.P., Hickson, T., Marr, J.G., Sheets, B., Paola, C., Parker, G., 2004. Surging Versus Continuous Turbidity Currents: Flow Dynamics and Deposits in an Experimental Intraslope Minibasin. *J. Sediment. Res.* 74, 148–155. doi:10.1306/062103740148
- Lanteaume, M., Beaudoin, B., Campredon, R., 1967. Figures sédimentaires du flysch “grès d’Annot” du synclinal de Peira-Cava. Editions du Centre national de la recherche scientifique.
- Lastras, G., Canals, M., Urgeles, R., De Batist, M., Calafat, A.M., Casamor, J.L., 2004. Characterisation of the recent BIG’95 debris flow deposit on the Ebro margin, Western Mediterranean Sea, after a variety of seismic reflection data. *Mar. Geol.* 213, 235–255. doi:10.1016/j.margeo.2004.10.008
- Law, A., Raymond, A., White, G., Atkinson, A., Clifton, M., Atherton, T., Dawes, I. a n., Robertson, E., Melvin, A., Brayley, S., 2000. The Kopervik fairway, Moray Firth, UK. *Pet. Geosci.* 6, 265–274. doi:10.1144/petgeo.6.3.265
- Le Friant, A., Ishizuka, O., Boudon, G., Palmer, M.R., Talling, P.J., Villemant, B., Adachi, T., Aljhdali, M., Breikreuz, C., Brunet, M., Caron, B., Coussens, M., Deplus, C., Endo, D., Feuillet, N., Fraas, A.J., Fujinawa, A., Hart, M.B., Hatfield, R.G., Hornbach, M., Jutzeler, M., Kataoka, K.S., Komorowski, J.C., Lebas, E., Lafuerza, S., Maeno, F., Manga, M., Martínez-Colón, M., McCanta, M., Morgan, S., Saito, T., Slagle, A., Sparks, S., Stinton, A., Stroncik, N., Subramanyam, K.S.V., Tamura, Y., Trofimovs, J., Voight, B., Wall-Palmer, D., Wang, F., Watt, S.F.L., 2015. Submarine record of volcanic island construction and collapse in the Lesser Antilles arc: First scientific drilling of submarine volcanic island landslides by IODP Expedition 340. *Geochemistry, Geophys. Geosystems* 16, 420–442. doi:10.1002/2014GC005652
- Lee, C., Nott, J.A., Keller, F.B., Parrish, A.R., 2004. Seismic Expression of the Cenozoic Mass Transport Complexes, Deepwater Tarfaya-Agadir Basin, Offshore Morocco, in: *Offshore Technology Conference*. doi:10.4043/16741-MS
- Lee, G.H., Kim, B., Chang, S.J., Huh, S., Kim, H.-J., 2004. Timing of trap formation in the southwestern margin of the Ulleung Basin, East Sea (Japan Sea) and

- implications for hydrocarbon accumulations. *Geosci. J.* 8, 369–380. doi:10.1007/BF02910473
- Lee, H.J., 2009. Timing of occurrence of large submarine landslides on the Atlantic Ocean margin. *Mar. Geol.* 264, 53–64. doi:10.1016/j.margeo.2008.09.009
- Lee, S.H., Jung, W.-Y., Bahk, J.J., Gardner, J.M., Kim, J.K., Lee, S.H., 2013. Depositional features of co-genetic turbidite–debrite beds and possible mechanisms for their formation in distal lobated bodies beyond the base-of-slope, Ulleung Basin, East Sea (Japan Sea). *Mar. Geol.* 346, 124–140.
- Leigh, S., Hartley, A.J., 1992. Mega-debris flow deposits from the Oligo-Miocene Pindos foreland basin, western mainland Greece: implications for transport mechanisms in ancient deep marine basins. *Sedimentology* 39, 1003–1012. doi:10.1111/j.1365-3091.1992.tb01993.x
- Lewis, K.B., 1971. Slumping on a continental slope inclined at 1–4. *Sedimentology* 16, 97–110.
- Lipman, P.W., Normark, W.R., Moore, J.G., Wilson, J.B., Gutmacher, C.E., 1988. The giant submarine Alika debris slide, Mauna Loa, Hawaii. *J. Geophys. Res.* 93, 4279–4299.
- Locat, J., 2001. Instabilities along ocean margins: a geomorphological and geotechnical perspective. *Mar. Pet. Geol.* 18, 503–512. doi:10.1016/S0264-8172(00)00076-3
- Locat, J., Lee, H.J., 2002. Submarine landslides: advances and challenges. *Can. Geotech. J.* 39, 193–212.
- Long, R.R., 1955. Some aspects of the flow of stratified fluids: 111. continuous density gradients. *Tellus* 7, 341–357.
- Loseth, H., Wensaas, L., Arntsen, B., Hovland, M., 2003. Gas and fluid injection triggering shallow mud mobilization in the Hordaland Group, North Sea. *Geol. Soc. London, Spec. Publ.* 216, 139–157. doi:10.1144/gsl.sp.2003.216.01.10
- Lourenço, S.D.N., Sassa, K., Fukuoka, H., 2006. Failure process and hydrologic response of a two layer physical model: implications for rainfall-induced landslides. *Geomorphology* 73, 115–130.
- Lowe, D.R., 1975. Water escape structures in coarse-grained sediments. *Sedimentology* 22, 157–204. doi:10.1111/j.1365-3091.1975.tb00290.x
- Lowe, D.R., 1979. Sediment gravity flows: their classification and some problems of application to natural flows and deposits. Doyle, N.J., Pilkey, O.H. (Eds.), *Geol. Cont. Slopes*, SEPM Spec. Publ. 27, 75–82.
- Lowe, D.R., 1982. Sediment Gravity Flows: II Depositional Models with Special Reference to the Deposits of High-Density Turbidity Currents. *SEPM J.*

- Sediment. Res. Vol. 52, 279–297. doi:10.1306/212F7F31-2B24-11D7-8648000102C1865D
- Lowe, D.R., 1988. Suspended-load fallout rate as an independent variable in the analysis of current structures. *Sedimentology*. doi:10.1111/j.1365-3091.1988.tb01250.x
- Lowe, D.R., Guy, M., 2000. Slurry-flow deposits in the Britannia Formation (Lower Cretaceous), North Sea: A new perspective on the turbidity current and debris flow problem. *Sedimentology* 47, 31–70. doi:10.1046/j.1365-3091.2000.00276.x
- Lowe, D.R., Guy, M., Palfrey, A., 2003. Facies of slurry-flow deposits, Britannian Formation (Lower Cretaceous), North Sea: Implications for flow evolution and deposit geometry. *Sedimentology* 50, 45–80.
- Lu, H., Shipp, R.C., 2011. Impact of a Large Mass-Transport Deposit on a Field Development in the Upper Slope of Southwestern Sabah, Malaysia, Offshore Northwest Borneo. *Mass-Transport Depos. Deep. Settings, SEPM Spec. Publ.* 96 96, 199–218. doi:-
- Lucente, C.C., 2002. Geometry and emplacement of an extensive submarine slide body (Marnoso-arenacea Fm, northern Apennines, Italy). *Boll. della Soc. Geol. Ital.* 1, 385–392.
- Lucente, C.C., Pini, G.A., 2003. Anatomy and emplacement mechanism of a large submarine slide within a Miocene foredeep in the northern Apennines, Italy: A field perspective. *Am. J. Sci.* 303, 565–602. doi:10.2475/ajs.303.7.565
- Lucente, C.C., 2004. Topography and palaeogeographic evolution of a middle Miocene foredeep basin plain (Northern Apennines, Italy). *Sediment. Geol.* 170, 107–134. doi:10.1016/j.sedgeo.2004.06.002
- Lucente, C.C., Pini, G.A., De Libero, C., 2006. The role of large-scale sedimentary failures at the wedge front-foredeep boundary: A case study from the northern Apennines, Italy. *GeoActa* 5, 113–128.
- Lucente, C.C., Pini, G.A., 2008. Basin-wide mass-wasting complexes as markers of the Oligo-Miocene foredeep-accretionary wedge evolution in the Northern Apennines, Italy. *Basin Res.* 20, 49–71. doi:10.1111/j.1365-2117.2007.00344.x
- Lykousis, V., Roussakis, G., Alexandri, M., Pavlakis, P., Papoulia, I., 2002. Sliding and regional slope stability in active margins: North Aegean Trough (Mediterranean). *Mar. Geol.* 186, 281–298.
- Macdonald, D.I.M., 1993. Controls on Sedimentation at Convergent Plate-Margins, in: *Tectonic Controls and Signatures in Sedimentary Successions*. Blackwell Publishing Ltd., Oxford, UK, pp. 223–257. doi:10.1002/9781444304053.ch13
- Machell, A.J., 2003. AAPG International Conference, in: *AAPG International*

Conference. p. 4.

- Magara, K., 1976. Thickness of removed sedimentary rocks, paleopore pressure, and paleotemperature, southwestern part of Western Canada Basin. *Am. Assoc. Pet. Geol. Bull.* 60, 554–565.
- Maltman, A. (Ed.), 1994. *The Geological Deformation of Sediments*. Springer Netherlands, Dordrecht. doi:10.1007/978-94-011-0731-0
- Marini, M., Felletti, F., Milli, S., Patacci, M., 2016a. The thick-bedded tail of turbidite thickness distribution as a proxy for flow confinement: Examples from tertiary basins of central and northern Apennines (Italy). *Sediment. Geol.* 341, 96–118. doi:10.1016/j.sedgeo.2016.05.006
- Marini, M., Patacci, M., Felletti, F., McCaffrey, W.D., 2016b. Fill to spill stratigraphic evolution of a confined turbidite mini-basin succession, and its likely well bore expression: The Castagnola Fm, NW Italy. *Mar. Pet. Geol.* 69, 94–111. doi:10.1016/j.marpetgeo.2015.10.014
- Marjanac, T., 1990. Reflected sediment gravity flows and their deposits in flysch of Middle Dalmatia, Yugoslavia. *Sedimentology* 37, 921–929.
- Marr, J.G., Shanmugam, G., Parker, G., Harff, P.A., Shanmugam, G., Parker, G., 2001. Experiments on subaqueous sandy gravity flows: The role of clay and water content in flow dynamics and depositional structures. *Geol. Soc. Am. Bull.* 113, 1377–1386. doi:10.1130/0016-7606(2001)113<1377:EOSSGF>2.0.CO;2
- Martín-Merino, G., Fernández, L.P., Colmenero, J.R., Bahamonde, J.R., 2014. Mass-transport deposits in a Variscan wedge-top foreland basin (Pisuerga area, Cantabrian Zone, NW Spain). *Mar. Geol.* 356, 71–87. doi:10.1016/j.margeo.2014.01.012
- Martinsen, O., 1994. Mass movements, in: *The Geological Deformation of Sediments*. Springer Netherlands, Dordrecht, pp. 127–165. doi:10.1007/978-94-011-0731-0_5
- Martinsen, O.J., Lien, T., Walker, R.G., 2000. Upper Carboniferous Deep Water Sediments, Western Ireland: Analogues for Passive Margin Turbidite Plays, in: *Deep-Water Reservoirs of the World: 20th Annual. SOCIETY OF ECONOMIC PALEONTOLOGISTS AND MINERALOGISTS*, pp. 533–555. doi:10.5724/gcs.00.15.0533
- Maslin, M., Mikkelsen, N., Vilela, C., Haq, B., 1998. Sea-level–and gas-hydrate–controlled catastrophic sediment failures of the Amazon Fan. *Geology* 26, 1107–1110.
- Maslin, M., Owen, M., Day, S., Long, D., 2004. Linking continental-slope failures and climate change: Testing the clathrate gun hypothesis. *Geology* 32, 53.

doi:10.1130/G20114.1

- Maslin, M., Vilela, C., Mikkelsen, N., Grootes, P., 2005. Causes of catastrophic sediment failures of the Amazon Fan. *Quat. Sci. Rev.* 24, 2180–2193. doi:10.1016/j.quascirev.2005.01.016
- Masson, D.G., Huggett, Q.J., Brunsten, D., 1993. The surface texture of the Saharan Debris Flow deposit and some speculations on submarine debris flow processes. *Sedimentology* 40, 583–598. doi:10.1111/j.1365-3091.1993.tb01351.x
- Masson, D.G., 1996. Catastrophic collapse of the volcanic island of Hierro 15 ka ago and the history of landslides in the Canary Islands. *Geology* 24, 231. doi:10.1130/0091-7613(1996)024<0231:CCOTVI>2.3.CO;2
- Masson, D.G., Van Niel, B., Weaver, P.P.E., 1997. Flow processes and sediment deformation in the Canary debris flow on the NW African continental rise. *Sediment. Geol.* 110, 163–179.
- Masson, D.G., Canals, M., Alonso, B., Urgeles, R., Huhnerbach, V., 1998. The Canary Debris Flow: Source area morphology and failure mechanisms. *Sedimentology* 45, 411–432. doi:10.1046/j.1365-3091.1998.0165f.x
- Masson, D., Watts, A., Gee, M.J., Urgeles, R., Mitchell, N., Le Bas, T., Canals, M., 2002. Slope failures on the flanks of the western Canary Islands. *Earth-Science Rev.* 57, 1–35. doi:10.1016/S0012-8252(01)00069-1
- Masson, D.G., Harbitz, C.B., Wynn, R.B., Pedersen, G., Lovholt, F., 2006. Submarine landslides: processes, triggers and hazard prediction. *Philos. Trans. R. Soc. A Math. Phys. Eng. Sci.* 364, 2009–2039. doi:10.1098/rsta.2006.1810
- Masson, D.G., Le Bas, T.P., Grevemeyer, I., Weinrebe, W., 2008. Flank collapse and large-scale landsliding in the Cape Verde Islands, off West Africa. *Geochemistry, Geophys. Geosystems* 9, n/a-n/a. doi:10.1029/2008GC001983
- Masson, D.G., Wynn, R.B., Talling, P.J., 2010. Large Landslides on Passive Continental Margins: Processes, Hypotheses and Outstanding Questions. *Submar. Mass Movements Their Consequences* 28, 153–165. doi:10.1007/978-90-481-3071-9_13
- Masson, D.G., Arzola, R.G., Wynn, R.B., Hunt, J.E., Weaver, P.P.E., 2011. Seismic triggering of landslides and turbidity currents offshore Portugal. *Geochemistry, Geophys. Geosystems* 12. doi:10.1029/2011GC003839
- Maxwell, J.C., 1959. Turbidite, tectonic and gravity transport, northern Apennine mountains, Italy. *Am. Assoc. Pet. Geol. Bull.* 43, 2701–2719. doi:-
- Maxwell, J.C., 1964. Influence of depth, temperature, and geologic age on porosity of quartzose sandstone. *Am. Assoc. Pet. Geol. Bull.* 48, 697–709.

- Mayall, M., Lonergan, L., Bowman, A., James, S., Mills, K., Primmer, T., Pope, D., Rogers, L., Skeene, R., 2010. The response of turbidite slope channels to growth-induced seabed topography. *Am. Assoc. Pet. Geol. Bull.* 94, 1011–1030. doi:10.1306/01051009117
- McAdoo, B., Pratson, L., Orange, D., 2000. Submarine landslide geomorphology, US continental slope. *Mar. Geol.* 169, 103–136. doi:10.1016/S0025-3227(00)00050-5
- McCaffrey, W.D., Kneller, B.C., 1996. Silurian turbidite provenance on the northern Avalonian margin. *J. Geol. Soc. London.* 153, 437–450.
- McCaffrey, W.D., Kneller, B.C., 2001. Process controls on the development of stratigraphic trap potential on the margins of confined turbidite systems and aids to reservoir evaluation. *Am. Assoc. Pet. Geol. Bull.* 85, 277–87. doi:10.1306/8626CA41-173B-11D7-8645000102C1865D
- McCaffrey, W.D., Choux, C.M., Baas, J.H., Houghton, P.D.W., 2003. Spatio-temporal evolution of velocity structure, concentration and grain size stratification within experimental particulate gravity currents. *Mar. Pet. Geol.* 20, 851–860. doi:10.1016/j.marpetgeo.2003.02.002
- McCaffrey, W.D., Kneller, B.C., 2004. Scale effects of non-uniformity on deposition from turbidity currents with reference to the Grès d'Annot of SE France. *Geol. Soc. London, Spec. Publ.* 221, 301–310. doi:10.1144/GSL.SP.2004.221.01.16
- McCave, I.N., Jones, K.P.N., 1988. Deposition of ungraded muds from high-density non-turbulent turbidity currents. *Nature* 333, 250–252.
- McGilvery, T.A. (Mac), Cook, D.L., 2003. The Influence of Local Gradients on Accommodation Space and Linked Depositional Elements Across a Stepped Slope Profile, Offshore Brunei, in: *Shelf Margin Deltas and Linked Down Slope Petroleum Systems: 23rd Annual. SOCIETY OF ECONOMIC PALEONTOLOGISTS AND MINERALOGISTS*, pp. 387–419. doi:10.5724/gcs.03.23.0387
- McGilvery, T.A. Mac, Cook, D.L., 2004. Depositional elements of the slope/basin depositional system offshore Brunei.
- Mckee, E.D., Weir, G.W., 1953. Terminology for stratification and cross-stratification in sedimentary rocks. *Geol. Soc. Am. Bull.* 64, 381–390.
- McKenzie, D., 1978. Some remarks on the development of sedimentary basins. *Earth Planet. Sci. Lett.* 40, 25–32.
- Meckel, L.D.L.D., 2011. Reservoir characteristics and classification of sand-prone submarine mass-transport deposits. *Mass-Transport Depos. Deep. Settings* 423–452. doi:-

- Meiburg, E., Kneller, B., 2010. Turbidity Currents and Their Deposits. *Annu. Rev. Fluid Mech.* 42, 135–156. doi:10.1146/annurev-fluid-121108-145618
- Middleton, G. V., 1967. Experiments on density and turbidity currents: III. Deposition of sediment. *Can. J. Earth Sci.* 4, 475–505.
- Middleton, G.V., 1970. Experimental studies related to problems of flysch sedimentation.
- Middleton, G. V., Hampton, M. a., 1973. Sediment gravity flows: mechanics of flow and deposition. *Turbid. Deep Water Sediment.* 1–38.
- Middleton, G. V, Hampton, M.A., 1976. Subaqueous sediment transport and deposition by sediment gravity flows, in: *Marine Sediment Transport and Environmental Management.*
- Middleton, G. V, Southard, J.B., 1984. *Mechanics of sediment movement.*
- Middleton, G. V., 1993. Sediment deposition from turbidity currents. *Annu. Rev. Earth Planet. Sci.* 21, 89–114.
- Mienert, J., Weaver, P., 2012. *European margin sediment dynamics: side-scan sonar and seismic images.* Springer Science & Business Media.
- Miller, M.C., McCave, I.N., Komar, P., 1977. Threshold of sediment motion under unidirectional currents. *Sedimentology* 24, 507–527.
- Milton-Worsell, R.J., Stoker, S.J., Cavill, J.E., 2006. Lower Cretaceous deep-water sandstone plays in the UK Central Graben. *Geol. Soc. London, Spec. Publ.* 254, 169–186. doi:10.1144/GSL.SP.2006.254.01.09
- Mohrig, D., Elverhoi, A., Parker, G., Anonymous, 1996. Experiments on the remobilization of antecedent deposits by subaqueous and subaerial debris flows. *Eos, Trans. Am. Geophys. Union* 77, 329.
- Mohrig, D., Marr, J.G., 2003. Constraining the efficiency of turbidity current generation from submarine debris flows and slides using laboratory experiments. *Mar. Pet. Geol.* 20, 883–899.
- Mohrig, D., Buttles, J., 2007. Deep turbidity currents in shallow channels. *Geology* 35, 155–158.
- Molyneux, S., Cartwright, J., Lonergan, L., 2001. Large scale deepwater sediment remobilisation: examples from North Sea 3D seismic and outcrop. *Rock Found. Conv.* 11. doi:10.1306/3FEF44FB-1741-11D7-8645000102C1865D
- Moore, J.G., Clague, D.A., Holcomb, R.T., Lipman, P.W., Normark, W.R., Torresan, M.E., 1989. Prodigious submarine landslides on the Hawaiian Ridge. *J. Geophys. Res.* 94, 17465. doi:10.1029/JB094iB12p17465
- Moore, J.G., Normark, W.R., Holcomb, R.T., 1994. Giant Hawaiian underwater landslides. *Science* (80). 264, 46–48.

- Moore, I., Jarvie, A., Fuzeau, T., 2009. Britannia Reservoir Model - Internal Reservoir Stratigraphy.
- Moretti, I., 2008. Working in complex areas: New restoration workflow based on quality control, 2D and 3D restorations. *Mar. Pet. Geol.* 25, 205–218. doi:10.1016/j.marpetgeo.2007.07.001
- Moscardelli, L., Wood, L., Mann, P., 2006. Mass-transport complexes and associated processes in the offshore area of Trinidad and Venezuela. *Am. Assoc. Pet. Geol. Bull.* 90, 1059–1088. doi:10.1306/02210605052
- Moscardelli, L., Wood, L., 2008. New classification system for mass transport complexes in offshore Trinidad. *Basin Res.* 20, 73–98. doi:10.1111/j.1365-2117.2007.00340.x
- Moscardelli, L., Ramnarine, S.K., Wood, L., Dunlap, D.B., 2013. Seismic geomorphological analysis and hydrocarbon potential of the Lower Cretaceous Cromer Knoll Group, Heidrun field, Norway. *Am. Assoc. Pet. Geol. Bull.* 97, 1227–1248. doi:10.1306/02081312155
- Moscardelli, L., 2014. Boulders of the Vastitas Borealis Formation: Potential origin and implications for an ancient martian ocean. *GSA Today* 24, 4–10. doi:10.1130/GSATG197A.1
- Moscardelli, L., Wood, L., 2016. Morphometry of mass-transport deposits as a predictive tool. *Bull. Geol. Soc. Am.* 128, 47–80. doi:10.1130/B31221.1
- Mosher, D.C., Moscardelli, L., Shipp, R.C., Chaytor, J.D., Baxter, C.D.P., Lee, H.J., Urgeles, R., 2010. Submarine Mass Movements and Their Consequences, in: *Submarine Mass Movements and Their Consequences*. pp. 1–8.
- Mulder, T., Cochonat, P., 1996. Classification of offshore mass movements. *J. Sediment. Res.* 66, 43–57. doi:10.1306/D42682AC-2B26-11D7-8648000102C1865D
- Mulder, T., Savoye, B., Syvitski, J.P.M., 1997. Numerical modelling of a mid-sized gravity flow: the 1979 Nice turbidity current (dynamics, processes, sediment budget and seafloor impact). *Sedimentology* 44, 305–326. doi:10.1111/j.1365-3091.1997.tb01526.x
- Mulder, T., Alexander, J., 2001. The physical character of subaqueous sedimentary density flows and their deposits. *Sedimentology* 48, 269–299. doi:10.1046/j.1365-3091.2001.00360.x
- Mulder, T., Migeon, S., Savoye, B., Faugeres, J.-C., 2001. Inversely graded turbidite sequences in the deep Mediterranean: a record of deposits from flood-generated turbidity currents? *Geo-Marine Lett.* 21, 86–93. doi:10.1007/s003670100071

- Mutti, E., Ricci Lucchi, F., 1972. Le torbiditi dell'Appennino settentrionale: introduzione all'analisi di facies. *Mem. dell Soc. Geol. Ital.* 11, 161–199.
- Mutti, E., Ricci Lucchi, F., 1975. Turbidite facies and facies association, in: IAS, Field Trip. *Guidebook Examples of Turbidites Facies and Facies Association From Selected Formations of the Northern Apennines.* pp. 21–36.
- Mutti, E., Ricci Lucchi, F., 1978. Turbidites of the northern Apennines: introduction to facies analysis. *Int. Geol. Rev.* 20, 125–166. doi:10.1080/00206817809471524
- Mutti, E., 1979. Turbidites et cones sous-marins profonds. *Sédimentation détritique (fluviale, littorale Mar.* 1, 353–419.
- Mutti, E., Normark, W.R., 1987. Comparing examples of modern and ancient turbidite systems: problems and concepts, in: *Marine Clastic Sedimentology.* Springer, pp. 1–38.
- Mutti, E., Normark, W.R., 1991. An integrated approach to the study of turbidite systems, in: *Seismic Facies and Sedimentary Processes of Submarine Fans and Turbidite Systems.* Springer, pp. 75–106.
- Mutti, E., 1992. Turbidite sandstones. Agip, Istituto di geologia, Università di Parma.
- Mutti, E., Ricci Lucchi, F., Roveri, M., 2002. Revisiting turbidites of the Marnoso-arenacea formation and their basin-margin equivalents: problems with classic models. *Excursion Guideb. Turbid. Work.* ... 27–30.
- Mutti, E., Tinterri, R., Benevelli, G., Biase, D. d., Cavanna, G., 2003. Deltaic, mixed and turbidite sedimentation of ancient foreland basins. *Mar. Pet. Geol.* 20, 733–755. doi:10.1016/j.marpetgeo.2003.09.001
- Mutti, E., Carminatti, M., Moreira, J.L.P., Grassi, A.A., 2006. Chaotic Deposits: es from the Brazilian offshore and from outcrop studies in the Spanish Pyrenees and Northern Apennines, Italy, in: *A.A.P.G. Annual Meeting.* Houston, Texas.
- Mutti, E., Bernoulli, D., Ricci Lucchi, F., Tinterri, R., 2009a. Turbidites and turbidity currents from Alpine “flysch” to the exploration of continental margins. *Sedimentology* 56, 267–318. doi:10.1111/j.1365-3091.2008.01019.x
- Mutti, E., Ogata, K., Tinterri, R., Care, D., 2009b. MTDs - Fine-grained unsorted matrix as evidence of excess pore pressure in sedimentary chaotic units. *Conf. Present.*
- Muzzi Magalhaes, P., 2009. *Stratigrafia fisica ed analisi di facies della Formazione Marnoso-arenacea, affiorante fra la Valle Santerno e la Valle Savio (Langhiano-Serravalliano, Appennino Settentrionale, Italia) - Vol II.* PhD Thesis. Università degli Studi di Parma.
- Muzzi Magalhaes, P., Tinterri, R., 2010. Stratigraphy and depositional setting of slurry and contained (reflected) beds in the Marnosoarenacea Formation

- (LanghianSerravallian) Northern Apennines, Italy. *Sedimentology* 57, 1685–1720. doi:10.1111/j.1365-3091.2010.01160.x
- Nardin, T.R., Hein, F.J., Gorsline, D.S., Edwards, B.D., 1979. A review of mass movement processes, sediment and acoustic characteristics, and contrasts in slope and base-of-slope systems versus canyon-fan-basin floor systems. *SEPM Spec. Publ.* 27, 61–73. doi:10.2110/pec.79.27.0061
- Naylor, M.A., 1980. The Origin of Inverse Grading in Muddy Debris Flow Deposits - A Review. *SEPM J. Sediment. Res. Vol.* 50. doi:10.1306/212F7B8F-2B24-11D7-8648000102C1865D
- Nelson, C.H., Escutia, C., Damuth, J.E., Twichell, D.C., 2011. Interplay of Mass-Transport and Turbidite-System Deposits in Different Active Tectonic and Passive Continental Margin Settings: External and Local Controlling Factors. *SEPM Spec. Publ.* 39–66. doi:-
- Nelson, C.H., Gutiérrez Pastor, J., Goldfinger, C., Escutia, C., 2012. Great earthquakes along the Western United States continental margin: Implications for hazards, stratigraphy and turbidite lithology. *Nat. Hazards Earth Syst. Sci.* 12, 3191–3208. doi:10.5194/nhess-12-3191-2012
- Nemec, W., 1990. Aspects of sediments movements on steep delta slopes, Coarse-Grained Deltas.
- Neuhuber, S., Wagneich, M., 2011. Geochemistry of Cretaceous Oceanic Red Beds - A synthesis. *Sediment. Geol.* 235, 72–78. doi:10.1016/j.sedgeo.2010.10.008
- Norem, H., Locat, J., Schieldrop, B., 1990. An approach to the physics and the modeling of submarine flowslides. *Mar. Georesources Geotechnol.* 9, 93–111.
- Normark, W.R., Posamentier, H., Mutti, E., 1993. Turbidite systems: state of the art and future directions. *Rev. Geophys.* 91–116. doi:10.1029/93RG02832
- Nygaard, A., Sejrup, H.P., Hafliðason, H., King, E.L., 2002. Geometry and genesis of glacial debris flows on the North Sea Fan: TOBI imagery and deep-tow boomer evidence. *Mar. Geol.* 188, 15–33. doi:10.1016/S0025-3227(02)00273-6
- O’Learly, D.W., 1986. The Munson-Nygreen slide: a major lower-slope slide off Georges Bank. *Mar. Geol.* 101–114.
- Oakman, C.D., Partington, M.A., 1998. Cretaceous. *Pet. Geol. North Sea Basic Concepts Recent Adv.* Fourth Ed. 294–349.
- Oakman, C.D., 2005. The Lower Cretaceous plays of the Central and Northern North Sea: Atlantean drainage models and enhanced hydrocarbon potential, in: Geological Society, London, Petroleum Geology Conference Series. Geological Society of London, pp. 187–198.

- Odone, F., Callot, P., Debroas, E.J., Sempere, T., Hoareau, G., Maillard, A., 2011. Soft-sediment deformation from submarine sliding: Favourable conditions and triggering mechanisms in examples from the Eocene Sobrarbe delta (Ainsa, Spanish Pyrenees) and the mid-Cretaceous Ayabacas Formation (Andes of Peru). *Sediment. Geol.* 235, 234–248. doi:10.1016/j.sedgeo.2010.09.013
- Ogata, K., 2010. Mass-transport complexes in bacini confinati a controllo strutturale: l'Unità Epiligure di Specchio (Appennino Settentrionale). PhD Thesis. Università degli Studi di Parma.
- Ogata, K., Mutti, E., Tinterri, R., 2010. Mass transport-related stratal disruption and sedimentary products, in: EGU. p. 9171. doi:10.1144/gsjgs.134.1.0019.-
- Ogata, K., Mutti, E., Tinterri, R., Pini, G.A., 2011. Mass transport complex in confined intra-slope basins: the case study of the Epiligurian Specchio unit (Northern Apennines, Italy). *Conf. Abstr.* 13, 4141.
- Ogata, K., Mutti, E., Pini, G.A., Tinterri, R., 2012a. Mass transport-related stratal disruption within sedimentary mélanges: Examples from the northern Apennines (Italy) and south-central Pyrenees (Spain). *Tectonophysics* 568–569, 185–199. doi:10.1016/j.tecto.2011.08.021
- Ogata, K., Pini, G.A., Carè, D., Zélic, M., Dellisanti, F., 2012b. Progressive development of block-in-matrix fabric in a shale-dominated shear zone: Insights from the Bobbio Tectonic Window (Northern Apennines, Italy). *Tectonics* 31, n/a-n/a. doi:10.1029/2011TC002924
- Ogata, K., Mountjoy, J.J., Pini, G.A., Festa, A., Tinterri, R., 2014a. Shear zone liquefaction in mass transport deposit emplacement: A multi-scale integration of seismic reflection and outcrop data. *Mar. Geol.* 356, 50–64. doi:10.1016/j.margeo.2014.05.001
- Ogata, K., Pini, G.A., Festa, A., Pogačnik, Ž., Tunis, G., Mountjoy, J.J., Senger, K., Strasser, M., 2014b. High-Resolution Studies of Mass Transport Deposits: Outcrop Perspective for Understanding Modern Submarine Slope Failure and Associated Natural Hazards, in: Lollino, G., Arattano, M., Rinaldi, M., Giustolisi, O., Marechal, J.-C., Grant, G.E. (Eds.), *Engineering Geology for Society and Territory - Volume 4*. Springer International Publishing, Cham, pp. 209–213. doi:10.1007/978-3-319-08660-6_40
- Ogata, K., Storti, F., Balsamo, F., Tinterri, R., Bedogni, E., Fetter, M., Gomes, L., Hatushika, R., 2017. Sedimentary facies control on mechanical and fracture stratigraphy in turbidites. *Geol. Soc. Am. Bull.* 129, 76–92. doi:10.1130/B31517.1
- Olafiranye, K., Jackson, C.A.L., Hodgson, D.M., 2013. The role of tectonics and

- mass-transport complex emplacement on upper slope stratigraphic evolution: A 3D seismic case study from offshore Angola. *Mar. Pet. Geol.* 44, 196–216. doi:10.1016/j.marpetgeo.2013.02.016
- Olowokere, M.T., 2011. Porosity and Lithology Prediction in Eve Field, Niger Delta Using Compaction Curves and Rock Physics Models. *Int. J. Geosci.* 2, 366–372. doi:10.4236/ijg.2011.23039
- Omeru, T., Cartwright, J.A., 2015. Multistage, progressive slope failure in the Pleistocene pro-deltaic slope of the West Nile Delta (Eastern Mediterranean). *Mar. Geol.* 362, 76–92. doi:10.1016/j.margeo.2015.01.012
- Omosanya, K.O., Alves, T.M., 2013. Ramps and flats of mass-transport deposits (MTDs) as markers of seafloor strain on the flanks of rising diapirs (Espírito Santo Basin, SE Brazil). *Mar. Geol.* 340, 82–97. doi:10.1016/j.margeo.2013.04.013
- Omosanya, K.O., 2014. Seismic character and interaction of intrabasinal mass-transport deposits in deep-water continental margins (Espírito Santo Basin, SE Brazil). PhD Thesis. Cardiff University.
- Ortiz-Karpf, A., Hodgson, D.M., McCaffrey, W.D., 2015. The role of mass-transport complexes in controlling channel avulsion and the subsequent sediment dispersal patterns on an active margin: The Magdalena Fan, offshore Colombia. *Mar. Pet. Geol.* 64, 58–75. doi:10.1016/j.marpetgeo.2015.01.005
- Ortiz-Karpf, A., Hodgson, D.M., Jackson, C.A.-L., McCaffrey, W.D., 2017. Influence of Seabed Morphology and Substrate Composition On Mass-Transport Flow Processes and Pathways: Insights From the Magdalena Fan, Offshore Colombia. *J. Sediment. Res.* 87, 189–209. doi:10.2110/jsr.2017.10
- Owen, G., 2003. Load structures: gravity-driven sediment mobilization in the shallow subsurface. *Geol. Soc. London, Spec. Publ.* 216, 21–34. doi:10.1144/GSL.SP.2003.216.01.03
- Parsons, J.D., García, M.H., 1998. Similarity of gravity current fronts. *Phys. Fluids* 10, 3209–3213. doi:10.1063/1.869848
- Parsons, B.S., Vogt, P.R., Hafliðason, H., Jung, W.Y., 2004. Seafloor reconnaissance and classification of the Storegga Slide headwall region, Norwegian Sea, using side-scan sonar, video, and photographs acquired on submarine NR-1. *Am. Assoc. Pet. Geol. Bull.* 88, 841–855. doi:10.1306/01260403097
- Patacci, M., Haughton, P.D.W., McCaffrey, W.D., 2014. Rheological Complexity In Sediment Gravity Flows Forced To Decelerate Against A Confining Slope, Braux, SE France. *J. Sediment. Res.* 84, 270–277. doi:10.2110/jsr.2014.26

- Patacci, M., Haughton, P.D.W., McCaffrey, W.D., 2015. Flow Behavior of Ponded Turbidity Currents. *J. Sediment. Res.* 85, 885–902. doi:10.2110/jsr.2015.59
- Patacci, M., 2016. A high-precision Jacob's staff with improved spatial accuracy and laser sighting capability. *Sediment. Geol.* 335, 66–69. doi:10.1016/j.sedgeo.2016.02.001
- Peakall, J., McCaffrey, B., Kneller, B., 2000. A Process Model for the Evolution, Morphology, and Architecture of Sinuous Submarine Channels. *J. Sediment. Res.* 70, 434–448. doi:10.1306/2DC4091C-0E47-11D7-8643000102C1865D
- Pickering, K.T., Hiscott, R.N., 1985. Contained (reflected) turbidity currents from the Middle Ordovician Cloridorme Formation, Quebec, Canada: an alternative to the antidune hypothesis. *Sedimentology* 32, 373–394.
- Pickering, K., Stow, D., Watson, M., Hiscott, R., 1986. Deep-water facies, processes and models: a review and classification scheme for modern and ancient sediments. *Earth-Science Rev.* 23, 75–174. doi:10.1016/0012-8252(86)90001-2
- Pickering, K.T., Hiscott, R.N., Hein, F.J., 1989. *Deep Marine Environments: Clastic Sedimentation and Tectonics*. London.
- Pickering, K.T., Corregidor, J., 2000. 3D Reservoir-Scale Study of Eocene Confined Submarine Fans, South-Central Spanish Pyrenees, in: *Deep-Water Reservoirs of the World: 20th Annual. SOCIETY OF ECONOMIC PALEONTOLOGISTS AND MINERALOGISTS*, pp. 776–781. doi:10.5724/gcs.00.15.0776
- Pickering, K.T., Corregidor, J., 2005. Mass-transport complexes, (MTCs) and tectonic control on basin-floor submarine fans, middle eocene, south Spanish Pyrenees. *J. Sediment. Res.* 75, 761–783. doi:10.2110/jsr.2005.062
- Pierson, T.C., Costa, J.E., 1987. A rheologic classification of subaerial sediment-water flows. *Rev. Eng. Geol.* 7, 1–12.
- Piper, D.J.W., Normark, W.R., 1982. Acoustic interpretation of Quaternary sedimentation and erosion on the channelled upper Laurentian Fan, Atlantic margin of Canada. *Can. J. Earth Sci.* 19, 1974–1984.
- Piper, D.J.W., Shor, A.N., Farre, J.A., O'Connell, S., Jacobi, R., 1985. Sediment slides and turbidity currents on the Laurentian Fan: Sidescan sonar investigations near the epicenter of the 1929 Grand Banks earthquake. *Geology* 13, 538–541.
- Piper, D.J.W., Shor, A.N., Hughes Clarke, J.E., 1988. The 1929 "Grand Banks" earthquake, slump, and turbidity current. *Sedimentol. consequences Convuls. Geol. events.* 229, 77–92. doi:-
- Piper, D.J.W., Pirmez, C., Manley, P.L., Long, D., Flood, R.D., Normark, W.R.,

- Showers, W., 1997. Mass-transport deposits of the Amazon Fan, in: Proceedings of the Ocean Drilling Program, 155 Scientific Results. Ocean Drilling Program, pp. 531–538. doi:10.2973/odp.proc.sr.155.212.1997
- Piper, D.J.W., Cochonat, P., Morrison, M.L., 1999. The sequence of events around the epicenter of the 1929 Grand Banks earthquake: Initiation of debris flows and turbidity currents inferred from sidescan sonar. *Sedimentology* 46, 79–97.
- Porter, J.R., Knipe, R.J., Fisher, Q.J., Farmer, a. B., Allin, N.S., Jones, L.S., Palfrey, a. J., Garrett, S.W., Lewis, G., 2000. Deformation processes in the Britannia Field, UKCS. *Pet. Geosci.* 6, 241–254. doi:10.1144/petgeo.6.3.241
- Posamentier, H.W., Kolla, V., 2003. Seismic Geomorphology and Stratigraphy of Depositional Elements in Deep-Water Settings. *J. Sediment. Res.* 73, 367–388. doi:10.1306/111302730367
- Posamentier, H.W., 2005. Application of 3D seismic visualization techniques for seismic stratigraphy, seismic geomorphology and depositional systems analysis: examples from fluvial to deep-marine depositional environments. *Pet. Geol.*
- Posamentier, H.W., Walker, R.G., 2006. Deep-Water Turbidites and Submarine Fans, Facies models revisited. doi:10.2110/pec.06.84.0339
- Posamentier, H.W., Martinsen, O.J., 2011. The character and genesis of submarine mass-transport deposits: insights from outcrop and 3D seismic data, SEPM special publication.
- Postma, G., Nemec, W., Kleinspehn, K.L., 1988. Large floating clasts in turbidites: a mechanism for their emplacement. *Sediment. Geol.* 58, 47–61. doi:10.1016/0037-0738(88)90005-X
- Prather, B.E., Booth, J.R., Steffens, G.S., Craig, P.A., 1998. Succession of Seismic Facies of Intraslope Basins, Deep-Water Gulf of Mexico 1. *Am. Assoc. Pet. Geol. Bull.* 82, 701–728. doi:10.1306/1D9BC5D9-172D-11D7-8645000102C1865D
- Prather, B.E., 2003. Controls on reservoir distribution, architecture and stratigraphic trapping in slope settings. *Mar. Pet. Geol.* 20, 529–545. doi:10.1016/j.marpetgeo.2003.03.009
- Prior, D.B., Bornhold, B.D., Johns, M.W., 1984. Depositional Characteristics of a Submarine Debris Flow. *J. Geol.* 92, 707–727. doi:10.1086/628907
- Prior, D.B., Bornhold, B.D., 1985. Sediment transport on subaqueous fan delta slopes, Britannia Beach, British Columbia. *Geo-marine Lett.* 5, 217–224.
- Pryor, W.A., 1973. Permeability-porosity patterns and variations in some Holocene sand bodies. *Am. Assoc. Pet. Geol. Bull.* 57, 162–189. doi:10.1306/819A4252-

16C5-11D7-8645000102C1865D

- PuigdefàBregas, C., Gjelberg, J., Vaksdal, M., 2004. The Grès d'Annot in the Annot syncline: outer basin-margin onlap and associated soft-sediment deformation. *Geol. Soc. London, Spec. Publ.* 221, 367–388.
- Pyles, D.R., Slatt, R.M., 2000. A High Frequency Sequence Stratigraphic Framework for Shallow through Deep-Water Deposits of the Lewis Shale and Fox Hills Sandstone, Great Divide and Washakie Basins, Wyoming, in: *Deep-Water Reservoirs of the World: 20th Annual. SOCIETY OF ECONOMIC PALEONTOLOGISTS AND MINERALOGISTS*, pp. 836–861. doi:10.5724/gcs.00.15.0836
- Qin, Z., Wu, S., Wang, D., Li, W., Gong, S., Mi, L., Spence, G., 2015. Mass transport deposits and processes in the north slope of the Xisha Trough, northern South China Sea. *Acta Oceanol. Sin.* 34, 117–125. doi:10.1007/s13131-015-0608-9
- Regione Emilia Romagna Geological, 1994. *Carta Geologica dell'Apennino Emilia Romagna - Scala 1:10000*. SELCA, Florence.
- Ricci Lucchi, F., 1978. Turbidite dispersal in a Miocene deep-sea plain: the Marnoso-Arenacea of the northern Apennines. *Geol. en Mijnb.* 57, 559–576.
- Ricci Lucchi, F., Valmori, E., 1980. Basin-wide turbidites in a Miocene, over-supplied deep-sea plain: a geometrical analysis. *Sedimentology* 27, 241–270. doi:10.1111/j.1365-3091.1980.tb01177.x
- Ricci Lucchi, F., 1981. The Miocene Marnoso-arenacea turbidites, Romagna and Umbria Apennines, in: *IAS, 2nd European Regional Meeting, Roma, Excursion Guidebook*. pp. 231–303.
- Ricci Lucchi, F., 1983. The Deep-Sea Fan deposits of the miocene Marnoso-Arenacea formation, northern Apennines. *Geo-Marine Lett.* 3, 203–210. doi:10.1007/BF02462469
- Ricci Lucchi, F., Ori, G.G., 1985. Field Excursion D: syn-orogenic deposits of a migrating basin system in the NW Adriatic Foreland: examples from Emilia Romagna region, Northern Apennines, in: *Excursion Guidebook: Cardiff, International Symposium on Foreland Basins*. pp. 137–176.
- Ricci Lucchi, F., 1986. The Oligocene to Recent foreland basins of the northern Apennines. *Forel. Basins, IAS Spec. Publ.* 8, 105–139. doi:10.1002/9781444303810.ch6
- Richardson, S.E.J., Davies, R.J., Allen, M.B., Grant, S.F., 2011. Structure and evolution of mass transport deposits in the South Caspian Basin, Azerbaijan. *Basin Res.* 23, 702–719. doi:10.1111/j.1365-2117.2011.00508.x
- Roberts, J.A., Cramp, A., 1996. Sediment stability on the western flanks of the

- Canary Islands. *Mar. Geol.* 134, 13–30.
- Rodine, J.D., Johnson, A.M., 1976. The ability of debris, heavily freighted with coarse clastic materials, to flow on gentle slopes. *Sedimentology* 23, 213–234. doi:10.1111/j.1365-3091.1976.tb00047.x
- Rouillard, P., 2010. Modèle architectural et lithologique du système de Rosetta (Delta du Nil, Méditerranée orientale): implication pour un analogue actuel de réservoir pétrolier. PhD Thesis.
- Rouse, H., 1939. Experiments on the mechanics of sediment suspension.
- Rovere, M., Gamberi, F., Mercorella, A., Leidi, E., 2013. Geomorphometry of a submarine mass-transport complex and relationships with active faults in a rapidly uplifting margin (Gioia Basin, NE Sicily margin). *Mar. Geol.* 356, 31–43. doi:10.1016/j.margeo.2013.06.003
- Roveri, M., Ricci Lucchi, F., Manzi, V., Mutti, E., 2002. Stratigraphy, facies and basin fill history of the Marnoso-arenacea Formation - part III 1–26.
- Royden, L., Keen, C.E., 1980. Rifting process and thermal evolution of the continental margin of eastern Canada determined from subsidence curves. *Earth Planet. Sci. Lett.* 51, 343–361.
- Royden, L., Sclater, J.G., Von Herzen, R.P., 1980. Continental margin subsidence and heat flow: important parameters in formation of petroleum hydrocarbons. *Am. Assoc. Pet. Geol. Bull.* 64, 173–187.
- Rupke, N.A., 1978. Deep clastic seas. *Sediment. Environ. facies* 372–415.
- Savoie, B., Cochonat, P., Piper, D.J.W., 1990. Seismic evidence for a complex slide near the wreck of the Titanic: model of an instability corridor for non-channeled gravity events. *Mar. Geol.* 91, 281–298.
- Sawyer, D.E., Flemings, P.B., Shipp, R.C., Winker, C.D., 2007. Seismic geomorphology, lithology, and evolution of the late Pleistocene Mars-Ursa turbidite region, Mississippi Canyon area, northern Gulf of Mexico. *Am. Assoc. Pet. Geol. Bull.* 91, 215–234. doi:10.1306/08290605190
- Sawyer, D.E., Flemings, P.B., Dugan, B., Germaine, J.T., 2009. Retrogressive failures recorded in mass transport deposits in the Ursa Basin, Northern Gulf of Mexico. *J. Geophys. Res. Solid Earth* 114, 1–20. doi:10.1029/2008JB006159
- Schlumberger Limited, 1974. *Log Interpretation: Applications*. Schlumberger Limited.
- Schnellmann, M., Anselmetti, F.S., Giardini, D., McKenzie, J.A., 2005. Mass movement-induced fold-and-thrust belt structures in unconsolidated sediments in Lake Lucerne (Switzerland). *Sedimentology* 52, 271–289.
- Sclater, J.G., Christie, P.A.F., 1980. Continental stretching: an explanation of the post-mid-Cretaceous subsidence of the Central North Sea basin. *J. Geophys.*

- Res. 85, 3711–3739.
- Selley, R.C., 1978. Porosity gradients in North Sea oil-bearing sandstones. *J. Geol. Soc. London*. 135, 119–132.
- Shanmugam, G., Lehtonen, L.R., Straume, T., Syvertsen, S.E., Hodgkinson, R.J., Skibeli, M., 1994. Slump and debris-flow dominated upper slope facies in the Cretaceous of the Norwegian and northern North Seas (61-67 N): Implications for sand distribution. *Am. Assoc. Pet. Geol. Bull.* 78, 910–937.
- Shanmugam, G., Bloch, R.B., Mitchell, S.M., Damuth, J.E., Beamish, G.W.J., Hodgkinson, R.J., Straume, T., Syvertsen, S.E., Shields, K.E., 1996. Slump and debris-flow dominated basin-floor fans in the North Sea: an evaluation of conceptual sequence-stratigraphical models based on conventional core data. *Geol. Soc. London, Spec. Publ.* 103, 145–176. doi:10.1144/GSL.SP.1996.103.01.09
- Shanmugam, G., 2000. 50 years of the turbidite paradigm (1950s—1990s): deep-water processes and facies models—a critical perspective. *Mar. Pet. Geol.* 17, 285–342. doi:10.1016/S0264-8172(99)00011-2
- Shanmugam, G., 2002. Ten turbidite myths. *Earth-Science Rev.* 58, 311–341. doi:10.1016/S0012-8252(02)00065-X
- Shanmugam, C., 2008. The constructive functions of tropical cyclones and tsunamis on deep-water sand deposition during sea level highstand: Implications for petroleum exploration. *Am. Assoc. Pet. Geol. Bull.* 92, 443–471. doi:10.1306/12270707101
- Sharman, G.R., Graham, S.A., Masalimova, L.U., Shumaker, L.E., King, P.R., 2015. Spatial patterns of deformation and paleoslope estimation within the marginal and central portions of a basin-floor mass-transport deposit, Taranaki Basin, New Zealand. *Geosphere* 11, 266–306. doi:10.1130/GES01126.1
- Sharp, A., Samuel, A., 2004. An example study using conventional 3D seismic data to delineate shallow gas drilling hazards from the West Delta Deep Marine Concession, offshore Nile Delta, Egypt. *Pet. Geosci.* 10, 121–129. doi:10.1144/1354-079303-588
- Sheldon, N.D., Retallack, G.J., 2001. Equation for compaction of paleosols due to burial. *Geology* 29, 247–250. doi:10.1130/0091-7613(2001)029<0247:EFCOPD>2.0.CO;2
- Shipp, R.C., Nott, J. a, Newlin, J. a, E, S.I., 2004. Physical Characteristics and Impact of Mass Transport Complexes on Deepwater Jetted Conductors and Suction Anchor Piles. *Offshore Technol. Conf.* 11. doi:10.4043/16751-MS
- Shipp, R.C., Weimer., Posamentier, H.W., 2011. Mass-Transport Deposits in

- Deepwater Settings. SEPM (Society for Sedimentary Geology). doi:10.2110/sepm.sp.096
- Shor, A.N., Piper, D.J.W., 1989. A large late pleistocene blocky debris flow on the central scotian slope. *Geo-Marine Lett.* 9, 153–160. doi:10.1007/BF02431042
- Shultz, M.R., Fildani, A., Cope, T.D., Graham, S.A., 2005. Deposition and stratigraphic architecture of an outcropping ancient slope system: Tres Pasos Formation, Magallanes Basin, southern Chile. *Geol. Soc. London, Spec. Publ.* 244, 27–50. doi:10.1144/GSL.SP.2005.244.01.03
- Sinclair, C.G., 1962. The limit deposit-velocity of heterogeneous suspensions. *Proc. Symp. Interact. between fluid Part.* A68–A76.
- Sinclair, H.D., Tomasso, M., 2002. Depositional Evolution of Confined Turbidite Basins. *J. Sediment. Res.* 72, 451–456. doi:10.1306/111501720451
- Slatt, R.M., 2000. Why Outcrop Characterization of Turbidite Systems. *Fine-grained Turbid. Syst.* 181–186. doi:-
- Smith, R.A., 1955. Experiments on the flow of sand-water slurries in horizontal pipes. *Chemistry & Industry. Chem. Ind.* 18, 501–504.
- Smith, R., Joseph, P., 2004. Onlap stratal architectures in the Grès d'Annot: geometric models and controlling factors. *Geol. Soc. London, Spec. Publ.* 221, 389–399. doi:10.1144/GSL.SP.2004.221.01.21
- Sobiesiak, M.S., Kneller, B.C., Alsop, G.I., 2013. Blocky Mass Transport Deposit, Argentina, in: *Submarine Mass Movements and Their Consequences.*
- Sobiesiak, M.S., Kneller, B., Alsop, G.I., Milana, J.P., 2016. Internal deformation and kinematic indicators within a tripartite mass transport deposit, NW Argentina. *Sediment. Geol.* 344, 364–381. doi:10.1016/j.sedgeo.2016.04.006
- Sobiesiak, M.S., Alsop, G.I., Kneller, B., Milana, J.P., 2017. Sub-seismic scale folding and thrusting within an exposed mass transport deposit: A case study from NW Argentina. *J. Struct. Geol.* 96, iii–iv. doi:10.1016/j.jsg.2017.01.006
- Southern, S.J., Patacci, M., Felletti, F., McCaffrey, W.D., 2015. Influence of flow containment and substrate entrainment upon sandy hybrid event beds containing a co-genetic mud-clast-rich division. *Sediment. Geol.* 321, 105–122. doi:10.1016/j.sedgeo.2015.03.006
- Stacey, M.W., Bowen, A.J., 1988. The vertical structure of turbidity currents and a necessary condition for self-maintenance. *J. Geophys. Res. Ocean.* 93, 3543–3553.
- Stow, D.A.V., Shanmugam, G., 1980. Sequence of structures in fine-grained turbidites: Comparison of recent deep-sea and ancient flysch sediments. *Sediment. Geol.* 25, 23–42. doi:10.1016/0037-0738(80)90052-4

- Stow, D.A. V, Cremer, M., Droz, L., Normark, W.R., O'Connell, S., Pickering, K.T., Stelling, C.E., Meyer, W.A.A., Deep Sea Drilling Project, L. 96 S.S., 1985. Mississippi Fan sedimentary facies, composition, and texture, in: *Submarine Fans and Related Turbidite Systems*. pp. 259–265. doi:-
- Stow, D.A.V., 1986. Deep clastic seas. *Sediment. Environ. facies* 2, 399–444.
- Stow, D.A. V, Wetzell, A., 1990. Hemiturbidite: a new type of deep-water sediment, in: *Proceedings of the Ocean Drilling Program, Scientific Results*. pp. 25–34.
- Stow, D.A. V, Reading, H.G., Collinson, J.D., 1996. Deep seas. *Sediment. Environ. Process. facies Stratigr.* 3, 395–453.
- Stow, D.A., Mayall, M., 2000. Deep-water sedimentary systems: New models for the 21st century. *Mar. Pet. Geol.* 17, 125–135. doi:10.1016/S0264-8172(99)00064-1
- Strachan, L.J., 2002. Slump-initiated and controlled syndepositional sandstone remobilization: An example from the Namurian of county Clare, Ireland. *Sedimentology* 49, 25–41. doi:10.1046/j.1365-3091.2002.00430.x
- Strachan, L.J., 2008. Flow transformations in slumps: A case study from the Waitemata Basin, New Zealand. *Sedimentology* 55, 1311–1332. doi:10.1111/j.1365-3091.2007.00947.x
- Strachan, L.J., Rarity, F., Gawthorpe, R.L., Wilson, P., Sharp, I., Hodgetts, D., 2013. Submarine slope processes in rift-margin basins, Miocene Suez Rift, Egypt. *Bull. Geol. Soc. Am.* 125, 109–127. doi:10.1130/B30665.1
- Strasser, M., Stegmann, S., Bussmann, F., Anselmetti, F.S., Rick, B., Kopf, A., 2007. Quantifying subaqueous slope stability during seismic shaking: Lake Lucerne as model for ocean margins. *Mar. Geol.* 240, 77–97. doi:10.1016/j.margeo.2007.02.016
- Stright, L., Bernhardt, A., Boucher, A., 2013. DFTopoSim: Modeling Topographically-Controlled Deposition of Subseismic Scale Sandstone Packages Within a Mass Transport Dominated Deep-Water Channel Belt. *Math. Geosci.* 45, 277–296. doi:10.1007/s11004-013-9444-7
- Sullivan, M.D., Jensen, G.N., Goulding, F.J., Jennette, D.C., Foreman, J.L., Stern, D., 2000. Architectural Analysis of Deep-Water Outcrops: Implications for Exploration and Development of the Diana Sub-Basin, Western Gulf of Mexico. *GCSSEPM Found. 20th Annu. Res. Conf. Deep. Reserv. World* 1010–1031. doi:10.5724/gcs.00.15.1010
- Sumner, W.R., Loutit, S., Tohill, E., Way, D., Criddle, D., Palfrey, A., Hakes, W.G., Archer, S.G., Colleran, J., Scott, A., Kaiser, K., Harding, A., Castellini, A., Clark, J., Lianshuang, Q.I., 2005. Managing reservoir uncertainty after five years of

- field life: Britannia Field, in: *Petroleum Geology: North-West Europe and Global Perspectives – Proceedings of the 6th Petroleum Geology Conference*. Geological Society of London, pp. 511–525. doi:10.1144/0060511
- Sumner, E.J., Talling, P.J., Amy, L.A., 2009. Deposits of flows transitional between turbidity current and debris flow. *Geology* 37, 991–994. doi:10.1130/G30059A.1
- Sylvester, Z., Lowe, D.R., 2004. Textural trends in turbidites and slurry beds from the Oligocene flysch of the East Carpathians, Romania. *Sedimentology* 51, 945–972. doi:10.1111/j.1365-3091.2004.00653.x
- Tagliaferri, A., Tinterri, R., 2016. The tectonically-confined Firenzuola turbidite system (Marnoso-arenacea Formation, northern Apennines, Italy). *Ital. J. Geosci.* 135, 425–443. doi:10.3301/IJG.2015.27
- Talling, P.J., Amy, L.A., Wynn, R.B., Peakall, J., Robinson, M., 2004. Beds comprising debrite sandwiched within co-genetic turbidite: origin and widespread occurrence in distal depositional environments. *Sedimentology* 51, 163–194. doi:10.1111/j.1365-3091.2004.00617.x
- Talling, P.J., Amy, L.A., Wynn, R.B., 2007a. New insight into the evolution of large-volume turbidity currents: comparison of turbidite shape and previous modelling results. *Sedimentology* 54, 737–769. doi:10.1111/j.1365-3091.2007.00858.x
- Talling, P.J., Amy, L., Wynn, R., Blackburn, G., Gibson, O., 2007b. Evolution of Turbidity Currents Deduced from Extensive Thin Turbidites: Marnoso Arenacea Formation (Miocene), Italian Apennines. *J. Sediment. Res.* 77, 172–196. doi:10.2110/jsr.2007.018
- Talling, P.J., Wynn, R.B., Masson, D.G., Frenz, M., Cronin, B.T., Schiebel, R., Akhmetzhanov, A.M., Dallmeier-Tiessen, S., Benetti, S., Weaver, P.P.E., Georgiopoulou, A., Zühlsdorff, C., Amy, L.A., 2007c. Onset of submarine debris flow deposition far from original giant landslide. *Nature* 450, 541–544. doi:10.1038/nature06313
- Talling, P.J., Masson, D.G., Sumner, E.J., Malgesini, G., 2012. Subaqueous sediment density flows: Depositional processes and deposit types. *Sedimentology* 59, 1937–2003. doi:10.1111/j.1365-3091.2012.01353.x
- Talling, P.J., 2013. Hybrid submarine flows comprising turbidity current and cohesive debris flow: Deposits, theoretical and experimental analyses, and generalized models. *Geosphere* 9, 460–488. doi:10.1130/GES00793.1
- Tappin, D.R., 2010. Mass Transport Events and Their Tsunami Hazard, in: *Submarine Mass Movements and Their Consequences*. Springer Netherlands, Dordrecht, pp. 667–684. doi:10.1007/978-90-481-3071-9_54
- Terlaky, V., Arnott, R.W.C., 2014. Matrix-rich and associated matrix-poor

- sandstones: avulsion splays in slope and basin-floor strata. *Sedimentology* 61, 1175–1197.
- Thornburg, T.M., Kulm, L.D., Hussong, D.M., 1990. Submarine-fan development in the southern Chile Trench: a dynamic interplay of tectonics and sedimentation. *Geol. Soc. Am. Bull.* 102, 1658–1680.
- Thorne, J.A., Watts, A.B., 1989. Quantitative analysis of North Sea subsidence. *Am. Assoc. Pet. Geol. Bull.* 73, 88–116.
- Tinterri, R., Muzzi Magalhaes, P., Milli, S., Marini, M., Moscatelli, M., Stanzione, O., 2009. Northern and Central Apennines Turbidites (Italy). *F. Trip Guid. 27th IAS Meet. Sedimentol. (Sedimentary Environ. Mediterr. Islands)*, Alghero, Italy 245–297. doi:-
- Tinterri, R., 2011. Combined flow sedimentary structures and the genetic link between sigmoidal-and hummocky-cross stratification. *GeoActa* 10, 1–43. doi:-
- Tinterri, R., Muzzi Magalhaes, P., 2011. Synsedimentary structural control on foredeep turbidites: An example from Miocene Marnoso-arenacea Formation, Northern Apennines, Italy. *Mar. Pet. Geol.* 28, 629–657. doi:10.1016/j.marpetgeo.2010.07.007
- Tinterri, R., Muzzi Magalhaes, P., Tagliaferri, A., 2012. Foredeep turbidites of the Miocene Marnoso-arenacea Formation (Northern Apennines). *Geol. F. trips* 4, 1–133. doi:10.3301/GFT.2012.03
- Tinterri, R., Muzzi Magalhaes, P., Tagliaferri, A., Cunha, R.S.S., 2015. Convolute laminations and load structures in turbidites as indicators of flow reflections and decelerations against bounding slopes. Examples from the Marnoso-arenacea Formation (northern Italy) and Annot Sandstones (south eastern France). *Sediment. Geol.* 344, 382–407. doi:10.1016/j.sedgeo.2016.01.023
- Tinterri, R., Tagliaferri, A., 2015. The syntectonic evolution of foredeep turbidites related to basin segmentation: Facies response to the increase in tectonic confinement (Marnoso-arenacea Formation, Miocene, Northern Apennines, Italy). *Mar. Pet. Geol.* 67, 81–110. doi:10.1016/j.marpetgeo.2015.04.006
- Tinterri, R., Laporta, M., Ogata, K., 2016. Cross-currents turbidite facies tract in a structurally-confined, asymmetrical mini-basin (Priabonian-Rupelian, Ranzano Sandstone, northern Apennines, Italy). *Sediment. Geol.* 352, 63–87. doi:10.1016/j.sedgeo.2016.12.005
- Trincardi, F., Argnani, A., 1990. Gela submarine slide: A major basin-wide event in the plio-quadernary foredeep of Sicily. *Geo-Marine Lett.* 10, 13–21. doi:10.1007/BF02431017
- Tripsanas, E.K., Piper, D.J.W., Jenner, K.A., Bryant, W.R., 2008. Submarine mass-

- transport facies: New perspectives on flow processes from cores on the eastern North American margin. *Sedimentology* 55, 97–136. doi:10.1111/j.1365-3091.2007.00894.x
- Twichell, D.C., Chaytor, J.D., Uri, S., Buczkowski, B., 2009. Morphology of late Quaternary submarine landslides along the US Atlantic continental margin. *Mar. Geol.* 264, 4–15.
- Uchman, A., 1995. Taxonomy and palaeoecology of flysch trace fossils: the Marnoso–arenacea Formation and associated facies (Miocene, Northern Apennines, Italy). *Beringeria* 15, 3–115.
- Urgeles, R., Canals, M., Baraza, J., Alonso, B., Masson, D., 1997. The most recent megalandslides of the Canary Islands: El Golfo debris avalanche and Canary debris flow, west El Hierro Island. *J. Geophys. Res. Solid Earth* 102, 20305–20323.
- Urgeles, R., Masson, D.G., Canals, M., Watts, A.B., Le Bas, T., 1999. Recurrent large-scale landsliding on the west flank of La Palma, Canary Islands. *J. Geophys. Res. Solid Earth* 104, 25331–25348. doi:10.1029/1999JB900243
- Urgeles, R., Locat, J., Lee, H.J., Martin, F., 2002. The Saguenay Fjord, Quebec, Canada: integrating marine geotechnical and geophysical data for spatial seismic slope stability and hazard assessment. *Mar. Geol.* 185, 319–340.
- Urlaub, M., Talling, P.J., Zervos, A., Masson, D., 2015. What causes large submarine landslides on low gradient (2°) continental slopes with slow (~0.15 m/kyr) sediment accumulation? *J. Geophys. Res. Solid Earth* 120, 6722–6739. doi:10.1002/2015JB012347
- Van der Merwe, W.C., Hodgson, D.M., Flint, S.S., 2009. Widespread syn-sedimentary deformation on a muddy deep-water basin-floor: The vischkuil formation (Permian), Karoo Basin, South Africa. *Basin Res.* 21, 389–406. doi:10.1111/j.1365-2117.2009.00396.x
- Van Der Merwe, W.C., Hodgson, D.M., Flint, S.S., 2011. Origin and terminal architecture of a submarine slide: A case study from the Permian Vischkuil Formation, Karoo Basin, South Africa. *Sedimentology* 58, 2012–2038. doi:10.1111/j.1365-3091.2011.01249.x
- Van Vliet, A., 1978. Early Tertiary deepwater fans of Guipuzcoa, northern Spain. *Sediment. Submar. canyons, fans trenches* 190–209.
- Varnes, D.J., 1978. Slope Movement Types and Processes. *Transp. Res. Board Spec. Rep.* doi:In Special report 176: Landslides: Analysis and Control, Transportation Research Board, Washington, D.C.
- Walker, R.G., 1967. Turbidite Sedimentary Structures and their Relationship to

Proximal and Distal Depositional Environments. *J. Sediment. Res.* 37.

- Walker, R.G., 1978. Deep-water sandstone facies and ancient submarine fans: models for exploration for stratigraphic traps. *Am. Assoc. Pet. Geol. Bull.* 62, 932–966.
- Walker, D., 2008. Topographic controls on deep-water sedimentation patterns - the Casaglia Monte della Colonna submarine slide, Marnoso-arenacea Formation (Miocene), Northern Italian Apennines. MSc Thesis.
- Waltham, D., 2004. Flow transformations in particulate gravity currents. *J. Sediment. Res.* 74, 129–134.
- Ward, W.H., 1945. The Stability of Natural Slopes. *Geogr. J.* 105, 170. doi:10.2307/1789732
- Watt, S.F.L., Talling, P.J., Vardy, M.E., Heller, V., Hühnerbach, V., Urlaub, M., Sarkar, S., Masson, D.G., Henstock, T.J., Minshull, T.A., Paulatto, M., Le Friant, A., Lebas, E., Berndt, C., Crutchley, G.J., Karstens, J., Stinton, A.J., Maeno, F., 2012a. Combinations of volcanic-flank and seafloor-sediment failure offshore Montserrat, and their implications for tsunami generation. *Earth Planet. Sci. Lett.* 319–320, 228–240. doi:10.1016/j.epsl.2011.11.032
- Watt, S.F.L., Talling, P.J., Vardy, M.E., Masson, D.G., Henstock, T.J., Hühnerbach, V., Minshull, T.A., Urlaub, M., Lebas, E., Le Friant, A., Berndt, C., Crutchley, G.J., Karstens, J., 2012b. Widespread and progressive seafloor-sediment failure following volcanic debris avalanche emplacement: Landslide dynamics and timing offshore Montserrat, Lesser Antilles. *Mar. Geol.* 323–325, 69–94. doi:10.1016/j.margeo.2012.08.002
- Watts, A.B., Masson, D.G., 1995. A giant landslide on the north flank of Tenerife, Canary Islands. *J. Geophys. Res. Solid Earth* 100, 24487–24498.
- Watts, A., Masson, D., 2001. New sonar evidence for recent catastrophic collapses of the north flank of Tenerife, Canary Islands. *Bull. Volcanol.* 63, 8–19.
- Weimer, P., 1989. Sequence stratigraphy of the Mississippi fan (Plio-Pleistocene), Gulf of Mexico. *Geo-Marine Lett.* 9, 185–272. doi:10.1007/BF02431072
- Weimer, P., Shipp, C., 2004. Mass Transport Complex: Musing on Past Uses and Suggestions for Future Directions. *Proc. Offshore Technol. Conf.* 1–10. doi:10.4043/16752-MS
- Weimer, P., Slatt, R.M., 2006. Deepwater-Reservoir Elements: Mass-Transport Deposits and Slides, in: *Introduction to the Petroleum Geology of Deepwater Setting*. American Association of Petroleum Geologists, Tulsa, Oklahoma, pp. 9-419–9-455. doi:10.1306/St571314C9
- Weimer, P., Slatt, R.M., 2006. Introduction to Deepwater Systems, in: *Introduction to*

- the Petroleum Geology of Deepwater Setting. American Association of Petroleum Geologists, Tulsa, Oklahoma, pp. 1-1-1–17. doi:10.1306/St571314C1
- Weimer, P., Slatt, R.M., 2008. Contents 4. *J. Am. Coll. Surg.* 206, A9. doi:10.1016/S1072-7515(08)00122-1
- White, N., Latin, D., 1993. Subsidence Analyses From the North-Sea Triple-Junction. *J. Geol. Soc. London.* 150, 473–488. doi:10.1144/gsjgs.150.3.0473
- Wilson, J.T., 1966. Did the Atlantic close and then re-open? *Nature.*
- Wilson, F., 2009. Reservoir heterogeneity in the Early Cretaceous Britannia Sandstone, Outer Moray Firth. MSc Thesis.
- Wood, A., Smith, A.J., 1958a. The sedimentation and sedimentary history of the Aberystwyth Grits (Upper Llandoveryan). *Q. J. Geol. Soc.* 114, 163–195.
- Wood, A., Smith, A.J., 1958b. Two undescribed structures in a greywacke series. *J. Sediment. Res.* 28.
- Wynn, R.B., Masson, D.G., Stow, D.A. V, Weaver, P.P.E., 2000. The Northwest African slope apron: A modern analogue for deep-water systems with complex seafloor topography. *Mar. Pet. Geol.* 17, 253–265. doi:10.1016/S0264-8172(99)00014-8
- Wynn, R.B., Kenyon, N.H., Masson, D.G., Stow, D.A. V, Weaver, P.P.E., 2002a. Characterization and recognition of deep-water channel-lobe transition zones. *Am. Assoc. Pet. Geol. Bull.* 86.
- Wynn, R.B., Weaver, P.P.E., Masson, D.G., Stow, D.A. V, 2002b. Turbidite depositional architecture across three interconnected deep-water basins on the north-west African margin. *Sedimentology* 49, 669–695.
- Zattin, M., Zuffa, G.G., 2004. Unravelling the source rocks of Late Eocene-Miocene orogenic wedge and foredeep arenites of the northern Apennines and southern Alps. *BOLLETTINO-SOCIETA Geol. Ital.* 123, 67–76.
- Zeng, J., Lowe, D.R., Prior, D.B., Wiseman, W.J., Bornhold, B.D., 1991. Flow properties of turbidity currents in Bute Inlet, British Columbia. *Sedimentology* 38, 975–996.
- Ziegler, P.A., 1975. The Geological Evolution of the North Sea Area in the Tectonic Framework of North Western Europe. *Norges Geol* 1–27.
- Ziegler, P.A., 1990. Collision related intra-plate compression deformations in Western and Central Europe. *J. Geodyn.* 11, 357–388.

Appendix A – Britannia Platform Area well-dataset

The work undertaken in the Platform Area of the Lower and Middle Britannia was based on wireline and core data from 47 wells. The new correlation framework and the facies analysis presented in this thesis forms a new database which is stored in tabulated excel file format and included in the attached CD-ROM.

The database is structured as follow:

A.1 Reservoir zones and beds (well; depths: top/base)

A.2 Lithology intervals (well; depths: top/base)

- Sandstone
- Mixed Sandstone/Mudstone
- Mudstone

A.3 Lithofacies intervals (well; depths: top/base) – only for cored wells (14)

- | | |
|----------------------------------|------------------|
| - Massive sandstone (SMa) | - Debrite (DSn) |
| - Laminated Sandstone (SLa) | - Mudstone (Mds) |
| - Banded Sandstone (SBa) | |
| - Injected Sandstone (SInj) | |
| - Mixed-slurried Sandstone (SMs) | (see Table 4.2) |

A.4 Detailed facies intervals (well; depths: top/base) – only for cored wells (14)

- | | |
|-----------------------------|------------------------------|
| - Massive sandstone | - Debrite “Starry-night” |
| - Laminated Sandstone | - Debrite “Non-Starry-night” |
| - Banded Sandstone | - Mudstone Undifferentiated |
| - Pseudobanded Sandstone | - Mudstone Red |
| - Wispy-laminated Sandstone | - Mudstone Grey |
| - Sandstone | - Mudstone Black |

The depth intervals for each well are shown as Measured Depth (MD) and as True Vertical Depth Subsea (TVDSS). All values are in feet.

Appendix B – Britannia Sandstone Fm. graphic logs

The graphic sedimentary logging of core from the Britannia Sandstone Formation in the Platform Area was undertaken at 1:20 scale (5 cm = 1 m) and incorporated ~1000 m of core from 12 wells. A standard sedimentary logging procedure was followed whereby lithology, grain size, internal fabric, sedimentary structures and other additional observations were recorded. Grain size was assessed visually using a hand lens and grain size comparator chart. The following pages include all the original logging sheets. Wells 16/26-24 and 16/27A-6 are two exploration wells and are shown first. The remaining 10 wells (B3, B4, B5, B6, B7, B8, B10, B13z, B17 and B33; all with the pre-fix 16/26-) are production wells.

For relative well positions see Figure 4.1 in Chapter 4.

Wells	Middle Reservoir Zone (This study)		Thickness logged (feet)
16/26-24	13030	12830	200
16/27A-6	13350	12870	480
B03	14030	13840	190
B04	14004	13600	404
B05	14120	13730	390
B06	13872	13842	30
B07	16660	16490	170
B08	16830	16600	230
B10	15370	15070	300
B13Z	19564	19325	239
B17	21100	20780	320
B33	15280	14965	315
TOT			3268

Lithology

Mudstone	Conglomerate	Limestone	Calcareous mudstone	Tuff
Siltstone	Breccia	Dolomitic limestone	Anhydrite	Chalk
Sandstone	Coal	Dolomite	Halite	Metamorphic

<h3>Stratification type</h3> <ul style="list-style-type: none"> Trough cross-bedding Planar cross-bedding Flat-lying lamination (dashed where indistinct) Climbing current ripple lamination Planar current ripple lamination Wave-ripple lamination 		<h3>Consolidation fabrics</h3> <ul style="list-style-type: none"> Consolidation lamination Dish structures Sheet and pillar structure (dashed where faint) Thick (>4mm) sheet and pillar structures Irregular fluidisation pipes and patches Contorted dewatering sheets and clean streaks (liquefaction) Disrupted fabric with dislocation surface and sheared sand lense Mudrock breccia produced by sand injection Pseudonodular/loaded fabric 	
--	--	--	--

<h3>Fractures</h3> <ul style="list-style-type: none"> Open fractures Closed fractures Cemented fractures Grain shear Zone of intense fracturing Stylolite 	<h3>Qualifiers</h3> <p>zoned: in order of fill e.g. q/ca/p</p> <p>indeterminate: e.g. q,ca,p</p> <table border="0"> <tr> <td>q - quartz</td> <td>sp - sphalerite</td> </tr> <tr> <td>ca - calcite</td> <td>ba - barite</td> </tr> <tr> <td>p - pyrite</td> <td>a - anhydrite</td> </tr> <tr> <td>h - haematite</td> <td>d - dolomite</td> </tr> <tr> <td>s - siderite</td> <td>cl - clay lined</td> </tr> <tr> <td>ga - galena</td> <td>ha - halite</td> </tr> </table>	q - quartz	sp - sphalerite	ca - calcite	ba - barite	p - pyrite	a - anhydrite	h - haematite	d - dolomite	s - siderite	cl - clay lined	ga - galena	ha - halite
q - quartz	sp - sphalerite												
ca - calcite	ba - barite												
p - pyrite	a - anhydrite												
h - haematite	d - dolomite												
s - siderite	cl - clay lined												
ga - galena	ha - halite												

Bed Boundaries

<h3>Clasts</h3> <ul style="list-style-type: none"> Quartz and lithic granules Green ?tuffaceous (or glauconitic) granules/pellets Intraformational mudclasts (including pseudoclasts produced by injection) Sandstone intraclasts Plant detritus/carbonaceous matter Comminuted carbonaceous detritus Mica Reworked intraformational nodules/pellets 	<h3>Extraformational clast qualifiers</h3> <p>Extraformational clasts are assumed to be sandstone unless qualified in the remarks column, or, e.g.</p> <table border="0"> <tr> <td>Gr - granitic</td> <td>Gs - gneiss</td> </tr> <tr> <td>Gb - gabbro</td> <td>Ch - chalk</td> </tr> <tr> <td>B - basaltic</td> <td>g - pelletal glauconite</td> </tr> <tr> <td>F - felsite</td> <td>ph - pelletal phosphate</td> </tr> <tr> <td>P - phyllite</td> <td>ca - calcrite</td> </tr> <tr> <td>Sc - schist</td> <td></td> </tr> </table>	Gr - granitic	Gs - gneiss	Gb - gabbro	Ch - chalk	B - basaltic	g - pelletal glauconite	F - felsite	ph - pelletal phosphate	P - phyllite	ca - calcrite	Sc - schist	
Gr - granitic	Gs - gneiss												
Gb - gabbro	Ch - chalk												
B - basaltic	g - pelletal glauconite												
F - felsite	ph - pelletal phosphate												
P - phyllite	ca - calcrite												
Sc - schist													

<h3>Cements</h3> <ul style="list-style-type: none"> Nodule Displacive nodule Cemented stringer Micronodules/framboids Weakly cemented Pervasively cemented Diffuse boundaries Sharp boundaries Disseminated cement (vertical slash = calcite, oblique slash = dolomite) 	<h3>Qualifiers</h3> <table border="0"> <tr> <td>si - silica</td> <td>ga - galena</td> <td>ca - calcite</td> </tr> <tr> <td>p - pyrite</td> <td>sp - sphalerite</td> <td>d - dolomite</td> </tr> <tr> <td>h - haematite</td> <td>ba - barite</td> <td>ha - halite</td> </tr> <tr> <td>g - glauconite</td> <td>a - anhydrite</td> <td></td> </tr> <tr> <td>ph - phosphate</td> <td>s - siderite</td> <td></td> </tr> </table>	si - silica	ga - galena	ca - calcite	p - pyrite	sp - sphalerite	d - dolomite	h - haematite	ba - barite	ha - halite	g - glauconite	a - anhydrite		ph - phosphate	s - siderite	
si - silica	ga - galena	ca - calcite														
p - pyrite	sp - sphalerite	d - dolomite														
h - haematite	ba - barite	ha - halite														
g - glauconite	a - anhydrite															
ph - phosphate	s - siderite															

<h3>Bioclasts</h3> <ul style="list-style-type: none"> Bivalves (articulated) Bivalves (disarticulated) Gastropod Ammonite Belemnites Echinoderm Crinoid ossicles Sponge spicules Coral Fish detritus Sharks teeth Arthropod Serpulids Ostracods 	<h3>Qualifiers</h3> <p>dc - decalcified, si - silicified, dp - dissolution porosity after bioclasts</p>
---	---

<h3>Burrows/Biogenic Structures</h3> <ul style="list-style-type: none"> Pellet lined burrows e.g. <i>Ophiomorpha</i> cm-scale horizontal sand-filled burrows e.g. <i>Thalassinoides</i> Simple vertical burrows e.g. <i>Skolithos</i> Vertical spreiten/backfilled burrows e.g. <i>Diplocraterion</i>, <i>Tigillites</i> Collapse/escape burrows e.g. <i>Monocraterion</i> Horizontal spreiten/meniscate burrows e.g. <i>Rhizocorallium</i> Arenicolites, <i>Diplocraterion</i> (with spreiten) Horizontal spreiten filled burrows e.g. <i>Teichichnus</i> Concentric burrow-fills e.g. <i>Asterosoma</i>, <i>Phoebichnus</i> Clustered burrows e.g. <i>Terebellina</i> mm-scale sand-filled burrows e.g. <i>Planolites</i>, <i>Anconichnus</i> Mud-lined burrows e.g. <i>Palaeophycus</i> Mud-filled burrows (intermediate) Meniscate/spreiten burrows e.g. <i>Zoophycus</i>, <i>Taenidium</i> Chondrites

Trends

- Major coarsening/fining-upward
- Minor coarsening/fining-upward
- Cleaning-upward package

Colours

- Dark grey/black
- Medium/dark grey
- Light/medium grey
- White/cream
- Brown/heavy hydrocarbon stain
- Buff/grey (light hydrocarbon stain)
- Dark grey/green
- Light grey/green
- Red
- Orange/brown

Stratigraphy	Samples	Depth (ft. d.d)	Core	Colour	Cements	Fractures	Graphic Lithology	Grain Size & Sedimentary Structures										Event beds	Depth ft. d.d	Lithotypes	Remarks	Depositional Environment	
								M'rock		Sandstone				Conglomerate									Trends
								Clay 0.004	Silt 0.062	V. fine 0.125	Fine 0.250	Medium 0.500	Coarse 1.00	V.Coarse 2.00	Granule 4.00	Pebble 64.00	Cobble 256.00						
		12867																					
		12868																					
		12869																					
		12870																					
		12871																					
		12872																					
		12873																					
		12874																					
		12875																					
		12876																					
		12877																					
		12878																					
		12879																					
		12880																					
		12881																					
		12882																					
		12883																					
		12884																					
		12885																					
		12886																					
		12887																					
		12888																					
		12889																					
		12890																					

Core Sedimentology Log

SHEET 1 OF 21 DATE: 25/06/12

WELL: 16/27A-6

SCALE: 1:20

STRATIGRAPHIC INTERVAL: BRITANNIA SS

PROJECT: RICCARDO TELONI

green granule *

very fractured:

↑ finishing upward with silt and clay on the top (dark grey)

white cream - there are 3-4 fluidifications with a different color of sand (white cream - light grey)

very pow (molto poroso)

Stratigraphy	Samples	Depth (ft. d.d.)	Core	Colour	Cements	Fractures	Graphic Lithology	Grain Size & Sedimentary Structures										Event beds	Depth ft. d.d.	Lithotypes	Remarks	Depositional Environment	
								M'rock		Sandstone				Conglomerate									Trends
								Clay 0.004	Silt 0.062	V. fine 0.125	Fine 0.250	Medium 0.500	Coarse 1.00	V.Coarse 2.00	Granule 4.00	Pebble 64.00	Cobble 256.00						
		12936																					
		12937																					
		12938																			few laminations cut by pillars and pipes		
		12939																			MULTI POROUS		
		12940																					
		12941																					
		12942																					
		12943																					
		12944																					
		12945																					
		12946																					
		12947																					
		12948																					
		12949																					
		12950																					
		12951																					
		12952																					
		12953																					
		12954																					
		12955																					
		12956																					
		12957																					
		12958																					
		12959																					

Core Sedimentology Log

SHEET 4 OF 21 DATE: 25/06/12

WELL: 16/27A-G
SCALE: 1:20

STRATIGRAPHIC INTERVAL: BRITANNIA SS
PROJECT: RICCA RDO TELONI



Stratigraphy Samples	Depth (ft. d.d.)	Core	Colour	Cements	Fractures	Graphic Lithology	Grain Size & Sedimentary Structures										Event beds	Depth (ft. d.d.)	Lithotypes	Remarks	Depositional Environment	
							M'rock		Sandstone				Conglomerate									Trends
							Clay 0.004	Silt 0.062	V. fine 0.125	Fine 0.250	Medium 0.500	Coarse 1.00	V. Coarse 2.00	Granule 4.00	Pebble 64.00	Cobble 256.00						
	13 120																					
	13 121																					
	13 122																					
	13 123	CORE 4																				
	13 124																					
	13 125																					
	13 126																					
	13 127																					
	13 128																					
	13 129																					
	13 130																					
	13 131	CORE 4																				
	13 132																					
	13 133																					
	13 134																					
	13 135																					
	13 136																					
	13 137																					
	13 138																					
	13 139	CORE 4																				
	13 140																					
	13 141																					
	13 142	CORE 5																				
	13 143																					

consolidations associated with pipes and piler with the same setting.
Very sloped

sand very clean.
No consolidation, only a big patches on the bottom of this event.

high porosity
NB → moderate sorted difficult recognizing the grain size.

nodule carbonate with clay in clasts and consolidations.

sand very clean without consolidation (only few) with high porosity and many very small clasts of clay that give the dark color to the sandstone.

starry night

starry night

clay very fractured and altered

starry night

clay *(very compacted, no fractured)

Stratigraphy	Samples	Depth (ft. d.d)	Core	Colour	Cements	Fractures	Graphic Lithology	Grain Size & Sedimentary Structures 454										Event beds	Depth ft. d.d	Lithotypes	Remarks	Depositional Environment	
								M'rock		Sandstone				Conglomerate									Trends
								Clay 0.004	Silt 0.062	V. fine 0.125	Fine 0.250	Medium 0.500	Coarse 1.00	V.Coarse 2.00	Granule 4.00	Pebble 64.00	Cobble 256.00						
		13328																					
		13329																					
		13330																					
		13331																					
		13332																					
		13333																					
		13334																					
		13335																					
		13336																					
		13337																					
		13338																					
		13339																					
		13340																					
		13341																					
		13342																					
		13343																					
		13344																					
		13345																					
		13346																					
		13347																					
		13348																					
		13349																					
		13350																					
		13351																					

Stratigraphy	Samples	Depth (ft. d.d)	Core	Colour	Cements	Fractures	Graphic Lithology	Grain Size & Sedimentary Structures										Event beds	Depth (ft. d.d)	Lithotypes	Remarks	Depositional Environment		
								M'rock		Sandstone				Conglomerate									Trends	
								Clay 0.004	Silt 0.062	V. fine 0.125	Fine 0.250	Medium 0.500	Coarse 1.00	V.Coarse 2.00	Granule 4.00	Pebble 64.00	Cobble 256.00							Boulder
		13856																						
		13857																						
		13858																			mudchips			
		13859																				high grey		
		13860																				calcite		
		13861																						
		13862																				consolidation lamination with high angle.		
		13863																						
		13864																					pilar structures	
		13865																						
		13866																					DW pipes and pilar structures.	
		13867																					NO consolidation/lamination.	
		13868																						
		13869																						
		13870																						mudclast
		13871																						mudclast
		13872																						
		13873																						

Core Sedimentology Log

SHEET 7 OF 7

DATE: 17/08/13

WELL: 16/26-803

SCALE: 1:20

STRATIGRAPHIC INTERVAL: BRITANNIA SST. FM

PROJECT: RICCARDO TELONI

Stratigraphy	Samples	Depth (ft. d.d)	Core	Colour	Cements	Fractures	Graphic Lithology	Grain Size & Sedimentary Structures										Event beds	Depth (ft. d.d)	Lithotypes	Remarks	Depositional Environment	
								M'rock		Sandstone				Conglomerate									Trends
								Clay 0.004	Silt 0.062	V. fine 0.125	Fine 0.250	Medium 0.500	Coarse 1.00	V. Coarse 2.00	Granule 4.00	Pebble 64.00	Cobble 256.00						
		13988																color: dark grey					
		13989																mudclast with sand and silt pebbles photo					
		13990																starry night motif. very well mixed quartz grainsize (0.05-0.1)					
		13991																					
		13992																					
		13993																					
		13994																					
		13995																					
		13996																					
		13997																					
		13998																					
		13999																					
		14000																					
		14001																background is composed of silt injections of VFU sand sand globules floating into mud background linked debris? or mudcap?					
		14002																light grey -> interval with presence of water, calcite between sand grains.					
		14003																					
		14004																					
		14005																some pipes and patches - dewatering					
		14006																					
		14007																					
		14008																					
		14009																					
		14010																					
		14011																					

Core Sedimentology Log

SHEET 1 OF 7

DATE: 16/08/13

WELL: 16/26 - 303

SCALE: 1:20

STRATIGRAPHIC INTERVAL: BRITANNIA SST FORM

PROJECT: RICCARDO TELONI

Stratigraphy	Samples	Depth (ft. d.d.)	Core	Colour	Cements	Fractures	Graphic Lithology	Grain Size & Sedimentary Structures											Event beds	Depth (ft. d.d.)	Lithotypes						Remarks	Depositional Environment			
								M'rock		Sandstone				Conglomerate							Trends										
								Clay 0.004	Silt 0.062	V. fine 0.125	Fine 0.250	Medium 0.500	Coarse 1.00	V.Coarse 2.00	Granule 4.00	Pebble 64.00	Cobble 256.00	Boulder													
		13913	CORE 4																				13.1							green granule - poorly sorted (4mm across)	
		13914	CORE 4																											alterate pyrite 12.6 transition sand fine lower and upper	
		13915	CORE 4																											- clasts granule of clay / medium pebbles	
		13916	CORE 4																											- many silt clasts and rounded granules - sandstone (size fine up/moderated sorted)	
		13917	CORE 4																											alterate pyrite sandstone	
		13918	CORE 4																												
		13919	CORE 4																											Trough cross-bedding planar flat-lying lamination	
		13920	CORE 4																											trough cross-bedding injection of silt?	
		13921	CORE 4																											planar cross bedding	
		13922	CORE 4																											planar and trough current ripple lamination	
		13923	CORE 4																											convolution - laminations	
		13924	CORE 4																											wavy and convolute laminations and soft shearing and faulting. Lamination are truncated at the top of each bed (at the transition of siltstone)	
		13925	CORE 4																											flat-lying lamination of the base and planar cross lamination on the top of the bed sheet	
		13926	CORE 4																											convolution and fluidifications of sand + clay and silt clast folded (80 mm across)	
		13927	CORE 4																											- bioturbation? sand pebble (2.4 mm across)	
		13928	CORE 4																											folded	
		13929	CORE 4																												
		13930	CORE 4																												
		13931	CORE 4																												
		13932	CORE 4																												
		13933	CORE 4																												
		13934	CORE 4																												
		13935	CORE 4																												
		13936	CORE 4																												

Core Sedimentology Log

SHEET 13 OF 16

DATE: 19-01-12

WELL: 16/26 - B04

SCALE: 1:20

STRATIGRAPHIC INTERVAL: BRITANNIA S.S.

PROJECT: RICCARDO TELONI

Stratigraphy	Samples	Depth (ft. d.d)	Core	Colour	Cements	Fractures	Graphic Lithology	Grain Size & Sedimentary Structures											Event beds	Depth ft. d.d)	Lithotypes	Remarks	Depositional Environment	
								M'rock		Sandstone				Conglomerate										Trends
								Clay 0.004	Silt 0.062	V. fine 0.125	Fine 0.250	Medium 0.500	Coarse 1.00	VCoarse 2.00	Granule 4.00	Pebble 64.00	Cobble 256.00	Boulder						
		13950	CORE 4															starry night						
		13951	CORE 4															" clay						
		13952	CORE 4															starry night						
		13953	CORE 4																					
		13954	CORE 4																					
		13955	CORE 4															starry night						
		13956	CORE 4															sand						
		13957	CORE 4															starry night						
		13958	CORE 4															silt > sand						
		13959	CORE 4															several injections of sand with different grain size						
		13960	CORE 4															lamination of sand + silt						
		13961	CORE 4															mixed sand/silt in laminations						
																		starry night						

Stratigraphy	Samples	Depth (ft. d.d)	Core	Colour	Cements	Fractures	Graphic Lithology	Grain Size & Sedimentary Structures											Event beds	Depth ft. d.d)	Lithotypes	Remarks	Depositional Environment			
								M'rock		Sandstone				Conglomerate										Trends		
								Clay 0.004	Silt 0.062	V. fine 0.125	Fine 0.250	Medium 0.500	Coarse 1.00	VCoarse 2.00	Granule 4.00	Pebble 64.00	Cobble 256.00	Boulder								
		16616																irregular fluidificational pipes and patches								
		16617																								
		16618																								
		16619																								
		16620																								
		16621																								
		16622																								
		16623																								
		16624																								
		16625																								
		16626																								
		16627																								
		16628																								
		16629																								
		16630																								
		16631																								
		16632																								
		16633																								
		16634																								
		16635																								
		16636																								
		16637																								
		16638																								
		16639																								

Stratigraphy	Samples	Depth (ft. d.d)	Core	Colour	Cements	Fractures	Graphic Lithology	Grain Size & Sedimentary Structures											Event beds	Depth ft. d.d	Lithotypes	Remarks	Depositional Environment	
								M'rock		Sandstone				Conglomerate										Trends
								Clay 0.004	Silt 0.062	V. fine 0.125	Fine 0.250	Medium 0.500	Coarse 1.00	V. Coarse 2.00	Granule 4.00	Pebble 64.00	Cobble 256.00	Boulder						
		19414																* clay/silt very disrupted and fractured						
		19415																						
		19416																						
		19417																silt with clay folded by sand injection						
		19418																						
		19419																laminations on silt due to sand injections and follow them.						
		19420																						
		19421																						
		19422																						
		19423																*-debris flow stary night with several injections and big clasts of clay - Some of these clasts are altered with pyrite. - the base of bed is massive with small clasts of clay.						
		19424																						
		19425																stary night darker than all bed stary night						
		19426																	? looks like only one event.					
		19427																irregular pipes with small clasts of clay						
		19428																						
		19429																same few irregular pipes	there are not signs of interruption on sedimentation but this part is clearer than the upper part. It is massive as well					
		19430																	May be the presence of pipes in this bed shows that only one event					
		19431																very fine low sand						
		19432																						
		19433																						
		19434																						
		19435																						
		19436																						
		19437																						

Core Sedimentology Log

SHEET 5 OF 11

DATE: 26/03/12

WELL: 16/26-8137

SCALE: 1:20

STRATIGRAPHIC INTERVAL: BRITANNIA SS.

PROJECT: RICCARDO TELONI



Appendix C – Britannia Sandstone Fm. decompaction

Decompaction of the Britannia Sandstone Fm. deposits in the Platform Area was conducted on the basis of the steps described in Section 6.1. This section aims to show what guided the choice of the specific values of each variable needed for the decompaction, together with an evaluation of the associated uncertainty.

C.1 Choice of the porosity (ϕ) and compaction factor (c)

The identification of the different lithologies making up the stratigraphy and the choice of the related coefficients has an important role because of the difference in compaction between the individual lithologies. This difference is a result of physical processes associated with increasing pressure and chemical cementation of the actual sedimentary matrix associated to a specific area and burial depth (e.g., Olowokere, 2011). The actual value of the compaction factor (c) of different lithologies in the Central North Sea is largely determined by sediment composition and thermal history related to the North Sea Basin (as is shown for the calculation of compaction coefficient for shales by White and Latin, 1993).

Values of initial porosity (0.63) and compaction factor (0.51) for the *shales* (Table C.1; Fig C.1) were calculated by Sclater and Christie (1980) from sonic log plots for a normally pressured section described by Schlumberger (1974). This was done using the sonic log velocity/porosity relation of Magara (1976a), and a relationship to calculate porosities from transit times for shales derived by Hanses (1996). Given the agreement within the literature on such values of initial porosity and compaction factor (e.g., see test for shales buried at 2600 metres for the North Sea; Sclater and Christie, 1980), it is assumed that these values are also applicable to Britannia reservoir shales buried at depths of 3700-3800 meters.

Values of initial porosity (0.49) and compaction factor (0.27) for *sands* (Table C-1) for the North Sea, are proposed by Sealey (1976) and supplemented with data calculated using observed sonic velocities and the velocity/porosity tables of Schlumberger (1974) (Fig. C-1).

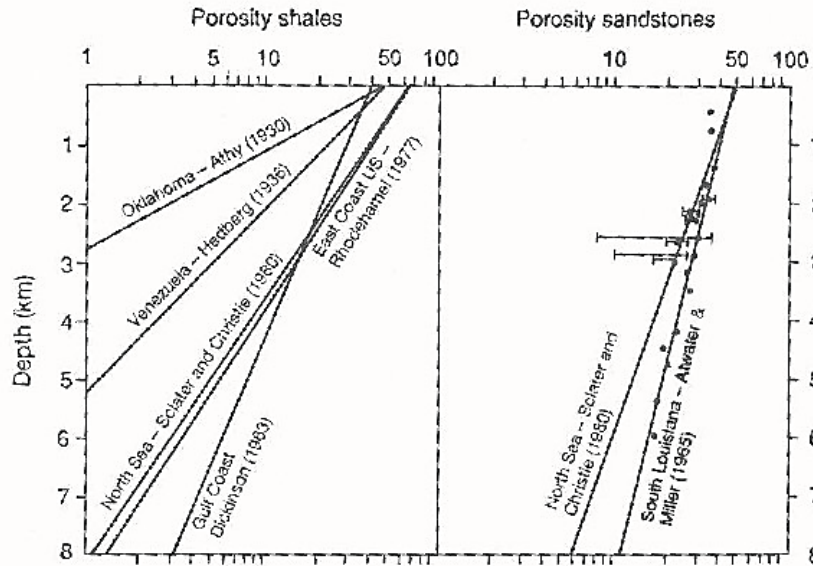


Fig. C-1 – Plots of log porosity versus depth for shales and sandstones (from Sclater and Christie, 1980)

However, sands initial porosity based on Pryor's (1973) data is considered too high (see Section 5.2.2.2) and it is here investigated through a comparative analysis of reconstructed porosity/depth curves from initial porosity of artificially mixed wet-packed sand and the real porosity of the sands at the Britannia reservoir depth, measured from core samples (by BOL).

Initial porosity (ϕ_0) value for the *sands* of Britannia Sandstone Fm. was selected from the artificially mixed wet-packed sand table proposed by Bear and Weyl (1973) and it was compared and tested against the Sclater and Christie (1980) porosity-depth curve. The porosity-depth curve for the Britannia sands can be reconstructed knowing the initial porosity value (at surface), and the exponent of the exponential relationship between the porosity and the depth (eq. 1). The equation can be inverted to calculate the exponent having the initial porosity and one value of porosity at depth. Present-day porosities at depth can be determined from petrophysical logs as downhole sonic or density logs calibrated on core with the associated facies scheme of Moore et al. (2009) and with the revised facies for this work (Table 6.2 in Chapter 6). Britannia sandstones at reservoir depths (i.e., between 3700 and 3800 meters) range in porosity from 13% to 16%, with variations mainly depending on the sorting and grain size of the sand fraction and the presence of silt and clay particles, characteristic of each lithofacies (Table C.1).

Sand Facies	Sand ϕ (Britannia sands) 3700/3800 meter	Sand ϕ_0 (Britannia near the surface) calculated after Bear and Weyl (1973)
Massive	16 %	39 %
Laminated	14-18 %	36 %
Banded	13 %	34 %
Injected	16 %	39 %
Mixed Slurried	10-14 %	34 %
Average values	15 %	37 %

Table C-1 – Summary of porosity values/facies in the Britannia Sandstone Fm. and reconstructed porosity near the surface calculated with the Table. 3.2 proposed by Bear and Weyl (1973).

The reconstruction of the porosity-depth curves for Britannia sands is based on the calculation of the compaction coefficient (c) of sands which can be directly calculated using the reverse decompaction equation (3):

$$c = \frac{-\log\left(\frac{\phi}{\phi_0}\right)}{y} \quad (4)$$

For sandstones with reservoir and near surface porosities of 13 and 34%, respectively, the compaction coefficient is 0.252 whereas for sandstone comparative values of 16 and 39% the coefficient is 0.234 (see also Section C.2 below). Assuming these values, the variation of porosity with depth was then calculated for Britannia sands of near surface porosity (ϕ_0) of 34% and 39% using equation (1). The results were plotted on a porosity-depth graph and compared with the Sclater and Christie curve in which they assigned 49% porosity for near surface sands. The graph highlights the decrease of porosity at different depths, with the curves ϕ_0 39% and 49% relatively close at the present Britannia depth (3700-3800 meters) (Fig. C-2). The difference between the real porosity and reconstructed porosities by the three curves at Britannia reservoir depths is on the order of 1% and 2% (Table C-2).

The reconstructed curves also highlight slightly different results between the three sand porosity models, with values of the 34% depth-porosity curve moderately farther from the average porosity measured on Britannia sands (Fig. C-2) On this basis the choice of near surface sand porosity of 39% is considered the most reliable value to be used for this study.

	Average measured Britannia reservoir sand ϕ (BOL)	Reconstructed d Sand 34(ϕ_0)	Reconstructed Sand 39(ϕ_0)	Reconstructed Sclater & Christie (ϕ_0)
Porosity at Britannia reservoir depth (3700-3800 m)	15%	13%	16%	17.5%

Table C-2 – Summary of the measured and reconstructed porosity at reservoir depth (3700-3800 m).

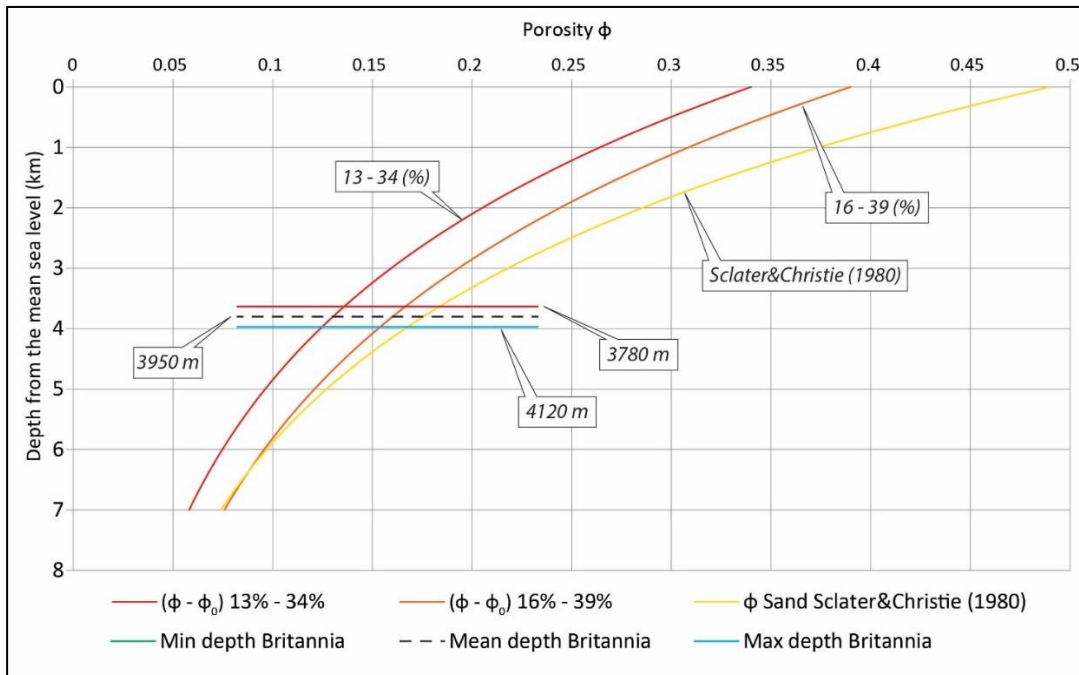


Fig. C-2 – Reconstructed porosity-depth curves for sands initial porosity taken by Bear and Weyl's (1973) table and reservoir porosities, compared against the Sclater and Christie curve.

C.2 Calculation of sand/mud decompaction coefficients for a chosen decompaction interval

An important step in the decompaction workflow is the calculation of the decompaction coefficients for sand and mud. These values will be then multiplied for the net/gross of each stratigraphic interval to be decompacted. The effect of moving the top of a stratigraphic package top y_1 vertically to a new shallower depth $y'_1 = 0$ (near surface) can be calculated by using the inverse function of the decompaction equation (3). In fact, as y_1 and y_2 are the present depths of the top and bottom of a section and ϕ_0 and c are constant and known, $y'_2 - y'_1$ can be evaluated, since y'_1

corresponds with the bottom of the previous layer (Fig. 5.1). Having calculated y'_1 by working down the sedimentary column, y'_2 can be evaluated by numerical methods.

$$y'_2 = (y_2 - y_1) - \frac{\varphi_0}{c} \{(\exp(-cy_1) - (\exp(-cy_2)))\} + \frac{\varphi_0}{c} \{(1 - \exp(-cy'_2))\} \quad (3)$$

The formula should be applied to each reservoir interval making up the Britannia Field stratigraphy for each well of the Platform Area. The solution to this general decompaction equation (3) essentially represents the exercise of sliding the sediment layers up along the exponential porosity-depth curve; it can be computed by numerical iteration which makes it ideal for solving using software. Considering the complexity of the dataset and the large amount of data a simplified solution based on a Microsoft Excel spreadsheet is proposed for this work. This requires adopting a series of approximations whose sensitivities were investigated and numbered assigning a percentage of uncertainty and possible error in the final calculation of the decompacted deposit thicknesses.

The first simplification adopted in this methodology consists in calculating decompaction coefficients for mud and sand that could be used to decompact any interval within the reservoir. In other words, a unique set of mud and sand decompaction coefficients was calculated by choosing a 'model' interval of 'model' thickness at a defined depth position within the Britannia reservoir. Different thicknesses of such 'model' interval (1, 5, 10, 25 and 50 meters) and different positions within the reservoir (top, base and centre) were tested to minimise the errors associated with the above simplification (Fig. C-3).

An interval of a thickness of 10 meters for both sand and mud as 'model' decompaction interval was chosen as this value best approximates the average thickness of the reservoir intervals used in the decompaction workflow. Decompaction coefficient for sand was calculated for a 'model' thickness interval of 10 meters placed at the average middle point of the reservoir thickness (3800.19 m). This average point was determined as the middle point between the maximum depth of Z10A-base measured in well B12, and the minimum depth of Z50-top measured in 16/26-19. These values correspond respectively to the base and top of Britannia Sandstone Fm. in the Platform Area. At this was subtracted the water depth measured on the present seafloor above the Britannia Field area (approx. 150 metres) (Fig. C-3).

a) MIN Brit. absolute depth (Z50 Top)	b) MAX Brit. absolute depth (Z10A Base)	c) Mudline Z50 Top depth (water d. 150 m)	d) Mudline Z10A Base depth (water d. 150 m)	e) Average Middle point reservoir from mudline	f) Mud decomp. coefficient	g) Sand decomp. coefficient
3780.19 m	4120.19 m	3630.19 m	3970.19 m	3800.19 m	2.4519	1.3752

Table C-3 – Britannia Field depth of intervals in the Platform Area: a-b) depths of base and top of Britannia Sandstone Fm.; c-d) depths of base and top of Britannia Sandstone Fm. without water depth; e) calculated average middle point of the reservoir; f-g) decompaction coefficients for mud and sand based on the simplification adopted in the model (see text for explanation).

The mud decompaction coefficient was instead calculated for a ‘model’ interval of 10 meters placed in the lower portion of the reservoir (3970.19 m); this choice is due to the high concentration of hemipelagic intervals in the lower Britannia stratigraphy.

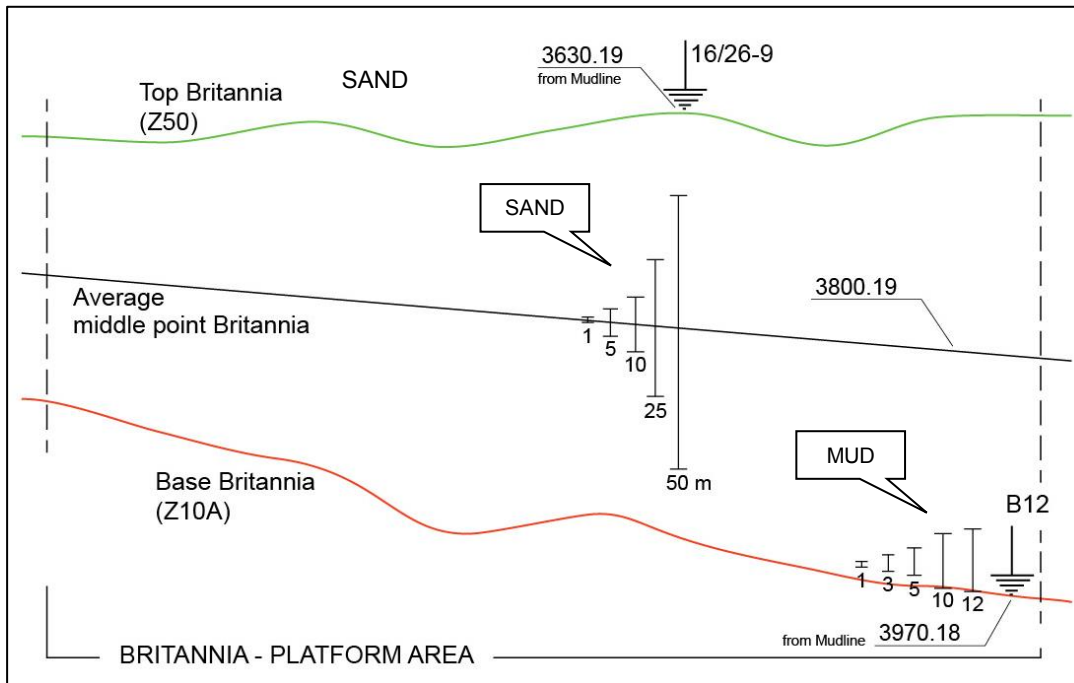


Fig. C-3 – Decompaction interval within the Britannia Field deposits. The sketch shows the decompaction intervals chosen for mud and sand, respectively placed at the base and middle average point of the reservoir.

C.3 Sand/mud decompaction coefficients sensitivities

The formula to calculate the decompaction coefficients for mud and sand includes two main parameters, the initial porosity and the compaction factors of each lithology, as described in the previous paragraph. The choice of the initial porosity and compaction values for mud and sand has a significant influence on the calculation of the decompaction coefficients for mud and sand and hence plays an important role in the decompaction analysis itself. Values for shales or shaley sandstones vary little in the literature (e.g., Sclater and Christie 1980; Egawa et al., 2013; Sheldon and Retallack, 2001), with a consensus that the depositional porosity in shales is generally around 60%. However, as detailed above (section C-1), a range of values for the sandstones were tested because of the different choices operated by various authors in the past (Maxwell, 1964; Selley, 1978; Atwater and Miller, 1965; Pryor, 1973; Sclater and Christie, 1980; Thorne and Watts, 1989).

For each of the three tested initial porosity and compaction coefficient values for the sand (models with initial porosity of 34%, 39% and 49%), the resulting decompaction coefficients were calculated. Note that as detailed in (see Section 5.2.2.2) the 39% is the model chosen. Three tests were undertaken to assess independently from each other the influence of the initial porosity and compaction coefficient choice, and that of the 'model' interval thickness and depth.

As expected, the choice of initial porosity and compaction coefficient results in the higher uncertainty and it is on the order of 4.59% between the models with 34% and 39% initial porosity. This uncertainty increases significantly if we compare the chosen model (39%) with Sclater and Christie's sand value (17.54%) (Table C-4).

The decompaction coefficients for each of the three models were also calculated at different reservoir depths in order to estimate the uncertainty associated with the choice of the 'model' interval depth. Decompaction coefficients for sand with initial porosity of 34% calculated at the base, top and middle reservoir depth shown a maximum difference of 1.29%. The maximum difference between decompaction coefficients for sand with initial porosity of 39% (the chosen value) was on the order of 1.53%, whereas for Sclater and Christie values (49% initial porosity) the uncertainty was 1.97% (Table C-4).

	Sand 13(ϕ)-34(ϕ_0)			Sand 16(ϕ)-39(ϕ_0)			Sclater&Christie 49% (ϕ_0)		
	Top Brit 3630.2	Middle 3800.2	Base 3970.2	Top Brit 3630.2	Middle 3800.2	Base 3970.2	Top Brit 3630.2	Middle 3800.2	Base 3970.2
Decom coeff.	1.3077	1.3163	1.3246	1.3645	1.3752	1.3854	1.597	1.6131	1.6284
Uncert. for reservoir depth	1.29%			1.53%			1.97%		
Uncert. for sand (ϕ)-(ϕ_0)	4.59% (based on 13-34 /16-39 comparison)						17.54% (based on 16-39 / Sclater&Christie comparison)		

Table C-4 – Summary of the calculated decompaction coefficients for sand for different intervals and mud in function of interval and depth.

The uncertainty in the calculated mud and sand decompaction coefficients associated with the choice of different ‘model’ interval thicknesses was also tested. The range of thicknesses investigated was between 1 and 50 meters for sands and between 1 and 12 meters for muds. These values correspond to the minimum and maximum thickness of reservoir intervals dominated by a single lithology (sand or mud respectively) in the Platform Area. It resulted that the maximum uncertainty related to the thickness of the chosen ‘model reservoir interval’ is equivalent to 0.47% for the sands and 1.19% for the muds (Table C-5).

THICKNESS DECOMPACTION INTERVAL FOR SAND AT MIDDLE BRIT. RESERVOIR (M) AT 3800.2 M	SAND 16% (Φ) - 39% (Φ_0)	THICKNESS DECOMPACTION INTERVAL FOR MUD IN AT BASE BRIT. RESERVOIR (M) AT 3970.2 M	MUD 63% (ϕ_0) WITH SCLATER & CHRISTIE (1980)
1	1.376	1	2.476
5	1.376	3	2.47
10	1.3752	5	2.4646
25	1.37308	10	2.4519
50	1.3696	12	2.4468
MAX DIFFERENCE IN UNCERTAINTY OF THICK. INTERVAL	0.47 %	Max uncertainty in function of thickness interval	1.19 %

Table C-5 – Calculated decompaction coefficients for sand and mud in function of different ‘model’ interval thicknesses.

C.4 Reservoir intervals thicknesses

Britannia stratigraphy was subdivided in 18 intervals based on their lithological and sedimentological character (see Chapter 4); these intervals formed the basis for the decompaction workflow. Intervals mainly composed of hemipelagites range in thickness between 1.2 and 12 m, whereas intervals dominated by sandstones and remobilised sediments range in thickness between 3.4 and 56.4, and between 16.5 and 53.7 meters respectively (Table C-6).

Reservoir Intervals / Thickness	Sandstone intervals (Turbidites, HEBs)	Debrite intervals (MTDs)	Mudstone intervals (Hemipelagites)
Min (m)	3.4	16.5	1.2
Max (m)	56.4	53.7	12.0

Table C-6 – Summary of the calculated min and max thickness value of the Britannia Field reservoir intervals.

C.5 Calculation of the net/gross through core inspection (a) and related sensitivities

All the 11 lithofacies identified on core were grouped according to their lithotypes (sandstones, debrites and mudstones) and uploaded into the Britannia Field Database managed via the ODM (Oilfield Data Manager) software in order to have the exact absolute depth (base and top) of each lithology and hence their thickness. Each of these thicknesses was multiplied for the net/gross value assigned to the lithotype (clean sandstone = 1; mixed sandstone/mudstone = 0.7; sandy debrite = 0.3; muddy debrite = 0.1; mudstone = 0). Precise net-to-gross values were calculated for each reservoir interval for each well subdividing the summed net/gross values of each lithology making up the interval, for the entire thickness of the reservoir interval.

$$1) \text{ net/gross} = \text{facies thickness (m)} * \text{coeff (1; 0.7; 0.3; 0.1; 0)}$$

$$2) \frac{\sum \text{calculated net/gross}}{\sum \text{facies thickness (m)}} = \text{Zone net/gross}$$

This methodology was applied to all the cored intervals logged for this study (Z10A-Bed 58 interval) and it was also applied for uncored-wells in the Z10A-Bed 58 interval, taking in consideration Moore's (2009) facies scheme, based on the integration of core investigation together with cuttings analysis.

The calculation of net/gross of the upper reservoir (Z45, MTD-6 and Z50) needed a different approach given that this interval was not object of this study and therefore a

facies classification from new core logging or from Moore's (2009) work was not available. Net/gross for the sandstone zones Z45 and Z50 was calculated using wireline log data. In order to extrapolate net/gross values for these zones, the relation between gamma ray values (GRREF: gamma ray data contained into the Britannia ODM database provided) and net/gross needed to be established. In particular this relationship was studied for those wells provided of core logs in the studied interval (Z10A-Bed 58) and with a net/gross calculated through core inspection and facies analysis. A reliable correlation between net/gross and GRREF was observed for the sandy intervals (Fig. C-4) and the linear best-fit was used to extrapolate the most likely net/gross for the upper Z45 and Z50 sand intervals.

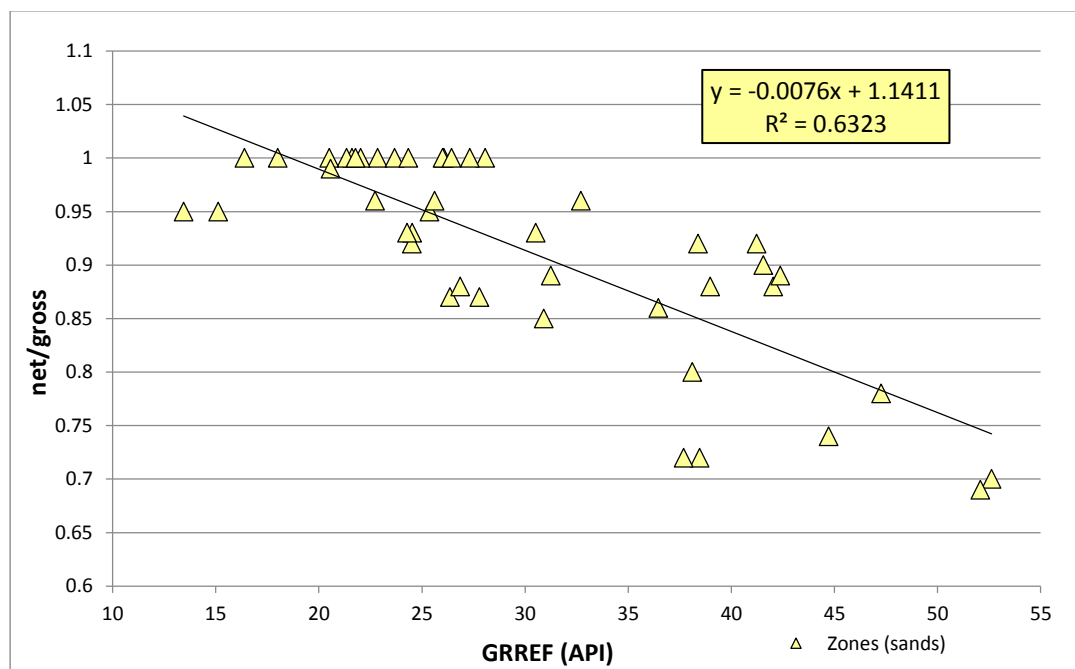


Fig. C-4 – Graph showing the relationship between net/gross and gamma ray value for sand intervals on cored wells (reservoir interval Z10A-Bed 58).

$$n/g = (-0.0076 * GRREF) + 1.1411$$

However, no correlation between net/gross and GRREF values could be observed for the reservoir intervals made up of debrites (i.e., mass-transport deposits, MTDs). Figure C-5 shows that their average gamma ray values do not correlate with the net/gross, likely due to the heterogeneous character of the deposits. Low values of GRREF and high net/gross likely represent reservoir intervals characterised by the presence of large sand clasts incorporated into a sandy matrix whereas a muddy matrix with mud clasts is usually associated with high values of gamma ray and low

net/gross ratio (Fig. C-5). For this reason the net-to-gross values for the MTD-6 was visually estimated by using wireline logs and cuttings charts.

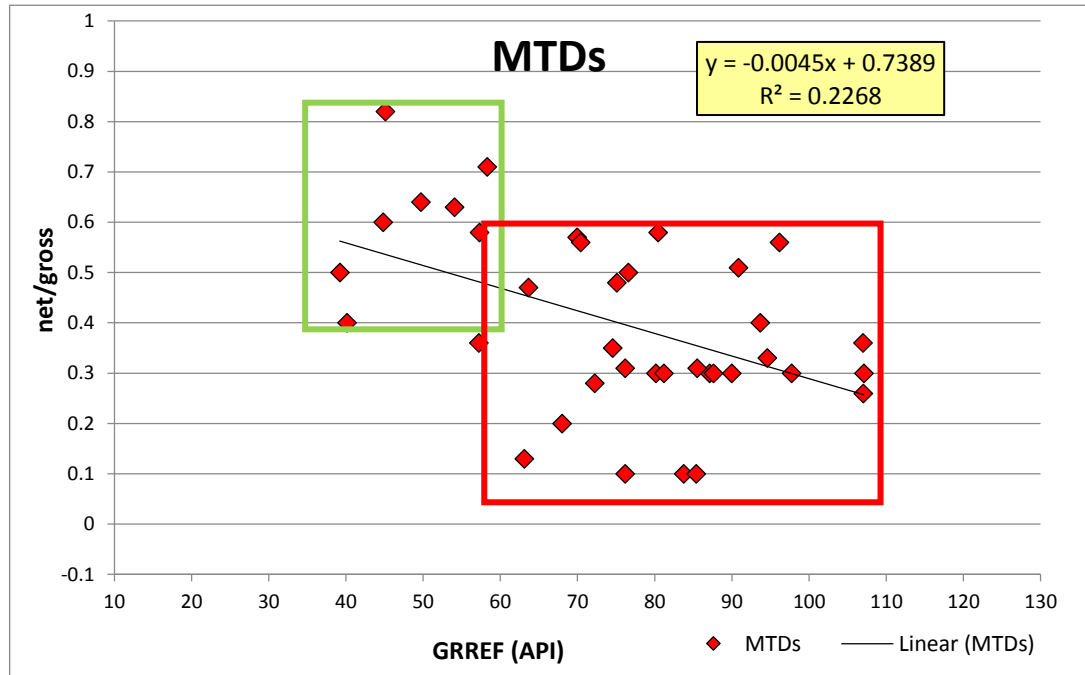


Fig. C-5 – Graph showing net/gross vs. gamma ray values for debritic intervals corresponding to MTDs on cored wells (reservoir interval Z10A-B58). Boxes show the concentration of sand clasts in MTDs: green = high; red = low.

The three methodologies used to calculate the gamma-ray (new core description and lithofacies scheme; lithofacies scheme by Moore, 2009 and estimation by best-fit-approach with GRREF) were tested for cored wells within the study interval where they could all be applied. The aim was to study the difference in the results between the three approaches. The average difference between the net-to-gross values for sandy intervals calculated using the new core-based facies schemes used in this work and that proposed by Moore, 2009 is 10% and that between the new facies scheme and the best-fit approach based on the GRREF is 16% (Table C-7). The differences arise due to differences in the facies schemes and to the difficulty in their identification from the cuttings analysis.

A high uncertainty characterises the choice of net/gross values for the MTDs, due to the high heterogeneity of these deposits. Differences between new core-based facies schemes used in this work and that proposed by Moore, 2009 can be up to 40-70% (Table C-7).

Well B01	Z10A	MTD1	Z10B	Z20	MTD2	Z40A	MTD3	Z40B	MTD4	Z40C	Z45	MTD6	Z50
RT	1	0.47	0.93	-	0.3	0.87	0.1	0.92	0.28	0.78	-	0.19	-
IDM	1	0.55	0.88	-	0.2	0.8	0.2	0.87	0.2	0.71	-	-	-
GRREF	1	-	0.95	-	-	0.93	-	0.95	-	0.78	0.91	-	0.87
RT vs IDM (%)	0.0	15.7	5.5	-	40.0	8.4	66.7	5.6	33.3	9.4	-	-	-
RT vs GRREF (%)	0.0	-	2.1	-	-	6.7	-	3.2	-	0.0	5.3	-	2.3

Table C-7 – Tab shows the net/gross for selected reservoir intervals of well B01. RT indicates the net-to-gross calculated from new facies analysis from core. IDM indicates net-to-gross calculated using the facies scheme of the Britannia Field by Moore (2009). Finally, GRREF indicates net-to-gross calculated using the empiric relationship between net to gross and GRREF. The last two rows, the difference in percentage between the net-to-gross calculated with different methodologies is shown.

C.6 Errors associated with the simplified decompaction workflow

A full decompaction workflow aiming at reconstructing the original thicknesses of a number of stratigraphic intervals at different times should also include a correction for the partial re-compaction of the decompacted sediment. However, to simplify the calculations this correction was not included in the used decompaction workflow. In other words, the thickness of one of the lower intervals of the reservoir even at the time of the deposition of the uppermost reservoir interval was considered to be as fully decompacted (i.e. as if that layer was actually at surface, rather than being buried below the entire reservoir).

In order to assess the error associated with this simplification, a full decompaction analysis including a correction for sediment re-compaction was conducted for the well B04 (Table C-8). Decompaction coefficients for mud and sand were progressively calculated for the exact thickness of each reservoir interval (rather than the 'model' interval thickness of 10m) and for the exact depth (rather than the fixed depth of the 'model' interval). Crucially, by doing so the effect of sediment re-compaction was also included. The decompacted thickness of the reservoir from the base of Z10A up to the top of Z50 was reduced by 5.13 metres (i.e., 187.5 m vs 182.4 m), equivalent to 2.8% of the decompacted stratigraphy (Table C-8-A).

As the chosen interval covers most of the reservoir thickness, this is the maximum possible error due to the simplified decompaction workflow (note that the resulting thicknesses will always be greater than those calculated with a full decompaction workflow). A comparable exercise was undertaken for a thinner interval, between the base of Z10A and the base of Z40A (Table C-8-B). Not surprisingly, the results show

a much smaller total error (0.07 m = 0.2%) as the amount of error is a function of the considered decompaction interval. It is also necessary to specify that such thick decompaction interval (~148 meters between Z10A and Z50 before decompaction) was never used with the methodology chosen for the Britannia Field, because of the presence of B58 and its use as a datum, therefore splitting the reservoir into two.

It should be noted that the overestimation in the thickness of the reservoir intervals associated with the simplification in the decompaction workflow has an opposite trend compared to the other approximations adopted in the various steps of the selected decompaction process. In addition it is also important to note that considering the depth-compaction curves of sand and mud (Fig. C-2) calculation of the compaction coefficients with the reverse decompaction formula (3) is very sensitive for shallow depths which could correspond to the Britannia stratigraphic thickness (100-200 meters) and therefore a full decompaction workflow could generate additional errors due to the shape of those curves.

a) B04 - Base of MTD6 - using Z10A as datum						
Reservoir Interval	Base (m)	Net/ Gross	Thickness (m)	Decomp Thickness current model (m)	Decomp Thickness progressive current model (m)	Decomp Thickness progressive - with sediment loading (m)
Z50	3734.97	0.83	18.13			
MTD-6	3744.57	0.1	9.60			0.00
Z45	3758.00	0.93	13.43	19.48	19.48	19.41
B58	3763.50	0.77	5.50	8.92	28.39	28.23
Z40C	3777.89	0.81	14.40	22.74	51.13	50.64
Mud Undiff.	3778.14	0	0.25	0.60	51.74	51.22
MTD-4	3782.26	0.56	4.12	7.62	59.36	58.62
Z40B	3787.29	0.9	5.03	7.46	66.81	65.96
Mud Red	3787.71	0.25	0.41	0.90	67.71	66.82
MTD-3	3796.94	0.4	9.24	18.66	86.37	84.63
Z40A	3842.60	1	45.66	62.78	149.15	146.48
Mud Grey	3846.07	0	3.47	8.49	157.64	154.07
MTD-2	3850.17	0.3	4.10	8.72	166.36	161.96
Z10B	3850.25	1	0.09	0.12	166.48	162.08
MTD-1	3851.20	0.35	0.94	1.95	168.43	163.85
Mud Black	3851.83	0	0.63	1.55	169.98	165.22
Z10A	3864.60	1	12.77	17.56	187.54	182.41
5.13 m = 2.8%						
b) B04 - Base of Z40A - using Z10A as datum						
Reservoir Interval	Base (m)	Net/ Gross	Thickness (m)	Decomp Thickness current model (m)	Decomp Thickness progressive current model (m)	Decomp Thickness progressive - with sediment loading (m)
Z40A	3842.60	1	45.66	62.78		0.00
Mud Grey	3846.07	0	3.47	8.49	8.49	8.50
MTD-2	3850.17	0.3	4.10	8.72	17.21	17.18
Z10B	3850.25	1	0.09	0.12	17.33	17.30
MTD-1	3851.20	0.35	0.94	1.95	19.28	19.24
Mud Black	3851.83	0	0.63	1.55	20.83	20.77
Z10A	3864.60	1	12.77	17.56	38.39	38.32
0.07 m = 0.2%						

Table C- 8 – Full decompaction step by step of the reservoir intervals (Z10A-MTD-6) in well B04 with comparison between the decompaction adopted for this work and the decompaction provided of sediment loading correction. b) Full decompaction step by step for shallower stratigraphy (Z10A-Z40A).

Appendix D – Correlation panel of the Casaglia MTD

Sedimentary graphic logs constructed in the field for the stratigraphic interval (~60 m) overlying the Casaglia MTD are shown in the correlation panel presented in Figure 7.12 of the Chapter 7. A high resolution version of this panel is included in the CD-ROM attached to this thesis. The correlation panel is built upon the 18 sedimentary logs across the four identified sectors, forming two hinged orthogonal transects 2.5 km and 9 km long.

A standard sedimentological logging procedure was followed for each log (1:20 scale), recording lithology, grain size, internal fabrics and sedimentary structures, palaeoflow indicators, bedding dips and strikes, fossils and additional observations.